Docket 71-9305

AREVA

TRUPACT-III

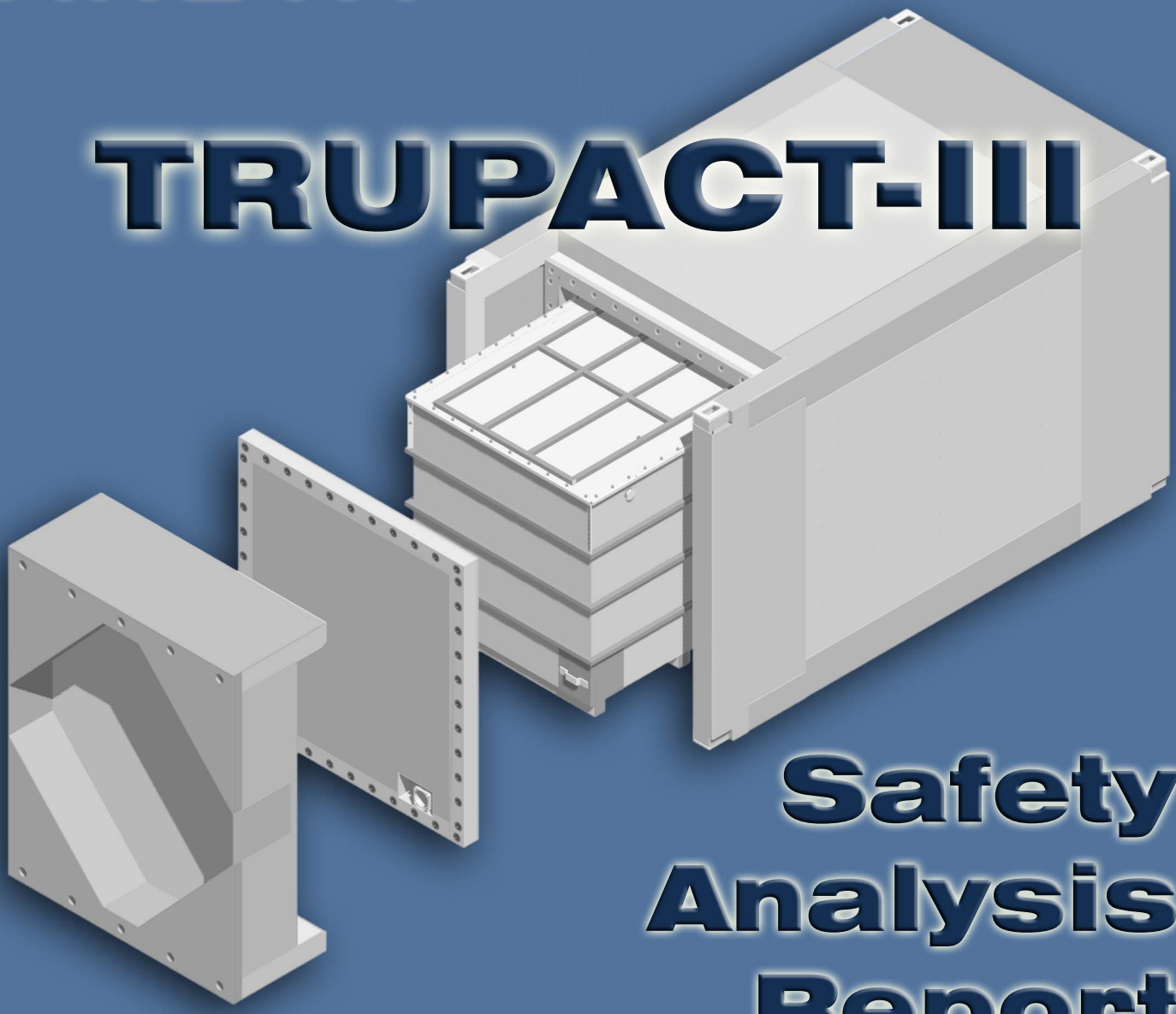

Safety Analysis Report

Revision 15
July 2013

AREVA Federal Services LLC

TABLE OF CONTENTS

This page intentionally left blank.

1.0 GENERAL INFORMATION

This chapter of the Safety Analysis Report (SAR) presents a general introduction and description of the TRUPACT–III contact–handled transuranic (CH–TRU) waste packaging. The major components comprising the TRUPACT–III packaging are presented in Figures 1.1-1 through 1.1-7. Figure 1.1-1 presents an exploded view of all major TRUPACT–III packaging components. Figure 1.1-2 presents a cross–section of the body, with Figure 1.1-3 presenting a cross–section detail of the body wall. Figure 1.1-4 presents the containment structural assembly (CSA). Figure 1.1-5 presents a detailed view of the closure lid and O–ring seal region. Figure 1.1-6 presents a cross–section of the overpack cover. Figure 1.1-7 presents a detailed view of the debris shield. Drawings of the TRUPACT–III packaging design are presented in Appendix 1.3.1, *Packaging General Arrangement Drawings*. All details relating to payloads and payload preparation for shipment in a TRUPACT–III package are presented in the *TRUPACT–III TRU Waste Authorized Methods for Payload Control (TRUPACT–III TRAMPAC)*[1]. Terminology and acronyms used throughout this document are presented as Appendix 1.3.2, *Glossary of Terms and Acronyms*.

1.1 Introduction

The model TRUPACT–III packaging has been developed by AREVA Federal Services LLC (AFS) as a safe method for transportation of CH–TRU waste materials. The TRUPACT–III packaging is intended primarily for truck transport, and may also be transported by rail. In truck transport, a single TRUPACT–III package is transported on a semi–trailer.

The structure of the TRUPACT–III packaging can sustain both normal conditions of transport (NCT) and hypothetical accident condition (HAC) structural and thermal loadings without loss of leaktight capability[2]. Two full–scale TRUPACT–III certification test units (CTU) were subjected to a series of free and puncture drop tests. These tests, together with structural, thermal, and criticality analyses, conclusively demonstrate the containment integrity of the TRUPACT–III package.

The CH–TRU waste material payload within the TRUPACT–III packaging will be confined within a single steel SLB2 container, supported by a payload loading system, such as a pallet and roller floor. Specifications for SLB2 payload containers and loading systems are provided in the TRUPACT–III TRAMPAC.

Based on the shielding and criticality assessments provided in Chapter 5.0, *Shielding Evaluation*, and Chapter 6.0, *Criticality Evaluation*, the Criticality Safety Index (CSI) for the TRUPACT–III package is zero (0.0), and the shielding Transport Index (TI) is determined at the time of shipment. Authorization is sought for shipment of the TRUPACT–III package by truck or railcar as a Type B(U)F –96 package per the definition delineated in 10 CFR §71.4[3].

[1] U.S. Department of Energy (DOE), *TRUPACT–III TRU Waste Authorized Methods for Payload Control (TRUPACT–III TRAMPAC)*, U.S. Department of Energy, Carlsbad Field Office, Carlsbad, New Mexico.

[2] Leaktight is defined as 1×10^{-8} reference Pascals – cubic meters per second (Pa–m^3/s), or less, air leakage per the definition in ANSI N14.5–1997 (or later), *American National Standard for Radioactive Materials – Leakage Tests on Packages for Shipment,* American National Standards Institute, (ANSI), Inc.

[3] Title 10, Code of Federal Regulations, Part 71 (10 CFR 71), *Packaging and Transportation of Radioactive Material*, 01–01–09 Edition.

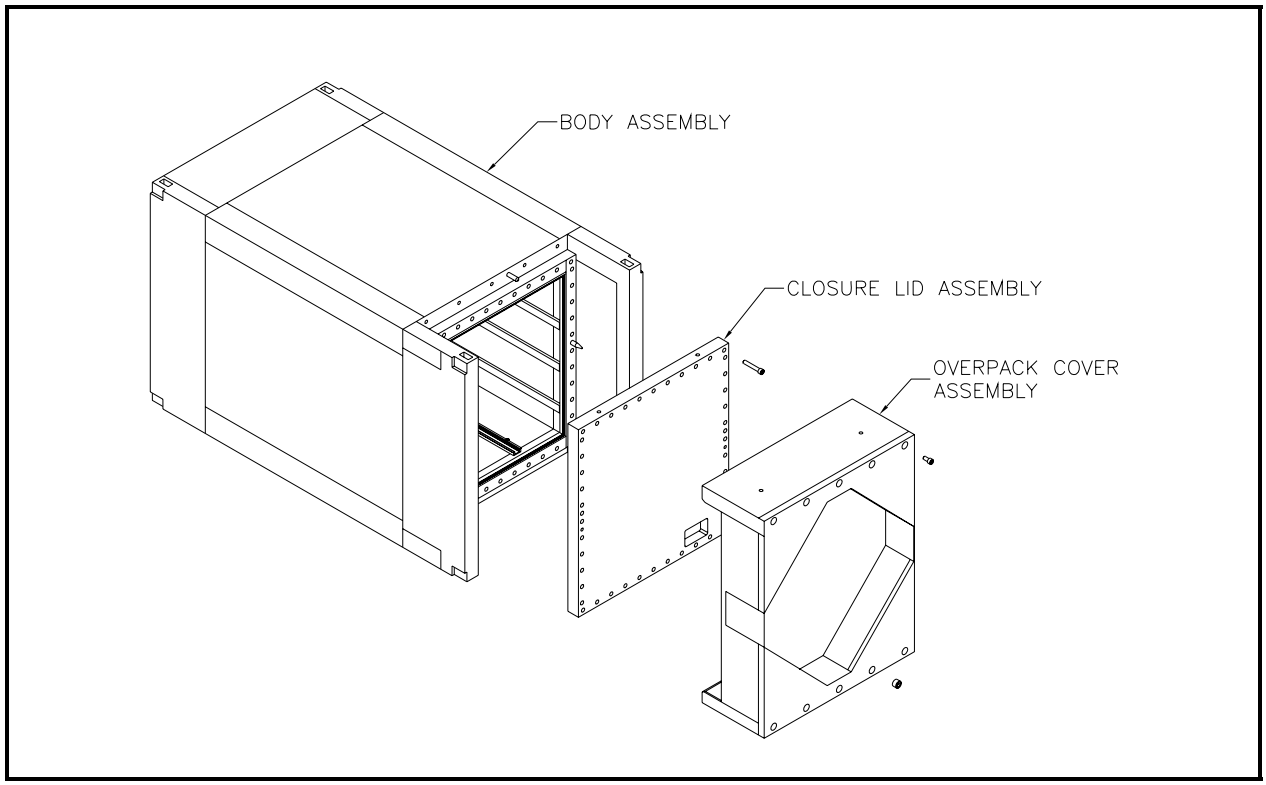

Figure 1.1-1 – TRUPACT–III Packaging Assembly

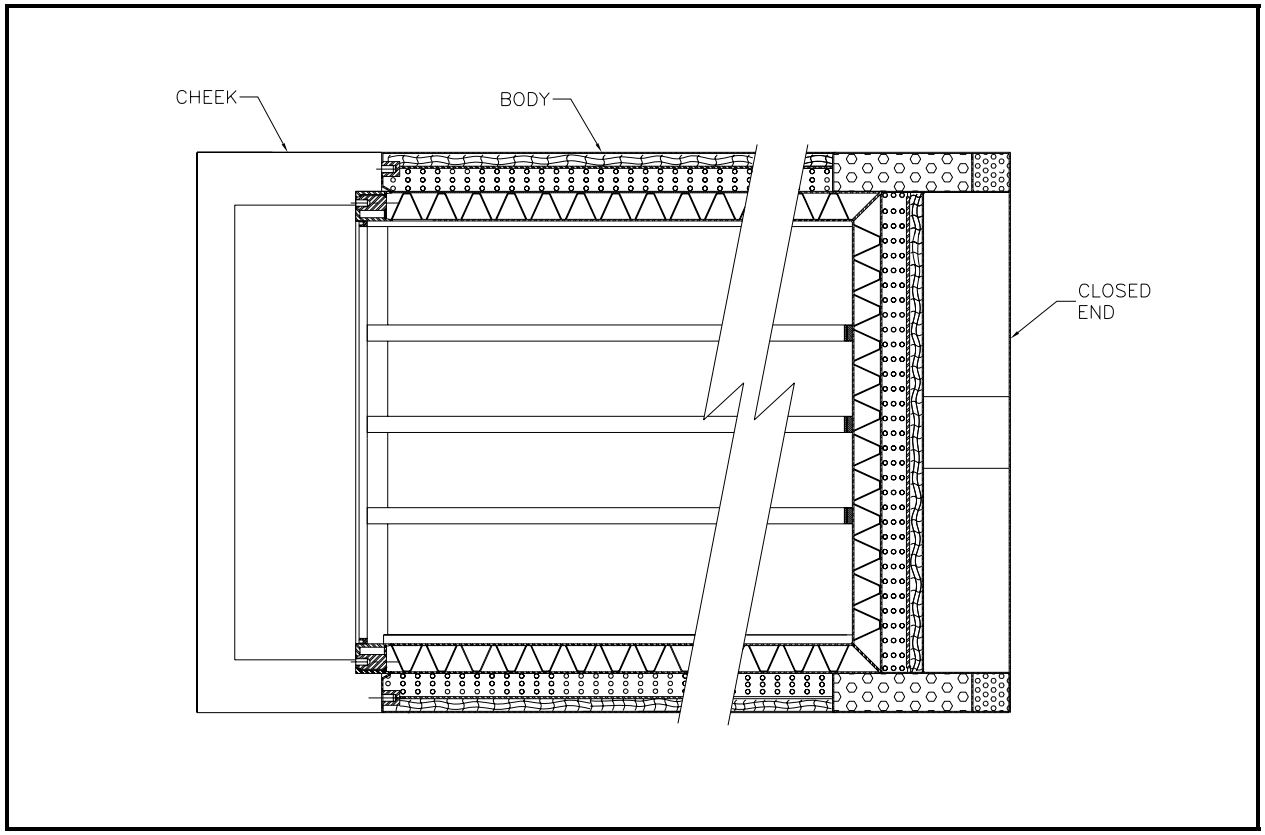

Figure 1.1-2 – TRUPACT–III Packaging Body Cross–Section

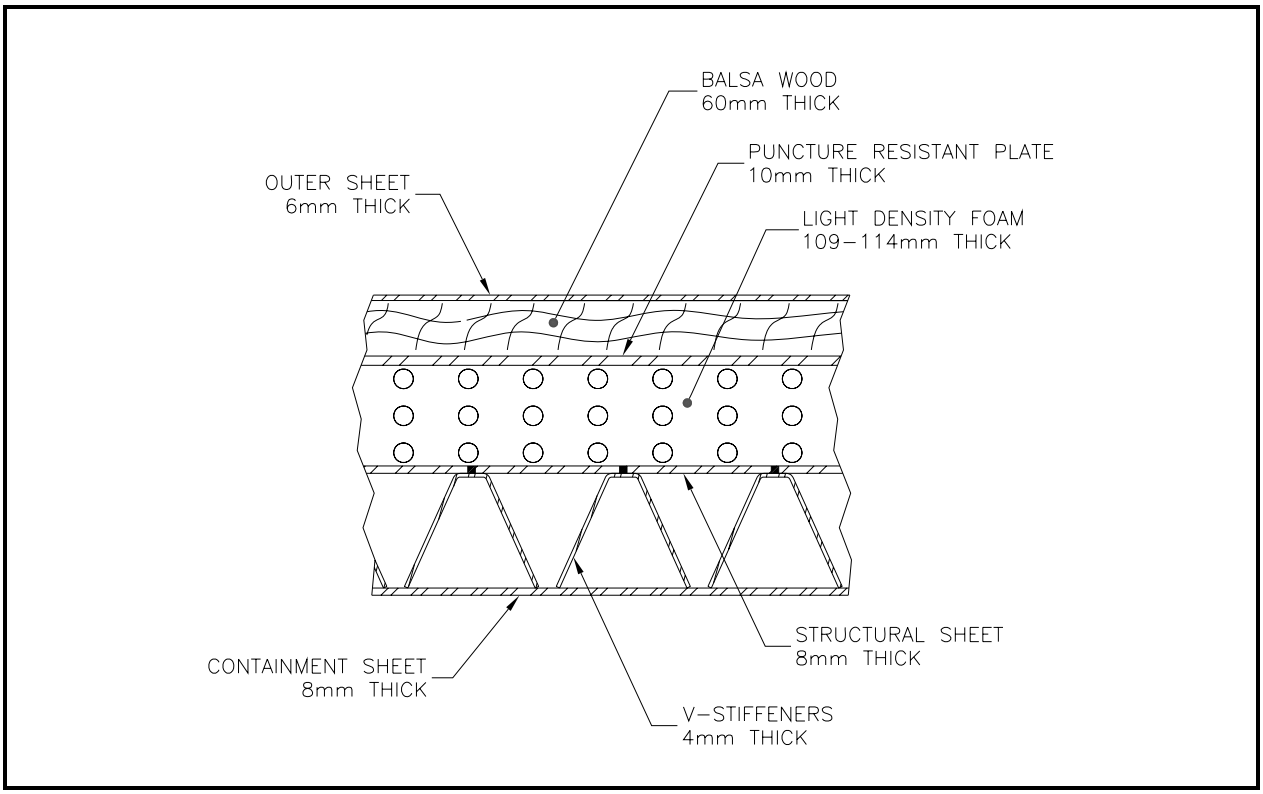

Figure 1.1-3 – TRUPACT–III Packaging Body Side Wall Cross–Section

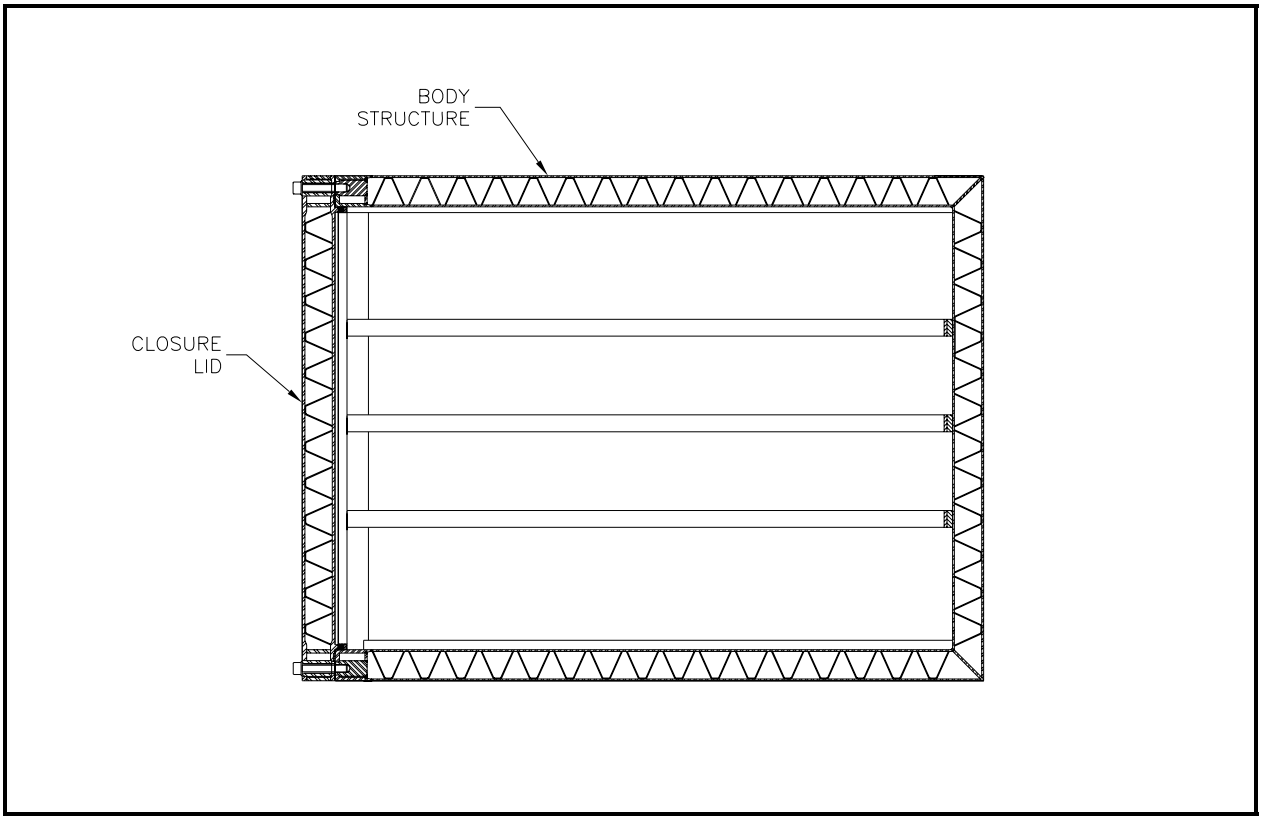

Figure 1.1-4 – TRUPACT–III Packaging Containment Structural Assembly

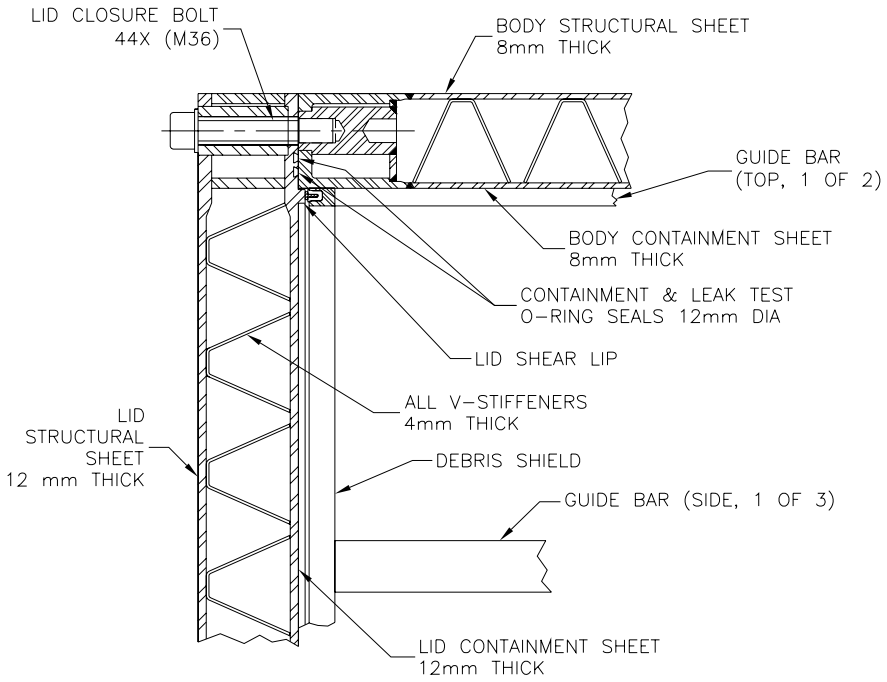

Figure 1.1-5 – TRUPACT–III Packaging Closure Lid/Seal Flange Details

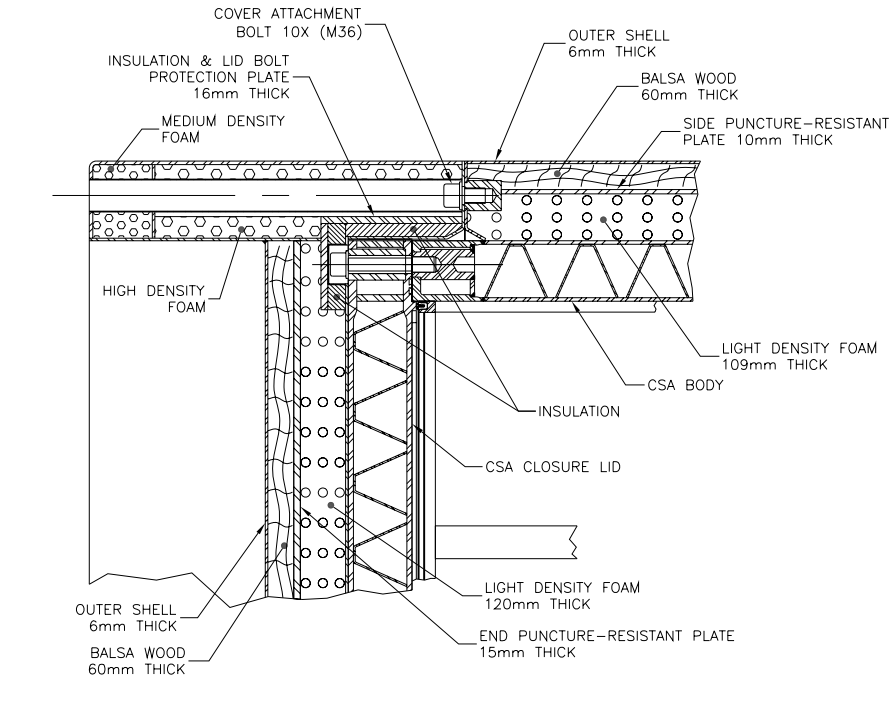

Figure 1.1-6 – TRUPACT–III Packaging Overpack Cover Cross–Section

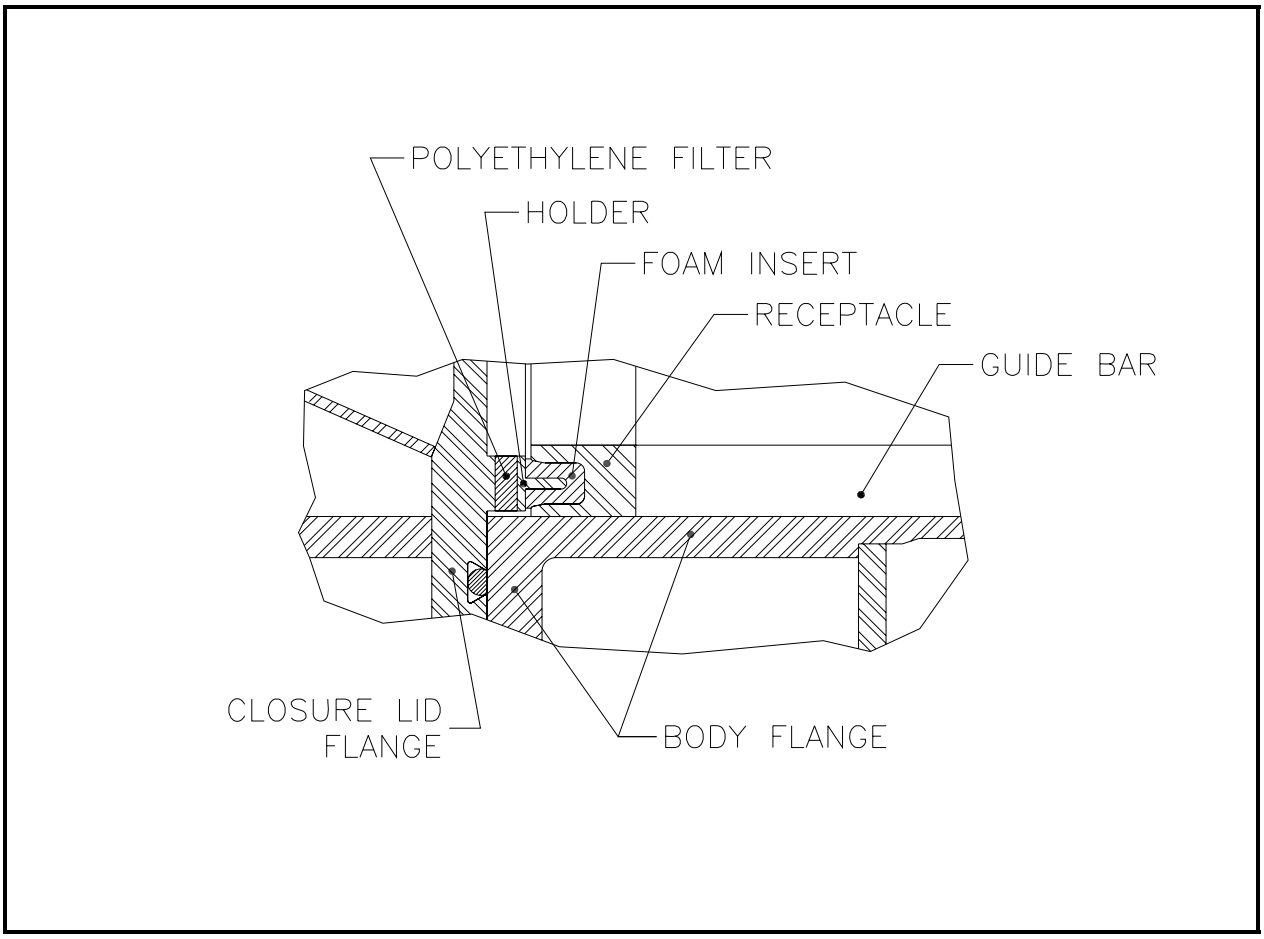

Figure 1.1-7 – TRUPACT–III Debris Shield Cross–Section

This page intentionally left blank.

1.2 Package Description

This section presents a basic description of the TRUPACT–III package. General arrangement drawings of the TRUPACT–III packaging are presented in Appendix 1.3.1, *Packaging General Arrangement Drawings*. Payload assembly details are presented in the TRUPACT–III TRAMPAC[1].

1.2.1 Packaging

The TRUPACT–III packaging is comprised of a body, a closure lid, and an overpack cover, as shown in Figure 1.1-1. The components may be briefly described as follows:

- The body is in the form of a rectangular box. It is comprised of the containment structural assembly (CSA, a rigid rectangular weldment) and an integral energy–absorbing overpack structure.
- The closure lid is a flat, rigid weldment having a construction similar to that of the CSA body, and when bolted in place, completes the CSA.
- The overpack cover is the only separable part of the overpack structure, and allows access to the closure lid and the vent/test ports.

The CSA (body plus bolted closure lid) is the rigid weldment that contains, supports, and reinforces the containment boundary. The containment boundary consists of:

- the inner stainless steel sheets of the CSA body (four sides plus the closed end),
- the closure lid inner sheet,
- the inner O–ring seal located in the flange of the closure lid,
- the vent port insert located in the closure lid,
- the vent port insert inner O–ring seal.

The body, closure lid, and overpack cover are fully described in the following subsections. All detail and sheet references in the following text refer to the drawings presented in Appendix 1.3.1, *Packaging General Arrangement Drawings*. Except for fasteners and some incidental parts as noted, all steel components are made from UNS S31803 duplex stainless steel.

1.2.1.1 Body

The body of the TRUPACT–III packaging is a rectangular box, open on one end. It consists of the body portion of the CSA with an integral overpack structure.

The CSA is a rigid stainless steel weldment consisting of sandwich panels which form the flat walls, as shown in Section BC–BC on Sheet 19. The wall sections are made of inner and outer, 8–mm thick sheets, connected by V–stiffeners of 4–mm thickness. The total wall section thickness of the CSA body is 140 mm. The V–stiffeners are connected to the outside surface of the inner sheets using continuous fillet welds. The outer sheets are connected to the V–stiffeners

[1] U.S. Department of Energy (DOE), *TRUPACT–III TRU Waste Authorized Methods for Payload Control (TRUPACT–III TRAMPAC)*, U.S. Department of Energy, Carlsbad Field Office, Carlsbad, New Mexico.

using either plug welds (on the four sides of the box) or continuous slot welds (on the closed end wall). The walls and V–stiffeners are joined at the edges of the box using diagonal sheets of 10–mm thickness as shown in Detail AX on Sheet 20. The CSA body flange is a rigid box beam structure having 15–mm inner and outer plates and a 25–mm seal face plate thickness, as shown in Detail BE on Sheet 21. The rear plate of the box beam is 10–mm in thickness. The threaded bolting bosses for the closure bolts and closure lid alignment pins pass through the box beam and are welded to both the outer plate and the rear plate. Optionally, alloy steel thread inserts may be used in the bolting bosses. By means of several 10–mm diameter holes in the diagonal corner plates and through other openings, all cavities between the inner (containment) and outer sheets of the CSA are interconnected. When evacuated of air and backfilled with helium, these cavities present a fully enveloping blanket of helium for use during leakage rate testing of the containment boundary. All containment boundary welds are radiograph inspected per Flag Note 15 and liquid penetrant inspected per Flag Note 16 on Sheet 1. All other CSA body welds are liquid penetrant inspected per Flag Note 16 on Sheet 1. The internal cavity dimensions are: 1,840 mm wide, 2,000 mm tall, and 2,790 mm long.

A debris shield receptacle is located on each side of the CSA inner cavity near the opening as shown on Sheet 4. The receptacle is a 26–mm × 38–mm cross section bar made of Type 304L or UNS S31803 duplex stainless steel with a 15–mm wide by approximately 20–mm deep groove cut along its length, as shown on Sheet 19. The groove interfaces with the debris shield insert, described in Section 1.2.1.2, *Closure Lid*. Guide bars are attached to the CSA inner cavity (as shown in Section F–F on Sheet 5 and Section H–H on Sheet 7), having a cross section of 25 mm × 76 mm, and running between the closed end of the CSA and the back edge of the debris shield receptacle. Three guide bars also run across the closed end of the CSA. The guide bars, made of ASTM Type 304/304L stainless steel, are located to correspond to the bumpers of the SLB2 payload container. There are three bars on each side of the cavity and on the closed end, and two on the top. Both the debris shield receptacle and guide bars are attached to the CSA containment sheets using a combination of groove welds and fillet welds.

Two 100–mm × 50–mm × 6–mm austenitic stainless steel channels are installed on the floor of the cavity, and continuously welded to the bottom containment stainless steel sheet. Austenitic stainless steel guide tracks are installed and continuously welded to the channels. Two M24 × 3 threaded bosses made from ASTM Type 304L stainless steel are welded to the channels to provide an anchorage for internal arrangements such as a roller floor, as shown in Detail AD on Sheet 21.

The overpack structure fully envelops the CSA body, and is designed to provide energy absorption, puncture resistance, and thermal insulation for the containment seals. Energy absorption is accomplished by the crushing of four different densities of polyurethane foam and by deformation of the outer sheets of the overpack structure, having a thickness of 6– or 8–mm. Puncture resistance is afforded by adjacent layers of balsa wood, stainless steel, and polyurethane foam. Thermal protection is provided by layers of stainless steel, foam, and calcium silicate insulation.

The overpack structure surrounding the CSA body is shown in Section F–F on Sheet 5 and Section G–G on Sheet 6. On the top and bottom walls, the thickness of the structure is 185 mm; on the vertical side walls, 190 mm; and in the octagonal recess on the closed end, the thickness is 201 mm. The overpack structure on the end (outside the octagonal recess) extends 610 mm beyond the CSA weldment, and the total length of the end overpack structure is 838 mm. At the open end of the body, two structures extend beyond the CSA flange face that envelops both sides of the overpack cover.

These structures, known as "cheeks", contain energy absorbing foam and thermal insulation. The cheeks extend 748 mm beyond the CSA flange face, and the total length of the cheek structure is 870 mm. The overall length of the Body assembly, which is equal to the overall length of the assembled packaging, is 4,288 mm. The external width is 2,500 mm, and the external height is 2,650 mm.

The puncture–resistant system of components occupies the central 2,574 mm of the package sides, top, and bottom, and the octagonal recess at the closed end. Starting adjacent to the CSA weldment, the system consists of a 109 – 120–mm thick layer of nominally 0.10 kg/dm^3 polyurethane foam, a puncture resistant plate made from stainless steel, a 60–mm thick layer of nominally 0.12 kg/dm^3 balsa wood, and an outer sheet made from 6–mm thick stainless steel. The puncture–resistant plate is 10–mm thick on the sides, top, and bottom, and 15–mm thick on the closed end. The puncture–resistant plates are fastened to the surrounding structures using pop rivets. As shown in Detail E on Sheet 4, the end faces of the top and bottom overpack structure by the open end each contain five threaded bosses (total of ten) for the attachment of the overpack cover. The threads are M36 × 4 and may optionally feature alloy steel thread inserts. As shown in Section C–C of Sheet 4, a single alignment pin is located between two bolt holes in the top row, used to aid in alignment during installation of the overpack cover.

As shown in Section H–H on Sheet 7, with further detail given in Detail K, the four edges of the overpack in the central 2,574 mm length between the end structures are protected by a chevron–shaped region filled with blocks of 0.29 kg/dm^3 polyurethane foam and enveloped by a 6–mm thick stainless steel sheet.

The end overpack region (228 mm overlapping the end of the CSA weldment and extending 610 mm beyond the end of the CSA for a total length of 838 mm) is composed of nominally 0.48 kg/dm^3 and 0.16 kg/dm^3 polyurethane foam. The heavier density foam is used for protection in corner drops, and is placed as shown in Section J–J on sheet 8. The lighter density foam is used primarily on the end face as shown in Section AU–AU on sheet 8. A puncture–resistant plate of 6–mm thickness separates the two densities of foam. Other views of the end overpack structure are shown in Partial Sections AR–AR and AS–AS on Sheet 9.

At the open end of the body, the cheek structures have a construction similar to the corresponding regions of the closed end overpack. An added feature in the cheeks is a 30–mm thick sheet of calcium silicate thermal insulation placed next to the CSA body flange. The insulation is protected by enveloping stainless steel plates of 16–mm thickness. The cheek is shown in Partial Sections AN–AN and AP–AP on Sheet 9. All welds pertaining to the overpack structure are liquid penetrant inspected per Flag Note 17 on Sheet 1.

A modified International Organization for Standardization (ISO) lifting corner fitting is incorporated into each corner of the body. These ISO fittings provide the handling interface for lifting the TRUPACT–III package from its conveyance and on–site movement for loading/unloading operations. Since these fittings are only designed for lifting and off–road movement of the package, the ISO fittings are disabled during transport to prevent their use as a potential tie–down device.

The payload cavity length is 2752 ± 3 mm. This tight tolerance is achieved in one of three ways: a) reducing the thickness of the three guide bars which run transversely across the closed end of the payload cavity, b) attaching hard plastic plates to the three guide bars, or c) a combination of guide bar thickness reduction and addition of plastic plates. The vertical locations of the transverse guide bars correspond to the bumpers on each end of the SLB2. For a minimum

length SLB2 of 107.38 inches, or 2,727 mm, the maximum axial free space between the package cavity and the SLB2 is 28 mm. A minimum clearance between the SLB2 and the closure lid inner surface of 2 mm will be assured at the time of package closure (see Section 7.1.4, *Loading the Payload into the TRUPACT–III Package*).

To prevent pressurization of the overpack structure in the event of the HAC fire, the outer sheets feature a total of (36) 1–inch NPT fusible plastic plugs. All external surfaces of the body assembly except the external bottom surface, surfaces covered by the overpack cover, and the ISO corner fittings, are coated with a low–halogen white paint. The external bottom surface may be painted as an option.

1.2.1.2 Closure Lid

The closure lid, shown on Sheets 13 and 14, is a rigid stainless steel weldment that completes the CSA. It consists of inner and outer, 12–mm thick sheets, connected by V–stiffeners of 4–mm thickness. The total thickness of the weldment is 148 mm (not including the shear lip), the width is 2,108 mm, and the height is 2,280 mm. The V–stiffeners are attached to the outside of the inner (containment) sheet using continuous fillet welds. The outer sheets are connected to the V–stiffeners using continuous slot welds (similar in kind to the corresponding welds on the closed end).

Around the outside of the lid is located a rigid box beam flange which mates with the flange on the CSA body. As shown in Detail Y on Sheet 14, the inner (seal side) plate of the flange is 20–mm thick. The opposite side of the flange is also 20–mm in thickness. The remaining two plates of the flange are of 16–mm thickness. Bolt tubes of 10–mm radial thickness are welded at each end to the inner and outer flange plates, and which carry the closure bolt loads through the thickness of the lid. A shear lip runs on all four sides of the lid and engages the opening of the CSA body. It has a shear thickness of 20 mm and a bearing width of 10 mm. All containment boundary welds are radiograph inspected per Flag Note 15 and liquid penetrant inspected per Flag Note 16 on Sheet 1. All other closure lid welds are liquid penetrant inspected per Flag Note 16 on Sheet 1. As with the CSA body, all cavities within the closure lid are interconnected. When evacuated of air and backfilled with helium, these cavities present a fully enveloping blanket of helium for use during leakage rate testing of the containment boundary. Access to these cavities (including those between the inner and outer sheets of the CSA body) is provided by small ports in the lower right–hand corner of the lid and CSA body flanges, as shown in Section Z–Z on Sheet 15.

Extending inward from the shear lip inner surface (as shown in Figure 1.1-7) is the debris shield holder, which is 4 mm thick and 15 mm long. It may be welded to, or be integral with the shear lip. The debris shield insert, shown on Sheet 4, has a U–shaped cross–section and is made of silicone foam rubber. It is attached to both sides of the holder using double–sided tape. The insert mates with the receptacle described in Section 1.2.1.1, *Body,* to form the completed debris shield, as shown on Sheet 4. Each of the four shear lips features two, 5/16–inch (7.9 mm) diameter filters made from porous polyethylene. These filtered passages prevent a pressure differential across the debris shield and permit helium to reach the containment O–ring seal during leakage rate testing.

In the lower right–hand corner on the exterior surface, a 200–mm × 320–mm recess is located, which contains the vent port and the seal test port, as shown in Section Z–Z on Sheet 15. The seal test port communicates with the cavity between the containment and test O–ring seals in the closure lid and is used during leakage rate or pressure rise testing. The vent port (a containment boundary penetration) is 50–mm in diameter. It is closed by an aluminum bronze insert and sealed by a butyl

O–ring seal. A test O–ring seal is also located in the vent port insert. The insert is retained in position using an aluminum bronze, M120 × 6 threaded retaining ring, which in turn is locked in place using an aluminum bronze locking ring. In the region of the 200 mm × 320 mm recess, the closure lid inner plate is 40–mm in thickness (20–mm elsewhere).

The closure lid is attached to the body by (44) M36 × 205 mm bolts that are tightened to 1,600 N–m (lubricated) torque. The bolts are made from ASTM A320, L43 alloy steel and are cadmium plated. Washers are used with the closure bolts, made of ASTM A564, Grade 630, Condition H1025 (17–4 PH) material. The sealing flange of the closure lid contains two dovetail grooves to retain the butyl rubber containment and test O–rings, each of which is nominally of 12–mm cross–sectional diameter. At each corner of the closure lid, the containment seal groove changes direction using a 50–mm radius, while the test O–ring groove utilizes a 74–mm radius. Both containment O–ring seals (i.e., the inner seal on the vent port and the inner seal of the closure lid) are made from Rainier Rubber R–0405–70 material, meeting the requirements of Section 8.1.5.3, *Butyl Rubber O–rings*.

Lifting of the closure lid is performed using two standard lifting eyes that are threaded into M36 threaded bosses installed on the top surface. During transport, these lifting points are covered by the overpack cover, making them inoperable.

One M36 threaded hole is located near the middle of each side of the lid (total of four holes). These holes are used if needed to separate the closure lid from the body. Two holes for the closure lid guide pins (attached to the CSA body flange) are located immediately above the horizontal centerline. As an option, thread inserts may be installed in all internal threads of the closure lid.

1.2.1.3 Overpack Cover

The overpack cover has a design very similar to that of the overpack structure on the closed end. When installed, the overpack cover fits between the cheeks on the body and completely envelops the closure lid and CSA body flange. It is designed to provide energy absorption, puncture resistance for the closure lid, and thermal insulation for the containment seals, and is depicted on Sheets 16 through 18.

The overpack cover of the TRUPACT–III packaging consists of a rectangular stainless steel sheet structure encasing an impact–absorbing and thermal insulation materials structure. Similar to the body closed end overpack structure, the central area of the overpack cover consists of a nominally 393–mm deep octagonal recess. The recess consists of a 6–mm cover sheet, a 60–mm thick balsa wood sheet, a 15–mm thick puncture–resistant stainless steel sheet, and a 120–mm thickness of 0.10 kg/dm^3 polyurethane foam, adjacent to a 6–mm thick inner cover sheet. Outside the recess, the overpack cover features 272 mm long, upper and lower flanges which envelop the CSA body flange. The remainder of the 870–mm total thickness is taken up by a 42–mm thick layer of calcium silicate insulation, a 16–mm thick stainless steel protective plate, a 382–mm thickness of 0.48 kg/dm^3 polyurethane foam, a 6–mm thick puncture–resistant plate, a 140–mm thickness of 0.16 kg/dm^3 polyurethane foam, and an outer 8–mm thick steel sheet. The calcium silicate thermal insulation and the 16–mm thick protective stainless steel sheet include a region that covers the vent test ports as shown in Section AF–AF on Sheet 17. The upper and lower flanges feature 30–mm thick thermal insulation (corresponding to the thermal insulation in the body cheeks), protected by 16–mm thick stainless steel plates.

The overpack cover is attached to the body by ten, M36 × 60 mm bolts that are tightened to 1,600 N–m (lubricated) torque. The bolts are made from ASTM A320, Type L43 alloy steel and are

cadmium plated. The bolts (five each along the top and bottom edges) are installed through thin–wall, ASTM Type 304L stainless steel access tubes that are located on the top and bottom edges. The bolts thread into 70–mm diameter stainless steel threaded bosses that are welded in the exterior stainless steel sheet of the body. Two of the access tubes (lower left and lower right) are configured to accept a tamper–indicating seal. On the inside surface, short, 3½–inch diameter cylindrical depressions are located around the perimeter to provide receptacles for the heads of the closure lid bolts. A 44–mm wide and 84–mm tall opening located on the top flange of the overpack cover interfaces with the guide pin installed in the mating flange of the body assembly.

Lifting of the overpack cover is performed using two standard lifting eyes that are threaded into M36 threaded bosses installed on the top surface. These threaded bosses are made inoperable during transport to prevent their use as a tie–down device and to prevent the collection of water. As an option, a thread insert may be installed in these internal threads. On one side of the overpack cover (protected by a side cheek), is located a recess in which a pressure relief valve is installed, and which will prevent an excessive pressure differential from developing inside the overpack cover shell. To prevent pressurization of the overpack cover in the event of the HAC fire, the outer face sheet features a total of (8) 1–inch NPT fusible plastic plugs.

The overpack cover has nominal external dimensions of 2,108–mm wide, 2,650–mm high, and 870–mm thick. All overpack cover welds are liquid penetrant inspected per Flag Note 17 on Sheet 1. All surfaces of the overpack cover that form the outside surface when installed on the TRUPACT–III, except the external bottom surface, are coated with a low–halogen white paint. The external bottom surface may be painted as an option.

1.2.1.4 Gross Weight

The gross shipping weight of a TRUPACT–III package is 25,000 kg (55,116 lbs) maximum. A summary of overall component weights is shown in Table 2.1-2 and discussed in Section 2.1.3, *Weights and Centers of Gravity*.

1.2.1.5 Neutron Moderation and Absorption

The TRUPACT–III package does not require specific design features to provide neutron moderation and absorption for criticality control. Fissile materials in the payload are limited to amounts that ensure safely subcritical packages for both NCT and HAC. The fissile material limits for a single TRUPACT–III package are based on an optimally moderated and reflected fissile material. The structural materials in the TRUPACT–III packaging are sufficient to maintain reactivity between the fissile materials in an infinite array of damaged TRUPACT–III packages at an acceptable level. Further discussion of neutron moderation and absorption is provided in Chapter 6.0, *Criticality Evaluation*.

1.2.1.6 Receptacles, Valves, Testing, and Sampling Ports

There are no receptacles used on the TRUPACT–III packaging. However, a vent port, a seal test port, and a body helium fill port access port are located in the closure lid as described in Section 1.2.1.2, *Closure Lid*. The vent port provides access to the payload cavity for sampling or venting the payload cavity during unloading operations. The vent port, in conjunction with the seal test port, is also used to perform leakage rate testing of the inner containment O–ring seal to verify

proper assembly of the TRUPACT–III package prior to shipment. The vent port and the seal test port are accessed through a recess located in the lower right corner of the closure lid. The body helium fill port access port is accessible on the surface of the closure lid, near the recess. All ports are inaccessible when the overpack cover is installed.

1.2.1.7 Heat Dissipation

The TRUPACT–III package design capacity is 80 thermal watts maximum. The TRUPACT–III package dissipates this low internal heat load entirely by passive heat transfer for both NCT and HAC. The TRUPACT–III packaging does not utilize any coolants. To improve the insolation resistance for NCT, the external surfaces of the packaging are painted with a low–halogen white paint. No other features or special devices are needed or utilized to enhance the dissipation of heat. Features are included in the design to enhance thermal performance in the HAC thermal event. These features include the use of a high temperature insulating material (calcium silicate insulating board) and polyurethane foam in the body and overpack cover. A more detailed discussion of the package thermal characteristics is provided in Chapter 3.0, *Thermal Evaluation*.

1.2.1.8 Lifting and Tie–down Devices

Lifting of the TRUPACT–III package is via the ISO fittings at each upper corner. Under excessive load, the ISO corner fittings are designed to fail in shear prior to compromising the structure of the packaging. The ISO corner fittings are covered during transport and rendered inoperable to preclude their use as a tie–down device.

The closure lid and the overpack cover are lifted via two M36 lifting eyes. These lifting points are designed for lifting only their respective component, and therefore, are covered during transport and rendered inoperable to preclude their use as a tie–down device.

There are no tie–down devices on the TRUPACT–III package. The TRUPACT–III package is secured to the transport vehicle (semi–trailer or rail car) by straps or a tie–down frame that is positioned over the top of the package.

A detailed discussion of lifting and tie–down designs, with corresponding structural analyses, is provided in Section 2.5, *Lifting and Tie–down Standards for All Packages*.

1.2.1.9 Pressure Relief System

There are no pressure relief systems included in the TRUPACT–III package design to relieve pressure from within the containment boundary. A pressure relief valve is utilized in the overpack cover to prevent a significant gage pressure from occurring within the overpack cover outer shell. In addition, fire–consumable, plastic vent plugs are employed on the exterior surface of the body and overpack cover.

1.2.1.10 Shielding

Due to the nature of the contact–handled transuranic (CH–TRU) payloads, no biological shielding is necessary or provided by the TRUPACT–III packaging.

1.2.2 Contents

The TRUPACT–III packaging is designed to transport contact–handled transuranic (CH–TRU) waste and other authorized payloads that do not exceed 10^5 A_2 quantities, as defined in the TRUPACT–III TRAMPAC. All users of the TRUPACT–III package shall comply with all payload requirements outlined in the TRUPACT–III TRAMPAC, using one or more of the methods described in that document.

1.2.3 Special Requirements for Plutonium

The TRUPACT–III package may contain plutonium in excess of 0.74 Tbq (20 Ci), which is in solid or solidified form.

1.2.4 Operational Features

The TRUPACT–III package is not operationally complex. All operational features are readily apparent from an inspection of the drawings provided in Appendix 1.3.1, *Packaging General Arrangement Drawings*, and the previous discussions presented in Section 1.2.1, *Packaging*. Operational procedures and instructions for loading, unloading, and preparing an empty TRUPACT–III package for transport are provided in Chapter 7.0, *Operating Procedures*.

1.3 Appendices

1.3.1 Packaging General Arrangement Drawings

1.3.2 Glossary of Terms and Acronyms

This page intentionally left blank.

1.3.1 Packaging General Arrangement Drawings

This section presents the TRUPACT–III packaging general arrangement drawing[1], consisting of 21 sheets entitled, *TRUPACT–III Packaging SAR Drawing*, Drawing Number 51199–SAR, Rev. 15.

Within the packaging general arrangement drawing, dimensions important to the packaging's safety are dimensioned and toleranced (e.g., sealing regions on the seal flanges). All other dimensions are provided as a reference dimension, and are toleranced in accordance with the general tolerance block.

[1] The TRUPACT–III packaging general arrangement drawing utilizes the uniform standard practices of ASME Y14.5M–1994, *Dimensioning and Tolerancing*, American National Standards Institute, Inc. (ANSI).

This page intentionally left blank.

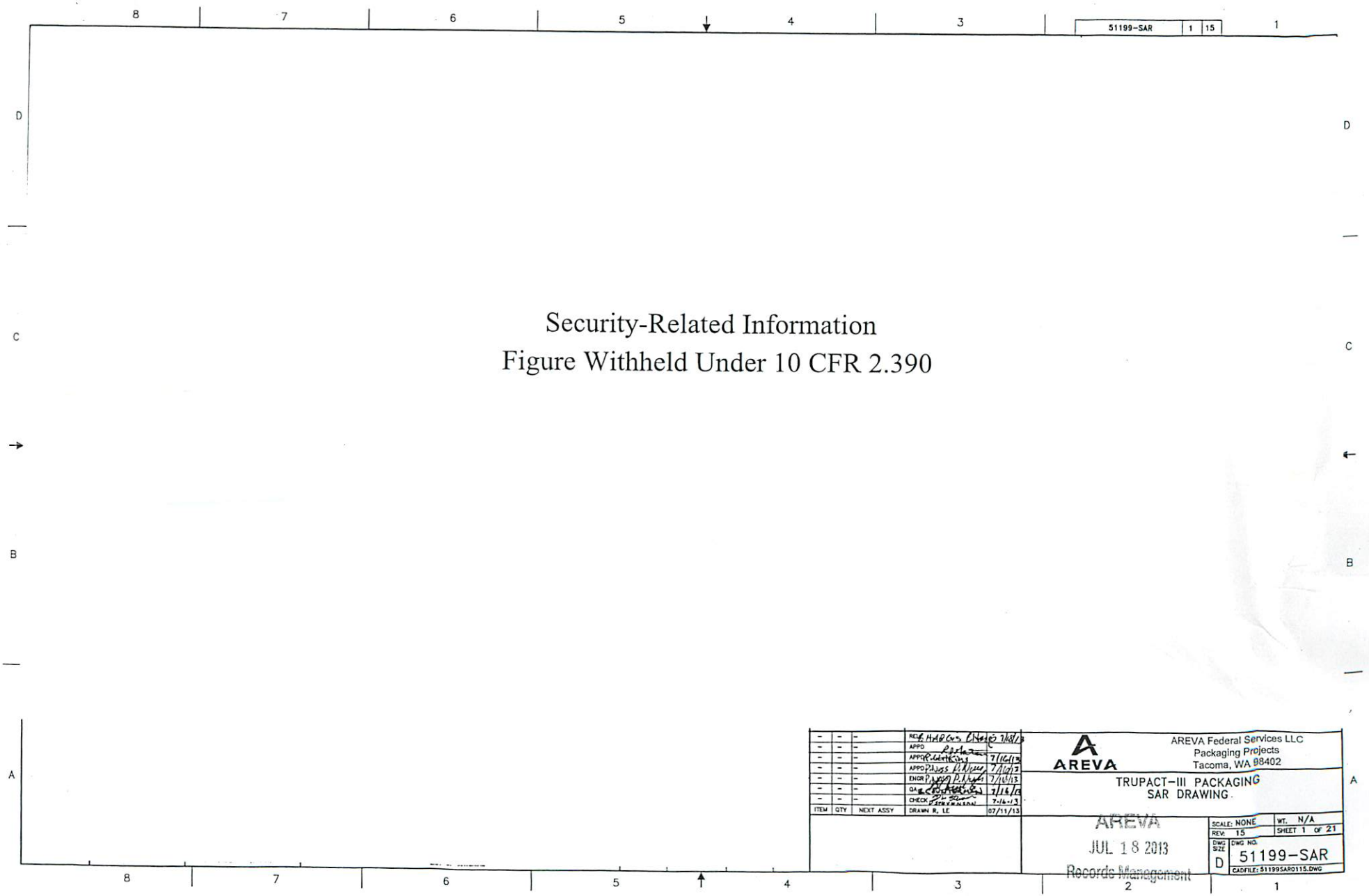
8
7
6
5
4
3
51199-SAR
1
15
1
D
C
B
A
Security-Related Information
Figure Withheld Under 10 CFR 2.390
ITEM
QTY
NEXT ASSY
DRAWN R. LE
07/11/13
CHECK
7-16-13
APPD
7/16/13
ENGR
7/16/13
AREVA
AREVA Federal Services LLC
Packaging Projects
Tacoma, WA 98402
TRUPACT-III PACKAGING
SAR DRAWING
AREVA
JUL 18 2013
Records Management
SCALE: NONE
WT. N/A
REV. 15
SHEET 1 OF 21
DWG SIZE D
DWG NO. 51199-SAR
CADFILE: 51199SAR0115.DWG

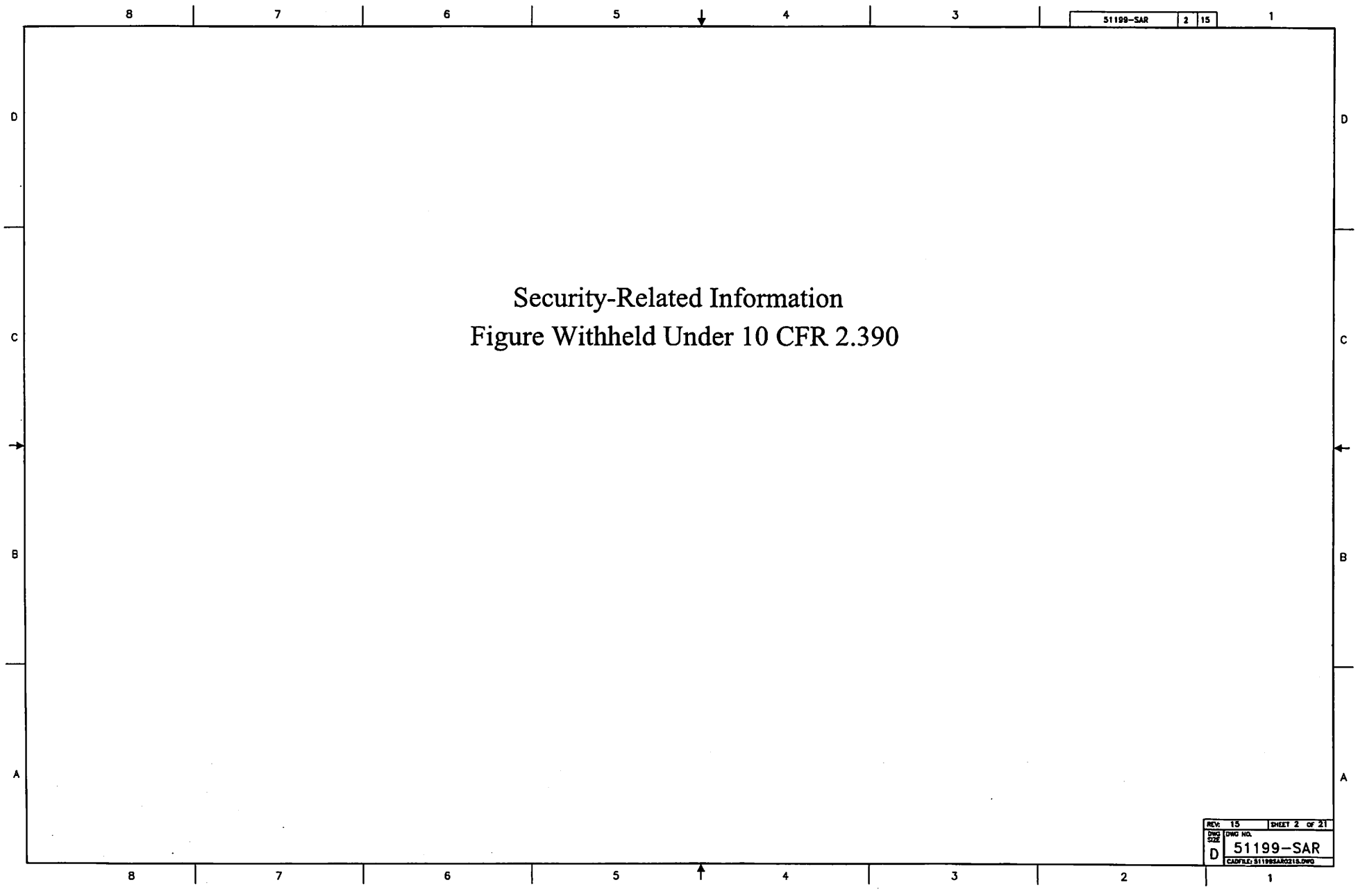
51199-SAR 2 15
Security-Related Information
Figure Withheld Under 10 CFR 2.390
REV: 15
SHEET 2 OF 21
DWG SIZE D
DWG NO. 51199-SAR
CADFILE: 51199SAR0215.DWG

Security-Related Information
Figure Withheld Under 10 CFR 2.390

Security-Related Information
Figure Withheld Under 10 CFR 2.390

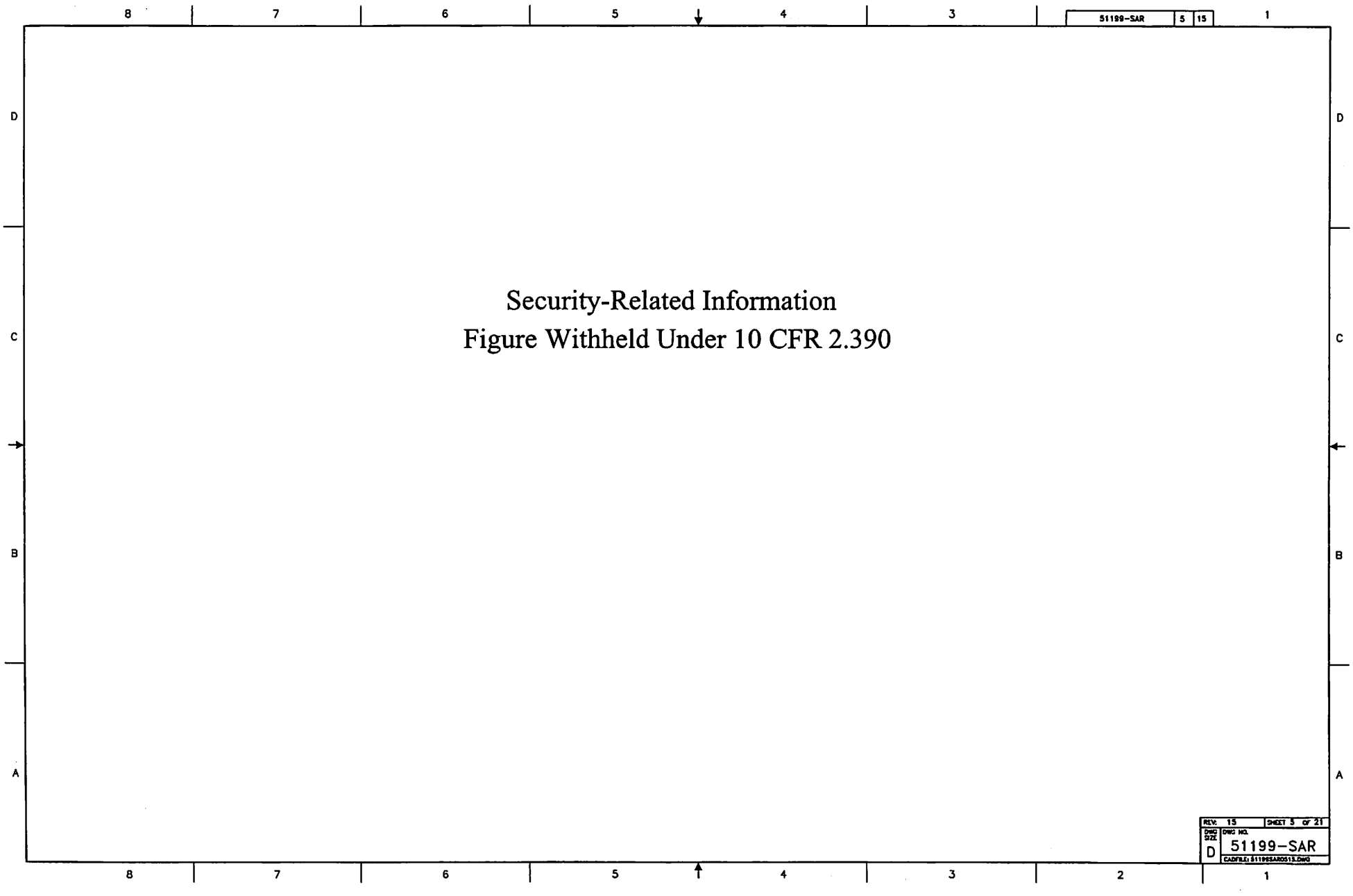
8
7
6
5
4
3
2
1
D
C
B
A
51199-SAR
5
15
Security-Related Information
Figure Withheld Under 10 CFR 2.390
REV. 15
SHEET 5 OF 21
DWG SIZE
D
DWG NO.
51199-SAR

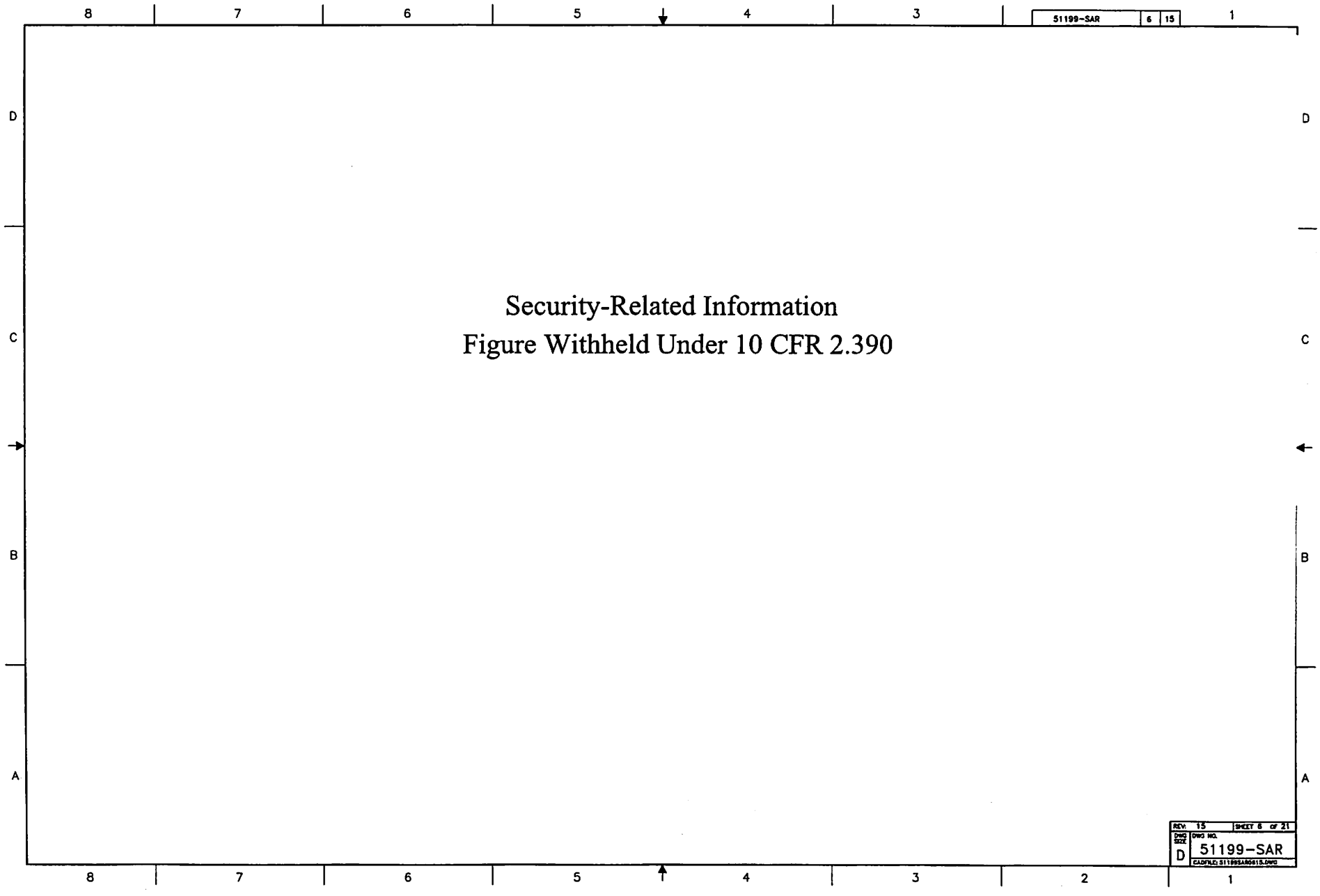
8
7
6
5
4
3
2
1
51199-SAR
6
15
D
C
B
A
Security-Related Information
Figure Withheld Under 10 CFR 2.390
REV. 15
SHEET 6 OF 21
DWG SIZE
D
DWG NO.
51199-SAR

Security-Related Information
Figure Withheld Under 10 CFR 2.390

Security-Related Information
Figure Withheld Under 10 CFR 2.390

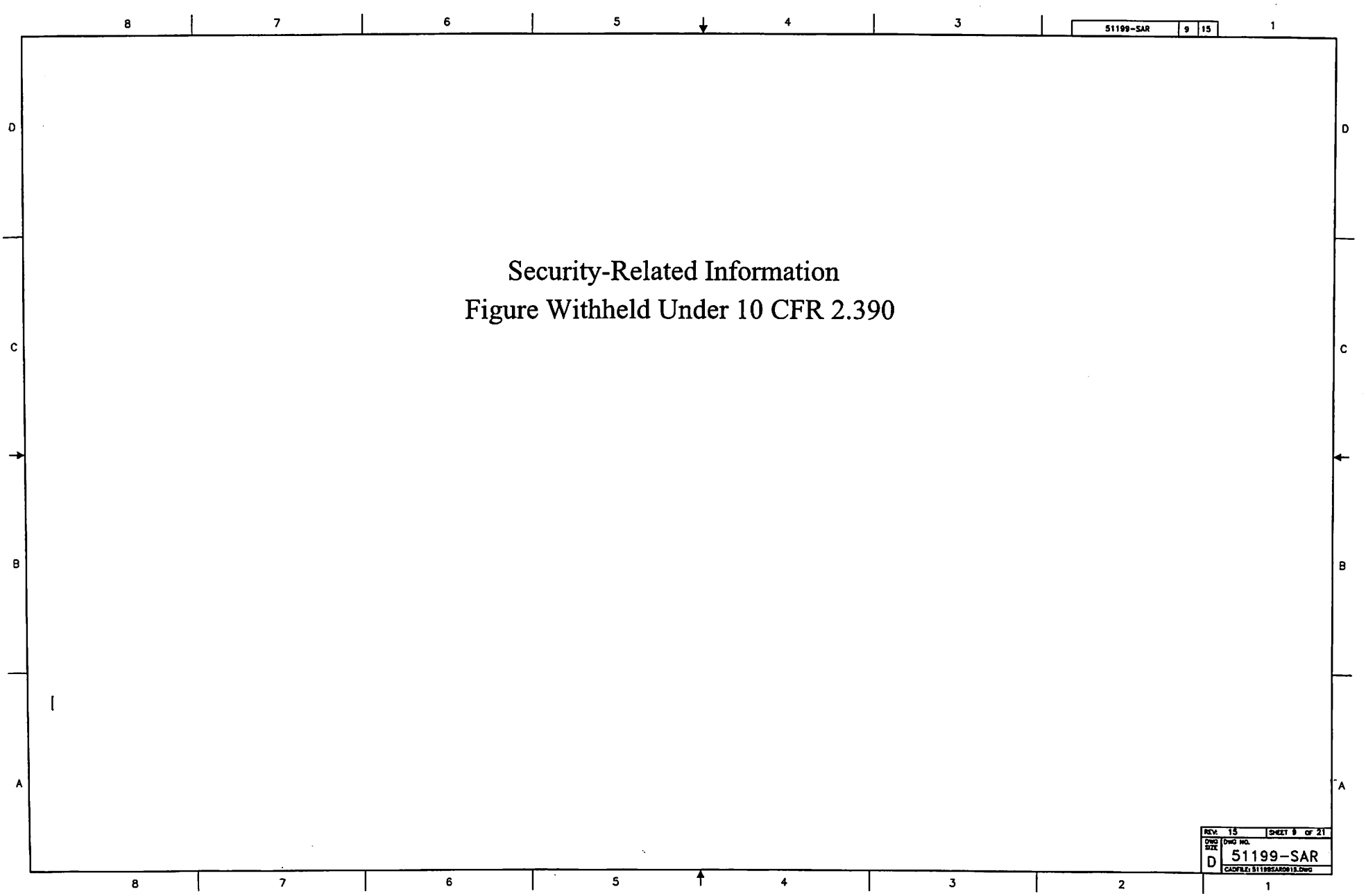
8
7
6
5
4
3
2
1
D
C
B
A
51199-SAR 9 15
Security-Related Information
Figure Withheld Under 10 CFR 2.390
REV. 15
SHEET 9 OF 21
DWG SIZE D
DWG NO. 51199-SAR
CADFILE: 51199SAR0915.DWG

Security-Related Information
Figure Withheld Under 10 CFR 2.390

Security-Related Information
Figure Withheld Under 10 CFR 2.390

Security-Related Information
Figure Withheld Under 10 CFR 2.390

Security-Related Information
Figure Withheld Under 10 CFR 2.390

Security-Related Information
Figure Withheld Under 10 CFR 2.390

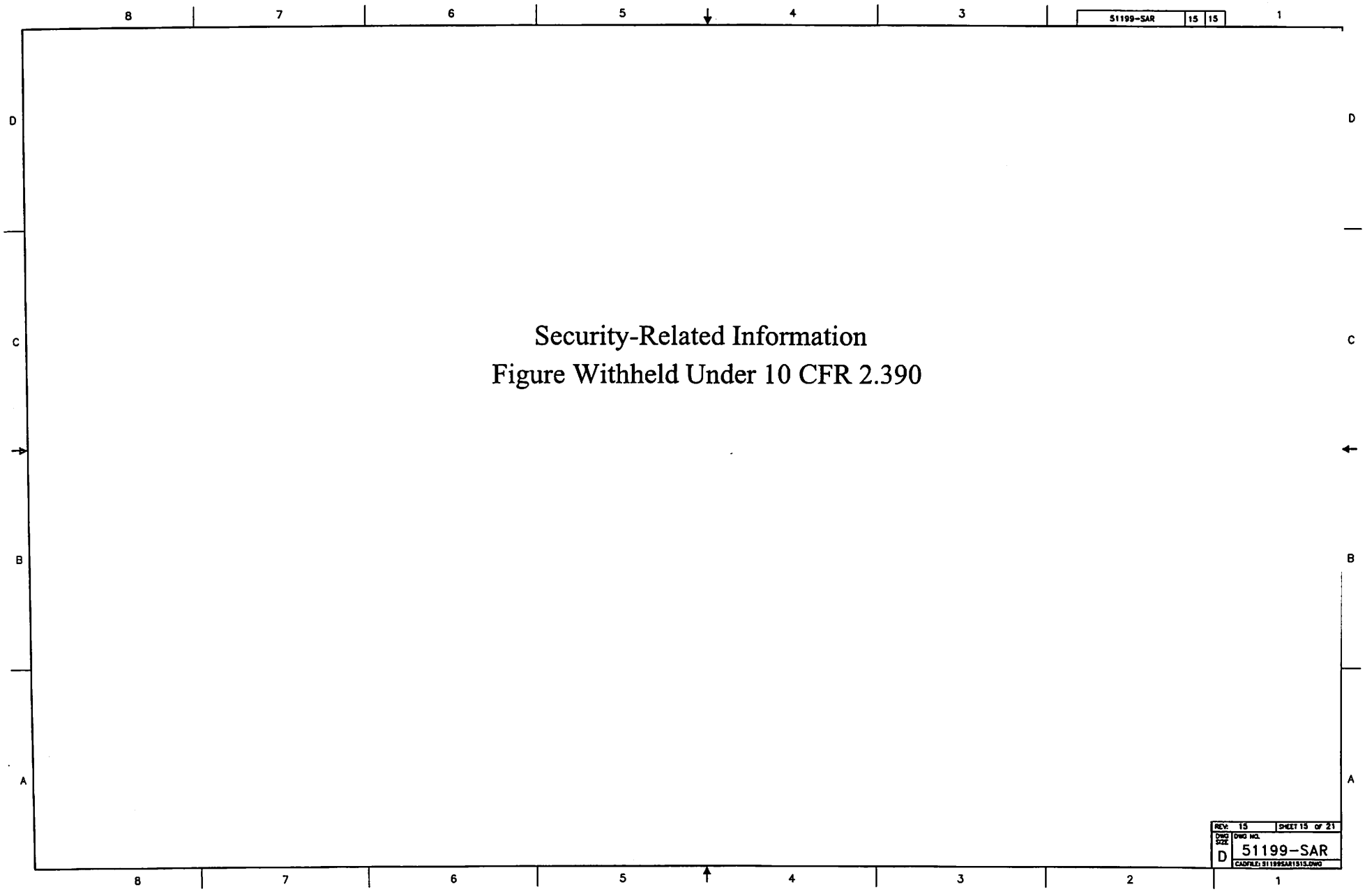
8
7
6
5
4
3
51199-SAR
15
15
1
D
C
B
A
Security-Related Information
Figure Withheld Under 10 CFR 2.390
REV: 15
SHEET 15 OF 21
DWG SIZE
D
DWG NO.
51199-SAR
CADFILE: 51199SAR1515.DWG
8
7
6
5
4
3
2
1

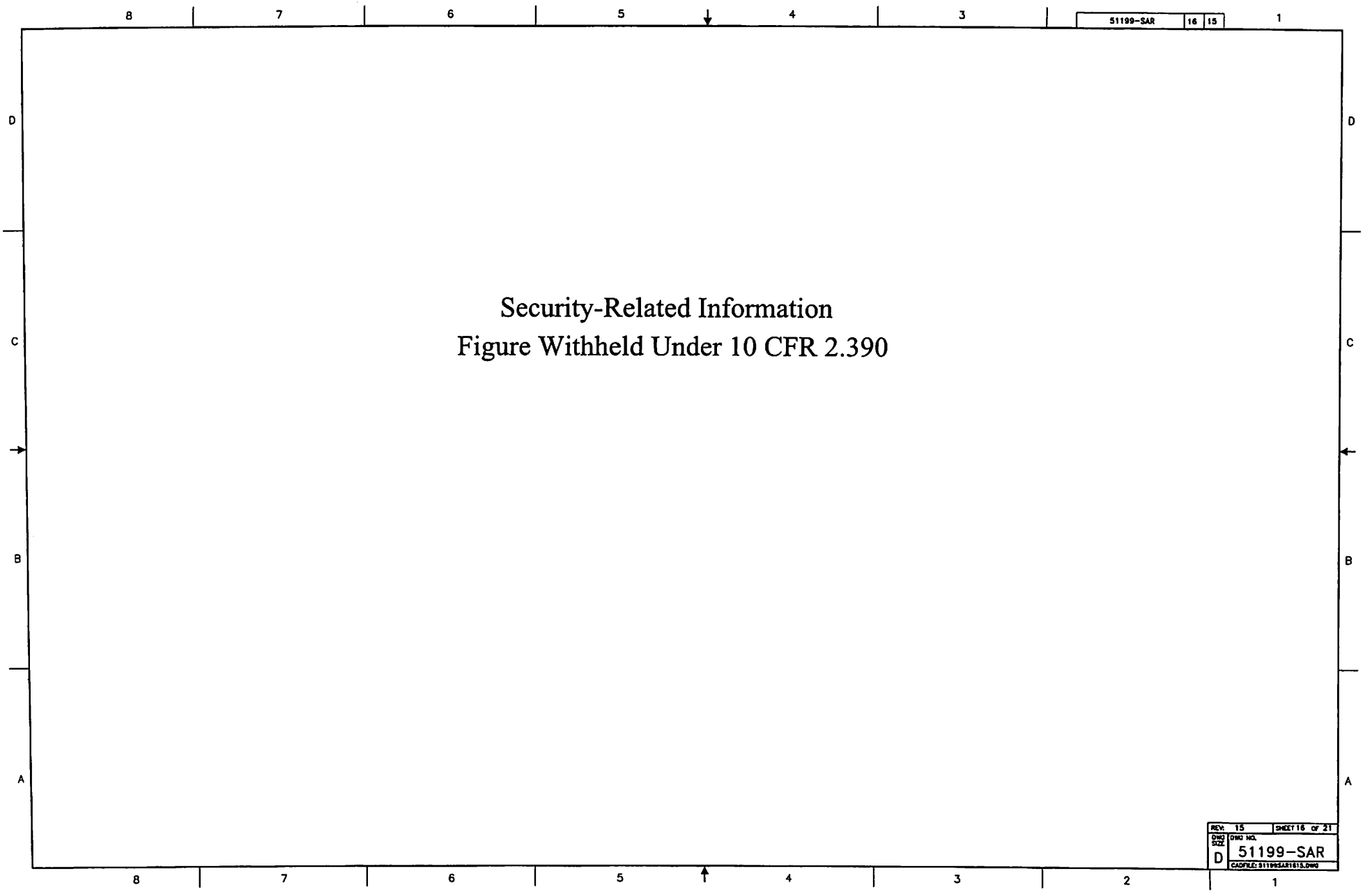
8
7
6
5
4
3
2
1
51199-SAR
16
15
D
C
B
A
Security-Related Information
Figure Withheld Under 10 CFR 2.390
REV: 15
SHEET 16 OF 21
DWG SIZE
D
DWG NO.
51199-SAR
CADFILE: 51199SAR1615.DWG

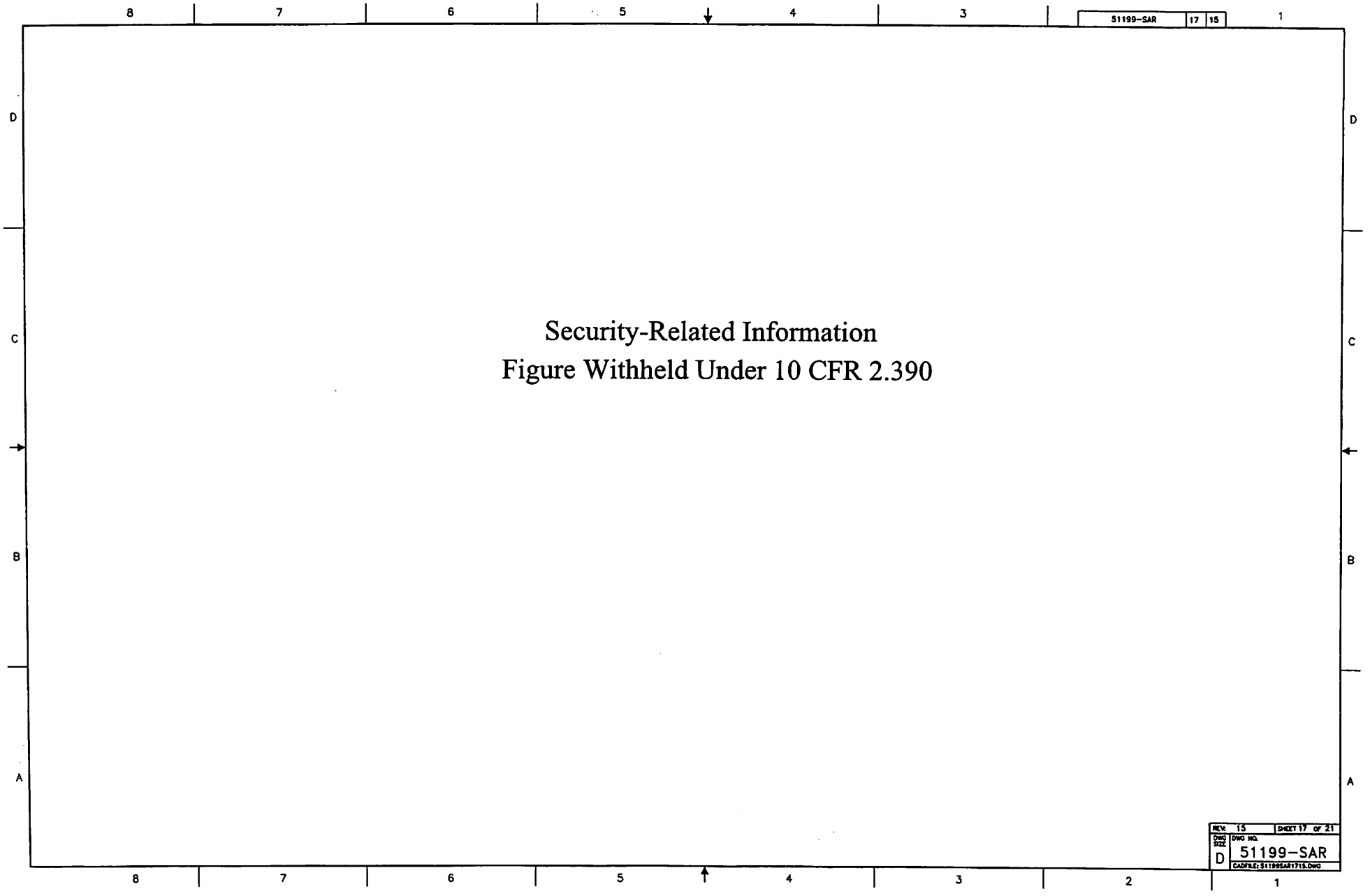
8
7
6
5
4
3
2
1
51199-SAR
17
15
D
C
B
A
Security-Related Information
Figure Withheld Under 10 CFR 2.390
REV: 15
SHEET 17 OF 21
DWG SIZE
D
DWG NO.
51199-SAR

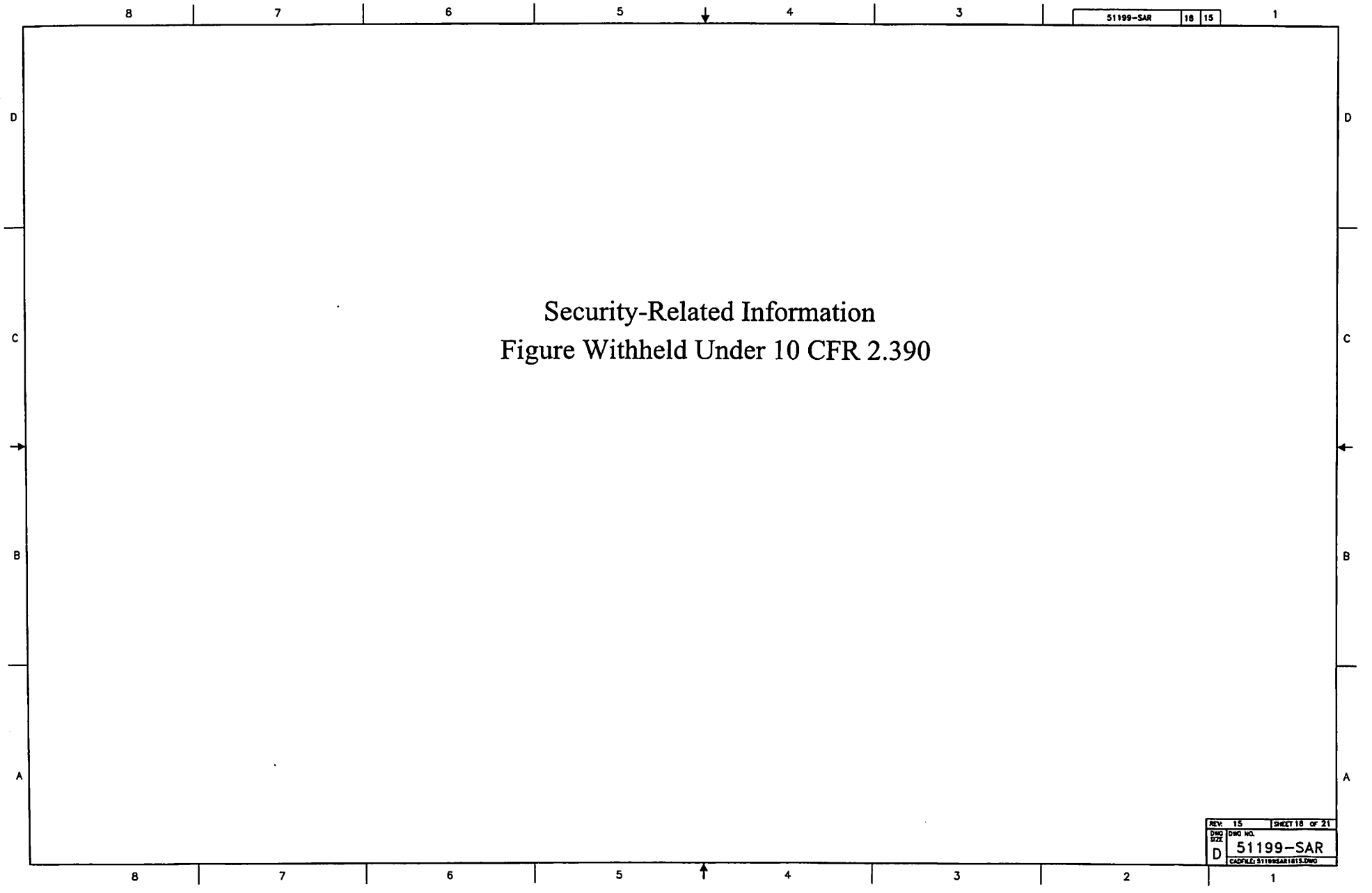
8
7
6
5
4
3
2
1
51199-SAR
18
15
D
C
B
A
Security-Related Information
Figure Withheld Under 10 CFR 2.390
REV: 15
SHEET 18 OF 21
DWG SIZE
D
DWG NO.
51199-SAR
CADFILE: 51199SAR1815.DWG

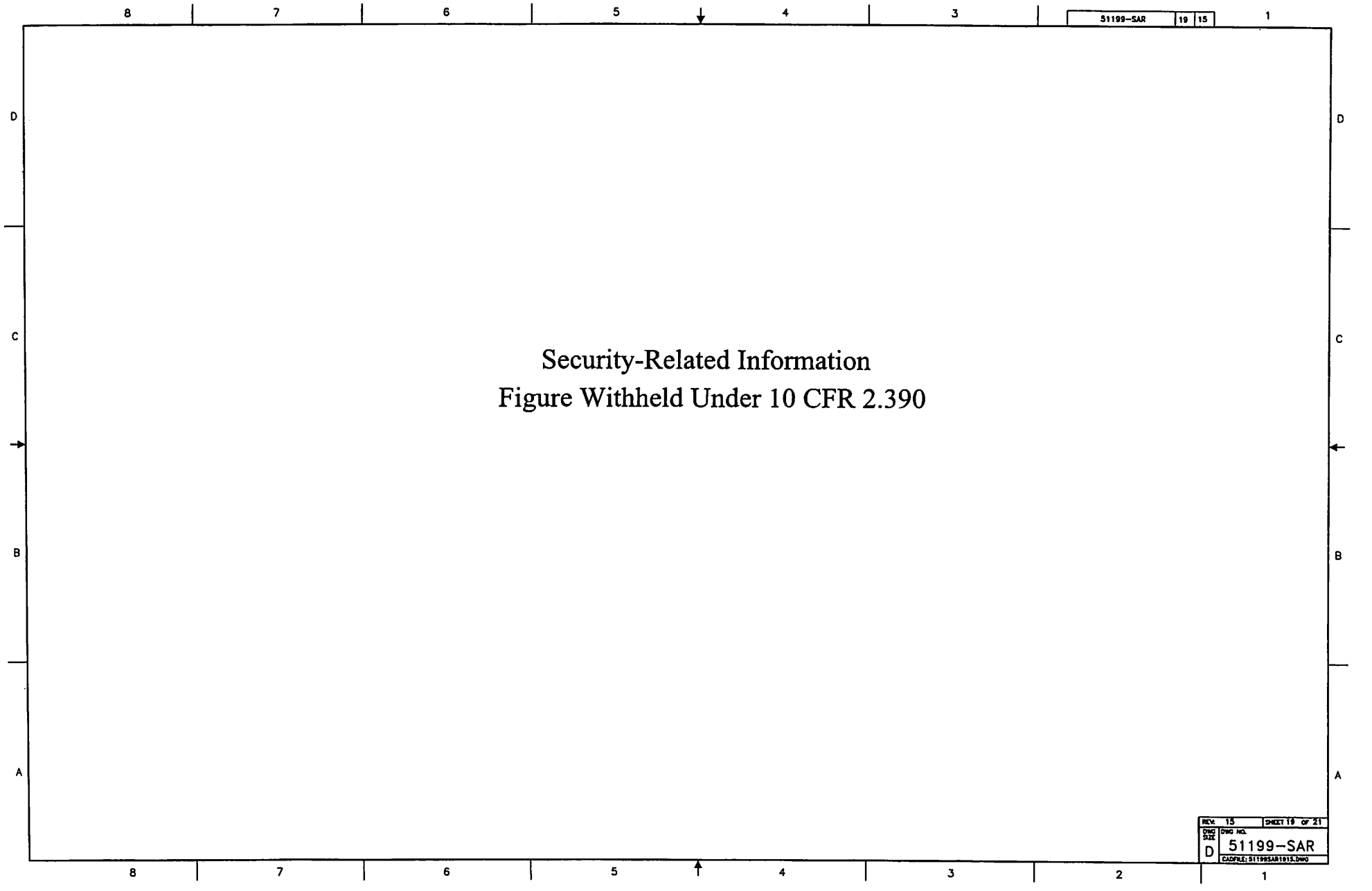
51199-SAR 19 15
Security-Related Information
Figure Withheld Under 10 CFR 2.390
REV. 15
SHEET 19 OF 21
DWG SIZE D
DWG NO. 51199-SAR

Security-Related Information
Figure Withheld Under 10 CFR 2.390

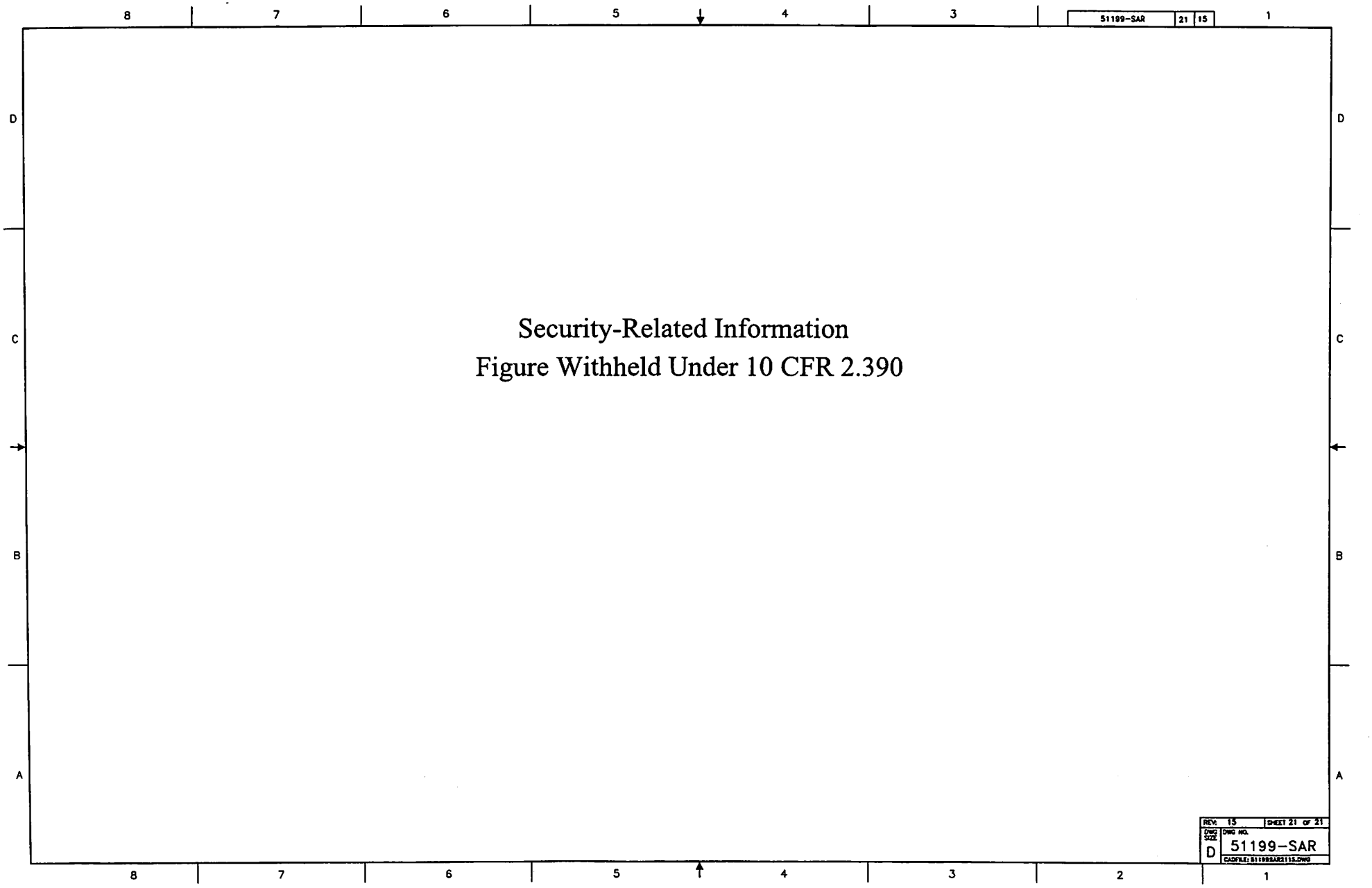
8
7
6
5
4
3
2
1
51199-SAR
21
15
D
C
B
A
Security-Related Information
Figure Withheld Under 10 CFR 2.390
REV: 15
SHEET 21 OF 21
DWG SIZE
D
DWG NO.
51199-SAR
CADFILE: 51199SAR2115.DWG

1.3.2 Glossary of Terms and Acronyms

ANSI – American National Standards Institute.

ASME – American Society of Mechanical Engineers.

ASME B&PVC – ASME Boiler and Pressure Vessel Code.

ASTM – American Society for Testing and Materials.

AWS – American Welding Society.

Body Assembly – The rectangular box, which together with the closure lid and overpack cover, constitutes the TRUPACT–III packaging.

Body Helium Fill Access Plugs – The threaded aluminum bronze plugs that seal the helium fill ports in the closure lid and body seal flange; consists of a plug on both sides of the closure lid.

Body Helium Fill Access Ports – The penetrations in the closure lid sealing flange to permit access to the body helium fill port; consists of a port on both sides of the closure lid.

Body Helium Fill Port – The penetration into the V–stiffener cavity of the sealing/bolting flange of the body that permits the introduction of helium for helium leakage rate testing of the containment boundary.

Body Helium Fill Port Plug – The threaded aluminum bronze plug that seals the body helium fill port.

Cheeks – The extensions of the body assembly which protect the sides of the overpack cover.

Closure Lid – The packaging component that closes and seals the payload cavity. The closure lid is part of the CSA.

Containment O–ring Seal – The inner O–ring seal located in the closure lid; forms part of the containment boundary.

Containment Structural Assembly – The rigid weldment that contains, supports, and reinforces the containment boundary. Consists of two vertical walls, the top and bottom walls, the closed end wall, the closure lid, and closure bolts.

CSA – Containment Structural Assembly.

CTU – Certification Test Unit.

CH–TRU Waste – Contact–Handled Transuranic Waste.

Debris Shield Receptacle, Holder, and Insert – The receptacle is attached to the body and receives the insert. The holder is attached to the closure lid, and supports the insert. The insert is the silicone rubber extrusion that provides the shield when interfacing with the receptacle.

Guide Bar – Steel component attached to the CSA inner cavity to guide the payload container and protect the debris shield from damage.

HAC – Hypothetical accident conditions.

Lifting Arms – Reinforced steel structures at each end of the package that carry the lifting loads from the ISO lift fittings into the CSA. The front lifting arms are identical with the cheeks.

NCT – Normal conditions of transport.

Overpack Cover – The protective cover that is installed over the closure lid, and which completes the packaging overpack.

Overpack Structure – The structures and materials attached to the outside of the CSA.

Packaging – The assembly of components necessary to ensure compliance with packaging requirements as defined in 10 CFR §71.4.

Package – The packaging with its radioactive contents, or payload, as presented for transportation as defined in 10 CFR §71.4.

Payload – Contact–handled transuranic (CH–TRU) waste or other authorized contents contained within the approved payload container. In this SAR, the payload includes a loaded SLB2 payload container and a payload loading system, such as a pallet and roller floor. Payload requirements are defined by the TRUPACT–III TRAMPAC.

Payload Container – The payload container is the SLB2.

Payload Loading Pallet – A lightweight pallet used for handling the payload containers.

Roller Floor – A structure supported by the floor of the TRUPACT–III interior cavity. It may be equipped with retractable rollers or equivalent means to facilitate insertion and removal of the payload loading pallet.

SAR – Safety Analysis Report (this document).

Seal Test Port – The penetration in the closure lid to evacuate for helium leakage rate testing or pressure rise testing of the main containment O–ring seal.

Seal Test Port Plug – The threaded aluminum bronze plug that seals the seal test port.

SLB2 – Standard Large Box, a payload container for use within the TRUPACT–III packaging.

Test O–ring Seal – The outer O–ring seal in the closure lid; forms the vacuum boundary for leakage rate testing.

TRUPACT–III Package – The package consisting of a TRUPACT–III packaging and payload.

TRUPACT–III Packaging – The packaging consisting of a body, closure lid, and an overpack cover.

TRUPACT–III TRAMPAC – TRUPACT–III TRU Waste Authorized Methods for Payload Control.

UNS – Unified National Standard.

Vent Port – The penetration into the cavity that is located in the closure lid; used to obtain an air sample, vent, and introduce helium into the payload cavity.

Vent Port Dust Plug – The threaded aluminum bronze plug that seals the vent port insert.

Vent Port Insert – The aluminum bronze solid plug that contains a containment and test O–ring seals; forms part of the containment boundary.

Vent Port Locking Ring – The threaded aluminum bronze ring that locks the vent port retaining ring into the closure lid.

Vent Port Retaining Ring – The threaded aluminum bronze ring that secures the vent port insert into the closure lid.

2.0 STRUCTURAL EVALUATION

This section presents evaluations demonstrating that the TRUPACT–III package meets all applicable structural criteria. The TRUPACT–III packaging, consisting of a body, a closure lid, and an overpack cover, is evaluated and shown to provide adequate protection for the payload. Normal conditions of transport (NCT) and hypothetical accident condition (HAC) evaluations, using analytic and empirical techniques, are performed to address 10 CFR 71[1] performance requirements. Analytic demonstration techniques, which apply to most NCT and some HAC evaluations, comply with the methodology presented in NRC Regulatory Guides 7.6[2] and 7.8[3]. Empirical demonstration techniques, which apply to free drop and puncture drop evaluations, consist of certification testing, utilizing two full-scale certification test units (CTU-1 and CTU-2). In all, the CTUs were subjected to a total of one 0.3-m NCT free drop, five 9-m HAC free drops, and six 1-m puncture drop tests. Results of the certification tests are provided in Appendix 2.12.3, *Certification Tests on CTU-1* and Appendix 2.12.6, *Certification Tests on CTU-2*. The design of the TRUPACT–III and the scope of the certification testing were guided by prior engineering tests on a half-scale test unit, as detailed in Appendix 2.12.1, *Engineering Tests*.

2.1 Description of Structural Design

2.1.1 Discussion

A comprehensive discussion of the TRUPACT–III packaging design and configuration is provided in Section 1.2, *Package Description*. A summary of that information follows.

From a structural viewpoint, the TRUPACT–III packaging consists of a rigid containment structural assembly (CSA) which is surrounded by energy-absorbing and thermally-protective overpack structure, shown in Section B-B on Sheet 4 of drawing 51199-SAR.

From an operational viewpoint, the TRUPACT–III packaging consists of a body assembly, a closure lid assembly, and an overpack cover assembly, as shown on Sheet 2 of drawing 51199-SAR. A detailed description of the TRUPACT–III body assembly is given in Section 1.2.1.1, *Body*; that of the closure lid assembly in Section 1.2.1.2, *Closure Lid*, and that of the overpack cover assembly in Section 1.2.1.3, *Overpack Cover*.

2.1.2 Design Criteria

Proof of performance for the TRUPACT–III packaging is achieved by a combination of analytic and empirical evaluations. The acceptance criteria for analytic assessments are in accordance with Regulatory Guide 7.6. The acceptance criterion for empirical assessments is a demonstration that the

[1] Title 10, Code of Federal Regulations, Part 71 (10 CFR 71), *Packaging and Transportation of Radioactive Material*, 01–01–09 Edition.

[2] U. S. Nuclear Regulatory Commission, Regulatory Guide 7.6, *Design Criteria for the Structural Analysis of Shipping Cask Containment Vessels*, Revision 1, March 1978.

[3] U. S. Nuclear Regulatory Commission, Regulatory Guide 7.8, *Load Combinations for the Structural Analysis of Shipping Casks for Radioactive Material*, Revision 1, March 1989.

containment boundary remains leaktight[4] following the imposed loading conditions. Additionally, package deformations obtained from certification testing must be such that deformed geometry assumptions used in subsequent thermal and criticality evaluations are validated.

The remainder of this section presents the detailed acceptance criteria used for analytic structural assessments of the TRUPACT–III packaging.

2.1.2.1 Analytic Design Criteria (Allowable Stresses)

This section defines the allowable stresses for primary membrane, primary bending, secondary, shear, peak, and buckling stresses for containment and non-containment structures. These allowable stresses are used for all analytic assessments of TRUPACT–III packaging structural performance.

2.1.2.1.1 Containment Structures

A summary of allowable stresses used for containment structures, which includes the CSA body, closure lid, and closure bolts, is presented in Table 2.1-1. These data are consistent with Regulatory Guide 7.6, and the ASME Boiler and Pressure Vessel Code, Section III, Subsection NB-3000 and Appendix F[5].

2.1.2.1.2 Non-Containment Structures

Overpack structures (both body and overpack cover) are expected to deform and absorb energy in the NCT and HAC free drop events and the HAC puncture drop event. Thus, specific design criteria are not applicable to overpack structures. The performance of the overpack structures is discussed in Sections 2.7.1, *Free Drop*, and 2.7.3, *Puncture*.

The allowable stress applicable to package lifting is limited to one-third of the material yield strength, consistent with the requirements of 10 CFR §71.45(a). Since there are no tie-down devices in the TRUPACT–III packaging design, allowable stress applicable to tie-down loading is not required.

2.1.2.2 Miscellaneous Structural Failure Modes

2.1.2.2.1 Brittle Fracture

By avoiding the use of ferritic steels in the TRUPACT–III packaging, brittle fracture concerns are precluded. Specifically, the primary structural components are fabricated of Alloy UNS S31803 duplex stainless steel. This material satisfies the brittle fracture requirements of

[4] Leaktight is defined as leakage of 1×10^{-8} Pascals - cubic meters per second (Pa-m^3/s), air, or less per ANSI N14.5–1997, *American National Standard for Radioactive Materials – Leakage Tests on Packages for Shipment,* American National Standards Institute, Inc. (ANSI).

[5] American Society of Mechanical Engineers (ASME) Boiler and Pressure Vessel Code, Section III, *Rules for Construction of Nuclear Facility Components*, Division 1 - Subsection NB, *Class 1 Components*, and Appendix F, *Rules for Evaluation of Service Loadings with Level D Service Limits,* 2004 Edition, 2005 and 2006 Addenda.

Regulatory Guide 7.11[6] and ASTM E604[7] at the minimum service temperature of -29 ºC required by 10 CFR §71.73(b). Therefore, the material is safe from brittle fracture.

The closure lid and overpack cover attachment bolts are socket head cap screws fabricated from ASTM A320, L43 material, ensuring that brittle fracture is not of concern. Other fasteners used in the TRUPACT–III packaging assembly, such as the vent port retaining ring, are made from copper alloy material, again eliminating brittle fracture concerns.

2.1.2.2.2 Fatigue Assessment

2.1.2.2.2.1 Normal Operating Cycles

Normal operating cycles do not present a fatigue concern for the TRUPACT–III components over a 35 year service life. The basis for this conclusion is reached using the six criteria of Article NB-3222.4(d) of the ASME Boiler and Pressure Vessel Code. A summary of the six criteria and their application are discussed below.

(1) Atmospheric to Service Pressure Cycle: The total number of atmospheric-to-operating pressure cycles during normal operations does not exceed the number of cycles on the fatigue curve corresponding to a value of $S_a = 3S_m$ for Alloy UNS S31803 stainless steel. From Section 2.2.1, *Material Properties and Specifications* at a bounding temperature of 71 °C per Section 2.6.1.1, *Summary of Pressures and Temperatures*, the S_m value for UNS S31803 stainless steel is 207 MPa, which corresponds to an alternating stress value of $S_a = 3S_m = 621$ MPa. The corresponding number of cycles for a value of $S_a = 621$ MPa is approximately 2,000 from Figure I-9.2.1 and Table I-9.1M of the ASME Code.[8] The package has a design life of 35 years, with the expected maximum number of shipments to be 50 per year. The package undergoes one atmospheric-to-operating pressure cycle per shipment, therefore the package will experience $35 \times 50 = 1{,}750$ atmospheric-to-operating pressure cycles in its life. Since the allowable number of cycles is greater than the maximum expected number of cycles, the first criterion is satisfied.

(2) Normal Service Pressure Fluctuation: The specified full range of pressure fluctuations during normal service does not exceed the quantity 1/3(Design Pressure)(S_a / S_m), where the design pressure is 172 kPa, S_a is the value obtained from the Alloy UNS S31803 stainless steel design fatigue curve for the total specified number of significant pressure fluctuations, and S_m is the allowable stress intensity for the material at the service temperature. The total number of service cycles is less than 10^6 cycles. From Table I-9.1M for Figure I-9.2.1 of the ASME Code, $S_a = 195$ MPa for 10^6 cycles as a lower bound. When adjusted for temperature to 71 ºC using the ratio of the modulus of elasticity from Section 2.2.1, *Material Properties and Specifications*, S_a becomes ($19.2(10^4)$/

[6] U.S. Nuclear Regulatory Commission, Regulatory Guide 7.11, *Fracture Toughness Criteria of Base Material for Ferritic Steel Shipping Cask Containment Vessels with Maximum Wall Thickness of 4 Inches (0.1 m)*, June 1991.

[7] ASTM E604–83 (2002), *Standard Test Method for Dynamic Tear Testing of Metallic Materials*, American National Standards Institute (ANSI), Inc.

[8] American Society of Mechanical Engineers (ASME) Boiler and Pressure Vessel Code, Section III, *Rules for Construction of Nuclear Facility Components*, Appendix I, *Design Stress Intensity Values, Allowable Stresses, Material Properties, and Design Fatigue Curves*, 2004 Edition, 2005 and 2006 Addenda.

$19.5(10^4)) \times 195 = 192$ MPa. The value of S_m was defined above as 207 MPa at service temperature. The significant pressure fluctuation (SPF) becomes:

$$SPF = 1/3(\text{Design Pressure})(S_a/S_m)$$

$$SPF = 1/3(172)(192/207) = 53 \text{ kPa}$$

Next, the maximum pressure fluctuations in the package will be determined. If the package temperature in storage varies between the extremes of $T_1 = -40$ ºC to $T_2 = 71$ ºC, the increase in internal pressure from atmospheric, $P_1 = 101$ kPa, is:

$$\frac{P_2}{P_1} = \frac{T_2}{T_1} \Rightarrow P_2 = P_1\left(\frac{T_2}{T_1}\right) = 101\left(\frac{71+273}{-40+273}\right) = 149 \text{ kPa}$$

The resulting pressure fluctuation is 149 - 101 = 48 kPa, which is less than 53 kPa presented above. Therefore, the second criterion is satisfied.

(3) Temperature Difference — Startup and Shutdown: The temperature between adjacent points of a package component during normal service does not exceed $1/2(S_a/E\alpha)$, where S_a is the design fatigue curve value taken from Table I-9.1M for Figure I-9.2.1 of the ASME Code for Alloy UNS S31803 stainless steel for the total specified number of temperature difference fluctuations, E is the modulus of elasticity, and α is the mean coefficient of thermal expansion, all evaluated at temperature. The total number of temperature fluctuations will not exceed the number of uses of the package, which is 1,750 as calculated above. It will be conservative to use the value of S_a from Table I-9.1M of the ASME Code for 2,000 cycles, which is 669 MPa. From Section 2.2.1, *Material Properties and Specifications* at a bounding temperature of 71 °C, the value of the mean thermal expansion coefficient is $13.0(10^{-6})$. Therefore, the value of $1/2(S_a/E\alpha) = 1/2(669/[19.2(10^4)13.0(10^{-6})] = 134$ ºC, which corresponds to 2,000 cycles. Since the package design temperature is 71 ºC under ambient conditions of 38 ºC, the temperature difference between any two adjacent points cannot approach the 134 ºC value. Thus, the third criterion is satisfied.

(4) Temperature Difference — Normal Service: The temperature difference between any two adjacent points does not change during normal service by more than the quantity $1/2(S_a/E\alpha)$, where S_a, E, and α are as defined above. However, normal operating temperatures of the CSA are largely decoupled from the fluctuations of the outer sheets, and any changes in temperature will be relatively slow and even due to the large thermal mass of the package. Therefore, the fourth criterion is satisfied.

(5) Temperature Difference — Dissimilar Materials: Except for the closure bolts (see below), there are only two other dissimilar materials used: UNS S31803 and Type 304L stainless steel. The total algebraic temperature range does not exceed the quantity $S_a/[2(E_1\alpha_1 - E_2\alpha_2)]$, where S_a is the design fatigue curve value taken from Table I-9.1M for Figure I-9.2.1 of the ASME Code at 10^6 cycles. The subscripts 1 and 2 refer to Type 304L and UNS S31803 material properties, respectively. The quantity defined above is the significant temperature fluctuation, or STF. The total temperature range is between the NCT cold temperature of -40 ºC and the design temperature of 71 ºC, or 111 ºC. The mean temperature, used for the evaluation of properties, is 55.5 ºC. At this temperature, from Section 2.2.1, *Material Properties and Specifications*, the modulus of elasticity $E_1 = E_2 = 19.27(10^4)$ MPa. From ASME Code, Section II, Part D, Table TE-1, the instantaneous value of α_1 (Material Group 3) is

equal to $15.84(10^{-6})$ per ºC, and the instantaneous value of α_2 (Material Group 2) is equal to $12.96(10^{-6})$ per ºC. From paragraph (2) above, the design fatigue strength for 10^6 cycles (conservatively adjusted for the maximum temperature of 71 ºC) is 192 MPa. The STF therefore is:

$$STF = \frac{S_a}{2(E_1\alpha_1 - E_2\alpha_2)} = \frac{192}{2\left[19.27(10^4)\times 15.84(10^{-6}) - 19.27(10^4)\times 12.96(10^{-6})\right]} = 173\ ^\circ C$$

Since the maximum temperature fluctuation range of 111 ºC is less than the STF of 173 ºC, the fifth criterion is not a concern.

(6) Mechanical Loads: The specified full range of mechanical loads does not result in load stresses whose range exceeds the S_a design fatigue curve taken from Table I-9.1M for Figure I-9.2.1 of the ASME Code for Alloy UNS S31803 stainless steel for the total specified number of load fluctuations. The only repeating mechanical loads will be those associated with lifting and handling. Since the package is handled twice for each transport cycle (load and unload), the maximum number of cycles is 2 × 1,750 = 3,500. From Table I-9.1M, S_a = 576 MPa for 3,500 cycles. The maximum temperature of the lifting arms (cheeks) is bounded by 83 ºC. When adjusted for a temperature of 83 ºC using the ratio of the modulus of elasticity, S_a becomes $(19.1(10^4)/19.5(10^4)) \times 576 = 564$ MPa. Lifting stress is limited by 10 CFR §71.45(a) to a value of one-third of the material's minimum yield strength. For a lifting temperature of 83 ºC, the minimum yield strength of UNS S31803 stainless steel is 408 MPa. Thus, one-third of the minimum yield strength is 1/3(408) = 136 MPa. Since the adjusted S_a is greater than this value, the sixth criterion is satisfied.

Summary: The previous discussion verifies that fatigue failure of the package body due to normal operating cycles is not a concern, per Section III, Subsection NB, Article NB-3222.4(d) of the ASME Code. Therefore the TRUPACT–III packaging's resistance to fatigue is adequate to ensure a minimum 35 year service life (assuming 50 shipments per year).

Closure Bolt Fatigue Evaluation: The maximum stress intensity developed in the closure bolts during normal operations, given in Section 2.6.1.6, *Closure Bolts*, is S_{max} = 446 MPa. This stress includes preload stress, thermal stress, and a conservative inclusion of 50% of the applied preload torque as a residual torsion stress. From Table 2.2-4, the ASME allowable stress, S_m, at 71 ºC is 233 MPa. From Table I-9.1M of the ASME B&PV Code, the Maximum Nominal Stress (MNS) of 446 MPa is less than $2.7S_m$ (2.7(233) = 629 MPa). Therefore, from Table I-9.1M for Figure I-9.4 for ASTM A320 L43 bolting material, the allowable number of cycles for a corresponding alternating stress above that of one-half the value of S_{max} (i.e., 1/2(446) = 223 MPa) is over 10,000 cycles. Per NB-3232.3, a stress concentration factor of four shall be applied to one-half the value of S_{max}, i.e., $4(1/2S_{max}) = 4 \times 223 = 892$ MPa. Per NB-3232.3(d), the alternating stress must be adjusted for the elastic modulus used in the fatigue curves. The modulus used for the fatigue curve, per Table I-9.1M is $207(10^3)$ MPa. Conservatively using the lower modulus for 93 ºC from Table 2.2-4 of $18.7(10^4)$ MPa, the adjusted alternating stress is:

$$S_{ALT} = \frac{20.7}{18.7}892 = 987\ \text{MPa}$$

The corresponding cycles allowed per Table I-9.1M for Figure I-9.4 is interpolated per Note 2 of the table:

$$N = N_i\left(\frac{N_j}{N_i}\right)^{[\log(S_i/S)]/\log(S_i/S_j)} = 500\left(\frac{1000}{500}\right)^{[\log(986/987)]/\log(986/690)} = 499 \text{ cycles}$$

Since closure bolts are tightened twice per package service cycle, the allowable number of package service cycles is half of this value. Therefore, the closure bolts should be replaced approximately every 499/2 = 250 service cycles for the package.

2.1.2.2.2.2 Normal Vibration Over the Road

Fatigue associated with normal vibration over the road is addressed in Section 2.6.5, *Vibration*.

2.1.2.2.2.3 Extreme Total Stress Intensity Range

Per paragraph C.7 of Regulatory Guide 7.6:

> The extreme total stress intensity range (including stress concentrations) between the initial state, the fabrication state, the normal operating conditions, and the accident conditions should be less than twice the adjusted value (adjusted to account for modulus of elasticity at the highest temperature) of S_a at 10 cycles given by the appropriate design fatigue curves.

Since the response of the TRUPACT–III packaging to accident conditions is evaluated empirically rather than analytically, the extreme total stress intensity range for all conditions has not been quantified. However, both full-scale certification test units were tested at minimum ambient temperatures during free drop testing. Both CTUs were also fabricated in accordance with the drawings in Appendix 1.3.1, *Packaging General Arrangement Drawings*, thus incurring prototypic fabrication induced stresses, stresses consistent with an increased internal pressure equal to 150% of MNOP applied during fabrication pressure testing, and stresses from reduced internal pressure (i.e., a full vacuum during leak testing), applied as part of initial acceptance. Exposure to these extreme conditions including stresses resulting from certification testing, while consistently demonstrating the leak tightness of the containment boundary, satisfies the intent of paragraph C.7 of Regulatory Guide 7.6.

2.1.2.2.3 Buckling Assessment

Buckling, per Regulatory Guide 7.6, is an unacceptable failure mode for the containment vessel. The intent of this provision is to preclude large deformations that would compromise the validity of linear analysis assumptions and quasi-linear stress allowable limits, as given in Paragraph C.6 of Regulatory Guide 7.6.

The methodology of corrugated-core sandwich sheets is applied to the containment structural assembly (CSA). Buckling from pressure loading is governed by the HAC immersion case. Analysis results are provided in Section 2.7.6, *Immersion – All Packages*, and details provided in Appendix 2.12.4, *HAC Immersion Buckling Evaluation*.

Consistent with Regulatory Guide 7.6 philosophy, factors of safety corresponding to ASME Boiler and Pressure Vessel Code, Level A and Level D service conditions are employed. For NCT (Service Level A), the factor of safety is 2.0, and for HAC (Service Level D), the factor of safety is 1.34.

It is noted that 9-m drop tests performed on the full-scale certification test unit with the package in various orientations produced no evidence of buckling of any part of the CSA structure (refer to Appendix 2.12.3, *Certification Tests*). Although certification testing does not provide a specific determination of the margin of safety against buckling, it is considered evidence that buckling will not occur.

2.1.3 Weights and Centers of Gravity

The maximum gross weight of the TRUPACT–III package, including a maximum payload weight of 5,210 kg (11,486 lbs), is 25,000 kg (55,116 lbs). The empty packaging therefore weighs 25,000 - 5,210 = 19,790 kg (43,630 lb). With reference to Figure 2.1-1, a detailed breakdown of the TRUPACT–III package component weights are summarized in Table 2.1-2.

Due to symmetry of design, the center of gravity (CG) of the empty package is located at the geometric center of the package cross-section: 1,325 mm (52.2 in) above the bottom outside surface of the package and 1,250 mm (49.2 in) from either outer side of the package on the longitudinal axis. The longitudinal CG of the empty package is located 2,356 mm (93 in) from the outer closed-end surface of the package. Since the thickness of the end material between the datum plane and the rear inside of the payload cavity is 750 mm, and given the length of the payload cavity as 2,790 mm, the location of the center of gravity of a uniformly loaded package relative to the datum plane is:

$$x = \frac{19{,}790(2{,}356) + 5{,}210\left(750 + \frac{2{,}790}{2}\right)}{25{,}000} = 2{,}312 \text{ mm}$$

The center of gravity is located 168 mm (6.6 in) towards the closure end from the longitudinal geometric center, based on an overall package length of 4,288 mm. The TRUPACT–III package will be so loaded that the center of gravity of the loaded package will not deviate more than ±150 mm (5.9 in) laterally or vertically, or ±200 mm (7.9 in) longitudinally from this location.

2.1.4 Identification of Codes and Standards for Package Design

The TRUPACT–III package contents potentially exceed an amount of $3{,}000A_2$, and according to Table 1 of Regulatory Guide 7.11, the TRUPACT–III is therefore a Category 1 package. Per the guidance of NUREG/CR-3854[9], the appropriate design criteria is Section III, Subsection NB of the ASME B&PV Code. Consequently, the design of the containment boundary is based on the methodology of Regulatory Guide 7.6, and load cases are applied and combined according to Regulatory Guide 7.8.

All welds in the containment boundary shell (see Section 1.2.1.1, *Body*, and Section 1.2.1.2, *Closure Lid*) are full penetration welds inspected by visual, dye penetrant, and radiographic methods. The fillet welds connecting the V-stiffeners to the outer surface of the containment sheets are classified as fillet welded attachments per ASME B&PV Code, Section III, Subsection NB, paragraph NB-3123.2. Welds outboard of these fillet welds (e.g., the plug welds connecting the V-stiffeners to the CSA outer sheets, and all overpack welds) do not qualify as Subsection

[9] L. E. Fischer, W. Lai, *Fabrication Criteria for Shipping Containers,* NUREG/CR–3854, UCRL–53544, U.S. Nuclear Regulatory Commission, March 1985.

NB weld types. These welds are evaluated using other codes, such as AWS D1.6, and inspected using visual and dye penetrant techniques as described in Section 2.3.2, *Examination*.

To fully ensure adequate package performance, a certification test unit was subjected to a series of free drop and puncture events as described in Section 2.7.1, *Free Drop*, and Section 2.7.3, *Puncture*. Additionally, during fabrication each package is subjected to an internal pressure equal to 150% of the design pressure, and a full vacuum. This combination of the use of codes, standards, and verification testing ensures satisfactory package performance.

Table 2.1-1 – Containment Structure Allowable Stress Limits

Stress Category	NCT	HAC
General Primary Membrane Stress Intensity	S_m	Lesser of: $2.4S_m$, $0.7S_u$
Local Primary Membrane Stress Intensity	$1.5S_m$	Lesser of: $3.6S_m$, S_u
Primary Membrane + Bending Stress Intensity	$1.5S_m$	Lesser of: $3.6S_m$, S_u
Range of Primary + Secondary Stress Intensity	$3.0S_m$	Not Applicable
Pure Shear Stress	$0.6S_m$	$0.42S_u$
Bearing	S_y	S_y
Peak	Per Section 2.1.2.2.2, *Fatigue Assessment*	
Buckling	Per Section 2.1.2.2.3, *Buckling Assessment*	
*Containment Fasteners:*①		
Average Tensile Stress Intensity	S_m②	Lesser of: $1.0S_y$, $0.7S_u$
Average Tensile + Average Shear + Bending + Residual Torsion Stress Intensity	$1.35S_m$②	Not Applicable
For Non-Linear Analysis:		
General Primary Membrane Stress Intensity	Not Applicable	Greater of: $0.7S_u$, $S_y + (1/3)(S_u - S_y)$
Maximum Primary Stress Intensity	Not Applicable	$0.9S_u$

Notes: ① Containment fastener stress limits are in accordance with NUREG/CR-6007.
② S_m is defined as $(2/3)S_y$ as recommended by NUREG/CR-6007.

Table 2.1-2 – TRUPACT–III Component Weights

Item	Weight, kg (lb)	
	Component	Assembly
Total Empty Package		19,790 (43,630)
Body	15,100 (33,290)	
Closure Lid	1,840 (4,057)	
Overpack Cover	2,850 (6,283)	
Payload and Payload Components		5,210 (11,486)
Loaded SLB2	4,763 (10,500)	
Payload Loading System (e.g., pallet and roller floor)	447 (986)	
Total Loaded Package (Maximum)		25,000 (55,116)

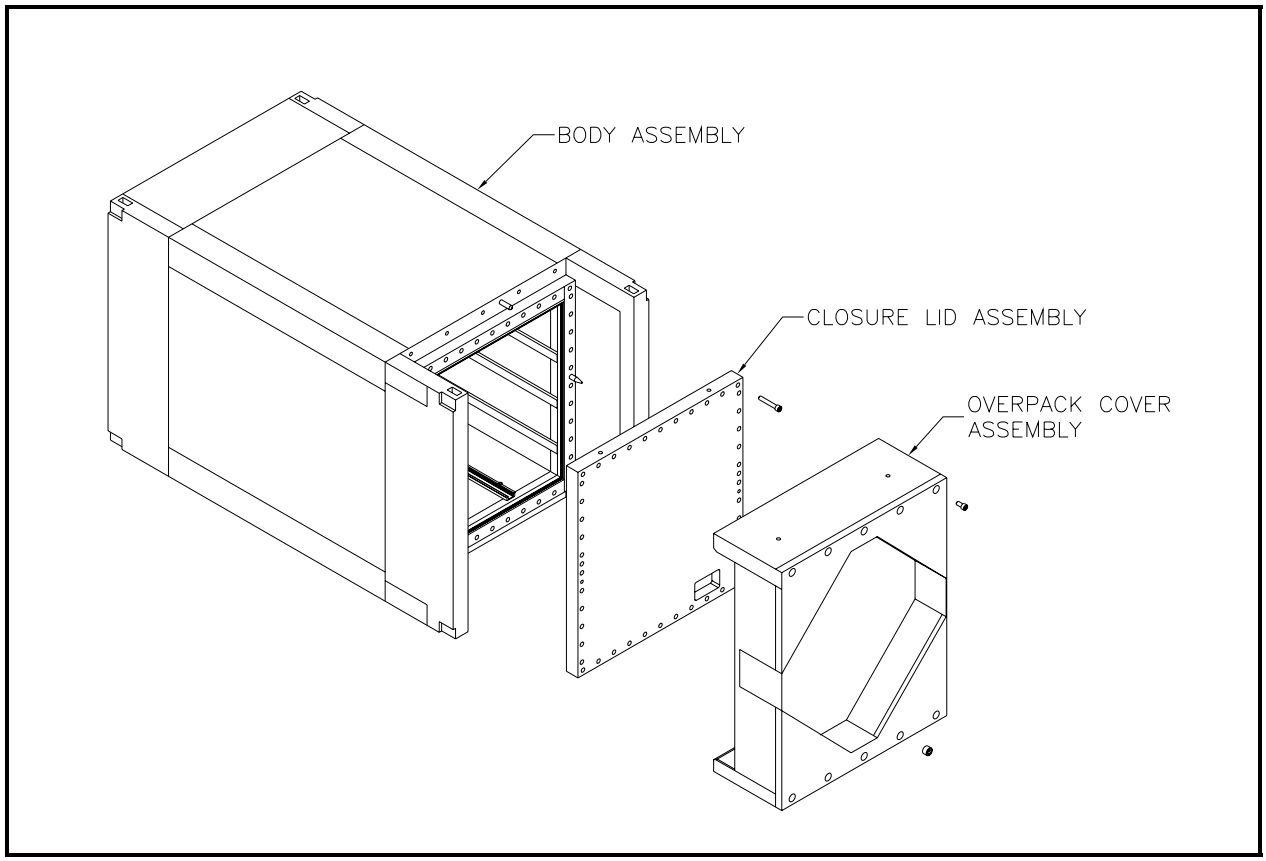

Figure 2.1-1 – TRUPACT–III Packaging Components

2.2 Materials

The TRUPACT–III CSA and overpack steel components are fabricated primarily from Alloy UNS S31803 duplex stainless steel. Polyurethane foam and balsa wood are used for impact resistance. Other materials performing a structural function are copper alloy UNS C63200 (for the vent port plug, retaining ring, and locking ring), and ASTM A320, L43, carbon steel (for the closure lid bolts and overpack cover attachment bolts). Type 304/304L stainless steel is utilized for a limited number of parts not having an important structural function, such as the lid guide pin, the overpack cover guide pin, the guide bars in the payload cavity, debris shield receptacle, and the bolt access tubes on the overpack cover. Several varieties of non-structural materials are also utilized. Representative non-structural materials include butyl rubber O-ring seals, calcium silicate insulation, and plastic fire consumable vent plugs used in the foam cavities. The drawings presented in Appendix 1.3.1, *Packaging General Arrangement Drawings*, delineate the specific materials used for each TRUPACT–III packaging component.

The remainder of this section presents the pertinent mechanical properties for the materials that perform a structural function.

2.2.1 Material Properties and Specifications

Tables 2.2-1 through 2.2-8 present the mechanical properties for the structural materials used in the TRUPACT–III packaging. Each of the mechanical properties of Alloy UNS S31803 stainless steel is taken from Code Case N-635-1 or Section II of the ASME Boiler and Pressure Vessel Code[1]. Any analyses of the CSA utilize the properties presented for Alloy UNS S31803, ASTM A240/A479 stainless steel. The density of stainless steel is taken as 7.89 kg/dm^3, and Poisson's Ratio is 0.3. Data is interpolated or extrapolated from the available data, as necessary, as noted in the tables.

Where required, non-linear material properties are utilized in the form of true stress-strain curves, developed in the following paragraphs. The material models for Alloy UNS S31803 and ASTM Type 304L are evaluated at the minimum temperature of -29 ºC for consistency with the maximum HAC cold free drop impact magnitudes. Alloy UNS S31803 is also evaluated at the maximum NCT temperature of 71 ºC.

For the Alloy UNS S31803 material, the non-linear properties are based on tensile tests of as-received specimens at temperature. The data set is then adjusted for the minimum yield strength given in Code Case N-635-1. The stress-strain curves thus obtained conservatively represent the minimum strength allowed for the material. Utilizing a standard Ramberg-Osgood[2] curve, the engineering stress-strain curve is developed up to the yield strength for each temperature using the following equations:

$$\varepsilon = \frac{\sigma}{E_0} + 0.002\left(\frac{\sigma}{S_y}\right)^n \qquad n = \frac{\ln(20)}{\ln\left(\frac{S_y}{\sigma_{0.01}}\right)}$$

[1] American Society of Mechanical Engineers (ASME) Boiler and Pressure Vessel Code, Section III, *Code Case N–635–1*.

[2] National Advisory Committee for Aeronautics – Technical Note No. 902, *Description of Stress–Strain Curves by Three Parameters*, Walter Ramberg and William R. Osgood, July 1943.

where: ε = strain, mm/mm

σ = stress, MPa

E_o= average elastic modulus of test samples, MPa

$\sigma_{0.01}$ = stress at 0.01% strain, MPa

S_y = yield strength, MPa

To develop the engineering stress-strain curve between the yield and ultimate strengths, a linear progression is used as follows:

$$\sigma'_{eng} = \sigma_{eng} - \left[\frac{\Delta S_u - \Delta S_y}{\varepsilon_2 - \varepsilon_1} \left(\varepsilon_{eng} - \varepsilon_1 \right) + \Delta S_y \right]$$

where: σ'_{eng} = resultant engineering stress, MPa

σ_{eng} = stress at a given strain ε, MPa

ΔS_u = difference between ASME and test sample ultimate strengths, MPa

ΔS_y = difference between ASME and test sample yield strengths, MPa

ε_{eng} = engineering strain at a given stress σ_{eng}, mm/mm

ε_1 = strain at average yield strength of test samples, mm/mm

ε_2 = strain at average ultimate strength of test samples, mm/mm

The engineering stress-strain values are converted into true stress-strain using the following equations:

$$\varepsilon_{true} = \ln (\varepsilon_{eng} + 1) \qquad \sigma_{true} = \sigma_{eng} \left(\varepsilon_{eng} + 1 \right)$$

The resulting true stress-strain curves for UNS S31803 at temperatures of -29 ºC and 71 ºC are given in Table 2.2-2 and shown graphically in Figure 2.2-1.

For Type 304L material, nonlinear properties are based on the following material model taken from the literature:[3]

$$\sigma = \sigma_p + A\left(\varepsilon_p - \varepsilon_L \right)^n$$

where: σ_p = 193.06 MPa [28,000 psi]

A = 1,329 MPa [192,746 psi]

n = 0.74819

ε_p = true plastic strain

ε_L = Luder's strain (equal to zero for stainless steel)

This model applies at room temperature. To adjust it to the properties at the minimum temperature of -29 ºC, the model is multiplied by the ratio:

$$\frac{\sigma_{true-y}}{\sigma_p} = \frac{201.2}{193.06} = 1.04$$

[3] Sandia National Laboratories, *Reexamination of Spent Fuel Shipment Risk Estimates*, NUREG/CR–6672, Vol. 1, U.S. Nuclear Regulatory Commission, March 2000, p. 5-7.

where σ_p is defined above and the true yield stress at temperature, $\sigma_{true\text{-}y}$, is found from:

$$\sigma_{true-y} = \sigma_{eng-y}\left(1 + \frac{\sigma_{eng-y}}{E}\right) = 201.2 \text{ MPa}$$

where the engineering yield strength and Young's modulus at a temperature of -29 ºC from Table 2.2-3 are:

$\sigma_{eng\text{-}y}$ = 201 MPa (extrapolated from 38 ºC and 93 ºC)[4]

E = $19.8(10^4)$ MPa

Further, since the model reports only plastic strain, the total strain used in analysis is obtained from:

$$\varepsilon_{tot} = \varepsilon_p + \frac{\sigma_{eng-y}}{E}$$

in which the last term is equal to the elastic strain, or 0.001. The resulting true stress-strain curve for Type 304L material at -29 ºC is given in Table 2.2-2 and shown graphically in Figure 2.2-1.

The performance of the TRUPACT–III in free drop and puncture events is dependent on polyurethane foam and balsa wood. The foam and wood are prepared for installation within the overpack as prefabricated blocks or panels. A total of four nominal foam densities and one balsa wood density are used. The drawings presented in Appendix 1.3.1, *Packaging General Arrangement Drawings*, show the placement of the various densities of foam and wood and the direction of the foam rise (or wood grain). Section 8.1.5.1, *Polyurethane Foam* and Section 8.1.5.2, *Balsa Wood* present the details of acceptance tests for these materials. The nominal, room-temperature crush properties of the polyurethane foam components are given in Table 2.2-5, and for balsa wood in Table 2.2-6. Bronze material properties are given in Table 2.2-7.

2.2.2 Chemical, Galvanic, or Other Reactions

The major materials of construction of the TRUPACT–III packaging (i.e., stainless steel, alloy steel, copper alloy, polyurethane foam, balsa wood, calcium silicate insulation board, and butyl rubber O-ring seals) will not have significant chemical, galvanic or other reactions in air, inert gas or water environments. These materials have been previously used, without incident, in radioactive material (RAM) packages for transport of similar payload materials. With the exception of butyl rubber and polyurethane foam, these materials of construction have been used in the TN–Gemini package[5] for several years without incident, carrying essentially identical payload materials as will be carried in the TRUPACT–III package. Polyurethane foam and butyl rubber have been used in many other RAM packagings, such as the TRUPACT–II.[6] A successful RAM packaging history combined with successful use of these fabrication materials in similar industrial environments ensures that the integrity

[4] According to MIL–HDBK–5F, Figure 2.7.1.1.1(a), the yield strength of Type 304L stainless steel varies essentially linearly between -29 ºC and 93 ºC.

[5] AREVA Cogema Logistics (ACL), *Safety Analysis Report for the TN–Gemini Package*, French Certificate of Approval F/343/B(U)F–85 Bg, AREVA Cogema Logistics, Paris, France.

[6] U. S. Department of Energy (DOE), *Safety Analysis Report for the TRUPACT–II Shipping Package*, USNRC Certificate of Compliance 71–9218, U.S Department of Energy, Carlsbad Field Office, Carlsbad, New Mexico.

of the TRUPACT–III package will not be compromised by any chemical, galvanic or other reactions. The materials of construction and the payload are further evaluated below for potential reactions.

2.2.2.1 Packaging Materials of Construction

The TRUPACT–III packaging is primarily constructed of UNS S31803 stainless steel. This material is highly corrosion resistant to most environments. The metallic structure of the TRUPACT–III packaging is composed entirely of this material and compatible weld material. The weld material and processes have been selected in accordance with the ASME Boiler and Pressure Vessel Code[7] to provide as good or better material properties, including corrosion resistance, as the base material. Since both the base and weld materials are essentially the same, they have nearly identical electrochemical potential thereby minimizing any galvanic corrosion that could occur.

The polyurethane foam and balsa wood that is used in the TRUPACT–III packaging is essentially identical to many previously licensed transportation packagings. All of these packagings have had a long and successful record of performance demonstrating that the polyurethane foam and/or wood does not cause any adverse conditions with the packaging. The polyurethane foam in the packaging is a rigid, closed-cell (non-water absorbent) foam that is free of halogens and chlorides, as discussed in Section 8.1.5.1, *Polyurethane Foam*. The balsa wood used in the outer overpack layer does not react with the stainless steel or foam. The foam and wood material cavities are sealed with plastic threaded plugs to exclude moisture.

The various copper alloy fittings used in the TRUPACT–III packaging are very corrosion resistant. Any damage that could occur to the material is easily detectable since the fittings are all handled and/or visible each time the TRUPACT–III package is loaded and unloaded.

The butyl rubber elastomer that is used for the O-ring seals and the silicone that is used for the debris seal foam insert contain no corrosives that would react with or adversely affect the TRUPACT–III packaging. These materials are organic in nature and non-corrosive to the stainless steel containment boundary of the TRUPACT–III packaging. The silicone foam debris shield is closed-cell, and will not retain corrosive fluids. Silicone rubber is an inert material with wide use in many industrial environments. Should any corrosion occur, it will not affect containment, and will be easily detectable since the debris shield is inspected for wear or damage (see Section 7.1.5, *Closure Lid Installation*, Step 4). Similarly, the polyethylene filters associated with the debris shield are made of an inert material which will not contribute to corrosion. The hard plastic plates used with the rear-wall guide bars are also inert and will not contribute to corrosion.

2.2.2.2 Payload Interaction with Packaging Materials of Construction

The materials of construction of the TRUPACT–III packaging are checked for compatibility with the various payload chemistries when the payloads are evaluated for chemical compatibility. All

[7] American Society of Mechanical Engineers (ASME) Boiler and Pressure Vessel Code, Section III, *Rules for Construction of Nuclear Facility Components*, 2004 Edition, 2005 and 2006 Addenda.

payload materials are in approved SLB2 payload containers meeting the specifications for payload containers delineated in the TRUPACT–III TRAMPAC.[8]

The payload configuration within payload containers ensures that the payload material has an insignificant level of contact with the TRUPACT–III packaging materials of construction. However, the evaluation of compatibility is based on complete interaction of payload materials with the packaging.

The design of the TRUPACT–III package is for transport of CH–TRU materials and other authorized payloads that are limited in form to solid or solidified material. Corrosive materials, pressurized containers, explosives, non-radioactive pyrophorics, and liquid volumes greater than 1% are prohibited. These restrictions ensure that the waste in the payload is in a non-reactive form for safe transport in the TRUPACT–III package. For a comprehensive discussion defining acceptable payload properties, refer to the TRUPACT–III TRAMPAC.

2.2.3 Effects of Radiation on Materials

Since the payload of the TRUPACT–III is contact handled transuranic waste material, the level of radiation inside the package is negligible. Furthermore, the materials of construction, including the butyl rubber containment seal, have been used for many years in RAM transport packagings without any incident relating to radiation exposure. For these reasons, there will be no radiation effects on the packaging, and the requirements of 10 CFR §71.43(d) are met.

[8] U.S. Department of Energy (DOE), *TRUPACT–III TRU Waste Authorized Methods for Payload Control (TRUPACT–III TRAMPAC)*, U.S. Department of Energy, Carlsbad Field Office, Carlsbad, New Mexico.

This page intentionally left blank.

Table 2.2-1 – Mechanical Properties① of Alloy UNS S31803 Stainless Steel Components

Material Specification	Temperature (°C)	Yield Strength, S_y (MPa)	② Ultimate Strength, S_u (MPa)	Allowable Strength, S_m (MPa)	③ Elastic Modulus, E ($\times 10^4$ MPa)	④ Thermal Expansion Coefficient, α ($\times 10^{-6}$ mm/mm/ºC)
Alloy UNS S31803 ASTM A240 ASTM A479	-40	-----	-----	-----	19.9	11.9
	-29	-----	-----	-----	19.8	12.0
	21	-----	-----	-----	19.5	12.6
	38	448	621	207	19.4	12.8
	93	399	621	207	19.0	13.1
	149	370	598	199	18.6	13.3
	204	353	576	192	18.3	13.7
	260	342	563	188	17.8	13.9
	316	330	556	185	17.4	14.0

Notes: ① Data from ASME Code Case N-635-1, unless otherwise noted. Table data converted from English units.

② ASME Code, Section II, Part D, Table U.

③ Modulus not given in ASME Code, Section II, Part D, Table TM-1; data is for Group G (selected based on chromium content.) Values for -40 ºC and -29 ºC interpolated from 21 ºC and -73 ºC.

④ ASME Code, Section II, Part D, Table TE-1, Material Group 2, Mean Coefficient. Values for -40 ºC and -29 ºC extrapolated from 21 ºC and 38 ºC.

Table 2.2-2 – True Stress-Strain Values for Alloy UNS S31803 and Type 304L Stainless Steel Components

Alloy UNS S31803 at -29 ºC		**Alloy UNS S31803 at 71 ºC**		**Type 304L at -29 ºC**	
Strain (%)	Stress (MPa)	Strain (%)	Stress (MPa)	Strain (%)	Stress (MPa)
0.00	0.0	0.00	0.0	0	0.0
0.16	317.9	0.08	151.7	0.10	200.8
0.22	414.4	0.16	276.5	0.20	208.7
0.32	484.0	0.23	345.4	0.30	214.0
0.47	528.8	0.42	420.6	0.50	223.0
0.70	568.8	1.92	497.1	1.10	244.9
4.31	681.9	4.66	572.3	4.10	325.1
10.89	779.8	10.89	654.3	10.10	447.6
22.31	888.8	26.24	806.7	25.10	690.7

Table 2.2-3 – Mechanical Properties① of Type 304L Stainless Steel

Material Specification	Temperature (°C)	② Yield Strength, S_y (MPa)	③ Ultimate Strength, S_u (MPa)	④ Allowable Strength, S_m (MPa)	⑤ Elastic Modulus, E ($\times 10^4$ MPa)	⑥ Thermal Expansion Coefficient, α ($\times 10^{-6}$ mm/mm/ºC)
ASTM A240 ASTM A249 ASTM A269 ASTM A479 Type 304L	-40	-----	-----	-----	19.9	-----
	-29	-----	-----	-----	19.8	-----
	21	-----	-----	-----	19.5	15.3
	38	172	483	115	19.4	15.5
	93	148	456	115	19.0	16.0
	149	132	422	115	18.6	16.6
	204	121	405	109	18.3	17.1
	260	113	396	102	17.8	17.5

Notes: ① Table data converted from English units.

② ASME Code, Section II, Part D, Table Y-1.

③ ASME Code, Section II, Part D, Table U.

④ ASME Code, Section II, Part D, Table 2A.

⑤ ASME Code, Section II, Part D, Table TM-1, Material Group G. Values for -40 ºC and -29 ºC interpolated from 21 ºC and -73 ºC.

⑥ ASME Code, Section II, Part D, Table TE-1, Material Group 3, Mean.

Table 2.2-4 – Mechanical Properties① of ASTM A320, Grade L43 Alloy Bolting Material

Material Specification	Temperature (°C)	② Yield Strength, S_y (MPa)	③ Ultimate Strength, S_u (MPa)	④ Allowable Strength, S_m (MPa)	⑤ ASME Allowable Strength, S_m (MPa)	⑥ Elastic Modulus, E ($\times 10^4$ MPa)	⑦ Thermal Expansion Coefficient, α ($\times 10^{-6}$ mm/mm/ºC)
ASTM A320 Grade L43	-40	-----	-----	-----	-----	19.5	10.8
	-29	-----	-----	-----	241	19.4	10.9
	21	-----	-----	-----	241	19.2	11.5
	38	724	862	483	241	19.1	11.7
	93	683	-----	455	228	18.7	12.1
	149	660	-----	440	220	18.4	12.4
	204	633	-----	422	211	18.0	12.8
	260	610	-----	407	203	17.7	13.1

Notes: ① Table data converted from English units.
② ASME Code, Section II, Part D, Table Y-3.
③ ASME Code, Section II, Part D, Table Y-3.
④ Computed as 2/3Sy per NUREG/CR-6007.
⑤ ASME Code, Section II, Part D, Table 4.
⑥ ASME Code, Section II, Part D, Table TM-1, Material Group B. Values for -40 ºC and -29 ºC interpolated from 21 ºC and -73 ºC.
⑦ ASME Code, Section II, Part D, Table TE-1, Material Group 1, Mean Coefficient. Values for -40 ºC and -29 ºC extrapolated from 21 ºC and 38 ºC.

Table 2.2-5 – Crush Strength of Polyurethane Foam

	Foam Nominal Density, kg/dm^3			
	0.10	0.16	0.29	0.48
Strain, %	**Crush Strength, MPa**			
Parallel to Rise				
10	0.98	2.30	6.88	18.0
40	1.05	2.53	8.42	24.3
60				44.9
70	2.15	6.58	24.8	
Perpendicular to Rise				
10	0.96	2.30	6.83	18.0
40	1.01	2.53	8.35	24.4
60				45.2
70	2.15	6.69	24.7	

Table 2.2-6 – Mechanical Properties of Balsa Wood

Property	**Direction**	**Nominal Value**
Compressive Strength, S	Parallel-to-Grain	8.0 MPa
Density, ρ	-----	0.11 kg/dm^3

Table 2.2-7 – Mechanical Properties of Bronze Material

Material	**Minimum Mechanical Properties**
ASTM B150, UNS C63200 Copper Alloy (Aluminum Bronze)	σ_y = 275 MPa σ_u = 620 MPa

Table 2.2-8 – Mechanical Properties① of Closure Bolt Washer Material

Material Specification	Temperature (°C)	② Yield Strength, S_y (MPa)	③ Ultimate Strength, S_u (MPa)	④ Elastic Modulus, E ($\times 10^4$ MPa)
ASTM A564 Grade 630 H1025	21	1,000	1,069	19.7
	93	925	1,069	19.2

Notes: ① Table data converted from English units.
② ASME Code, Section II, Part D, Table Y-1.
③ ASME Code, Section II, Part D, Table U.
④ ASME Code, Section II, Part D, Table TM-1, for S17400.

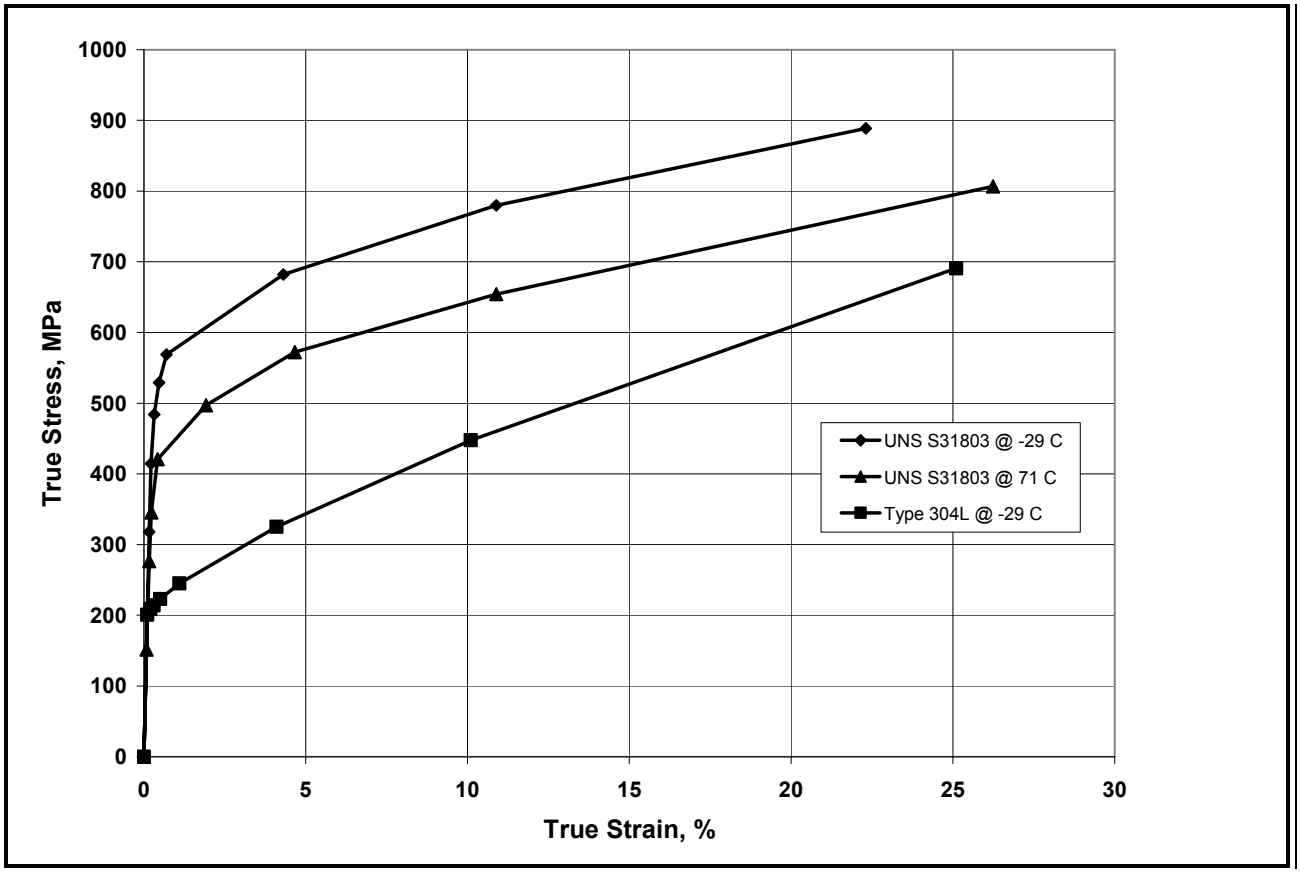

Figure 2.2-1 – True Stress-Strain Curves for Alloy UNS S31803 and Type 304 Stainless Steel

2.3 Fabrication and Examination

2.3.1 Fabrication

The TRUPACT–III packaging is fabricated using conventional metal forming and joining techniques. All welding procedures and welding personnel must be qualified in accordance with Section IX of the ASME Boiler and Pressure Vessel Code.[1] Where possible, containment boundary weld joints are made in flat sections and are full penetration butt joints. Where a corner joint is necessary, such as at the closed end of the containment boundary or at the body flange inner corner joints, the joint is a full penetration corner joint. Threaded parts are fabricated according to ASME B1.13M.[2] All non-containment joints, such as those connecting the CSA outer sheets, are fabricated in accordance with the requirements delineated on the drawings in Appendix 1.3.1, *Packaging General Arrangement Drawings*.

The polyurethane foam, calcium silicate insulation, balsa wood, and butyl rubber O-rings are procured using written procedures. See Section 8.1.5, *Component Tests*, for details of the fabrication and performance requirements of these components.

2.3.2 Examination

Each of the materials performing a significant safety function must meet the ASTM specifications delineated on the drawings in Appendix 1.3.1, *Packaging General Arrangement Drawings*. Safety-significant materials not having an ASTM designation are controlled by means of written procedures whose requirements are summarized in Section 8.1.5, *Component Tests*.

All welds are subject to visual examination per AWS D1.6.[3] Welds of the containment boundary plates and flanges are examined additionally by radiographic inspection in accordance with the ASME Boiler and Pressure Vessel Code, Section III, Division 1, Subsection NB, Article NB-5000, and Section V, Article 2,[4] and by liquid penetrant inspection on the final pass in accordance with the ASME Boiler and Pressure Vessel Code, Section III, Division 1, Subsection NB, Article NB-5000, and Section V, Article 6.[5] Fillet welds attaching the V-stiffeners to the containment sheets, and all other welds of the CSA outboard of that location, are inspected in the same way, omitting the radiographic inspection. Welds between components of the overpack structures (including welds to the outside of the CSA) are inspected visually as noted above, and additionally using liquid

[1] American Society of Mechanical Engineers (ASME) Boiler and Pressure Vessel Code, Section IX, *Qualification Standard for Welding and Brazing Procedures, Welders, Brazers, and Welding and Brazing Operators*, 2004 Edition, 2005 and 2006 Addenda.

[2] American Society of Mechanical Engineers (ASME) B1.13M, *Metric Screw Threads – M Profile*.

[3] ANSI/AWS D1.6:1999, *Structural Welding Code–-Stainless Steel*, American Welding Society (AWS).

[4] American Society of Mechanical Engineers (ASME) Boiler and Pressure Vessel Code, Section III, *Rules for Construction of Nuclear Facility Components*, Division 1 - Subsection NB, *Class 1 Components*, and Section V, *Nondestructive Examination*, Article 2, *Radiographic Examination*, 2004 Edition, 2005 and 2006 Addenda.

[5] American Society of Mechanical Engineers (ASME) Boiler and Pressure Vessel Code, Section V, *Nondestructive Examination*, Article 6, *Liquid Penetrant Examination*, 2004 Edition, 2005 and 2006 Addenda.

penetrant inspection on the final pass in accordance with the ASME Boiler and Pressure Vessel Code, Section III, Division 1, Subsection NF, Article NF-5000, and Section V, Article 6.[6]

In cases where radiographic examination cannot be performed, containment boundary welds are inspected by ultrasonic examination in accordance with the ASME Boiler and Pressure Vessel Code, Section III, Division 1, Subsection NB, Article NB-5000, and Section V, Article 4[8]. The use of multi-pass liquid penetrant examination for repair of containment boundary welds is identified in General Note 48 on the drawings in Appendix 1.3.1, *Packaging General Arrangement Drawings*. Subsequent to repairs of containment boundary welds, the CSA containment boundary will be subjected to the pressure and leakage rate tests described below.

Each TRUPACT–III packaging will also be subjected to the following three tests:

- CSA internal pressure test, in which the containment boundary is pressurized to at least 150% of the MNOP. The pressure test requirements are described in Section 8.1.3.2, *Containment Vessel Pressure Testing*.
- Containment boundary leakage rate test, which includes helium leakage rate tests of the structural containment boundary, the containment O-ring seal, and the vent port containment O-ring seal. The requirements are described in Section 8.1.4, *Fabrication Leakage Rate Tests*.
- Load test of the upper ISO lift fittings, in which each fitting is tested to 150% of its maximum working load. The load test requirements are described in Section 8.1.3.1, *Lifting Device Load Testing*.

[6] American Society of Mechanical Engineers (ASME) Boiler and Pressure Vessel Code, Section III, *Rules for Construction of Nuclear Facility Components*, Division 1 - Subsection NF, *Supports*, 2004 Edition, 2005 and 2006 Addenda.

[8] American Society of Mechanical Engineers (ASME) Boiler and Pressure Vessel Code, Section III, *Rules for Construction of Nuclear Facility Components*, Division 1 - Subsection NB, *Class 1 Components*, and Section V, *Nondestructive Examination*, Article 4, *Ultrasonic Examination*, 2004 Edition, 2005 and 2006 Addenda.

[1] Title 10, Code of Federal Regulations, Part 71 (10 CFR 71), *Packaging and Transportation of Radioactive Material*, 01–01–09 Edition.

2.4 General Requirements for All Packages

This section defines the general standards for all packages. The TRUPACT–III package meets all requirements delineated for this section.

2.4.1 Minimum Package Size

The minimum dimension of the TRUPACT–III package is 2,500 mm (the package width). Thus, the 10–cm minimum requirement of 10 CFR §71.43(a)[1] is satisfied.

2.4.2 Tamper-Indicating Feature

Tamper-indicating seals are installed through two of the access tubes for the overpack cover, as delineated on the drawings in Appendix 1.3.1, *Packaging General Arrangement Drawings*. A lock wire device is used between two tie-points. Failure of the tamper-indicating devices provides evidence of possible unauthorized access. Thus, the requirement of 10 CFR §71.43(b) is satisfied.

2.4.3 Positive Closure

The TRUPACT–III package cannot be opened unintentionally. The overpack cover, which is secured with ten (10) M36 socket head cap screws, fully conceals the closure lid and the vent port. The closure lid is secured with (44) M36 closure bolts (socket head cap screws). Thus, the requirements of 10 CFR §71.43(c) are satisfied.

2.4.4 Valves

The containment boundary of the TRUPACT–III packaging does not contain any valves. The overpack cover features one pressure relief valve to relieve any large internal pressure differential which could occur within the overpack cover shells due to atmospheric or temperature conditions. Besides the closure lid, the TRUPACT–III packaging has a vent port penetration into the containment cavity. This vent port penetration is closed using an aluminum bronze insert that is held in place by a threaded retaining ring, and sealed using a butyl rubber O–ring seal. In addition to the retaining ring, access to the vent port penetration is prevented by the overpack cover, as discussed in Section 2.4.3, *Positive Closure*. Thus, the requirements of 10 CFR §71.43(e) are satisfied.

2.4.5 Package Design

As shown in Chapter 2.0, *Structural Evaluation*, Chapter 3.0, *Thermal Evaluation*, Chapter 5.0, *Shielding Evaluation*, and Chapter 6.0, *Criticality Evaluation*, the structural, thermal, shielding, and criticality requirements, respectively, of 10 CFR §71.43(f) are satisfied for the TRUPACT–III package.

[1] Title 10, Code of Federal Regulations, Part 71 (10 CFR 71), *Packaging and Transportation of Radioactive Material*, 01–01–09 Edition.

2.4.6 External Temperatures

As shown in Table 3.3-2 from Section 3.3.1, *Heat and Cold*, the maximum accessible surface temperature with maximum internal decay heat load and no insolation is 42 ºC. Since the maximum external temperature does not exceed 50 ºC, the requirements of 10 CFR §71.43(g) are satisfied for non–exclusive use shipments.

2.4.7 Venting

The TRUPACT–III package does not include any features intended to allow continuous venting of the containment boundary during transport. Thus, the requirements of 10 CFR §71.43(h) are satisfied.

2.5 Lifting and Tie-down Standards for All Packages

For analysis of the lifting and tie-down components of the TRUPACT–III packaging, material properties from Section 2.2.1, *Material Properties and Specifications*, are taken at a temperature of 86 °C. This temperature is essentially identical to the overpack outer skin maximum temperature of 86.6 ºC given in Section 2.6.1.1, *Summaries of Pressures and Temperatures*. The primary structural material for lifting is Alloy UNS S31803 stainless steel.

A loaded TRUPACT–III package is only lifted by the four upper ISO fittings, located at each corner of the body. Properties of Alloy UNS S31803 stainless steel are summarized below.

Material Property	Value	Reference
Alloy UNS S31803 Stainless Steel at 86 ºC		
Elastic Modulus, E	19.1×10^4 MPa	Table 2.2-1
Yield Strength, σ_y	405 MPa	
Shear Stress, equal to $(0.6)\sigma_y$	243 MPa	

2.5.1 Lifting Devices

This section demonstrates that the ISO corner fittings, the only attachments designed to lift the TRUPACT–III package, are designed with a minimum safety factor of three against yielding, per the requirements of 10 CFR §71.45(a)[1]. Figure 2.5-1 illustrates the lifting device configuration for the TRUPACT–III package.

2.5.1.1 Lifting Forces

When lifting the entire TRUPACT–III package, the applied lift force without yielding is simply three times the total package weight of 25,000 kg, as given in Section 2.1.3, *Weights and Centers of Gravity*.

$$F_L = (3)(25{,}000) = 75{,}000 \text{ kg}$$

The entire package is lifted via four ISO fittings located at each corner of the body. For the purposes of this analysis, it is conservatively assumed that only two, diagonally opposed ISO fittings support the applied load. An additional conservatism is applied by offsetting the center of gravity (CG) by the maximum offset. According to Section 2.1.3, *Weights and Centers of Gravity*, the CG of a uniformly loaded package is located 2,312 mm from the outer surface of the closed-end of the package. In this analysis, the essentially identical value of 2,313 mm will be used. In addition, the package will be loaded so that the CG will translate no more than ±200 mm from that location. Therefore, the most biased position is 2,313 + 200 = 2,513 mm from the outside closed-end wall, with the maximum lifting load on the ISO fitting occurring at the closure lid end of the package. The extreme ends of the package are utilized as essentially equivalent to the lift locations of the ISO fittings. This assumption is also conservative for the bending analysis performed below. The maximum load is:

[1] Title 10, Code of Federal Regulations, Part 71 (10 CFR 71), *Packaging and Transportation of Radioactive Material*, 01–01–09 Edition.

$$F_{ISO} = \left(\frac{2{,}513}{4{,}288}\right)(75{,}000) = 43{,}954 \text{ kg} = 431{,}189 \text{ N}$$

where 4,288 mm is the overall length of the package.

2.5.1.2 Lifting Failure Modes

Several failure modes are considered for the ISO corner fitting due to the lifting force. The failure modes that are considered are:

(a) Shear tearout of the ISO twistlock in top ISO fitting plate,

(b) Shear failure of the welds attaching the top ISO fitting plate,

(c) Bending failure in the lifting arm structures.

2.5.1.2.1 Shear Tearout of Twistlock Top Plate

Figure 2.5-2 presents the dimensional details of the twistlock top plate for evaluation of shear tearout due to lifting forces. The top plate shear area is the length of the twistlock cam multiplied by the top plate thickness. The length of the twistlock cam outline is determined from the following expression:

$$l = 2\left[\frac{2r\alpha\pi}{180} + (w_1 - w_2)\right] = 2\left[\frac{2(50)\left[\sin^{-1}\frac{28.5}{50}\right]\pi}{180} + (82 - 63.5)\right] = 158 \text{ mm}$$

The top plate thickness, t, is 28.5 mm. Thus, the total shear area, A_s, is:

$$A_s = l \times t = 158 \times 28.5 = 4{,}503 \text{ mm}^2$$

The maximum shearing force, V, is the maximum lifting force on the ISO fitting, F_{ISO} = 431,189 N from Section 2.5.1.1, *Lifting Forces*, resulting in a corresponding shear stress of:

$$\tau_V = \frac{F_{ISO}}{A_s} = \frac{431{,}189}{4{,}503} = 95.8 \text{ MPa}$$

The allowable shear stress for UNS S31803 material is 243 MPa. Therefore, the margin of safety is:

$$MS = \frac{243.0}{95.8} - 1.0 = +1.54$$

2.5.1.2.2 Shear Failure of Twistlock Top Plate Attachment Welds

Figure 2.5-3 presents the dimensional details for the top plate attachment welds. The total length of the weld is 2(149 + 178 + 28.5) = 711 mm. The effective weld thickness for the attachment welds is equal to the thickness of the lifting arm, i.e., 8 mm. Thus, the total shear area for the attachment weld is:

$$A_{weld} = (711)(8) = 5{,}688 \text{ mm}^2$$

The maximum shearing force, V, is the maximum lifting force on the ISO fitting, F_{ISO} = 431,189 N from Section 2.5.1.1, *Lifting Forces*, resulting in a corresponding shear stress of:

$$\tau_{weld} = \frac{F_{ISO}}{A_{weld}} = \frac{431{,}189}{5{,}688} = 75.8 \text{ MPa}$$

The allowable shear stress for UNS S31803 material is 243 MPa. Therefore, the margin of safety is:

$$MS = \frac{243.0}{75.8} - 1.0 = +2.21$$

2.5.1.2.3 Bending Stress in Lifting Arm Structures

Figure 2.5-4 presents the configuration of the lifting arm structures that react the lifting loads. A breakdown of the material thicknesses for the lifting arm structure is presented in Figure 2.5-5. The lifting arm structures are fabricated entirely from Alloy UNS S31803 stainless steel.

The front and rear lifting arms are constructed differently. The front lifting arm design utilizes a longer length sheet than the rear lifting arm design. In addition, the rear lifting arm design utilizes thinner sheet materials than the front lifting arm design. For conservatism, the thinner sheet material of the rear lifting arm design and the longer length sheet of the front lifting arm design will be utilized in the analysis. The lifting arm structure is approximated by a varying cross-section and will be analyzed as a fixed cantilever beam, as illustrated in Figure 2.5-6. For simplicity, the "open" end of the cantilever (located 532 mm from the fixed end as shown in Figure 2.5-6) will be used to calculate the section properties. The open section has less material than the fixed end, and when combined with the larger bending moment of the fixed end, the resulting bending stress will be conservative.

Because of symmetry, the centroid of the cantilever beam, relative to the base, is located at a height of:

$$\bar{x} = \frac{2{,}500}{2} = 1{,}250 \text{ mm}$$

The moment of inertia at the open end is:

$$I = \frac{188(2{,}500)^3}{12} - \frac{174(2{,}488)^3}{12} - \frac{6(2{,}000)^3}{12} = 1.75 \times 10^{10} \text{ mm}^4$$

The cross-sectional area at the open end is:

$$A = 2{,}500(188) - 2{,}488(174) - 6(2000) = 25{,}088 \text{ mm}^2$$

The maximum bending moment, M, is the maximum lifting force at the base, F_{ISO}, with a moment arm of 870 – 102 = 768 mm, resulting in a corresponding bending stress of:

$$\sigma_{closed} = \frac{M\bar{x}}{I} = \frac{431{,}189(768)1{,}250}{1.75 \times 10^{10}} = 23.7 \text{ MPa}$$

The maximum shearing force, V, is the maximum lifting force at the base, F_{ISO}, resulting in a corresponding shear stress of:

$$\tau_{closed} = \frac{F_{ISO}}{A} = \frac{431{,}189}{25{,}088} = 17.2 \text{ MPa}$$

The yield stress for Alloy UNS S31803 stainless steel is 405 MPa and the shear yield stress is 243 MPa. The margin of safety on bending stress at the extreme fiber is:

$$MS = \frac{405.0}{23.7} - 1.0 = +16.1$$

The margin of safety on maximum shear at the neutral axis is:

$$MS = \frac{243.0}{17.2} - 1.0 = +13.1$$

The weld of the lifting arm to the fixed end is a complex structure consisting of a combination of complete-joint-penetration and full-thickness-leg fillet welds. However, its configuration is bounded by a hypothetical, 6 mm fillet weld having the same dimensions as used above to calculate the full section properties. The weld may therefore be conservatively modeled as a rectangle 2,500 mm tall, 188 mm wide, with 2,000 mm removed from one long side (see Figure 2.5-6), and a width of 6 × 0.707 = 4.24 mm. The moment of inertia of the weld is:

$$I_w = \frac{188(2{,}500)^3}{12} - \frac{(188 - 2\times 4.24)(2{,}500 - 2\times 4.24)^3}{12} - \frac{4.24(2{,}000)^3}{12} = 1.06\times 10^{10} \text{ mm}^4$$

The cross-sectional area of the weld is:

$$A_w = 2{,}500(188) - (2{,}500 - 2\times 4.24)(188 - 2\times 4.24) - 4.24(2{,}000) = 14{,}296 \text{ mm}^2$$

Using the same fixed-end moment as calculated above, the bending stress in the weld is:

$$\sigma_w = \frac{M\bar{x}}{I_w} = \frac{431{,}189(768)1{,}250}{1.06\times 10^{10}} = 39.1 \text{ MPa}$$

The shear stress in the weld is:

$$\tau_w = \frac{F_{ISO}}{A_w} = \frac{431{,}189}{14{,}296} = 30.2 \text{ MPa}$$

The maximum combined shear stress in the weld is:

$$\tau_T = \sqrt{\sigma_w^2 + \tau_w^2} = \sqrt{39.1^2 + 30.2^2} = 49.4 \text{ MPa}$$

Using the shear yield stress for the weld, the margin of safety is:

$$MS = \frac{243.0}{49.4} - 1.0 = +3.92$$

2.5.1.3 Summary

All margins of safety for the lifting devices are positive relative to a minimum factor of safety of three against yielding, per 10 CFR §71.45(a). The smallest tensile or shear margin of safety, i.e., MS = +1.54, is for shear tearout failure of the top plate on the ISO fitting, indicating that this item will be the mode of failure for lifting devices under excessive load condition. In accordance with

10 CFR §71.45(a), this failure mode does not compromise the performance capabilities of the TRUPACT–III package since no main structural part of the package is affected.

2.5.2 Tie–down Devices

During transport, the TRUPACT–III package is secured to its conveyance by tie-rods (or equivalent) which connect to a frame installed over the top of the package. Horizontal restraint is provided by structural pockets on the conveyance in the vicinity of the four lower ISO fittings. However, no attachment is made to any (upper or lower) ISO fittings during transport. As such, the TRUPACT-III has no integral tie-down devices that are part of the package. Therefore, per 10 CFR §71.45(b)(1), no analysis of tie–down devices is required.

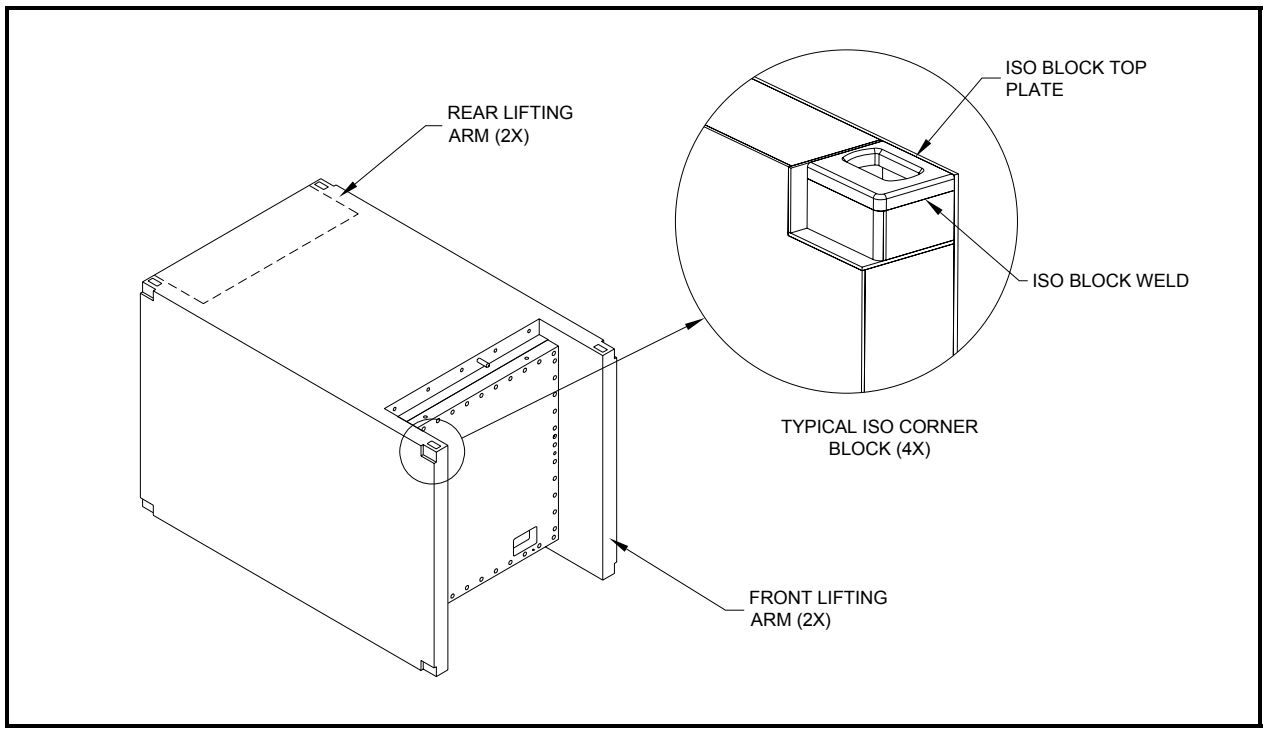

Figure 2.5-1 – Lifting Device Configuration

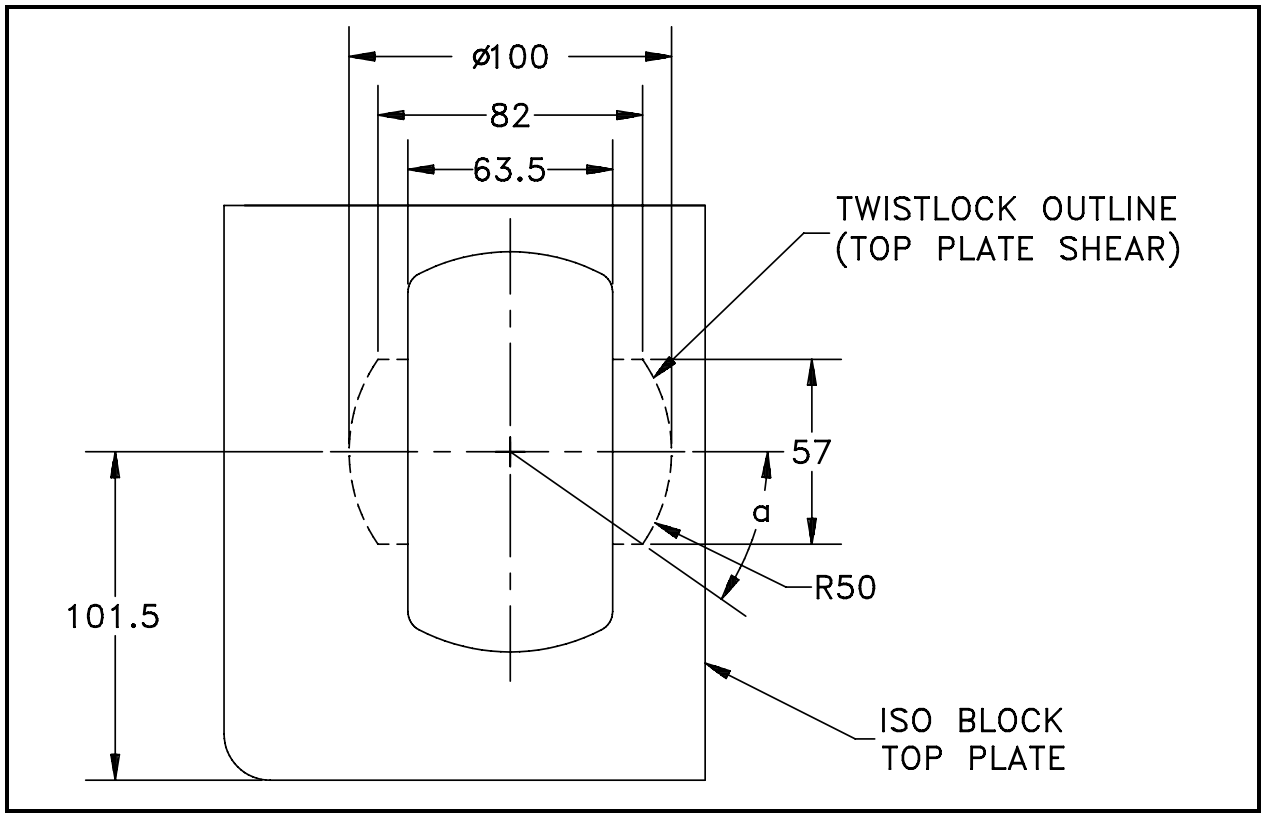

Figure 2.5-2 – Shear Tearout of Twistlock Top Plate

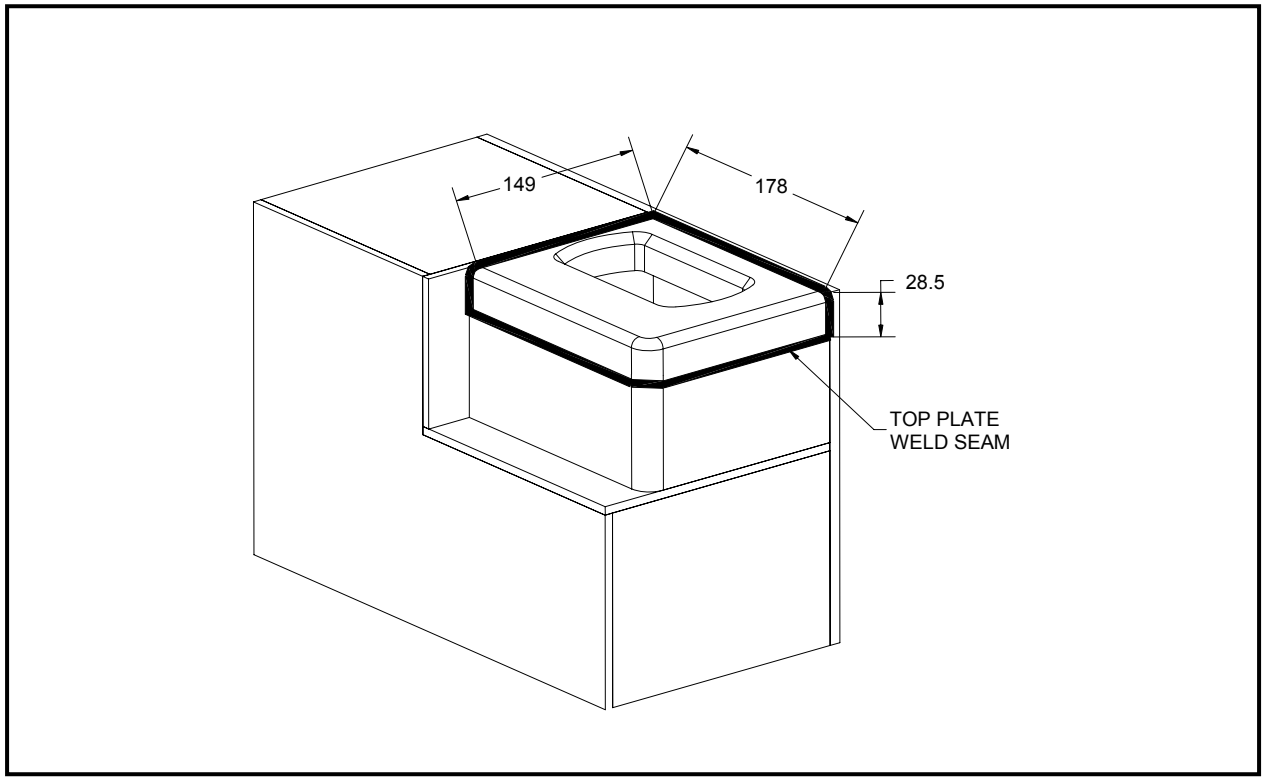

Figure 2.5-3 – Shear Failure of Twistlock Top Plate Attachment Welds

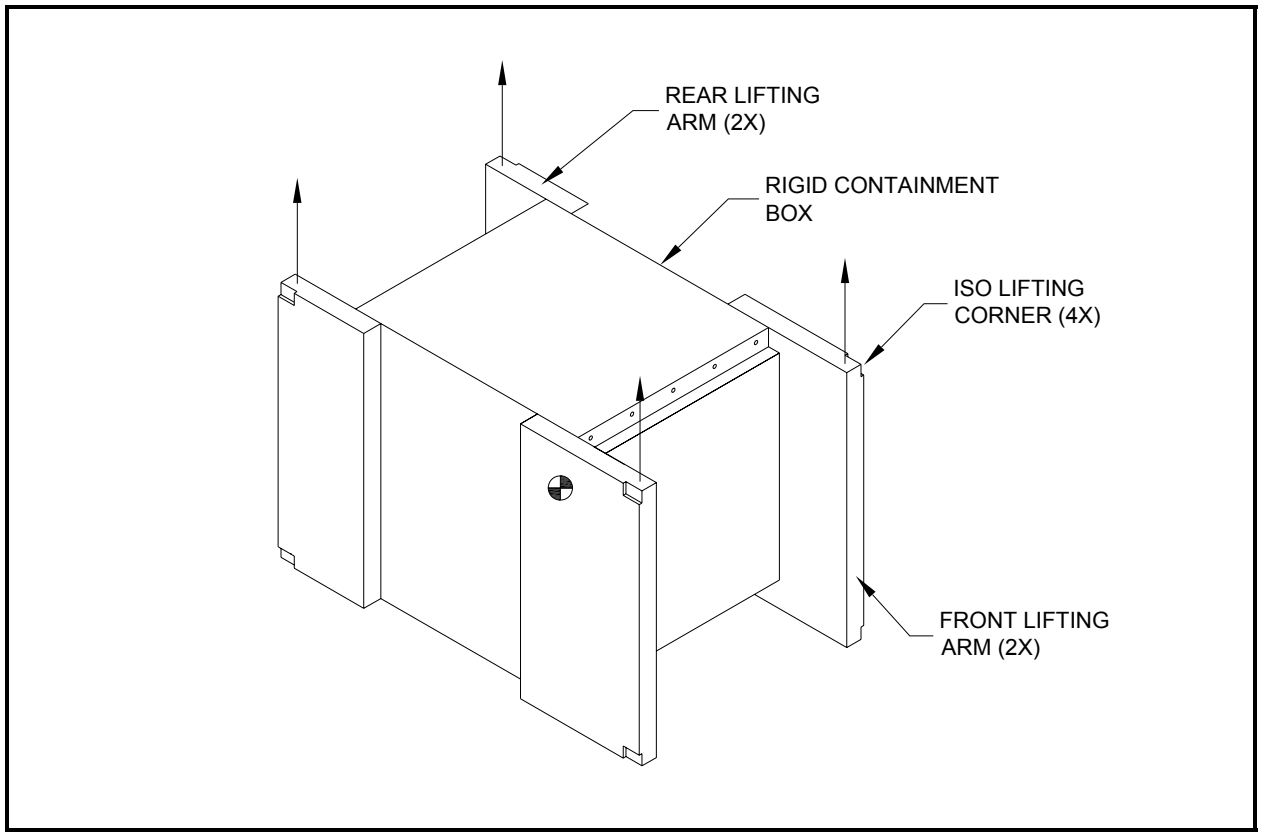

Figure 2.5-4 – Lifting Arm Structure Bending

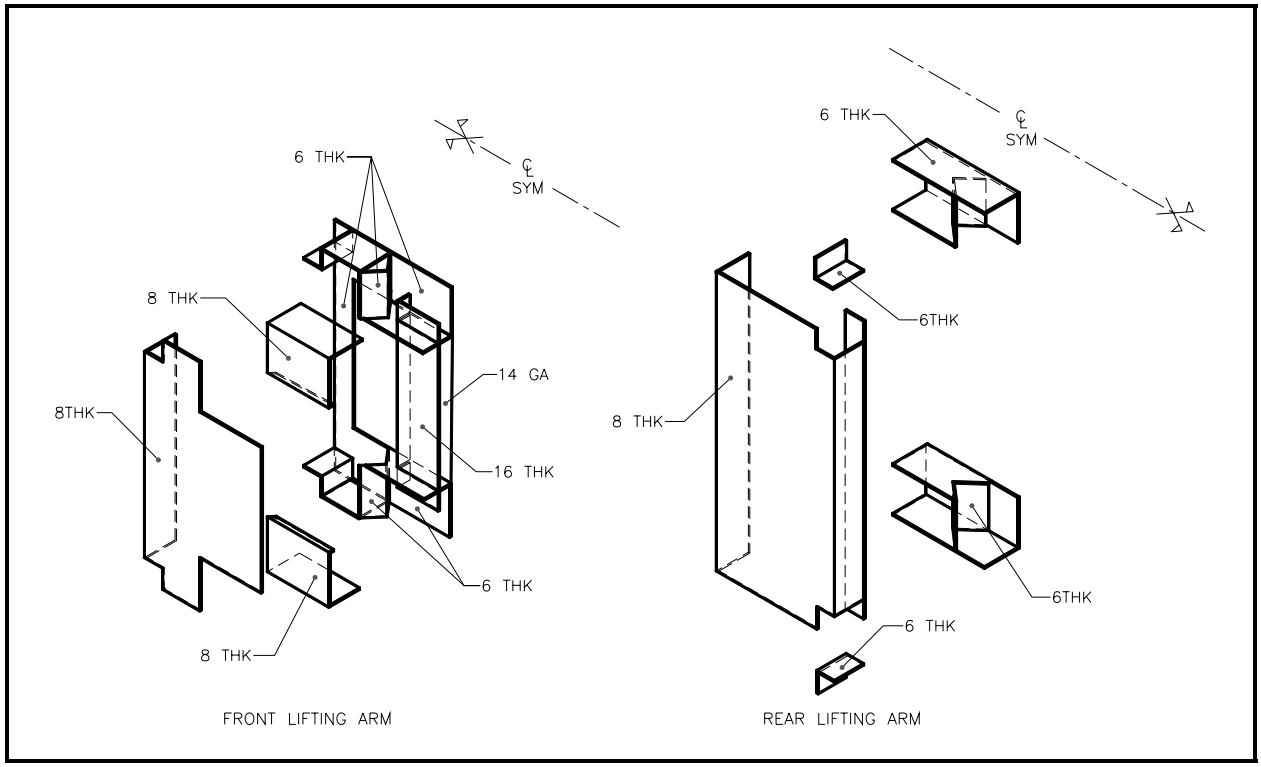

Figure 2.5-5 – Lifting Arm Material Thicknesses

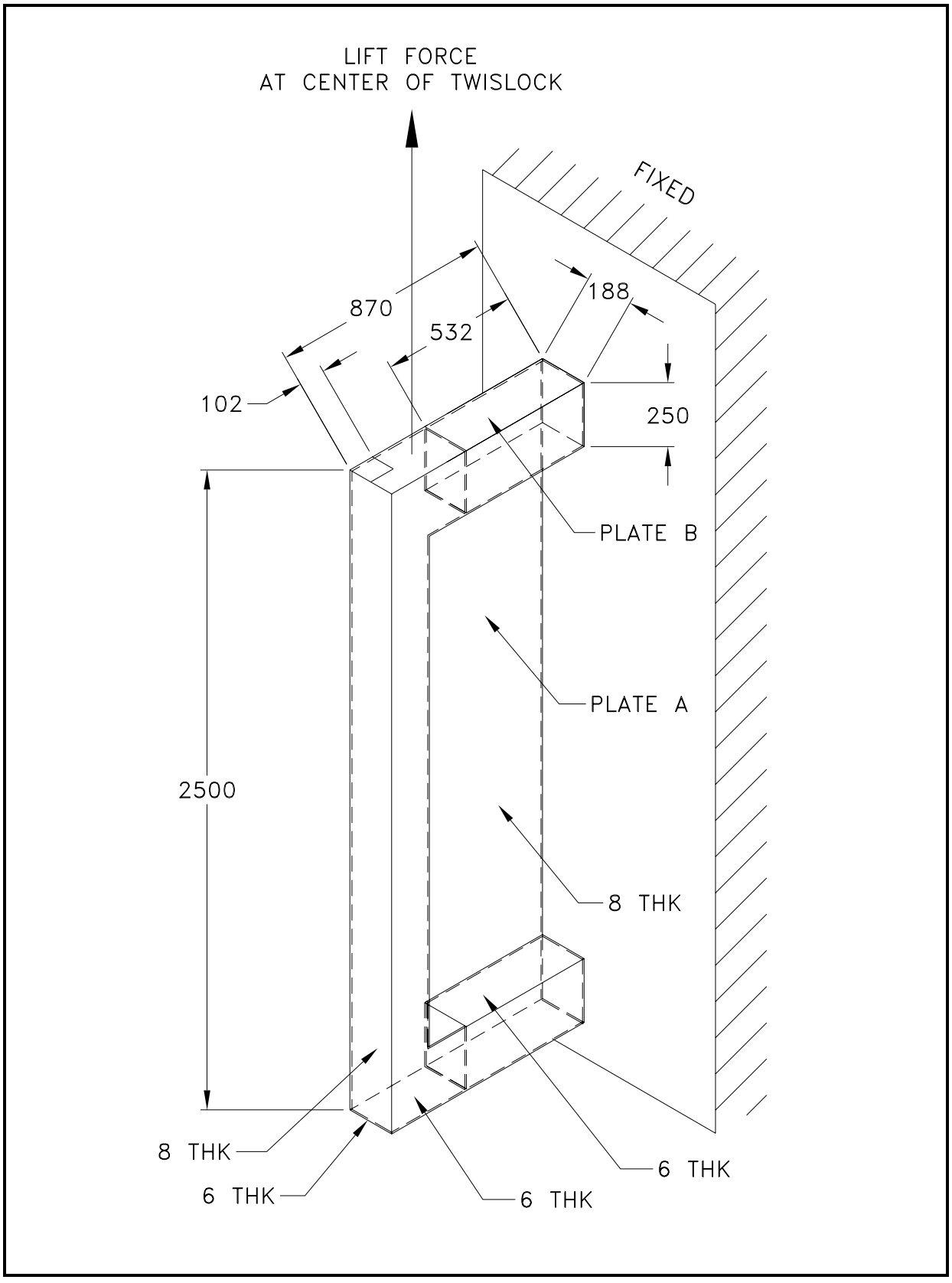

Figure 2.5-6 – Lifting Arm Analysis Model

2.6 Normal Conditions of Transport

The TRUPACT–III package, when subjected to the normal conditions of transport (NCT) specified in 10 CFR §71.71[1], is shown to meet the performance requirements specified in Subpart E of 10 CFR 71. As discussed in the introduction to this chapter, the primary proof of NCT performance is via analytic methods. Regulatory Guide 7.6[2] criteria are demonstrated as acceptable for all NCT analytic evaluations presented in this section. Specific discussions regarding brittle fracture and fatigue are presented in Section 2.1.2.2, *Miscellaneous Structural Failure Modes*, and are shown not to be limiting cases for the TRUPACT–III packaging design. The performance capabilities of the butyl containment O-ring seals are documented in Appendix 2.12.2, *Elastomer O-ring Seal Performance Tests*.

NCT analyses for heat, cold, reduced external pressure, increased external pressure, and vibration are performed in this section. The NCT free drop demonstration is by test as discussed in Section 2.6.7, *Free Drop*. Dimensions are taken from the drawings in Appendix 1.3.1, *Packaging General Arrangement Drawings*. Allowable stress limits are consistent with Table 2.1-1 in Section 2.1.2.1, *Analytic Design Criteria (Allowable Stresses)*, using temperature-adjusted material properties taken from the tables in Section 2.2.1, *Material Properties and Specifications.* Properties at selected temperatures are summarized below.

Table 2.6-1 – NCT Material Properties

Material Property	Material Property Value (MPa)			Reference
	-29 ºC	21 ºC	71 ºC	
ASTM A240 & ASTM A479, UNS S31803 Stainless Steel				Table 2.2-1
Elastic Modulus, E	19.8×10^4	19.5×10^4	19.2×10^4	
Design Stress Intensity, S_m	207	207	207	
Yield Strength, S_y	448	448	419	
ASTM A320 Grade L43 Bolting Material				Table 2.2-4
Elastic Modulus, E	19.4×10^4	19.2×10^4	18.9×10^4	
Yield Strength, S_y	724	724	699	

2.6.1 Heat

The NCT thermal analyses presented in Section 3.3, *Thermal Evaluation for Normal Conditions of Transport*, consist of exposing the TRUPACT–III package to direct sunlight and 38 ºC still air per the requirements of 10 CFR §71.71(b). Although the actual internal heat load depends on the particular payload being transported, this section utilizes the maximum internal heat allowed within a TRUPACT–III package of 80 thermal watts, and which results in the maximum temperature gradients throughout the TRUPACT–III package.

[1] Title 10, Code of Federal Regulations, Part 71 (10 CFR 71), *Packaging and Transportation of Radioactive Material*, 01–01–09 Edition.

[2] U. S. Nuclear Regulatory Commission, Regulatory Guide 7.6, *Design Criteria for the Structural Analysis of Shipping Cask Containment Vessels*, Revision 1, March 1978.

2.6.1.1 Summary of Pressures and Temperatures

The maximum normal operating pressure (MNOP) is 172 kPa gauge (273 kPa absolute), as determined in Section 3.3.2, *Maximum Normal Operating Pressure*. The pressure stress analyses within this section combine the internal pressure of 172 kPa gauge due to MNOP with a reduced external pressure, per 10 CFR §71.71(c)(3), of 25 kPa absolute. Therefore, the net resulting internal pressure utilized in all NCT structural analyses considering internal pressure is 273 - 25 = 248 kPa.

The NCT heat input results in modest temperatures and temperature gradients throughout the TRUPACT–III package. Maximum temperatures for the major packaging components are summarized in Table 3.1-1 from Section 3.1.4, *Summary Tables of Temperatures*. As shown in the table, the maximum temperature of the containment structural assembly (CSA) is 57.6 ºC (for the outer structural sheet). The maximum temperature of the CSA containment sheet is 55.6 ºC. Due to the relatively small temperature gradients between CSA components, temperature gradients are of no concern. For conservatism, structural analyses of the package for NCT utilize a bounding uniform temperature of 71 ºC. The maximum temperature of overpack outer skin is 86.6 ºC.

2.6.1.2 Differential Thermal Expansion

In the absence of significant temperature gradients, concern with differential expansions is limited to regions of the TRUPACT–III packaging that employ adjacent materials with sufficiently different coefficients of thermal expansion. The CSA is a double-wall, composite construction of inner and outer stainless steel sheets that are joined by a stainless steel V-stiffener interior structure. The CSA double-wall construction is composed entirely of the same material and subsequently does not exhibit differential expansions. The guide bars attached to the inside of the containment sheets are made of ASTM Type 304/304L material. Any fatigue concerns with this construction are evaluated and dismissed in Section 2.1.2.2.2.1, *Normal Operating Cycles*. The only potential for meaningful differential expansion is between the closure lid bolts, composed of ASTM A320, Grade L43, alloy steel, and the material clamped by the bolts, composed of UNS S31803 stainless steel. The effect of varying temperature on the closure lid bolt stress and clamping force is evaluated in Section 2.6.1.6, *Closure Bolts*.

2.6.1.3 Stress Calculations

The internal pressure considers the effects of a maximum normal operating pressure (MNOP) of 172 kPa gauge (273 kPa absolute) internal, coupled with a reduced external pressure of 25 kPa absolute. The net result is an internal pressure of 273 – 25 = 248 kPa. This evaluation will use classical methods to find the stresses in the CSA walls. Bending and membrane stresses will conservatively be directly added. The margins of safety will be conservatively evaluated using mechanical properties at 71°C.

The side longitudinal and rear walls of the CSA will be evaluated for maximum membrane-plus-bending stresses. The TRUPACT–III longitudinal walls support global bending along their span and local bending between the V-stiffeners from pressure loading. The walls also support axial and lateral loads from the pressure loads acting on the adjacent walls. The contribution of the V-stiffeners to the bending moment of inertia is conservatively neglected. Figure 2.6-1(f) shows the typical wall section used for the global bending and membrane evaluations. Figure 2.6-1(g) and Figure 2.6-1(h) show the cross sections used for the local bending evaluations. The axial and lateral loads are translated by

neighboring walls as membrane stresses through the combined thickness of the adjoining inner and outer sheets of each wall. The side longitudinal walls have a greater span, which makes them the more vulnerable to bending stresses than the top and bottom containment walls.

Assumptions

1. The edge loads (resulting from pressure loads on the adjacent walls) will be evaluated with the areas shown in Figure 2.6-1(a) through Figure 2.6-1(e).
2. The height of the side wall extends from the center of the bottom wall cross section to the center of the top wall cross section. Similarly, the width of the top/bottom wall extends from the center of one side wall cross section to the center of the other side wall cross section. The length of any wall extends from the center of the end wall to the bolted seal flange. These dimensions are:

   H = height of side wall = 2,140 mm

   W = width of top/bottom sheets = 1,980 mm

   L = length of any wall = 2,860 mm
3. Referring to Figure 2.6-1(a), the pressure load acting on Area 1 of the rear wall applies forces to the end edges of the side wall.
4. From the same figure, the pressure load on Area 2 of the top wall loads the top and bottom edges of the side wall.
5. Referring to Figure 2.6-1(b), the pressure load acting on Area 3 of the top wall loads the top and bottom edges of the rear wall.
6. From the same figure, the pressure load on Area 4 of the side wall loads the side edges of the rear wall.
7. All edges are conservatively assumed to be simply supported. Since the closure lid has sheets which are 50% thicker than the body walls, the assumption of simply supported edges means that the closure lid does not need to be considered.

Calculation Input Parameters

Internal design pressure differential: P = 248 kPa =248,000 Pa

Thickness of inner and outer sheets: t = 8 mm = 0.008 m

Distance between inner & outer sheet neutral axes: d = 132 mm = 0.132 m

Area of one face sheet per unit width, b: $A = b(t) = 8\ mm^2 = 8.0 \times 10^{-6}\ m^2$

Membrane and maximum fiber distances from central axis:

$$c_m = \frac{d}{2} = 0.066\ m \qquad c_o = \frac{d+t}{2} = 0.070\ m$$

Second moment of area (about central axis):

$$I_1 = 2A\left(\frac{d}{2}\right)^2 = 2(8\times10^{-6}\ m^2)\left(\frac{0.132\ m}{2}\right)^2 = 6.97\times10^{-8}\ m^4$$

Stress Analysis of the Governing CSA Wall

Due to local bending stress, the inner containment sheet is governing. Coordinate directions are shown on Figure 2.6-1(b). The x-direction is parallel to the V-stiffeners and y is perpendicular to the V-stiffeners. The following stresses are evaluated and combined:

- Membrane stress on the neutral axis, and membrane-plus-bending stress on the inner surface of the inner sheet due to global bending of the side wall (x-direction)
- Local bending stress generated by pressure acting over the span of the inner sheet between V-stiffener supports (y-direction)
- Axial membrane stress (parallel to V-stiffeners) generated by pressure on Area 2 (x-direction)
- Lateral membrane stress (perpendicular to V-stiffeners) generated by pressure on Area 1 (y-direction)

Stresses due to global bending:

Maximum moment, conservatively assuming the walls are pinned at the edge:

$$M_{side} = \frac{PbH^2}{8} = \frac{(248{,}000\ \text{Pa})(0.001\ \text{m})(2.140\ \text{m})^2}{8} = 141.97\ \text{N-m}$$

Membrane stress, σ_{mbx}:

$$\sigma_{mbx} = \frac{M_{side} c_m}{I_1} = \frac{(141.97\ \text{N-m})(0.066\ \text{m})}{(6.97\times10^{-8}\ \text{m}^4)} \times 10^{-6}\ \frac{\text{MPa}}{\text{Pa}} = 134.4\ \text{MPa}$$

Maximum global bending stress, σ_{gbx}:

$$\sigma_{gbx} = \frac{M_{side} c_o}{I_1} = \frac{(141.97\ \text{N-m})(0.070\ \text{m})}{(6.97\times10^{-8}\ \text{m}^4)} \times 10^{-6}\ \frac{\text{MPa}}{\text{Pa}} = 142.6\ \text{MPa}$$

Local bending stress:

Unsupported span of inner sheet between V-stiffeners: S = 145 mm = 0.145 m

Area moment of inertia for inner sheet:

$$I_2 = \frac{bt^3}{12} = \frac{(0.001\ \text{m})(0.008\ \text{m})^3}{12} = 4.27\times10^{-11}\ \text{m}^4$$

Maximum moment, conservatively assuming the sheet has pinned edges at the locations supported by V-stiffeners:

$$M_{side\text{-}local} = \frac{P\,b\,S^2}{8} = \frac{(248{,}000\ \text{Pa})(0.001\ \text{m})(0.145\ \text{m})^2}{8} = 0.652\ \text{N-m}$$

Maximum local bending stress:

$$\sigma_{lby} = \frac{(t/2)M_{side\text{-}local}}{I_2} = \frac{(0.008\ \text{m}/2)(0.652\ \text{N-m})}{(4.27\times10^{-11})} \times 10^{-6}\ \frac{\text{MPa}}{\text{Pa}} = 61.1\ \text{MPa}$$

Axial membrane stress:

Load supplied by area A_2 (see Figure 2.6-1(d)): $A_2 = 2(0.5)0.990^2 + 0.880 \times 0.990 = 1.851\ m^2$

Edge load per unit length in the x-direction (parallel to the core longitudinal axis):

$$N_x = \frac{PA_2}{L} = \frac{(248{,}000\ Pa)\,(1.851\ m^2)}{(2.860\ m)} \times 10^{-3}\ \frac{kN}{N} = 160.5\ kN/m$$

Axial stress in the x-direction (parallel to the core longitudinal axis):

$$\sigma_x = \frac{N_x}{2t} = \frac{160.5\ kN/m}{2(0.008\ m)} \times 10^{-3}\ \frac{MPa}{kPa} = 10.0\ MPa$$

Lateral membrane stress:

Load supplied by area A_1 (see Figure 2.6-1(c)): $A_1 = 2(0.5)0.990^2 + 0.160 \times 0.990 = 1.139\ m^2$

Edge load per unit length in the y-direction (perpendicular to the core longitudinal axis):

$$N_y = \frac{PA_1}{H} = \frac{(248{,}000\ Pa)\,(1.139\ m^2)}{(2.140\ m)} \times 10^{-3}\ \frac{kN}{N} = 132.0\ kN/m$$

Lateral stress in the y-direction (perpendicular to the core longitudinal axis):

$$\sigma_y = \frac{N_y}{2t} = \frac{132.0\ kN/m}{2(0.008\ m)} \times 10^{-3}\ \frac{MPa}{kPa} = 8.3\ MPa$$

Conservatively combining all membrane stresses arithmetically, regardless of direction:

$$SI_{pm} = \sigma_{mbx} + \sigma_x + \sigma_y = 134.4 + 10.0 + 8.3 = 152.7\ MPa$$

The allowable stress for this case is S_m, or 207 MPa for Alloy UNS S31803 stainless steel at 71°C. Therefore, the margin of safety (MS) is:

$$MS = \frac{207}{SI_{pm}} - 1.0 = +0.36$$

Conservatively combining all membrane-plus-bending stresses arithmetically, regardless of direction,

$$SI_{pmb} = \sigma_{gbx} + \sigma_{lby} + \sigma_x + \sigma_y = 142.6 + 61.1 + 10.0 + 8.3 = 222.0\ MPa$$

The allowable stress this case is $1.5S_m$. Therefore, the margin of safety is:

$$MS = \frac{1.5\,(207)}{SI_{pmb}} - 1.0 = +0.40$$

Wall stiffener weld evaluation

As previously described, the CSA walls have a sandwich construction. V-stiffeners are welded to the inner and outer sheets of each wall. The V-stiffeners are attached to the inner containment sheet by continuous skewed fillet welds, which have an equivalent throat thickness of at least 4 mm. The V-stiffeners are attached to the outer structural sheet by equally spaced 20-mm diameter plug welds. As shown below, the equivalent shear width of the plug welds is 5.5 mm, and

therefore, this shear width is bounding compared to the inner sheet welds that have a combined effective throat of 2 × 4 = 8 mm. The calculation parameters are:

Number of plug welds per V-stiffener: N = 40

Diameter of plug welds, D: D = 20 mm = 0.020 m

Conservative V-stiffener length, L: L = 2,280 mm = 2.280 m

Distance between plug weld rows, d_p: d_p = 164 mm = 0.164 m

Equivalent plug weld shear width, t_e, per V-stiffener:

$$t_e = \frac{(\pi/4)\, D^2\, N}{L} = \frac{(\pi/4)\,(0.020\,\text{m})^2\,(40)}{(2.280\,\text{m})} = 0.0055\,\text{m}$$

Equivalent plug weld shear width, t_{eb}, per unit width b:

$$t_{eb} = \frac{t_e b}{164\,\text{mm}} = \frac{(0.0055\,\text{m})\,(0.001\,\text{m})}{(0.164\,\text{m})} = 3.354\times10^{-5}\ \text{m}$$

Shear Force, V: V = ½P(b)(H) = ½(248,000 Pa)(0.001 m)(2.140 m) = 265.4 N

Plug Weld Shear Stress, $\tau_{\text{plug weld}}$:

$$\tau_{\text{plug weld}} = \frac{VQ}{I_1 t_{eb}} = \frac{(265.4\,\text{N})\,(5.28\times10^{-7}\ \text{m}^3)}{(6.97\times10^{-8}\,\text{m}^4)\,(3.354\times10^{-5}\ \text{m})}\times10^{-6}\ \frac{\text{MPa}}{\text{Pa}} = 59.9\ \text{MPa}$$

where: Q = (cm)(t)(b) = (0.066 m)(0.008 m)(0.001 m) = 5.28 × 10^{-7} m^3

The allowable shear stress for this case is $0.6S_m$ = 124.2 MPa for Alloy UNS S31803 stainless steel at 71 °C. Therefore, the margin of safety is:

$$\text{MS} = \frac{124.2}{\tau_{\text{plug weld}}} - 1.0 = +1.07$$

Of note, the rear wall has the same fillet welds to the containment sheet, but has continuous welds to the structural sheet, and is therefore bounded by the analysis of the side wall shown here.

The fillet welds attaching the V-stiffeners to the containment sheets are classified as fillet welded attachments per ASME Code, paragraph NB-3123.2. For this application, a fatigue analysis of the welds must be performed. The applied loading range is for the full internal pressure differential of P = 248 kPa to the full internal vacuum and normal ambient external pressure differential of 101 kPa.

The fillet weld shear width per unit width b, t_{fb}, is:

$$t_{fb} = \frac{(\text{combined fillet throat})\,b}{164} = \frac{(0.008\,\text{m})(0.001\,\text{m})}{0.164\,\text{m}} = 4.878\times10^{-5}\ \text{m}$$

The fillet weld shear stress due to the internal pressure differential is:

$$\tau_{\text{fw-ip}} = \frac{VQ}{I_1 t_{fb}} = \frac{(265.4\,\text{N})\,(5.28\times10^{-7}\ \text{m}^3)}{(6.97\times10^{-8}\,\text{m}^4)\,(4.878\times10^{-5}\ \text{m})}\times10^{-6}\ \frac{\text{MPa}}{\text{Pa}} = 41.2\ \text{MPa}$$

For the internal vacuum case, the differential pressure arises from the normal atmospheric external absolute pressure of 101 kPa and an internal pressure of zero. The corresponding fillet weld stress may be determined by scaling to be:

$$\tau_{fw-ep} = \tau_{fw-ip}\frac{101}{248} = 16.8 \text{ MPa}$$

The range of stress between these two states is 41.2 + 16.8 = 58 MPa. Since this stress is a shear stress in a fillet weld, the stress intensity is twice this value, or 116 MPa. The maximum stress is increased by a stress concentration factor of 4 in accordance with ASME B&PV Code, paragraph NB-3232.3. The alternating stress intensity is equal to half of this result, or:

$$S_{alt} = 0.5(116)(4) = 232 \text{ MPa}$$

This value must be adjusted for the modulus of elasticity at temperature. The modulus of elasticity at a temperature of 71 ºC is 19.2(10^4) MPa from Table 2.6-1. The modulus at a temperature of 21 ºC, for which the fatigue curve is prepared, is 19.5(10^4) MPa. The temperature-adjusted value of S_{alt} is:

$$S_{alt-adj} = S_{alt}\frac{19.5}{19.2} = 235.6 \text{ MPa}$$

The allowable cycles are taken from Table I-9.1M (for Figure I-9.2.1M) of the ASME Code. Conservatively assuming that the stress $S_{alt-adj}$ is equal to a value of 248 MPa, the allowable fatigue cycles are 2(10^5). This value is well above the requirement calculated in Section 2.1.2.2.2.1, *Normal Operating Cycles*, of 1,750 cycles. Thus, the fatigue of the V-stiffener fillet welds is not of concern.

Stress Analysis of the Rear Wall

As for the side wall, the inner containment sheet is governing. Coordinate directions are shown on Figure 2.6-1(b). The x-direction is perpendicular to the end V-stiffeners and z is parallel to the end V-stiffeners. The following stresses are evaluated and combined:

- Membrane stress on the neutral axis, and membrane-plus-bending stress on the inner surface of the inner sheet due to global bending of the side wall (z-direction)
- Local bending stress generated by pressure acting over the span of the inner sheet between V-stiffener supports (x-direction)
- Axial membrane stress (parallel to V-stiffeners) generated by pressure on Area 4 (z-direction)
- Lateral membrane stress (perpendicular to V-stiffeners) generated by pressure on Area 3 (x-direction)

<u>Stresses due to global bending:</u>

Maximum moment, $M_{end,}$ conservatively assuming the walls are pinned at the edge:

$$M_{end} = \frac{P\,(b)W^2}{8} = \frac{(248{,}000 \text{ Pa})\,(0.001)\,(1.980 \text{ m})^2}{8} = 121.5 \text{ N - m}$$

Membrane Stress, σ_{mbx}:

$$\sigma_{mbz} = \frac{M_{end}c_m}{I_1} = \frac{(121.5 \text{ N - m})\,(0.066 \text{ m})}{(6.97\times10^{-8} \text{ m}^4)}\times10^{-6}\,\frac{\text{MPa}}{\text{Pa}} = 115.1 \text{ MPa}$$

Maximum Global Bending Stress, σ_{gbx}:

$$\sigma_{gbz} = \frac{M_{end} c_o}{I_1} = \frac{(121.5\,\text{N-m})\,(0.070\,\text{m})}{(6.97\times10^{-8}\,\text{m}^4)} \times 10^{-6}\ \frac{\text{MPa}}{\text{Pa}} = 122.0\,\text{MPa}$$

Local bending stress:

Unsupported span of inner sheet between V-stiffeners: S = 151 mm = 0.151 m

Area moment of inertia for inner containment sheet:

$$I_2 = \frac{bt^3}{12} = \frac{(0.001\,\text{m})\,(0.008\,\text{m})^3}{12} = 4.27\times10^{-11}\ \text{m}^4$$

Maximum moment, $M_{end\text{-}local}$, conservatively assuming sheet has pinned edges at locations supported by V-stiffeners:

$$M_{end\text{-}local} = \frac{bPS^2}{8} = \frac{(0.001\,\text{m})\,(248{,}000)\,(0.151\,\text{m})^2}{8} = 0.707\,\text{N-m}$$

Maximum Local Bending Stress, σ_{lbz}:

$$\sigma_{lbx} = \frac{t/2\,(M_{end-local})}{I_2} = \frac{(0.008\,\text{m}/2)(0.707\,\text{N-m})}{(4.27\times10^{-11}\,\text{m}^4)} \times 10^{-6} = 66.2\,\text{MPa}$$

Axial membrane stress:

Loading is supplied by area A_4 (see Figure 2.6-1(e)): $A_4 = ½(1.070)(2.140) = 1.14\ \text{m}^2$

Edge load per unit length in the z-direction, N_z, (parallel to the V-stiffener):

$$N_z = \frac{PA_4}{H} = \frac{(248{,}000\,\text{Pa})\,(1.14\,\text{m}^2)}{(2.140\,\text{m})} \times 10^{-3}\ \frac{\text{kN}}{\text{N}} = 132.1\,\text{kN/m}$$

Axial stress in the z-direction, σ_z, (parallel to the core longitudinal axis):

$$\sigma_z = \frac{N_z}{2t} = \frac{132.1\,\text{kN/m}}{2(0.008\,\text{m})} \times 10^{-3}\ \frac{\text{MPa}}{\text{kPa}} = 8.3\,\text{MPa}$$

Lateral membrane stress

Loading is supplied by area A_3 (see Figure 2.6-1(d)): $A_3 = ½(0.990)1.980 = 0.98\ \text{m}^2$

Edge load per unit length in the x-direction, N_x, (perpendicular to the core longitudinal axis):

$$N_x = \frac{PA_3}{W} = \frac{(248{,}000\,\text{Pa})\,(0.980\,\text{m}^2)}{(1.980\,\text{m})} \times 10^{-3}\ \frac{\text{kN}}{\text{N}} = 122.7\,\text{kN/m}$$

Lateral stress in the x-direction, σ_x, (perpendicular to the core longitudinal axis):

$$\sigma_x = \frac{N_x}{2t} = \frac{122.7\,\text{kN/m}}{2(0.008\,\text{m})} \times 10^{-3}\ \frac{\text{MPa}}{\text{kPa}} = 7.7\,\text{MPa}$$

Conservatively combining all membrane stresses arithmetically, regardless of direction,

$$SI_{pm} = \sigma_{mbx} + \sigma_x + \sigma_z = 115.1 + 7.7 + 8.3 = 131.1\ \text{MPa}$$

The allowable stress for this case is S_m, or 207 MPa, for Alloy UNS S31803 stainless steel at 71°C. Therefore, the margin of safety is:

$$MS = \frac{207}{SI_{pm}} - 1.0 = +0.58$$

Conservatively, combining all membrane-plus-bending stresses arithmetically, regardless of direction:

$$SI_{pmb} = \sigma_{gbx} + \sigma_{lbz} + \sigma_x + \sigma_z = 122.0 + 66.2 + 7.7 + 8.3 = 204.2 \text{ MPa}$$

The allowable stress for this case is $1.5S_m$ for Alloy UNS S31803 stainless steel at 71 °C. Therefore, the margin of safety is:

$$MS = \frac{1.5\,(207)}{SI_{pmb}} - 1.0 = +0.52$$

2.6.1.4 Comparison with Allowable Stresses

Section 2.1.2, *Design Criteria*, presents the design criteria for structural evaluation of the TRUPACT–III packaging. The containment vessel design criteria for NCT analyses are in accordance with Regulatory Guide 7.6, which uses as a basis the criteria defined for Level A service limits in Section III of the ASME Boiler and Pressure Vessel Code.[3] Load combinations follow the guidelines of Regulatory Guide 7.8.[4]

From Table 2.6-1, the design stress intensity for Alloy UNS S31803 stainless steel is S_m = 207 MPa at 71°C. From Table 2.1-1, the allowable stress intensities for the NCT hot condition are S_m for general primary membrane stress intensity (P_m), $1.5S_m$ for local primary membrane stress intensity (P_L), $1.5S_m$ for primary membrane (general or local)-plus-primary bending stress intensity ($P_m + P_b$ or $P_L + P_b$).

Maximum stress intensity, allowable stress intensity, and minimum margins of safety for each stress category and each load case are summarized in Table 2.6-2. Since all margins of safety are positive, the design criteria are satisfied.

[3] American Society of Mechanical Engineers (ASME) Boiler and Pressure Vessel Code, Section III, *Rules for Construction of Nuclear Power Plant Components*, 2004 Edition, 2005 and 2006 Addenda.

[4] U. S. Nuclear Regulatory Commission, Regulatory Guide 7.8, *Load Combinations for the Structural Analysis of Shipping Casks for Radioactive Material*, Revision 1, March 1989.

Table 2.6-2 – Margins of Safety for NCT Hot Case

Stress Type	Stress, MPa	Location	Allowable, MPa	Margin of Safety
Membrane	152.7	Side wall inner and outer sheets	207.0	+0.36
Membrane + Bending	222.0	Side wall inner containment sheet	310.5	+0.40
Weld Shear	59.9	Outer sheet plug welds	124.2	+1.07
Membrane	131.1	Rear wall inner and outer sheets	207.0	+0.58
Membrane + Bending	204.2	Rear wall inner containment sheet	310.5	+0.52

2.6.1.5 Range of Primary-Plus-Secondary Stress Intensities

Per Paragraph C.4 of Regulatory Guide 7.6, the maximum range of primary-plus-secondary stress intensity for NCT must be less than $3.0S_m$. This limitation on stress intensity range applies to the entire history of NCT loadings and not only to the stresses from each individual load transient. To conservatively encompass the maximum stress intensity range, the maximum stress condition in the CSA was doubled to account for the worst possible stress reversal. From the table above, the maximum CSA stress is 222 MPa in the side wall containment sheet, for the maximum internal pressure with reduced external pressure. Doubling this value results in a maximum stress intensity range of 444 MPa. The allowable stress, at NCT temperatures, is $3.0S_m$, or 3(207) = 621 MPa. The margin of safety is then:

$$\text{MS} = \frac{621}{444} - 1.0 = +0.40$$

Therefore, the criterion of Paragraph C.4 of Regulatory Guide 7.6 is met.

2.6.1.6 Closure Bolts

The closure lid bolt stresses are determined using the recommendations of NUREG/CR 6007[5] and Shigley, *Mechanical Engineering Design*[6]. Allowable stresses are defined in Table 2.1-1 and obtained from Table 2.2-4 for the ASTM A320, Grade L43 bolting material. The maximum bolt stress occurs during the NCT hot operating condition. The resulting tensile stress is 327.9 MPa, which includes the preload and effects of differential thermal expansion. When compared to the allowable tensile stress of S_m, where S_m is $2/3S_y$ (or 466 MPa), the corresponding margin of safety is +0.42. Due to the magnitude of the closure lid bolt preload compared to the internal pressure load, there is no significant prying stress on the bolts. The portion of the internal pressure load taken by the closure lid bolts is 6.3

[5] G. C. Mok, L. E. Fischer, S. T. Hsu, *Stress Analysis of Closure Bolts for Shipping Casks*, NUREG/CR-6007, U.S. Nuclear Regulatory Commission, Washington, DC 20555, January 1993.

[6] Shigley, J. E., Mischke, C. R., *Mechanical Engineering Design*, Fifth Edition, McGraw-Hill, 1989, New York, NY.

kN, which is less than 3% of the 222.2 kN preload. Adding the residual torsion to the tensile stress, the total stress intensity is 445.6 MPa. The corresponding margin of safety on the allowable of $1.35S_m$ (or 629.1 MPa) is +0.41. Details of this analysis are provided below. A depiction of the various bolting parameters is provided in Figure 2.6-2.

Calculation Input Parameters

Nominal bolt diameter:	$d = 36$ mm
Nominal shank diameter:	$d_s = 30$ mm
Thread pitch:	$p = 4$ mm
Pitch diameter:	$d_m = d - 0.649519(p) = 33.0$ mm $= 0.033$ m
Minor diameter:	$d_r = d - 1.226869(p) = 31.0$ mm $= 0.031$ m
Mean of pitch and minor diameters, d_{rm}:	$d_{rm} = \frac{d_m + d_r}{2} = 0.032$ m
Threaded tensile area, A_t, of fastener:	$A_t = \pi/4 (d_{rm}^2) = 8.042 \times 10^{-4}$ m^2
Length of threaded portion of grip:	$L_t = 0$ mm
Shank tensile area, A_d, of fastener:	$A_d = \pi/4 (d_s^2) = 7.069 \times 10^{-4}$ m^2
Length of unthreaded portion of grip:	$L_d = 155$ mm $= 0.155$ m
Total grip length:	$L = L_d + L_t = 0.155$ m
Elastic modulus of bolt:	E_b at 21 °C $= 19.2 \times 10^4$ MPa (ASTM A320 L43)
Elastic modulus of clamped material:	E_m at 21 °C $= 19.5 \times 10^4$ MPa (UNS S31803)
Installation torque :	T = 1,600 N-m
Installation torque factor :	K = 0.20

Bolt Calculations at 21 ºC

The bolt stiffness, k_b, is:

$$k_b = \frac{A_d E_b}{L_d} = \frac{(7.069 \times 10^{-4}\ \text{m}^2)(19.2 \times 10^4\ \text{MPa})}{(0.155\ \text{m})} = 875.6\ \text{MN/m}$$

The cross-sectional area of the closure lid boss, A_m (i.e., the tube forming the bolt hole in the lid, having an outer diameter of 64 mm and an inner diameter of 44 mm) is:

$$A_m = \pi/4 (D_o^2 - D_i^2) = \pi/4 (64^2 - 44^2) \times 10^{-6} = 1.696 \times 10^{-3}\ \text{m}^2$$

The member stiffness, k_m, is:

$$k_m = \frac{A_m E_m}{L} = \frac{(1.696 \times 10^{-3}\ \text{m}^2)(19.5 \times 10^4\ \text{MPa})}{(0.155\ \text{m})} = 2133.7\ \text{MN/m}$$

The preload, F_i, is:

$$F_i = \frac{T}{Kd} = \frac{1600\ \text{N - m}}{(0.20)(0.036\ \text{m})} \times 10^{-3}\ \frac{\text{kN}}{\text{N}} = 222.2\ \text{kN}$$

The external tensile load per bolt, P, is found using the MNOP (248 kPa), the square dimensions of the containment O-ring seal (1.888 m by 2.048 m), and the quantity of closure bolts (44):

$$P = \frac{\text{Pressure (Area)}}{\text{Number of Bolts}} = \frac{(248\ \text{kPa})(1.888\ \text{m})(2.048\ \text{m})}{44} = 21.8\ \text{kN}$$

The portion of P reacted by bolt, P_b, is:

$$P_b = \frac{k_b P}{k_b + k_m} = \frac{(875.6\ \text{MN/m})\,(21.8\ \text{kN})}{(875.6\ \text{MN/m} + 2133.7\ \text{MN/m})} = 6.3\ \text{kN}$$

And the portion of P reacted by members, P_m, is:

$$P_m = \frac{k_m P}{k_b + k_m} = \frac{(2133.7\ \text{MN/m})\,(21.8\ \text{kN})}{(875.6\ \text{MN/m} + 2133.7\ \text{MN/m})} = 15.5\ \text{kN}$$

As shown, the bolt preload is significantly greater than the applied pressure load per bolt, and is the dominant factor in determining the bolt stress.

The resultant bolt load is: $F_b = P_b + F_i = 6.3 + 222.2 = 228.5$ kN

The resultant load on members is: $F_m = P_m - F_i = 15.5 - 222.2 = -206.7$ kN

The maximum bolt tensile stress, $\sigma_{tensile}$, is:

$$\sigma_{tensile} = \frac{F_b}{A_d} = \frac{228.5\ \text{kN}}{7.069 \times 10^{-4}\ \text{m}^2} \times 10^{-3}\ \frac{\text{MPa}}{\text{kPa}} = 323.2\ \text{MPa}$$

The residual bolt torque is: $T_r = 0.5(T) = 800$ N-m

The residual bolt torsion stress, τ_r, is:

$$\tau_r = \frac{T_r d_s}{\pi(d_s/2)^4} = \frac{(800\ \text{N - m})\,(0.030\ \text{m})}{\pi(0.030\ \text{m}/2)^4} \times 10^{-6}\ \frac{\text{MPa}}{\text{Pa}} = 150.9\ \text{MPa}$$

The stress intensity, SI, is:

$$SI = \sqrt{\sigma_{tensile}^2 + 4\tau_r^2} = \sqrt{(323.2\ \text{MPa})^2 + 4(150.9\ \text{MPa})^2} = 442.2\ \text{MPa}$$

The margin of safety for tensile stress using the allowable of $(2/3)S_y$ at 21°C is:

$$MS = \frac{(2/3)S_y}{\sigma_{tensile}} - 1.0 = \frac{2/3\,(724)}{323.2} - 1.0 = +0.49$$

The margin of safety for tensile-plus-residual torsion using the allowable of $1.35*(2/3)S_y$ at 21°C is:

$$MS = \frac{1.35(2/3)S_y}{SI} - 1.0 = \frac{652}{442.2} - 1.0 = +0.47$$

Bolt Calculations at -40 ºC

Assuming that the bolts are installed and pretensioned at a temperature of 21 ºC, the remaining preload under cold (-40 °C) conditions is evaluated as follows. The required mechanical and physical properties are given in the table below.

Elastic modulus of bolt, $E_{b\text{-}40}$, at -40 ºC	19.5×10^4 MPa
Coefficient of thermal expansion of bolt, $\alpha_{b\text{-}40}$, at -40 °C	10.8×10^{-6} mm/mm/°C
Coefficient of thermal expansion of clamped material (UNS S31803), $\alpha_{ss\text{-}40}$, at -40 °C	11.9×10^{-6} mm/mm/°C

The initial preload bolt displacement, δ_I, is:

$$\delta_1 = \frac{F_i L}{A_d E_b} = \frac{(222.2\times10^3\ \text{N})(0.155\ \text{m})}{(7.069\times10^{-4}\ \text{m}^2)(19.2\times10^{10}\ \text{Pa})} = 2.54\times10^{-4}\ \text{m}$$

The change in bolt length due to the temperature change is:

$$\delta_{t1} = \alpha_{b\text{-}40}\, L\, (-40 - 21) = (10.8 \times 10^{-6}\ \text{m/m/°C})\ (0.155\ \text{m})\ (-40\ °\text{C} - 21\ °\text{C}) = -1.02 \times 10^{-4}\ \text{m}$$

The change in closure lid height due to the temperature change is:

$$\delta_{t2} = \alpha_{ss\text{-}40}\, L\, (-40 - 21) = (11.9 \times 10^{-6}\ \text{m/m/°C})\ (0.155\ \text{m})\ (-40\ °\text{C} - 21\ °\text{C}) = -1.13 \times 10^{-4}\ \text{m}$$

The net change in displacement between the bolt and the closure lid is:

$$\delta_{net} = \delta_{t2} - \delta_{t1} = (-1.13 \times 10^{-4}\ \text{m}) - (-1.02 \times 10^{-4}\ \text{m}) = -1.10 \times 10^{-5}\ \text{m}$$

The decrease in initial preload bolt displacement from the temperature change is:

$$\delta_2 = \delta_1 + \delta_{net} = (2.54 \times 10^{-4}\ \text{m}) + (-1.10 \times 10^{-5}\ \text{m}) = 2.43 \times 10^{-4}\ \text{m}$$

The remaining bolt preload at -40 °C is:

$$F_{ri} = \frac{\delta_2 A_d E_{b\text{-}40}}{L} = \frac{(2.43\times10^{-4}\ \text{m})(7.069\times10^{-4}\ \text{m}^2)(19.5\times10^{10}\ \text{Pa})}{(0.155\ \text{m})} \times 10^{-3}\ \frac{\text{kN}}{\text{N}} = 216.1\ \text{kN}$$

$$\text{Percent Reduction} = \frac{F_{ri} - F_i}{F_i} \times 100 = \frac{(216.1\ \text{kN}) - (222.2\ \text{kN})}{(222.2\ \text{kN})} \times 100 = -2.7\%$$

This small reduction in preload force at -40 ºC may be neglected.

Bolt Calculations at 71 ºC

Assuming that the bolts are installed and pretensioned at a temperature of 21 ºC, the effects of NCT hot (71 °C) conditions are evaluated as follows. The required mechanical and physical properties are given in the table below.

Elastic modulus of bolt, E_{b71}, at 71 ºC	18.8×10^4 MPa
Coefficient of thermal expansion of bolt, α_{b71}, at 71 °C	11.9×10^{-6} mm/mm/°C
Coefficient of thermal expansion of clamped material (UNS S31803), α_{ss71}, at 71 °C	13.0×10^{-6} mm/mm/°C

The change in bolt length due to the temperature change is:

$$\delta_{t1} = \alpha_{b71} L (71 - 21) = (11.9 \times 10^{-6} \text{ m/m/°C}) (0.155 \text{ m}) (71 \text{ °C} - 21 \text{ °C}) = 9.22 \times 10^{-5} \text{ m}$$

The change in closure lid height due to the temperature change is:

$$\delta_{t2} = \alpha_{ss71} L (71 - 21) = (13.0 \times 10^{-6} \text{ m/m/°C}) (0.155 \text{ m}) (71 \text{ °C} - 21 \text{ °C}) = 1.01 \times 10^{-4} \text{ m}$$

The net change in displacement between the bolt and the closure lid boss is:

$$\delta_{net} = \delta_{t2} - \delta_{t1} = (1.01 \times 10^{-4} \text{ m}) - (9.22 \times 10^{-5} \text{ m}) = 8.80 \times 10^{-6} \text{ m}$$

The increase in initial preload bolt displacement from the temperature change is:

$$\delta_2 = \delta_1 + \delta_{net} = (2.54 \times 10^{-4} \text{ m}) + (8.80 \times 10^{-6} \text{ m}) = 2.63 \times 10^{-4} \text{ m}$$

The increased bolt preload at 71 °C is:

$$F_{ii} = \frac{\delta_2 A_d E_{b71}}{L} = \frac{(2.63\times10^{-4} \text{ m})(7.069\times10^{-4} \text{ m}^2)(18.8\times10^{10} \text{ Pa})}{(0.155 \text{ m})} \times 10^{-3} \frac{\text{kN}}{\text{N}} = 225.5 \text{ kN}$$

$$\text{Percent Increase} = \frac{F_{ii} - F_i}{F_i} \times 100 = \frac{(225.5 \text{ kN}) - (222.2 \text{ kN})}{(222.2 \text{ kN})} \times 100 = 1.5\%$$

The resultant bolt load is: $F_{b71} = P_b + F_{ii} = 6.3 + 225.5 = 231.8$ kN

(Note: the slight change in P_b due to changes in bolt and joint stiffness which result from the temperature difference between 21 ºC and 71 ºC is negligible.) The maximum bolt tensile stress, $\sigma_{tensile}$, is:

$$\sigma_{tensile} = \frac{F_{b71}}{A_d} = \frac{231.8 \text{ kN}}{7.069\times10^{-4} \text{ m}^2} \times 10^{-3} \frac{\text{MPa}}{\text{kPa}} = 327.9 \text{ MPa}$$

From above, the residual bolt torsion stress, $\tau_r = 150.9$ MPa. The stress intensity, SI, is:

$$SI = \sqrt{\sigma_{tensile}^2 + 4\tau_r^2} = \sqrt{(327.9 \text{ MPa})^2 + 4(150.9 \text{ MPa})^2} = 445.6 \text{ MPa}$$

The margin of safety for tensile stress using the allowable of $(2/3)S_y$ at 71°C is:

$$MS = \frac{(2/3)S_y}{\sigma_{tensile}} - 1.0 = \frac{2/3(699)}{327.9} - 1.0 = +0.42$$

The margin of safety for tensile-plus-residual torsion using the allowable of $1.35*(2/3)S_y$ at 71°C is:

$$MS = \frac{1.35(2/3)S_y}{SI} - 1.0 = \frac{1.35(2/3)(699)}{445.6} - 1.0 = +0.41$$

Internal Thread Evaluation

The internal thread stripping area,[7] A_{in}, per engagement length of the M36 × 4 threads is 84.1 mm^2/mm. With a thread engagement length, L_t, of 50 mm, the shear stress of the internal closure bolt threads, $\tau_{int\ threads}$, is then:

[7] Industrial Fasteners Institute, *Manufacturer's Capability Guide*, Table 2, 1986, Cleveland, Ohio.

$$\tau_{\text{int threads}} = \frac{F_{b71}}{A_{in} L_t} = \frac{(231.8\ \text{kN})}{(0.0841\ \text{m}^2/\text{m})\,(0.050\ \text{m})} \times 10^{-3}\ \frac{\text{MPa}}{\text{kPa}} = 55.1\ \text{MPa}$$

The allowable stress for the Alloy UNS S31803 boss material is $0.6S_m$. Therefore, the margin of safety for the internal threaded material is:

$$MS_{\text{shear}} = \frac{0.6S_m}{\tau_{\text{int threads}}} - 1.0 = \frac{0.6(207)}{55.1} - 1.0 = +1.25$$

The optional alloy steel thread insert has material strength properties equal to or greater than the Alloy UNS S31803 material. Therefore, the shear stress for thread insert is bounded by the base material.

The maximum stresses and minimum margins of safety for each closure bolt load case are summarized in Table 2.6-3. Since all margins of safety are positive, the design criteria are satisfied.

Table 2.6-3 – Summary of Closure Lid Bolt and Thread Analysis

Condition	Stress, MPa	Allowable Stress	Margin of Safety
Tensile stress at 21 ºC	323.2	$(2/3)S_y = 482.7$	+0.49
Tensile plus residual torsion stress at 21 ºC	442.2	$1.35(2/3)S_y = 651.6$	+0.47
Tensile stress at 71 ºC	327.9	$(2/3)S_y = 466$	+0.42
Tensile plus residual torsion stress at 71 ºC	445.6	$1.35(2/3)S_y = 629.1$	+0.41
Internal Thread Shear Stress (UNS S31803)	55.1	$0.6S_m = 124.2$	+1.25

2.6.2 Cold

For the NCT cold condition, a -40 ºC steady state ambient temperature is utilized per 10 CFR §71.71(c)(2), with zero insulation and zero decay heat. This results in a uniform temperature of -40 ºC throughout the package. With no internal heat load (i.e., no contents to produce heat and, therefore, pressure), the net pressure differential is assumed to be zero (101 kPa absolute internal, 101 kPa absolute external). The materials of construction for the TRUPACT–III packaging are not adversely affected by the -40 ºC condition.

Brittle fracture at -40 ºC is addressed in Section 2.1.2.2.1, *Brittle Fracture*. Performance of the O-ring seals at -40 ºC is discussed in Appendix 2.12.2, *Elastomer O-ring Seal Performance Tests*.

The closure bolts are fabricated of ASTM A320, Grade L43 having a coefficient of thermal expansion which is lower than that of the cask body and closure lid bosses, as presented in Section 2.2.1, *Material Properties and Specifications*. Therefore, under cold conditions, the initial bolt preload force is reduced below the value at room temperature. However, a significant positive preload force remains, and bolt stresses developed are well within allowable limits, as described above in Section 2.6.1.6, *Closure Bolts*. The minimum bolt preload force under cold conditions is 216.1 kN per bolt. This force is only 2.7% less than the installation preload and is more than adequate to compress the elastomer O-ring seals.

2.6.3 Reduced External Pressure

The effect of a reduced external pressure of 25 kPa absolute, per 10 CFR §71.71(c)(3), is negligible for the TRUPACT–III packaging. This conclusion is based on the analyses presented in Section 2.6.1, *Heat*, addressing the ability of the CSA to independently withstand a maximum normal operating pressure (MNOP) of 172 kPa gauge internal pressure at the same reduced external pressure, equivalent to a 248 kPa gauge internal pressure.

2.6.4 Increased External Pressure

The effect of an increased external pressure of 140 kPa absolute (39 kPa gauge external pressure), per 10 CFR §71.71(c)(4), is negligible for the TRUPACT–III packaging. The external pressure induces small compressive stresses in the containment boundary that are limited by stability (buckling) requirements. The bounding buckling case is in fact the HAC load case of immersion under 15 meters head of water, which corresponds to an external gauge pressure of 150 kPa. From Appendix 2.12.4, *HAC Immersion Buckling Evaluation*, using the greater HAC external gauge pressure, the combined stress in the critical sidewall is 88.7 MPa, and the allowable inelastic buckling load is 391 MPa. The factor of safety against buckling is:

$$FS = \frac{(\sigma_{cr})_x}{\sigma} = \frac{391}{88.7} = 4.41$$

This is considerably in excess of the minimum factor of safety of 2.0 for NCT per ASME Code Case N-284-1, corresponding to ASME Code, Service Level A conditions. Note that the factor of safety requirement for NCT is easily met using the HAC pressure, which is 150/39 = 3.8 times larger than the required pressure. Therefore, the NCT external pressure of 39 kPa gauge is not of concern. Details of the analysis are given in Appendix 2.12.4, *HAC Immersion Buckling Evaluation*. Of note, the containment vessel is designed to withstand a full vacuum equivalent to 101 kPa external pressure during acceptance leakage rate testing of the TRUPACT–III package, as described in Section 8.1.4, *Fabrication Leakage Rate Tests*.

2.6.5 Vibration

By comparing the alternating stresses arising during NCT with the established endurance limits of the TRUPACT–III packaging materials of construction, the effects of vibration normally incident to transport are shown to be acceptable. By conservatively comparing NCT stresses with endurance stress limits for an infinite service life, the development of accurate vibratory loading cycles is not required.

ANSI N14.23[8] provides a basis for estimating peak truck trailer vibration inputs. A summary of peak vibratory accelerations for a truck semi-trailer bed with light loads (less than 15 tons) is provided in Table 2 of ANSI N14.23. The component accelerations are given in Table 2 as 1.3*g* longitudinally, 0.5*g* laterally, and 2.0*g* vertically. A fully loaded TRUPACT–III package on a single trailer will exceed the light load limit, but acceleration magnitudes associated with light loads are conservative for heavy loads per Table 2 of ANSI N14.23. The commentary provided within Section 4.2, *Package*

[8] ANSI N14.23, *Design Basis for Resistance to Shock and Vibration of Radioactive Material Packages Greater than One Ton in Truck Transport* (Draft), 1980, American National Standards Institute, Inc, (ANSI).

Response, of ANSI N14.23 states that recent "…*tests conducted by Sandia National Laboratories have shown that the truck bed accelerations provide an upper bound on cask (response) accelerations*." Based upon these data, conservatively assume the peak acceleration values from Table 2 are applied to the TRUPACT–III package in a continuously cycling fashion.

As described in Section 2.5.2, *Tie-down Devices*, the TRUPACT-III is supported during transport by structural pockets on the conveyance in the vicinity of the four lower ISO fittings. Lifting the package by the upper ISO fittings is structurally equivalent to supporting the package by the bottom ISO fittings. Only the magnitude of loading is different. As shown in Section 2.5.1, *Lifting Devices*, the shear stress in the lifting arm (i.e., cheek) attachment welds, for a lifting load of 3g, is 49.4 MPa. Scaling the stress for a 2g vertical acceleration gives a shear stress of (2/3) × 49.4 = 32.9 MPa. In calculating this stress, a conservative assumption was made that only two of the four lifting arms actually support any load. Since the package weight during transport is supported by a relatively lightweight and therefore structurally compliant trailer, a uniform load distribution on all four ISO fittings may be reasonably assumed. Therefore the stress in the attachment weld will be half as much as calculated above, so that the stress in transport is 32.9/2 = 16.5 MPa. Including a stress concentration factor of 4 as described in ASME B&PV Code, Subsection NB-3232.3, gives an adjusted shear stress of 16.5 × 4 = 66 MPa. As calculated below in this section, the temperature-adjusted fatigue value for 10^6 cycles in shear is $\tau_{fatigue}$ = 115.2 MPa. The margin of safety is:

$$MS = \frac{115.2}{66} - 1 = +0.75$$

Therefore, the TRUPACT-III lifting arms do not exhibit any fatigue limitations resulting from normal transportation vibration.

The bottom wall of the CSA supports the payload in normal transport and may be subject to vibration. The vibration analysis is performed by calculating the stress in the wall (i.e., the CSA floor) assuming an upper bound mass for the wall and including the mass of the payload, under the action of a 2g inertia force. The total inertia load on the wall is then analyzed as an applied pressure. For conservatism, the wall is assumed to be simply supported on all four edges. The length of the wall, which is conservatively assumed to extend from the center of the rear wall to the bolted seal flange, is L = 2,860 mm. The width, which extends to the centers of the side walls, is W = 1,980 mm. The wall self-mass is very conservatively assumed to be equal to one quarter of *total* empty packaging mass.

Calculation Input Parameters

Bottom containment wall self-mass: $M_1 = 19{,}825/4 = 4{,}956$ kg

Payload mass: $M_2 = 5{,}175$ kg

The total pressure distributed over the wall (including 2g factor):

$$P = 2g\left[\frac{M_1 + M_2}{LW}\right] = 2 \times (9.81\ m/s^2)\left[\frac{(4{,}956\ kg) + (5{,}175\ kg)}{(2.860\ m) \times (1.980\ m)}\right] \times 10^{-3}\ \frac{kPa}{Pa} = 35\ kPa$$

Thickness of inner and outer sheets: t = 8 mm = 0.008 m

Distance between inner & outer sheet centroids: d = 132 mm = 0.132 m

Area of one face sheet per unit width: $A = 1 \times 10^{-6}\ (t) = 8 \times 10^{-6}$ m

Outer fiber distance: $c_o = \frac{d+t}{2} = 70\text{ mm} = 0.070\text{ m}$

Area moment of inertia (see Section 2.6.1.3): $I_1 = 6.97 \times 10^{-8}\text{ m}^4$

Bottom Containment Wall Fatigue Evaluation

The maximum moment in the wall, assuming pinned edges, is:

$$M_{max_1} = \frac{PbW^2}{8} = \frac{(35\text{ kPa})(0.001\text{ m})(1.98\text{ m})^2}{8} \times 10^3\ \frac{\text{Pa}}{\text{kPa}} = 17.15\text{ N-m}$$

The maximum global bending stress, σ_{gbx}, is:

$$\sigma_{gbx} = \frac{M_{max_1} c_o}{I_1} = \frac{(17.15\text{ N-m})(0.070\text{ m})}{(6.97\times10^{-8}\text{ m}^4)} \times 10^{-6}\ \frac{\text{MPa}}{\text{Pa}} = 17.2\text{ MPa}$$

The local bending stress in the region between the V-stiffeners will next be considered. The unsupported span of the wall between V-stiffeners is S = 145 mm. The area moment of inertia for the wall inner sheet is:

$$I_2 = \frac{bt^3}{12} = \frac{(0.001\text{ m})(0.008\text{ m})^3}{12} = 4.267\times10^{-11}\text{ m}^4$$

The maximum local moment, again assuming pinned edges at the V-stiffeners, is:

$$M_{max_2} = \frac{PbS^2}{8} = \frac{(35\text{ kPa})(0.001\text{ m})(0.145\text{ m})^2}{8} \times 10^3\ \frac{\text{Pa}}{\text{kPa}} = 0.092\text{ N-m}$$

The maximum local bending stress is:

$$\sigma_{lby} = \frac{(0.008\text{ m}/2)(0.092\text{ N}-\text{m})}{(4.267\times10^{-11}\text{ m}^4)} \times 10^{-6}\ \frac{\text{MPa}}{\text{Pa}} = 8.6\text{ MPa}$$

The maximum primary membrane-plus-bending stress intensity is:

$$SI_{pmb} = \sigma_{gbx} + \sigma_{lby} = 17.2 + 8.6 = 25.8\text{ MPa}$$

The fatigue allowable stress for Alloy UNS S31803 stainless steel corresponding to 1.0×10^6 cycles is 195 MPa, per Table I-9.1M for Figure I-9.2.1 of the ASME Code. The fatigue allowable is then factored by the ratio of the modulus of elasticity at 21 °C and 71 °C to adjust for service at temperature, where $E_{21} = 19.5 \times 10^4$ MPa is the modulus at 21 ºC and $E_{71} = 19.2 \times 10^4$ MPa is the modulus at 71 ºC:

$$\sigma_{fatigue} = \frac{E_{71}}{E_{21}}(195) = \frac{19.2\times10^4}{19.5\times10^4}(195) = 192\text{ MPa}$$

The maximum stress intensity is increased by a stress concentration factor of 4 in accordance with ASME B&PV Code, Subsection NB 3232.3.

$$\sigma_{factored} = 4SI_{pmb} = 4 \times 25.8\text{ MPa} = 103.2\text{ MPa}$$

The maximum factored stress of 103.2 MPa is less than the fatigue allowable of 192 MPa at a service temperature of 71 °C. The margin of safety is:

$$MS = \frac{\sigma_{fatigue}}{\sigma_{factored}} - 1.0 = \frac{192}{103.2} - 1.0 = +0.86$$

Therefore, the bottom containment wall does not exhibit any fatigue limitations resulting from normal transportation vibration.

Bottom Containment Wall Weld Fatigue Evaluation

The V-stiffeners are attached to the inner containment sheet by continuous skewed fillet welds, which have an equivalent throat thickness of 4 mm. The V-stiffeners are attached to the outer structural sheet by a series of 20-mm diameter plug welds. As shown below, the equivalent shear width of the plug welds is 5.9 mm, and therefore, this shear width is bounding compared to the inner sheet welds that have a combined effective throat of 2 × 4 = 8 mm. The calculation parameters are:

Number of plug welds per V-stiffener: N = 40

Diameter of plug welds, D: D = 20 mm = 0.020 m

V-stiffener length, L: L = 2,120 mm = 2.120 m
(conservatively equal to the full width of the CSA)

Distance between plug weld rows, d_p: d_p = 164 mm = 0.164 m

The equivalent plug weld shear width, t_e, per V-stiffener is:

$$t_e = \frac{(\pi/4)\, D^2\, N}{L} = \frac{(\pi/4)\,(0.020\ \text{m})^2\,(40)}{(2.120\ \text{m})} = 0.0059\ \text{m}$$

The equivalent plug weld shear width, t_{eb}, per unit width is:

$$t_{eb} = \frac{t_e b}{164\ \text{mm}} = \frac{(0.0059\ \text{m})\,(0.001\ \text{m})}{(0.164\ \text{m})} = 3.60 \times 10^{-5}\ \text{m}$$

The weld shear force, V, is:

$$V = \tfrac{1}{2}P(b)(W) = \tfrac{1}{2}(35\ \text{kPa})(0.001\ \text{m})(1.980\ \text{m}) = 34.7\ \text{N}$$

The plug weld shear stress, $\tau_{plug\ weld}$, is:

$$\tau_{plug\ weld} = \frac{VQ}{I_1 t_{eb}} = \frac{(34.7\ \text{N})(5.28 \times 10^{-7}\ \text{m}^3)}{(6.97 \times 10^{-8}\ \text{m}^4)(3.60 \times 10^{-5}\ \text{m})} \times 10^{-6}\ \frac{\text{MPa}}{\text{Pa}} = 7.30\ \text{MPa}$$

where: d = 132 mm t = 8 mm b = 1 mm

$I_1 = 6.97 \times 10^{-8}\ \text{m}^4$ $Q = (\tfrac{1}{2}d)(t)(b) = 5.28 \times 10^{-7}\ \text{m}^3$

As determined above, the fatigue allowable stress for Alloy UNS S31803 stainless steel at 71°C is 192 MPa. Factoring this value for 0.6 for shear loading, the shear fatigue allowable is:

$$\tau_{fatigue} = 0.6(192) = 115.2\ \text{MPa}$$

The maximum stress is increased by a stress concentration factor of 4 in accordance with ASME B&PV Code, Subsection NB 3232.3.

$$\tau_{factored} = 4\tau_{plug\ weld} = 4(7.30\ \text{MPa}) = 29.2\ \text{MPa}$$

The maximum factored stress of 29.2 MPa is less than the fatigue allowable of 115.2 MPa at a service temperature of 71 °C. The margin of safety is:

$$\text{MS} = \frac{\tau_{\text{fatigue}}}{\tau_{\text{factored}}} - 1.0 = \frac{115.2}{29.2} - 1.0 = +2.95$$

Therefore, the bottom containment wall plug welds do not exhibit any fatigue limitations resulting from transportation vibration.

2.6.6 Water Spray

The materials of construction utilized for the TRUPACT–III package are such that the water spray test identified in 10 CFR §71.71(c)(6) will have a negligible effect on the package.

2.6.7 Free Drop

10 CFR §71.71(c)(7) requires a NCT free drop from a height of 0.3 m for packages weighing more than 15,000 kg. The TRUPACT–III is designed to withstand the effects of a 9-m free drop while maintaining leaktight containment. The NCT free drop height of 0.3-m represents a potential energy at impact of only 3.3% of the HAC, 9-m free drop. A 0.3-m free drop was performed during full-scale certification testing of CTU-1, resulting in negligible visible damage to the test unit. This test was followed by four HAC, 9-m free drops. The structural performance of the TRUPACT–III was demonstrated to be acceptable as described in Section 2.7, *Hypothetical Accident Conditions*. Therefore, the requirements of 10 CFR §71.71(c)(7) are met.

2.6.8 Corner Drop

This test does not apply, since the package weight is in excess of 100 kg, as delineated in 10 CFR §71.71(c)(8).

2.6.9 Compression

This test does not apply, since the package weight is in excess of 5,000 kg, as delineated in 10 CFR §71.71(c)(9).

2.6.10 Penetration

The one meter drop of a 6 kilogram, hemispherically-headed, 3.2-cm diameter steel cylinder, as delineated in 10 CFR §71.71(c)(10), is of negligible consequence to the TRUPACT–III package. This conclusion is due to the fact that the TRUPACT–III package is designed to minimize the consequences associated with the much more limiting case of a one meter drop of the entire package onto a puncture bar as discussed in Section 2.7.3, *Puncture*. The 6-mm minimum thickness outer sheet is not damaged by the penetration event.

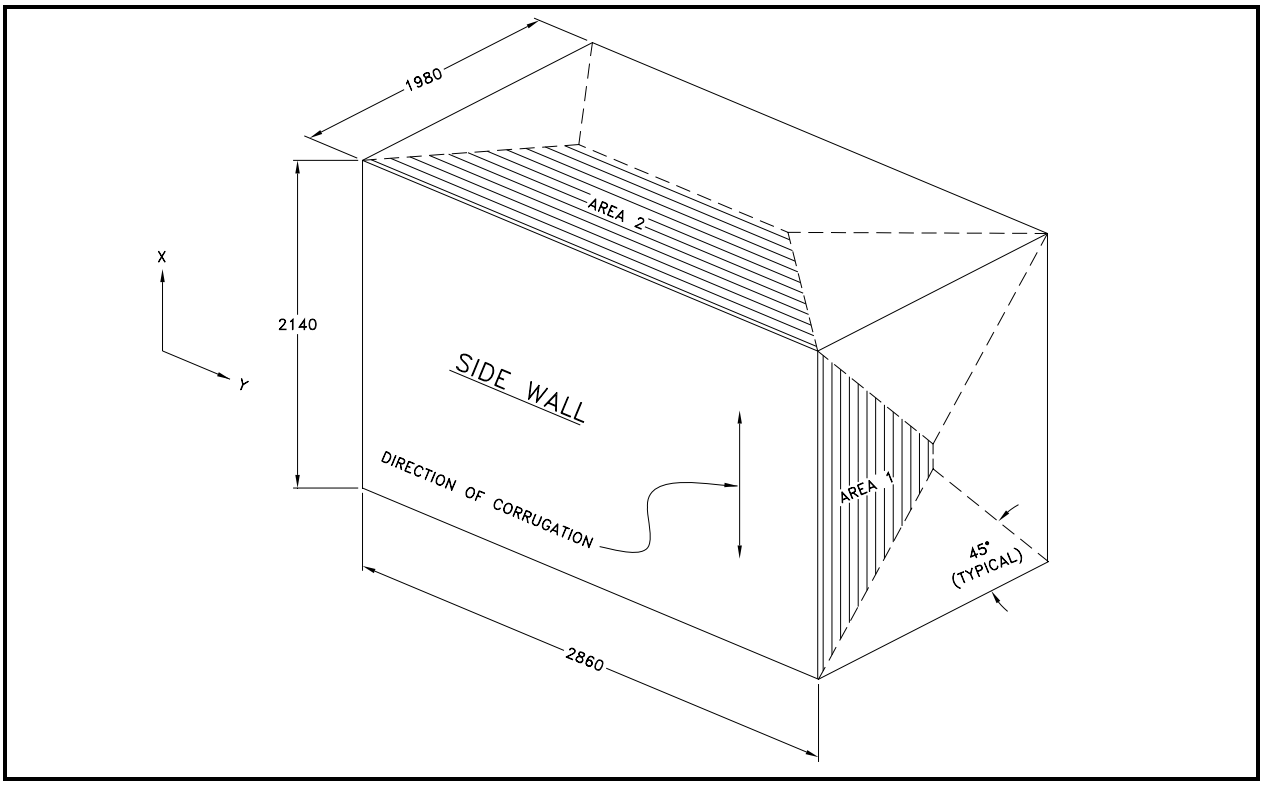

Figure 2.6-1(a) – View of Side Walls and Adjacent Walls, Showing Areas Used to Calculate Edge Loads for Side Walls

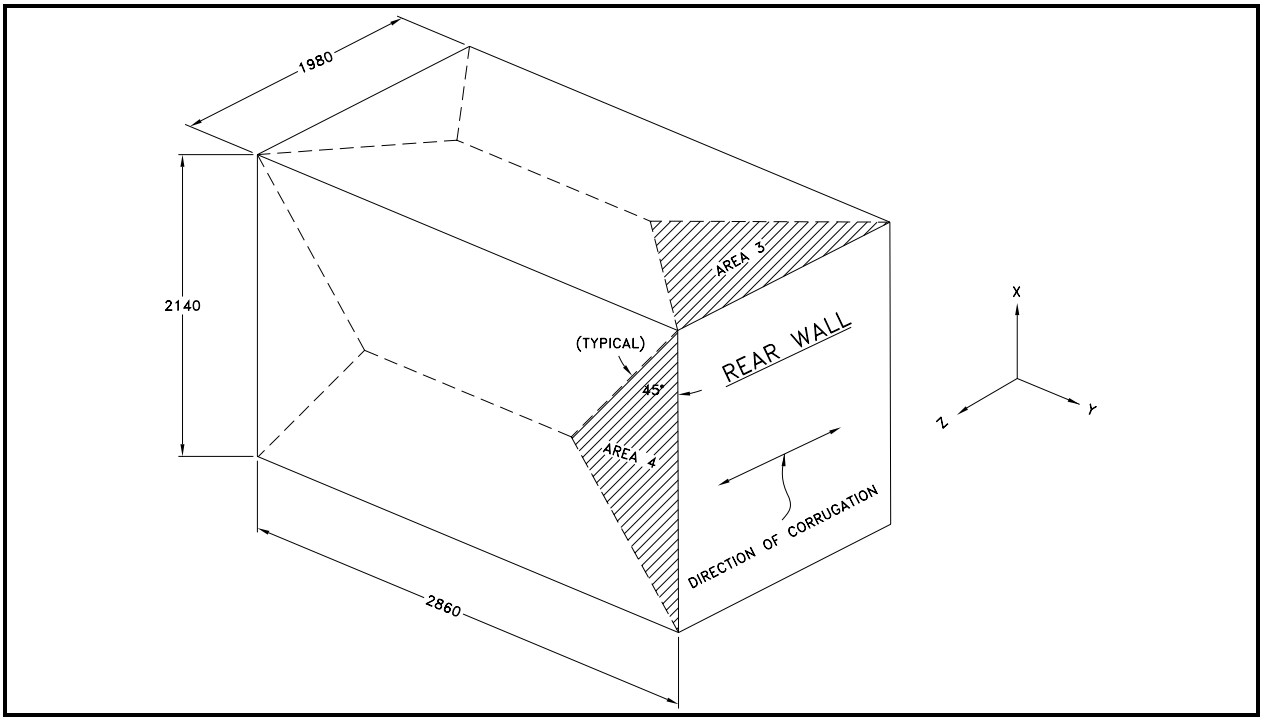

Figure 2.6-1(b) – View of Rear Wall and Adjacent Walls, Showing Areas Used to Calculate Edge Loads for the Rear Wall

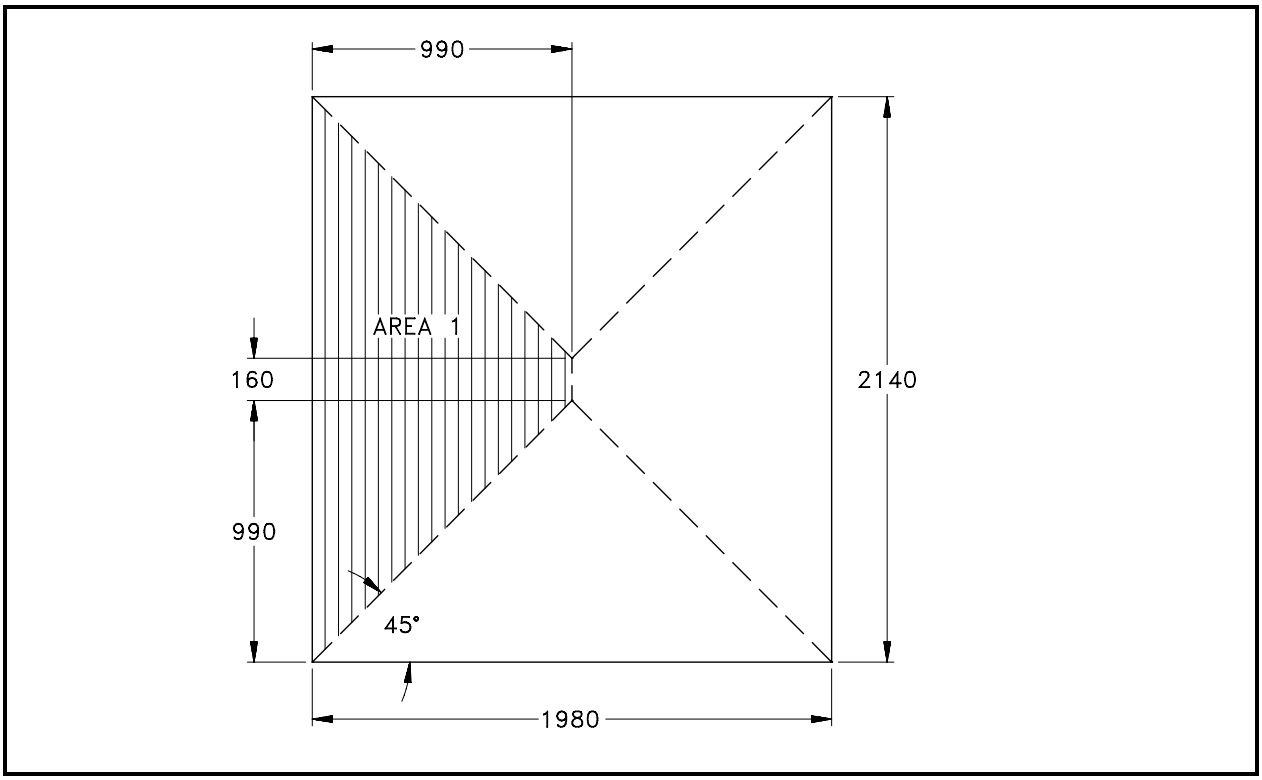

Figure 2.6-1(c) – View of Area 1 on End Wall Used to Calculate End Edge Load on Side Wall

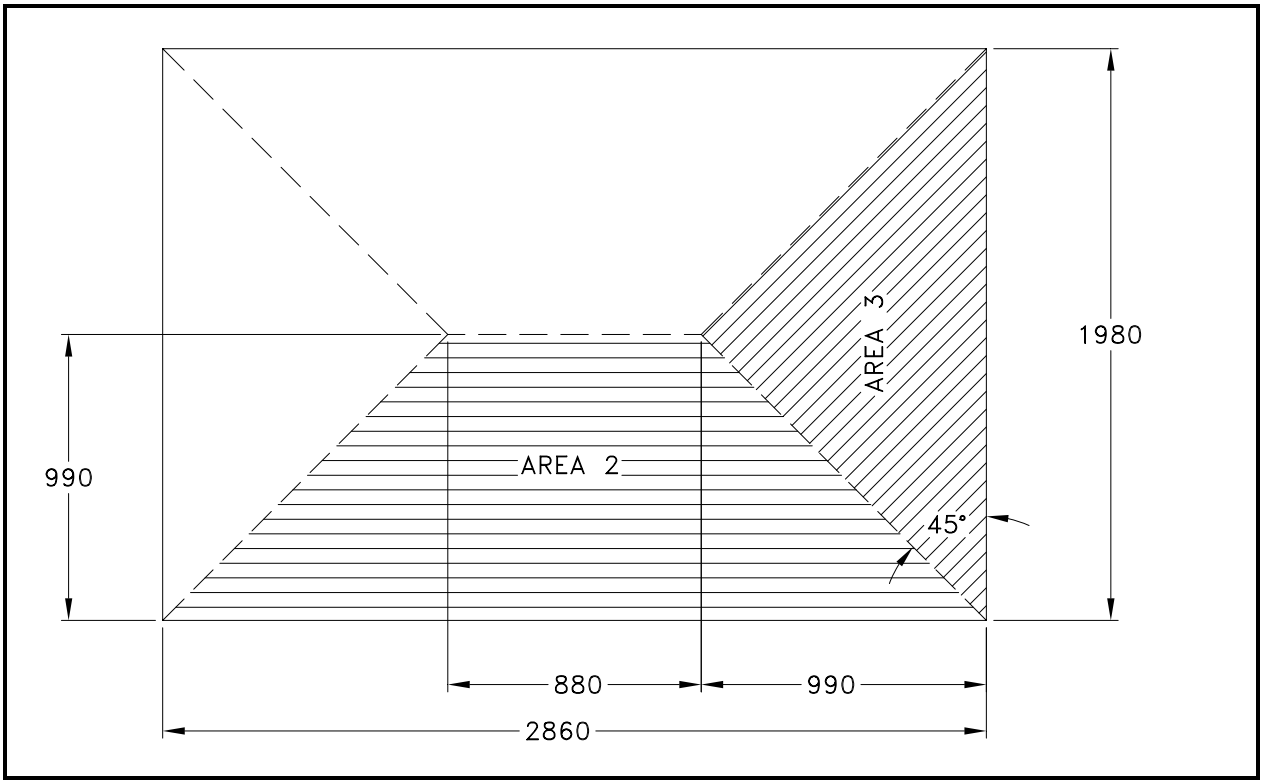

Figure 2.6-1(d) – View of Areas 2 & 3 on Top Wall Used to Calculate Edge Loads on Side & Rear Walls

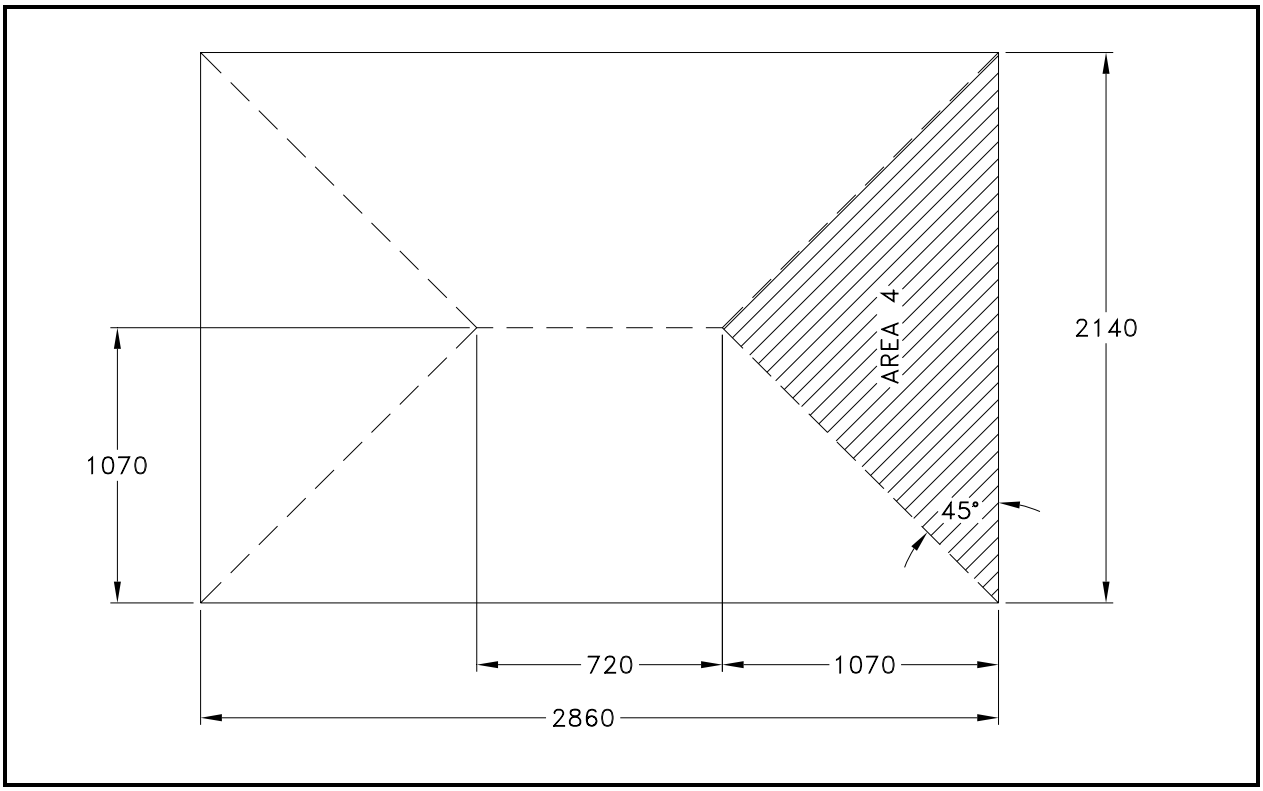

Figure 2.6-1(e) – View of Area 4 on Side Wall Used to Calculate Edge Load on Rear Wall

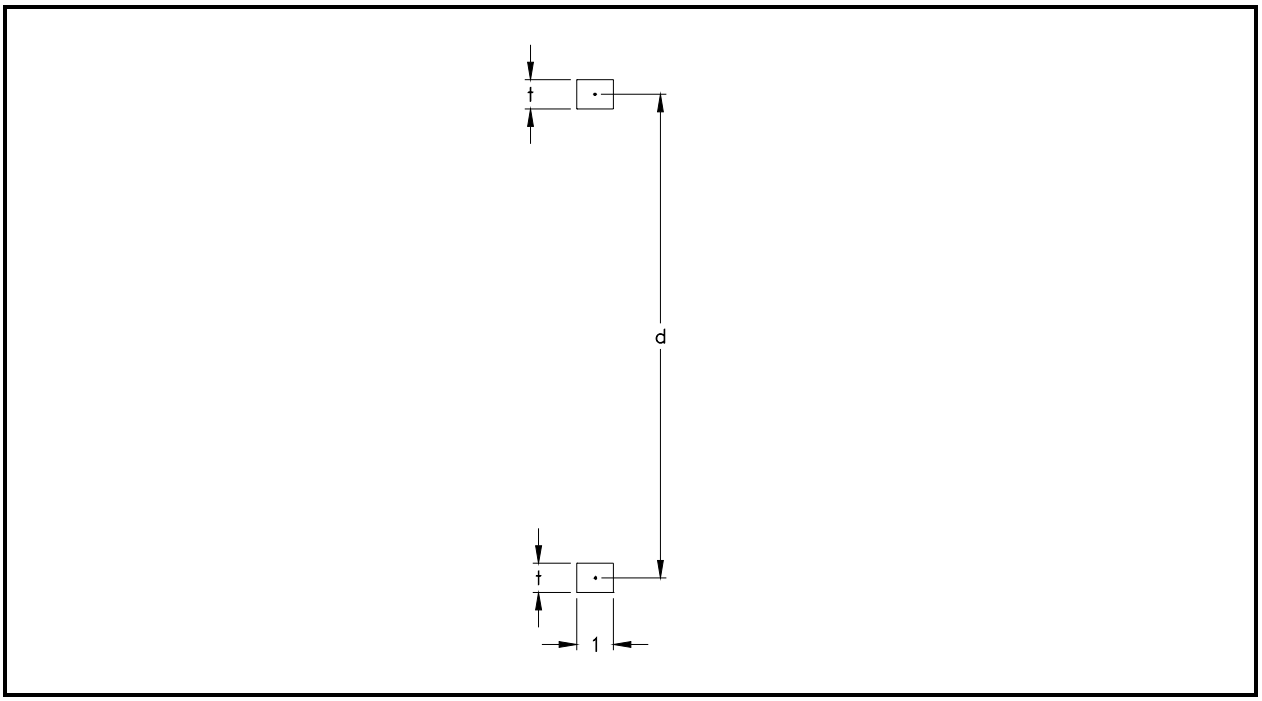

Figure 2.6-1(f) – Typical Wall Section for Global Bending and Membrane Analysis

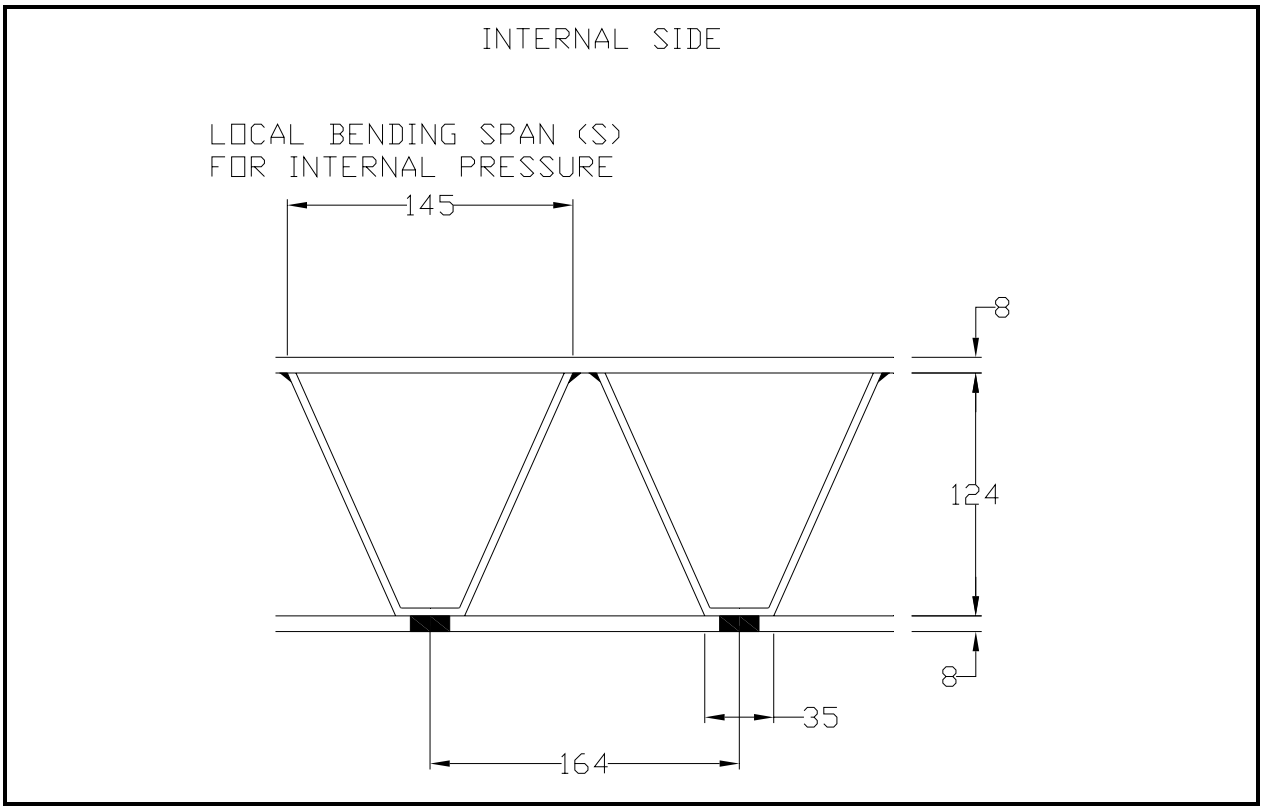

Figure 2.6-1(g) – Local Bending Spans for Side Wall

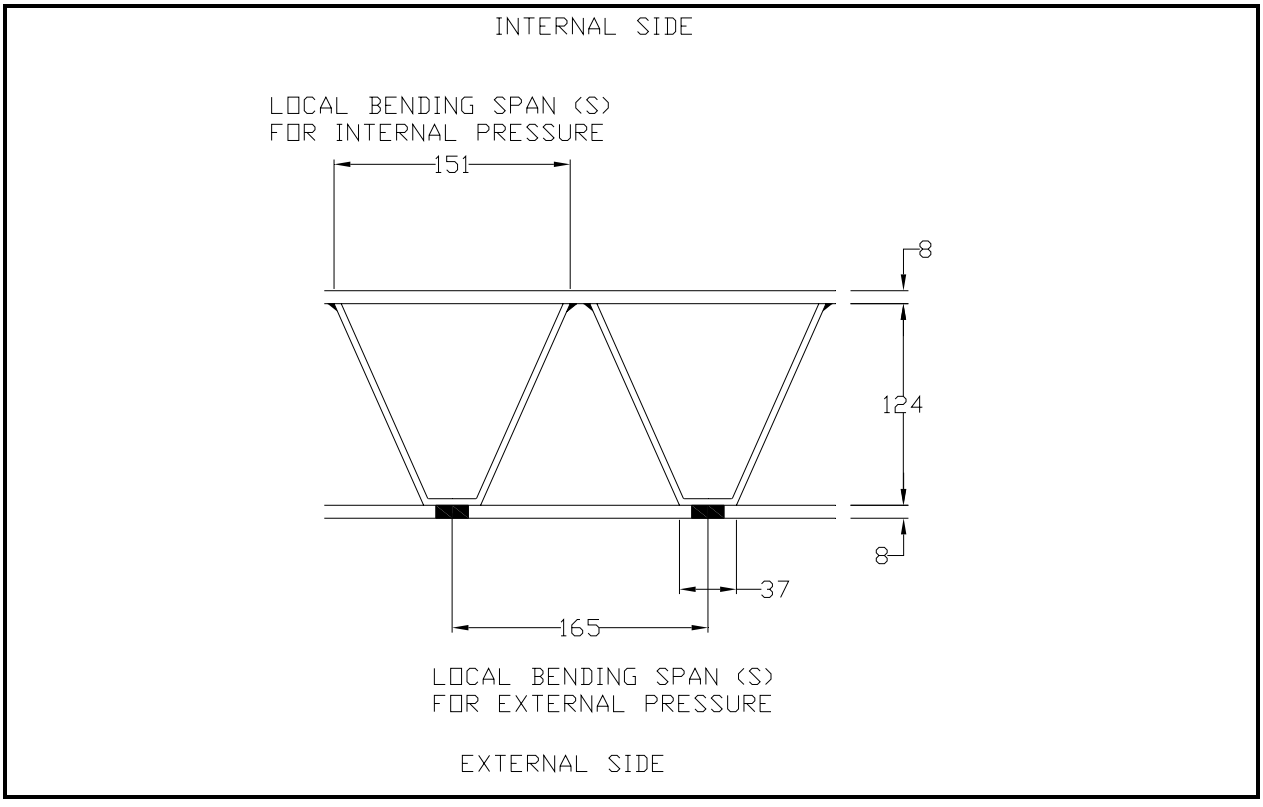

Figure 2.6-1(h) – Local Bending Spans for Rear Wall

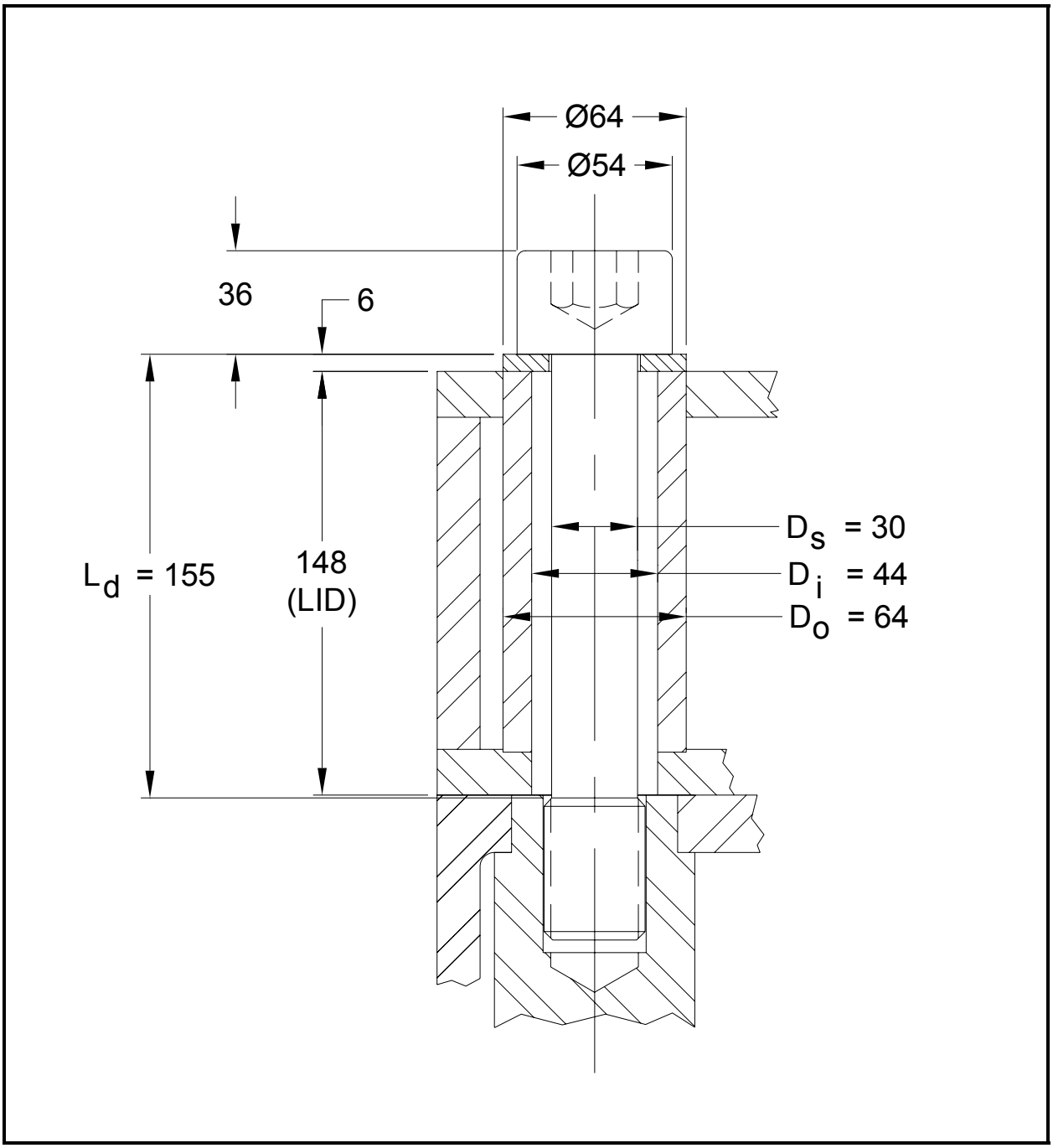

Figure 2.6-2 – Closure Bolt Analysis Parameters

This page intentionally left blank.

2.7 Hypothetical Accident Conditions

The TRUPACT–III package, when subjected to the sequence of hypothetical accident condition (HAC) tests specified in 10 CFR §71.73, subsequent to the sequence of normal conditions of transport (NCT) tests specified in 10 CFR §71.71, is shown to meet the performance requirements specified in Subpart E of 10 CFR 71[1]. Demonstration of compliance with the requirements is by a combination of test and analysis. Analysis is used for all NCT events except the free drop, and for the HAC thermal and immersion cases. Testing is used for the NCT & HAC free drop events, and for the HAC puncture drop event. Two full-scale certification test units (CTU-1 and CTU-2) were used for all test demonstrations. Test results are summarized in Section 2.7.8, *Summary of Damage*, with details provided in Appendix 2.12.3, *Certification Tests on CTU-1* and Appendix 2.12.6, *Certification Tests on CTU-2*. An analytical evaluation of the debris shield, which was included in CTU-2, is provided in Section 2.12.5, *Closure Lid Debris Shield*. A significant number of engineering tests using a half-scale prototype test unit were performed, as documented in Section 2.12.1, *Engineering Tests*.

2.7.1 Free Drop

Subpart F of 10 CFR 71 requires performing a free drop test in accordance with the requirements of 10 CFR §71.73(c)(1). The free drop test involves performing a 9-m free drop onto a flat, essentially unyielding, horizontal surface, with the package striking the surface in an orientation for which maximum damage is expected. The ability of the TRUPACT–III package to adequately withstand this specified free drop is demonstrated by testing of a full-scale CTU. A total of four, 9-m HAC free drops were performed on CTU-1, preceded by one, 0.3-m NCT free drop. One, 9-m HAC free drop was performed on CTU-2.

2.7.1.1 Technical Basis for the Free Drop Tests

In order to determine the worst-case free drop orientation, an exhaustive consideration of all uniquely different free drop orientations was made. Each was evaluated to determine if bounding forces, stresses, strains, or damage to the containment sealing area would occur. The criteria used to evaluate each free drop were based on the following considerations:

- Rupture of containment boundary
- Buckling of the CSA
- Excessive deformation in the containment sealing area (body and closure lid flanges)
- Separation of the closure lid from the body
- Separation of the overpack cover from the package
- Excessive compression, damage, or exposure of the overpack structures (e.g., foam or calcium silicate insulation).

[1] Title 10, Code of Federal Regulations, Part 71 (10 CFR 71), *Packaging and Transportation of Radioactive Material*, 01–01–09 Edition.

Of note, shielding integrity is not of concern since the payload is contact-handled transuranic waste. For the criticality analysis, deformations are conservatively bounded as shown in Section 6.0, *Criticality Evaluation*. All of the free drops considered are individually evaluated below.

Note: In the following, an *edge* is defined as a line where two sides meet at a right angle. A *corner* is defined as a point where three sides meet.

Drops on the Ends (Total of 12)

A. Flat end (package vertical). Total of two drops. Although the overpack construction is essentially the same at each end, the CSA construction is somewhat different.

B. Near vertical on each edge. Total of four drops, since each end has only two unique edges.

C. C.g.-over-end edges. Total of four drops, since each end has only two unique edges.

D. C.g.-over-each corner. Total of two drops, since there is one unique corner per end.

Drops on the Sides (Total of 9)

A. Flat side (package horizontal). Total of two drops, since there are only two unique sides.

B. On side edges (package horizontal). Total of one drop, since all four side-edges are identical.

C. Slapdown on flat side, lid primary. Total of two drops, since there are two unique sides.

D. Slapdown on flat side, lid secondary. Total of two drops, since there are two unique sides.

E. Slapdown on side-edge, lid primary. Total of one drop, since all side-edges are identical.

F. Slapdown on side-edge, lid secondary. Total of one drop, since all side-edges are identical.

Each drop orientation is evaluated to determine whether it is unique and whether it places bounding loads on the package, or represents bounding damage to the containment sealing area that could affect thermal performance. The result of all of these evaluations is summarized in Table 2.7-1 and illustrated in Figure 2.7-1. As documented in Section 2.12.1, *Engineering Tests*, many orientations have been tested in prior testing programs using a half-scale test article. The results of these tests provided a database of information which was used to guide the choice of bounding tests to be performed on the full-scale CTU. Tables 2.12.1-2 through 2.12.1-4 show the extent of previous testing using the half-scale article. The following detailed discussions justify the orientations chosen for certification testing. In the following small figures, a number in parentheses (e.g., *LD1*), indicates that the orientation has been specifically evaluated by full-scale certification testing as summarized in Table 2.7-1. All references in the following paragraphs to prior testing are discussed in more detail in Section 2.12.1, *Engineering Tests*. The test performed on CTU-2 is discussed in Section 2.7.1.1.3, *Free Drop Test on CTU-2*.

2.7.1.1.1 Drops on the Ends

A. Flat End Free Drops (Package Vertical). The overpack construction at each end is essentially identical, and therefore the impacts are considered identical at each end. However, the CSA structure is different at each end: the closed end has 8 mm plates and is continuously connected to the sides, whereas the lid has 12 mm plates and is connected to the sides by closure bolts.

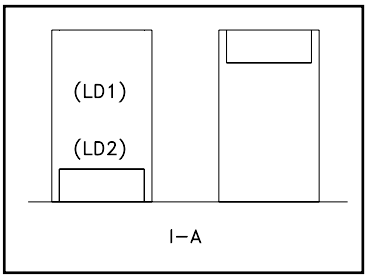

Consequently, the closed end structure is a plate with essentially fixed edges and the lid is a plate which is essentially simply supported. Under a distributed load (such as the payload in a vertical drop), the bending stress at the edges of the closed end is about 50% greater than at the center of the lid. However, the lid flange may rotate and affect the ability of the containment seal to remain leaktight. From these considerations, it is not obvious whether the lid down or closed end down drops would present a bounding case. The lid end down orientation places the greatest loads on the lid structure and on the closure, potentially deforming the sealing area; the closed end down potentially creates bounding stresses in the containment boundary.

During the certification testing of the TN–Gemini in France in 1994, the half-scale test article was dropped 9 m on the closed end with an equivalent full scale impact of 179g. No damage or deformation was noted in the closed end region of the CSA after this, and several subsequent tests. Since the construction of the CSA of the TRUPACT–III package is essentially identical to that of the TN-Gemini, and since the maximum end drop impact of the TRUPACT–III package was of a similar magnitude at 204g, it was not necessary to test the closed end down orientation. The robust nature of the TRUPACT–III package closed end has been adequately demonstrated in the half-scale test. But since the lid end down orientation places the greatest loads on the lid structure and closure, the TRUPACT–III package was tested in a lid-down orientation under maximum-impact (cold) conditions in both the NCT (0.3-m) and HAC (9-m) free drop configurations.

B. Near-Vertical End Free Drops. The impact magnitude drops off rapidly with the off-vertical angle of impact, and consequently the near-vertical impact will be much less than the vertical impact. This was demonstrated in the half-scale tests described in Section 2.12.1.7.2.1, *Free Drop Test No. FD1* and Section 2.12.1.7.2.3, *Free Drop Test No. FD3*. In the bottom-down end drop, the impact occurred at an angle of approximately 6º - 7º from the vertical, with an equivalent full scale impact of 109g. An equivalent impact under the same conditions on the opposite end of the article, in which the orientation was essentially perfectly vertical, and where the impact absorbing structures were essentially identical, was 327g, or three times higher. Therefore, near-vertical impacts have a significantly lower magnitude compared to vertical. Also, since the lid is supported by the overpack cover only in the vicinity of its four corners, it will still be left unsupported near the middle of its four sides, even in a pure vertical drop. Finite element analyses show that the deflections of the lid will be greatest at the middle of the sides. In other words, whether the package orientation is vertical or near vertical, the most vulnerable areas of the closure and sealing structures are unsupported by impact absorbing structures. Therefore, since the forces driving seal area deformation fall off rapidly, even for small off-vertical angles, but the vulnerability of the closure structures are essentially unchanged, the near-vertical end free drops are not bounding and do not need to be performed.

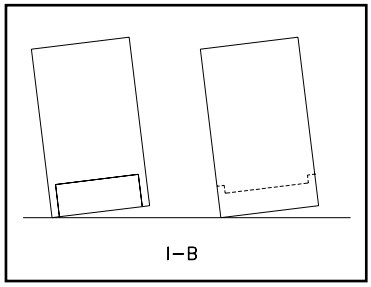
I–B

C. C.g.-Over-End Edges. These orientations provide neither maximum component loading nor maximum seal area stress, as discussed in the section above. Further, the thermally-relevant crush in the seal area is less than the softer corner case discussed below.

If dropped on one edge of the cover, an "overturning moment" might be applied to the cover attachments. However, since the

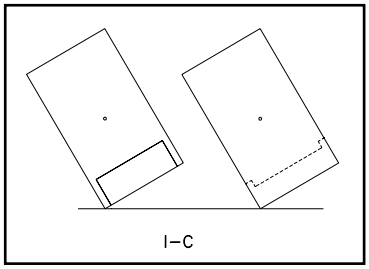
I–C

cover is relatively soft, allowing the crush to be localized, there is no risk of sufficient load transfer to the opposite side so as to fail the cover attachment bolts. This condition was demonstrated in the certification testing described in Section 2.12.1.7.1.4, *Free Drop Test No. A4*, in which a 9-m, c.g.-over-lid-end edge test was performed, without any apparent challenge to the cover attachment. Therefore, this free drop is not bounding and does not need to be performed.

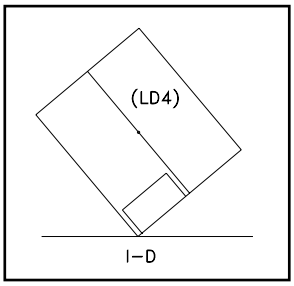

D. C.g.-Over-Corner. This orientation produces the greatest total deformation, since the crushed area is relatively small compared to other orientations. The impact-absorbing structures are essentially identical on each end. However, due to the presence of the thermal shield and associated protective structures on the lid end, the TRUPACT–III package was tested in the lid-down, c.g.-over-corner orientation. This was one of the two orientations producing the greatest thermally-relevant free drop damage (the other is discussed in Section 2.7.1.1.2(B), *Side-Edge Free Drop*). The test was performed at ambient temperature. More deformation would have occurred at maximum NCT temperature, but as shown in Section 2.7.1.5, *Crush Deformation Extrapolations*, the additional deformation caused by the accumulation of damage of this drop with the vertical end drop (see paragraph 2.7.1.1.1(A), *Flat End Free Drops, Package Vertical*) is essentially the same. In other words, the crush damage as measured after the test, including damage accumulation from the two free drops, was essentially the same as if the c.g.-over-corner drop had occurred at maximum NCT temperature without damage accumulation. This test was repeated at the cold, -29 ºC temperature as discussed in Section 2.7.1.1.3, *Free Drop Test on CTU-2*.

2.7.1.1.2 Drops on the Sides

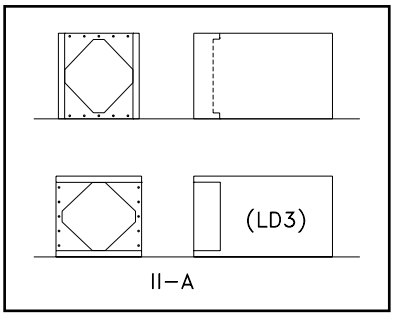

A. Flat Side Free Drops. In these orientations (upper side/bottom side or left side/right side), the wall towards the ground is squeezed by the payload, and the upper flat wall is in bending under its own weight. Impact loads in the left side/right side orientation are bounding due to their slightly larger size. Slapdown is not governing as discussed below. The TRUPACT–III package was dropped on the side opposite the special test ports, with the impact surface horizontal, under maximum-impact (cold) conditions.

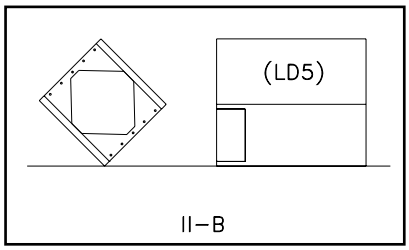

B. Side-Edge Free Drop. In this orientation, the package is horizontal, with one side edge down and the opposite side edge directly above (c.g.-over-edge). This is a single orientation since all four edges are alike. A side-edge drop was performed as described in Section 2.12.1.7.1.9, *Free Drop Test No. A6*. The greatest risk in this orientation is to the thermal insulation shield, since excessive deformation along the crush axis could damage the shield or the thermal insulation behind it. Therefore, the TRUPACT–III package was tested in the side-edge orientation. The test was performed at ambient temperature. To obtain the maximum deformation, the test results were extrapolated to maximum temperatures by analysis as discussed in

Section 2.7.1.5, *Crush Deformation Extrapolations*. This test is discussed further in Section 2.7.1.1.3, *Free Drop Test on CTU-2*.

C. Slapdown on Flat Sides, Lid Primary. There are two orientations, one with the cheeks vertical (normal transport orientation), and one with the cheeks horizontal. The cheeks vertical case would presumably put greater loads on dislodging the cover, but the cheeks horizontal case would be overall a larger load since it represents a slightly larger impact area. Since the difference in side length is less than 6%, the distinction between sides can be ignored, and the orientation of interest is the short side down, with the cover vertical. In this orientation, the apparent loads on cover attachments would be greatest.

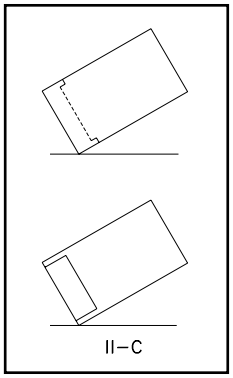

However, the loads on the cover attachments are not significant. Based on the fact that the impact limiting cover is "soft" (see I-C above), the primary impact of the cover will not place any important "moment" loads on the cover. The initial impact is in a direction to drive the cover on, but there will be little moment transfer to the top row of attachment bolts. The loads on the lid itself are bounded in the axial direction by the vertical drop (Section 2.7.1.1.1(B), *Near-Vertical End Free Drops*) and in the lateral direction by the flat side drop (Section 2.7.1.1.2(A), *Flat Side Free Drops*). Therefore, this drop is not bounding and does not need to be performed.

D. Slapdown on Flat Sides, Lid Secondary. Again, there are two orientations, one with the cheeks vertical, and one with the cheeks horizontal. However, since the secondary impact angle is nearly horizontal, very little crush damage is experienced either way, as described in Section 2.12.1.7.2.4, *Free Drop Test No. FD4*. In that test, the crush deformation at the secondary end of the package was only about 50 mm (in equivalent full scale), or less than 2% of the total height of the package. The secondary impact of the package, perpendicular to the ground, was 325g, and decreased rapidly going toward the package center. As a result of changes to the overpack energy absorbing materials, and to the fact that the package is shorter than the one tested previously, the slapdown secondary impact will fall well below 325g, and is instead bounded by the flat side drop discussed in Section 2.7.1.1.2(A), *Flat Side Free Drops*. Since the flat side drop impact will bound the slapdown secondary impact, and since the flat side orientation is essentially the same as the slapdown secondary orientation (i.e., essentially horizontal), the flat side drop bounds the impact conditions of the slapdown drop, particularly at the closure lid, and the slapdown free drop test does not need to be performed.

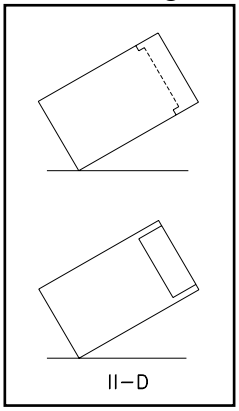

E. Slapdown on Side Edge, Lid Primary. Since the side edge drop is softer in impact than the flat side drop, the impact in this case is not governing. Further, since the c.g.-over-corner end drop puts all of the package energy into a single corner, but the diagonal slapdown divides the energy between corners, the damage to the corner will be governed by the c.g.-over-corner drop (Section 2.7.1.1.1(D), *C.G.-over-Corner*). Therefore, this free drop is not bounding and does not need to be performed.

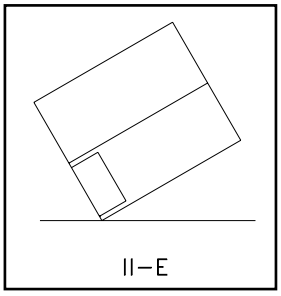

F. Slapdown on Side Edge, Lid Secondary. For the same reasons stated above, neither the crush deformations nor the impacts will be governing, and consequently, this free drop does not need to be performed.

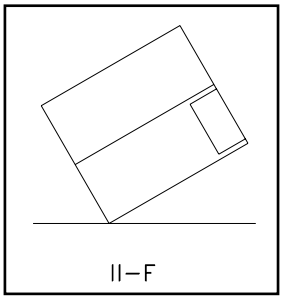

Summarizing the above discussions, the free drop tests performed on CTU-1 were (9-m, HAC unless stated otherwise):

- Vertical, Lid Down (0.3-m, NCT) (Section 2.7.1.1.1(A))
- Vertical, Lid Down (Section 2.7.1.1.1(A))
- C.G.-over-Corner (Section 2.7.1.1.1(D))
- Flat Side (Section 2.7.1.1.2(A))
- Side-Edge (Section 2.7.1.1.2(B))

This information is summarized in greater detail in Table 2.7-1 and depicted in Figure 2.7-1.

2.7.1.1.3 Free Drop Test on CTU-2

As discussed in Section 2.7.8, *Summary of Damage*, the closure lid containment seal of CTU-1 was not leaktight subsequent to the full series of tests. The cause was judged to be the intrusion of internal debris on the sealing surface, but some closure bolts had become bent as well, involving some loss of preload. Therefore the cause could not be ascertained with absolute certainty. A debris shield was added to the design subsequent to the tests on CTU-1. To test the performance of the debris shield and to obtain positive confirmation of the leaktight ability of the package, additional certification testing was required.

During the testing of CTU–1, intermediate vacuum tests of the containment seal were used to track the performance of the package as testing progressed. The vacuum test was successful after the first three free drops (0.3 m NCT free drop LD1, the 9 m end drop LD2, and the 9 m side drop LD3), but not after the last two (the 9 m side–edge drop LD5 and the 9 m c.g.–over–corner drop LD4). Therefore, the one worst–case free drop must be one of those two free drops. All other orientations have been either justified as not requiring test, or successfully tested in either a prior engineering or certification test.

As stated above, the items of concern relative to the leaktight condition of the containment seal are a) the bending of bolts, and b) the function of the debris shield. Therefore, the c.g.–over–corner and the side–edge orientations will be evaluated relative to these considerations. The following discussion relies on the evaluations of CTU-1 presented in Section 2.7.8, *Summary of Damage*.

The bending of the bolts was caused by contact with the overpack cover recess cups. This result was made possible by the sliding motion of the overpack cover during impact deformation. The direction of bolt bending correlated to the 11 o'clock direction, facing the closure lid. The overpack cover would have slid in a direction approximately halfway between 10 and 11 o'clock in the c.g.–over–corner orientation, and in a direction approximately halfway between 7 and 8 o'clock in the side–edge orientation. In both cases, the direction of motion is taken to be in a direction opposite to

the ground, driven by the crush deformation of the overpack structures. Therefore, it is concluded that the c.g.–over–corner orientation was responsible for the bending of the closure bolts.

It is further noted that the driving force for overpack cover motion may be greater in the c.g.–over–corner case. As observed from testing, the deformation of the cover at the corner nearest to the ground in the c.g.–over–corner case (see Figure 2.12.3-19) is significantly larger than for the side–edge case (see Figure 2.12.3-16). The deformation of the cover correlates to the force applied to the cover. Even though the cover is nominally located between fixed bounds (e.g., the limits of the side cheeks and the top and bottom lips of the cover), a larger force has a larger potential for deforming the bounds, and thus moving the cover further, than a smaller force would.

The function of the debris shield is to prevent internal debris from reaching the closure lid containment seal during the impact event. The debris shield is designed to function in the presence of both axial and lateral relative motions of the lid. However, from the design of the debris shield, it is clear that lateral motions in either direction only serve to compress the foam rubber component on one side or the other and improve its function, as shown in Figure 2.12.5-2. Only axial motions could possibly compromise the shield, if the motion exceeds the insertion length of the foam rubber component into the receptacle. Therefore, of the two candidate orientations, the one with the greatest potential for axial motion is clearly the worst case. The side–edge orientation has no component of impact force which is axial to the package; the closure lid is loaded by only its own inertia, in its own plane, against the lid lips. During testing of CTU–1, it was demonstrated that the lid lips and the interfacing body flange were adequate to support the closure lid in the lateral direction against the impact forces of the side–edge free drop. Any lateral motion of the body flange due to outward deformation of the body walls would only compress the debris shield foam rubber as stated above, with no effect on its performance. In the c.g.–over–corner orientation, although the total impact is smaller than the side–edge case, an axial component exists which applies the inertia loading of both the payload as well as the closure lid against the closure joint, creating the potential for some axial relative motion across the debris shield. Therefore, although the axial motion is not expected to come anywhere near the design capacity of the debris shield, the c.g.–over–corner orientation is again judged to be the worst case.

The appropriate temperature of the c.g.–over–corner drop is evident from the preceding considerations. The force applied to the overpack cover, and thus its potential to move far enough to contact the bolt heads and possibly bend the bolts, is greatest for the largest impact load. Likewise, for the greatest axial motion at the debris shield, the greatest deflection of the closure lid will occur with the greatest impact force, which corresponds to the cold case. Therefore the worst–case free drop is the c.g.–over–corner orientation, performed at the cold, -29 ºC condition.

Of the four corners available for the c.g.–over–corner free drop, the bottom left corner should be used. The left side is remote from the side containing the CTU test ports, lowering the likelihood of damage to this important area, needed for leakage rate testing. The bottom side should be used since the possible sliding of the overpack cover is important, and the vertical gap between the overpack cover and the body is present only on the bottom. Since the cover can only slide upward, the impact must therefore be on the bottom corner.

In summary, the worst-case test on CTU-2 was a 9 m, c.g.–over–corner orientation, striking the lower left corner (viewed from the closure end), with the region of deformation at cold temperature (-29 ºC). Two puncture drop tests were also performed on CTU-2 as described in Section 2.7.3, *Puncture*.

2.7.1.2 Certification Test Unit and Test Conditions

CTU-1

CTU-1 was an essentially prototypic representation, in full-scale, of the TRUPACT–III packaging. Any differences between it and the drawings of Appendix 1.3.1, *Packaging General Arrangement Drawings*, were insignificant, and are discussed and justified in Section 2.12.3.3, *Test Unit Configuration*. Since internal pressure has the effect of increasing containment boundary stress, for the free drops the CSA was pressurized at ambient temperature to an internal pressure of 172 kPa, equal to the design pressure. The simulated payload used inside the CTU consisted primarily of a quantity of aluminum bars. Since the structures normally present within the packaging (the payload container(s), the pallet, and the roller floor) may contribute some beneficial energy absorption under impact, these structures were conservatively omitted. However, their weight was included in the simulated payload. The total weight of the test payload was 6,746 kg, which is 29.5% more than the maximum TRUPACT–III payload of 5,210 kg. This condition is particularly conservative for impact loads on the closure lid. The gross weight of the CTU was 25,052 kg, essentially equal to the maximum allowed weight of 25,000 kg.

CTU-2

CTU-2 was an essentially prototypic representation, in full-scale, of the TRUPACT–III packaging. Any differences between it and the drawings of Appendix 1.3.1, *Packaging General Arrangement Drawings*, were insignificant, and are discussed and justified in Section 2.12.6.3, *Test Unit Configuration*. An internal pressure of 172 kPa (ambient basis) was again used. The simulated payload consisted of a prototypic roller floor, pallet, and SLB2 container. The SLB2 was loaded with aluminum bars and weighed 5,543 kg, which is conservatively 16% more than the maximum loaded SLB2 weight of 4,763 kg. The sum of the weight of the contents was 5,974 kg, which is significantly more than the maximum contents weight of 5,210 kg. The total weight of CTU-2 was 25,154 kg, which is essentially equal to the maximum allowed weight of 25,000 kg. To test the performance of the debris shield, approximately one quart of fine, granular debris was dumped into the payload cavity (external to the SLB2) prior to installing the closure lid.

The significance of temperature, and the choice of temperature for each free drop test, is discussed in Section 2.7.1.1, *Technical Basis for the Free Drop Tests*. For cold temperature tests, the temperature of the polyurethane foam energy absorbing material which was crushed in each case was at a temperature of -29 ºC or less. Foam material which was outside the region of crushing deformation in a given impact orientation was not required to be at this temperature. For ambient temperature tests, the foam material experiencing crush was required to be at least +7 ºC at impact.

The certification testing took place at the Sandia National Laboratories. For CTU-1, the tests occurred between November 1 and November 10, 2006. For CTU-2 the tests occurred on November 20, 2009. A discussion of the test facilities and CTU instrumentation is provided in Section 2.12.3.2, *Test Facilities*.

2.7.1.3 Test Criteria

The following are the acceptance criteria for both the free drop and puncture drop testing of the TRUPACT–III package:

1. When combined with damage due to the puncture test (see Section 2.7.3, *Puncture*), the worst-case sequence of free drop and puncture damage must not affect the ability of the containment boundary to remain leaktight per ANSI N14.5[2], as demonstrated by post-test leakage rate testing. Since several free drop and puncture tests were performed on CTU-1 and CTU-2, the containment boundary must be leaktight at the conclusion of all free and puncture drop testing.
2. The worst-case combination of free drop and puncture damage must not be of such a magnitude that the maximum temperature limit of the containment seals or of the CSA material would be exceeded in a subsequent HAC fire.

2.7.1.4 Summary of Results of the Free Drop Analyses and Tests

The results of each of the free drops evaluated are described below indicating the reference number as listed in Table 2.7-1. Under each heading, the results of the free drop test are described. A detailed test description, test results, and photographs are given in Appendix 2.12.3, *Certification Tests on CTU-1* and in Appendix 2.12.6, *Certification Tests on CTU-2*. The discussion below begins with test LD2, since the results of the NCT free drop, test LD1, are discussed in Section 2.6.7, *Free Drop*. Post-test leakage rate testing demonstrated that the containment metallic boundary and vent port insert O-ring seal remained leaktight per ANSI N14.5 after the conclusion of all certification testing for both CTU-1 and CTU-2, and the closure lid O-ring seal remained leaktight per ANSI N14.5 for CTU-2. The closure lid O-ring seal of CTU-1 did not meet the leakage rate criteria of ANSI N14.5, most likely due to the presence of debris in the sealing nip[3]. The debris shield, which was not present in CTU-1, is analytically evaluated in Section 2.12.5, *Closure Lid Debris Shield*. The debris shield was present in CTU-2, and was evaluated in free drop test LD91.

The closure bolt washers used on CTU-1 were made from Type 304 stainless steel. The material used for CTU-2 and subsequent production units is ASTM A564 Grade 630 H1025 (17-4 PH) precipitation hardened stainless steel. A finite element evaluation of the function of the closure bolt washer under high loads is given in Appendix 2.12.7, *Closure Lid, Bolt, and Washer Interaction*. This analysis shows that, if the closure joint were to be loaded up to the yield load of the bolt shank, the washer made of 17-4PH material would not experience any permanent deformation.

2.7.1.4.1 Vertical, Lid Down Free Drop Results (CTU-1, Ref. No. LD2)

The TRUPACT–III CTU was dropped at a foam material temperature of approximately -34 ºC and with an internal pressure of 172 kPa. The CTU struck the ground on the end face of the overpack cover and cheeks. The resulting impact was 204g. The axial crush from test LD2 was 29 mm. This combined with the crush from test LD1 of 7 mm for a total of 36 mm of axial crush from the two

[2] ANSI N14.5–1997 (or later), *American National Standard for Radioactive Materials – Leakage Tests on Packages for Shipment,* American National Standards Institute, Inc. (ANSI).

[3] After removal of the debris, the closure lid containment O-ring seal did pass the ANSI N14.5 criteria in two separate tests: one using a torque of only 149 N-m on all 44 bolts (9.3% of the nominal preload torque of 1,600 N-m) and a second test, using a torque of 149 N-m on only the four corner bolts. Of note, all leakage rate tests performed subsequent to the removal of the debris passed the criteria. These leakage rate tests are discussed fully in Section 2.7.8.2, *Closure Bolts*.

tests. Some cracks occurred in the welds of the overpack cover near the corners of the octagonal opening in the cover, ranging from approximately 51 mm to 152 mm in length. Small cracks and deformations occurred close to the ISO fittings due to the translation of the stiff fittings relative to the cheeks. In addition, the impact load was carried into the overpack cover attachment flange on the body, and caused some deformation and outward bending of the body top and bottom outer shell sheets. Overall, however, deformation of the CTU was modest from the test. As shown from measurements of the payload cavity before and after all testing, there was no indication of any buckling behavior in the CSA structure (see Section 2.12.3.8.2, *CTU Measurements*).

2.7.1.4.2 Flat Side Free Drop Results (CTU-1, Ref. No. LD3)

The TRUPACT–III CTU was dropped at a material temperature of approximately -39 ºC and with internal pressure of 172 kPa. The resulting impact was 407g. As expected given the large impact surface, the impact magnitude was relatively high, and the deformations correspondingly small. Other than a few more weld cracks around the ISO corners, there was essentially no externally identifiable damage. By means of four small drilled holes, it was determined that the CSA moved toward the impact surface by approximately 7 mm, by inside-out action. This movement could be accommodated by relatively small deformations of internal structures. There was no indication of contact of the lid shear lip with the body flange in this test.

2.7.1.4.3 CG-Over-Corner Free Drop Results (CTU-1, Ref. No. LD4)

For convenience in rigging the package during the free drops, test LD4 was performed after test LD5. The TRUPACT–III CTU was dropped at a material temperature of approximately +12 ºC and with internal pressure of 172 kPa. The resulting impact and deformation, perpendicular to the ground, was 53g and 323 mm, respectively. The deformation was calculated from the measurements of the triangular crushed surface, as follows. The three sides of the triangle (i.e., the plane of contact with the ground) were: a = 800 mm, b = 838 mm, and c = 1,054 mm. The area of the triangle was (noting that angle A is opposite side a, B opposite side b, and C opposite side c, and A1 is the area of the crush plane):

$$A = \cos^{-1}\frac{b^2 + c^2 - a^2}{2bc} = 48.386°$$

$$B = \sin^{-1}\frac{b}{a}\sin A = 51.550°$$

$$C = 180 - A - B = 80.064°$$

$$A1 = \frac{ab}{2}\sin C = 330{,}172\ \text{mm}^2$$

From Section 2.7.1.5.1, *CG-Over-Corner Free Drop Extrapolation*, the crush distance and the area of the crush plane are related by:

$$A1 = \frac{d^2}{2\sin^2\theta\cos\theta}\left[\frac{H}{W} + \frac{W}{H}\right]$$

from which the crush distance, d, is:

$$d = \left(A1 \sin^2\theta \cos\theta\right)^{1/2} = 323 \text{ mm}$$

where, since the package height, H = 2,650 mm and width, W = 2,500 mm, the term in brackets cancels the numeral 2 in the denominator, and the angle of impact of the end face to the ground is θ = 90 – 50 = 40º.

The combined damage from all of the free drops caused a slight bowing of the right cheek, and a gap of up to 76 mm at the center between the cheek and the overpack cover right edge. The gap was however blocked with buckled material starting about 89 mm deep into the gap, and the gap reduced to zero width at the top and bottom of the cheek-to-cover joint. No significant weld seam failures were noted from this test, and no significant exposure of foam was found.

The free crush distance (i.e., the length of crushable material in the direction of impact) is calculated between the struck corner and the corner of the 16-mm thick box which surrounds the calcium silicate insulation (i.e., the thermal shield). In calculating this distance, only polyurethane foam is considered. Any intervening steel sheets and the entire lift point structure (even though hollow and not rigid) are conservatively excluded. First, the distance along the three primary coordinate axes (axial = T_X; lateral = T_Y; and vertical = T_Z) are calculated.

T_X: From the SAR drawings given in Section 1.3.1, *Packaging General Arrangement Drawings*, Sheet 9, Section AN-AN, the length of the cheek is 870 mm. After subtracting the thermal shield length of 334 mm, the lift point length of 178 mm, the rear sheet of the lift point of 6 mm, and the thickness of the chevron shaped piece of 6 mm, the remaining axial crushable distance is $T_X = 870 – 334 – 178 – 6 – 6 = 346$ mm.

T_Y: From the SAR drawing Sheet 6, Section G-G (lower left corner of view), the full thickness of the overpack side region is equal to 190 mm. After subtracting the inner and outer side sheet thickness of 6 mm and 8 mm, respectively, the thermal shield of 16 mm, and the insulation board of 30 mm, the remaining crushable distance on the side is $T_Y = 190 – 6 – 8 – 16 – 30 = 130$ mm.

T_Z: The overall height of the package is 2,650 mm. After subtracting the height of the thermal shield of 2,436 mm (from SAR drawing Sheet 5, Section F-F), dividing by two, and subtracting the outer sheet thickness of 8 mm, the remaining crushable distance vertically is:

$$T_Z = \frac{2{,}650 - 2{,}436}{2} - 8 = 99 \text{ mm}$$

The diagonal distance from the outer corner of the thermal shield to the inner corner of the overpack (i.e., in a plane perpendicular to the package axis) is:

$$T_{YZ} = \left(T_Y^2 + T_Z^2\right)^{1/2} = 163 \text{ mm}$$

The shortest crushable distance from the inner surface at the c.g. over corner impact point to the thermal shield corner is:

$$T = \left(T_X^2 + T_{YZ}^2\right)^{1/2} = 382 \text{ mm}$$

The angle between the end face of the package and hypotenuse T is:

$$\lambda = \tan^{-1}\left(\frac{T_X}{T_{YZ}}\right) = 64.8^\circ$$

In the c.g.-over-corner orientation, the angle between the end face and the ground is θ = 40º, as stated above. Therefore, during impact, the angle between the distance T and the vertical is equal to δ = θ + λ – 90 = 14.8º. The total crushable distance along the line of impact is equal to:

$$D = T\cos(\delta) = 369 \text{ mm}$$

The distance of crush in test LD4 was equal to 323 mm, and as shown in Section 2.7.1.5.1, *CG-Over-Corner Free Drop Extrapolation*, does not require correction for maximum NCT temperature. The remaining crush distance is equal to 369 – 323 = 46 mm. The amount of available crush used in the worst case is:

$$\frac{323}{369} \times 100 = 87.5\%$$

This amount of crush is acceptable since it represents only the minimum at the corner point, and is much larger elsewhere.

2.7.1.4.4 Side-Edge Free Drop Results (CTU-1, Ref. No. LD5)

For convenience in rigging the package during the free drops, test LD5 was performed before test LD4. The TRUPACT–III CTU was dropped at a material temperature of approximately +7 ºC and with internal pressure of 172 kPa. The resulting impact, perpendicular to the ground, was 142g. The deformation is found from:

- The initial clear distance between the inside of the edge and the near corner of the calcium silicate protection box (i.e., thermal shield), found above as T_{YZ} = 163 mm
- The measured distance between the inside of the crush surface and the near corner of the thermal shield after test, $T_{Remaining}$ = 95 mm

The crush deformation distance was therefore $T_{YZ} - T_{Remaining}$ = 68 mm.

During the impact, a length of the weld at the front edge of the large outer side sheet on the right side of the CTU opened up for a distance of approximately 914 mm. The fissure started in the folded region associated with the side-edge deformation. The maximum opening distance was approximately 51 mm. The opening exposed the forward edge of the outer layer of balsa wood. The puncture-resistant plate, the underlying 0.10 kg/dm^3 foam, and the CSA were not affected. The weld was specified to be 6-mm full penetration, but examination of the failed edges of the fissure revealed that penetration was typically only half of this value. The inadequate weld penetration was traced to the process and technique used. For production units, the weld process and technique will be changed to ensure full penetration occurs on all TRUPACT-III welds. As discussed in Section 3.5.2.6, *Description of Thermal Model for HAC Conditions*, the thermal fire analysis conservatively assumes that the worst case puncture damage occurred directly on this weld fissure.

As stated above, the remaining free distance between the inside of the crushed surface and the nearest corner of the thermal shield, which is taken as a "hard corner", was measured to be 95 mm. As shown in Section 2.7.1.5.2, *Side-Edge Free Drop Extrapolation*, the crush distance must be increased by 30 mm to account for the effect of maximum NCT temperature. The crush deformation distance calculated above is 68 mm. Under NCT maximum temperature conditions the distance is 68 + 30 = 98 mm. The amount of available crush used in the worst case is:

$$\frac{98}{163} \times 100 = 60\%$$

This amount of crush is well within the capability of the foam to provide a margin of safety on crush distance as well as thermal protection in the HAC fire.

2.7.1.4.5 CG-Over-Corner Free Drop Results (CTU-2, Ref. No. LD91)

CTU-2 was dropped at a material temperature of -33.6 ºC and with internal pressure of 172 kPa (at ambient). The resulting impact, perpendicular to the ground, was 80.8g. As in the case of the c.g.-over-corner drop on CTU-1, the deformation surface was a triangle with lengths 737 mm along the overpack cover, 864 mm along the bottom, and 787 mm along the left side of the CTU. Since these values are less than those for the CTU-1 test (as expected, since the CTU-1 test was performed at a temperature of approximately +12 ºC), the crush deformation is less than that of the prior test and not bounding. Consequently the crush extrapolation performed in Section 2.7.1.5.1, *CG-Over-Corner Free Drop Extrapolation*, remains bounding. No significant weld seam failures or exposed foam was noted.

After the test, a vacuum was applied to the annulus between the two O-rings in the closure lid. The lowest vacuum achieved was below 200 millitorr, indicating a good seal. After the two subsequent puncture tests, a helium leakage rate test was performed, and the leakage rate of the containment boundary, the closure lid containment seal, and the vent port seal met the leaktight criteria of ANSI N14.5. Detailed test results are given in Appendix 2.12.6, *Certification Tests on CTU-2*.

2.7.1.5 Crush Deformation Extrapolations

Since two of the free drops on CTU-1 (the c.g.-over-corner free drop, ref. no. LD4, and the side-edge free drop, ref. no. LD5) were performed in order to obtain the worst-case deformation damage, the damage actually incurred at the test temperature must be extrapolated to the damage that would occur at maximum NCT temperatures.

2.7.1.5.1 CG-Over-Corner Free Drop Extrapolation

The damage present after the c.g.-over-corner free drop (LD4) includes the damage incurred during the two vertical, lid down free drops (ref. nos. LD1, NCT and LD2, HAC). The following analysis shows that the combination of damage from the c.g.-over-corner free drop (performed at ambient temperature) and the vertical, lid down free drops (performed at cold temperature) is essentially the same as would occur from the c.g.-over-corner free drop alone, if performed at the maximum NCT temperature. In other words, the damage observed in the certification testing is equivalent to the maximum damage which could occur if the c.g.-over-corner free drop were performed alone at NCT temperature.

Energy is absorbed in the c.g.-over-corner orientation by the deformation of the outer steel shell, by the crush of the forward slab (140-mm thick) of low density, 0.16 kg/dm^3 foam, and by the crush of the internal block of high density, 0.48 kg/dm^3 foam. Each of these quantities can be calculated by knowing the geometry of the package, the crush strength of the crushable media,

and the deformation force of the steel. The latter quantity is calculated using the test results from the engineering testing of the half-scale test unit.

Since the increment of shell deformation energy is equal to the crush area perimeter times the deformation force per unit length times the crush increment, the total energy absorbed by the deformation of the shell is equal to the crush area times the deformation force per unit length, or:

$$E_s = AF$$

where A is the crush area and F is the force to deform the steel shell per unit length. Similarly, since the increment of foam crush energy is equal to the crush area times the crush stress times the crush increment, the total energy absorbed by crush of the foam is equal to the total crushed volume times the crush stress, or:

$$E_c = V\sigma$$

where V is the total volume of the crushed region, and σ is equal to the foam crush strength.

Next, the relation between the crush area, A, the crushed volume, V, and the crush depth, d, will be determined. From the left side of Figure 2.7-2, which is a depiction of a diagonal section of the package during impact, the crush distance perpendicular to the ground is d. The measurement of the crushed region parallel to the package side-edge is h. It may be seen that:

$$h = \frac{d}{\cos\theta}$$

where θ is the orientation of the package, defined as the angle between the ground and the end face. From the right side of the figure, which depicts the crush area projected onto the undeformed package end face, the two areas A_1 and A_2 are:

$$A_1 = \frac{1}{2}a^2 \tan\alpha$$

$$A_2 = \frac{1}{2}a^2 \tan\beta$$

where:

$$a = \frac{d}{\sin\theta}, \qquad \tan\alpha = \frac{H}{W}, \qquad \tan\beta = \frac{W}{H}$$

On the plane of the package end face, the total area affected by impact is:

$$A_B = A_1 + A_2 = \frac{d^2}{2\sin^2\theta}\left[\frac{H}{W} + \frac{W}{H}\right]$$

The crushed volume is a wedge-shaped pyramid. One large face of the pyramid (on the ground) is area A_B, and which is associated with a height of h. The other large face (on the package) is the crush area, A, associated with height d. Since the volume of any pyramid is equal to (1/3) × baseplane area × height, then:

$$V = \frac{1}{3}A_B h = \frac{1}{3}Ad$$

This may be rearranged to give:

$$A = \frac{A_B h}{d}$$

Substituting for h and d:

$$A = \frac{d^2}{2\sin^2\theta\cos\theta}\left[\frac{H}{W} + \frac{W}{H}\right]$$

Since the package height, H = 2,650 mm and the width, W = 2,500 mm, it can be seen that the term in brackets cancels the numeral 2 in the denominator, and the area can be simplified to:

$$A = \frac{d^2}{\sin^2\theta\cos\theta} = C_A d^2$$

By integration, the volume is:

$$V = \frac{Ad}{3} = \frac{d^3}{3\sin^2\theta\cos\theta} = C_V d^3$$

In a HAC free drop, the low density material local to the impact is fully crushed, and a maximum stroke of 80% of its thickness may be assumed. Therefore the usable crush distance (parallel to dimension d) in the low density material is:

$$T = 0.8T_B\cos\theta$$

where T_B is the axial thickness of the low density material, or 140 mm.

It is now possible to state the energy relationships in the c.g.-over-corner impact as follows:

$$W(9.81)(9+d) = C_V\sigma_{LD}\left[d^3 + (d-T)^3\right] + C_V\sigma_{HD}(d-T)^3 + C_A F d^2$$

where the term on the left is the total impact energy of the package, and the terms on the right are the energy absorbed by the low density foam, the energy absorbed by the high density foam, and the energy absorbed by the steel shell, respectively. Notations not previously defined are:

W = package mass, kg

σ_{LD} = crush strength of low density material, N/m^2

σ_{HD} = crush strength of high density material, N/m^2

F = deformation force of the steel shell, N/m

The c.g.-over-corner angle defined above is readily calculated by noting that it is equal to the angle between the package diagonal and the vertical. The end face diagonal is:

$$x_d = \sqrt{H^2 + W^2} = 3{,}643 \text{ mm}$$

The c.g.-over-corner angle is:

$$\theta = \tan^{-1}\left(\frac{x_d}{L}\right)$$

where L is the package length. For the TN Gemini, L = 6,058 mm, and $\theta_G = 31°$. For the TRUPACT–III, L = 4,288 mm, and $\theta_{TP3} = 40.4°$.[4]

In order to evaluate the above equation, the crush strengths of the crushable materials and the deformation strength of the steel shell need to be evaluated. As stated above, the deformation strength of the steel shell is found using the above equation with known parameters, including total crush distance, from a prior engineering test. The crushable media strengths are evaluated as follows. Since the engineering test in question used redwood and balsa, an evaluation of these materials is needed, as well as an evaluation of the foams used in the TRUPACT–III.

All of the crushable materials have orthotropic properties (axes of orthotropy being parallel or perpendicular, respectively, to the grain or rise of the material.) The crush strength at a given intermediate angle is found using the well-known Hankinson formula[5]:

$$\sigma_\theta = \frac{\sigma_{par}\sigma_{per}}{\sigma_{per}\sin^2\theta + \sigma_{par}\cos^2\theta}$$

where σ_{par} is the strength parallel to the grain or rise, σ_{per} is the strength perpendicular to the grain or rise, and θ is the orientation angle.

The engineering test is described in Section 2.12.1.7.1.6, *Free Drop No. C7*. In that test, a half-scale test unit was dropped 9-m in the c.g.-over-corner orientation at ambient temperature. The configuration of the steel in the cheeks and overpack cover were essentially identical to that of the TRUPACT–III. For this reason, the results of this test can be used to obtain the average steel deformation force. The unit was fabricated with materials having crush strengths shown in the table below. The aggregate crush strengths in the drop orientation are calculated using the Hankinson formula with an orientation angle of 31°. To account for the dynamic effect, the static strengths were multiplied by a factor of 1.5[3].

Material	Crush strength parallel to grain, MPa	Crush strength perpendicular to grain, MPa	Crush strength, Hankinson, 31°, MPa	Including dynamic factor of 1.5, MPa
Balsa	8	1	2.80	$\sigma_{LD} = 4.20$
Redwood	46	10	23.5	$\sigma_{HD} = 35.3$

Using an angle of $\theta_G = 31°$ and the formulas above, the area coefficient, $C_A = 4.40$, and the volume coefficient, $C_V = 1.47$. In full scale, the mass of the test unit would have been 30,000 kg, and the front slab thickness, $T_B = 0.14$ m. The crush distance in the direction of the drop, in full scale, was d = 0.36 m. Using these parameters, the energy equation can then be solved for a steel deformation force of $F = 2.85(10^6)$ N/m.

It now remains to compare the deformation under certification test conditions with the deformation under NCT maximum temperature conditions using TRUPACT–III-specific parameters. The

[4] This result assumes the c.g. is at the geometric center of the package. As shown in Section 2.1.3, *Weights and Centers of Gravity*, it is actually shifted slightly towards the overpack cover end. However, since the effect of this shift on the c.g.-over-corner angle is only about 2°, it may be neglected for the purposes of this analysis.

[5] Cramer, Steven M., Hermanson, John C., and McMurtry, Wayne M., *Characterizing Large Strain Crush Response of Redwood*, SAND96-2966, Sandia National Laboratories, December 1996.

polyurethane foam crush strengths are found under dynamic conditions from the foam manufacturer's data, and are listed in the table below. Each value represents the average of crush strengths at 20, 30, and 40% strain. The average foam temperature during the c.g.-over-corner certification test (LD4) was 12 ºC, and for the NCT maximum temperature, 60 ºC is used, which is conservatively higher than the bulk average temperature of the foam in the cheek of 49.7 ºC recorded in Chapter 3, Table 3.1-1. The angle used in the Hankinson formula for the TRUPACT–III is 41º, which is sufficiently close to the angle of $\theta_{TP3} = 40.4º$ found above. Finally, the maximum temperature foam crush strength is further conservatively modified by a factor of 0.9, which reflects the minimum crush strength tolerance allowed on the foam, while the foam strength at test temperature is based on the actual density of the foam taken from the fabrication records of the CTU.

Foam, kg/dm^3	Crush strength parallel to rise, σ_{par}, MPa	Crush strength perp. to rise, σ_{per}, MPa	Crush strength, used, σ_θ, MPa (Hankinson @ 41º)
Test foam at 12 ºC, dynamic, actual density basis			
0.16	3.77	3.63	$\sigma_{LD} = 3.71$
0.47	30.1	32.7	$\sigma_{HD} = 31.2$
NCT max temp (60 ºC), dynamic, min strength basis (90% of nominal)			
0.16	2.74	2.55	$\sigma_{LD} = 2.65$
0.48	18.2	20.1	$\sigma_{HD} = 18.9$

Using an angle of $\theta_{TP3} = 40.4º$ and the formulas above, the area coefficient, $C_A = 3.13$, and the volume coefficient, $C_V = 1.04$. The mass of the TRUPACT–III CTU was 25,052 kg, and the front slab thickness, $T_B = 0.14$ m. For the maximum temperature case, the steel force F is reduced by 5% based on the difference between the steel flow stress (that is, the average of yield and ultimate strength) at temperatures of 38 ºC and 93 ºC, using data from Table 2.2-1. The value of the steel deformation force, F, at maximum NCT temperature is then:

$$F_{HOT} = F(0.95) = 2.71(10^6)\,N/m$$

Using these parameters, the crush distance in the ambient, actual strength case is d = 386 mm, and in the maximum NCT temperature, minimum strength case, d = 420 mm. Note that these values are not certification test predictions, but analytical results which can be compared with each other on the same basis. The difference between these results is the additional crush distance which would be expected to occur if the CTU had been tested using minimum strength foam at maximum NCT temperature, and is equal to 420 – 386 = 34 mm.

However, as shown in Section 2.7.1.4.1, *Vertical, Lid Down Free Drop Results*, the measured deformation (along the package axis) from the sum of end drop tests LD1 and LD2 was 36 mm. Along the line of action of the c.g.-over-corner free drop, the value is:

$$d = 36\cos(\theta_3) = 27.4 \text{ mm}$$

That is, the c.g.-over-corner free drop damage as actually measured on the CTU is 27.4 mm greater than if the c.g.-over-corner free drop had been performed on a "virgin" corner. Since difference between the additional damage due to maximum NCT temperature (34 mm) and the additional damage due to the prior free drop (27.4 mm) is only 6.6 mm, it may be neglected.

Thus, the actual measured crush of the CTU subsequent to the c.g.-over-corner free drop (LD4) does not require further adjustment.

2.7.1.5.2 Side-Edge Free Drop Extrapolation

The damage present after the side-edge free drop includes some damage incurred during the two vertical, lid-down drops, but since the damage is relatively small and since the end drop damage is at right angles to the side-edge damage, its effect is negligible and may be conservatively neglected. The procedure in this case is similar to the c.g.-over-corner case. First, the effect of the steel is found using engineering test results. Then, crush results at ambient, actual-strength conditions are calculated and compared to crush results at maximum NCT temperature, minimum-strength conditions. The difference between these two results is the added crush which would be expected to occur under worst case conditions.

In the side-edge orientation, one long edge is down, and the diagonally opposite edge is at the top. Since the height and width of the package are nearly the same, an angle of 45º is assumed for analysis purposes. Energy is absorbed by the deformation of the outer steel shell, and by the crush of the following foam components:

- The two end slabs of 0.16 kg/dm^3 foam, each 140 mm long, perpendicular to rise. (Low density balsa was used in the engineering test.)
- Two sections of 0.48 kg/dm^3 foam, 722 mm (front) and 682 mm (rear) long, 45º to rise. (Redwood was used in the engineering test, perpendicular to grain.)
- One section of 0.29 kg/dm^3 foam, 2,574 mm long, parallel to rise (High density balsa, 4,344 mm long, equivalent full-scale, was used in the engineering test.)

The side-edge orientation free drop test was performed on the half-scale test unit at ambient temperature as described in Section 2.12.1.7.1.9, *Free Drop No. A6*. The equivalent full-scale deformation was 138 mm and the impact was 112g. The crush strengths of the various wood components are shown in the table below. (Since crush takes place either parallel or perpendicular to the grain, strengths are given only in the relevant directions.) As for the c.g.-over-corner analysis, a dynamic increase factor of 1.5 is applied to the static strengths.

Material	Crush strength parallel to grain, MPa	Crush strength perpendicular to grain, MPa	Including dynamic factor of 1.5, MPa	Length, mm
LD balsa	N/A	1	$\sigma_1 = 1.50$	$L_1 = (2 \times 140) = 280$
Redwood	N/A	10	$\sigma_2 = 15.0$	$L_2 = (722 + 682) = 1{,}404$
HD balsa	12	N/A	$\sigma_3 = 18.0$	$L_3 = 4{,}344$

As shown in Section 2.7.1.5.1, *CG-Over-Corner Free Drop Extrapolation*, the total energy absorbed by the deformation of the shell is:

$$E_s = AF$$

and the total energy absorbed by the crush of foam (or wood) is:

$$E_c = V\sigma$$

As shown in Figure 2.7-3, the area of crush is equal to 2dL, where L is the total length of the package. By integration, the volume is equal to d^2L, or for a particular crush component, equal to d^2L_x, where L_x represents the length of the component. For example, the energy absorbed by a single wood component having a length L_x and a crush strength σ_x would be:

$$E_x = d^2 L_x \sigma_x$$

The energy relationships in the side-edge impact are therefore as follows:

$$W(9.81)(9+d) = d^2(L_1\sigma_1 + L_2\sigma_2 + L_3\sigma_3) + 2d(L_1 + L_2 + L_3)F$$

where the term on the left is the total impact energy, the first term on the right is the crush energy for the three components, and the second term on the right is the steel deformation energy. W is again the package mass of 30,000 kg, and F is the steel deformation force per unit length.

Using these parameters and a deformation distance of 138 mm, the energy equation can be solved for a steel deformation force of $4.70(10^5)$ N/m. (This value is less than the corresponding c.g.-over-corner case since the majority of the steel deformation strain in the side-edge case is much less severe.) As a check, the impact force can be found from:

$$I = [2d(L_1\sigma_1 + L_2\sigma_2 + L_3\sigma_3) + 2(L_1 + L_2 + L_3 + 2d)F]/W = 114g$$

which compares well with the equivalent full-scale engineering test average impact of 112g.

It now remains to compare the deformation under certification test conditions with the deformation under NCT maximum temperature conditions using TRUPACT–III-specific parameters. The polyurethane foam crush strengths are found under dynamic conditions from the foam manufacturer's data[6], and are listed in the table below. Each value represents the average of crush strengths at 20, 30, and 40% strain. The foam temperature during the side-edge certification test (LD5) was 7 ºC, and for the NCT maximum temperature, 60 ºC is used, which is conservatively higher than the bulk average temperature of the foam of 50 ºC for the package body recorded in Chapter 3, Table 3.1-1. The maximum temperature foam crush strength is further conservatively modified by a factor of 0.9, which reflects the minimum crush strength tolerance allowed on the foam, while the foam strength at test temperature is based on the actual density of the foam taken from the fabrication records of the CTU.

[6] *General Plastics Last-a-Foam® FR-3700 for Crash and Fire Protection of Nuclear Material Shipping Containers*, General Plastics Manufacturing Company.

Foam, kg/dm^3	Crush strength parallel to rise, MPa	Crush strength perpendicular to rise, MPa	Crush strength, used, MPa	Basis
Test foam at 7 ºC, dynamic, actual density basis				
0.16	3.96	3.78	$\sigma_1 = 3.78$	Perpendicular to rise
0.47	30.6	33.5	$\sigma_2 = 32.0$	Hankinson formula at 45º
0.27	11.1	11.2	$\sigma_3 = 11.1$	Parallel to rise
NCT max temp (60 ºC), dynamic, min strength basis (90% of nominal)				
0.16	2.74	2.55	$\sigma_1 = 2.55$	Perpendicular to rise
0.48	18.2	20.1	$\sigma_2 = 19.1$	Hankinson formula at 45º
0.29	8.36	8.54	$\sigma_3 = 8.36$	Parallel to rise

Similar to Section 2.7.1.5.1, *CG-Over-Corner Free Drop Extrapolation*, the steel force, F, in the maximum temperature case is reduced by 5% as follows:

$$F_{HOT} = F(0.95) = 4.465(10^5)\,N/m$$

Component lengths L_1 and L_2 are the same as in the engineering test, but L_3 = 2,574 mm in the TRUPACT–III case. Using these parameters, the crush distance in the ambient, actual strength case is d = 149 mm, and in the maximum NCT temperature case, d = 179 mm. Note that these values are not certification test predictions, but analytical results which can be compared with each other on the same basis. The difference between these results is the additional crush distance which would be expected to occur if the CTU had been tested using minimum strength foam at maximum NCT temperature, and is equal to 179 – 149 = 30 mm.

Table 2.7-1 – Summary of Free Drops Performed on the TRUPACT–III

Test Description①	Discussion Paragraph	Test Ref. No.②	Test Temperature③	Purpose
Vertical, Lid Down, (NCT 0.3-m, CTU-1)	Section 2.7.1.1.1(A)	LD1	Cold	Test closure lid attachments & O-ring seal area under maximum NCT impact conditions.
Vertical, Lid Down, HAC (CTU-1)	Section 2.7.1.1.1(A)	LD2	Cold	Test closure lid attachments & O-ring seal area under maximum impact conditions.
Flat Side (CTU-1)	Section 2.7.1.1.2(A)	LD3	Cold	Test closure lid attachments, O-ring seal area, lid lateral support, and unsupported wall under maximum impact conditions.
C.G.-over-Corner (CTU-1)	Section 2.7.1.1.1(D)	LD4	Ambient	Quantifies maximum crush for use in thermal analysis
Side-Edge (CTU-1)	Section 2.7.1.1.2(B)	LD5	Ambient	Quantifies maximum crush for use in thermal analysis
C.G.-over-Corner (CTU-2)	Section 2.7.1.1.3	LD91	Cold	Test debris shield and confirm ability to remain leaktight in worst-case free drop

Notes:

① The free drop distance was equal to 9-m, except when stated otherwise.

② The test sequence on CTU-1 was: LD1, LD2, LD3, LD5, LD4.

③ In this column, *cold* means -29 ºC or less. The conversion of ambient temperature results to maximum NCT temperature results is discussed in Section 2.7.1.5.1, *Crush Deformation Extrapolation*.

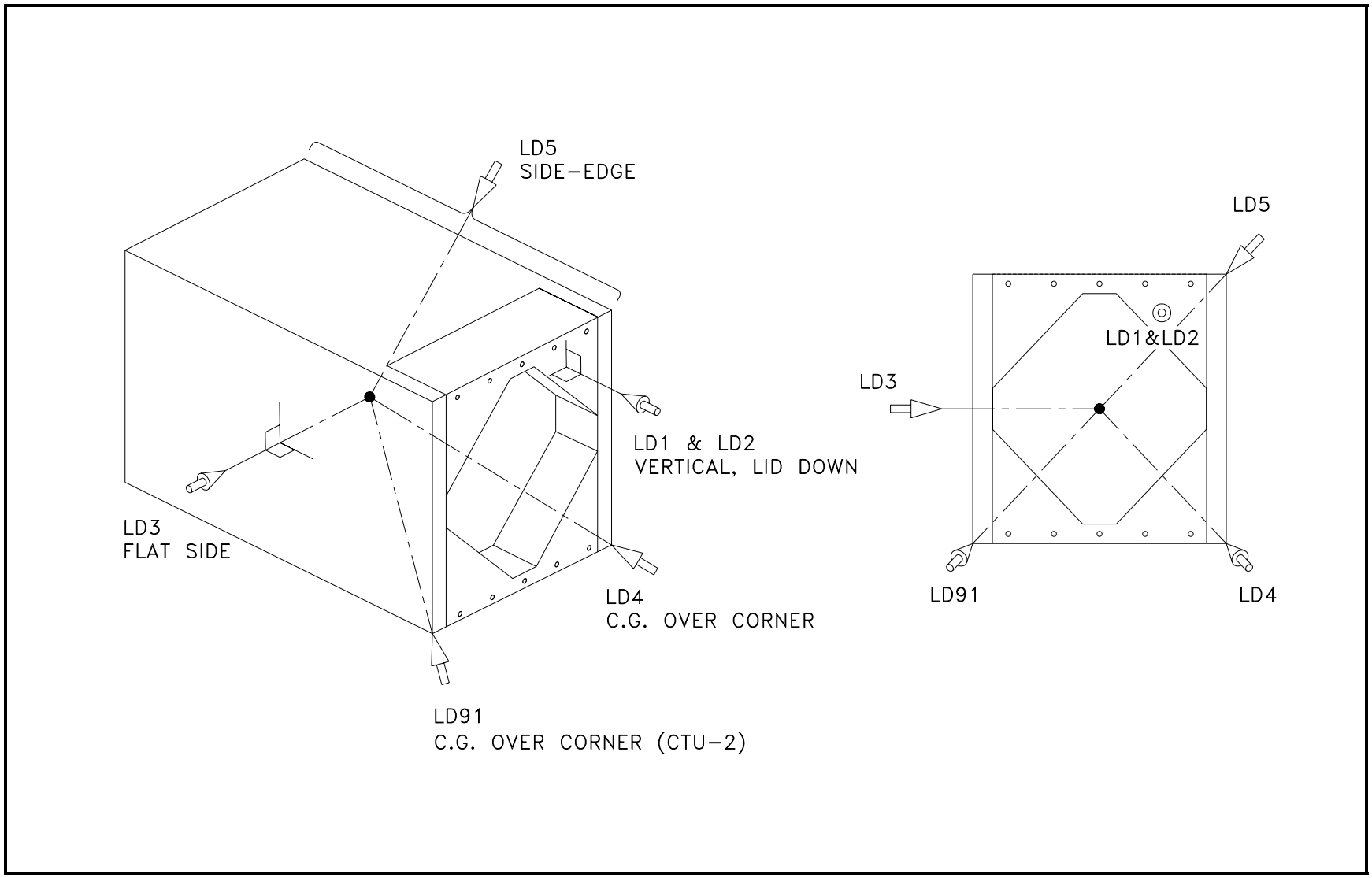

Figure 2.7-1 – Schematic of TRUPACT–III Free Drop Orientations

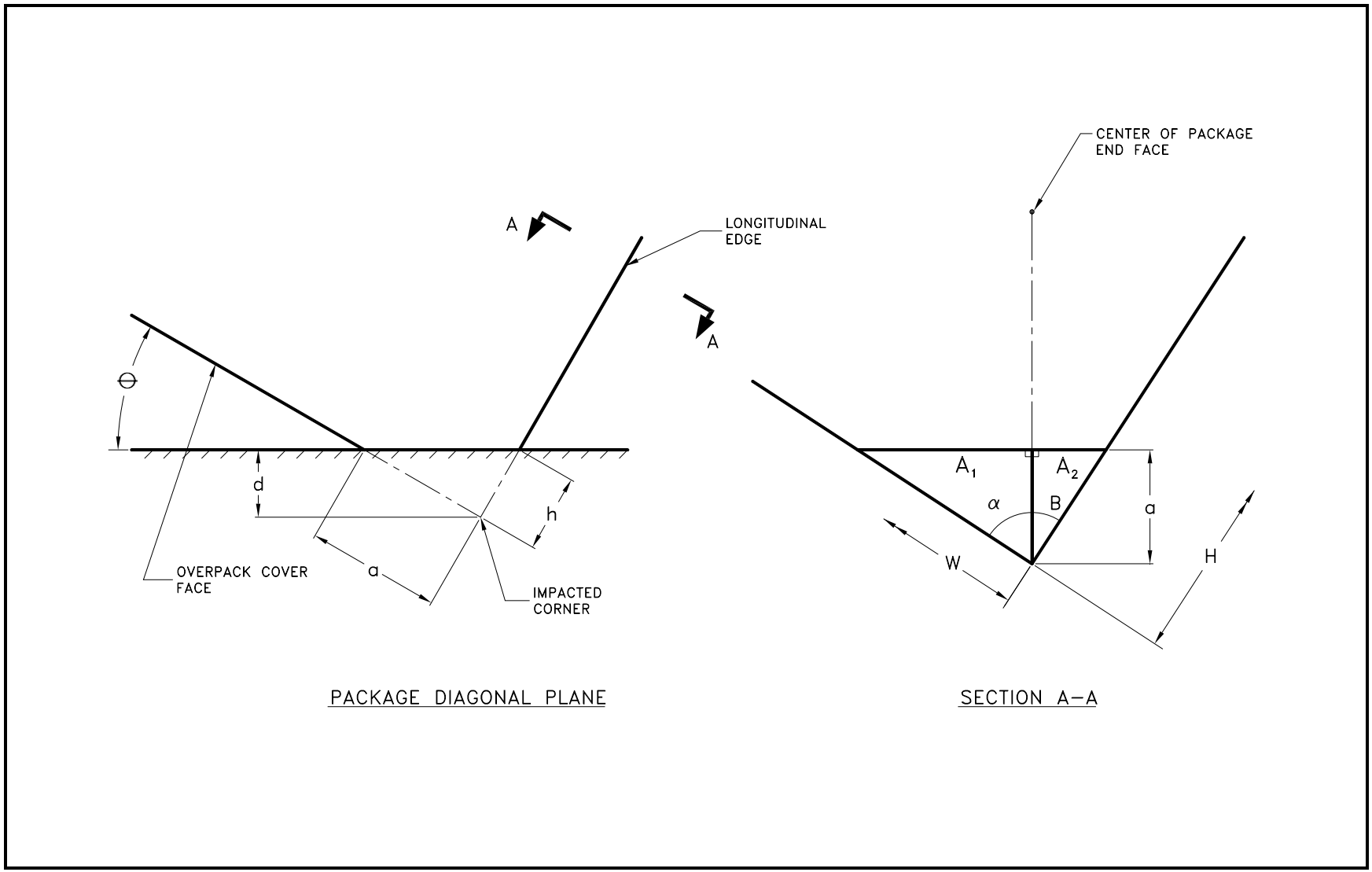

Figure 2.7-2 – CG-Over-Corner Impact Crush Area Relationships

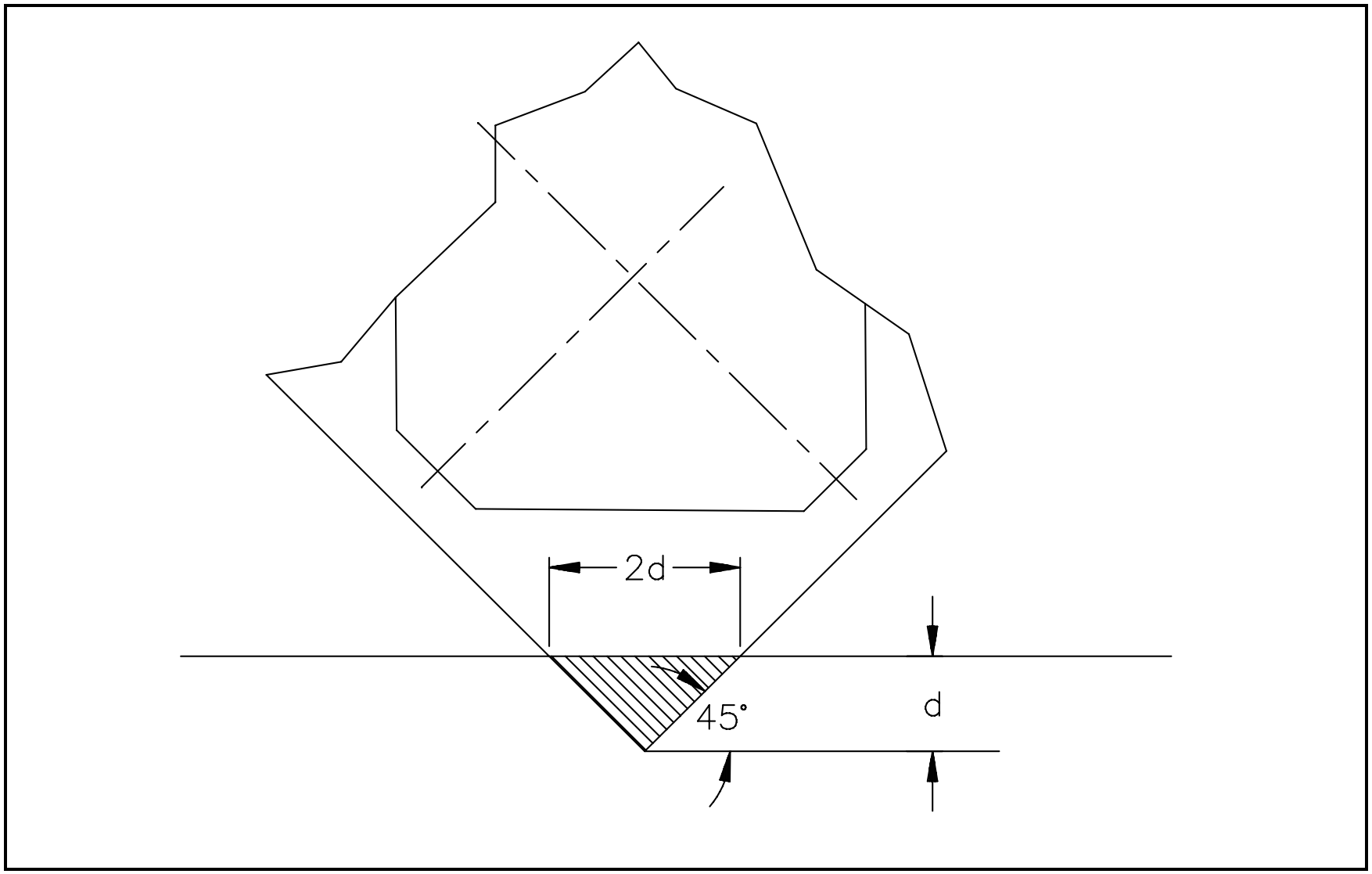

Figure 2.7-3 – Side-Edge Impact Crush Area Relationships

2.7.2 Crush

Subpart F of 10 CFR 71 requires performing a dynamic crush test in accordance with the requirements of 10 CFR §71.73(c)(2). Since the TRUPACT–III package weight exceeds 500 kg, the dynamic crush test is not required.

2.7.3 Puncture

Subpart F of 10 CFR 71 requires performing a puncture test in accordance with the requirements of 10 CFR §71.73(c)(3). The ability of the TRUPACT–III package to adequately withstand the specified puncture drop is demonstrated by testing of a full-scale CTU. A total of four puncture tests were performed on CTU-1 and two were performed on CTU-2. Each puncture drop was over a minimum distance of one meter between the top of the puncture bar and the target point on the CTU. The mild steel puncture bar had a nominal diameter of 150 mm and an edge radius not exceeding 6 mm. The puncture bar assembly was welded securely to the drop pad.

2.7.3.1 Technical Basis for the Puncture Drop Tests

In order to determine the worst-case puncture orientation, consideration of a number of possible orientations was made. Primary focus was on the ability of the TRUPACT–III package to withstand the puncture drop event without compromise to leaktight containment, and on the ability of the thermally-relevant structures located in the region of the closure lid containment O-ring seal to resist damage that could compromise their ability to adequately limit the temperature of the seal in the HAC thermal event. The criteria used to evaluate each puncture drop were based on the following considerations:

- Rupture of containment boundary
- Excessive deformation in the containment sealing area, particularly in combination with free drop damage
- Separation of the overpack cover from the package
- Excessive compression, damage, or exposure of the polyurethane foam or calcium silicate insulation.

Shielding and criticality are not of concern as discussed in Section 2.7.1.1, *Technical Basis for the Free Drop Tests*. A brief summary of the test unit configuration and test conditions is given in Section 2.7.1.2, *Certification Test Unit and Test Conditions*.

The following puncture drops (through the package CG unless stated otherwise) were considered in the worst-case evaluation:

A. Puncture on the side drop damage.

B. Puncture on the overpack cover.

C. Puncture on the overpack cover center.

D. Puncture on the closed end center.

E. Puncture on the overpack cover joint (front side). (non-CG)

F. Puncture on the overpack cover joint (top or bottom). (non-CG)

G. Puncture on the c.g.-over-corner drop damage.

H. Puncture on the side-edge drop damage. (non-CG)

I. Puncture on the region outside the puncture-resistant structure (non-CG)

Each puncture orientation is evaluated to determine whether it represents bounding damage to the containment boundary or to the containment sealing area that could affect thermal performance. The result of all of these evaluations is summarized in Table 2.7-2, and illustrated in Figure 2.7-5 and Figure 2.7-6. Note: in the following small figures, a number in parentheses (e.g., *LP1*), indicates that the particular test has been performed as summarized in Table 2.7-2.

A. Puncture on the Side. In this orientation, the bar axis is aimed through the c.g. of the package, and is oriented at 70° to the package surface (i.e., the package is oriented 20° from horizontal). The puncture took place on the side of the package which experienced the flat side free drop impact. The angle was chosen based on the results of a series of engineering puncture tests at different orientations using the half-scale test article as described in Section 2.12.1.7.3.2, *Puncture Drop Tests P105 through P405*. Other engineering tests performed in this orientation are described in Section 2.12.1.7.1.5, *Puncture Drop Test No. F5* and Section 2.12.1.7.1.8, *Puncture Drop Test No. F9*.

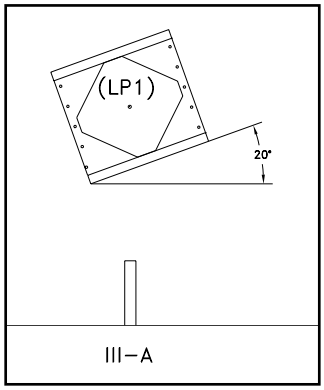

B. Puncture on the Overpack Cover. In this orientation, the bar axis was aimed through the c.g. of the package, at an angle which is oblique as possible considering the geometry of the overpack cover octagonal recess. The impact point was on the recessed octagonal surface. This puncture challenged the puncture-resistant plate near its edge. The impact point was also near the closure bolts and elastomeric containment seal. A similar puncture test was performed on the ends of the half-scale engineering test article as described in Section 2.12.1.7.2.5, *Puncture Drop Test No. P1* and Section 2.12.1.7.2.8, *Puncture Drop Test No. P4*. Based on the results of those tests, the puncture-resistant plates on both ends have been increased in thickness to 15 mm. The effectiveness of this measure was confirmed in another engineering test described in Section 2.12.1.7.3.3, *Puncture Drop Test No. P505*.

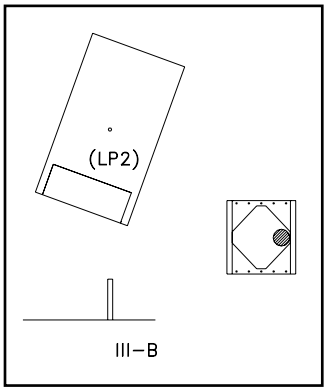

C. Puncture on the Overpack Cover Center. In this orientation, the puncture bar impacts the center of the overpack cover through the package c.g. Since the bar axis is not oblique to the surface, this test is not considered as severe as the oblique impact described in Section 2.7.3.1(B), *Puncture on the Overpack Cover*. Furthermore, an engineering test in this orientation was performed as described in Section 2.12.1.7.1.3, *Puncture Drop Test No. F3*. In that case, the overpack cover did not have a puncture-resistant plate, and the bar penetrated through the thickness of the octagonal region and left a depression in the lid outer sheet. However, the inner (containment boundary) sheet of the lid showed only insignificant deformation, and the test unit was leaktight. Due to the addition of the puncture-resistant plate to the overpack cover, and to the somewhat lighter

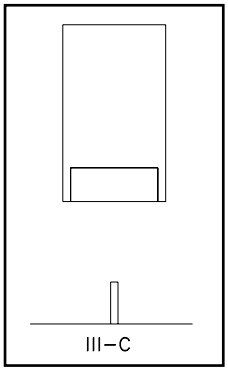

weight of the TRUPACT–III package compared to the full-scale equivalent weight of the engineering test unit, the margin of safety demonstrated in prior testing will be increased, and this puncture drop does not need to be performed.

D. Puncture on the Closed end Center. This orientation is similar to the one discussed in Section 2.7.3.1(C), *Puncture on the Overpack Cover Center*, except that the location is the center of the closed end octagonal area instead of the overpack cover. For the same reasons given in that section, this puncture drop does not need to be performed.

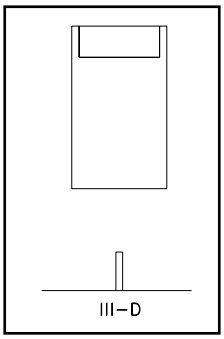

E. Puncture on the Overpack Cover Joint (Front Side). The purpose of this puncture is to damage the thermal protection of the lid elastomeric containment seal by compromising the integrity of the cheek structure. It is at an angle away from the package, in an attempt to tear the cheek away from the package, exposing the edge of the lid. Although the bar axis is not through the c.g., the damage is done before the package can rotate very far. The angle between the bar and package is not critical. The impact point is essentially on the ISO corner fitting, since this structure is a fairly rigid region and will help to distribute the load to the cantilever root of the cheek. An engineering test in this orientation was performed as described in Section 2.12.1.7.2.5, *Puncture Drop Test No. P2*. Essentially no damage resulted from this test. This demonstrated the effective resistance of the TRUPACT–III package to this mode of failure, and this puncture drop does not need to be performed.

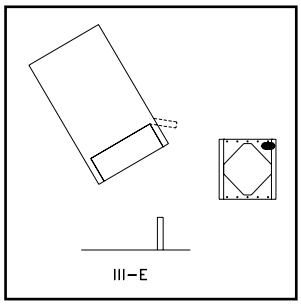

F. Puncture on the Overpack Cover Joint (Top/Bottom). The purpose of this puncture is to damage the thermal protection of the lid containment seal by opening up the joint between the overpack cover and body along the top or bottom of the package. This is an oblique impact on the overpack cover joint, aimed toward the package end so as to penetrate as deeply as possible. The bar axis is aimed away from the c.g., since damage is likely to be greater if the bar force is towards the nearby package end. If the bar were aimed toward the package c.g., the structure is more resistant to puncture due to the presence of the puncture-resistant plate, and any damage that occurred would tend to be further from the lid sealing area. The angle between the bar and package is not critical. An engineering test in this orientation was performed as described in Section 2.12.1.7.2.6, *Puncture Drop Test No. P3*. The impact point was in the region of slapdown secondary free drop damage. The resulting combined damage was not bounding compared to the combination of c.g.-over-corner free drop and puncture damage. For this reason, this puncture drop does not need to be performed.

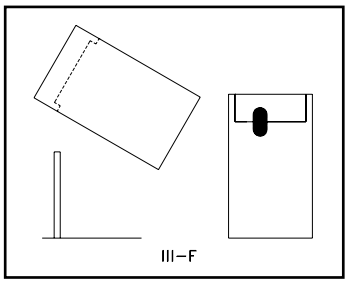

G. Puncture on the C.G.-over-Corner Drop Damage. The damage from the c.g.-over-corner free drop resulted in the greatest local crush distance, as described in Section 2.7.1.4.1, *Vertical, Lid Down Free Drop Results*. Therefore, the addition of puncture damage to the free drop damage may be bounding. This puncture drop was performed on CTU-1 using the same orientation as in the free drop test. It was also performed on CTU-2 to maximize the damage following free drop LD91.

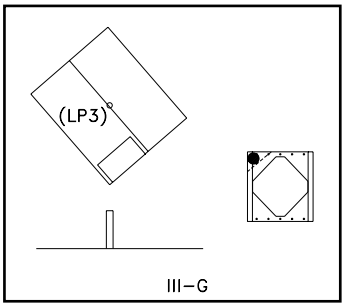

H. Puncture on the Side-Edge Drop Damage. The side-edge drop damage will result in deformation in the vicinity of the thermal shield (see Section 2.7.1.1.2(B), *Side-Edge Free Drop*). Puncture on this damage might interfere with the function of the thermal shield. The puncture bar should attack the package in a manner to cause the greatest compromise of the thermal shield. A puncture bar alignment through the package c.g. would be too steep (~45º) for maximum damage to occur. If the bar impacted the package at a lesser angle, more damage would likely occur even though it was not through the c.g. This puncture was performed with the package axis oriented at 30° to the horizontal for the worst case ripping effect on the damaged area opposite the thermal shield.

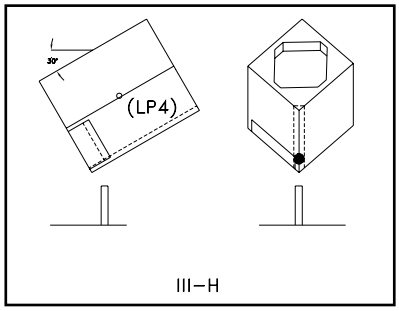

I. Puncture on the Region Outside the Puncture-Resistant Structure. As seen in Detail AX on sheet 20 of the drawings in Appendix 1.3.1, *Packaging General Arrangement Drawings*, there is a small region, 96 mm long, between the end of the puncture-resistant structures in the overpack sides and the inside end of the containment (inner shell of the CSA). Since this region lacks the puncture-resistant structures, it should be tested to ensure containment boundary integrity. Aiming the puncture bar through the package c.g. is not worst-case for two reasons. First, the angle between the bar and the package would be too small to allow it to rip into the outer skin. In other words, the bar axis and the package axis would differ by only 35º, which would likely cause the bar to glance off of the side and not penetrate the outer skin. Second (assuming that the bar did penetrate the outer skin), for a test through the package c.g., because of the small size of the subject region, the bar would strike either the strong corner-diagonal plate of the CSA (10-mm plate) or the strong end plate of the puncture-resistant region (8-mm plate). However, an angle of the package to the ground of 40º allows the bar to miss these structures, and aim at the weakest part of this region, as shown in Figure 2.7-4. It is also in the range of orientations where ripping into the outer skin is likely. This puncture was performed on the bottom side of the package between the rails, since the two vertical sides and the top side have significant reinforcements on the inner containment walls (i.e., the guide bars, see Figure 1.1-5).

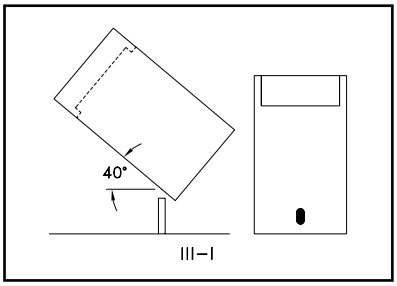

Summarizing the above discussions, the puncture drop tests performed on CTU-1 were:

- On Side Free Drop Damage (Section 2.7.3.1(A))
- On Overpack Cover (Section 2.7.3.1(B))

- On CG-Over-Corner Free Drop Damage (Section 2.7.3.1(G))
- On Side-Edge Free Drop Damage (Section 2.7.3.1(H))

The puncture drop tests performed on CTU-2 were:

- On CG-Over-Corner Free Drop Damage (Section 2.7.3.1(G))
- On the Region Outside the Puncture-Resistant Structure (Section 2.7.3.1 (I))

This information is summarized in greater detail in Table 2.7-2 and depicted in Figure 2.7-5 and Figure 2.7-6. To facilitate rigging CTU-1, the order of tests was LP3, LP4, LP1, and LP2.

2.7.3.2 Temperature of Puncture Drops

Since the puncture resistance of the TRUPACT–III is not significantly affected by temperature, all puncture drop tests were performed at ambient temperatures. The primary means of puncture resistance is afforded by the use of puncture-resistant plates, which are embedded in the overpack materials all over the package. There are three types of puncture-resistant plate. (1) On the longitudinal faces of the package, the plates are made of 10-mm thick Alloy UNS S31803 stainless steel, with a 60-mm thick layer of balsa wood on the outside. The inside layer is 0.10 kg/dm^3 polyurethane foam which is 109 mm thick on the top and bottom sides and 114 mm thick on the vertical sides. (2) On the recessed regions of the ends (overpack cover and closed end), the stainless steel plates are 15-mm thick. The outer layer is 60-mm thick balsa wood, and the inner layer is 120-mm thick, 0.10 kg/dm^3 polyurethane foam. (3) On the thicker, non-recessed regions of the ends, the sheets are fabricated of 6 mm thick Alloy UNS S31803 stainless steel, sandwiched between a 140-mm thick layer of 0.16 kg/dm^3 polyurethane foam on the outside and a massive block of 0.48 kg/dm^3 polyurethane foam on the other side. The edges of the puncture-resistant plates are essentially free to deform, since they are attached locally only by rivets or short tack welds. The material has been tested for ductility at cold temperatures according to ASTM E604[7]. Test specimens were as thick as or thicker than the puncture-resistant plates, and fabricated from fully certified material. Five specimens of the steel were tested at a temperature of -29 ºC, and the results demonstrated 100% shear (i.e., ductile behavior) on each of the broken surfaces. Therefore, the behavior of the material at the regulatory cold temperature is ductile in nature. Since the puncture behavior is primarily dependent on a material that is ductile at both the cold and ambient temperatures, the extent and type of puncture damage will be essentially the same at ambient temperature as it would be at cold temperature.

2.7.3.3 Summary of Results from Puncture Drop Tests

The results of each of the puncture tests evaluated are described below indicating the reference number as listed in Table 2.7-2. Under each heading, the results of the puncture test are described. For puncture drop tests on CTU-1, detailed descriptions, results, and photographs are given in Appendix 2.12.3, *Certification Tests on CTU-1*. For puncture drop tests on CTU-2, see Appendix 2.12.6, *Certification Tests on CTU-2*. No puncture test caused significant weld tears or exposed significant amounts of foam.

[7] ASTM E604-83, *Standard Test Method for Dynamic Tear Testing of Metallic Materials.*

2.7.3.3.1 Puncture on Side Results (CTU-1, Ref. No. LP1)

The ambient temperature for this test was 22 ºC. The puncture bar penetrated both the outer skin and the puncture-resistant plate, and left a dent of approximately 51 mm deep in the CSA outer structural sheet. There was no cutting or cracking of the CSA outer structural sheet, demonstrated by placing the CSA annular region under a vacuum. There was no deformation of the inner CSA containment sheet. The opening in the overpack was 254 mm long and 178 mm wide.

2.7.3.3.2 Puncture on Overpack Cover Results (CTU-1, Ref. No. LP2)

The ambient temperature for this test was 17 ºC. The puncture bar struck the overpack cover approximately 292 mm from the left edge of the octagonal recess. The bar penetrated the outer sheet, and left a dent in the puncture-resistant plate approximately 145 mm deep. However, the puncture-resistant plate was not penetrated nor cracked. Removal of the overpack cover showed the impact to have been aligned between two V-stiffeners in the closure lid. A dent of approximately 5 mm deep was left in the outer sheet of the closure lid at the puncture location. There was no deformation of the inner closure lid containment sheet.

2.7.3.3.3 Puncture on CG-Over-Corner Results (CTU-1, Ref. No. LP3)

The ambient temperature for this test was 17 ºC. The puncture bar struck at essentially the center of the prior c.g.-over-corner free drop (LD4) damage and created a further deformation of approximately 102 mm deep and 178 mm in diameter. The effect of the impact was to further locally compress the deformed materials in the damaged zone. Small amounts of foam were visible from the free drop test damage, and the puncture test did not significantly alter this. After cutting away the damaged material, a minimum distance of 51 mm was measured between the deformed steel resulting from the puncture drop and the nearest part of the calcium silicate protection box (i.e., thermal shield). This distance was filled with compressed, 0.48 kg/dm^3 foam.

2.7.3.3.4 Puncture on Side-Edge Results (CTU-1, Ref. No. LP4)

The ambient temperature for this test was 16 ºC. The puncture bar struck on the prior damage from free drop test LD5, with the center of the bar placed approximately 584 mm from the cover end of the package, with the package inclined 30º from the horizontal. The bar penetrated the outer skin and struck the top corner of the thermal shield. This structure, made from 16 mm-thick plate material, is very rigid. Later disassembly showed relatively minor weld cracks in this region and only approximately 3 mm of deformation of the thermal shield, local to the impact. There was no damage to the calcium silicate insulating board, which maintained full integrity without crumbling or breaking.

No puncture drop test was able to significantly deform the closure lid sealing area, nor was any test able to impart significant damage to the thermally-relevant overpack structures protecting the containment sealing area. For thermal analysis, the worst-case damage from puncture was combined with the worst-case damage from free drop, as discussed in Section 3.5.2.6, *Description of Thermal Model for HAC Conditions.* The results of the puncture tests demonstrate that the TRUPACT–III can withstand the HAC puncture drop event without significant damage.

2.7.3.3.5 Puncture on CG-Over-Corner Results (CTU-2, Ref. No. LP91)

The ambient temperature for this test was 15 ºC and the package surface temperature was 19 ºC. The puncture bar struck on the overpack cover portion of the prior c.g.-over-corner free drop (LD91) damage. The depth of puncture, measured to the center of the damage hole in an axial direction from the undeformed surface of the overpack cover, was 146 mm. The damage loosened the entire lower quadrant of the overpack cover outer sheet and a significant portion of the low density (0.16 kg/dm^3) foam fell out. The bar corner partially sheared into the 6-mm thick puncture resistant plate located between the low density and high density (0.48 kg/dm^3) foam by an amount of 38 mm. However, little of the high density foam was exposed and essentially none was lost.

2.7.3.3.6 Puncture on Region Outside Puncture-Resistant Structure (CTU-2, Ref. No. LP-92)

The ambient temperature for this test was 12 ºC, and the package surface temperature was 15 ºC. The puncture bar struck as shown in Figure 2.7-6. The bar penetrated the outer skin and impacted the CSA outer structural sheet, creating a crack in the weld between the structural sheet and the rear diagonal corner stiffener of the CSA, and in some of the adjacent plug welds which connect the outer structural sheet to the V-stiffener nearest the impact. However, there was no evidence of any dent or bulge in the CSA inner (containment) sheet at the puncture site. In addition, the containment boundary was leaktight after all testing was completed.

Table 2.7-2 – Summary of Puncture Drops Performed on the TRUPACT–III

Test Description	Discussion Paragraph	Test Ref. No.	Orientation	Purpose
On Side Free Drop Damage (CTU-1)	Section 2.7.3.1(A)	LP1	Bar axis 70º to surface, thru c.g.	Test ability of puncture-resistant design to resist penetration at worst-case oblique angle.
On Overpack Cover (CTU-1)	Section 2.7.3.1(B)	LP2	Bar axis 65º to surface, thru c.g., impact in octagonal recess	Test ability of puncture-resistant design to resist penetration on package end.
On C.G.-over-Corner Free Drop Damage (CTU-1)	Section 2.7.3.1(G)	LP3	Bar axis thru c.g., centered on free drop damage	Quantifies possible maximum accumulation of free drop and puncture damage.
On Side-Edge Free Drop Damage (CTU-1)	Section 2.7.3.1(H)	LP4	Bar axis 60º to edge, not thru c.g., centered on thermal shield/seal area	Quantifies possible maximum accumulation of free drop and puncture damage.
On C.G.-over-Corner Free Drop Damage (CTU-2)	Section 2.7.3.1(G)	LP91	Bar axis thru c.g., centered on free drop damage	Quantifies possible maximum accumulation of free drop and puncture damage following free drop LD91.
On Region Outside Puncture-Resistant Structure (CTU-2)	Section 2.7.3.1(I)	LP92	Package 40º to horizontal, bar not thru c.g., contact approx. 476 mm from closed end	Test ability of puncture-resistant design to resist penetration in subject region.

Note: For convenience in rigging the tests on CTU-1, the order of testing was LP3, LP4, LP1, and LP2.

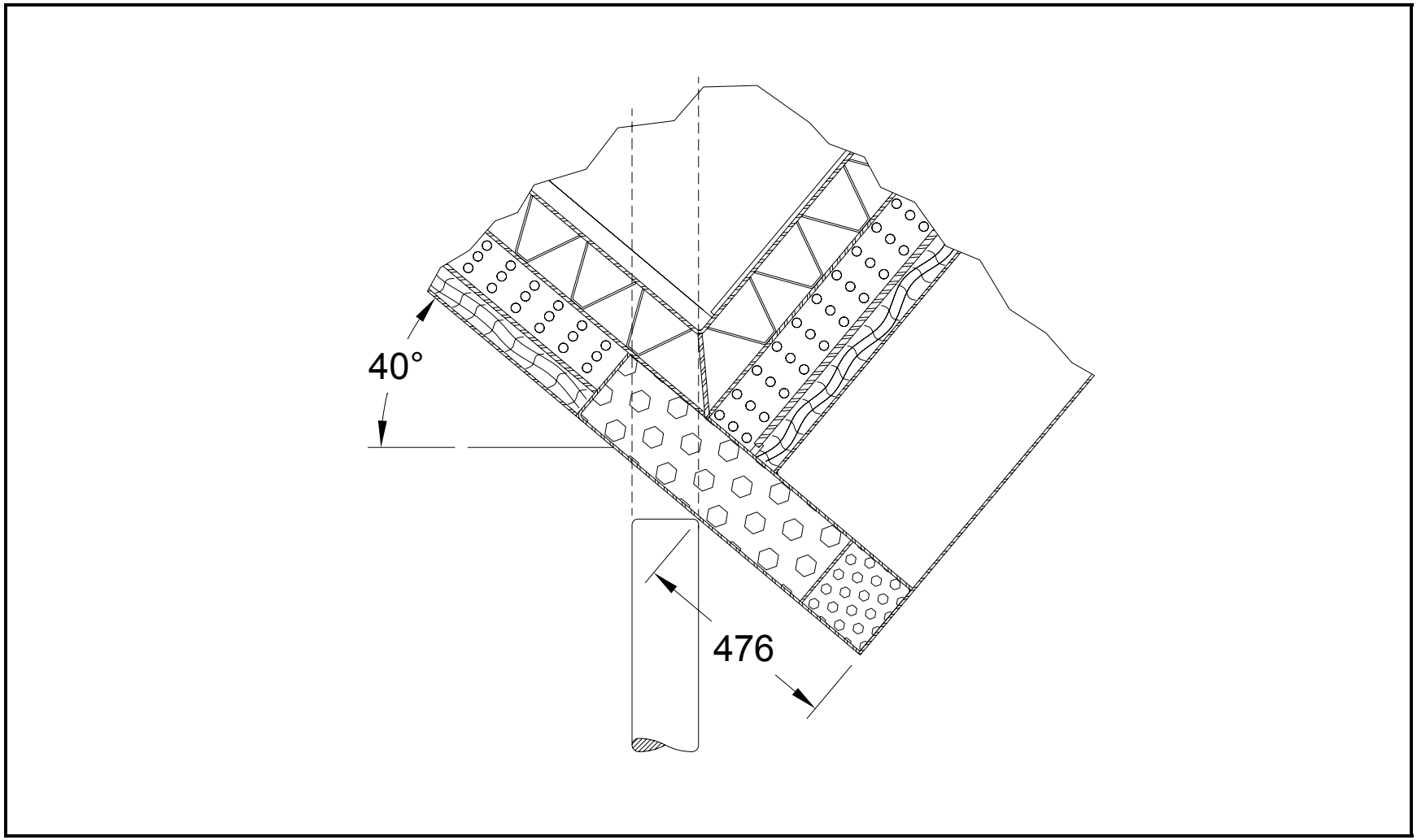

Figure 2.7-4 – Puncture On Region Outside Puncture Resistant Structure

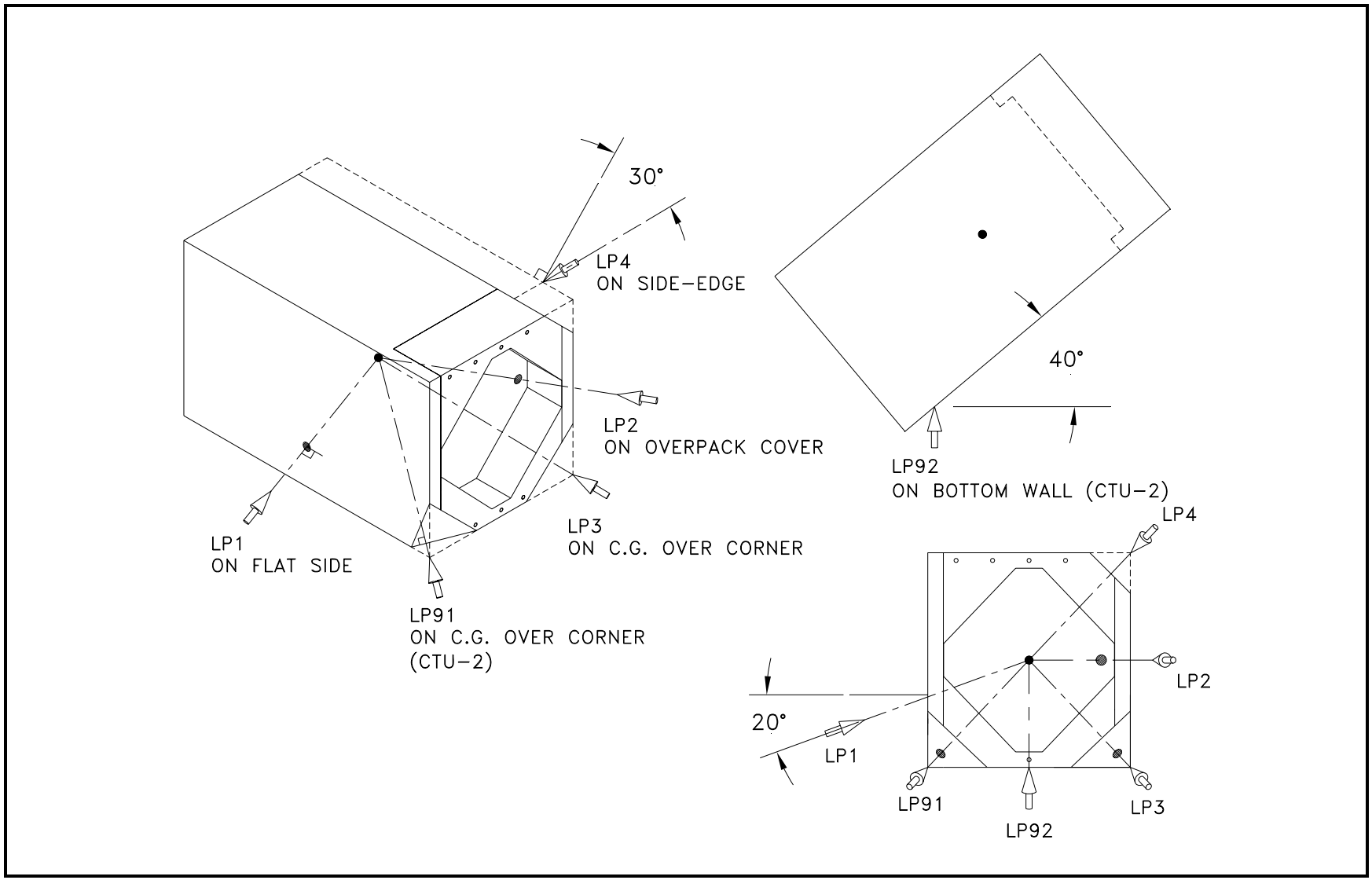

Figure 2.7-5 –TRUPACT–III Package Puncture Drop Orientations

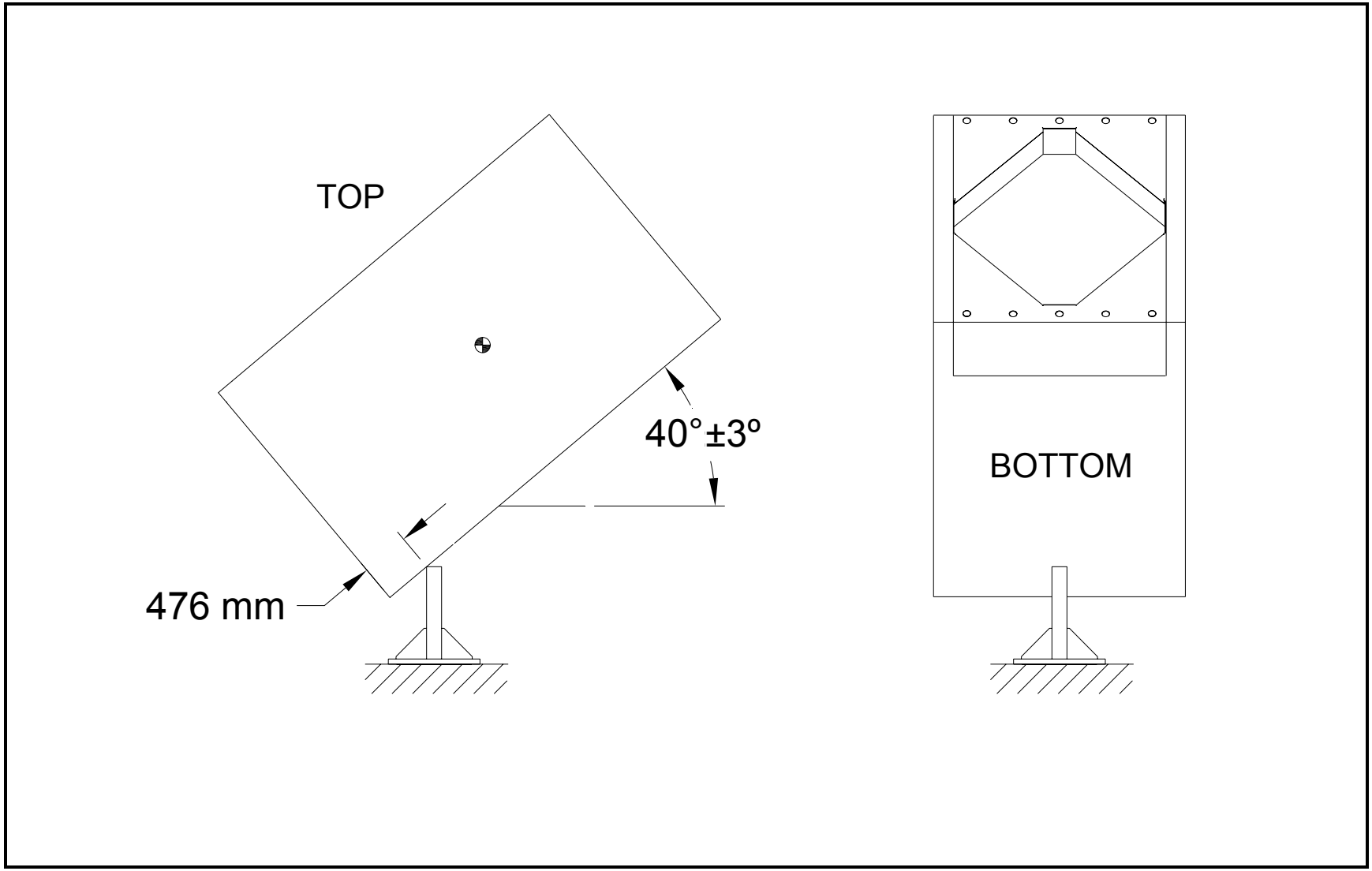

Figure 2.7-6 –TRUPACT–III Package Puncture Drop Orientation LP92

This page intentionally left blank.

2.7.4 Thermal

The TRUPACT–III is designed to withstand the HAC 30 minute fire specified in 10 CFR §71.73(c)(4). The thermal evaluation is presented in Section 3.4, *Thermal Evaluation under Hypothetical Accident Conditions*.

2.7.4.1 Summary of Pressures and Temperatures

As determined in Section 3.3.2, *Maximum Normal Operating Pressure*, the maximum normal operating pressure (MNOP) in the TRUPACT–III, including the effects of heat-up of ambient pressure air, generation of water vapor, and payload gas generation, is 172 kPa gauge. As discussed in Section 3.4.3, *Maximum Temperatures and Pressure*, the change in pressure due to the HAC thermal event is 77.3 kPa. This value conservatively considers the combination of the worst-case damage scenario and the bounding payload. From Table 3.4-1, the peak temperature of the CSA structural sheet is 689 ºC, which is reached at the end of the 30-minute fire, and falls rapidly thereafter. This temperature is limited to a small region local to the modeled puncture damage. Although it exceeds the stated limit of 316 ºC of the UNS S31803 material, it will not affect the ability of the package to maintain containment nor significantly inhibit post-accident recovery operations as discussed in Section 3.4.3.1, *Maximum HAC Temperatures*. The CSA containment sheet reaches a peak temperature of 222 ºC, and the closure lid bolt peak temperature is 187 ºC.

2.7.4.2 Differential Thermal Expansion

Differential thermal expansion is not of concern for the TRUPACT–III package. The package has a single containment, thus interference between two containment vessels is not possible. It has no shielding components such as lead or neutron shielding, and therefore no interference between package structures and shielding materials is possible. The maximum temperature for the CSA outer sheet stated in Section 2.7.4.1, *Summary of Pressures and Temperatures*, is for an area local to the puncture damage, and which is very small in relation to the CSA as a whole. Since the CSA outer sheet and containment sheets are connected with a large number of V-stiffeners which conduct heat, their overall temperatures do not differ significantly (except local to the puncture damage), and since they are made of the same material, differential thermal expansion between the CSA outer and containment sheets may also be neglected.

The only structurally significant components not made of UNS S31803 stainless steel are the lid closure bolts, which are made of ASTM A320, L43-material. Since the bolt is in intimate contact with the closure lid, the lid and bolt temperatures are essentially equal. The difference in thermal expansion coefficient between the two materials is small, as seen from Section 2.2.1, *Material Properties and Specifications*. At a temperature of 204 ºC (greater than the peak closure bolt temperature), the difference is less than 7%. Since the closure lid is made of the material having the greater coefficient, an increase in temperature of the closure lid and bolt components leads to an increase in bolt clamping load, although due to the proximity of thermal expansion coefficients, the change is negligible. Therefore, differential thermal expansion of the closure bolts is not of concern.

2.7.4.3 Stress Calculations

Stresses in the TRUPACT–III package CSA are calculated for NCT in Section 2.6.1.3, *Stress Calculations*. Since those calculations included the MNOP of 172 kPa gauge along with the reduced external pressure of 25 kPa absolute, the stress computed corresponded to a net differential pressure of (172 + 101.3 – 25) = 248.3 kPa. Under HAC, the reduced external pressure is not required, and considering the HAC thermal event maximum pressure increase of 77.3 kPa, the HAC net differential pressure is only (172 + 77.3) = 249.3 kPa. The NCT calculated stresses may therefore be increased by the ratio 249.3/248.3 = 1.004 for HAC. From Section 2.6.1.3, *Stress Calculations*, the maximum membrane stress at any location is 153 MPa and the maximum membrane-plus-bending stress is 222 MPa. The equivalent stresses for HAC are:

Membrane:	153 × 1.004 =	154 MPa
Membrane-plus-bending:	222 × 1.004 =	223 MPa

2.7.4.4 Comparison with Allowable Stresses

As discussed in Section 3.4.3.1, *Maximum HAC Temperatures*, a small region of the CSA structural (outer) sheet will experience a maximum temperature whereby some reduction in ductility of the material may occur, although the time at temperature is not sufficient for the full embrittlement effect to occur. A reduction in ductility of the CSA structural sheet is not of concern for two reasons:

- The containment boundary components, having a maximum temperature of 222 ºC, do not exceed the continuous-use temperature limit given by ASME Code Case N-635-1 (i.e., the highest temperature in the material property table of 316 ºC). Therefore no reduction of ductility of the containment boundary components will occur.
- The fire test is the last hypothetical accident condition which is applicable per 10 CFR 71. As such, the only subsequent structural loads occurring for the package will arise from accident recovery operations. Therefore, even if reduction in ductility does occur over a small portion of the CSA structural sheet, no safety impact will result since sufficient ductility will remain to allow recovery operations. Of note, the average CSA structural sheet temperature equals 75 ºC.

From Table 2.2-1 at a temperature of 316 ºC, S_m = 185 MPa, and S_u = 556 MPa. From Table 2.1-1, the membrane stress allowable is the lesser of $2.4S_m$ or $0.7S_u$, which in this case equals 389 MPa. The membrane-plus-bending allowable is the lesser of $3.6\ S_m$ or S_u, which in this case is 556 MPa. The margin of safety on CSA membrane stress is:

$$\text{MS} = \frac{389}{154} - 1.0 = +1.53$$

The margin of safety on CSA membrane-plus-bending stress is:

$$\text{MS} = \frac{556}{223} - 1.0 = +1.49$$

Therefore, stresses in the TRUPACT–III package in the HAC thermal event are acceptable.

Per Regulatory Guide 7.6, paragraph C.7, the extreme range of stress must be considered. Of all the various allowable stresses corresponding to the different conditions evaluated (including fabrication stresses and normal conditions of transport), the largest allowable stress is equal to the material ultimate strength S_u. It is therefore conservative to assume that S_u bounds all stresses actually developed in the structure. For Alloy UNS S31803 stainless steel, S_u = 621 MPa at 38 ºC. The maximum possible stress intensity range is twice this value, or 1,242 MPa. Applying a factor of four to account for possible stress concentrations at structural discontinuities gives a total stress range of 4,968 MPa. The alternating component is one-half of this value, or 2,484 MPa. To account for temperature effects, this value of alternating stress is factored by the ratio of modulus of elasticity. The ratio is formed between the modulus of elasticity at 38 ºC and the design temperature of 71 ºC. The adjusted stress is:

$$S_{alt} = 2{,}484\frac{E_{38}}{E_{71}} = 2{,}515 \text{ MPa}$$

where E_{38} = 194,000 MPa and E_{71} = 191,600 MPa. Per Table I-9.1M of the ASME Code (conservatively using the lower curve, for UTS of 793 - 896 MPa), the allowable value for S_{alt} at 10 cycles is 2,896 MPa. The margin of safety is:

$$MS = \frac{2{,}896}{2{,}515} - 1.0 = +0.15$$

Considering the significant conservatism used in the underlying assumptions (e.g., use of allowable stress rather than smaller actual stresses, assuming worst-case stresses are fully reversing, use of the maximum factor of stress concentration, use of the lower fatigue curve), it is apparent that the actual margin of safety is larger than 0.15. Thus, the requirement of paragraph C.7 of Regulatory Guide 7.6 is met.

2.7.5 Immersion – Fissile Material

Subpart F of 10 CFR 71 requires performing an immersion test for fissile material packages in accordance with the requirements of 10 CFR 71.73(c)(5). The criticality evaluation presented in Chapter 6.0, *Criticality Evaluation*, assumes optimum hydrogenous moderation of the contents, thereby conservatively addressing the effects and consequences of water in-leakage.

2.7.6 Immersion – All Packages

Subpart F of 10 CFR 71 requires performing an immersion test for all packages in accordance with the requirements of 10 CFR 71.73(c)(6). This condition is evaluated by analysis of the effects of a 150 kPa gauge pressure applied to the outside of the CSA.

The stress results are bounded by the analysis presented in Section 2.6.1.3, *Stress Calculations*, in which an internal gauge pressure of 172 kPa is used. Therefore, the immersion case is governed by allowable buckling loads. The buckling analysis for the TRUPACT–III package is presented in Section 2.12.4, *HAC Immersion Buckling Evaluation*. In that analysis, an external gauge pressure of 150 kPa is applied to the package, conservatively assuming an internal pressure of zero gauge. As shown, the stress in the most critical sidewall due to a combination

of normal pressure loading and wall edge loads is 88.7 MPa. The allowable inelastic buckling load is 391 MPa. The factor of safety against buckling is

$$FS = \frac{(\sigma_{cr})_x}{\sigma} = \frac{391}{88.7} = 4.41$$

This is considerably in excess of the minimum factor of safety of 1.34 for HAC per ASME Code Case N-284-1, corresponding to ASME Code, Service Level D conditions. Therefore, the immersion load of 150 kPa gauge is not of concern.

2.7.7 Deep Water Immersion Test (for Type B Packages Containing More than 10^5 A_2)

Subpart E of 10 CFR71 requires performing a deep water immersion test in accordance with 10 CFR §71.61. Since the TRUPACT–III does not transport payloads with an activity of greater than 10^5 A_2, this requirement does not apply.

2.7.8 Summary of Damage

From the discussions presented in Section 2.7.1 through 2.7.7, it is shown that the hypothetical accident sequence does not result in any significant structural damage to the TRUPACT–III package, and that the criteria established for hypothetical accident conditions in Section 2.1.2, *Design Criteria*, are satisfied. Full-scale physical model testing, including free drop and puncture tests on two certification test units, have shown that:

- The package can sustain a worst case free drop and puncture while remaining leaktight using the leak rate criterion of 1×10^{-8} Pa-m^3/s, air, per ANSI N14.5. Post-test leakage rate testing demonstrated that the containment metallic boundary, closure lid O-ring seal, and vent port insert O-ring seal remained leaktight after the conclusion of all certification testing on CTU-2. On CTU-1, the containment metallic boundary and the vent port insert O-ring seal remained leaktight, but the closure lid O-ring seal did not, due to the presence of debris in the sealing nip. The results from the testing of CTU-1 are further discussed in Section 2.7.8.1, *Debris Contamination of the Containment Seal on CTU-1*. The debris shield, which was fully implemented in CTU-2, was not present in CTU-1. The performance of the debris shield in preventing contamination of the containment O-ring seal was successfully demonstrated in the CTU-2 tests.
- Closure bolts retained an average of 56% of the initial tightening torque on CTU-1 after four HAC free drops and four puncture drops, and 79% of the initial tightening torque on CTU-2 after one HAC free drop and two puncture drops. The performance of the closure bolts is discussed in Section 2.7.8.2, *Closure Bolts*.
- The containment boundary was unaffected by any puncture test. The outer structural sheets of the CSA were subject to insignificant deformations or weld cracks local to the puncture bar impact, but no deformation of the inner containment components of the CSA was observed to occur from any puncture test on CTU-1 or CTU-2.
- Distortion or buckling of the CSA does not occur (see Section 2.7.1.4.1, *Vertical, Lid Down Free Drop Results*).

- The overpack cover is securely retained on both CTU-1 and CTU-2. At the conclusion of all testing, the overpack cover was still securely fastened to the body.
- Criticality assumptions regarding package reconfiguration are supported.
- Thermal fire event analysis assumptions regarding the integrity of thermal insulation and exposure of polyurethane foam are supported.

In addition, calculations have shown that the stress criteria of Table 2.1-1 are satisfied for the thermal and immersion events (see Section 2.7.4.4, *Comparison With Allowable Stresses* and Section 2.7.6, *Immersion – All Packages*, respectively).

Therefore, the TRUPACT–III package satisfies all of the requirements of 10 CFR §71.73.

2.7.8.1 Debris Contamination of the Containment Seal on CTU-1

As discussed in Section 2.12.5.2, *Contamination of the Containment O-ring Seal During Certification Testing*, the initial helium leakage rate test performed on the closure lid containment O-ring seal of CTU-1 at the conclusion of the certification test was not successful due to contamination of the sealing nip. The contamination was found to be in the form of small shards and flakes of aluminum, which were generated by the numerous collisions of the aluminum round bars which made up the CTU simulated payload. As a result of free drop impact, a transient gap can open between the CSA body and closure lid flanges. In certification testing, the debris from the simulated payload was transported across the containment seal with the aid of the internal air pressure, equal to MNOP. Even though the flanges returned to contact after only a few milliseconds, the seal was not leaktight per the criterion of 1×10^{-8} Pa-m^3/s, air, per ANSI N14.5. Since small amounts of grit or dirt could be present in the payload cavity in normal operation, a debris shield is utilized to ensure maintenance of a leaktight containment seal under all free drops and puncture drops. The debris shield shown in the drawings of Appendix 1.3.1, *Packaging General Arrangement Drawings*, is effective in preventing containment seal contamination, as demonstrated by the tests performed on CTU-2. A discussion of how the debris contaminated the CTU-1 containment seal, the design considerations for the debris shield, and an analytical evaluation of the effectiveness of the shield, are presented in Section 2.12.5, *Closure Lid Debris Shield*.

2.7.8.2 Closure Bolts

During the post-test disassembly of CTU-2, all of the closure bolts were found to be in good condition, having an average residual loosening torque of 79% of the initial tightening torque. The loosening torque is generally expected to be on the order of 75% of the tightening torque, even if no external loads are applied to the joint. Therefore, an average residual torque of 79% after application of HAC test loads is in the expected range. None of the bolts showed any bending deformation, nor was there evidence of any bolt heads being contacted by the overpack cover recess cups. Many of the closure bolt washers did show evidence of contact with the overpack cover recess cups, (evident also in the corresponding cups). However, evidence of contact of a washer with a cup did not correlate to lower residual loosening torque for the corresponding bolt. Details of the CTU-2 post-test results are given in Section 2.12.6.8, *Leakage Rate Tests and Post-Test Measurements*.

During post-test disassembly of CTU-1, it was discovered that some of the closure bolts, particularly on the right flange, had a residual torque which was significantly below the average for

all bolts. The bolts having below-average residual torque were found to be bent. There was strong correlation between the amount of bending and the lowness of the residual torque. The greatest bending and lowest residual torque occurred close to the center of the right side of the lid. Moving towards each end of the right side (i.e., the top right corner and the lower right corner), bolt bending approached the as-fabricated average runout, and the residual torque approached the non-bent average value. Each of the affected bolts was bent in two opposite directions, with the axes of the threaded portion and of the bolt head nearly parallel, but with an offset. These bolts showed evidence of having been struck laterally on the bolt head, and the location of the strike aligned with the direction of bending. It was noted that the direction of bending, relative to the CTU, generally aligned with the 11:00 o'clock azimuth. The right side of the lid moved upward along the same orientation, and the guide pin on the right side was sheared by approximately 4.3 mm in the same direction. More details regarding the CTU-1 post-test findings are provided in Section 2.12.3.8.2.1, *Body Flange and Closure Lid Observations*, and Section 2.12.3.8.2.2, *Closure Lid Bolt Removal Torque and Related Observations*. It is apparent that the bolt bending was caused by the side impact on the bolt heads from the overpack cover recess cups, that struck the heads during a lateral translation of the overpack cover, which in some cases also struck the edge of the washer. Contact may have occurred in more than one free drop, but most likely the primary case was free drop LD4, the CG-over-corner orientation, based on the direction of bending. Because of the number of tests performed on CTU-1 (four HAC free drops and four puncture drops), the condition of the bolts was likely caused by, or at least exacerbated by, over-testing.

Two helium leakage rate tests were performed on CTU-1 to determine whether the non-leaktight condition of the closure lid O-ring seal was due to the reduced clamping load of the bolts on the right side, or due to the debris on the seal. For the first test, the seal surfaces were wiped clean of debris (without removing them from the lid), and the lid was reinstalled with all 44 closure bolts tightened to the lowest residual tightening torque of all bolts, equal to 149 N-m (see Table 2.12.3-4). This was very conservative since it represented only one-sixth of the average measured residual tightening torque of all 44 bolts of 898 N-m. Upon repeating the standard helium leakage rate test for the CTU, the testing criterion of a leakage rate less than 1×10^{-8} Pa-m^3/s, air, per ANSI N14.5, was achieved. For the second test, the lid was removed and reinstalled with only the four corner bolts installed and tightened to 149 N-m. This configuration represented a hypothetical case of the loss of preload on all four sides of the lid. The standard helium leakage rate test for the closure lid seal was repeated, and was again successful to the same criterion. These two tests demonstrated that only a negligible clamping force is required to obtain a leaktight seal between the lid and body of the TRUPACT–III, and that a significant preload reduction due to closure bolt damage can be sustained without affecting the leaktight condition of the closure O-ring seal as long as the seal is not contaminated by debris. With the implementation of the debris shield that was successfully demonstrated in CTU-2, the TRUPACT-III package will remain leaktight in the presence of any damage to the closure bolts that could credibly occur.

2.7.8.3 Structural Steel Plates of 15 mm and 16 mm Thickness

As shown on the drawings in Appendix 1.3.1, *Packaging General Arrangement Drawings*, nominally 16 mm thick, ASTM A240, UNS31803 stainless steel plate, item 23, is specified for two different structures. One is the structure that encloses the calcium silicate insulating boards. The plates that are associated with these boards in the front cheeks are shown on sheet 10 of the drawings, in zone B/C-6. For the calcium silicate boards in the overpack cover, the plates are

shown on sheet 17, Section AF-AF, and in the detail located in zone B/C-1/2. The second structure is the closure lid flange, where the item 23 plates form the inner and outer edge, as shown on sheet 14, Detail Y. The following analysis demonstrates that plates that are nominally 15 mm thick may be used in lieu of nominally 16 mm thick plates, with no effect on the margin of safety, provided the material strength of the 15 mm plates and of the weld filler metal exceeds the minimum ASTM values by an amount that is identified in the analysis.

The minimum thickness of the nominally 16 mm plate is T_{min16} = 15.7 mm, and the minimum thickness of the nominally 15 mm plate is T_{min15} = 14.7 mm, per ASTM A480/A480M. Three types of loading of the plates are considered: tension, shear, and bending.

Tensile stress is equal to load over area. A characteristic stress may be identified in which the area used is based on a unit length of one mm and the thickness of the plate. Therefore, the characteristic tensile stress in the 16 mm plate is:

$$\sigma_{16} = \frac{P}{(1)T_{min16}}$$

where P is the tensile load occurring in the HAC free drop or puncture drop events. From Table 2.1-1, the allowable stress under HAC for general membrane stress is the lesser of $2.4S_m$ or $0.7S_u$, which for UNS 31803 material is $0.7S_u$. The resulting margin of safety is:

$$MS_{16} = \frac{0.7S_u}{\sigma_{16}} - 1 = \frac{0.7S_u T_{min16}}{P} - 1$$

Similarly, the tensile stress in the 15 mm plate is:

$$\sigma_{15} = \frac{P}{(1)T_{min15}}$$

where the load P is the same as before. The margin of safety is:

$$MS_{15} = \frac{0.7F_T S_u}{\sigma_{15}} - 1 = \frac{0.7F_T S_u T_{min15}}{P} - 1$$

where the factor F_T has been introduced to indicate that the allowable stress must be higher in the case of 15 mm plate, if the margin of safety is to be the same as for 16 mm plate. Setting the two margins of safety equal,

$$MS_{15} = MS_{16} \Rightarrow \frac{0.7F_T S_u T_{min15}}{P} - 1 = \frac{0.7S_u T_{min16}}{P} - 1$$

Solving for F_T,

$$F_T = \frac{T_{min16}}{T_{min15}} = \frac{15.7}{14.7} = 1.07$$

In other words, if the 15 mm thick plate material is 7% stronger than the minimum strength permitted by the ASTM standard, the margin of safety under tensile loading will be the same as for a 16 mm plate that has the same minimum strength.

Shear stress in the plates will have the same formula as tensile stress, just by substituting the shear area for the tensile area, and shear area will be based on the same plate thicknesses as for the tensile

load case. Although the allowable stress is equal to $0.42S_u$ instead of $0.7S_u$ (see Table 2.1-1), it can be seen that this will have no effect on the allowable factor, F. Therefore, $F_S = F_T = 1.07$.

The bending stress in a typical flat plate subjected to moment loading is proportional to M/t^2, where M is a general moment loading term and t is the plate thickness, as shown in the various stress cases listed in Table 26 of Roark[8]. The characteristic bending stress in the 16 mm plate is:

$$\sigma_{16} = \frac{M}{T_{min16}^2}$$

where M is the moment load term resulting from the HAC free drop or puncture drop events. From Table 2.1-1, the allowable stress under HAC for primary membrane plus bending stress is the lesser of $3.6S_m$ or S_u, which for UNS 31803 material is S_u. The resulting margin of safety is:

$$MS_{16} = \frac{S_u}{\sigma_{16}} - 1 = \frac{S_u T_{min16}^2}{M} - 1$$

Similarly, the bending stress in the 15 mm plate is:

$$\sigma_{15} = \frac{M}{T_{min15}^2}$$

where the load M is the same as before. The margin of safety is:

$$MS_{15} = \frac{F_B S_u}{\sigma_{15}} - 1 = \frac{S_u F_B T_{min15}^2}{M} - 1$$

where the factor F_B has been introduced to indicate that the allowable stress must be higher in the case of a 15 mm plate, if the margin of safety is to be the same as a 16 mm plate. Setting the two margins of safety equal,

$$MS_{15} = MS_{16} \quad => \quad \frac{F_B S_u T_{min15}^2}{M} - 1 = \frac{S_u T_{min16}^2}{M} - 1$$

Solving for F_B,

$$F_B = \frac{T_{min16}^2}{T_{min15}^2} = \left(\frac{15.7}{14.7}\right)^2 = 1.14$$

In other words, if the 15 mm thick plate material is 14% stronger than the minimum strength permitted by the ASTM standard, the margin of safety under moment loading will be the same for a 16 mm plate that has the same minimum strength.

Therefore, the minimum strength requirement for any 15 mm plate that has been substituted for 16 mm plate in the calcium silicate protection structures or in the closure lid is governed by moment loading, and is equal to +14% or a factor of 1.14. SAR drawing flag note 53 requires that any 15 mm plate which is used in the place of 16 mm plate have a tensile ultimate strength of at least 744 MPa. This requirement also applies to the weld filler metal. Since this is equal to 1.2 times the ASTM A240/A240M minimum value of 620 MPa, this requirement is conservatively met.

[8] Young, Warren C., *Roark's Formulas for Stress and Strain*, Sixth Edition, McGraw-Hill, 1989.

2.8 Accident Conditions for Air Transport of Plutonium

This section does not apply, since air transport is not used with the TRUPACT–III package.

This page intentionally left blank.

2.9 Accident Conditions for Fissile Material Packages for Air Transport

This section does not apply, since air transport is not used with the TRUPACT–III package.

This page intentionally left blank.

2.10 Special Form

This section does not apply, since special form is not claimed for the TRUPACT–III package.

This page intentionally left blank.

2.11 Fuel Rods

This section does not apply, since fuel rods are not included as an approved payload configuration for the TRUPACT–III package.

This page intentionally left blank.

2.12 Appendices

2.12.1 Engineering Tests

2.12.2 Elastomer O-ring Seal Performance Tests

2.12.3 Certification Tests on CTU-1

2.12.4 HAC Immersion Buckling Evaluation

2.12.5 Closure Lid Debris Shield

2.12.6 Certification Tests on CTU-2

2.12.7 Closure Lid, Bolt, and Washer Interaction

This page intentionally left blank.

2.12.1 Engineering Tests

This appendix documents the results of engineering free drop and puncture tests that have been performed in support of the TRUPACT–III certification. The results of these tests are used to guide the choice of test orientations and conditions in the full-scale certification test program, and to support calculations documented in Section 2.7.1.5, *Crush Deformation Extrapolations*. The certification test results are documented in Appendix 2.12.3, *Certification Tests on CTU-1* and in Appendix 2.12.6, *Certification Tests on CTU-2*.

2.12.1.1 Introduction

A large number of free drop and puncture tests were performed on the engineering test unit (ETU), which was fabricated as prototypical, in half-scale, to the TN-Gemini packaging. The TRUPACT–III packaging is a close derivative of the TN-Gemini, and for this reason, the test results recorded in this appendix are applicable to the TRUPACT–III. Differences between the ETU and the TRUPACT–III are detailed in Section 2.12.1.3, *Test Unit Configuration*. All of these tests were performed on the same half-scale test unit. Some refurbishment of the test unit occurred during the course of testing as described below.

A total of 23 engineering tests were performed: two NCT, 0.3-m free drops, eight HAC, 9-m free drops, and 13 puncture drops. Free drop tests were performed on a flat, essentially unyielding surface from a height of either 0.3 m (NCT) or 9 m (HAC). Puncture tests were performed using the puncture bar described in 10 CFR 71.73(c)(3), in half-scale, dropped from a height of 1 m. Free drop tests were performed at ambient and cold (-29 ºC) temperatures. Most free drops were instrumented with accelerometers. Details concerning test parameters are given below.

The engineering tests comprised primarily three separate test series: The first, performed in support of the French certification of the TN-Gemini, took place in France in 1994. After refurbishment of the overpack structures and the closure lid, the second series took place in the U.S. in 2003. Further testing occurred in the U.S. in 2005. Each of these test series is described and documented in the following sections.

The engineering test results demonstrate the robust nature of the TN-Gemini and TRUPACT–III packaging designs. It is noteworthy that the ETU containment structural assembly (CSA) body structure experienced all 23 tests without refurbishment, only two different closure lids were used, and the external overpack structures were refurbished only once (a small region on the closed end was refurbished twice). With the exception of a single puncture test in 1994 (see below), the test unit was leaktight (a leak rate not exceeding 1×10^{-8} Pacals–cubic meters per second (Pa–m^3/s), air, as defined in ANSI N14.5) after each test.

2.12.1.2 Test Facilities

The test facilities utilized in France and the U.S. are described below.

2.12.1.2.1 Sandia National Laboratories (U.S.)

Most engineering free drop tests not performed in France were performed at Sandia National Laboratories' Coyote Canyon Aerial Cable Facility in Albuquerque, New Mexico. The drop pad

is designed to accommodate test packages weighing up to 90,000 kg. The embedded steel plate target has a varying thickness of approximately 100 to 200 mm. The pad therefore constituted an essentially unyielding surface for the ETU, which weighed approximately 3,775 kg.

2.12.1.2.2 Engineered Products Department (U.S.)

All puncture tests not performed in France were performed at Washington Group International's (WGI's) Engineered Products Department (EPD) in Carlsbad, New Mexico. In addition, one free drop test was performed there. The drop pad is designed to accommodate test packages weighing up to 12,600 kg. The steel plate target has a thickness of 44 mm, embedded in a reinforced concrete pad.

In accordance with the requirements of 10 CFR §71.73(c)(3), half-scale puncture bars were fabricated from a solid, 75 mm diameter mild steel with three different lengths: 750 mm, 1,200 mm, and 1,800 mm. Each puncture bar was welded with gussets perpendicularly to a 25-mm thick, mild steel, 610-mm square plate. The top edge of each puncture bar was finished to a 3-mm radius maximum. Each puncture bar assembly was securely welded to the impact surface.

2.12.1.2.3 CEA/CESTA (France)

The first series of free drop and puncture testing of the engineering test unit was performed at the Centre d'Etudes Scientifiques et Techniques d'Aquitaine du Commissariat à l'Energie Atomique (CEA/CESTA) in France. The drop pad is designed to accommodate test packages weighing up to 13,800 kg. The steel target consists of a 100-mm thick steel plate anchored in a reinforced concrete pad.

Half-scale puncture bars were fabricated from a solid, 75-mm diameter mild steel of varying length. Each puncture bar was welded perpendicularly to a 20-mm thick, mild steel, 300-mm square plate. The top edge of each puncture bar was finished to a 3-mm radius maximum. Each puncture bar assembly was securely welded to the impact surface.

2.12.1.3 Test Unit Configuration

2.12.1.3.1 U.S. Testing

The ETU was an essentially prototypic representation of the TN-Gemini package, in half-scale. The ETU differed from the TRUPACT–III in several details, however, most differences were either conservative (i.e., tending to lead to greater impact or damage) or not significant (i.e., the ETU test response would be similar to that of the TRUPACT–III.) Any ETU test results that might not be representative of the response of the TRUPACT–III were not used in certification test planning. A discussion of test article scaling is given in Section 2.12.1.4, *Scale Model Testing*.

All plate thicknesses, weld sizes, closure features, and structural dimensions were scaled by a factor of one-half. Over-reinforcement of weld beads was precluded during fabrication. The relatively large size of the ETU facilitated prototypic fabrication. The following list details the differences between the ETU and the full-scale TRUPACT–III.

1. Package length: The ETU full-scale equivalent length was 6,058 mm, whereas the TRUPACT-III length is 4,288 mm. This difference might affect drop performance in some orientations. However, this difference had no effect on data actually utilized from the ETU test results.

2. Package weight: The ETU full-scale equivalent weight was 30,000 kg, whereas the weight of the TRUPACT–III is 25,000 kg. This difference would affect free drop and puncture performance, but generally the differences would be conservative (i.e., the ETU results would in general be worse due to the greater weight).
3. Energy-absorbing materials: The phenolic foam, redwood, and most balsa wood utilized in the ETU are replaced by four different densities of polyurethane foam in the TRUPACT–III (some balsa is retained). The polyurethane foam densities used are engineered to provide similar or better performance (i.e., lower impacts and acceptable maximum deformations) compared to the ETU. Therefore, this substitution is conservative.
4. Debris shield: The ETU did not have a debris shield or guide bars. This had no effect on data utilized from the ETU test results.
5. Overpack seam welds: The configurations of some seam welds on the TRUPACT–III are of a more robust configuration than that utilized on the ETU. This difference had no effect on data utilized from the ETU test results.
6. Puncture-resistant plate design difference: The TRUPACT–III includes a 15-mm puncture-resistant plate in the octagonal recess on both ends, but the ETU (during the 2003 test series) had no puncture-resistant plate in the overpack cover, and a 10-mm thick puncture-resistant plate in the closed end. This difference had no effect on data utilized from the ETU 2003 test results. During the 2005 test series, the octagonal recess at the closed end of the ETU was refurbished to be fully prototypic to the TRUPACT–III design. The puncture test subsequently performed on this structure was therefore directly applicable to the TRUPACT–III design.
7. No thread inserts: The ETU utilized no thread inserts. However, the TRUPACT–III thread inserts are optional, and since the parent material is weaker than the thread inserts, the ETU conservatively represented the minimum pull-out strength possible in a TRUPACT–III.
8. Threaded boss: The thread bosses for the closure bolts of the TRUPACT–III are made from Alloy UNS S31803 material, while the ETU material was Type 304L. Since Alloy UNS S31803 is stronger than Type 304L, this substitution is conservative. In addition, the ETU thread bosses were connected only to the front flange face, where the TRUPACT–III bosses connect to front and rear flange faces. Since the ETU had a weaker, less rigid design, this difference is conservative.
9. Body flange: The body flange on the ETU was made by bending a plate into a U-shape, whereas the TRUPACT–III flange has a welded box structure with thicker inner and outer sheets, as shown in Figure 2.12.1-1. This difference is conservative.
10. CSA Rear Corner Containment Weld Joint: The corner weld joint on the closed end containment sheets was a two-sided fillet weld on the ETU, whereas the weld joint for the TRUPACT–III is a complete joint penetration (CJP) weld with fillet reinforcement. This difference had no effect on data utilized from the ETU test results.
11. Body vents and relief valves: The plastic plugs and pressure-relief valves located in the outer sheets are not included on the ETU. Since these plugs and valves are very small relative to the puncture bar, they would have no effect on structural behavior of the ETU.
12. ISO corner fittings: The ISO corner fittings used in the ETU were not exact replicas, but were fabricated to have equivalent rigidity to the full scale ISO corner fitting.

13. Payload dunnage: No rails, pallets, or energy absorbing dunnage were included in the half-scale test unit. Absence of these structures was conservative, since their beneficial capacity to absorb impact energy was not present. Their weight, however, was included in the simulated payload bundles, which are shown in Figure 2.12.1-2.
14. Special test ports: The ETU had special test ports on one side which were used for helium leakage rate testing during the test series. These ports were located outside any region of damage, and had no effect on data utilized from the ETU test results.

As noted previously, the ETU was manufactured by refurbishing the test unit originally tested in France in 1994. However, only the CSA body (the body weldment consisting of the inner containment boundary sheets, the structural outer sheets, the V-stiffeners, the body O-ring seal flange, and threaded holes) was original. All of the other components (the closure lid, closure lid bolts, O-ring seals, overpack, overpack cover bolts, phenolic foam, wood, calcium silicate insulating board, puncture-resistant plates, and external sheets) were newly fabricated.

Each payload bundle, which consisted of square-ended, 50 mm diameter aluminum bars, weighed approximately 29½ kg. For the 2003 engineering test series, the ETU was loaded with enough payload bundles to ensure that the total gross weight was at least equal to the equivalent half-scale weight of the TN-Gemini. The gross weight of the ETU was 3,776 kg, or 0.7% more than the maximum gross weight (in half-scale) of the TN-Gemini package.

For the 2005 engineering test series, the ETU from the 2003 test series was utilized. As noted previously, the octagonal recess on the closed end was refurbished to be prototypic to the TRUPACT–III. No other alterations were made. The same payload bars were loaded inside the ETU until a gross weight of 3,163 kg was achieved, or approximately 1% more than the maximum gross weight (in half scale) of the TRUPACT–III.

2.12.1.3.2 French Testing

The ETU utilized for the French tests was essentially the same ETU discussed in Section 2.12.1.3.1, *U.S. Testing*. The purpose of this section is to describe the configuration of the ETU for engineering tests conducted in France.

The first group of tests was performed in April, 1994, and included one NCT, 0.3-m free drop, three HAC, 9 m free drops, and three puncture drops. After each test, both the containment O-ring seal and the containment boundary were individually leaktight. The testing was halted when the last puncture test ruptured the containment boundary. The ETU was then refitted with a revised sidewall overpack design as described below. Testing was resumed in July, 1994, which repeated the same puncture test that had previously caused failure (with a successful outcome), and followed by one, 9-m free drop.

The following list itemizes differences between the ETU utilized in the French tests and the TRUPACT–III, which are in addition to the differences noted in Section 2.12.1.3.1, *U.S. Testing*.

1. Containment seal: The containment O-ring seals used were made of EPDM rubber. In the TRUPACT–III, the O-ring seals are made of butyl rubber. In addition, the width of the dovetail groove opening in the closure lid was slightly smaller than that specified for the TRUPACT–III. This difference had no effect on data utilized from the tests.

2. Puncture-resistant plates: The original configuration of the ETU had a somewhat different sidewall overpack design relative to puncture resistance. As shown in Figure 2.12.1-3, the sidewall overpack construction along the long sides (including lower and upper sides) and in the octagonal recess in the closed end was originally a layer of phenolic foam retained by a single stainless steel outer sheet. After this design proved inadequate to resist puncture, a puncture-resistant plate design was adopted. The single layer of phenolic foam was replaced by a sandwich of phenolic foam, a 5-mm thick (10-mm in full-scale) stainless steel puncture-resistant plate, and low-density balsa wood. Additionally, the outer sheet thickness was reduced to one-half of its former thickness over the same wall regions. Since the added plates were riveted in place in only a few locations, there was no significant change in any impact load paths. Since the only test which could be affected by this change was the puncture test that had failed, this change had no effect on any prior free drop and puncture tests, all of which are therefore applicable to the TRUPACT–III.
3. Closure lid bolts: The material used for the closure lid bolts was Class 8.8, which has somewhat lower yield and ultimate strengths, and lower elongation than the ASTM A320, L43 material specified for the TRUPACT–III. Since all of the important material properties were lower, this substitution was conservative.
4. Closure lid bolt length: The closure lid bolt length was shorter than the scaled specified length (98 mm vs. 102.5 mm). This difference resulted in slightly less thread engagement, which is conservative.

As with the U.S. testing, the simulated payload consisted of a large number of square-ended, round aluminum bars, varying in diameter between 50 mm and 65 mm. The bars were placed within simulated drums made of sheet metal. The ETU was loaded with enough payload bundles to ensure that the total gross weight was at least equal to the equivalent half-scale weight of the TN-Gemini. Prior to the puncture-resistant plate redesign, the gross weight of the ETU was 3,700 kg, or only 1.3% less than the maximum gross weight (in half scale) of the TN-Gemini package. Due to the added material present after implementation of the redesign, the gross weight of the ETU was 3,860 kg, or 2.9% more than the maximum gross weight of the TN-Gemini package.

2.12.1.4 Scale Model Testing

The engineering tests of the half-scale ETU were planned and executed according to the recommendations of Mok, *et al*.[1] Following the terminology of the reference, the ETU scale model used is of Type A-4, where length is the only independent scaling factor. Several important dependent parameters are discussed below.

When using a scale model to test a package design, it is important to control the essential parameters of the problem. One such parameter is fabrication. To be representative of the full-scale package, the methods and effects of fabrication must be properly scaled. To ensure proper scaling of fabrication for the ETU, a modest scaling factor of 1/2 was chosen. Since the full-scale package is very large, a half-scale model is sufficiently large to be readily fabricated prototypically.

[1] Mok, Gerald C., Carlson, Roger W., Lu, Stephen C., and Fischer, Larry E., *Guidelines for Conducting Impact Tests on Shipping Packages for Radioactive Material*, UCRL-ID-121673, Lawrence Livermore National Laboratory, September 1995.

Model Type A-4 is a general purpose scale model that has been used successfully in the past. With this model, all dimensions are scaled using the same value. Material properties, including impact limiting materials, as well as drop height and impact orientation, are identical to the full-scale package. As a result of this scaling, the model weight is 1/8 of the full-scale package. The duration of impact is 1/2, impact force is 1/4, and acceleration is twice that of the full-scale package. Resulting ETU deformations are 1/2, and material stress and strain is identical to that of the full-scale package, which is particularly relevant to regulatory compliance demonstrations. Scaling factors for other model parameters is given in Table 2.12.1-1.

Despite its general applicability, model Type A-4 suffers from some limitations in use. For the engineering tests performed, each of the stated limitations is avoided or accounted for as discussed below.

- The model should not be used in cases where impact loads are small compared to gravity. In the case of the ETU, test impact levels range up to 654g (vertical end drop.) The lowest test impact, that for the 0.3-m, NCT free drop, was 69g. These impacts are all large compared to gravity, and this issue is not of concern.
- The model should not be used in cases where strain rate-sensitive materials are used. In the case of the ETU, the primary strain rate-sensitive material is the crushable wood used in the impact limiting overpack structures. However, since the strain rate scales as S_L^{-1} per Table 2.12.1-1, the strain rate in the model wood is higher than the full-scale package, which results in a greater strain rate effect and conservatively higher impact loads applied to the CSA. For the stainless steel materials used in the CSA, the effect of a scale factor of 1/2 is not important. Therefore, strain rate sensitivity is not of concern.
- The model should not be used for materials having a coarse microstructure, such as concrete or honeycomb. In the case of the ETU, no materials having a coarse microstructure are scaled. The wood impact limiting materials are not scaled in microstructure, and therefore this issue is not of concern.
- The model should not be used to demonstrate the leak tightness of bolted closure joints. In the case of the ETU, the leakage rate test results of the scale model are not utilized to demonstrate the leak tightness of the closure joint in full-scale. However, while not conclusive, it is nonetheless significant that the closure joint of the half-scale ETU was leaktight after each test.
- The model should not be used to demonstrate structural and material failure modes such as brittle fracture and certain modes of buckling. In the case of the ETU, results relative to brittle fracture or buckling are not utilized. However, it is significant that, even though the initial out-of-flat of the ETU CSA sidewalls was conservatively larger than the maximum out-of-flat allowed by the general arrangement drawings, no evidence of bucking was present after the engineering tests.

Based on the foregoing discussion, the use of model Type A-4 is appropriate for the ETU scale model testing. The specific results of greatest importance are the rigid body impact acceleration and resulting deformations of the CSA. According to the scaling laws, the acceleration of the full-scale package will be one-half of the acceleration of the ETU, and the resulting deformations will be twice as large.

Table 2.12.1-1 – Scaling Parameters

Parameter	Value	Parameter	Value
Length	S_L	Acceleration	S_L^{-1}
Time	S_L	Deformation	S_L
Weight	S_L^3	Force	S_L^2
Drop height	1	Stress	1
Impact angle	1	Strain	1
Material properties	1	Strain rate	S_L^{-1}

Note: Contents of table are adapted from Mok, *et al*; S_L is the primary scale factor, equal to 1/2 for the ETU.

2.12.1.5 Test Conditions and Measurement

2.12.1.5.1 Accelerometers

Accelerometers were utilized to record each free drop impact in the U.S. 2003 engineering test series. A total of 24 single axis accelerometers were used: 12 placed parallel to the package longitudinal axis, and 12 placed perpendicular to the package longitudinal axis. The accelerometers were attached to solid stainless steel blocks that were fillet welded to the outer sheet on the body at the locations shown in Figure 2.12.1-4. The accelerometer type used in the tests was piezoresistive. Data was recorded, conditioned, and reduced by the Sandia Mobile Instrumentation Data Acquisition System (MIDAS). A Fast Fourier Transform (FFT) of the raw data was performed to determine the appropriate cutoff, or filtering frequency. The accelerometer data was filtered using a six-pole Butterworth filter with the cutoff set no lower than 300 Hz. No accelerometers were used for the one free drop performed in the 2005 engineering test series, nor were any used for any U.S. puncture drop tests.

In the test series conducted in France, accelerometers were utilized to record each free drop and puncture drop impact. A minimum of two single axis accelerometers were used for each drop test. The accelerometers were screwed into aluminum blocks that were bonded to the outer sheet on the body at various locations, and aligned with the axis of the drop test. Each accelerometer used in the tests had a minimum capacity of 5,000g. Data was recorded, conditioned, and reduced by a data acquisition system. The appropriate cutoff or filtering frequency was then determined by examining the spectral response. The cutoff frequency was set to encompass the initial peaks and correspond to the overall structure mode. Depending on the drop orientation, the accelerometer data was filtered using a cutoff frequency of either 150 Hz or 300 Hz.

2.12.1.5.2 Thermocouples

Maximum impact occurs at the minimum initial temperature condition of -29 °C, as defined in 10 CFR §71.73(b). For the U.S. 2003 engineering free drop tests, Type K thermocouples were installed and numbered in each end of the package to measure the temperatures of the critical impact absorbing material (wood). The thermocouple locations that were utilized for the free drop tests are shown in Figure 2.12.1-5. The thermocouples were utilized to monitor both the balsa and

redwood temperatures. Since only the balsa undergoes crush in end drops, the balsa temperature was of primary importance for these orientations. Consequently, for the end drops, only the balsa wood temperature on the impacting end was considered critical. For the slapdown free drop, only the wood temperatures on the impacting side were considered critical. No effort was made to ensure that temperatures in non-critical areas were below -29 ºC. The data was monitored by Sandia's MIDAS data acquisition system during the chilling period, and continued after the ETU was removed from the insulated box. Monitoring ceased when the thermocouples were removed just prior to the actual drops. Temperature of the wood at the moment of impact was extrapolated from the data collected just prior to removal of the thermocouples. In the near-horizontal, slapdown free drop, the thermocouples were not removed, and data was collected up to and during impact. Temperature monitoring was not utilized in the French testing or in the U.S. 2005 testing.

2.12.1.5.3 Internal Pressure

Since internal pressure has the effect of increasing the stress on the containment boundary, in the U.S. 2003 test series, the ETU was pressurized (at ambient temperature) to an internal pressure of 172 kPa, equal to the design pressure. Since resistance to puncture is not significantly affected by internal pressure, the ETU was not pressurized for the puncture tests. Since the pressure is only an initial condition, monitoring the pressure was not performed. The U.S. 2005 testing and the French testing was performed with ambient internal pressure. The effect of internal pressure is not important for puncture drops.

2.12.1.6 Engineering Tests Performed

As stated previously, the engineering tests occurred in three separate series:

- Testing in France in 1994: One, 0.3-m free drop, four, 9-m free drops, and four, 1-m puncture drops. These tests are summarized in Table 2.12.1-2 and Figure 2.12.1-6, and discussed in Section 2.12.1.7.1, *French Engineering Test Results.*
- Testing in the U.S. in 2003: One, 0.3-m free drop, three, 9-m free drops, and four, 1-m puncture drops. These tests are summarized in Table 2.12.1-3 and Figure 2.12.1-7, and discussed in Section 2.12.1.7.2, *U.S. 2003 Engineering Test Results.*
- Testing in the U.S. in 2005: One, 9-m free drop and five, 1-m puncture drops. These tests are summarized in Table 2.12.1-4 and Figure 2.12.1-8, and discussed in Section 2.12.1.7.3, *U.S. 2005 Engineering Test Results.*

2.12.1.7 Engineering Test Results

The results of the engineering tests are described in chronological test order.

2.12.1.7.1 French Engineering Test Results

After installation of the simulated payload into the ETU payload cavity, helium leakage rate tests were performed on the main O-ring seal, the sampling/vent port plug O-ring seal, and the structural containment metallic boundary. Helium leakage rate tests of the main O-ring seal and the metallic boundary were also performed following each free drop and puncture drop test. The sampling/vent port plug O-ring seal was given a final test at the end since it was inaccessible during the test series.

All free drop and puncture drop testing was performed in accordance with IAEA Safety Series No. 6, §622 and §627, utilizing a test procedure prepared for the French certification testing program.

Orientation designations of the package utilized in the French tests are an alpha-numeric designator. The alpha characters are as follows: "A" designates an "edge", "F" designates a "face", and "C" designates a corner. The numeric character designates the sequence, so that test F2 follows test A1, etc. The only exception is test A6, which was performed last in the series.

2.12.1.7.1.1 Free Drop Test No. A1 (NCT, CG-over-Cheek Edge)

Free Drop Test No. A1 was a NCT edge drop from a height of 0.3-m, impacting the edge on the body cheek. As shown in Figure 2.12.1-6, the ETU was oriented at an angle of 68° from horizontal relative to the impact surface (essentially CG-over-edge), with the closure lid end down. The pre-test orientation is shown in Figure 2.12.1-10. The following list summarizes the test parameters:

- longitudinal axis 68°, closure lid end down
- free drop height 0.32 m
- conducted test on 4/25/94

The impact resulted in a slight bulge of the side wall (approx. 7 – 10 mm). The accelerometer signal was filtered using a cutoff frequency of 150 Hz, with a peak accelerometer reading of 56g.

2.12.1.7.1.2 Free Drop Test No. F2 (HAC, Vertical, Closed End Down)

Free Drop Test No. F2 was a HAC flat end drop from a height of 9-m, impacting the closed end. As shown in Figure 2.12.1-6, the ETU was oriented at an angle of 90° from horizontal relative to the impact surface, with the closed end down. The following list summarizes the test parameters:

- longitudinal axis 90°, closed end down
- free drop height 9.05 m
- conducted test on 4/26/94

The impact resulted in small bulges on the side walls. The side bulges ranged from 19 to 32 mm, with the bulge length approximately 92.5 mm long. The principal damage to the body was the failure of three outer edge weld joints in the octagonal recess (largest split approximately 5 mm wide × 400 mm long), and a failure of the short edge weld joint over its width. The post-test damage is shown in Figure 2.12.1-11. The accelerometer signals were filtered using a cutoff frequency of 300 Hz. The peak readings of the two accelerometers were 382g and 333g (average 358g).

2.12.1.7.1.3 Puncture Drop Test No. F3 (Puncture on Overpack Cover Center)

Puncture Drop Test No. F3 impacts the center of the overpack cover/closure lid. As shown in Figure 2.12.1-6, the ETU was oriented at an angle of 90° from horizontal relative to the impact surface, with the closed end down and the CG over the bar. The following list summarizes the test parameters:

- longitudinal axis 90°, closure lid end down
- free drop height 1.18 m
- conducted test on 4/28/94

The puncture bar impacted the ETU very close to the center of the overpack cover. The puncture bar penetrated through to the inner sheet of the recess in the overpack cover. The resulting deformation in the closure lid structural sheet was approximately 21 mm deep. No penetration of the closure lid structural sheet occurred. The orientation is shown in Figure 2.12.1-12, and the damage is shown in Figure 2.12.1-13. The accelerometer signals were filtered using a cutoff frequency of 150 Hz. The peak readings of the two accelerometers were 31g and 32g.

2.12.1.7.1.4 Free Drop Test No. A4 (HAC, CG-over-Overpack Cover Edge)

Free Drop Test No. A4 was a HAC edge drop from a height of 9-m, impacting the closure lid end short edge. As shown in Figure 2.12.1-6, the ETU was oriented at an angle of 66° from horizontal relative to the impact surface (essentially CG-over-edge), with the closure lid end down. The following list summarizes the test parameters:

- longitudinal axis 66°, closure lid end down
- free drop height 9.15 m
- conducted test on 4/29/94

The impact resulted in a flat contact area of approximately 267 mm wide on the cheeks and overpack cover. The resultant side bulge in the center of the overpack cover was approximately 85 mm wide × 170 mm long. The principal damage to the overpack cover was the failure of an outer edge weld joint in the octagonal recess in the impact zone. The width of the resultant opening was a maximum of 30 mm. The orientation is shown in Figure 2.12.1-14 and the post-test damage is shown in Figures 2.12.1-15 through 2.12.1-16. The accelerometer signal was filtered using a cutoff frequency of 150 Hz, with the peak reading of the accelerometer of 196g.

2.12.1.7.1.5 Puncture Drop Test No. F5 (Puncture on Side)

Puncture Drop Test No. F5 impacted the center of the side wall at an oblique angle of 30°. Shown in Figure 2.12.1-6, the ETU longitudinal axis was horizontal and rotated at an angle of 30° relative to the impact surface, with the CG over the bar. The following list summarizes the test parameters:

- longitudinal axis 0°
- rotational axis 30°
- free drop height 1.20 m
- conducted test on 5/02/94

The puncture bar impacted the ETU side wall and penetrated all the way through the CSA containment sheet, which resulted in a breach of the containment boundary. The orientation is shown in Figure 2.12.1-17 and the damage is shown in Figures 2.12.1-18 through 2.12.1-20. Since this test was a failure, the accelerometer data is not meaningful.

As a result of this puncture drop test, the design of the side wall was modified to the current specified configuration. After performing two further tests on the closure lid end (test nos. C7 and C8), the sidewalls of the ETU were refurbished to the new design, as shown in Figure 2.12.1-3, for the final two tests.

2.12.1.7.1.6 Free Drop Test No. C7 (HAC, CG-over-Corner, Lid Down)

Free Drop Test No. C7 was a HAC corner drop from a height of 9-m, impacting the closure lid end lower right corner. As shown in Figure 2.12.1-6, the ETU diagonal edge was oriented at an angle of 59° from horizontal relative to the impact surface (essentially CG-over-corner), with the closure lid end down. The following list summarizes the test parameters:

- longitudinal axis 59° and 43°, closure lid end down
- free drop height 9.20 m
- conducted test on 5/04/94

The impact resulted in deforming the corner to a flat measuring approximately 210 mm deep along the package side × 530 mm wide × 500 mm high. Some cracking of the welds around the ISO corner fitting occurred, but were very minor. No wood or foam was exposed in the deformed area. The orientation is shown in Figure 2.12.1-21 and the damage is shown in Figures 2.12.1-22 through 2.12.1-23. The accelerometer signal was filtered using a cutoff frequency of 150 Hz, with a peak reading of 122g.

2.12.1.7.1.7 Puncture Drop Test No. C8 (Puncture on Overpack Cover/Body Gap)

Puncture Drop Test No. C8 impacts the gap between the overpack cover and the body cheek, on the lower left corner. As shown in Figure 2.12.1-6, the ETU diagonal edge was oriented at an angle of 59° from horizontal relative to the impact surface, with the closure lid end down and the CG over the bar. The impact point was in an undamaged area. The following list summarizes the test parameters:

- longitudinal axis as 59°, closure lid end down
- free drop height 1.35 m
- conducted test on 5/05/94

The puncture bar impacted the edge of the overpack cover and next to the body cheek. The puncture bar penetrated the outer sheet of the overpack cover to an approximate depth of 100 mm. The gap between the body "cheek" and the overpack cover increased to approximately 100 mm wide × 90 mm long. The orientation is shown in Figure 2.12.1-24 and the damage is shown in Figure 2.12.1-25. The accelerometer signal was filtered using a cutoff frequency of 150 Hz, with a peak reading of 14g.

2.12.1.7.1.8 Puncture Drop Test No. F9 (Puncture on Side)

Puncture Drop Test No. F9 impacts the center of the side wall at an oblique angle of 30° (repeat of Puncture Drop Test F5). As shown in Figure 2.12.1-6, the ETU longitudinal axis was horizontal and rotated at an angle of 30° relative to the impact surface, with the CG over the bar. The following list summarizes the test parameters:

- longitudinal axis 0°
- rotational axis 30°
- free drop height 1.12 m
- conducted test on 7/04/94

The puncture bar impacted the ETU side wall directly opposite from the one attacked in F5. The puncture bar penetrated to the puncture resistant plate, but did not perforate it. No penetration and no deformation of the CSA structural sheet occurred. The maximum depth of the puncture bar was approximately 90 mm. The orientation is shown in Figure 2.12.1-26 and the damage is shown in Figure 2.12.1-27. The accelerometer signal was filtered using a cutoff frequency of 150 Hz, with a peak reading of 12g.

2.12.1.7.1.9 Free Drop Test No. A6 (HAC on Side-Edge)

Free Drop Test No. A6 was a HAC edge drop from a height of 9-m, impacting the long side edge (essentially CG-over-edge). See Figure 2.12.1-6. The ETU was oriented at a small angle of 5° from horizontal relative to the impact surface, with the closed end lower. The following list summarizes the test parameters:

- longitudinal axis 5°, closed end lower
- rotational axis 46°, long side edge down
- free drop height 9.15 m
- conducted test on 7/04/94

The impact resulted in a flat along the entire length of the edge, which ranged from 120 mm to 175 mm in width. The orientation is shown in Figure 2.12.1-28 and the damage is shown in Figures 2.12.1-29 through 2.12.1-30. The accelerometer signals were filtered using a cutoff frequency of 150 Hz. The peak readings of the three accelerometers were 122g, 220g, and 227g. Discarding the low reading, the average of the two higher readings is 224g.

2.12.1.7.1.10 Post-Test Disassembly

Post-test disassembly of the ETU was performed in two stages. The initial disassembly was performed following Puncture Drop Test No. C8 in May 1994. Following the refurbishment with the puncture-resistant design, reassembly, and performing Puncture Drop Test No. F9 and Free Drop Test No. A6, the final disassembly was performed in July 1994. Prior to removing the closure lid in the final disassembly, helium leakage rate tests of the containment main O-ring seal and the metallic boundary were performed on 7/5/94. Helium leakage rate testing of the sampling/vent port O-ring seal was performed on 7/6/94. A view of the simulated payload after testing is shown in Figure 2.12.1-31, and the payload cavity in Figure 2.12.1-32.

During the removal of the closure lid, the residual tightness of the closure bolts was checked. Ten of the forty-four bolts exhibited slightly less tightening torque than the nominal installation torque of 200 N-m. However, the decrease was less than one-quarter turn. A view of the damage to the closure lid from puncture test F3 is shown in Figure 2.12.1-33.

Following removal of the loose simulated payload, the inner surfaces of the CSA containment sheets were examined and revealed no measurable deformations. Four dents from the aluminum rods used for simulated payload were noted in the CSA containment sheets. The depth of these dents ranged from 6 mm to 9 mm.

Demonstration of containment boundary leak tightness of the ETU was accomplished by utilizing the test ports located on the side of ETU (main O-ring seal and metallic boundary) and

the sampling/vent port plug (O-ring seal). The interior cavity was evacuated sufficiently to operate a mass spectrometer leak detector (MSLD). The cavity on the outside of the main and sampling/vent port O-ring seals were evacuated and subsequently backfilled with helium gas. For the CSA metallic structure, the annulus between the CSA containment and the structural sheets was evacuated and subsequently backfilled with helium gas. Results of the successful mass spectrometer helium leakage rate testing are summarized below:

Sealing Component	Leakage Rate
Main O-ring Seal	1.6×10^{-8} Pa-m^3/s, helium
Sampling/Vent Port Plug O-ring Seal	1.6×10^{-9} Pa-m^3/s, helium
CSA Metallic Structure	1.6×10^{-8} Pa-m^3/s, helium

When accounting for the conversion between air leakage (per ANIS N14.5) and helium leakage, a 2.2 factor applies for standard temperatures and pressures. Thus, a reported helium leakage rate of 1.6×10^{-8} Pa-m^3/s, helium, is equivalently 7.3×10^{-9} Pa-m^3/s, air, a level below the "leaktight" criterion of 1×10^{-8} Pa-m^3/s, air, per ANSI N14.5.

In conclusion, based on visual inspection and on leakage rate testing, there was no evidence of buckling of the CSA containment sheets, gross distortion of the O-ring sealing flanges that would cause a sealing failure, or rupture of the containment boundary for the final puncture-resistant plate design.

2.12.1.7.2 U.S. 2003 Engineering Test Results

Prior to performing any free or puncture drop tests, extensive pre-test measurements of the ETU were made. They were compared to post-test measurements as discussed in Section 2.12.1.7.2.10, *ETU Measurements*. A pressure test using an internal pressure of 1.5 times MNOP was performed, and then the simulated payload was installed into the cavity. Helium leakage rate tests were then performed on the main O-ring seal and the sampling/vent port plug O-ring seal. The structural containment boundary leakage rate test was performed as a part of ETU acceptance testing. All free drop and puncture drop measurements and testing were performed in accordance with a written test plan. The alpha-numeric test designator includes the letters "FD" for free drops and "P" for punctures, followed by a sequence number. The order of testing was FD1 to FD4, followed by P1 to P4.

In the three vertical drops, acceleration readings increased with increasing distance from the ground. That is, the vertical accelerations nearest the ground were least, the accelerations farthest from the ground were greatest, and the accelerations at the package axial middle were in between. For example in free drop FD3, the average acceleration of the four accelerometers located farthest from the ground was about 23% greater than the average of the four nearest the ground. Since this phenomenon was likely a result of a global elastic response of the package in an axial mode, the accelerometers nearest the ground therefore represented the best approximation to the rigid-body acceleration of the package upon impact. All of the accelerometer summaries presented herein are for the accelerometers nearest the ground.

2.12.1.7.2.1 Free Drop Test No. FD1 (HAC Vertical, Closed End Down)

Free Drop Test No. FD1 was a HAC flat end drop from a height of 9-m, impacting the closed end (package vertical). As shown in Figure 2.12.1-7, the ETU was oriented at an angle of 90°

from horizontal relative to the impact surface, with the closed end down. The following list summarizes the test parameters:

- verified internal pressure as 172 kPa, +25/-0 kPa
- package temperature was accepted at -21 °C
- verified longitudinal axis as 90° ± 5°, closed end down
- verified free drop height as 9-m, +75/-0 mm
- measured ambient temperature as 19 °C at time of test
- conducted test at 9:16 a.m. on 9/16/03

Although the ETU was suspended in the correct orientation (90° ± 5°), the ETU impacted at an angle between 83° – 85°. This impact angle was apparently caused by a very slight delay in cutting one of the four cables. The impact surface (judged by rust transfer from the pad) covered approximately 2/3 of the closed end face of the ETU. Viewed from the end, the lower left corner impacted first, and deformed approximately 67 mm. The diagonally opposite corner crushed approximately 1.5 mm. The vertical left and bottom weld seams between the side and end sheets split open, although the openings were nearly filled with deformed steel material from the outer sheets. Some weld seams also split around the edge of the octagonal recess, with a maximum gap opening of approximately 6 mm. Openings also occurred around the ISO fitting on the initially impacted corner. The post-test damage is shown in Figures 2.12.1-34 through 2.12.1-35.

The accelerometer signals were filtered using a cutoff frequency of 300 Hz. The peak readings of the four accelerometers nearest to the impact surface are as follows:

Accelerometer	A3	A4	A9	A10	Avg.
Peak Value (g)	229	219	185	236	217

After the test, the overpack cover was removed and the closure lid bolts retightened. Out of the forty-four closure lid bolts, only one bolt turned slightly when retightened to 200 N-m torque. The overpack cover was replaced and its ten bolts were retightened to 200 N-m torque.

2.12.1.7.2.2 Free Drop Test No. FD2 (NCT Vertical, Lid End Down)

Free Drop Test No. FD2 was a NCT flat end drop from a height of 0.3-m, impacting the closure lid end (package vertical). As shown in Figure 2.12.1-7, the ETU was oriented at an angle of 90° from horizontal relative to the impact surface with the closure lid end down. The following list summarizes the test parameters:

- verified internal pressure as 172 kPa, +25/-0 kPa
- measured package temperature as -37 °C
- verified longitudinal axis as 90° ± 5°, closure lid end down
- verified free drop height as 0.3-m, +25/-0 mm
- measured ambient temperature as 16 °C at time of test
- conducted test at 8:36 a.m. on 9/17/03

There was almost no visible damage from the impact. No weld seams failed. As shown in Figure 2.12.1-36, the only deformation was a small bulge on one side. The maximum

deformation of the closure lid end was approximately 6 mm near the upper right corner, as viewed in the normally transported horizontal orientation.

The accelerometer signals were filtered using a cutoff frequency of 300 Hz. The peak readings of the four accelerometers nearest to the impact surface are as follows:

Accelerometer	A1	A6	A7	A12	Avg.
Peak Value (g)	78	51	82	64	69

2.12.1.7.2.3 Free Drop Test No. FD3 (HAC Vertical, Lid End Down)

Free Drop Test No. FD3 was a HAC flat end drop from a height of 9-m, impacting the closure lid end (package vertical). As shown in Figure 2.12.1-7, the ETU was oriented at an angle of 90° from horizontal relative to the impact surface with the closure lid end down. The following list summarizes the test parameters:

- verified internal pressure as 172 kPa, +25/-0 kPa
- measured package temperature as -28 °C
- verified longitudinal axis as 90° ± 5°, closure lid end down
- verified free drop height as 9-m, +75/-0 mm
- measured ambient temperature as 12 °C at time of test
- conducted test at 8:47 a.m. on 9/18/03

A review of the video recording of the drop demonstrated that the impact was essentially perfectly flat on the closure lid end. Post-test photographs are shown in Figures 2.12.1-37 through 2.12.1-38. There were no significant weld seam splits as a result of this free drop. The maximum crush distance of the ETU closure lid end was an additional 17 mm (measured from the post-Free Drop Test No. FD2 position).

The accelerometer signals were filtered using a cutoff frequency of 400 Hz, rather than 300 Hz, based on consideration of the FFT of the data. The peak readings of the four accelerometers nearest to the impact surface are as follows:

Accelerometer	A1	A6	A7	A12	Avg.
Peak Value (g)	781	641	671	521	654

2.12.1.7.2.4 Free Drop Test No. FD4 (HAC Slapdown, Lid End Secondary)

Free Drop Test No. FD4 was a HAC free drop from a height of 9-m, impacting 25° from horizontal with primary impact on the closed end and secondary impact on the closure lid end, as shown in Figure 2.12.1-7. The top short edge on the closed end was the primary impact point. The following list summarizes the test parameters:

- verified internal pressure as 172 kPa, +25/-0 kPa
- measured balsa temperature as -34 °C, and redwood temperature as -31 ºC
- verified longitudinal axis as 30° ± 5°, top edge of closed end down
- verified free drop height as 9-m, +75/-0 mm

- measured ambient temperature as 13 °C at time of test
- conducted test at 9:47 a.m. on 9/19/03

Primary Impact: The principal damage to the closed end was the relatively wide split of weld joints in the octagonal recess near the impacted edge, as shown in Figure 2.12.1-39. Although affected by prior damage from Free Drop No. FD1, it was concluded that the damaged weld joints would occur even in the absence of damage accumulation.

The accelerometer signals were filtered using a cutoff frequency of 300 Hz. The peak readings of the eight accelerometers at the primary impact end (closed end) are as follows:

Direction	Perpendicular to Axis				Parallel to Axis			
Accelerometer	A15	A16	A21	A22	A3	A4	A9	A10
Peak Value (g)	200	193	221	368	26	No Data	550	-98

The high reading shown for A9 was not consistent with the readings of other accelerometers (for example, A3), and was therefore considered to be a test anomaly.

Secondary Impact: The secondary impact occurred at an inclination of approximately 2º – 4º to the horizontal. The maximum crush distance at the outside edge of the overpack cover was approximately 25 mm, and the length of the impact zone, measured from the overpack cover end, was approximately 483 mm. A gap of up to 35 mm developed between the overpack cover and the side cheeks, but this gap was not open all the way to the root of the cheek. As shown in Figure 2.12.1-40, the gap was blocked by buckled sheet material from the inside face of the cheek. Some weld seams on the overpack cover split (approximately 10 mm wide), while many of the split weld seams remained essentially closed after impact. An overall view of the impact damage and a close-up view of the ISO fitting damage are shown in Figures 2.12.1-41 and 2.12.1-42, respectively.

The peak readings of the eight accelerometers at the center and at the secondary impact end (closure lid) during secondary impact are as follows:

Position	Direction	Perpendicular to Axis				Parallel to Axis			
Center	Accelerometer	A14	A17	A20	A23	A2	A5	A8	A11
	Peak Value (g)	No Data	350	286	No Data	-131	222	-208	186
End	Accelerometer	A13	A18	A19	A24	A1	A6	A7	A12
	Peak Value (g)	631	671	657	640	-103	202	-168	175

Note: The average acceleration at the package end, perpendicular to the package axis, was equal to (631 + 671 + 657 + 640)/4 = 650g.

2.12.1.7.2.5 Puncture Drop Test No. P1 (Puncture on Overpack Cover Near Bolts)

Puncture Drop Test No. P1 impacted the recess on the overpack cover. As shown in Figure 2.12.1-7, the ETU was oriented at an angle of 71° from horizontal relative to the impact surface, with the closure lid end down. The following list summarizes the test parameters:

- verified 750 mm long puncture bar welded to pad

- verified longitudinal axis as 71° ± 5°, closure lid end down
- verified free drop height as 1-m, +25/-0 mm
- measured ambient temperature as 27 °C at time of test
- conducted test at 9:00 a.m. on 9/23/03

Due to the characteristics of the rigging, the ETU translated slightly to the side on release so that the puncture bar impact occurred approximately 200 mm from the recess edge. The puncture bar penetrated the overpack cover end and created a 216 mm long tear on the closure lid outer structural sheet. The CSA containment boundary sheet was not damaged. Post-test photographs are shown in Figures 2.12.1-43 through 2.12.1-45.

2.12.1.7.2.6 Puncture Drop Test No. P2 (Puncture on Overpack Cover Joint)

Puncture Drop Test No. P2 impacted the lower corner joint between the side cheek and the overpack cover. As shown in Figure 2.12.1-7, the ETU was oriented at a compound angle of 120° and 45° from horizontal relative to the impact surface, with the closure lid end down. The following list summarizes the test parameters:

- verified 1,200 mm long puncture bar welded to pad
- verified longitudinal axis as 120° & 45° ± 5°, closure lid end down
- verified free drop height as 1-m, +25/-0 mm
- measured ambient temperature as 32 °C at time of test
- conducted test at 11:20 a.m. on 9/23/03

The puncture bar impacted on the gap between the overpack cover and the cheek, approximately 232 mm from the bottom edge of the lower right cheek structure (viewed as normally transported from the overpack cover end). The bar struck as desired, and did essentially no damage to the ETU structure, as shown in Figure 2.12.1-46.

2.12.1.7.2.7 Puncture Drop Test No. P3 (Puncture on Slapdown Damage)

Puncture Drop Test No. P3 impacted the joint between the body and the overpack cover. As shown in Figure 2.12.1-7, the ETU was oriented at an angle of 30° from horizontal relative to the impact surface, with the closed end down. The following list summarizes the test parameters:

- verified 1,800 mm long puncture bar welded to pad
- verified longitudinal axis as 30° ± 5°, closed end down
- verified free drop height as 1-m, +25/-0 mm
- measured ambient temperature as 34 °C at time of test
- conducted test at 3:05 p.m. on 9/23/03

The puncture bar impacted the upper overpack cover joint, in the same area as the secondary slapdown impact damage from Free Drop No. FD4. The impact point was about halfway between overpack cover bolt Nos. 3 and 4. The resulting deformation covered approximately 46

mm on the body, and 83 mm on the overpack cover, with a maximum depth of 36 mm. The puncture drop damage is shown in Figures 2.12.1-47 through 2.12.1-49.

2.12.1.7.2.8 Puncture Drop Test No. P4 (Puncture on Closed End)

Puncture Drop Test No. P4 impacted the recess on the closed end, adjacent to the wall of the recess. As shown in Figure 2.12.1-7, the ETU was oriented at an angle of 71° from horizontal relative to the impact surface, with the closed end down. The following list summarizes the test parameters:

- verified 750 mm long puncture bar welded to pad
- verified longitudinal axis as 71° ± 5°, closed end down
- verified free drop height as 1-m, +25/-0 mm
- measured ambient temperature as 21 °C at time of test
- conducted test at 7:57 a.m. on 9/30/03

The puncture bar impacted the ETU approximately 152 mm from the octagonal recess edge. The puncture bar penetrated through to the outer structural sheet of the CSA. The deformation in the CSA structural sheet was approximately 29 mm deep, and a section approximately 1/3 of the bar circumference (~80 mm) sheared completely through the sheet. The damage is shown in Figures 2.12.1-50 through 2.12.1-52.

2.12.1.7.2.9 ETU Post-Test Disassembly

Post-test disassembly of the ETU was performed in two stages. The initial disassembly was performed following Puncture Drop test No. P3 on 9/24/03. Following removal of the overpack cover and inspection of the damage to the exterior of the closure lid, a helium leakage rate test of the containment O-ring seals was performed. Following detailed inspection and measurement of the O-ring sealing flange on the closure lid and body, the ETU was reassembled for Puncture Drop Test No. P4. Final helium leakage rate testing of the metallic boundary was performed on 10/1/03.

Demonstration of containment boundary leak tightness of the ETU was accomplished by utilizing the test ports located on the side of ETU (main O-ring seal and metallic boundary) and the sampling/vent port plug (O-ring seal). The interior cavity was evacuated sufficiently to operate a mass spectrometer leak detector (MSLD). The cavities on the outside of the main and sampling/vent port O-ring seals were evacuated and subsequently backfilled with helium gas. For the CSA metallic structure, the annulus between the CSA containment and the structural sheets was evacuated and subsequently backfilled with helium gas. Results of the successful mass spectrometer helium leakage rate testing are summarized below:

Sealing Component	Leakage Rate
Main O-ring Seal	$<1.0 \times 10^{-9}$ Pa-m^3/s, helium
Sampling/Vent Port Plug O-ring Seal	$<1.0 \times 10^{-9}$ Pa-m^3/s, helium
CSA Metallic Structure	$<1.0 \times 10^{-9}$ Pa-m^3/s, helium

When accounting for the conversion between air leakage (per ANIS N14.5) and helium leakage, a 2.2 factor applies for standard temperatures and pressures. Thus, a reported helium leakage

rate of 1.0×10^{-9} Pa-m^3/s, helium, is equivalently 4.6×10^{-10} Pa-m^3/s, air, a level well below the "leaktight" criterion of 1×10^{-8} Pa-m^3/s, air, per ANSI N14.5. Views of the disassembled ETU are shown in Figures 2.12.1-53 through 2.12.1-56.

2.12.1.7.2.10 ETU Measurements

Extensive measurements of the ETU were made both before and after testing. Measurements of the payload cavity dimensions, closure bolt residual torque, closure lid lateral position, closure lid global flatness, and the local flatness of the body and closure lid sealing flanges were made. The following is a summary of the results.

- The length, width, height, and diagonals of the payload cavity were measured. The length, width, and diagonal measurements remained essentially unchanged. The only measurable change was in the height of the cavity at the open end, which decreased by approximately 2 mm. This was probably due to the forces resulting from the slapdown secondary impact. Some waviness in the containment sheets, parallel to the v-stiffeners, was noted before testing, most likely due to welding distortion. The depth of several "waves" were measured before and after testing, and no significant change in their depth or shape was noted.
- Closure bolt residual torque was measured prior to removing the closure lid. The average residual torque of all 44 bolts was 145 N-m, and the minimum value was 83 N-m. Since the applied torque was 200 N-m, the average represents a residual torque of 72%, and the minimum, 41%, of the originally applied value.
- The position of the closure lid was measured in order to characterize its behavior in the slapdown drop, where large lateral forces were generated. Post test measurements showed that the lid moved 2 mm toward the normally transported bottom of the package. Since the slapdown drop occurred on the top of the package, the lid moved away from the ground under the forces generated by the overpack cover structures in the secondary impact event. The direction of motion is parallel to the sealing flange face, and therefore had no consequences to the containment seal leakage rate. The amount of movement, 2 mm, was much less than the 7 mm clearance between the closure bolts and lid holes, and no visual evidence of contact between the lid shear lip and the body opening was present.
- Lid global flatness was checked to see if the forces from the payload (primarily from free drop FD3 or from puncture drop P1) could cause permanent deformation of the lid structure. The result showed that essentially no permanent deformation of the inside sheet of the closure lid occurred as a consequence of the testing.
- The body and closure lid flanges were measured before and after testing to determine if the test loads caused any permanent deformation of the flanges, and specifically, if any significant permanent reduction in the compression of the containment O-ring seal occurred. This was done using a multi-axis machine tool holding a dial indicator. Two rows of 13 points each were measured on each of the four sides of both the body and the lid flanges for a total of 208 individual measurements each time. The inner row of points was located 12 mm from the inner edge of the flange, and the outer row was located 10 mm from the outer edge. Points 1 – 4, 6, 8, 10, and 11 – 13 were located halfway between two bolts, and points 5, 7, and 9 were located at bolt locations near the center of the flange length. Thus, the density of measurement points increased near the center of each side. Refer to Figure 2.12.1-9. Each

point on the body was nominally coincident with a point on the lid. The position of the flange face in a direction axial to the ETU was measured relative to a common, arbitrary datum plane. From the raw measurements of the body and lid, gaps were calculated for all of the measurement locations around the flange. Each gap value represents the distance between the body and lid flange faces at the outside edge of the flange for the assembled, post-test configuration. Since the flange measurements were made with the lid removed, the calculations omit the effect of the closure bolt residual tightness, and are therefore very conservative. Note that the gap value is not necessarily equal to a change due to testing, but the total present after testing, which includes the effect of any pre-testing gaps. The flange gaps are given in Table 2.12.1-5. The maximum gap is 0.89 mm, located in the top flange at position 2. For comparison, a post-test feeler gauge measurement of the same location showed a gap of only 0.28 mm, demonstrating the conservatism of this calculation method.

Since all of the gaps between the body and the lid were located on the outside edge of the flange face, the movement at the containment O-ring seal, which is located near the inside edge of the flange, is much less. The seal is located 12.5 mm from the inside edge of the flange, and the total width of the top flange is 70.5 mm. Using linear interpolation, the maximum movement at the containment O-ring seal is:

$$M_{max} = \left(\frac{12.5}{70.5}\right)0.89 = 0.16 \text{ mm}$$

In full scale, the maximum movement would be twice this amount, or 0.32 mm. This is a very small movement compared to the compression of the elastomer seal of nominally 3 mm.

In conclusion, there was very little accumulated damage to the CSA structure resulting from the four free drops and four puncture drops. There was no evidence of buckling of the CSA containment sheets, gross distortion of the O-ring sealing flanges that would cause a sealing failure, or rupture of the containment boundary.

2.12.1.7.3 U.S. 2005 Engineering Test Results

The U.S. 2005 testing was performed at EPD in Carlsbad, NM, in September, 2005. The objectives of this test were:

1. To determine the effectiveness of the 15-mm thick (equivalent full-scale) puncture-resistant plate on the bottom end and in the overpack cover. Results were evaluated by general observations and measurements.
2. To determine the worst-case puncture attack angle for the side panels. Results were evaluated by comparison of the dent depth in the CSA outer sheet as described below.
3. To ensure that the package can withstand the 30 ft, horizontal side drop. Results were evaluated by general observation of the puncture damage.

Prior to testing, the internal width and height at mid-length of the CSA were measured for comparison with post-test measurements. After installation of the closure lid, a hard vacuum was placed between the two O-ring seals to ensure proper installation. Since the vent/test port had not been disturbed since the prior test series, it was not retested. No thermocouples or accelerometers were used. No internal pressure was used, and all tests occurred at ambient

temperature. Prior damage and weathering may have had an effect on the free drop results, and possibly on two of the five puncture tests. However, since the free drop was considered an order-of-magnitude test, the ETU pre-condition was not disqualifying. The effect of ETU condition on the punctures is discussed below. The free drop test is designated "FD05". The puncture tests are designated "P*x*05" where *x* = 1 through 5.

2.12.1.7.3.1 Free Drop Test FD05 (Flat Side)

In this test, the ETU was dropped flat on the (normally) vertical side opposite the special test ports. The test was planned as an order-of-magnitude test of the large impact forces that can be expected on the certification test of the same orientation. Although the actual impact magnitude was not recorded, the results demonstrate that the TRUPACT–III can withstand this impact without deformation of the CSA or damage to the closure flange and containment sealing area. Post-test measurements showed no change to the CSA-internal height and width measurements and only a very small (approximately 2-mm full scale) lateral slip of the closure lid. The closure bolts had essentially undiminished removal torque, and the containment seal was capable of a hard vacuum (application of a hard vacuum was utilized in lieu of a helium leak test.) Due to the large size of the impact area of the ETU, the impact deformation was too small for meaningful measurements.

2.12.1.7.3.2 Puncture Drop Tests P105 through P405 (Oblique on Sides)

In this series of puncture tests, the sides of the ETU, which were not damaged from prior testing, were used. In all cases, the line of puncture was through the center of gravity. The tests differed only in the oblique angle between the package surface and the puncture bar axis. The ETU axis was horizontal, and rotated by different amounts about that axis to achieve the desired orientations.

The results are shown in Table 2.12.1-6. In most cases, the puncture bar impact caused a shear fracture in the puncture-resistant plate. In no case did a shear fracture occur in the outer sheet of the CSA.

To fully support the conclusions drawn from the engineering puncture tests, the results in Table 2.12.1-6 are augmented by the results from puncture test P4 (see Section 2.12.1.7.2.8, *Puncture Drop Test No. P4*) that occurred during the U.S. 2003 test series. In that test, the puncture drop energy was approximately only 7% greater than in the U.S. 2005 puncture test series, and the impacted structure was identical, and therefore it may be included along with the other puncture tests documented here. Of note, a small fracture did occur in the CSA outer sheet in that test as shown in Figure 2.12.1-52.

As shown in the table, the puncture test severity, measured as the dent depth of the CSA outer sheet, increases with decreasing oblique angle, until a maxima is reached in the range of 20º to 25º. Of note, inspection of the puncture damage after test P305 showed that the outer layer of balsa wood contained moisture due to weathering during storage of the ETU. Since it was unclear what effect that might have on the results, the test at 25º was repeated (as test P405) in a different location. In that case, the impact occurred on a patch made in the CSA outer sheet subsequent to the test F5 in France, causing a small fracture in the patch material. The depth of the dent shown in the table for test P405 on the patch may not be representative of the response of prototypical CSA structure. Figures of the puncture damage for puncture tests P105 through P405 are shown in Figures 2.12.1-57 through 2.12.1-60.

2.12.1.7.3.3 Puncture Drop Test P505 (On Closed End)

The purpose of this test was to confirm the performance of the 15-mm puncture-resistant plates in the overpack cover and closed end octagonal recess areas. The angle of impact was as oblique as possible given the need to enter the recessed area with the puncture bar. The ETU axis was inclined 71º from the horizontal. The orientation of the closed end wall was equal to 90 – 71 = 19º from horizontal. The results showed that the puncture-resistant plate dented, but did not experience any shear fracturing. The puncture damage is shown in Figure 2.12.1-61.

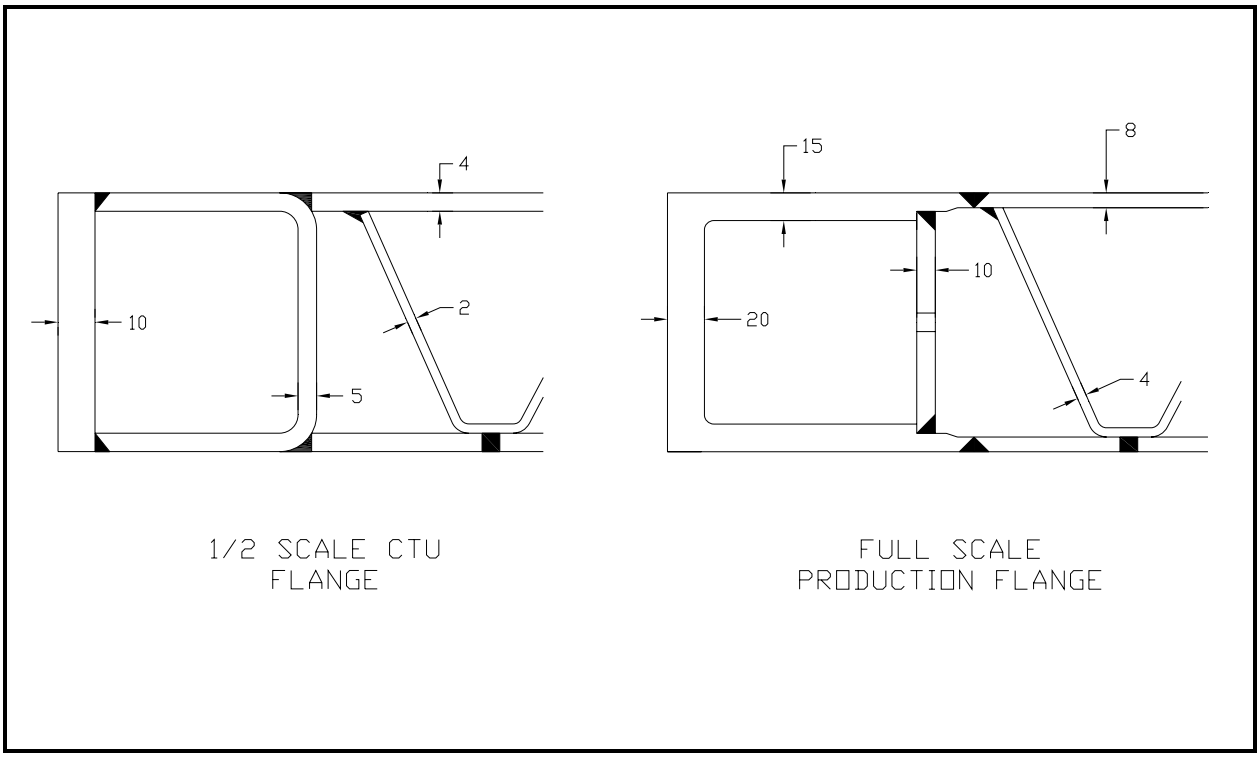

Figure 2.12.1-1 – ETU and TRUPACT–III Body Flange Construction Comparison

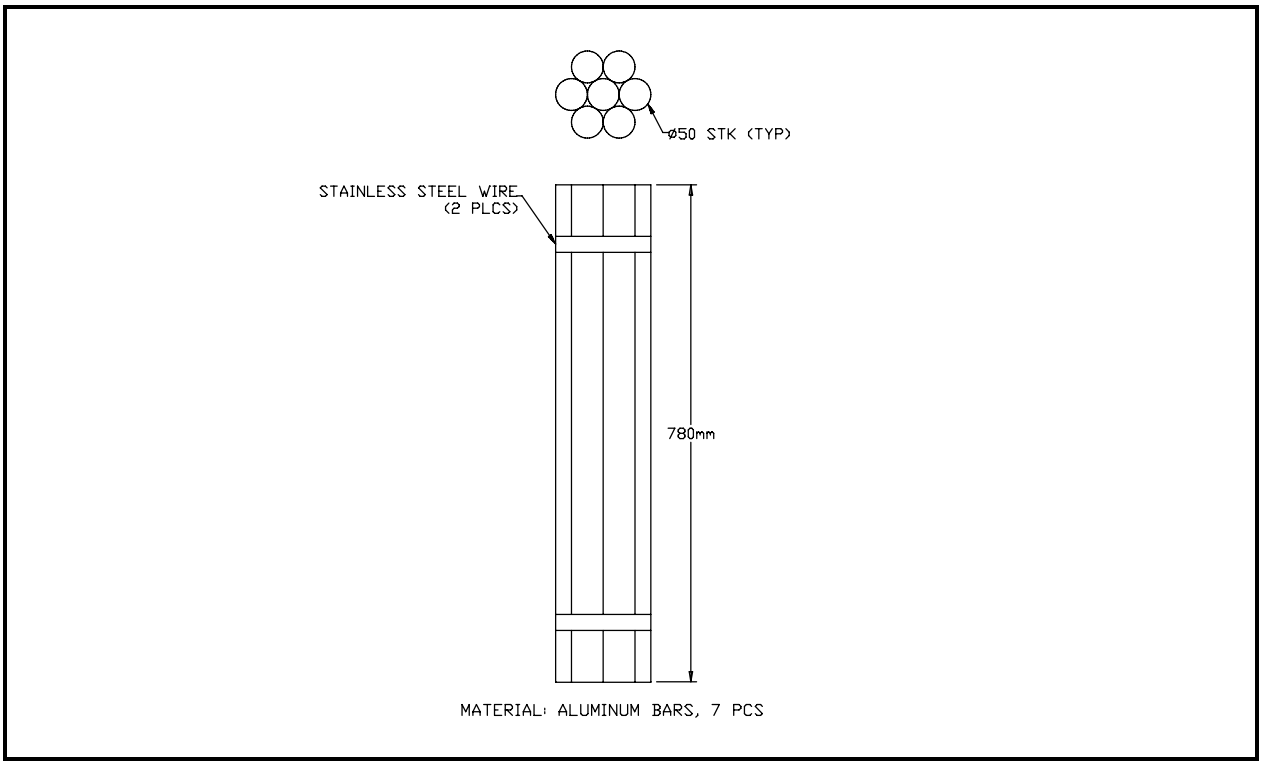

Figure 2.12.1-2 – ETU Simulated Payload Bundle – U.S. 2003 Testing

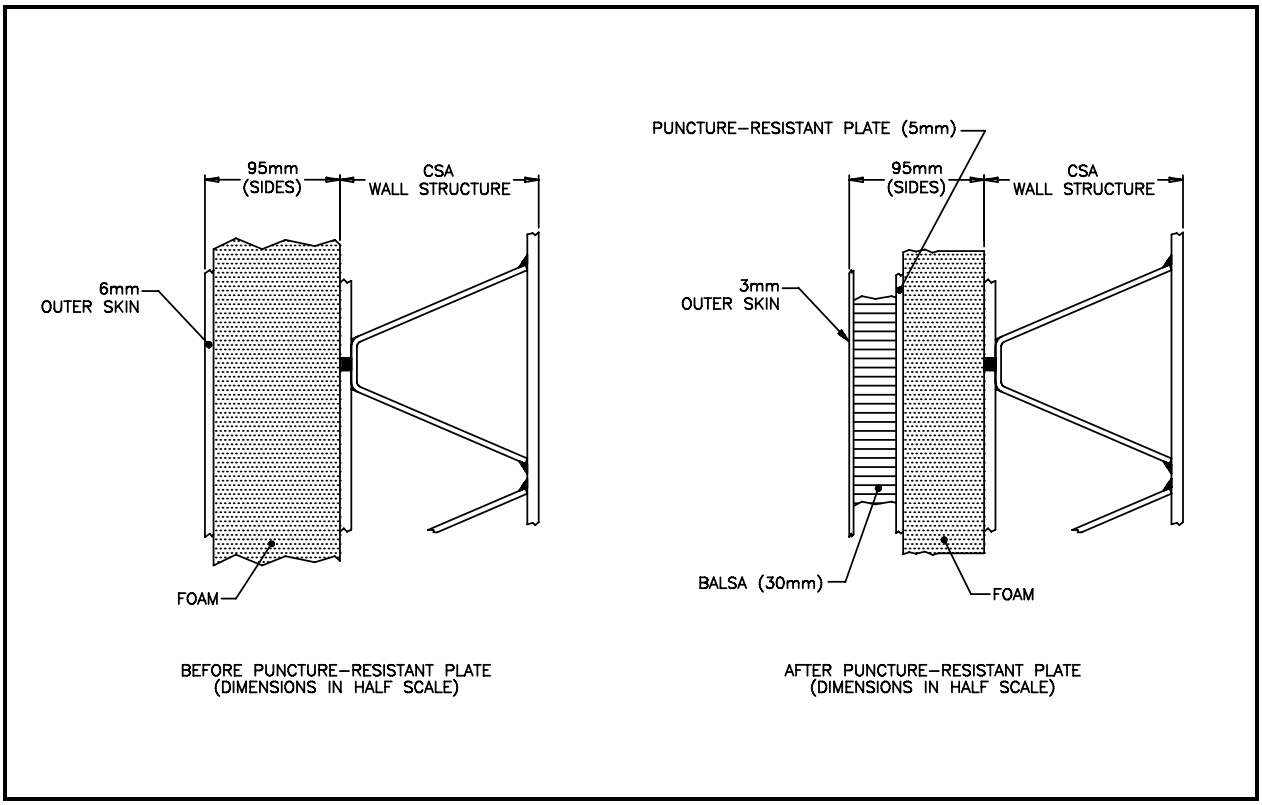

Figure 2.12.1-3 – Comparison of ETU Sidewall Designs in French Testing

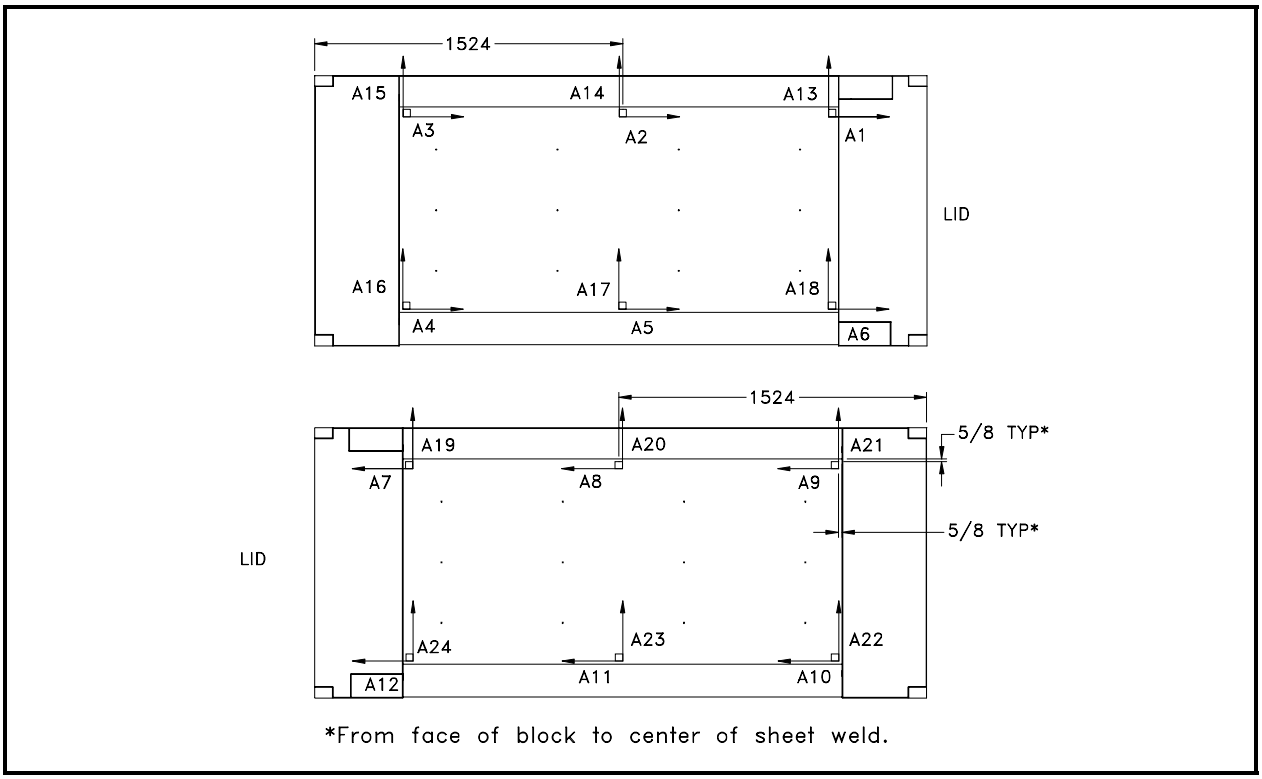

Figure 2.12.1-4 – Accelerometer Locations – U.S. 2003 Testing

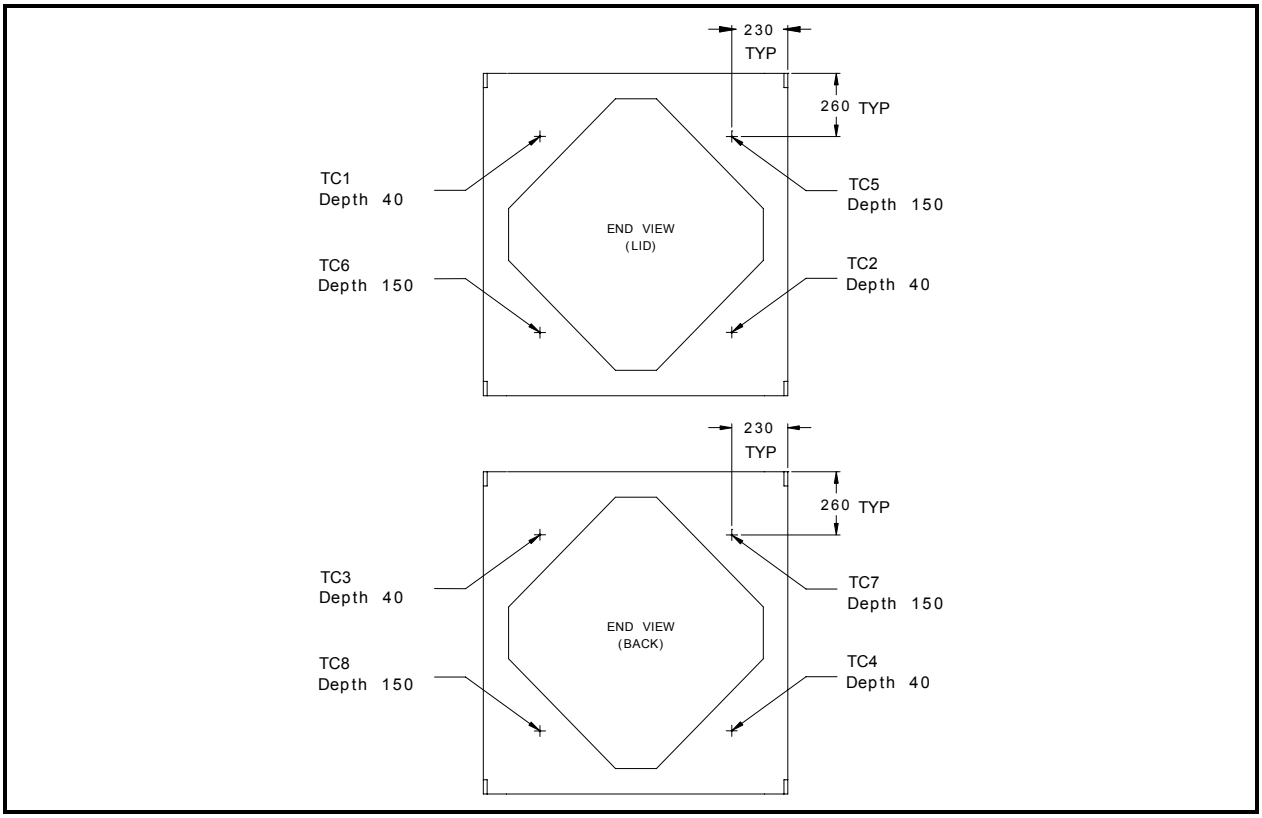

Figure 2.12.1-5 – Thermocouple Locations and Depths – U.S. 2003 Testing

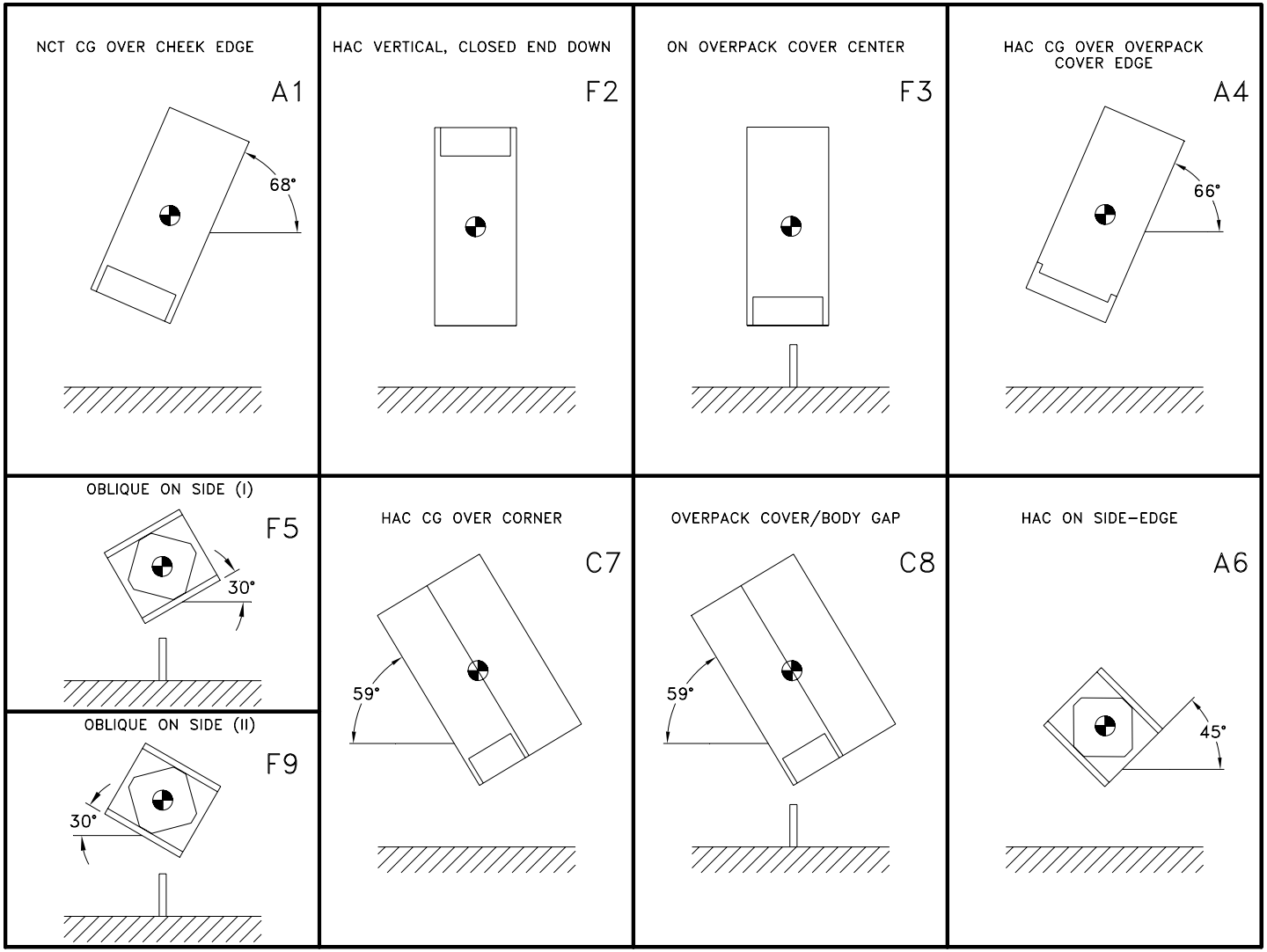

Figure 2.12.1-6 – Schematic of French Engineering Tests

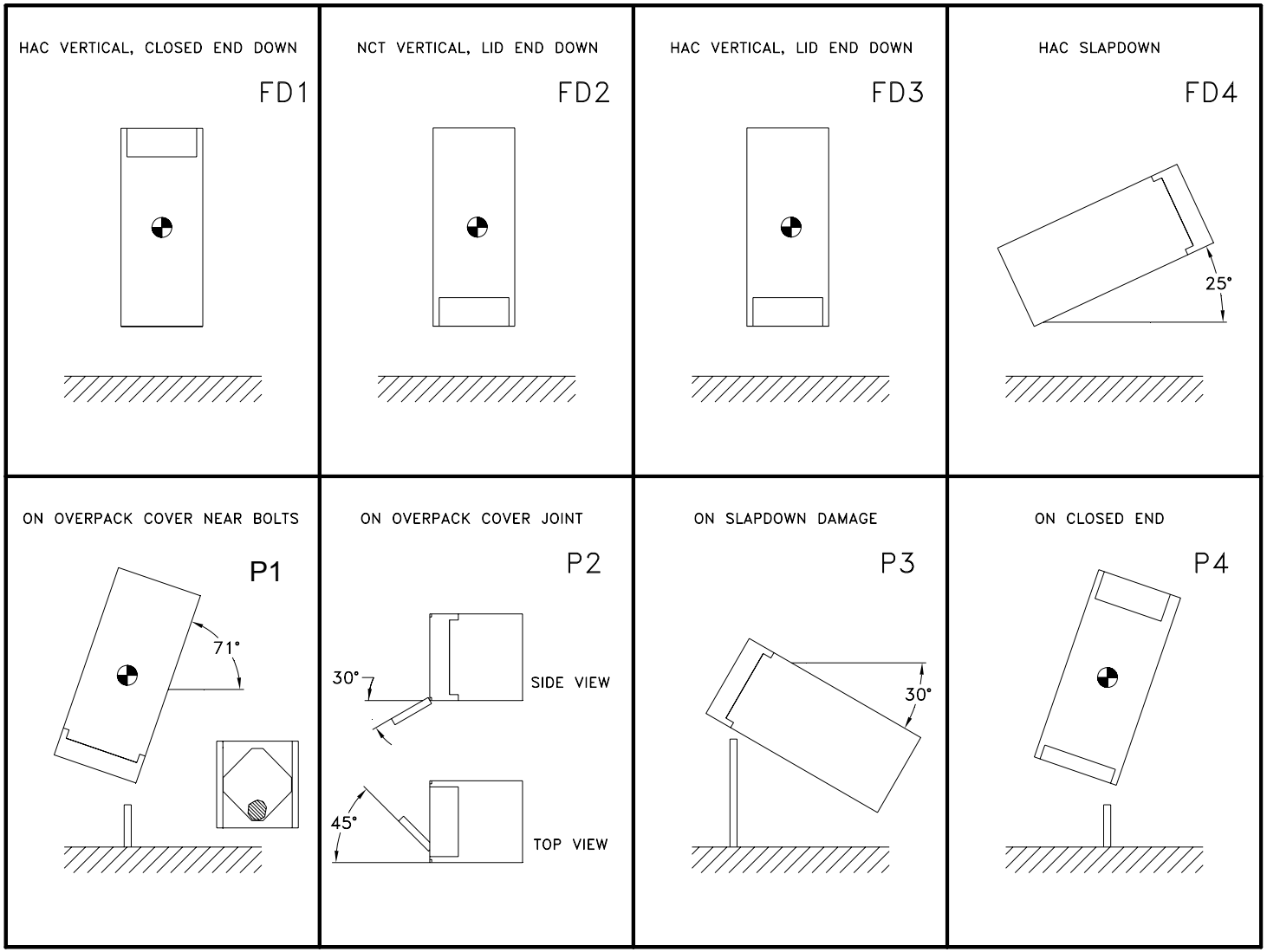

Figure 2.12.1-7 – Schematic of U.S. 2003 Engineering Tests

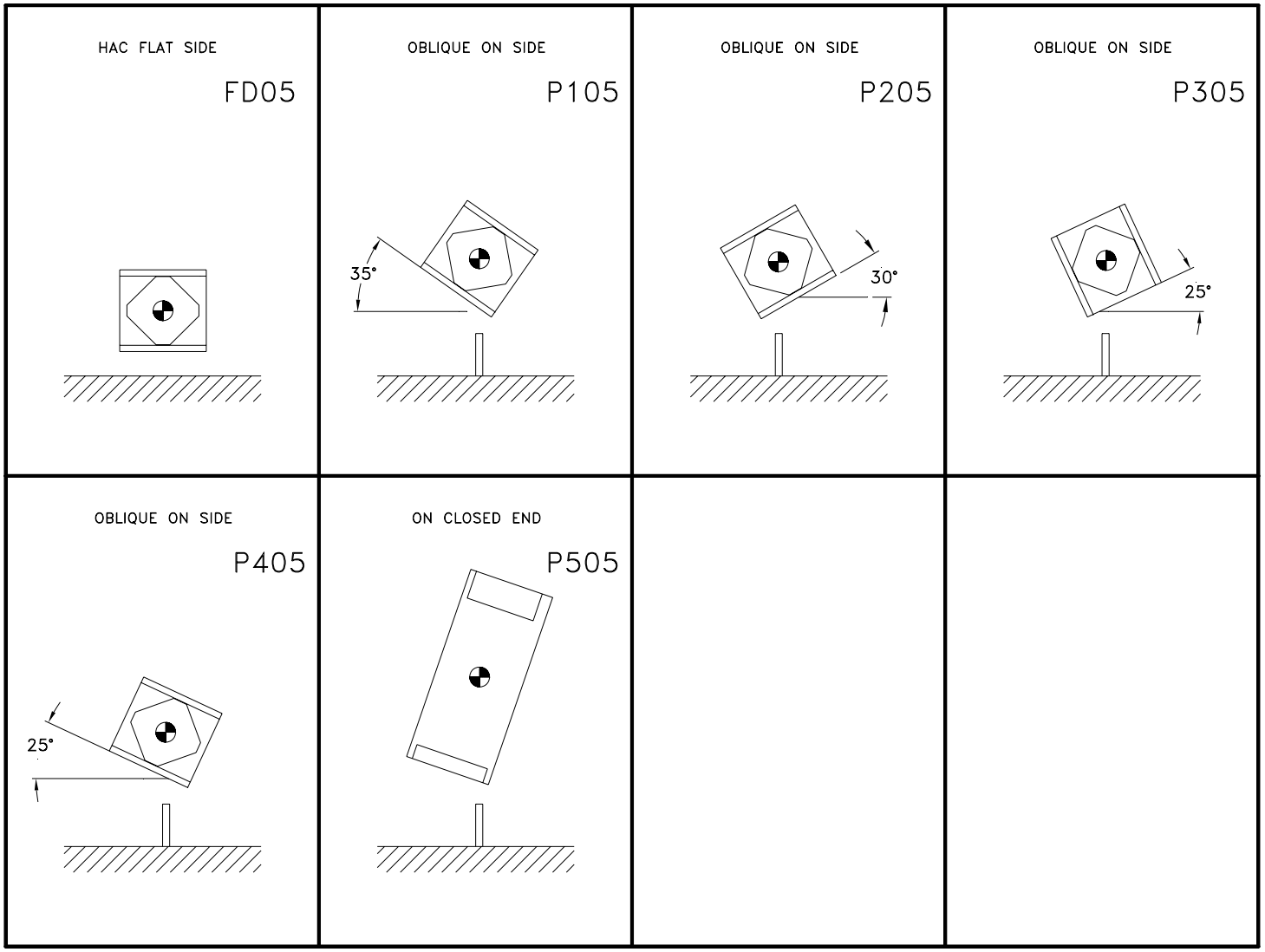

Figure 2.12.1-8 – Schematic of U.S. 2005 Engineering Tests

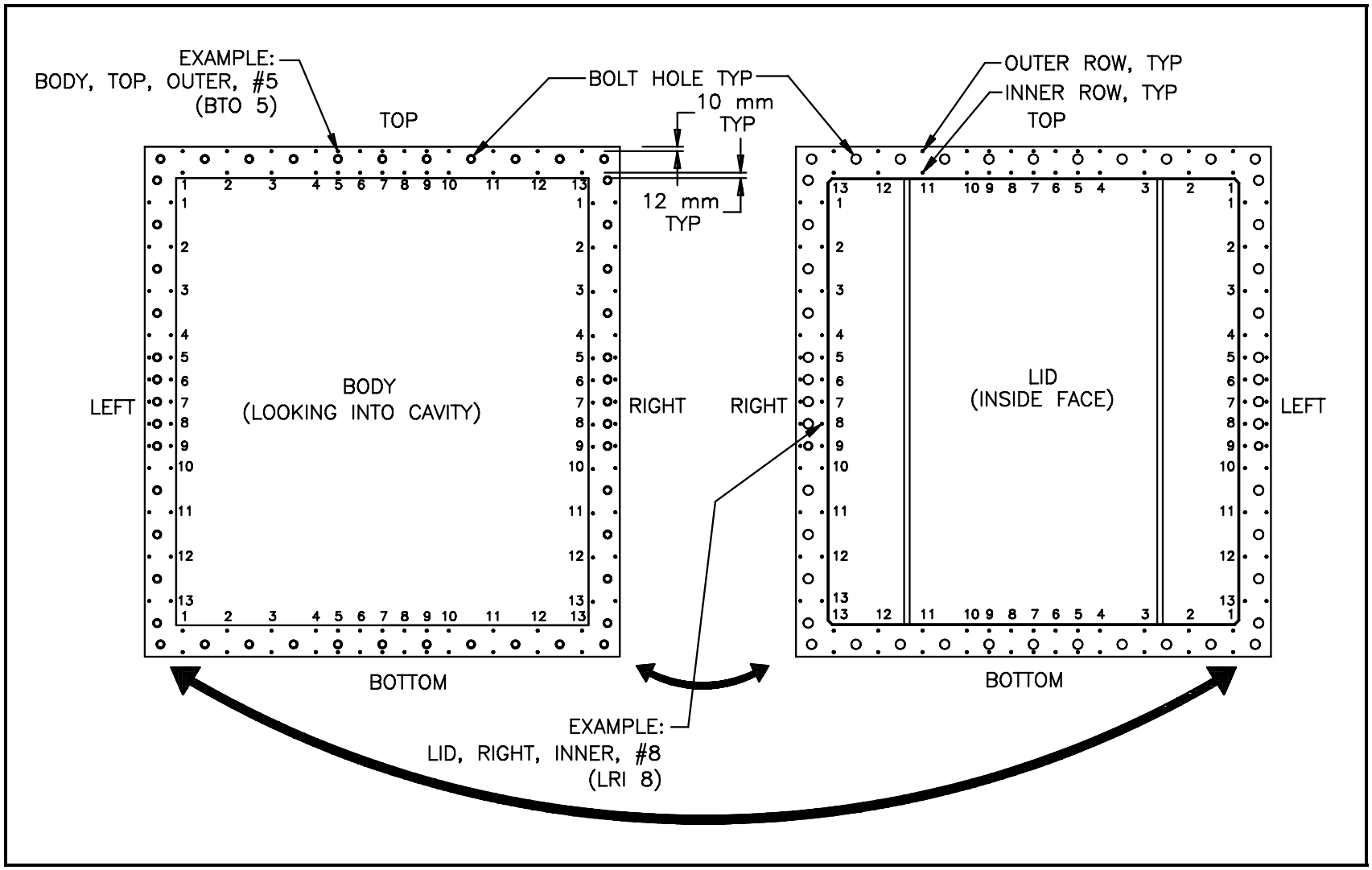

Figure 2.12.1-9 – Body and Lid Flange Measurement Locations

Table 2.12.1-2 – Summary of French Engineering Tests①

Test No.	Test Description	Orientation②	Test Temperature	Observations and Results
A1	NCT CG-over-cheek edge	68°	All tests performed at ambient temperatures.	~7 - ~10 mm bulge on side walls
F2	HAC vertical, closed end down	90°		Ave ~25 mm bulge on side walls, failure of three weld joints in octagon recess
F3	Puncture drop on cover center	90°		~21 mm dent in closure lid structural sheet
A4	HAC CG-over-cover edge	66°		~267 mm wide flat, max ~30 mm wide split in failed weld joint in octagon recess
F5	Puncture drop on side (30º oblique impact)	0°		Penetration through CSA containment sheet.
C7	HAC CG-over-corner, lid end	Fig. 2.12.1-6		~210 mm deep × ~530 mm wide × ~500 mm high flat
C8	Puncture on overpack cover/body gap	Fig. 2.12.1-6		~100 mm wide × ~100 mm deep gap
F9	Puncture drop on side (30º oblique impact)	0°		~90 mm penetration to CSA structural sheet
A6	HAC on side-edge	5°		~120 mm to ~175 mm wide flat along edge

Notes:

① Tested 4/25/94 – 7/4/94.

② Orientation is longitudinal axis of the package relative to the horizontal impact surface.

Table 2.12.1-3 – Summary of U.S. 2003 Engineering Tests①

Test No.	Test Description	Orientation②	Test Temperature③	Observations and Results
FD1	HAC vertical, closed end down	90°	-21 °C	~32 mm max crush (lower corner), creating a ~64 mm bulge. Some weld joints failed in octagon recess (maximum opening ~6 mm wide × ~686 mm long).
FD2	NCT vertical, lid end down	90°	-37 °C	~16 mm high × ~254 mm long bulge, no weld joint failures.
FD3	HAC vertical, lid end down	90°	-28 °C	~17 mm maximum crush, ~25 mm bulge of inner horizontal sheet in octagon, (2) small weld cracks (maximum width ~6 mm).
FD4	HAC slapdown, lid end secondary	25°	-34/-31 °C	~57 mm × ~152 mm flat (primary end), ~25 mm × ~483 mm flat (secondary end)
P1	Puncture drop on cover near bolts	71°	Ambient	Penetration to closure lid structural sheet, creating a ~216 mm long tear.
P2	Puncture drop on overpack cover joint	Fig. 2.12.1-7	Ambient	~19 mm wide scuff mark on cheek surface.
P3	Puncture drop on slapdown damage	30°	Ambient	~36 mm deep dent, ~46 mm on body, & ~83 mm on overpack cover (no penetration).
P4	Puncture drop on closed end	71°	Ambient	Penetration to CSA structural sheet, creating a dent ~29 mm deep, ~80 mm long tear. Dent depth on CSA structural sheet 29 mm

Notes:

① Tested 9/15/03 – 9/30/03.

② Orientation is longitudinal axis of the package relative to the horizontal impact surface.

③ Temperatures listed for wood. Ambient temperatures ranged between 21 ºC and 34 ºC for the puncture tests.

Table 2.12.1-4 – Summary of U.S. 2005 Engineering Tests①

Test No.	Test Description	Orientation②	Test Temperature	Observations and Results
FD05	HAC Flat Side Drop	0º	All tests performed at ambient temperatures.	Little external deformation; no permanent deformation of CSA, good retention of closure bolt torque, seals held hard vacuum
P105	Oblique Puncture on Side	35º		Least damaging of the P105 – P405 series
P205	Oblique Puncture on Side	30 º		Shear fracture of PRP③, moderate damage
P305	Oblique Puncture on Side	25º		Shear fracture of PRP, deepest CSA dent
P405	Oblique Puncture on Side	25º		Approximately the same as P305
P505	Oblique Puncture on Closed End	71º		No shear fracture of PRP, moderate dent only

Notes:

① Tested 9/2005.

② Orientation is longitudinal axis of the package relative to the horizontal impact surface.

③ Puncture-resistant plate (PRP).

This page intentionally left blank.

Table 2.12.1-5 – Lid-to-Body Gaps at Outside Edge of Flange (mm)

Position	Left Flange	Top Flange	Right Flange	Bottom Flange
1	0.30	0.81	0.46	0.25
2	0.30	0.89	0.43	0.36
3	0.23	0.84	0.30	0.33
4	0.18	0.79	0.33	0.25
5	0.18	0.79	0.25	0.28
6	0.08	0.86	0.28	0.18
7	0.00	0.84	0.33	0.08
8	0.08	0.66	0.38	0.10
9	0.18	0.84	0.38	0.23
10	0.18	0.84	0.38	0.36
11	0.15	0.79	0.30	0.48
12	0.23	0.84	0.25	0.56
13	0.36	0.86	0.15	0.48

Table 2.12.1-6 – U.S. 2005 Engineering Puncture Test Results

Test No.	Angle, degrees①	CSA Dent Depth, mm
P105	35	②
P205	30	14
P305	25 #1	29
P405	25 #2	24
U.S. 2003, P4	19	29

Notes:

① Angle defined as between ETU impact surface and the ground as shown in Figure 2.12.1-8. For U.S. 2003 P4 test, 71º orientation of ETU axis to ground is equivalent to 19º orientation of closed end surface to ground.

② Since the puncture-resistant plate did not shear, the dent depth is assumed negligible.

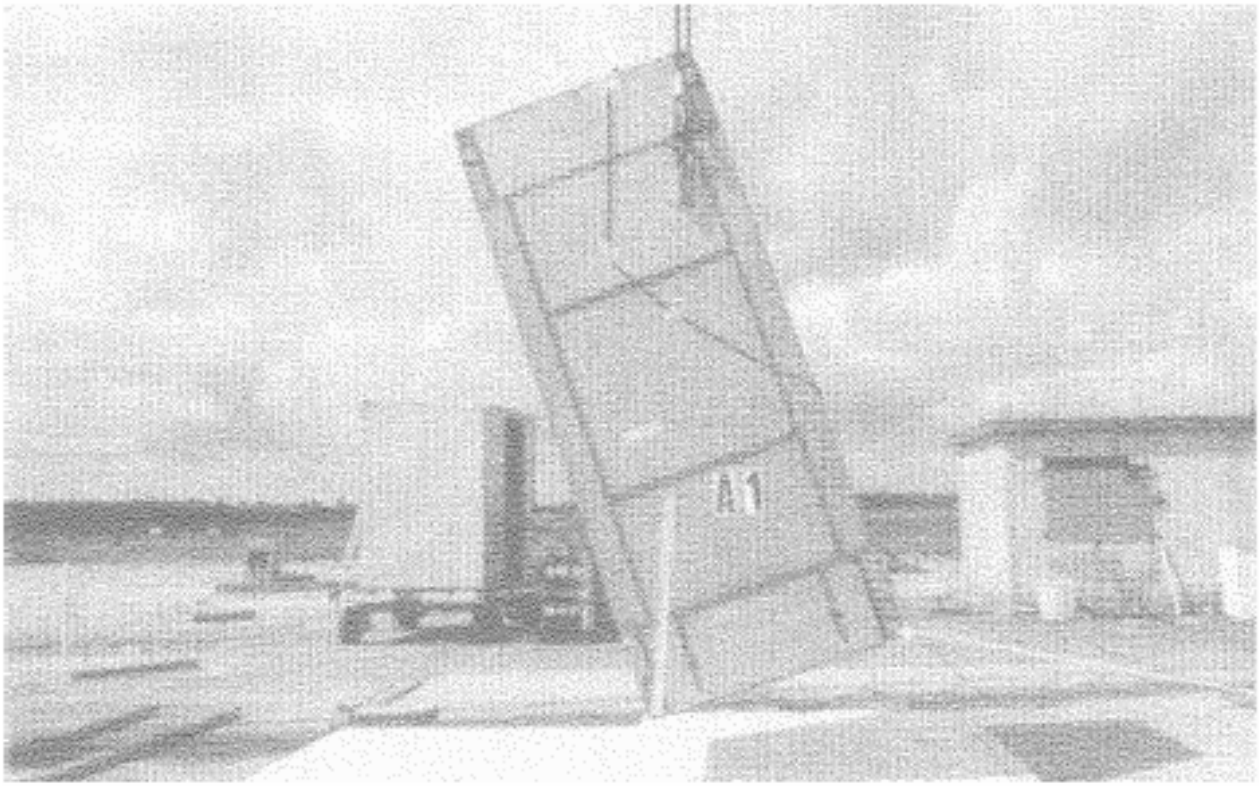

Figure 2.12.1-10 – Free Drop Test A1: Pre-Test View of CTU Orientation

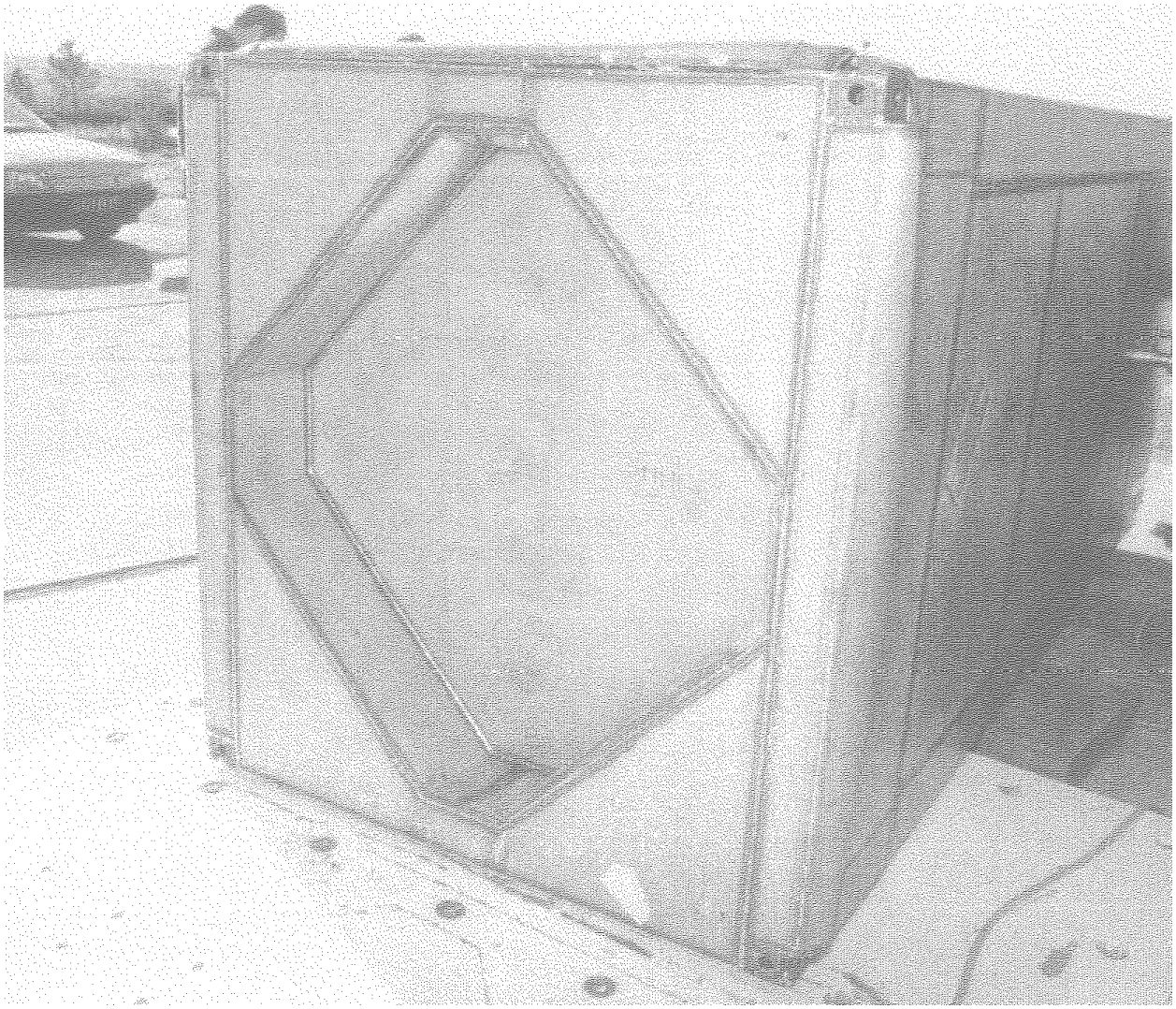

Figure 2.12.1-11 – Free Drop Test F2: Overall View of Closed End Damage

Figure 2.12.1-12 – Puncture Drop Test F3: Pre-Test View of CTU Orientation

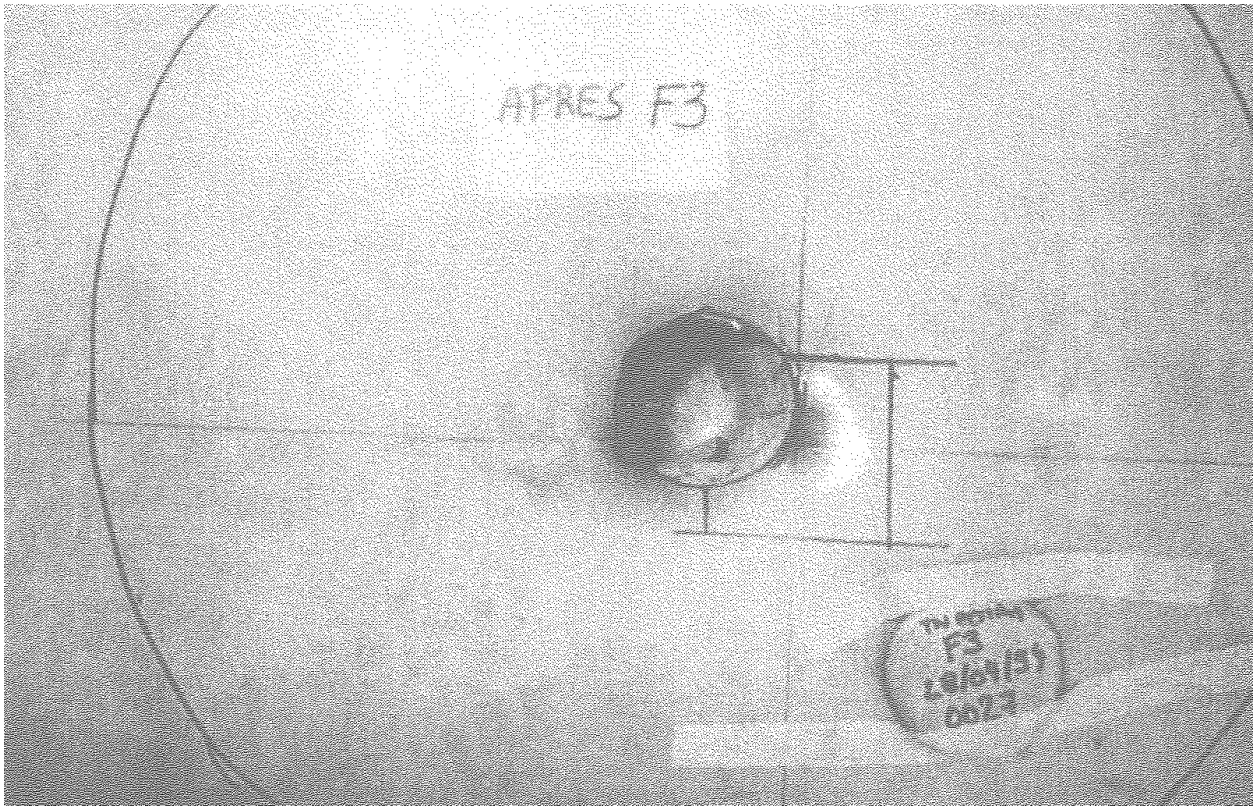

Figure 2.12.1-13 – Puncture Drop Test F3: Close-up View of Damage, ~120 mm Deep

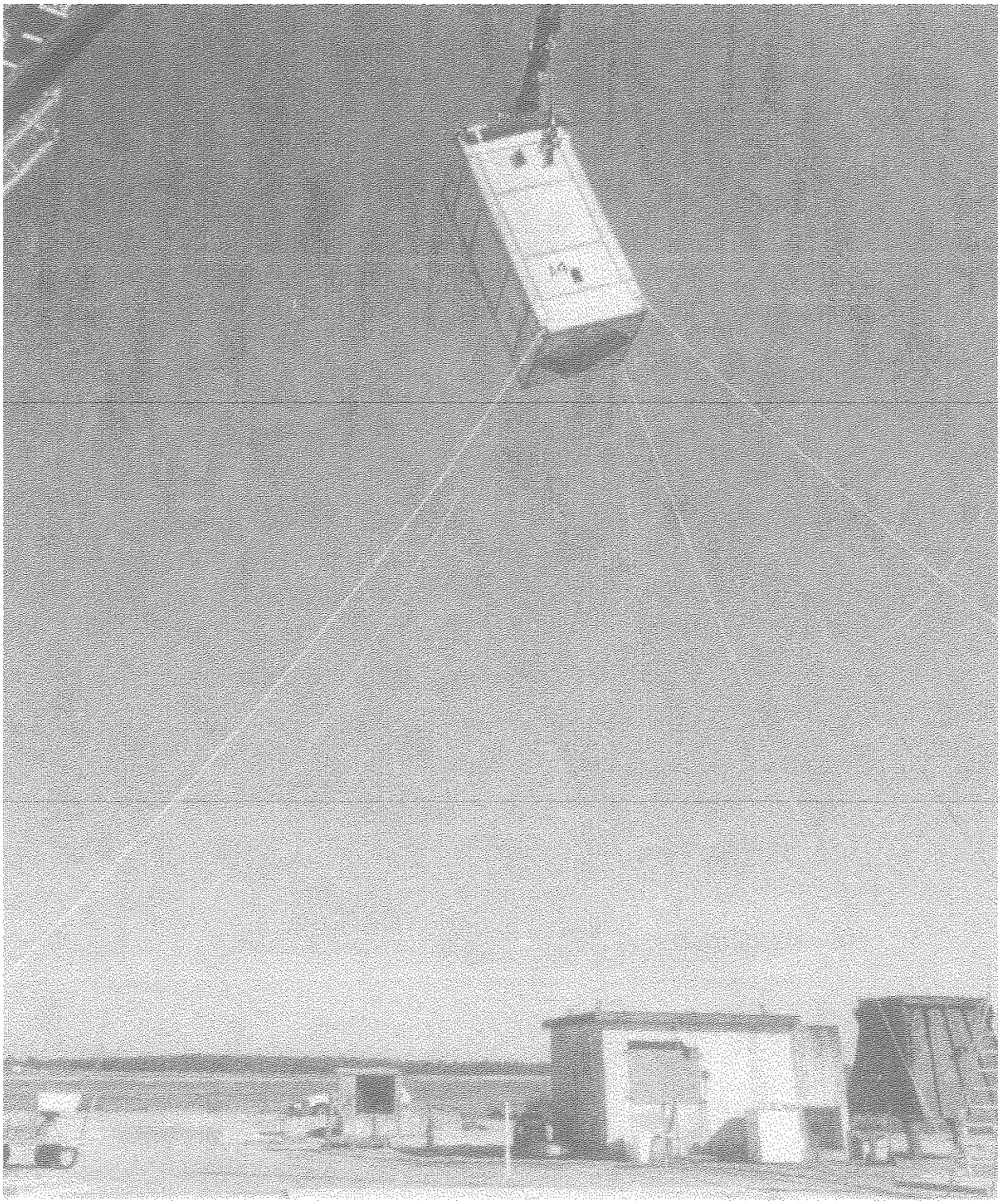

Figure 2.12.1-14 – Free Drop Test A4: Pre-Test View of CTU Orientation

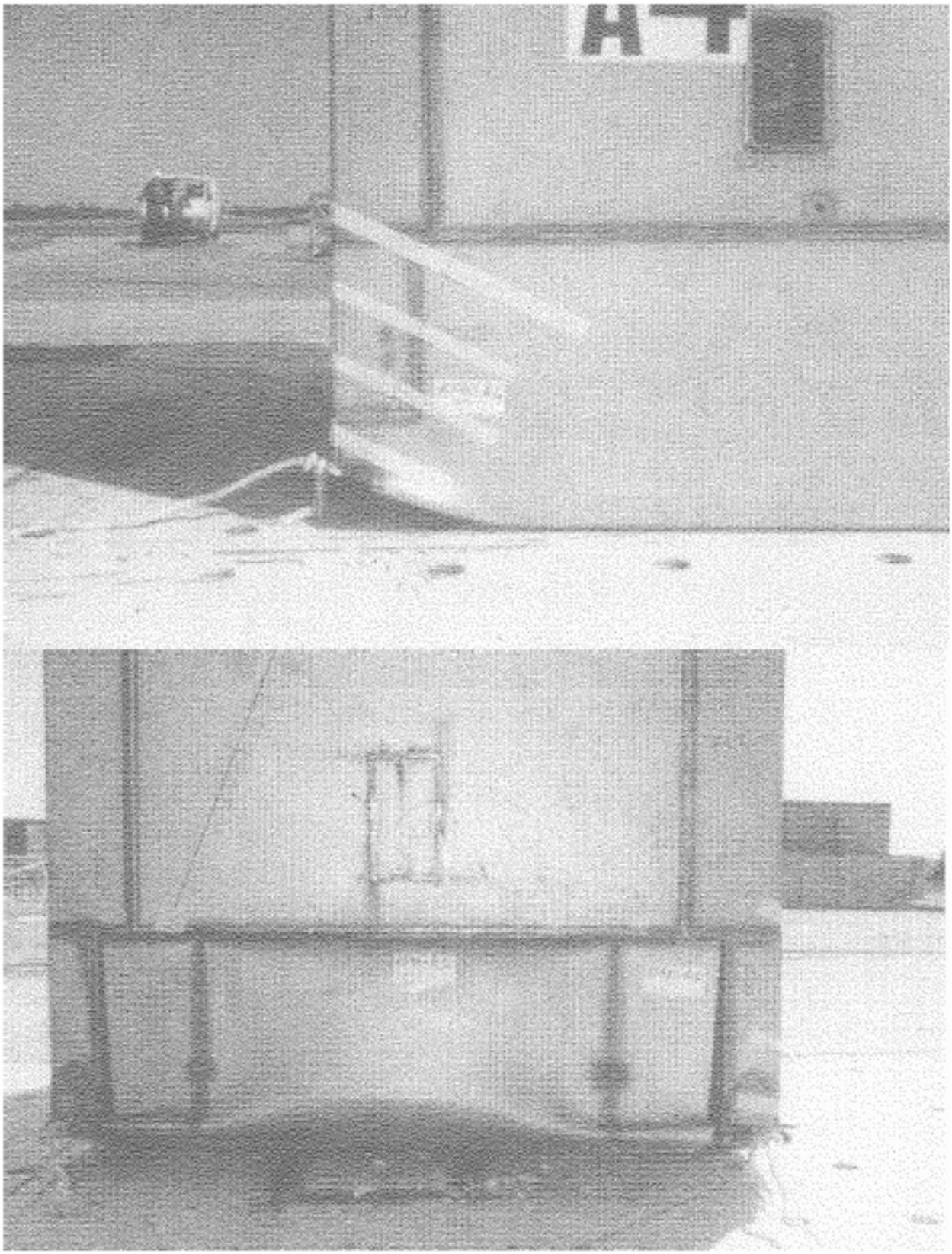

Figure 2.12.1-15 – Free Drop Test A4: Close-up Views of Edge Damage

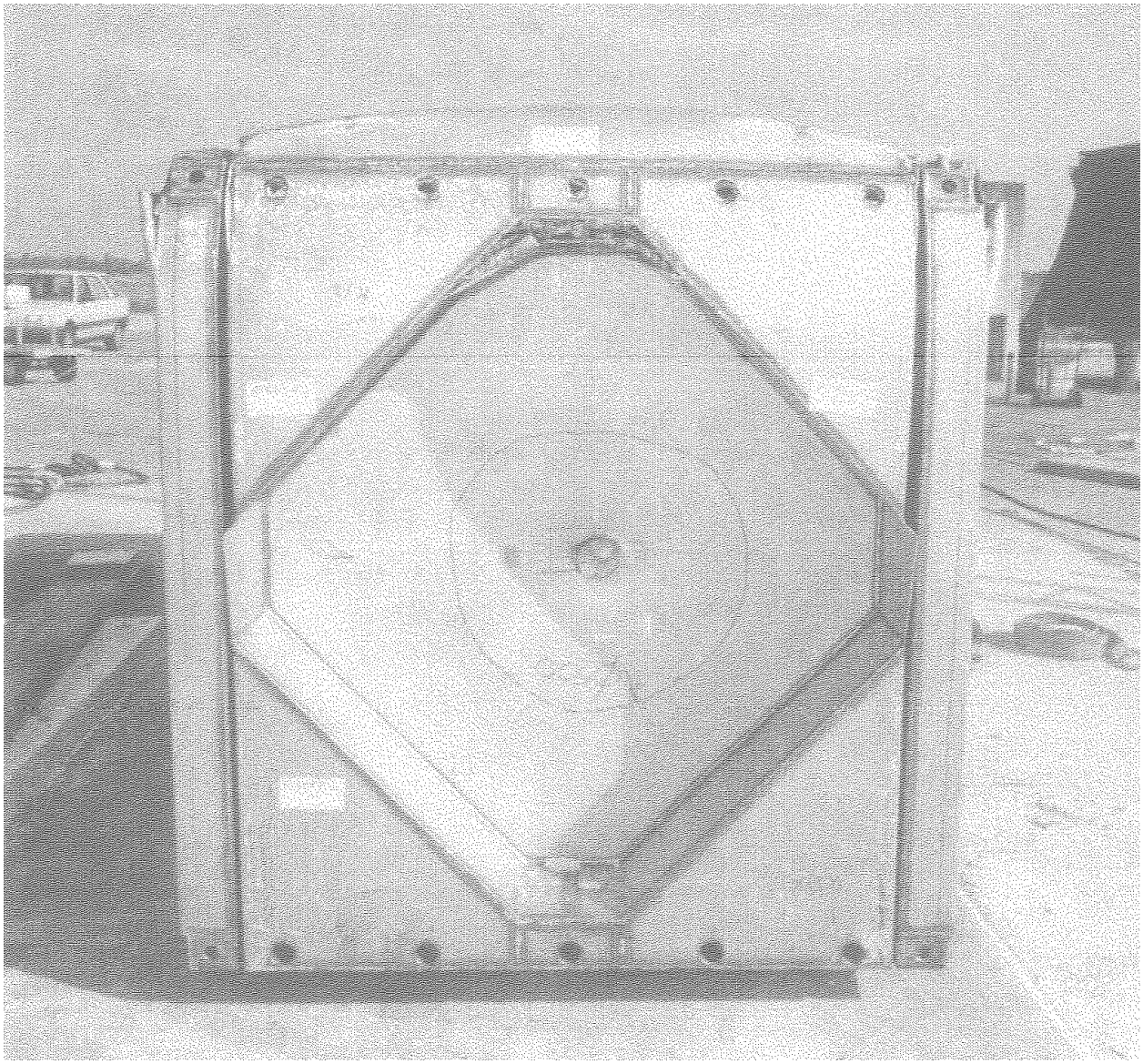

Figure 2.12.1-16 – Free Drop Test A4: Overall View of Overpack Cover Damage

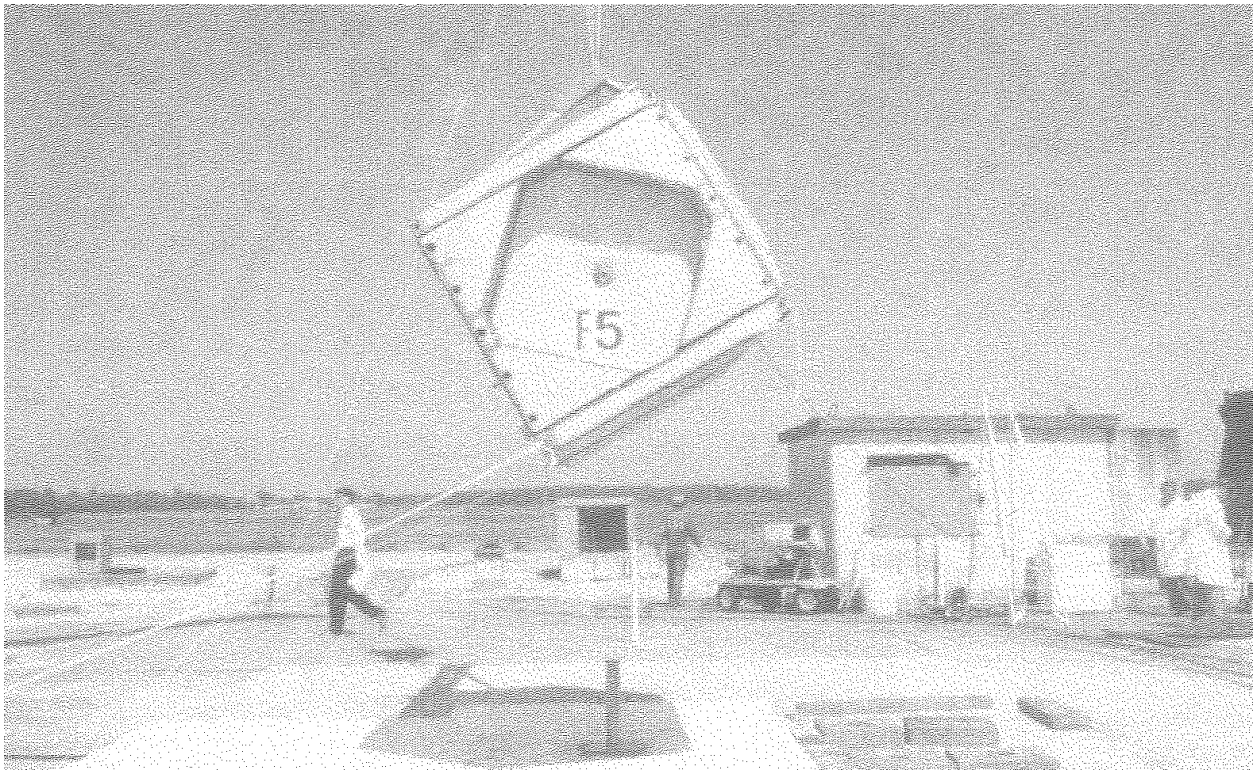

Figure 2.12.1-17 – Puncture Drop Test F5: Pre-Test View of CTU Orientation

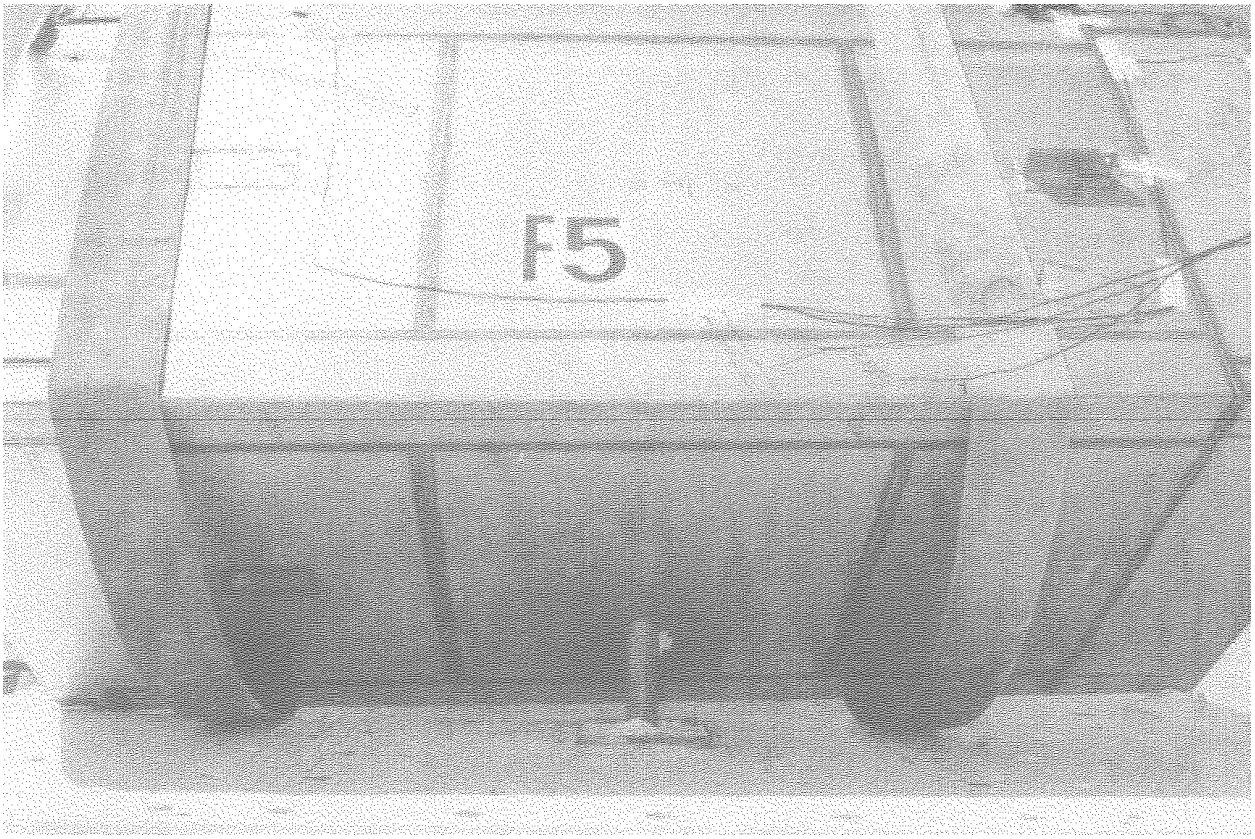

Figure 2.12.1-18 – Puncture Drop Test F5: View Immediately Following Impact

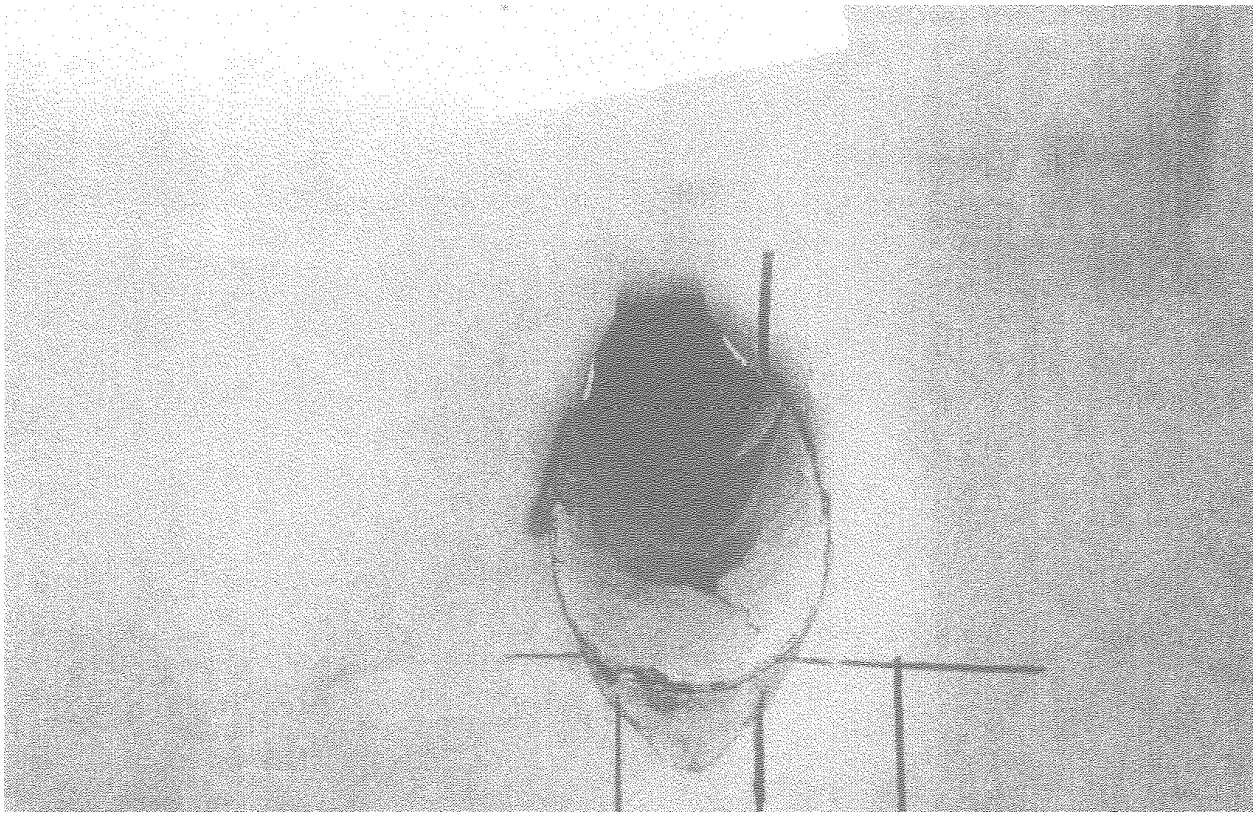

Figure 2.12.1-19 – Puncture Drop Test F5: Close-up View of Damage

Figure 2.12.1-20 – Puncture Drop Test F5: View of Internal Damage (with Welded Patch)

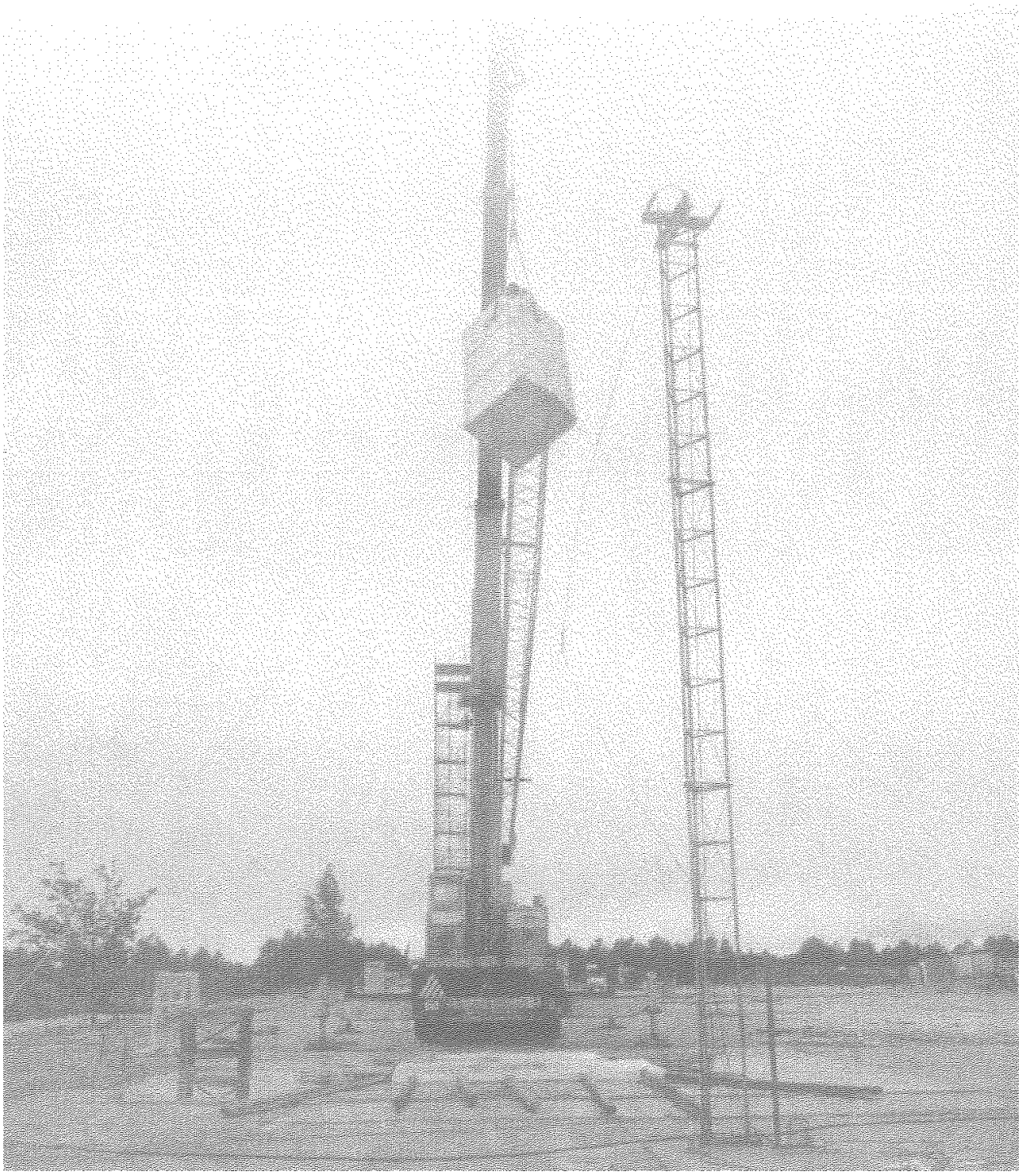

Figure 2.12.1-21 – Free Drop Test C7: Pre-Test View of CTU Orientation

Figure 2.12.1-22 – Free Drop Test C7: View Immediately Following Impact

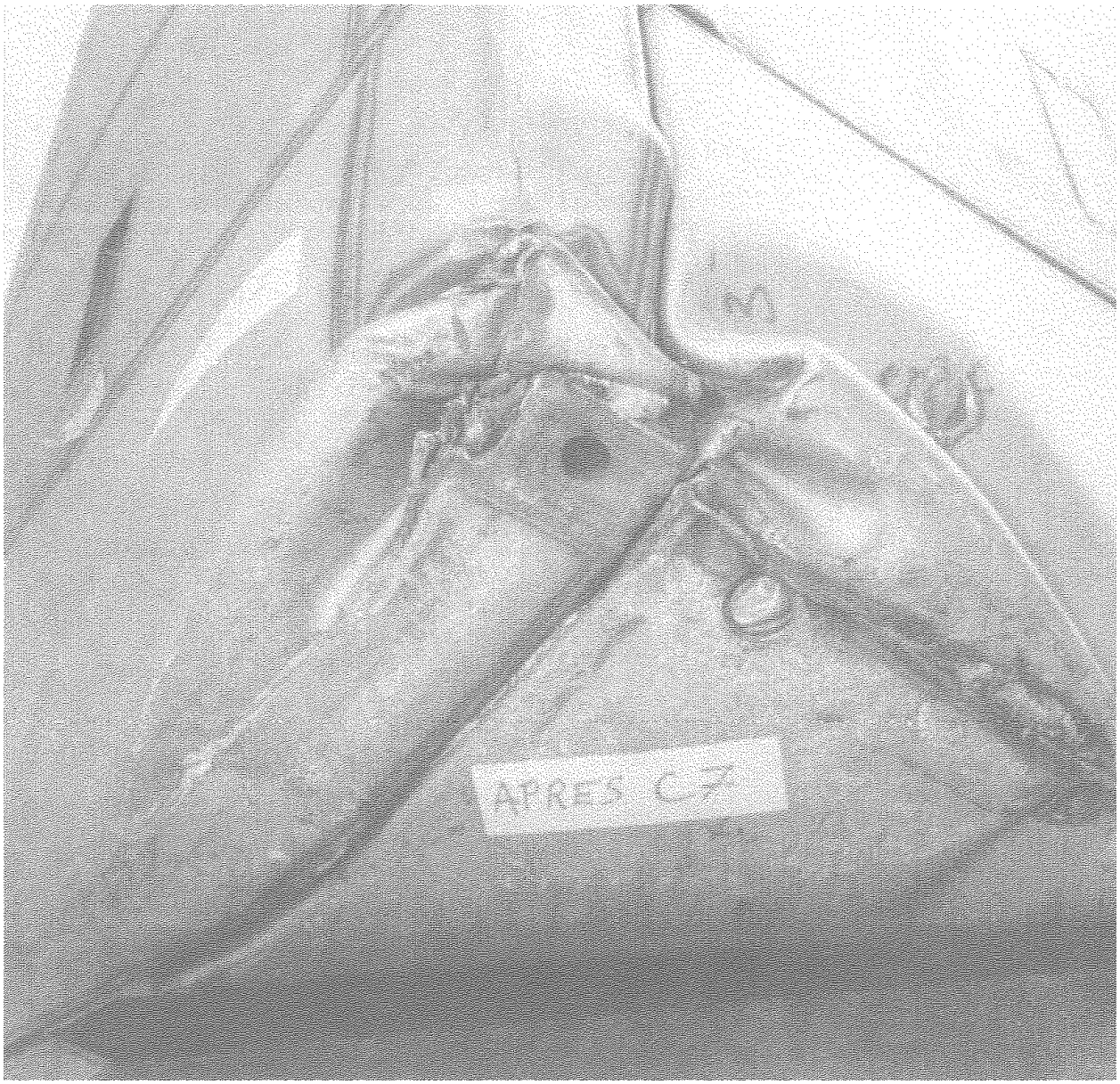

Figure 2.12.1-23 – Free Drop Test C7: Close-up View of Overpack Cover/Cheek Damage

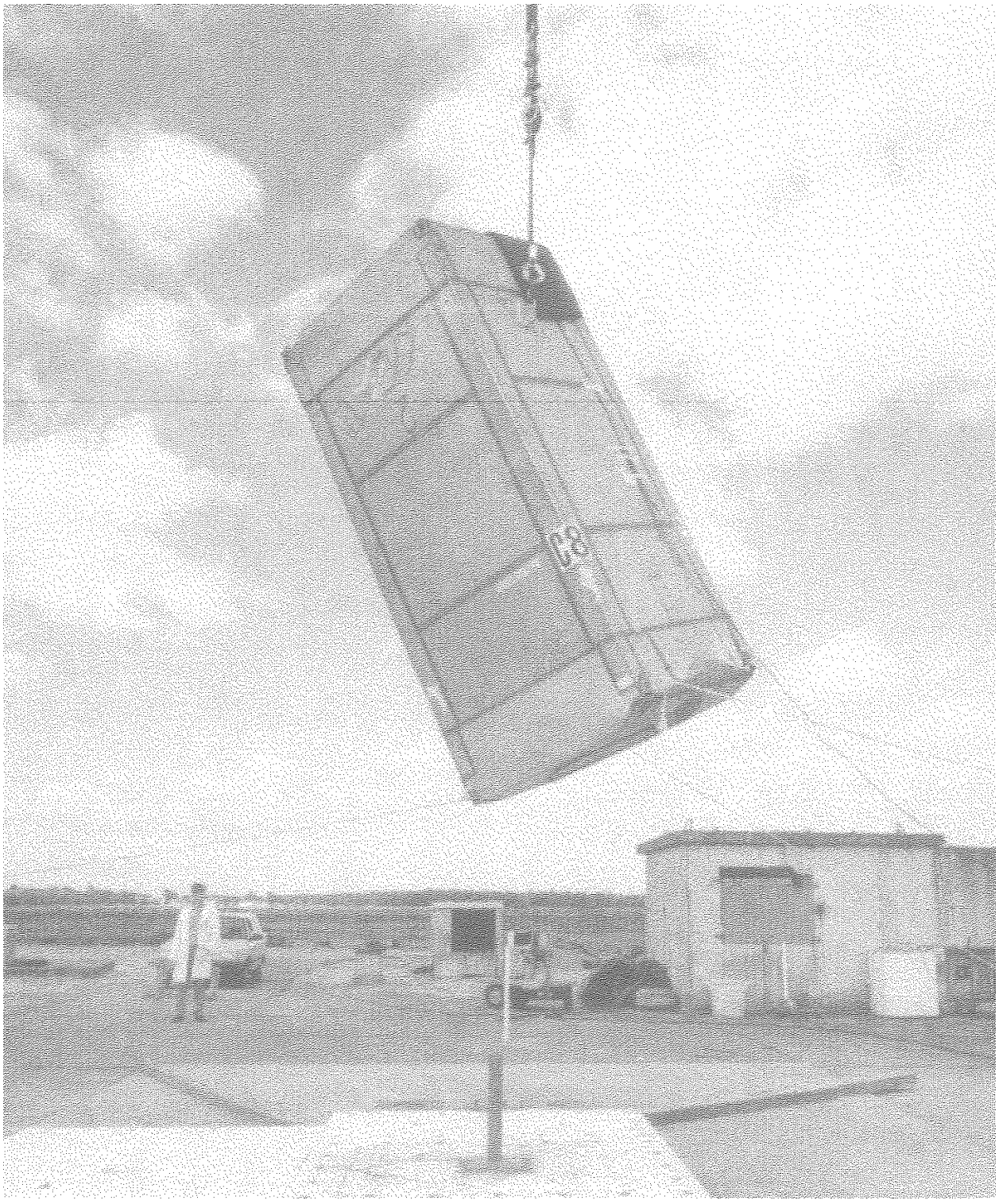

Figure 2.12.1-24 – Puncture Drop Test C8: Pre-Test View of CTU Orientation

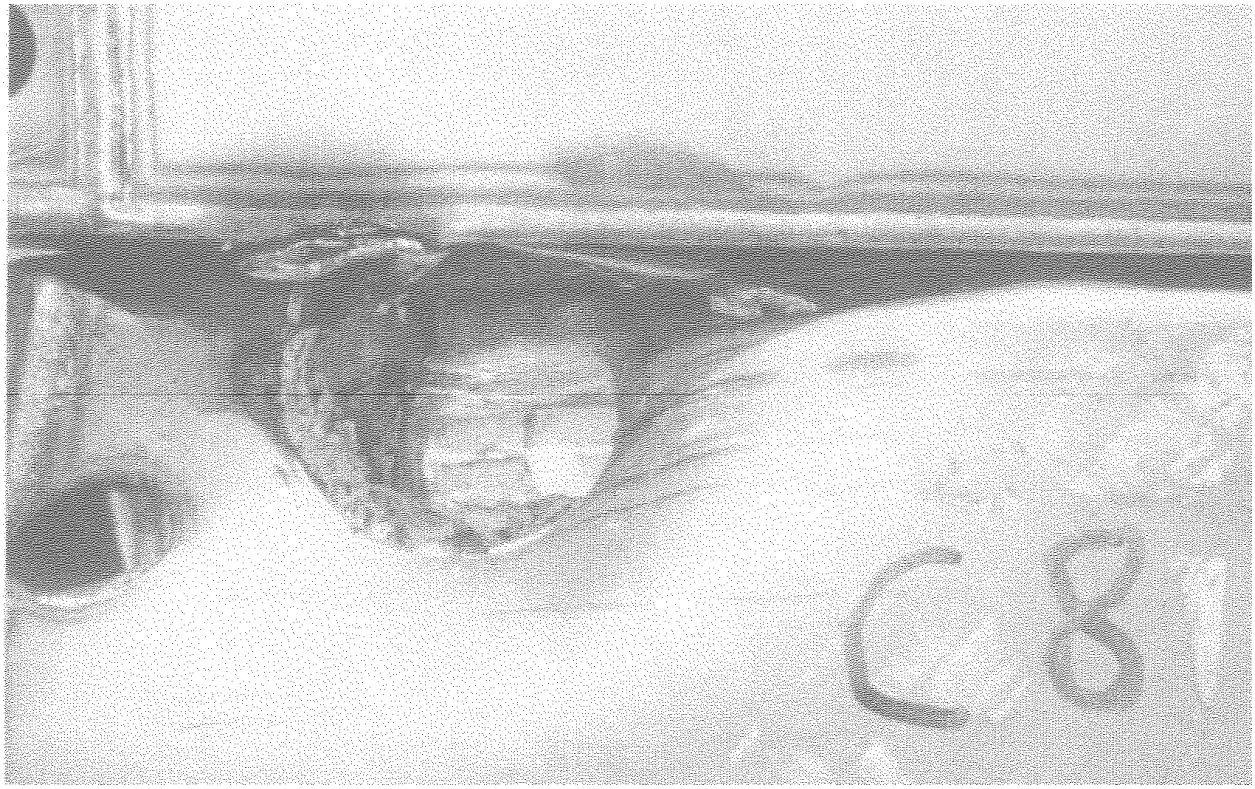

Figure 2.12.1-25 – Puncture Drop Test C8: Close-up of Overpack Cover/Cheek Damage

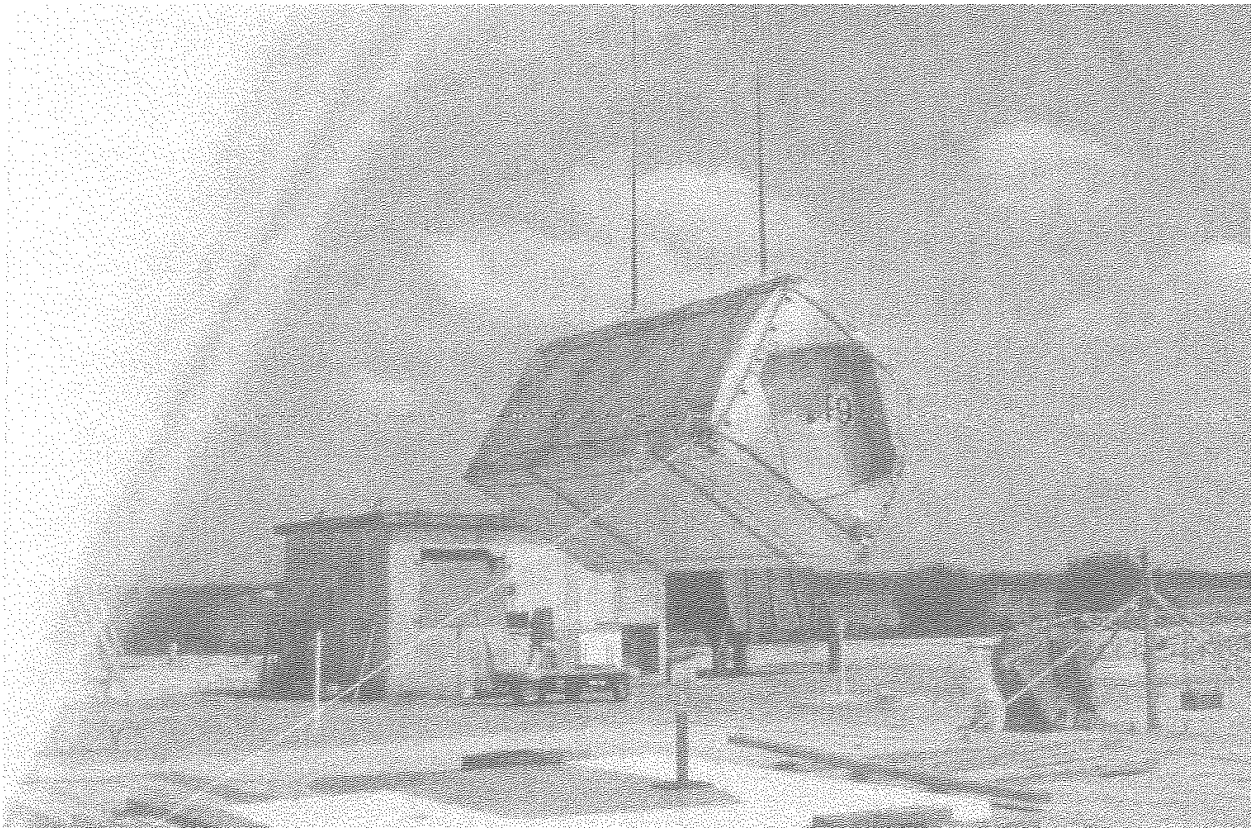

Figure 2.12.1-26 – Puncture Drop Test F9: Pre-Test View of CTU Orientation

Figure 2.12.1-27 – Puncture Drop Test F9: Close-up View of Damage

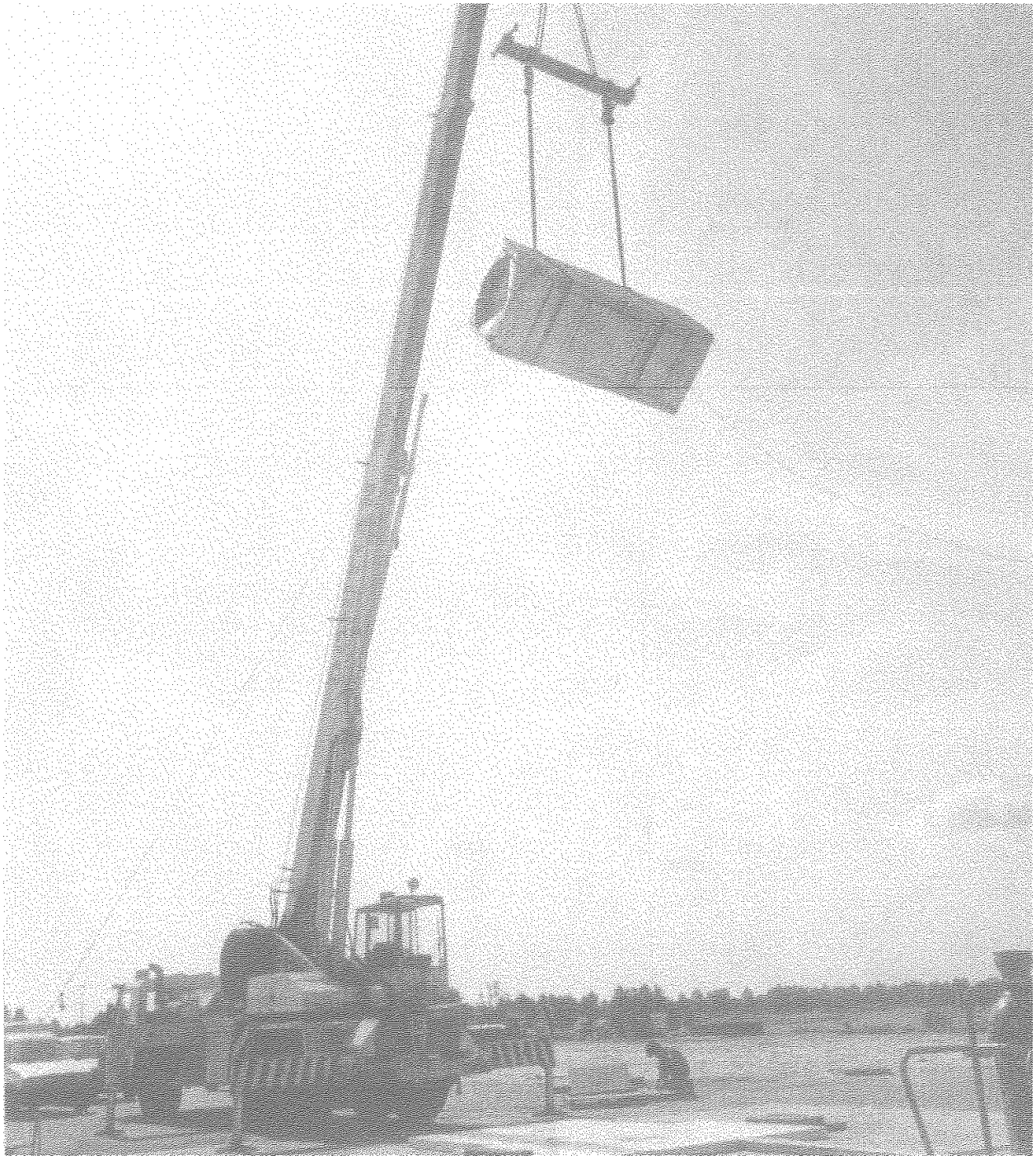

Figure 2.12.1-28 – Free Drop Test A6: Pre-Test View of CTU Orientation

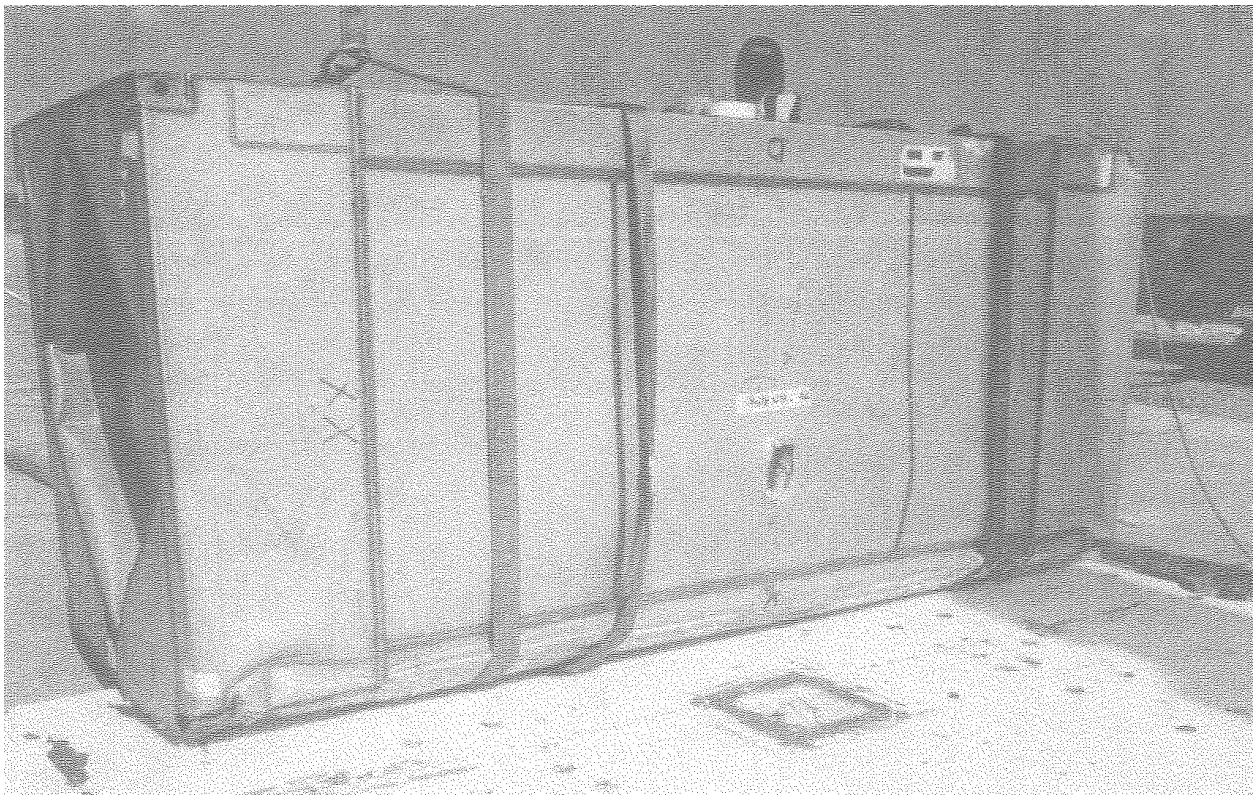

Figure 2.12.1-29 – Free Drop Test A6: Overall View of Damage Following Impact

Figure 2.12.1-30 – Free Drop Test A6: Overall View of Long-Edge Damage

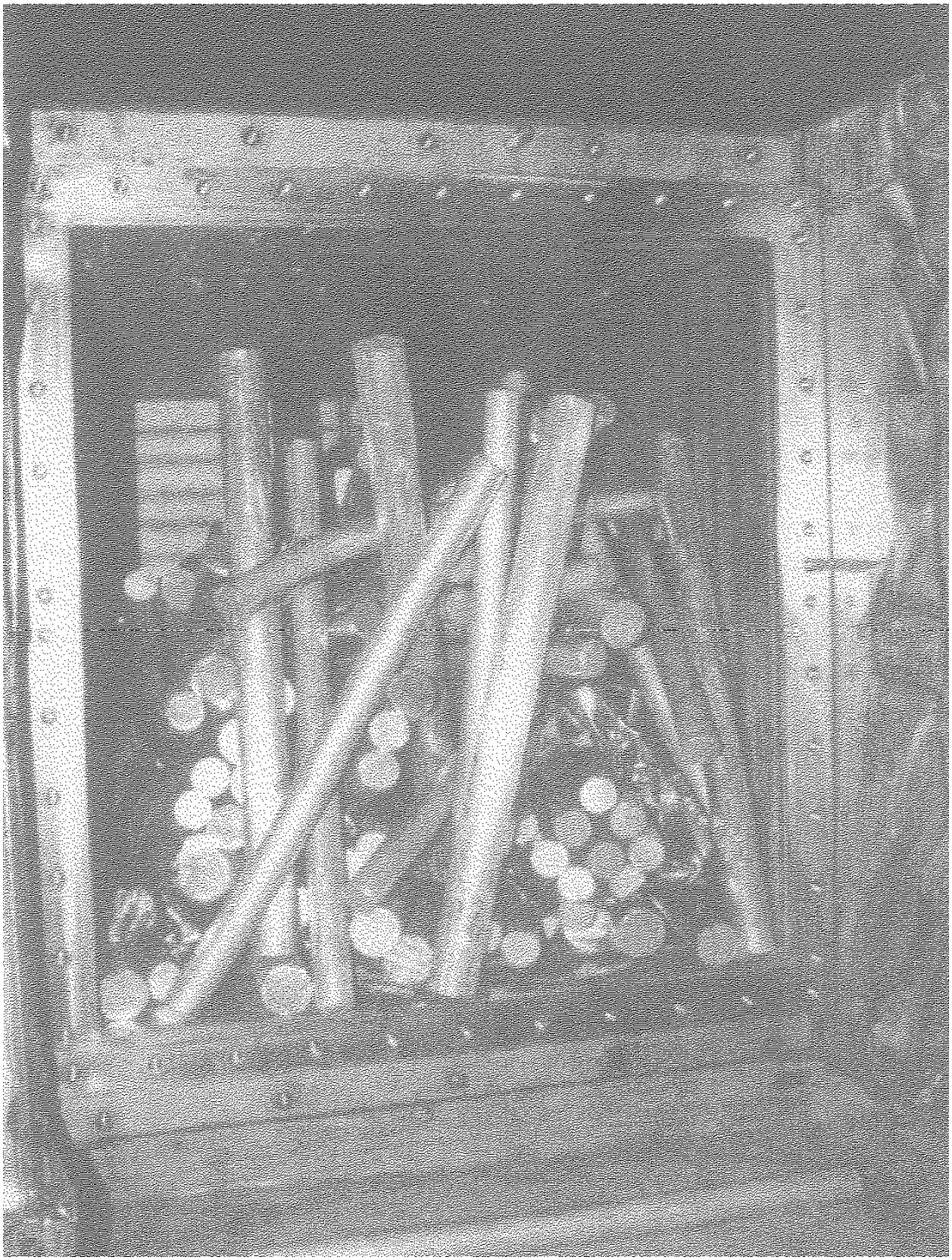

Figure 2.12.1-31 – Post-Test Disassembly: View of Loose Simulated Payload in Cavity

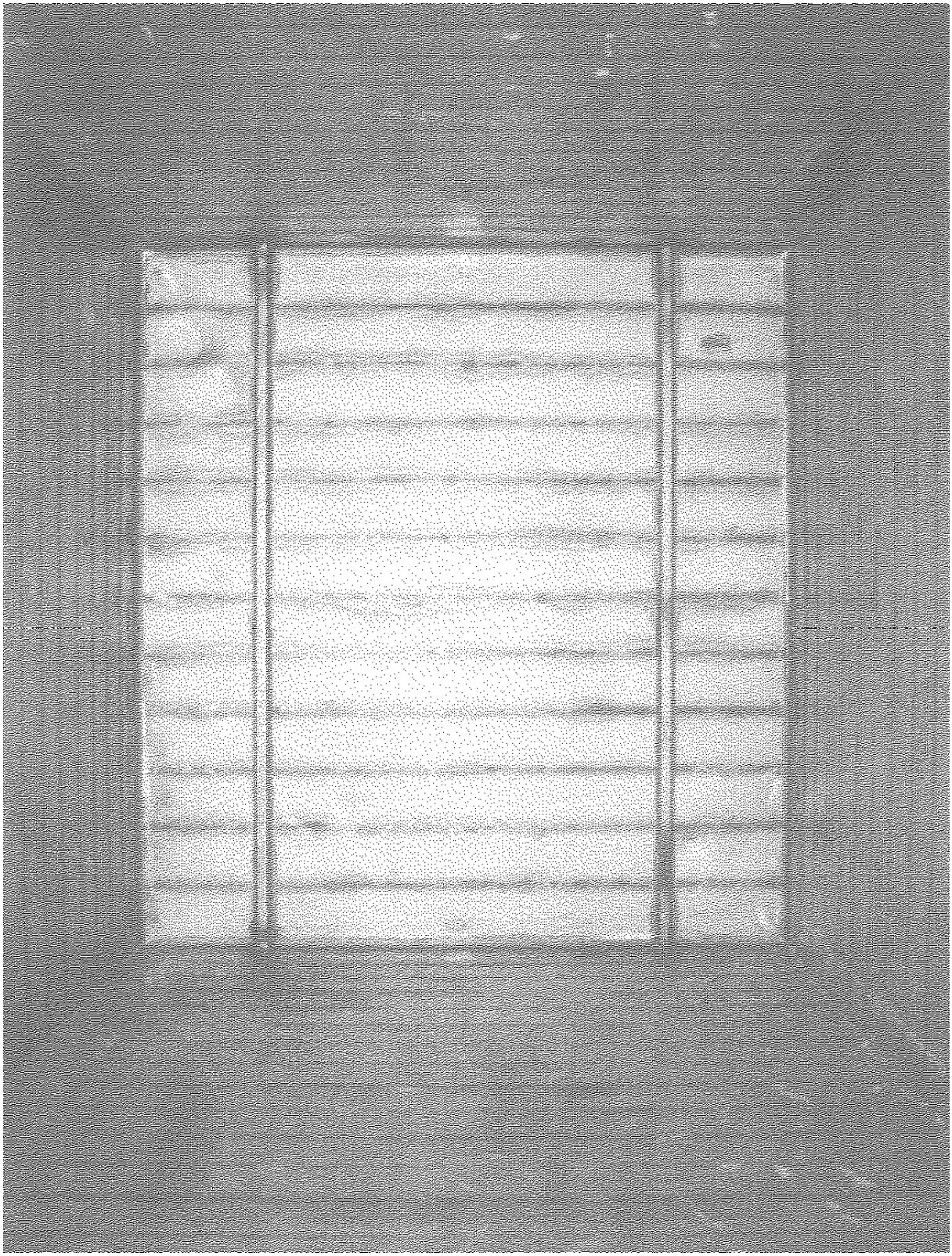

Figure 2.12.1-32 – Post-Test Disassembly: View of Cavity with Simulated Payload Removed

Figure 2.12.1-33 – Post-Test Disassembly: Close-up View of Closure Lid Puncture Damage

Figure 2.12.1-34 – Free Drop Test FD1: Close-up View of Weld Joint Damage

Figure 2.12.1-35 – Free Drop Test FD1: Close-up View of ISO Fitting Damage

Figure 2.12.1-36 – Free Drop Test FD2: View of Overpack Cover Edge Damage

Figure 2.12.1-37 – Free Drop Test FD3: Overall View of Overpack Cover Damage

Figure 2.12.1-38 – Free Drop Test FD3: Close-up View of ISO Fitting Damage

Figure 2.12.1-39 – Free Drop Test FD4: Overall View of Primary Impact Damage

Figure 2.12.1-40 – Free Drop Test FD4: Close-up View of Secondary Impact Damage

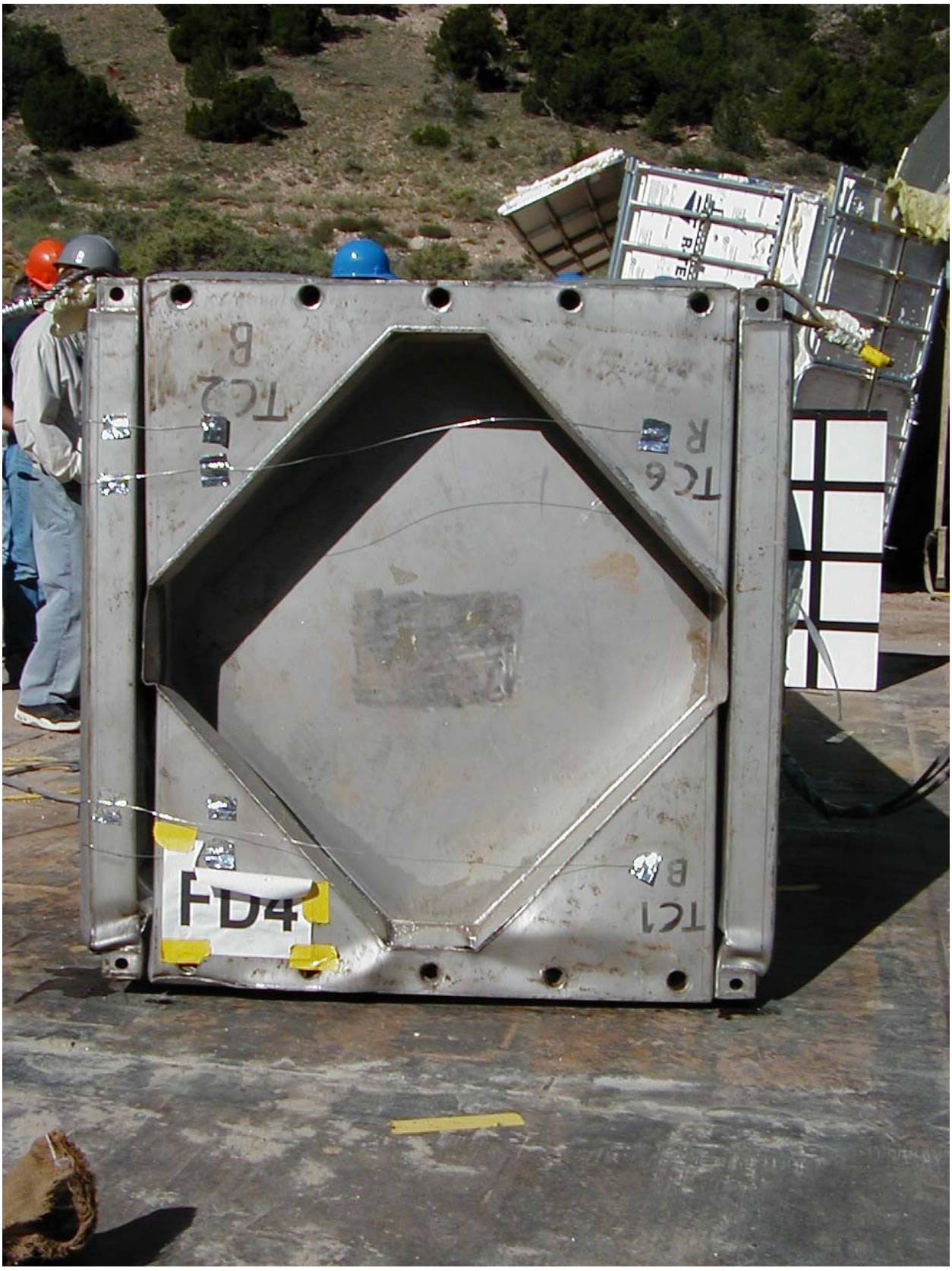

Figure 2.12.1-41 – Free Drop Test FD4: Overall View of Secondary Impact Damage

Figure 2.12.1-42 – Free Drop Test 4: View of ISO Fitting Damage, Secondary Impact

Figure 2.12.1-43 – Puncture Drop Test P1: Overall View Immediately After Impact

Figure 2.12.1-44 – Puncture Drop Test P1: Close-up View of Overpack Cover Damage

Figure 2.12.1-45 – Puncture Drop Test P1: Close-up View of Closure Lid Damage

Figure 2.12.1-46 – Puncture Drop Test P2: Overall View of Cheek Damage

Figure 2.12.1-47 – Puncture Drop Test P3: Overall View Immediately After Impact

Figure 2.12.1-48 – Puncture Drop Test P3: Overall View of Damage to Overpack Cover-Body Joint

Figure 2.12.1-49 – Puncture Drop Test P3: Close-up of Damage to Overpack Cover-Body Joint

Figure 2.12.1-50 – Puncture Drop Test P4: Overall View of Damage to Closed End

Figure 2.12.1-51 – Puncture Drop Test P4: View of Damage to CSA Structural Sheet

Figure 2.12.1-52 – Puncture Drop Test P4: Close-up of CSA Structural Sheet Damage

Figure 2.12.1-53 – Post-Test Disassembly: View of Loose Simulated Payload in Cavity

Figure 2.12.1-54 – Post-Test Disassembly: View of Cavity with Payload Removed

Figure 2.12.1-55 – Post-Test Disassembly: Overall View of Closure Lid, Inner Surface

Figure 2.12.1-56 – Post-Test Disassembly: Close-up View Closure Lid O-ring Seal Grooves

Figure 2.12.1-57 – Puncture Drop Test P105 at 35º

Figure 2.12.1-58 – Puncture Drop Test P205 at 30º

Figure 2.12.1-59 – Puncture Drop Test P305 at 25º

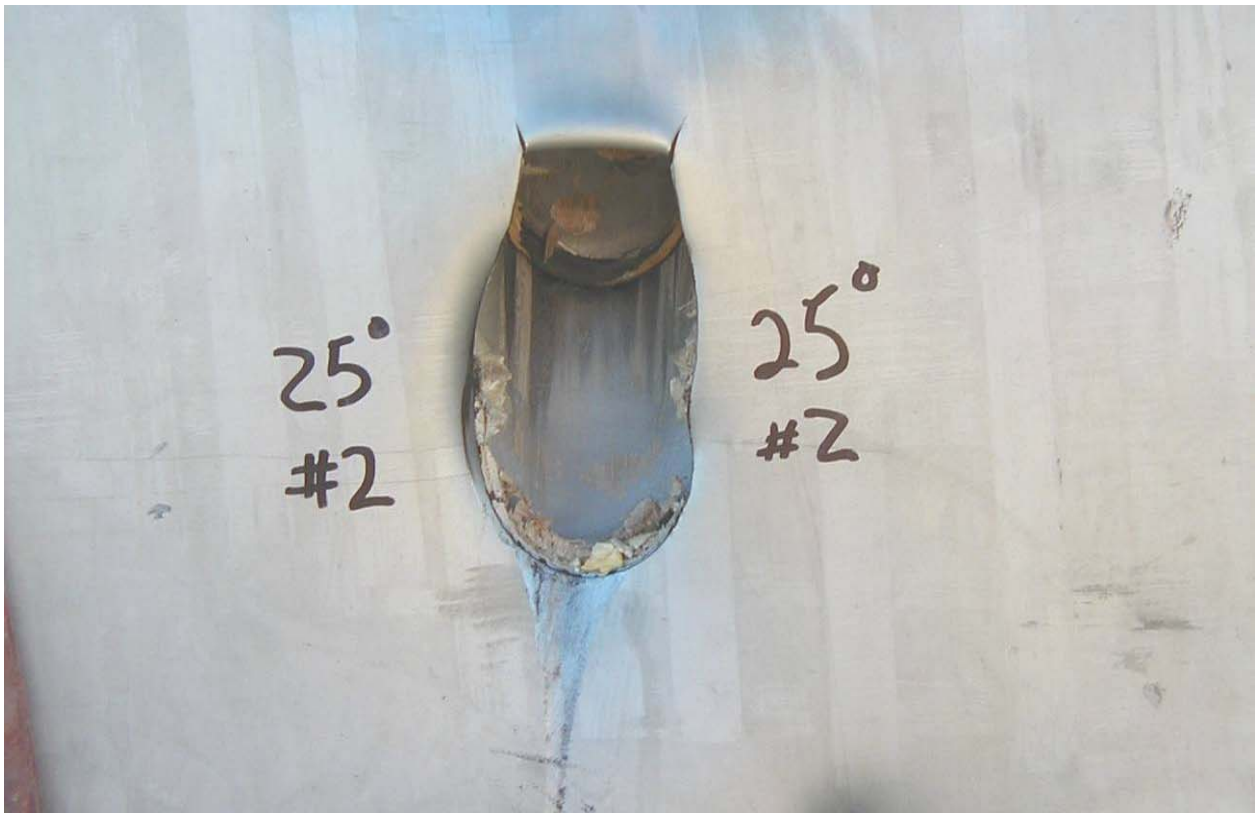

Figure 2.12.1-60 – Puncture Drop Test P405 at 25º

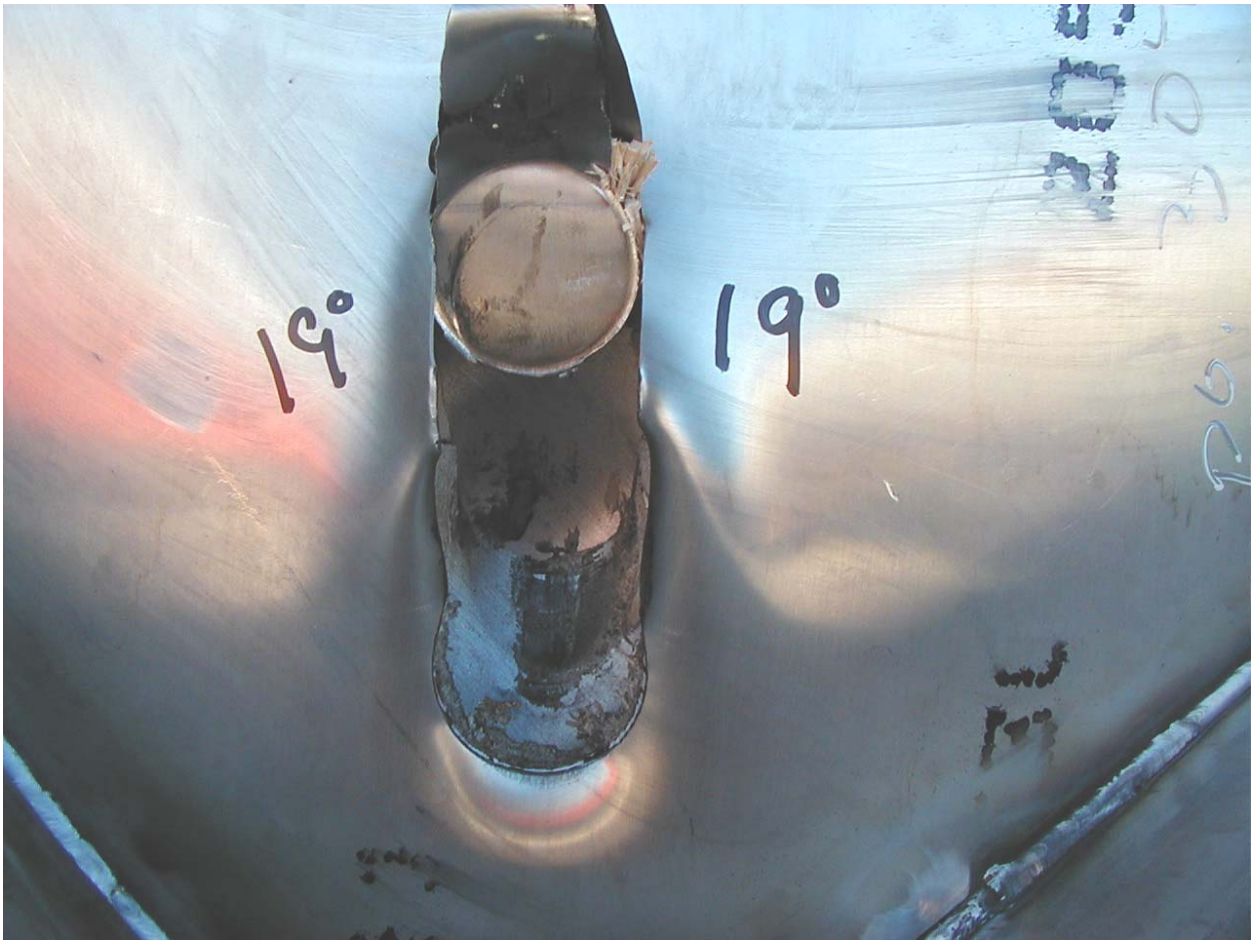

Figure 2.12.1-61 – Puncture Drop Test P505 at 19º (ETU longitudinal axis 71º)

2.12.2 Elastomer O-ring Seal Performance Tests

2.12.2.1 Introduction

Elastomer O-ring seal testing was performed in support of the certification of the TRUPACT–III package. The elastomer O-ring seal tests demonstrated the ability of a butyl rubber compound that meets the acceptance requirements of Section 8.1.5.3, *Butyl Rubber O-rings*, to maintain a leaktight[1] containment boundary under a reduced compression for the face-seal configuration. In addition, previous butyl O-ring seal testing performed for the certification of the TRUPACT–II packaging[2] and the Radioisotope Thermoelectric Generator (RTG) Transportation System Packaging[3] has demonstrated the ability of the butyl O-ring seal compound to maintain a leaktight containment boundary under worst-case conditions of compression and temperature duration that are beyond the conditions for the TRUPACT–III package. The results of the previous TRUPACT–II butyl O-ring tests are summarized in Table 2.12.2-1.

2.12.2.2 Test Specimen and Equipment

A production TN-Gemini package, which has an identical closure lid/seal design as the TRUPACT–III, was utilized to perform variable O-ring seal compression tests. An O-ring seal of prototypic cross-section, overall diameter, and butyl material, as delineated on the drawings in Appendix 1.3.1, *Packaging General Arrangement Drawings*, was installed in each dovetail groove on the closure lid.

2.12.2.3 Test Conditions

Since previous TRUPACT-II tests demonstrated the leaktight capability of the butyl O-ring compound at extreme temperatures and extended durations, the O-ring seal compression helium leakage rate tests were only performed at ambient temperature (e.g., 20 °C to 30 °C).

---

[1] Leaktight is defined as leakage of 1×10^{-8} reference Pascals – cubic meter per second (Pa–m^3/s), air, or less, per Section 6.3, *Application of Referenced Air Leakage Rate (L_R)*, of ANSI N14.5–1997 (or later), *American National Standard for Radioactive Materials – Leakage Tests on Packages for Shipment,* American National Standards Institute, Inc. (ANSI).

[2] U. S. Department of Energy (DOE), *Safety Analysis Report for the TRUPACT–II Shipping Package*, USNRC Certificate of Compliance 71–9218, U.S Department of Energy, Carlsbad Field Office, Carlsbad, New Mexico.

[3] DOE Docket No. 94–6–9904, *Radioisotope Thermoelectric Generator Transportation System Safety Analysis Report for Packaging*, WHC-SD-RTG-SARP-001, prepared for the U.S. Department of Energy Office of Nuclear Energy under Contract No. DE-AC06-87RL10930 by Westinghouse Hanford Company, Richland, WA. Per Appendix 2.10.6, elevated temperature tests were performed on Rainier Rubber Company butyl rubber compound No. RR–0405–70 O-ring seals with compressions as low as 10%. The specific time-temperature test parameters evaluated were 193 ºC for 24 hours followed by 177 ºC for 144 hours, for a total of 168 hours (1 week). At these temperatures, all elastomeric compounds are susceptible to relatively high helium permeability; thus, helium leak testing was not performed. Instead, a hard vacuum of less than 20 Pa was maintained on the test O-ring seals with no measurable pressure loss that would indicate leakage. At the end of the entire test sequence, the test O-ring seals were stabilized at -29 ºC and shown, via helium leak testing, to be leaktight (i.e., a leak rate less than 1×10^{-8} reference Pascals – cubic meter per second (Pa–m^3/s), air leakage).

2.12.2.4 Test Procedure

To vary the O-ring face-seal compression, 30-mm diameter metallic shims of varying thickness were installed between each of the forty-four closure lid bolts. By varying the thickness of the shims, the percentage of O-ring seal compression was varied. The process of leakage rate testing an O-ring seal is as follows:

1. Install the inner and outer O-ring seals in the TN–Gemini closure lid.
2. Install shims of a given thickness between each of the closure lid bolt holes on the body.
3. Install the closure lid onto the body. Tighten the closure lid bolts to 20 N-m torque. This is conservatively less than the installation torque used in transport.
4. Perform a helium leakage rate test of the main O-ring containment seal.

2.12.2.5 Example of O–ring Seal Compression Calculation

The minimum and maximum O-ring seal compressions were calculated based on as-measured dimensions for the cross-sectional diameter and inner diameter of the test O-ring seals, and the O-ring seal groove depth of the TN–Gemini package. Stretch was determined using the as-measured length of the O-ring groove in the closure lid.

Four quantities are required for the compression calculation: 1) the cross-sectional diameter, D, of the O-ring seal, 2) stretch, S, of the O-ring seal, 3) groove depth, d, of the O-ring groove, and 4) the thickness of the shim, *e*. The minimum O-ring seal compression for Test No. 2 is determined as follows:

1. Extract the pertinent data from Table 2.12.2-2.

   D_{min} = 12.01 mm, the minimum O-ring seal cross-sectional diameter

   D_{max} = 12.14 mm, the maximum O-ring seal cross-sectional diameter

   d_{min} = 8.31 mm, the minimum groove depth

   d_{max} = 8.40 mm, the maximum groove depth

   e = 1.24 mm, the thickness of the shim

2. Determine the reduction in O-ring seal cross-sectional diameter due to stretch.

   From Table 2.12.2-2, the stretch of the O-ring seal diameter in the groove length was 3.0%. From Figure 3-3 for the calculated curve of the Parker O-ring Handbook[4], the resulting reduction in O-ring seal cross-sectional diameter is 1.5%. The reduced cross-sectional diameter, D_{Rmin} and D_{Rmax}, is therefore 1.5% less than the non-stretched diameters, D_{min} and D_{max}, or:

   $D_{Rmin} = (1 - 0.015)D_{min} = 11.83$ mm

   $D_{Rmax} = (1 - 0.015)D_{max} = 11.96$ mm

3. Calculate the O-ring seal compression.

[4] ORD 5700, *Parker O-ring Handbook*, 2007, Parker Hannifin Corporation, Cleveland, OH.

Using the quantities determined in (1) and (2) above, the seal compression, C_{seal}, is calculated as follows:

$$C_{seal} = \left[1 - \left(\frac{e + d}{D_R}\right)\right] \times 100$$

$$C_{seal\text{-}min} = \left[1 - \left(\frac{1.24 + d_{max}}{D_{Rmin}}\right)\right] \times 100 = 18.5\%$$

$$C_{seal\text{-}max} = \left[1 - \left(\frac{1.24 + d_{min}}{D_{Rmax}}\right)\right] \times 100 = 20.2\%$$

Following the procedure used above, the minimum and maximum O-ring seal compressions are calculated for all tests, and summarized in Table 2.12.2-2.

2.12.2.6 Test Results

Test results are summarized in Table 2.12.2-2. As shown in the table, the minimum O-ring seal compression that the butyl rubber material maintained a leaktight seal for the TRUPACT–III face seal configuration was 18.5%. Since the O-ring seal will contract more than the groove depth with temperature change, the minimum tested compression of 18.5% must be adjusted for minimum temperature of -40 ºC. From the Parker O-ring Handbook, Table A3-2, an upper bound coefficient of expansion for all elastomer materials listed (butyl is not listed) is 2×10^{-4} mm/mm-ºC. The O-ring cross-sectional diameter is 12 mm, and the temperature change between 21 ºC and -40 ºC is 61 ºC. The contraction of the stainless steel is conservatively neglected. Therefore, the cross-sectional diameter contraction, C_{seal}, of the O-ring seal is:

$$C_{seal} = (2 \times 10^{-4})(12)(61) = 0.15 \text{ mm}$$

This contraction represents 1.3% of the cross-sectional diameter. Therefore, the minimum O-ring seal compression at room temperature for a leaktight seal is 18.5 + 1.3 = 19.8%, which ensures that the tested compression of 18.5% is still present at the minimum temperature of -40 ºC.

These results, in conjunction with prior TRUPACT–II testing, confirm that the butyl O-ring seals used in the TRUPACT–III package will remain leaktight if subjected to worst-case seal compressions over the range of NCT and HAC cold and hot temperatures. Additionally, following a HAC thermal event, the O-ring seals will remain leaktight when cooled to a temperature of -29 ºC, as demonstrated in the TRUPACT–II O-ring seal tests.

An additional test using a maximum elevated temperature of 232 ºC was performed (see Test 2 in Table 2.12.2-1). In this case, the O-ring seals were not leaktight during the final, post-heat, -29 ºC leak test, a vacuum at the high temperature could not be rapidly achieved, and the seals evidenced loss of elasticity and visible cracking was evident. Such was not the case for tests where the maximum temperature was 204 ºC. It is therefore concluded that the upper temperature limit for this butyl compound is somewhere between 204 ºC and 232 ºC, but an upper temperature limit of 204 ºC is conservatively utilized for analysis purposes.

This page intentionally left blank.

Table 2.12.2-1 – TRUPACT–II O-ring Seal Performance Test Results[5]

Test Number	O-ring Seal Cross-Sectional Diameter (inches)①				Stretch (%)		Maximum Gap (inches)		Minimum Compression (%)				Temperature for "Leaktight" Leak Test (Leakage ≤ 2.0×10^{-9} Pa-m^3/s, He)				
	O-ring Seal No. 1		O-ring Seal No. 2				Center Disk	Offset Disk	Center Disk		Offset Disk		Center Disk④		Offset Disk④		
	Min	Max	Min	Max	Min	Max			Min	Max	Min	Max	Ambient	-40 ºC	-29 ºC	8 hrs⑤	-29 ºC
1	0.387	0.397	0.387	0.396	2.0	4.1	0.026	③	22.1	25.6	14.9	20.0	Yes	Yes	Yes	177 ºC	Yes
2	0.388	0.398	0.387	0.398	2.0	4.1	0.029	0.050	21.3	25.1	15.7	19.7	Yes	Yes	⑥	232 ºC	No
3	0.387	0.397	0.387	0.399	2.0	4.1	0.027	0.052	21.9	25.8	15.2	19.4	Yes	Yes	Yes	204 ºC	Yes
4	②	②	②	②	2.0	4.1	0.027	0.053	21.9	25.8	14.9	19.1	Yes	Yes	Yes	204 ºC	Yes
5	②	②	②	②	2.0	4.1	0.026	0.050	22.1	26.0	15.7	19.9	Yes	Yes	Yes	204 ºC	Yes

Notes:

① Material for all O-ring seal test specimens is butyl rubber compound RR-0405-70, Rainier Rubber Co., Seattle, WA.

② Not measured; calculations assume the worst case range as taken from Tests Numbers 1 - 3 (i.e., Ø0.387 minimum to Ø0.399 maximum).

③ Range of values is 0.048 minimum to 0.053 maximum due to an indirect method of gap measurement (used for this test only).

④ A "Yes" response indicates that helium leakage testing demonstrated that the leak rate was ≤ 1.0×10^{-8} Pa-m^3/s, air (i.e., "leaktight" per ANSI N14.5). In all cases, measured leak rates were ≤ 2.0×10^{-9} Pa-m^3/s, helium, for tests with a "Yes" response.

⑤ No helium leak tests were performed at elevated temperatures due to O-ring seal permeation and saturation by helium gas. The ability of the test fixture to establish a rapid, hard vacuum between the O-ring seals was used as the basis for leak test acceptance at elevated temperatures. All tests rapidly developed a hard vacuum, with the exception of Test Number 2 at an elevated temperature of 232 ºC, which slowly developed a vacuum.

⑥ Initial leakage of 1.0×10^{-6} Pa–m^3/s, helium; became leaktight (≤ 2.0×10^{-9} Pa–m^3/s, He) approximately one minute later.

[5] U. S. Department of Energy (DOE), §2.10.2, *Elastomer O-ring Seal Performance Tests*, *Safety Analysis Report for the TRUPACT-II Shipping Package*, USNRC Certificate of Compliance 71–9218, U.S Department of Energy, Carlsbad Field Office, Carlsbad, New Mexico.

Table 2.12.2-2 – TRUPACT–III Containment O-ring Seal Performance Test Results

Test Number	O-ring Seal Cross-Sectional × Inner Diameter (mm)①		O-ring Groove Depth (mm)		Shim Thickness (mm)	Stretch (%)②	Compression (%)		"Leaktight" Leak Test (Leakage Rate ≤ 1.0 × 10^{-8} Pa-m^3/s, air)
	Min	Max	Min	Max			Min	Max	
1	12.01 × 2393	12.14 × 2393	8.31	8.40	0.00	3.0	29.0	30.5	Yes
2					1.24		18.5	20.2	Yes
3					1.56		15.8	17.4	No
4					2.27		9.8	11.5	No
5					2.29		9.6	11.3	No
6					2.32		9.4	11.1	No

Notes:

① Material for all O-ring seal test specimens is butyl rubber compound RR–0405–70, Rainier Rubber Co., Seattle, WA.

② Stretch, S, computed based on as-measured O-ring groove length (1,887.2 mm × 2,048.0 mm × R50 mm) with actual diameter measurements of O-ring seals per the following formula:

$$S = \frac{(\text{Groove Length}) - (\text{O-ring Length})}{(\text{O-ring Length})} \times 100$$

2.12.3 Certification Tests on CTU-1

This appendix presents the results of normal conditions of transport (NCT) and hypothetical accident condition (HAC) tests that address the free drop and puncture test performance requirements of 10 CFR 71[1]. This appendix summarizes the information presented in the test report[2] for the first TRUPACT–III certification test unit (CTU-1). Wherever the acronym "CTU" is used in this section, it is to be understood as meaning CTU-1.

2.12.3.1 Introduction

Demonstration of the compliance of the design of the TRUPACT–III transportation package with the requirements of 10 CFR §71.73 was primarily achieved using formal certification testing. Analysis was used for all NCT events except the free drop, and for HAC thermal and immersion cases. Performance of the debris shield, which was not present in the testing, was also evaluated by analysis. The NCT and HAC free drop events and HAC puncture event were demonstrated by testing. This appendix describes the results of the free drop and puncture testing, including post-test measurements and evaluations. One NCT free drop, four HAC free drops, and four HAC puncture tests were performed. The primary success criterion was that, subsequent to all free drop and puncture testing, the CTU containment boundary, including the closure lid and vent port seals, be leaktight per ANSI N14.5[3]. Other supporting data, including accelerations and physical measurements, was collected as described herein.

The TRUPACT–III CTU was fabricated in prototypic full-scale, which was in full compliance with the drawings given in Section 1.3.1, *Packaging General Arrangement Drawings* (except for differences noted and justified below). The results of extensive engineering tests on a half-scale engineering test unit (ETU) are provided in Section 2.12.1, *Engineering Tests*.

2.12.3.2 Test Facilities

Free drop and puncture testing of the TRUPACT–III package test unit was performed at Sandia National Laboratories' Coyote Canyon Aerial Cable Facility in Albuquerque, New Mexico. The drop pad is designed to accommodate test packages weighing up to 90,000 kg. The embedded steel plate target has a varying thickness of approximately 100 to 200 mm. The pad therefore constituted an essentially unyielding surface for the CTU, which weighed approximately 25,052 kg.

In accordance with the requirements of 10 CFR §71.73(c)(3), puncture bars were fabricated from a solid, 150 mm diameter mild steel. The length of each bar was designed to allow the puncture event to proceed to completion before the CTU gained any support from the unyielding surface, but without excessive length. Each puncture bar was welded with gussets perpendicularly to a thick

[1] Title 10, Code of Federal Regulations, Part 71 (10 CFR 71), *Packaging and Transportation of Radioactive Material*, 01–01–09 Edition.

[2] *TRUPACT–III Full–Scale Certification Test Report*, TR-024, Packaging Technology, Inc.

[3] "Leaktight" is a leakage rate not exceeding 1×10^{-8} Pascals – cubic meters per second (Pa–m^3/s), air, as defined in ANSI N14.5–1997 (or later), *American National Standard for Radioactive Materials – Leakage Tests on Packages for Shipment,* American National Standards Institute, Inc. (ANSI).

mild steel square plate. The top edge of each puncture bar was finished to a 6-mm radius maximum. Each puncture bar assembly was securely welded to the impact surface.

2.12.3.3 Test Unit Configuration

The CTU was an essentially prototypic, full-scale model of the TRUPACT–III package. The CTU was fabricated according to the drawings given in Section 1.3.1, *Packaging General Arrangement Drawings*. Prior to testing, the CTU data package was examined and a certificate of conformance was issued. Any differences between the CTU and a regular production TRUPACT–III unit are discussed and justified below.

1. The CTU utilized no thread inserts. The production unit inserts are stronger than threads made directly in the parent material. However, the production unit thread inserts are optional, therefore the CTU conservatively represented the minimum pull-out strength possible in a production unit.
2. The CTU utilized washers for closure bolts and overpack cover attachment bolts made from ASTM Type 304L material. The production unit washers are made from ASTM A564, Grade 630, Condition H1025 (17-4 PH) material. The production unit washers are significantly stronger than the CTU washers, thus, this substitution is conservative.
3. To reduce the effect of polyurethane crush strength tolerance on free drop impact and deformation results, the allowable range of properties in certain critical regions was reduced. In regions where the crush strength of the foam would affect maximum impact (the same drop tests for which cold temperature was used), the foam was fabricated using only the upper (stronger) half of the normally acceptable tolerance range. This helped ensure that the resulting impact magnitudes were not significantly affected by lower strength foam. In production units, expanding the crush strength tolerance to include the lower half of the range is conservative, since impacts could only be reduced. Likewise, in regions where the crush strength of the foam would affect maximum deflection (the same drop tests for which ambient temperature was used), the foam was fabricated using only the lower (weaker) half of the normally acceptable tolerance range. This helped ensure that the resulting deformations were not significantly affected by higher strength foam. In production units, expanding the crush strength tolerance to include the upper half of the range is conservative, since deformation could only be reduced. Of note, this use of biased strength tolerances was possible because the free drop tests were performed on different areas of the package, and interference of test results was not significant. Foam crush strength tolerances were biased according to the following table. Note that the 0.10 kg/dm^3 foam, located behind the puncture-resistant plates only, played a negligible role in free drops and was fabricated using the full production unit tolerance range.

CTU Reduced Foam Tolerance		
Density, kg/dm^3	**Tolerance Bias**	**Test Purpose**
0.16 (all locations)	Upper half-range	Primarily affects the end (LD1 & LD2) and side (LD3) orientations, for maximum impact.
0.29 (all locations)	Lower half-range	Primarily affects the CG-over-side-edge (LD5) orientation, for maximum deformation.
0.48 (left side only)	Upper half-range	Primarily affects the side (LD3) orientation, for maximum impact.
0.48 (all other locations)	Lower half-range	Primarily affects the CG-over-side-edge (LD5) and CG-over-corner (LD4) orientations, for maximum deformation.

4. To ensure conservative leakage rate measurement of the CTU containment O-ring seal, care was taken to ensure that the compression of the seal was near the minimum compression of the production unit seal. The as-built depth of the containment seal O-ring groove was d_G = 8.72 mm, and the cross-sectional diameter of the containment O-ring was D_R = 11.99 mm. From Section 4.1.3.1, *Seals*, the cross sectional diameter reduction due to O-ring stretch is 1.5%. The effective O-ring diameter is therefore:

$$D_{Re} = (1 - 0.015)D_R = 11.81 \text{ mm}$$

The compression of the CTU containment seal was therefore:

$$C_{CTU} = \left[1 - \left(\frac{d_G}{D_{Re}}\right)\right] \times 100 = 26.2\%$$

This is conservatively less than the minimum standard production unit containment seal compression of 27.8% calculated in Section 4.1.3.1, *Seals*.

5. Special vent and test ports were added to the side of the CTU that do not occur on the production unit. These were provided to allow leakage rate testing of the CTU without the need to remove the overpack cover or disturb the prototypic vent and test ports. They were located away from structural damage areas, and did not affect the behavior of the CTU.

6. The roller floor guide rails, the roller floor, and the pallet were not included in the test unit. Absence of these structures was conservative, since their beneficial capacity to absorb impact energy was not present. Their gross weight was included as part of the simulated payload.

7. The debris shield, including the receptacle, holder, foam rubber seal, and associated payload guide bars were not included. Absence of these components allowed debris contamination of the containment seal, as discussed in Section 2.12.3.8.1, *Leakage Rate Tests*. Their absence was also structurally conservative, since they would have a tendency to strengthen the containment boundary.

8. Several minor package features were omitted from the CTU: Package nameplate, tamper-indicating device, pressure relief valve on the overpack cover, paint, and the optional rubber bumper strips in the payload cavity. Lack of these items did not affect the outcome of the certification tests.
9. Small steel accelerometer mounting blocks and threaded steel lifting bosses were welded to the outside surface of the CTU. Since they were not directly involved in test damage, their presence did not affect results.
10. Several nonconformances were encountered during fabrication of the CTU. All are recorded in the data package for the CTU, and were dispositioned according to the Quality Assurance program and approved by Packaging Technology. The nonconformances were very minor in nature and did not have a significant effect on the performance of the CTU during testing. The most significant nonconformances are noted in the following list.

    - Twelve V-stiffeners having a design for the closed end of the CSA were placed on the top and bottom sides (six each). Since the V-stiffeners for the end and sides are of a very similar design, this had no effect.
    - The body flange face thickness should be 20 - 30 mm. The thickness of the CTU flange face ranges from 16 to 22 mm. The regions of under-thickness were not extensive. In any case, the resulting strength of the flange was less than a production unit, and was therefore conservative.
    - The internal length of the CTU was 2,783 – 2,785 mm [109.57 – 109.65 inches] versus the specified dimension of 2,790 +20/-5 mm [109.84 +0.79/-0.20 inches]. This had no effect on test results.
    - The thickness of the calcium silicate insulation was 1-inch and 1½ inches thick instead of 30 mm and 42 mm thick. This had no effect on test results.
    - The M120 threads for the vent port retaining ring were mis-cut for a depth of 86 mm. This would tend to reduce slightly the strength of the vent port closure, and is conservative.
    - The weld connecting the front edge of the right side outer skin sheet to the CTU had poor penetration. This caused an excessively long weld tear during a free drop. This is further discussed in Section 2.12.3.7.4, *Free Drop, Side-Edge, HAC (Test LD5)*.
    - The washers used with the overpack cover attachment bolts had an outer diameter of 54 mm instead of the 64 mm required by the drawings. In addition, the 44-mm diameter mounting holes on the top of the overpack cover were elongated similar to the mounting holes on the bottom of the cover. Since both of these conditions would increase the likelihood of the bolt head being pulled through the hole, they conservatively reduce attachment integrity.
    - The width to the outside of the front cheeks was 2,155 mm versus the specified dimension of 2,120 ±25 mm due to weld distortion. This condition would tend to apply lateral forces to the cheeks during end impacts, and is conservative for testing.

Except for these differences, the CTU was in full compliance with the SAR drawings of the TRUPACT–III package. Prior to any certification testing, the CTU was subject to acceptance testing, including a lifting load test, an internal pressure (1.5 times MNOP) test, and leakage rate tests of the containment boundary.

The test payload consisted primarily of a large quantity of square-ended, two-inch and four-inch diameter aluminum bars, with additions of other items made from brass and aluminum. The total weight of the test payload was 6,747 kg, which is 30.4% more than the maximum TRUPACT–III payload of 5,175 kg. This condition is particularly conservative for impact loads on the closure lid. The gross weight of the CTU was 25,052 kg, slightly more than the maximum gross weight of the TRUPACT–III package of 25,000 kg.

2.12.3.4 Instrumentation

2.12.3.4.1 Accelerometers

Accelerometers were utilized to record each free drop impact. No accelerometers were used for puncture drop tests. At least four single axis accelerometers were used to record each free drop event. The accelerometers were attached to solid stainless steel blocks that were fillet welded to the outer sheet on the body at the locations shown in Figure 2.12.3-1. The accelerometer type used in the tests was piezoresistive. Data was recorded, conditioned, and reduced by the Sandia Mobile Instrumentation Data Acquisition System (MIDAS). A Fast Fourier Transform (FFT) of the raw data was performed to determine the appropriate cutoff, or filtering frequency. The accelerometer data was filtered using a six-pole Butterworth filter with the cutoff set no lower than 250 Hz.

2.12.3.4.2 Thermocouples

As discussed in Section 2.12.3.5.2, *Temperature*, maximum impact will occur at the minimum initial temperature condition of -29 °C, as defined in 10 CFR §71.73(b). Type K thermocouples were installed and numbered in each end of the package to measure the temperatures of the polyurethane foam in the critical regions. The thermocouple locations that were utilized for the free drop tests are shown in Figure 2.12.3-2. Temperatures were monitored only in critical areas, i.e., those experiencing deformation in the free drop event. The data was monitored by Sandia's MIDAS data acquisition system during the chilling period, and continued until impact.

2.12.3.5 Initial Test Conditions

2.12.3.5.1 Internal Pressure

Since internal pressure has the effect of increasing the stress on the containment boundary, the CTU was pressurized (at ambient temperature) to an internal pressure of 172 kPa, equal to the design pressure. Since resistance to puncture is not significantly affected by internal pressure, the CTU was not pressurized for the puncture tests. Since the pressure is only an initial condition, monitoring the pressure was not performed.

2.12.3.5.2 Temperature

The free drop tests evaluated the integrity of the containment boundary under maximum impact, as well as the maximum deformation of the overpack for analysis of the HAC fire event. The greatest impact corresponds to the minimum regulatory temperature condition of -29 ºC, due to

the increase in crush strength of the impact limiting materials with decreasing temperature. Consequently, in free drops LD1, LD2, and LD3, the CTU was tested at a material temperature below -29 ºC. Ambient temperature was used for all puncture drop tests. For those free drop orientations where maximum deformation was of concern (free drops LD4 and LD5), the test was performed at a temperature of at least 7 ºC and extrapolated using analysis to the deformation corresponding to maximum NCT temperature.

2.12.3.6 Certification Tests Performed

The evaluation and selection of tests to be performed for certification testing is discussed in Section 2.7.1, *Free Drop*, and Section 2.7.3, *Puncture Drop*. A total of four HAC free drops and one NCT free drop were performed, as summarized in Table 2.12.3-1. A total of four puncture drops were performed, as summarized in Table 2.12.3-2. The free drops (except for tests LD1 and LD2, which are flat on the closure lid end, and LD3, which is flat on the side) are shown schematically in Figure 2.12.3-3 and Figure 2.12.3-4, and the punctures in Figure 2.12.3-5 through Figure 2.12.3-8.

2.12.3.7 Test Results

Five free drop tests were performed: one from a height of 0.3 m and four from a height of 9 m. After certain key drop tests, a vacuum was placed between the closure lid seals as an approximate confirmation of the sealing integrity of the seals, using the special test port on the CTU side. An adequate vacuum could not be obtained after the last free drop had been performed, likely as a consequence of the debris contamination of the containment seal as discussed in Section 2.12.3.8.1, *Leakage Rate Tests*. The tests were performed in the sequence: LD1, LD2, LD3, LD5, and LD4.

Four puncture drop tests were performed, all from a height of one meter. The internal pressure was bled off to approximately 2 psig. Accelerations were not recorded. All puncture tests occurred at prevailing CTU temperatures, which, based on ambient temperatures and the temperature of the last free drop, were between approximately 13 ºC and 18 ºC. The puncture bars typically did not survive the tests without damage. Two became bent, and one completely broke off subsequent to impact. However, the baseplate joints and attachment to the impact pad remained intact in all cases. For rigging convenience, the puncture tests were performed in the order: LP3, LP4, LP1, and LP2.

Prior to performing any free or puncture drop tests, helium leakage rate tests were performed on the containment metallic boundary, the main O-ring seal, and the sampling/vent port plug O-ring seal. All free drop and puncture drop measurements and testing were performed in accordance with a written test plan prepared for the TRUPACT–III certification testing program. Photos of certification testing are provided in Figure 2.12.3-9 to Figure 2.12.3-34.

2.12.3.7.1 Free Drop, Vertical, Overpack Cover Down, NCT (Test LD1)

Test LD1 was a free drop from a height of 0.3 m, oriented with the CTU axis vertical, striking the overpack cover flat on the surface. In order to preclude the necessity of re-chilling the CTU before the following test, the CTU was over-chilled for test LD1. The average temperature of thermocouples T1 and T3 was -42 ºC. The average temperature of the deeper thermocouples T2 and T4 was -40 ºC. The ambient temperature was 23 ºC. Accelerations were obtained from gages A1A, A3A, and A4A. The raw signals were filtered at 250 Hz, and the resulting acceleration plots are shown in Section 2.12.3.9, *Acceleration Time History Plots*. The peak accelerations and overall average maximum acceleration

are shown in the table below. After the drop, there was little visible damage to the CTU. However, the overpack cover, which had projected an average of 22 mm beyond the end faces of the cheeks, was uniformly crushed by an average of 7 mm. Photos of the post-test condition are not provided since no damage was visible.

A1A	A3A	A4A	Avg.
36.8g	49.1g	26.1g	**37.3g**

2.12.3.7.2 Free Drop, Vertical, Overpack Cover Down, HAC (Test LD2)

Test LD2 was a free drop from a height of 9 m, oriented with the CTU axis vertical (same as LD1), striking the overpack cover flat on the surface. The average temperature of thermocouples T1 and T3 was -34 ºC. The average temperature of the deeper thermocouples T2 and T4 was also -34 ºC. The ambient temperature was 12 ºC. Accelerations were obtained from gages A1A and A3A. (Note: velocity integrations of gages A2A and A4A showed velocities which are not physically possible, thus these gages were ignored.) The raw signals were filtered at 250 Hz, and the resulting acceleration plots are shown in Section 2.12.3.9, *Acceleration Time History Plots*. The peak accelerations and overall average maximum acceleration are shown in the table below.

A1A	A3A	Avg.
208.9g	199.8g	**204.4g**

In this case, both the overpack cover and the cheeks came into contact with the ground. There was very little rebound after impact. The additional crush was an average of 29 mm for a total end crush of 36 mm. There were a number of small weld cracks around the impacted end, but they were not significant relative to exposure of foam. The gaps between the cheeks and the overpack cover on the left and right sides were essentially closed by the buckling deformation of the 14-ga [0.0751-inch] thick sheets located on the cheeks and overpack cover. A hard vacuum was obtained between the closure lid O-ring seals after the test. Photos of the damage are shown in Figure 2.12.3-9 through Figure 2.12.3-12.

2.12.3.7.3 Free Drop, Flat Side, HAC (Test LD3)

Test LD3 was a free drop from a height of 9 m, oriented with the CTU axis horizontal, striking flat on the left side of the package. The average temperature of thermocouples T5 through T8 was -39 ºC. The ambient temperature was 12 ºC. Accelerations were obtained from gages A1L, A4L, A5L, A8L, A9L, and A10L. The raw signals were filtered at 300 Hz, and the resulting acceleration plots are shown in Section 2.12.3.9, *Acceleration Time History Plots*. The peak accelerations and overall average maximum acceleration are shown in the table below.

A1L	A4L	A5L	A8L	A9L	A10L	Avg.
529.2g	378.5g	438.2g	455.4g	352.2g	288.3g	**407.0g**

Some slight additional damage was noted in the areas around the ISO fittings, but little other external damage could be found. Measurements were taken at the four corners of the package between the outside surface and the surface of the internal containment structural assembly (CSA) using small drilled holes in the outer skin. These holes, designated S1 – S4, are located as shown in Figure 2.12.3-2. The depth of the holes was measured before any testing and

compared to measurements after test LD3, and show the magnitude of any "inside-out" deformations of the CSA relative to the outside of the CTU. The average decrease in the four measurements (i.e., the amount that the CSA approached the impact surface from inside of the body overpack) was 7 mm. A hard vacuum was obtained between the closure lid seals after the test. Photos of the damage are shown in Figure 2.12.3-13 through Figure 2.12.3-15.

2.12.3.7.4 Free Drop, Side-Edge, HAC (Test LD5)

Test LD5 was performed prior to Test LD4 for expediency in rigging. Test LD5 was a free drop from a height of 9 m, oriented with the CTU axis horizontal, and rotated about that axis so that it impacted with the center of gravity (CG) over one long edge (the upper right edge), as shown in Figure 2.12.3-3. The average temperature of thermocouples T6 and T8 was 7 ºC. The temperature of the body overpack skin was between 17 and 24 ºC. The ambient temperature was 18 ºC. Accelerations were obtained from gages A1L, A3L, A5L, and A7L. The raw signals were filtered at 250 Hz, and the resulting acceleration plots are shown in Section 2.12.3.9, *Acceleration Time History Plots*. The peak accelerations and overall average maximum acceleration lateral to the CTU are shown in the table below. A resolution of the average acceleration to the vertical direction is performed using the following equation:

$$A_{\perp} = \frac{A_L}{\cos(47)} = 142.2\text{g}$$

where A_L is the overall average lateral acceleration and the lateral direction is oriented at an angle of 47º to the vertical as defined in Figure 2.12.3-3.

A1L	A3L	A5L	A7L	A_L	Resolved Average
118.4g	90.2g	94.3g	85.2g	**97.0g**	**142.2g**

The impact caused a flat region along the central side-edge approximately 305 mm wide. This tapered down to approximately 178 mm toward each end. During post-test disassembly, it was noted that the minimum perpendicular distance between the inside surface of the outer skin and the corner of the relatively rigid weldment which protects the calcium silicate insulation was 95 mm. A gap opened up between the front cheek and the steel plate encasing the 0.29 kg/dm^3 foam equal to approximately 16 mm across the crush width. Additionally, the weld between the side outer skin and the front cheek unzipped for a distance of approximately 914 mm, and was a maximum of 51 mm wide, exposing the balsa wood in the side panel. It was subsequently determined that this weld was substandard. A vacuum test on the closure lid seals was not performed. Photos of the damage are shown in Figure 2.12.3-16 through Figure 2.12.3-18.

2.12.3.7.5 CG-Over-Corner, Overpack Cover Down, HAC (Test LD4)

Test LD4 was a free drop from a height of 9 m, oriented with the CTU axis oriented approximately 50º to the ground, striking the lower right corner of the package as shown in Figure 2.12.3-4. The center of gravity of the package was over the point of initial impact. The average temperature of thermocouples T1 and T2 was 12 ºC. These two temperatures were the shallow and deep readings on the opposite corner of the package, and were representative of the temperature of the impacted corner. The ambient temperature was 14 ºC. Accelerations were obtained from gages A1A, A2A,

A3A, and A4A. The raw signals were filtered at 250 Hz, and the resulting acceleration plots are shown in Section 2.12.3.9, *Acceleration Time History Plots*. The peak accelerations and overall average maximum acceleration axial to the CTU are shown in the table below. A resolution of the average acceleration to the vertical direction is performed using the following equation:

$$A_{\perp} = \frac{A_A}{\cos(40)} = 52.7g$$

where A_A is the overall average axial acceleration and the axial direction is oriented at an angle of 40º to the vertical as defined in Figure 2.12.3-4.

A1A	A2A	A3A	A4A	A_A	Resolved Average
35.4g	44.1g	39.8g	42.3g	**40.4g**	**52.7g**

The impact caused a triangular flat region having dimensions of 1,054 mm along the overpack cover, 838 mm along the bottom, and 800 mm along the right side of the CTU. The combined damage from all of the free drops caused a slight bowing of the right cheek, and a gap of up to 76 mm at the center between the cheek and the overpack cover right edge. The gap was however blocked with buckled material starting about 89 mm deep into the gap, and the gap reduced to zero width at the top and bottom of the cheek-to-cover joint. No significant weld seam failures were noted from this test. A hard vacuum could not be obtained between the closure lid seals, but the leak was not significant enough to have a measureable effect on the internal cavity pressure. Photos of the damage are shown in Figure 2.12.3-19 and Figure 2.12.3-20.

2.12.3.7.6 Puncture Drop On CG-over-Corner Damage (Test LP3)

The ambient temperature for this test was 17 ºC. The puncture bar struck at essentially the center of the prior c.g.-over-corner free drop (LD4) damage and created a further deformation of approximately 178 mm in diameter and 102 mm deep. The effect of the impact was to further locally compress the deformed materials in the damaged zone. Small amounts of foam were visible from the free drop test damage, and the puncture test did not significantly alter this. After cutting away the damaged material, a minimum distance of 51 mm was measured between the deformed steel resulting from the puncture drop and the nearest part of the calcium silicate protection box. This distance was filled with compressed, 0.48 kg/dm^3 foam. A photograph of the damage is shown in Figure 2.12.3-21.

2.12.3.7.7 Puncture Drop On Side-Edge Damage (Test LP4)

The ambient temperature for this test was 16 ºC. The puncture bar struck on the prior damage from free drop test LD5, with the center of the bar placed approximately 584 mm from the cover end of the package, with the package inclined 30º from the horizontal. The bar penetrated the outer skin (creating an approx. 178 mm diameter disk), and struck the top corner of the heavy structural box which protects the calcium silicate insulation in the cheek. This box is only 52 mm across, and is made from 16 mm thick material, and is therefore very rigid. Later disassembly showed relatively minor weld cracks in this region and only approximately 3 mm of deformation of the protective box. There was no damage to the calcium silicate insulating board, which maintained full integrity without crumbling or breaking. Note: the puncture bar fractured completely at a plane just above the reinforcement gussets as the package tipped off of the bar

following impact. However, all puncture bar welds, including those to the drop pad, remained intact. Photos of the damage are shown in Figure 2.12.3-22 and Figure 2.12.3-23.

2.12.3.7.8 Puncture Drop On Side Damage (Test LP1)

The ambient temperature for this test was 22 ºC. The puncture bar penetrated both the outer skin and the puncture-resistant plate, and left a dent of approximately 51 mm deep in the CSA outer structural sheet. There was no cutting or cracking of the CSA outer sheet, demonstrated by placing the CSA annular region under a vacuum. There was no deformation of the inner CSA containment sheet. The opening in the overpack was 254 mm long and 178 mm wide. Photos of the damage are shown in Figure 2.12.3-24 through Figure 2.12.3-26.

2.12.3.7.9 Puncture Drop On Overpack Cover (Test LP2)

The ambient temperature for this test was 17 ºC. The puncture bar struck the overpack cover approximately 292 mm from the left edge of the octagonal recess. The depth of penetration of the bar, measured from the outside surface, was 210 mm. From this value, the calculated depth of the dent in the puncture-resistant plate is approximately 145 mm deep. However, the puncture-resistant plate was not penetrated nor cracked. Removal of the overpack cover showed the impact to have been aligned between two V-stiffeners in the closure lid. A dent of approximately 5 mm deep was noted in the outer sheet of the closure lid at the puncture location. There was no deformation of the inner closure lid containment sheet. Photos of the damage are shown in Figure 2.12.3-27 and Figure 2.12.3-28.

2.12.3.8 Leakage Rate Tests and Post-Test Measurements

2.12.3.8.1 Leakage Rate Tests

Post-test leakage rate testing of the containment boundary was performed using helium test gas and a mass spectrometry leak detector (MSLD). The testing consisted of three elements:

- Metallic portion of the containment boundary
- Closure lid containment O-ring seal
- Vent port containment O-ring seal

The metallic portion of the containment boundary was tested by evacuating the payload (interior) cavity and then replacing the air in the annulus between the containment and structural sheets of the CSA with helium. The closure lid and vent/test port containment seals were both tested by evacuating the space between the containment seal and the test seal and then filling the payload cavity with helium. The metallic containment boundary leakage rate test was successful, with an adjusted leakage rate of 8.00×10^{-10} Pa-m^3/s, He, against a criterion of 2.2×10^{-8} Pa-m^3/s, He. The vent port containment O-ring seal leakage rate test was also successful, with an adjusted leakage rate of 4.07×10^{-9} Pa-m^3/s, He, against the same criterion.

The leakage rate test of the closure lid containment O-ring seal was, however, not initially successful. After removal of the closure lid, an amount of small debris was found to be present on both the containment and test O-ring seals, as shown in Figure 2.12.3-32 through Figure

2.12.3-34. Examination of the debris proved it to be made from thin shards or chips of aluminum that had been generated from the dummy payload bars in the testing. Some grain-like material may have come from some broken aluminum castings in the payload. Since the cavity was pressurized to 172 kPa, it is concluded that a transient opening of the closure joint during the impact event allowed debris to be blown outward by escaping air pressure over the sealing surfaces. Note: this does not mean that the gap size was larger than the amount by which the O-ring seal was initially compressed. Rather, the elastomer containment seal could not elastically respond in the very brief gap opening duration (on the order of milliseconds).

After cleaning the exposed surface of the O-rings (without removing them) and the body flange, the closure lid was reinstalled and all of the closure bolts were retightened to the smallest recorded residual tightening torque (that of bolt no. 16) of 149 N-m. See Section 2.12.3.8.2.2, *Closure Lid Bolt Removal Torque and Related Observations*, for a definition of residual torque. The leakage rate test of the closure lid containment seal was repeated and was successful, with an adjusted leakage rate of 1.76×10^{-9} Pa-m^3/s, He. As a further demonstration that the lack of leaktight condition was wholly attributable to the presence of debris, and not to low residual closure bolt torques, a third leak test was performed with only the four bolts in the corners of the closure lid installed (bolt nos. 1, 11, 23, and 33), again tightened to only 149 N-m. This test was also successful, with an adjusted leakage rate of zero. Note that since the internal pressure during the tests was atmospheric, there was no assistance from atmospheric pressure in holding the closure lid against the body. Furthermore, as the package was oriented horizontally, there was no assistance from the lid deadweight. These two supplemental leakage rate tests of the closure lid containment O-ring seal were performed for information only. They do not replace the initial, failed leakage rate test, but rather demonstrate leaktight capability in the absence of debris. The leakage rate test results are recorded in Table 2.12.3-3.

2.12.3.8.2 CTU Measurements

Besides measurement of the damage reported above, various measurements were taken of the CTU during disassembly as discussed below. A view of the payload cavity showing the state of the simulated payload after testing is shown in Figure 2.12.3-29.

The interior dimensions of the payload cavity were measured both prior to and subsequent to testing, and comparison of the measurements indicated only one negligible change. The diagonal of the open end which was in line with the impact from the Side-edge free drop impact LD5, having a nominal measurement of 2,718 mm, decreased by approximately 2 mm. Of note, this deformation was in the plane of the closure flange, and did not affect the closure seal. Careful measurements of the containment surface undulations indicated no evidence of actual or incipient local or global buckling. The inner walls of the CSA featured numerous dents as a result of impact with the simulated payload bars. The dents were of modest depth and there was no indication of failure of the containment sheet material.

2.12.3.8.2.1 Body Flange and Closure Lid Observations

The closure lid shear lip contacted the top right corner of the body (on both the top and right side flanges) corresponding to the side-edge free drop impact. The maximum indent was approximately 1.3 mm deep (See Figure 2.12.3-30). There was a local waviness of the body flange face of approximately 0.61 mm, possibly the result of bulged metal which was associated

with the shear lip impacts. There were no other indications of contact with the shear lips. In addition, the body flange exhibited a consistent slope on all four sides. Looking into the cavity, the inner flange edge of the CSA was nearest the observer, and the outer flange edge was farthest from the observer, on all four sides. The taper amounts varied between 0.25 to 0.50 mm, over the distance between the inner surface edge and the bolt line. This effect is probably due to the distortion caused by welding the body overpack parts in place after final flange machining. The small magnitude of this slope makes it of negligible importance. In addition, the direction of the taper is such that greater lid deformation would be necessary to open the containment seal.

To determine the lateral clearance which existed between the lid shear lip and the body flange, measurements of the lip and body flange were taken at three points along each side. Taking into account the shape and orientation of the interfacing edges, the maximum clearance (i.e., maximum possible movement) between the lid and the body in the lateral (side-to-side) direction was 3.37 mm, and in the vertical (top-bottom) direction, 4.49 mm.

2.12.3.8.2.2 Closure Lid Bolt Removal Torque and Related Observations

The residual torque of the closure bolts was checked by turning them counter-clockwise until impending motion of the bolt was sensed, and recording the torque achieved (the 'loosening' value). The bolt was subsequently turned clockwise, and the torque for impending motion was again recorded (the 'tightening' value). Both readings are given in Table 2.12.3-4. It was found that bolts on the right side, and some on the right ends of the top and bottom sides, featured relatively low residual torques compared to the other bolts. Upon removal of all bolts, it was also discovered that many bolts were bent. There was very good correlation between lower-than-expected residual torque and the degree of bending. The worst bolts (lowest torque, greatest bending) were located near the center of the right flange. Each bolt was bent in two opposite directions, with the axes of the threaded portion and of the bolt head nearly parallel, but with the axes offset. All bolts were chucked in a lathe to measure the runout between the head and the threads. The indicator was placed approximately 6 mm from the lower bearing surface of the head. The results as total indicator reading (TIR) are given in Table 2.12.3-5. The worst bolt was no. 17, having a TIR of 10.7 mm. A plot showing the correlation between runout and tightening torque is given in Figure 2.12.3-35. The direction of bolt bending relative to the package was toward the 11:00 o'clock direction, viewed from the open end, and was essentially uniform for all bent bolts. Each of the bent bolts also showed evidence of a side impact on the head. A smaller number of washers showed a similar side impact. As shown in Figure 2.12.3-31, the impact occurred near the lower bearing surface of the bolt head. The impact on the head aligned with the direction of bending and with evidence of contact in the overpack cover bolt head clearance cups. The location of the contact between the closure bolts and the overpack cover cups indicates that the overpack cover, most likely in the CG-over-corner free drop, moved into contact with the bolt heads and bent them.

Most of the clearance cups also showed some axial collapse due, presumably, to the lid down free drop. In some cases, the flat top of the bolt head contacted the inside bottom of the cups. This contact was most likely to occur near the center of each side of the lid. However, as noted, only the bolts on the right side had below-average residual torque.

The lid guide pin on the right side was sheared by approximately 4.3 mm towards the 11:00 o'clock direction. The guide pin on the left was sheared approximately 1.0 mm towards the 3:00 o'clock

direction. All closure bolt washers showed evidence of a thickness reduction, due to initial preload torque, applied impact loads, or both.

Table 2.12.3-1 – Free Drop Test Summary

Test	Description[1]	Orientation	Temperature[2]	Accelerometers & Direction[3]	Temperature Monitors
LD1	Vertical, overpack cover down, NCT	CTU axis vertical, impacting flat on cover end. (No figure)	Cold	A1A thru A4A	T1 & T3
LD2	Vertical, overpack cover down, HAC	CTU axis vertical, impacting flat on cover end. (No figure)	Cold	A1A thru A4A	T1 & T3
LD3	Flat side, HAC	CTU axis horizontal, impacting flat on left side. (No figure)	Cold	A1L, A4L, A5L, A8L, A9L, A10L	T5 thru T8
LD4	CG-over-corner, overpack cover down, HAC	CTU axis inclined 50º from horizontal, impacting on lower right corner. See Figure 2.12.3-4.	Prevailing, >7 ºC	A1A thru A4A	T1 & T2
LD5 [4]	Side-edge, HAC	CTU axis horizontal, rotated 47º from horiz., impacting on upper right edge. See Figure 2.12.3-3.	Prevailing, >7 ºC	A1L, A3L, A5L, A7L	T6 & T8

Notes:
1. NCT drop height 0.3 m; HAC drop height 9 m.
2. Recorded temperatures of the energy absorbing material are reported in Section 2.12.3.7.
3. Accelerometer designations are as follows: A1A is location no. 1, axial direction; A5L is location no. 5, lateral direction, etc. (lateral is defined as perpendicular to the package side as normally transported).
4. Test LD5 was performed before test LD4.

Table 2.12.3-2 – Puncture Drop Test Summary

Test No.	Description	Orientation
LP1*	On side damage	Impact on left side, inclined at 20º from horizontal, through CG. See Figure 2.12.3-5.
LP2	On overpack cover	Impact overpack cover in the octagonal recess, inclined at 25º to horizontal, through CG. See Figure 2.12.3-6.
LP3	On c.g.-over-corner damage	Impact on crushed corner at same orientation as test LD4, through CG. See Figure 2.12.3-7.
LP4	On side-edge damage	Impact on crushed edge from test LD5, inclined 30º from horizontal. See Figure 2.12.3-8.

*Sequence of test performance was LP3, LP4, LP1, LP2.

Table 2.12.3-3 – Leakage Rate Test Results

Test Date	Test Performed	Adjusted Leak Rate (Pa-m^3/s, He)	Pass/Fail①
12/12/06	Metallic containment boundary	8.00×10^{-10}	Pass
12/14/06	Closure lid containment seal	Test terminated	Fail
12/14/06	Vent port containment seal	4.07×10^{-9}	Pass
12/20/06	Closure lid containment seal, after debris removal (all 44 bolts × 149 N-m)	1.76×10^{-9}	Pass
3/2/07	Closure lid containment seal, after debris removal (4 corner bolts only × 149 N-m)	Zero②	Pass

Notes:
1. Pass criterion equals 2.2×10^{-8} Pa–m^3/s, He.
2. Zero leakage rate means that the final MSLD test reading was lower than the initial reading.

Table 2.12.3-4 – Closure Lid Bolt Residual Torques, N-m

Bolt No.	Residual Torque, Top Flange	Bolt No.	Residual Torque, Right Flange	Bolt No.	Residual Torque, Bot. Flange	Bolt No.	Residual Torque, Left Flange
1	759/1,248	12	475/658	23	542/664	34	814/1,112
2	868/1,166	13	522/583	24	678/868	35	976/1,220
3	1,003/>1,356	14	400/549	25	732/732	36	814/814
4	759/1,275	15	346/434	26	814/814	37	895/895
5	1,085/1,356	16	149/149	27	841/841	38	841/949
6	732/1,085	17	393/393	28	841/841	39	841/1,166
7	868/1,112	18	136/190	29	678/678	40	163/271
8	814/1,112	19	353/420	30	976/1,329	41	841/1,139
9	949/1,275	20	441/542	31	1,003/1,003	42	732/1,112
10	922/1,139	21	447/542	32	1,112/1,356	43	949/1,166
11	651/997	22	590/664	33	922/949	44	922/>1,356

Note: The value to the left of the slash character is the residual loosening torque, and the value to the right is the residual tightening torque, in N–m. See Section 2.12.3.8.2.2, *Closure Lid Bolt Removal Torque and Related Observations* for a definition of these quantities.

Table 2.12.3-5 – Closure Bolt Runout, TIR, mm

Bolt No.	Bolt Runout, Top Flange	Bolt No.	Bolt Runout, Right Flange	Bolt No.	Bolt Runout, Bot. Flange	Bolt No.	Bolt Runout, Left Flange
1	1.17	12	3.18	23	6.07	34	0.64
2	0.71	13	4.37	24	5.05	35	0.89
3	0.81	14	5.82	25	2.44	36	0.61
4	0.74	15	7.11	26	0.74	37	0.91
5	0.81	16	7.75	27	0.41	38	1.35
6	1.37	17	10.67	28	1.19	39	1.35
7	1.32	18	7.49	29	0.86	40	0.91
8	0.51	19	7.67	30	0.61	41	1.42
9	0.94	20	10.19	31	0.79	42	0.79
10	0.97	21	8.03	32	1.07	43	1.07
11	0.58	22	4.57	33	0.51	44	1.22

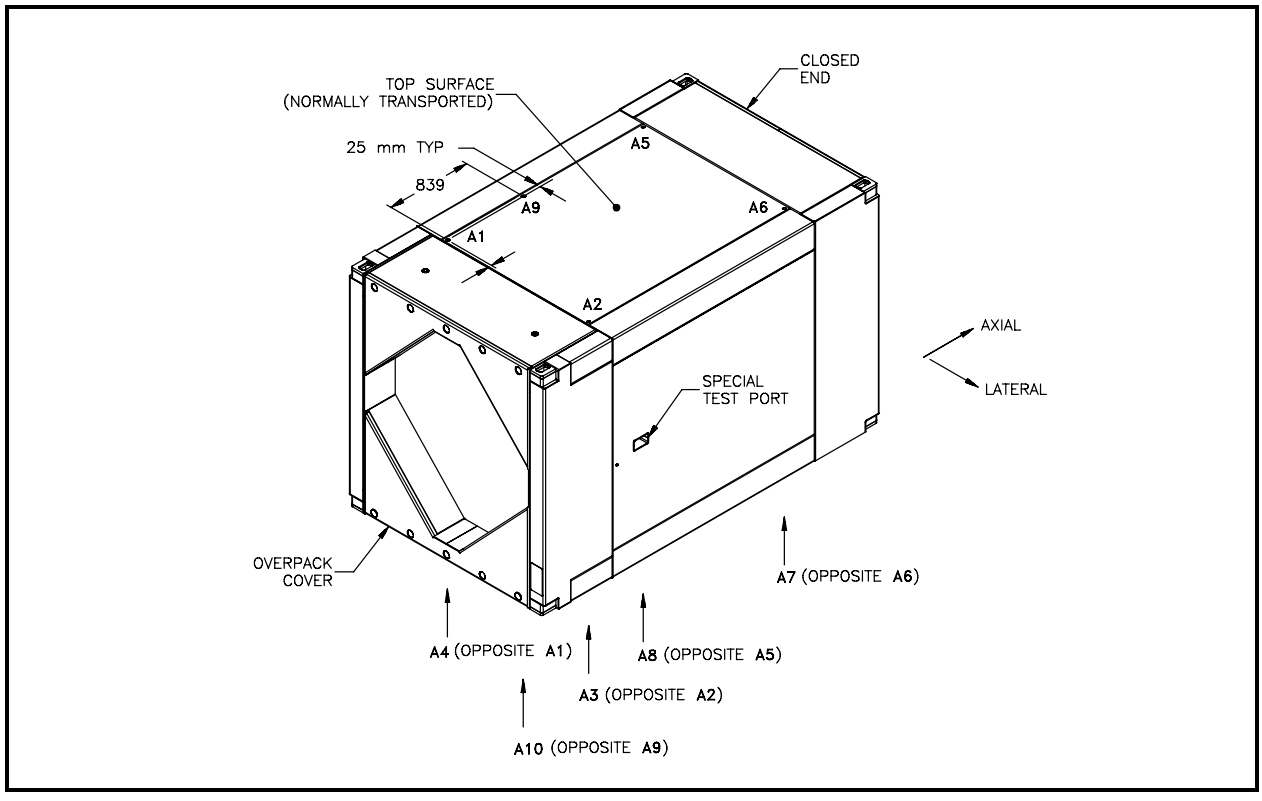

Figure 2.12.3-1 – Accelerometer Locations

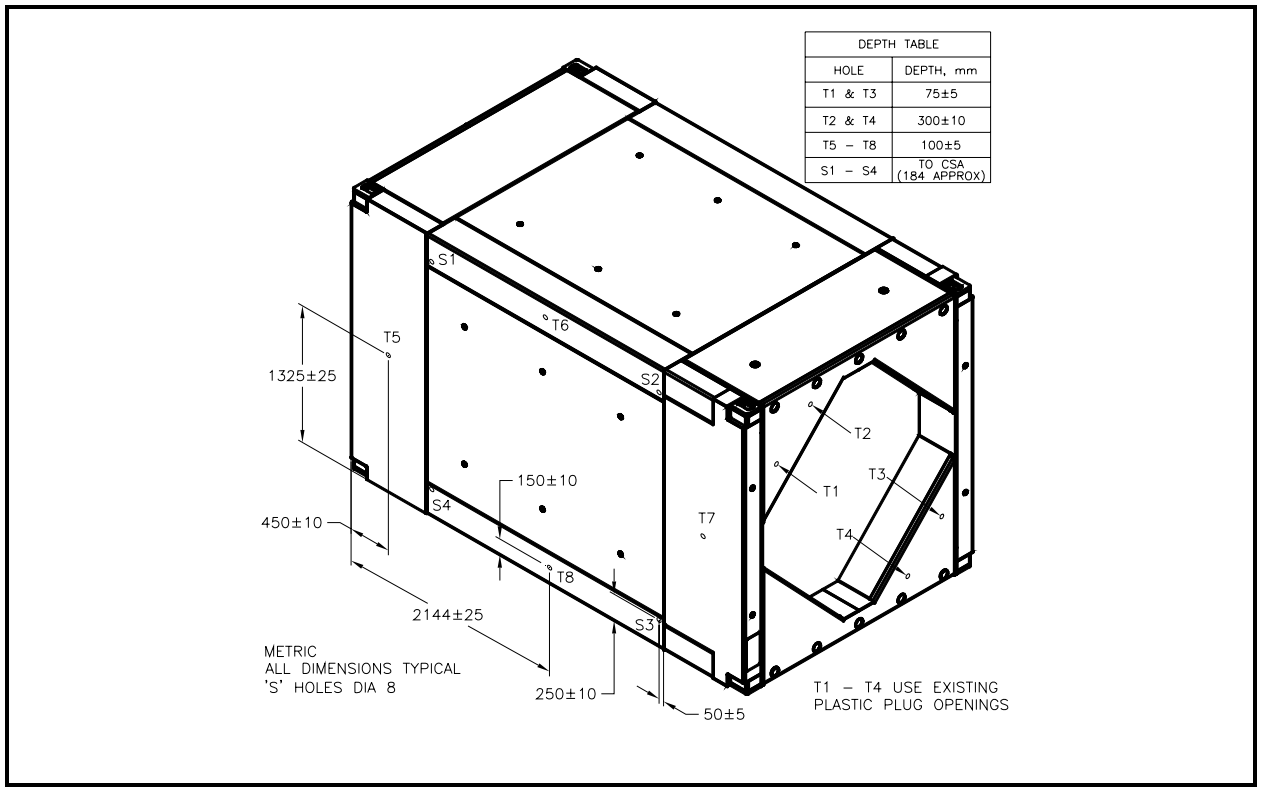

Figure 2.12.3-2 – Thermocouples (Tx) and Depth Measurement Holes (Sx)

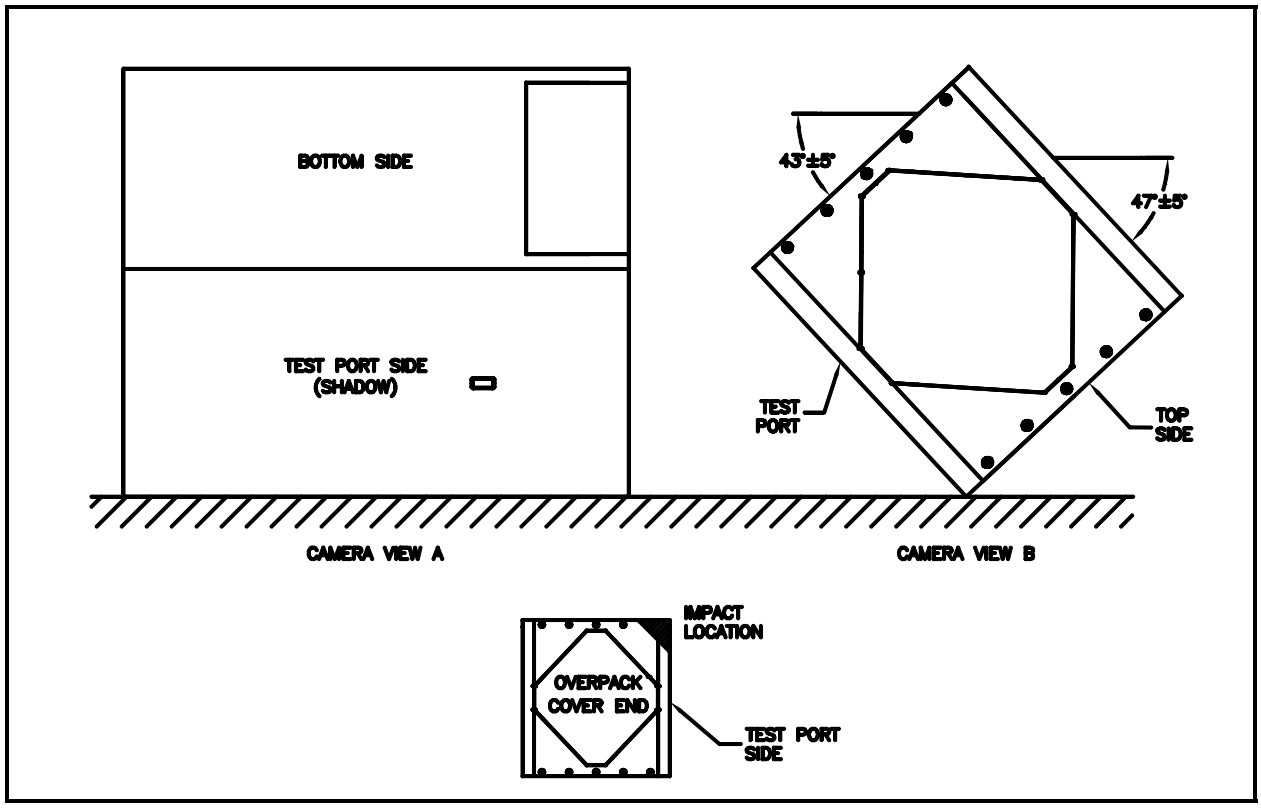

Figure 2.12.3-3 – Side – Edge Free Drop Orientation, Test LD5

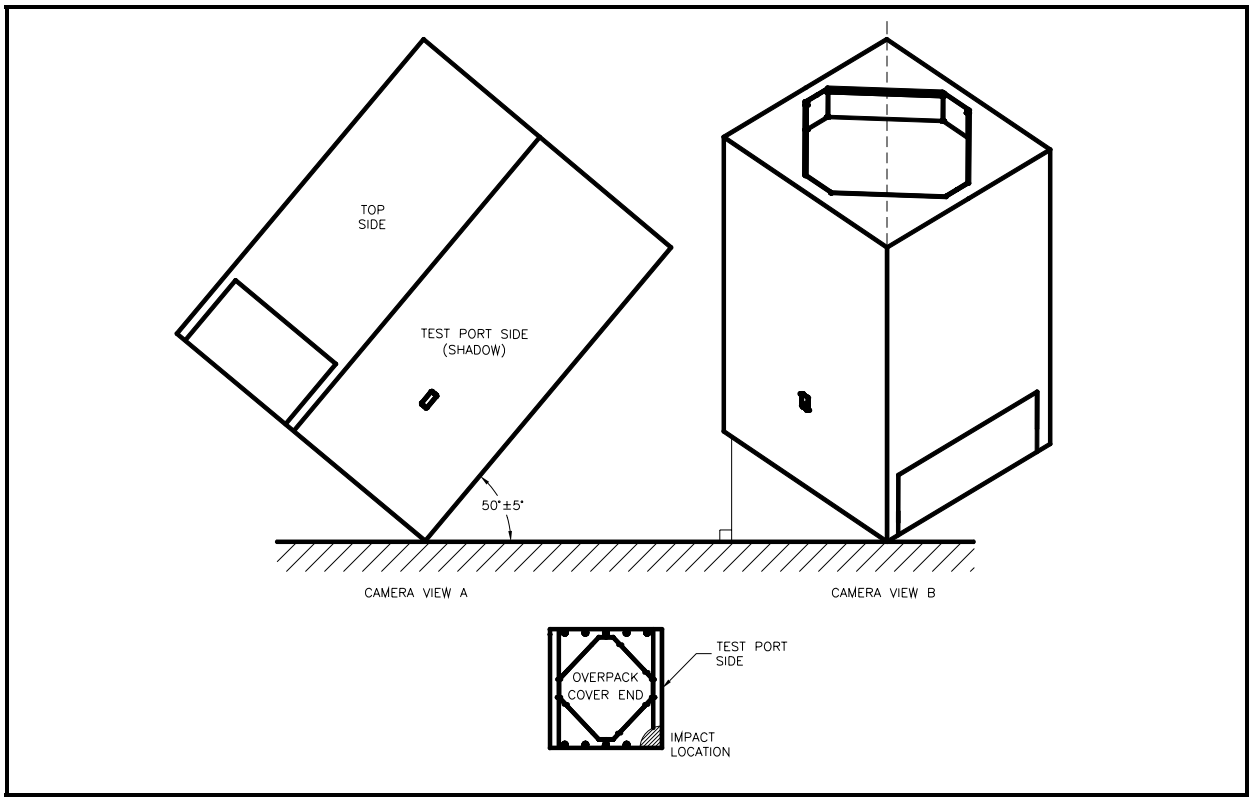

Figure 2.12.3-4 – CG-Over-Corner Free Drop Orientation, Test LD4

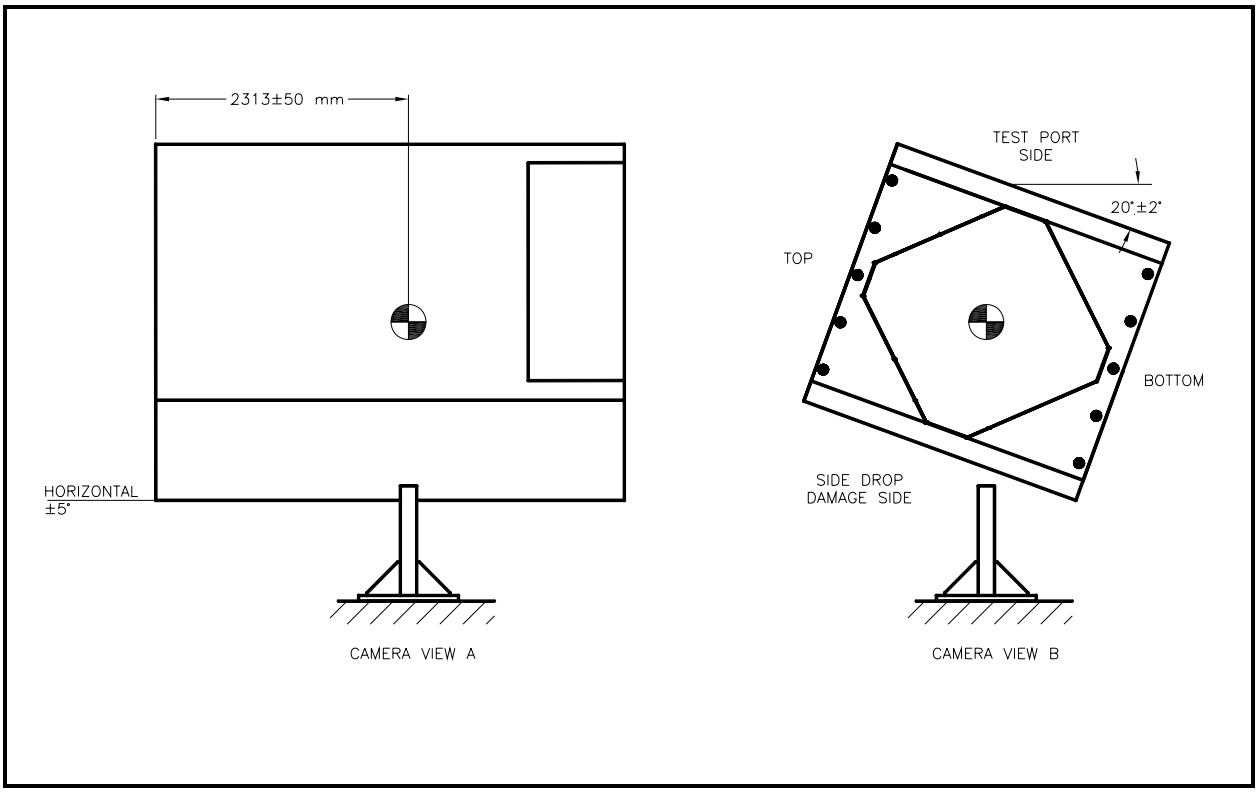

Figure 2.12.3-5 – Puncture on Side Damage Orientation, Test LP1

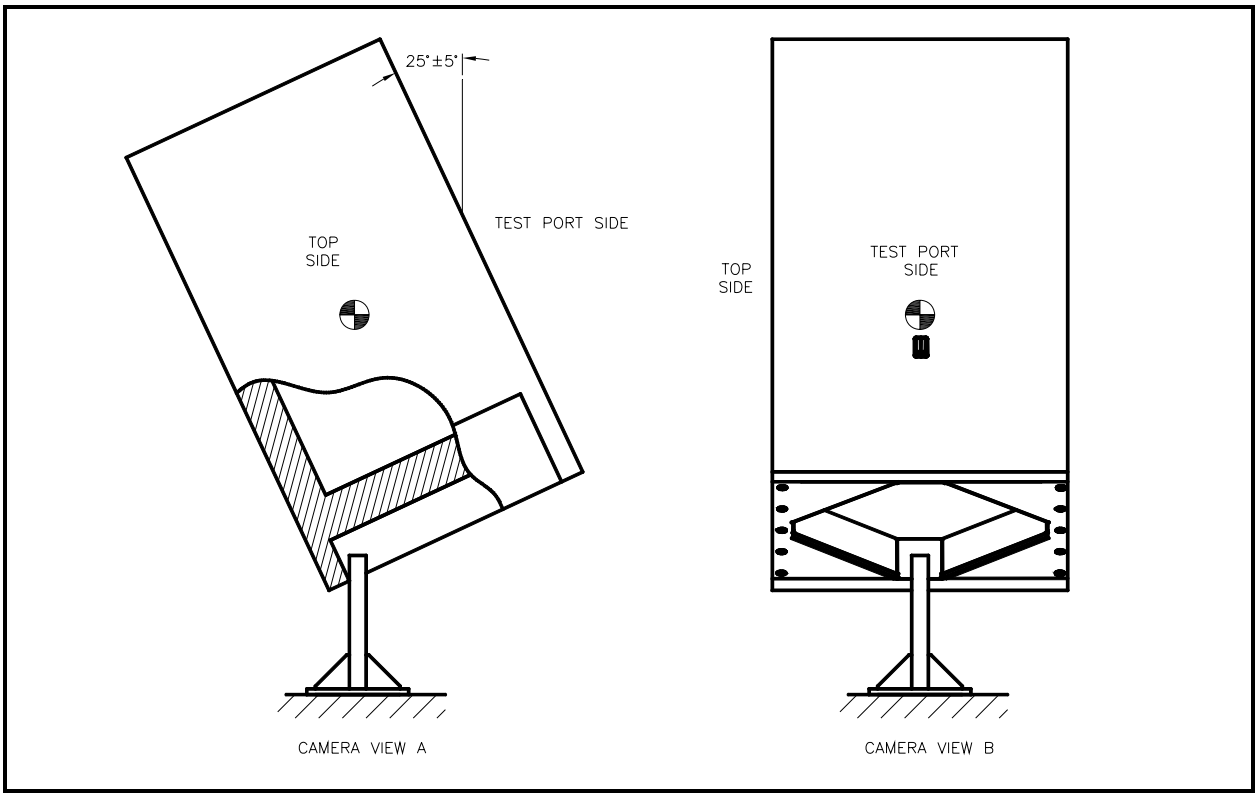

Figure 2.12.3-6 – Puncture on Overpack Cover Orientation, Test LP2

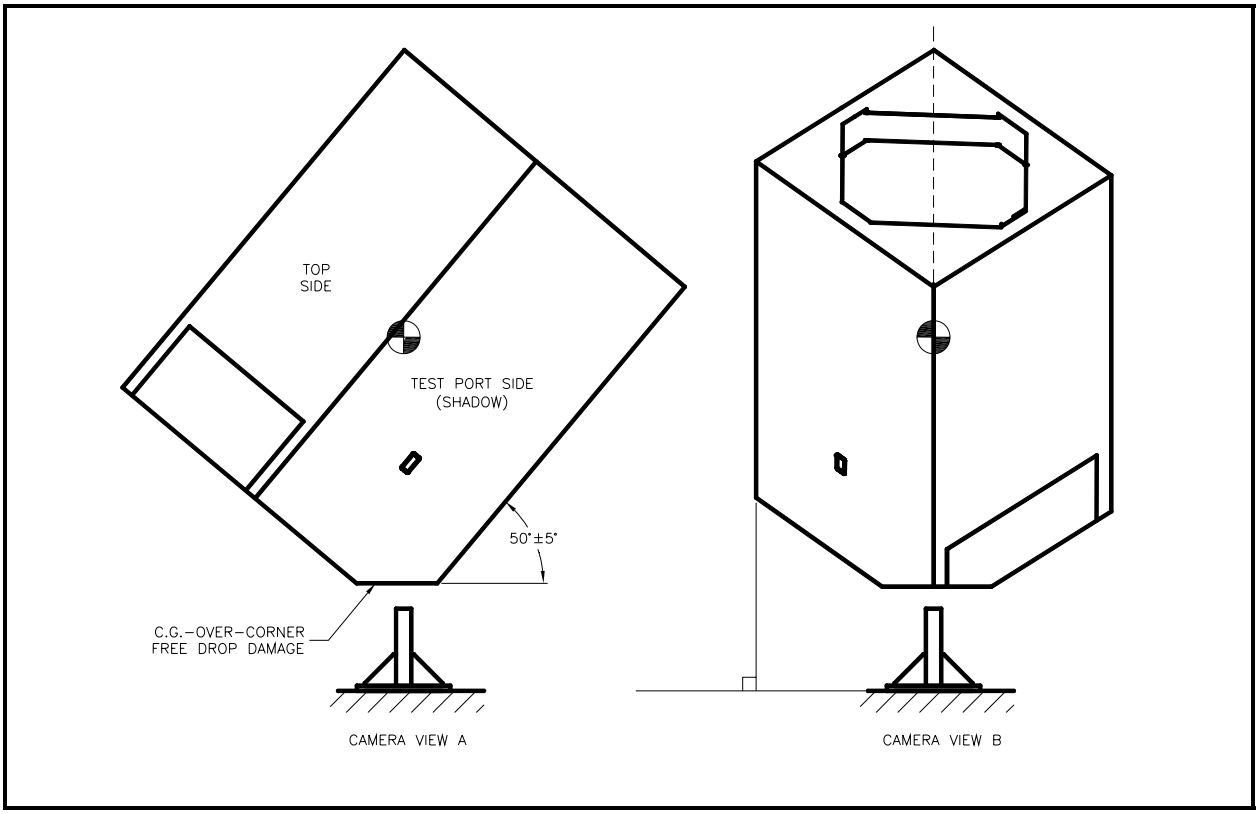

Figure 2.12.3-7 – Puncture on Prior CG-Over-Corner Damage, Test LP3

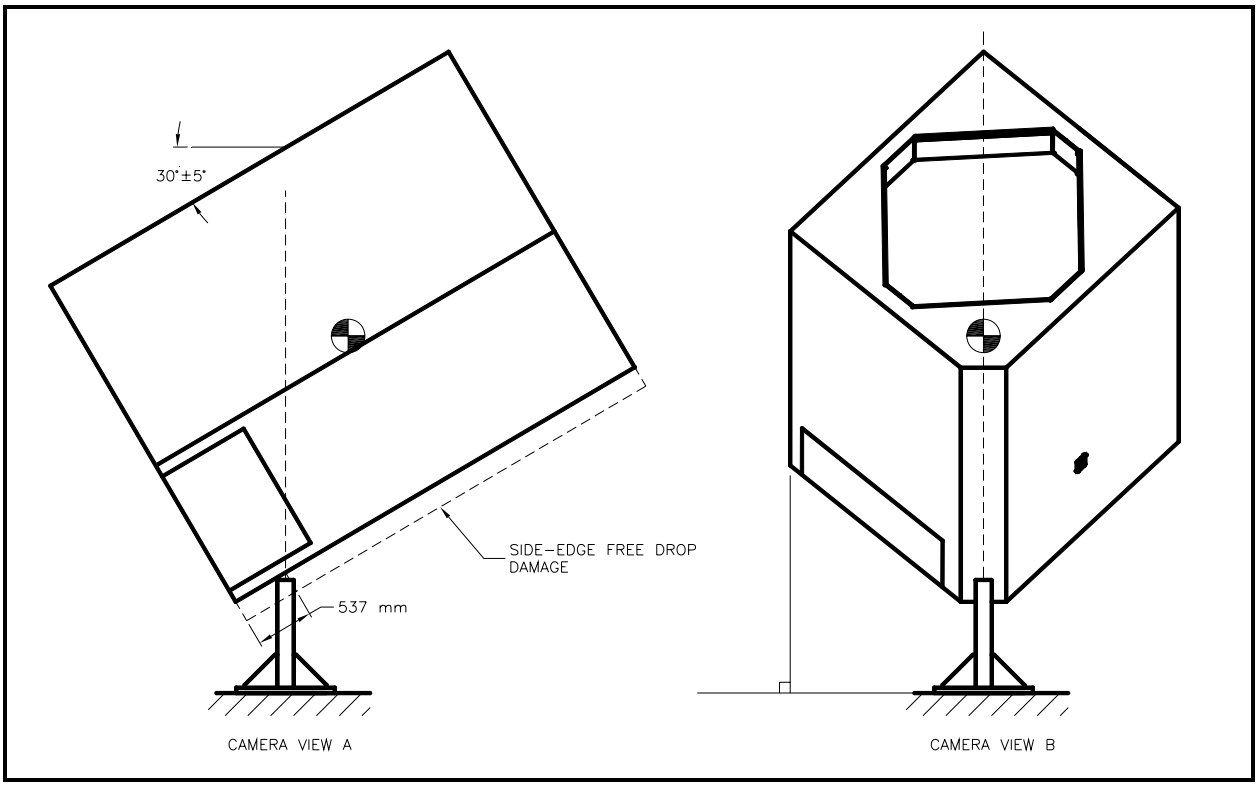

Figure 2.12.3-8 – Puncture on Prior Side – Edge Damage, Test LP4

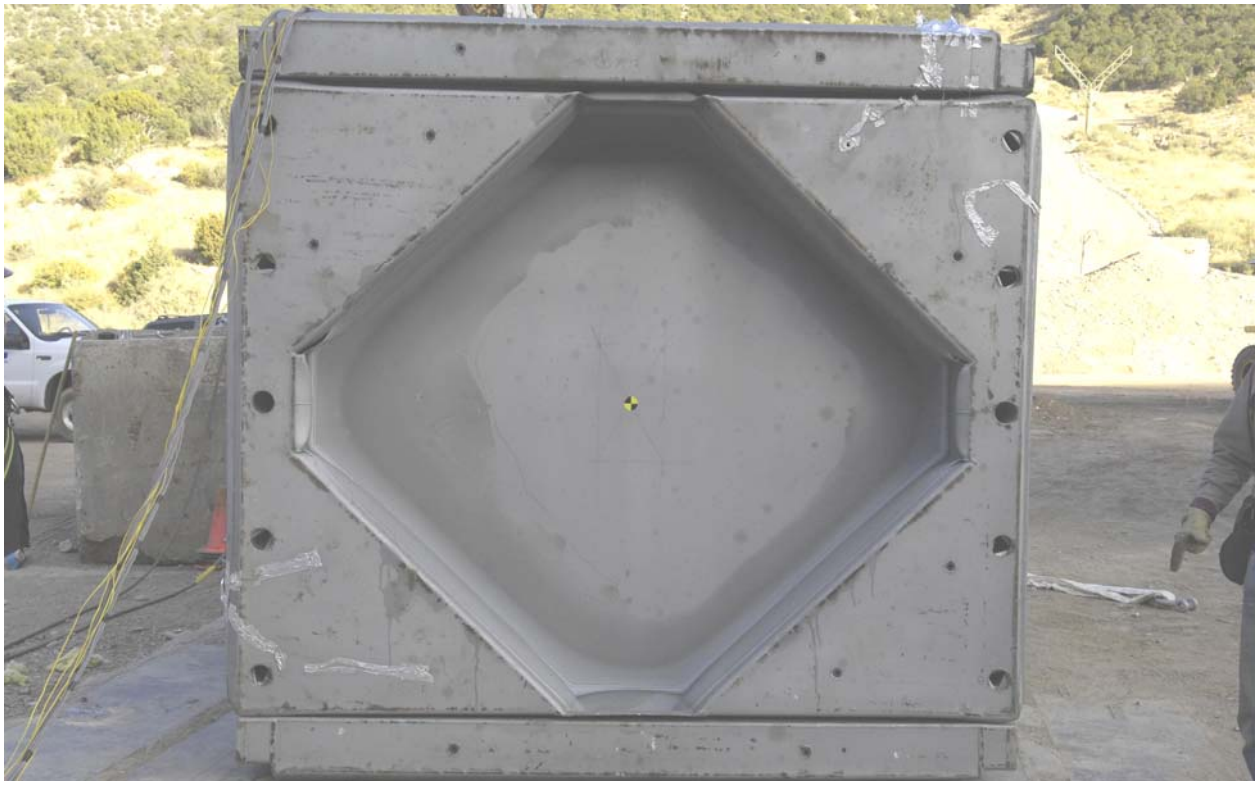

Figure 2.12.3-9 – Test LD2, Overall View of Impact Surface

Figure 2.12.3-10 – Test LD2, Typical Deformations at Closure End

Figure 2.12.3-11 – Test LD2, Typical Torn Welds on Overpack Cover

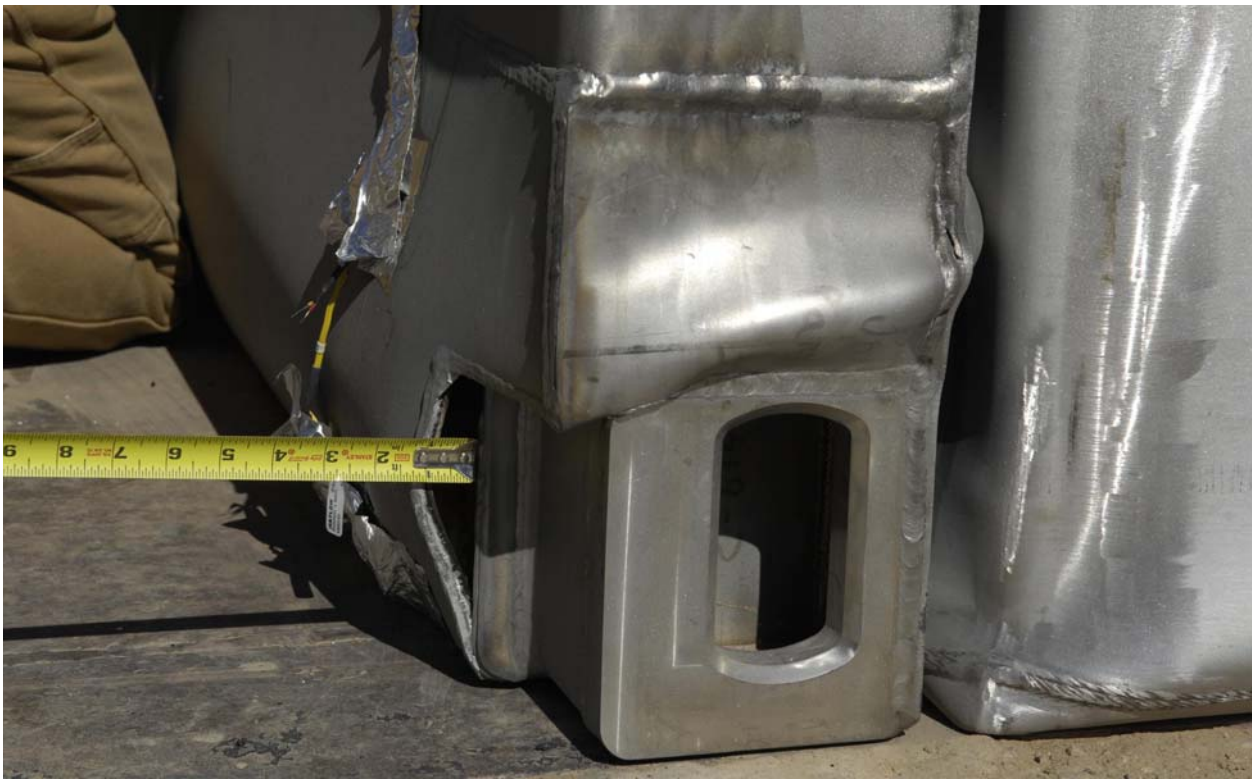

Figure 2.12.3-12 – Test LD2, Close-up of Deformation and Torn Welds Around ISO Fitting

Figure 2.12.3-13 – Test LD3, Typical Side Deformations (Impact Side Down)

Figure 2.12.3-14 – Test LD3, Impact Side

Figure 2.12.3-15 – Test LD3, Weld Tear Near Bottom of Left Cheek

Figure 2.12.3-16 – Test LD5, Typical Deformation

Figure 2.12.3-17 – Test LD5, Weld Tear Along Forward Edge of Side Outer Sheet (2-inch gap)

Figure 2.12.3-18 – Test LD5, Weld Tear Between Cheek (left half) and Body Edge (right half)

Figure 2.12.3-19 – Test LD4, Typical Deformations

Figure 2.12.3-20 – Test LD4, Close-up of Deformations

Figure 2.12.3-21 – Test LP3. Puncture Bar Damage Indicated by Arrow

Figure 2.12.3-22 – Test LP4 Puncture Damage. Note Broken Puncture Bar

Figure 2.12.3-23 – Test LP4, Close-up of Damage. Note Corner of 16-mm Thick Insulation Protection Box Inside Hole

Figure 2.12.3-24 – Test LP1, Before Removal of CTU From Bar

Figure 2.12.3-25 – Test LP1, After Removal of Bar

Figure 2.12.3-26 – Test LP1, Close-up of Damage. Bottom of Hole is CSA Outer Structural Sheet

Figure 2.12.3-27 – Test LP2 Puncture Damage

Figure 2.12.3-28 – Test LP2, Close-up of Damage. Bottom of Hole is Puncture-Resistant Plate

Figure 2.12.3-29 – View of Simulated Payload After Testing

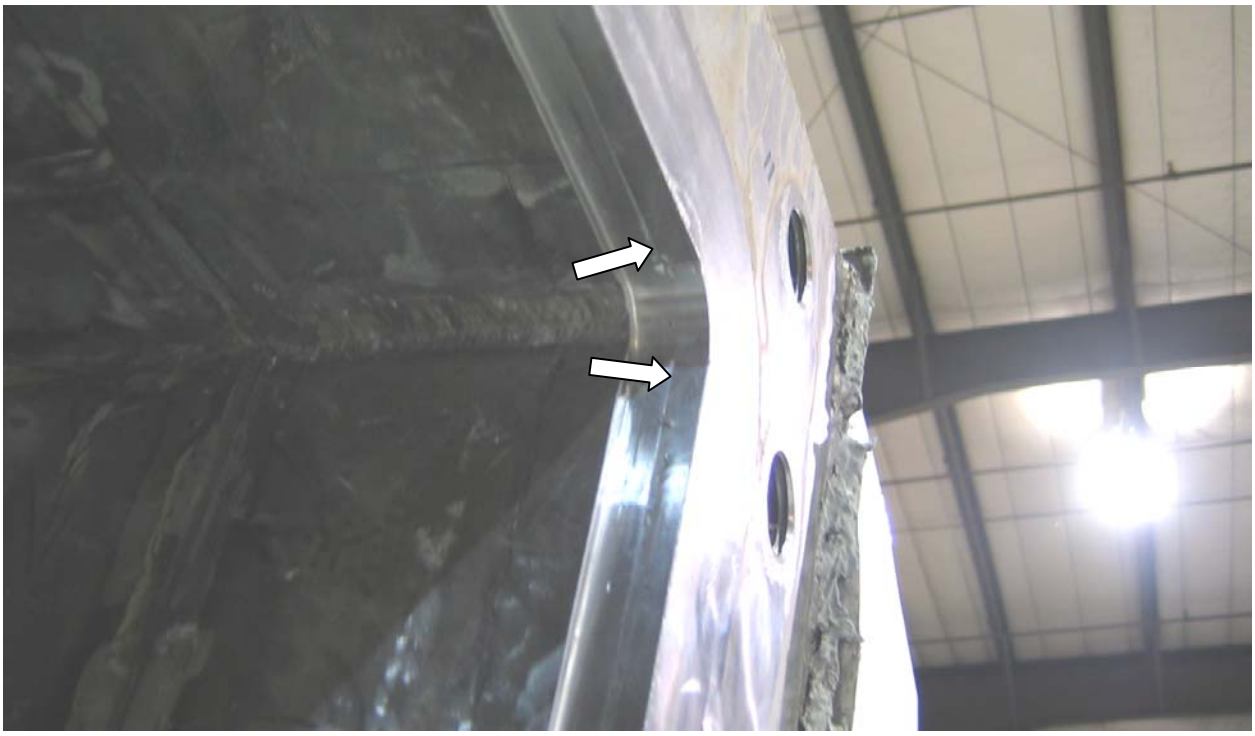

Figure 2.12.3-30 – View of Contact Between Lid Shear Lips and Body Upper Right Corner

Figure 2.12.3-31 – View of Contact on Closure Bolt Head and Washer (Typical)

Figure 2.12.3-32 – Debris on Closure Lid Seals (Right Side, Bolt Hole #15 in Center)

Figure 2.12.3-33 – Debris on Closure Lid Seals (Showing Large Chips)

Figure 2.12.3-34 – Debris on Closure Lid Seals (Lower Left Corner of Lid)

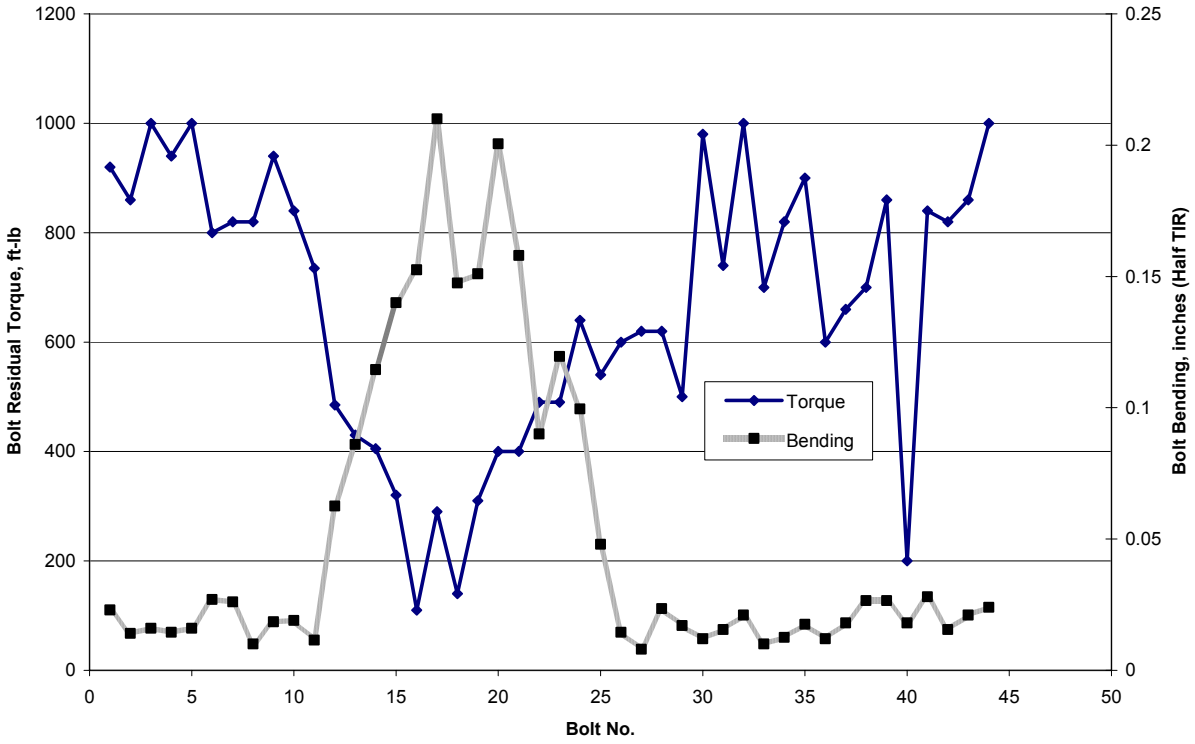

Figure 2.12.3-35 – Correlation of Residual Torque (Tightening) with Bolt Bending

2.12.3.9 Acceleration Time History Plots

Individual accelerometer time history output plots are given in this section in the following order. The designator is the test number followed by the accelerometer location number and direction. For example, 'LD2 – A2A' is test LD2, accelerometer location 2, axial direction; 'LD5 – A5L' is test LD5, accelerometer location 5, lateral direction.

No.	Designator	No.	Designator	No.	Designator
1	LD1 – A1A	8	LD3 – A1L	15	LD4 – A2A
2	LD1 – A3A	9	LD3 – A4L	16	LD4 – A3A
3	LD1 – A4A	10	LD3 – A5L	17	LD4 – A4A
4	LD2 – A1A	11	LD3 – A8L	18	LD5 – A1L
5	LD2 – A2A	12	LD3 – A9L	19	LD5 – A3L
6	LD2 – A3A	13	LD3 – A10L	20	LD5 – A5L
7	LD2 – A4A	14	LD4 – A1A	21	LD5 – A7L

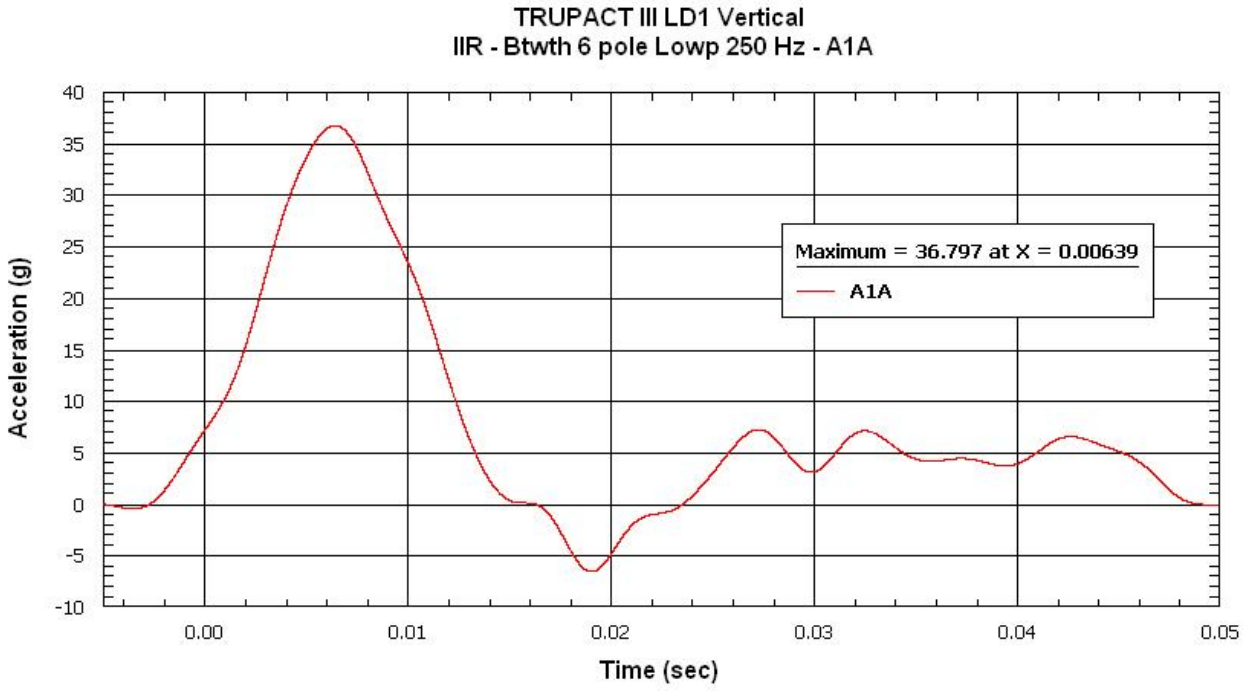

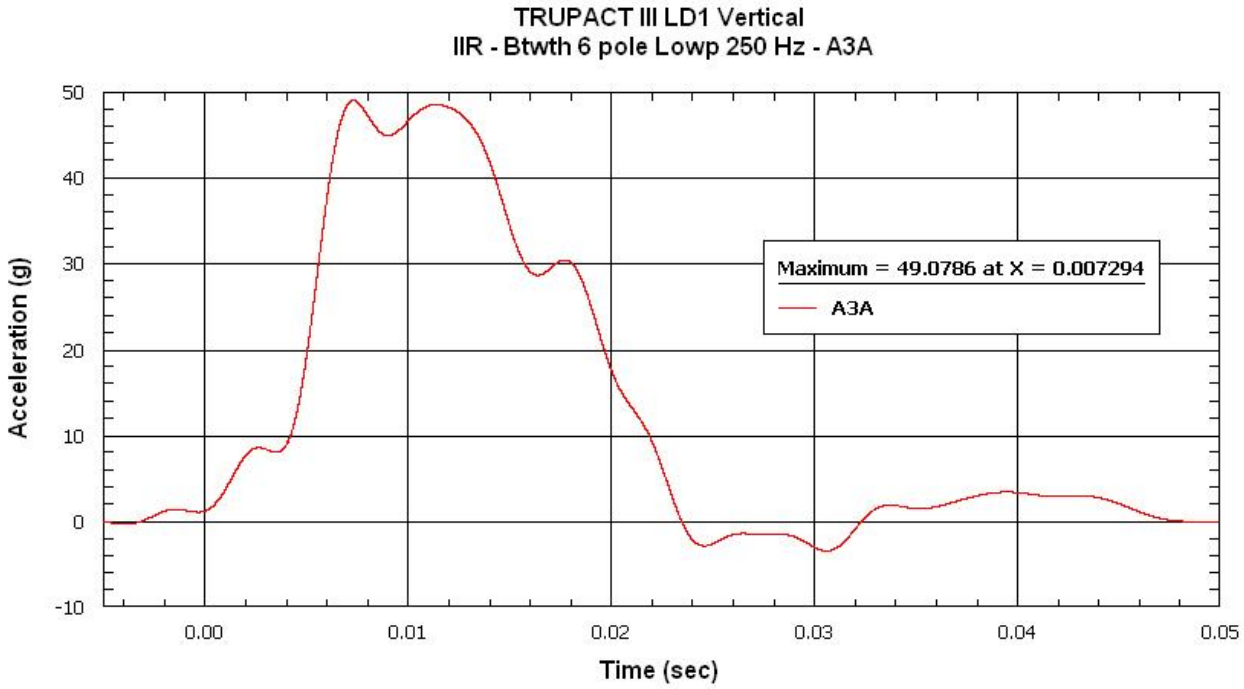
TRUPACT III LD1 Vertical
IIR - Btwth 6 pole Lowp 250 Hz - A3A
Acceleration (g)
Time (sec)
Maximum = 49.0786 at X = 0.007294
A3A
50
40
30
20
10
0
-10
0.00
0.01
0.02
0.03
0.04
0.05

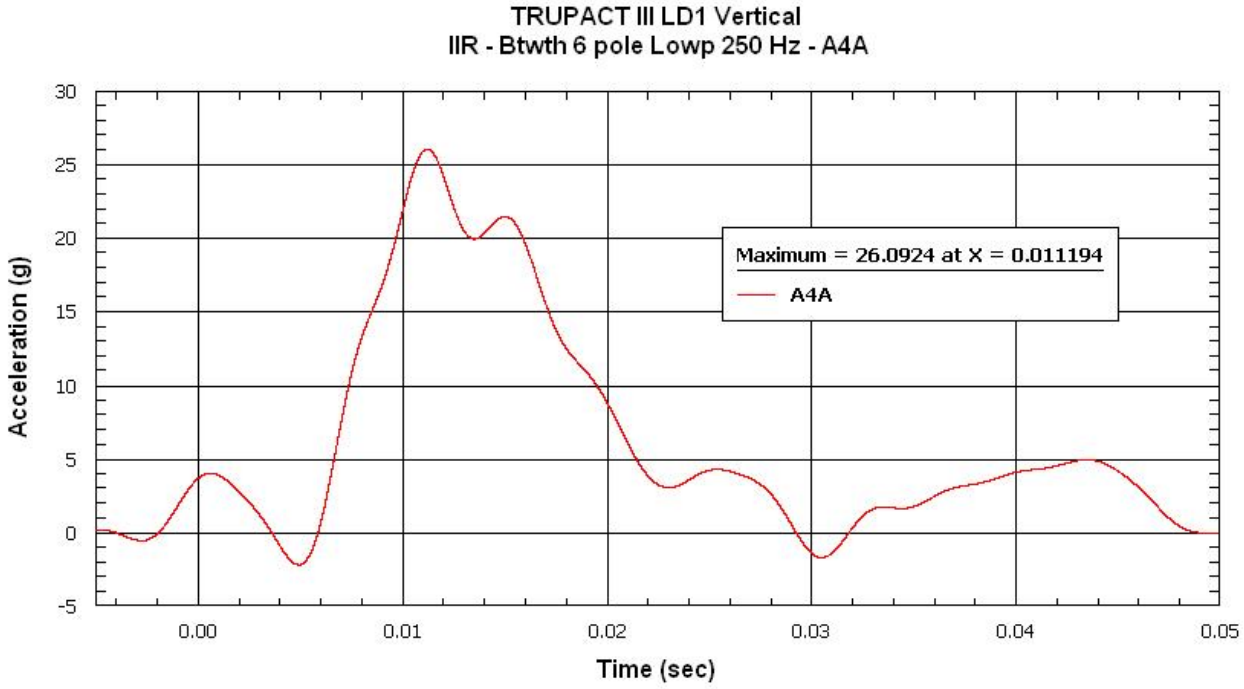
TRUPACT III LD1 Vertical
IIR - Btwth 6 pole Lowp 250 Hz - A4A
Acceleration (g)
Time (sec)
Maximum = 26.0924 at X = 0.011194
A4A
30
25
20
15
10
5
0
-5
0.00
0.01
0.02
0.03
0.04
0.05

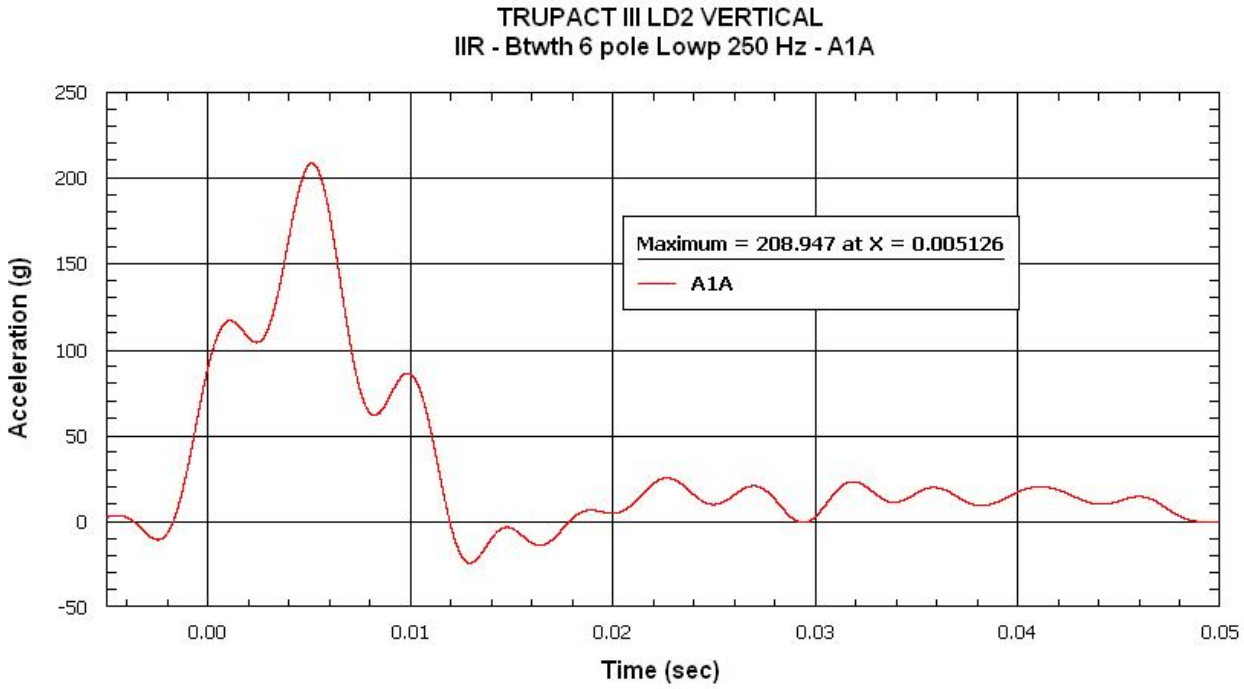
TRUPACT III LD2 VERTICAL
IIR - Btwth 6 pole Lowp 250 Hz - A1A
Maximum = 208.947 at X = 0.005126
A1A
Acceleration (g)
Time (sec)
250
200
150
100
50
0
-50
0.00
0.01
0.02
0.03
0.04
0.05

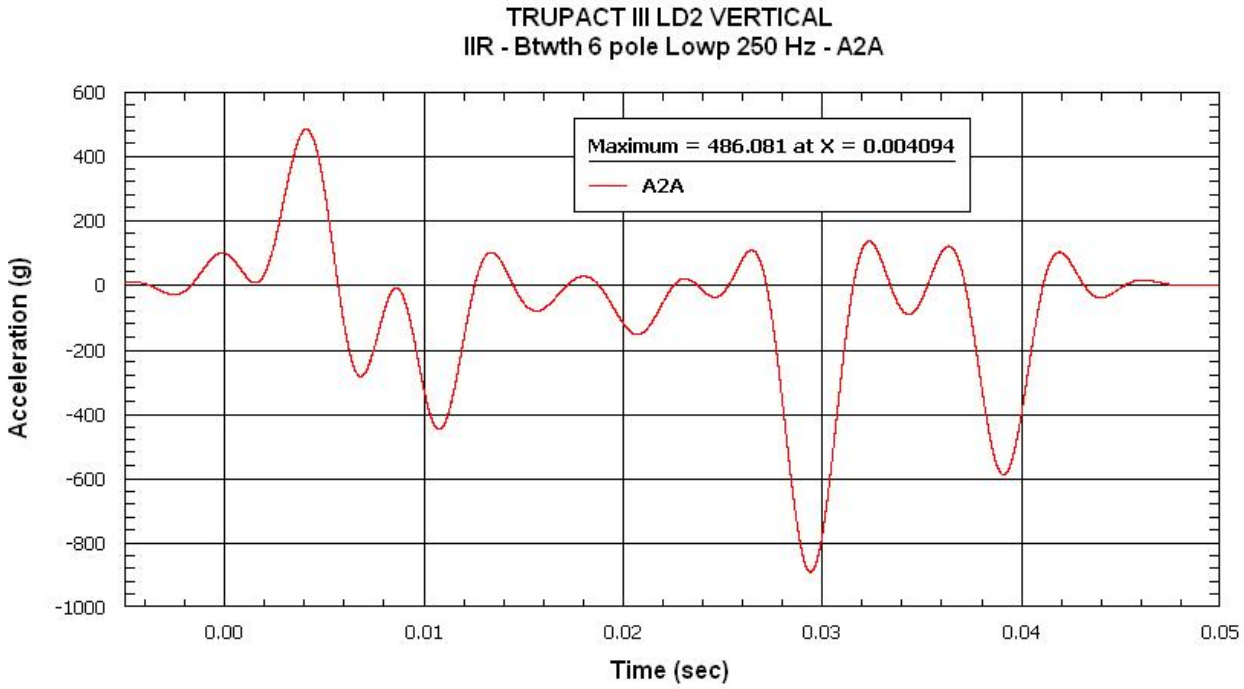
TRUPACT III LD2 VERTICAL
IIR - Btwth 6 pole Lowp 250 Hz - A2A
Maximum = 486.081 at X = 0.004094
A2A
Acceleration (g)
Time (sec)
600
400
200
0
-200
-400
-600
-800
-1000
0.00
0.01
0.02
0.03
0.04
0.05

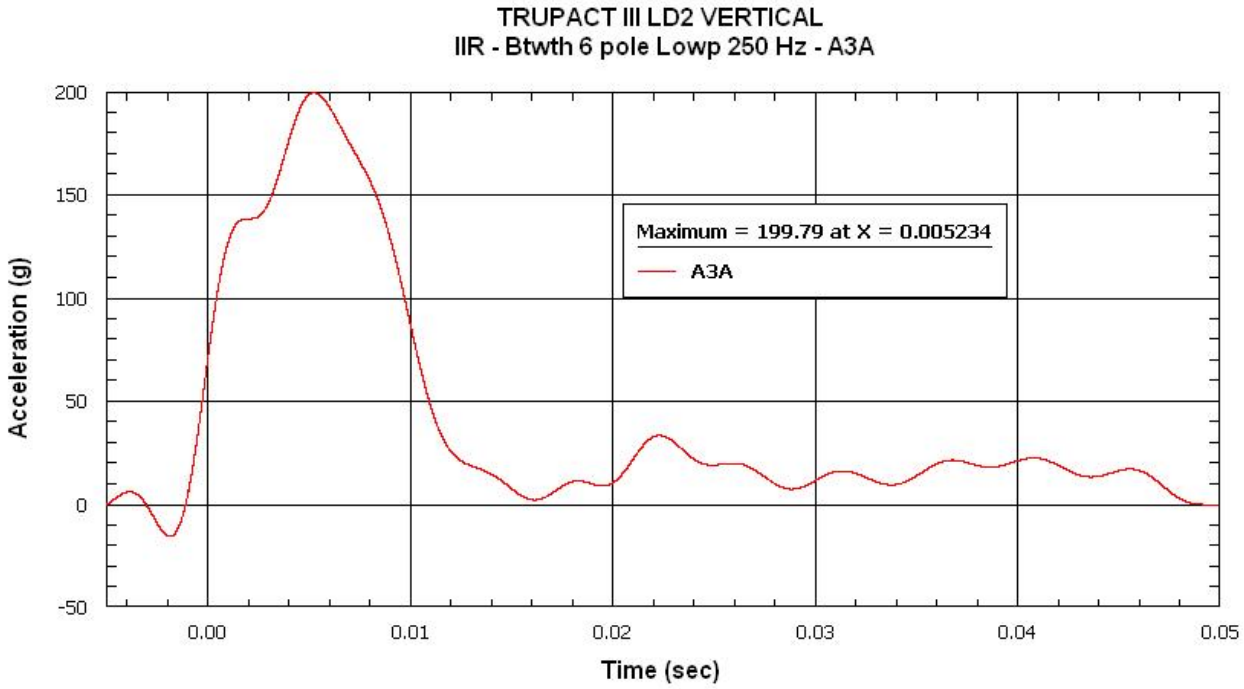
TRUPACT III LD2 VERTICAL
IIR - Btwth 6 pole Lowp 250 Hz - A3A
Maximum = 199.79 at X = 0.005234
A3A
Acceleration (g)
Time (sec)
200
150
100
50
0
-50
0.00
0.01
0.02
0.03
0.04
0.05

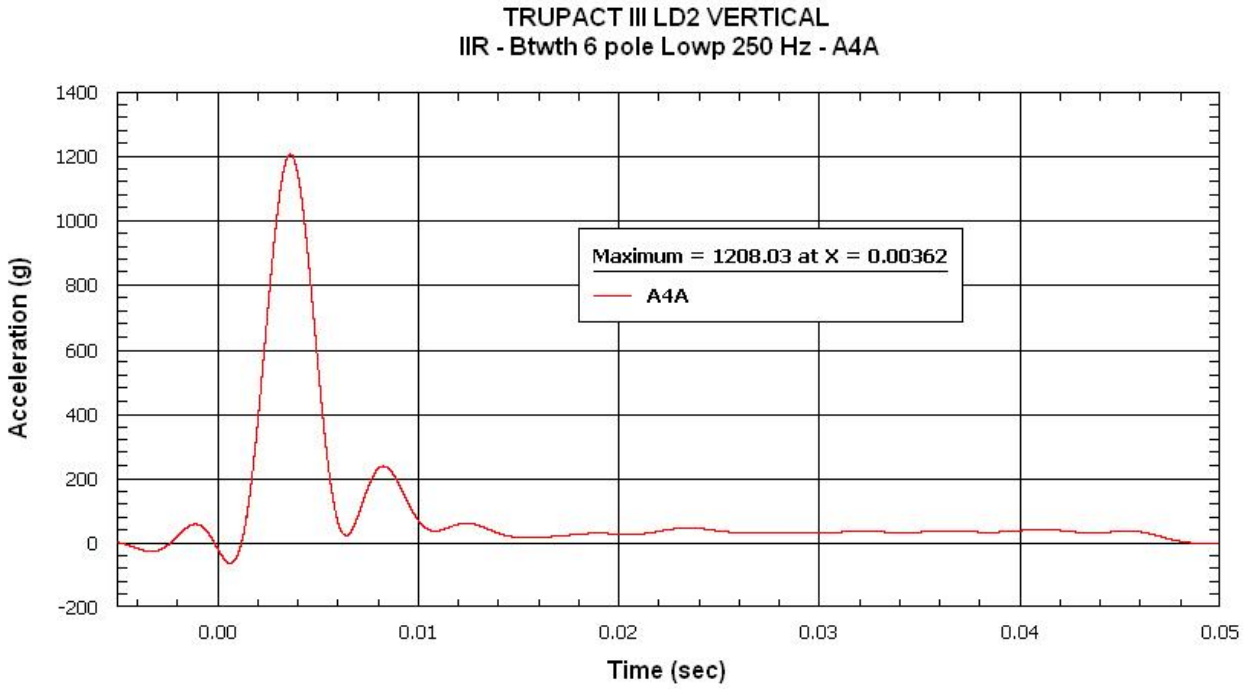
TRUPACT III LD2 VERTICAL
IIR - Btwth 6 pole Lowp 250 Hz - A4A
Maximum = 1208.03 at X = 0.00362
A4A
Acceleration (g)
Time (sec)
1400
1200
1000
800
600
400
200
0
-200
0.00
0.01
0.02
0.03
0.04
0.05

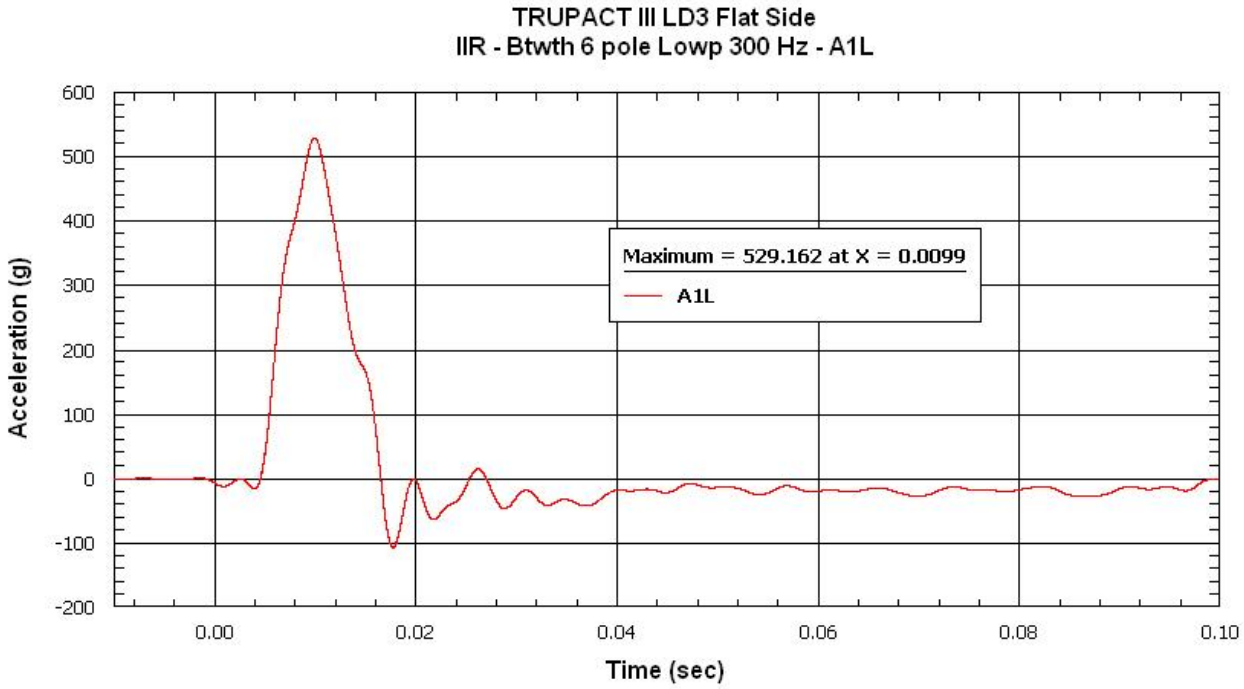
TRUPACT III LD3 Flat Side
IIR - Btwth 6 pole Lowp 300 Hz - A1L
Maximum = 529.162 at X = 0.0099
A1L
Acceleration (g)
Time (sec)
600
500
400
300
200
100
0
-100
-200
0.00
0.02
0.04
0.06
0.08
0.10

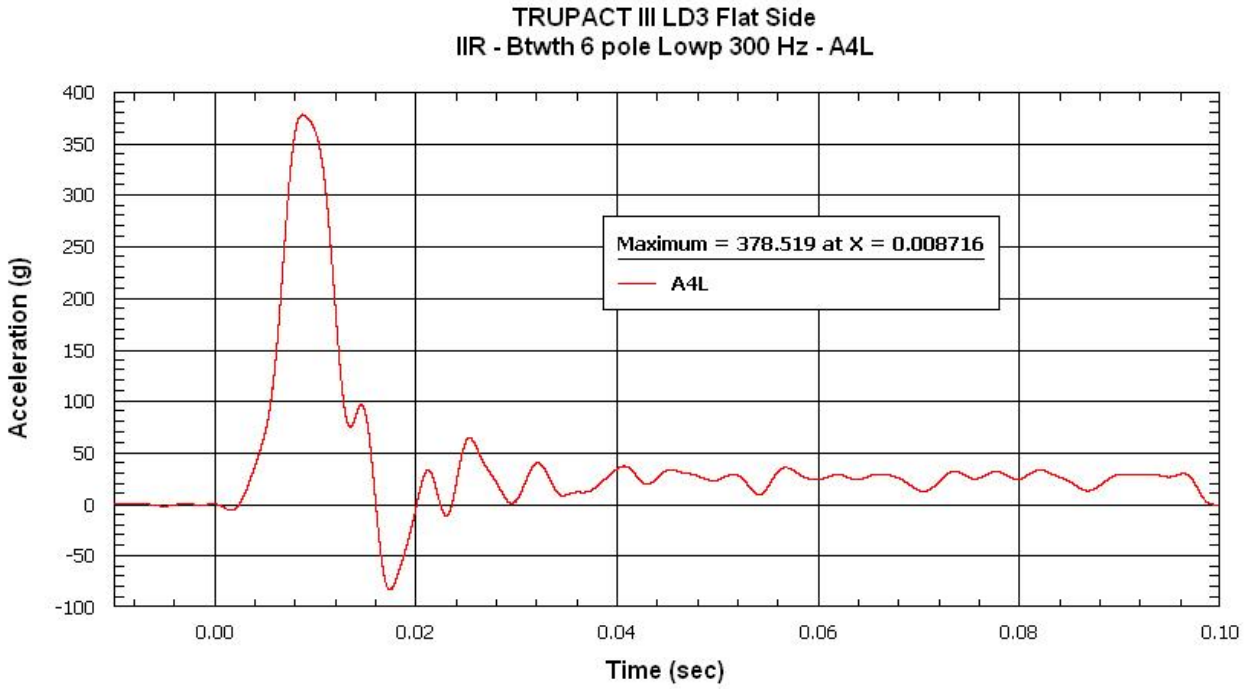
TRUPACT III LD3 Flat Side
IIR - Btwth 6 pole Lowp 300 Hz - A4L
Maximum = 378.519 at X = 0.008716
A4L
Acceleration (g)
Time (sec)
400
350
300
250
200
150
100
50
0
-50
-100
0.00
0.02
0.04
0.06
0.08
0.10

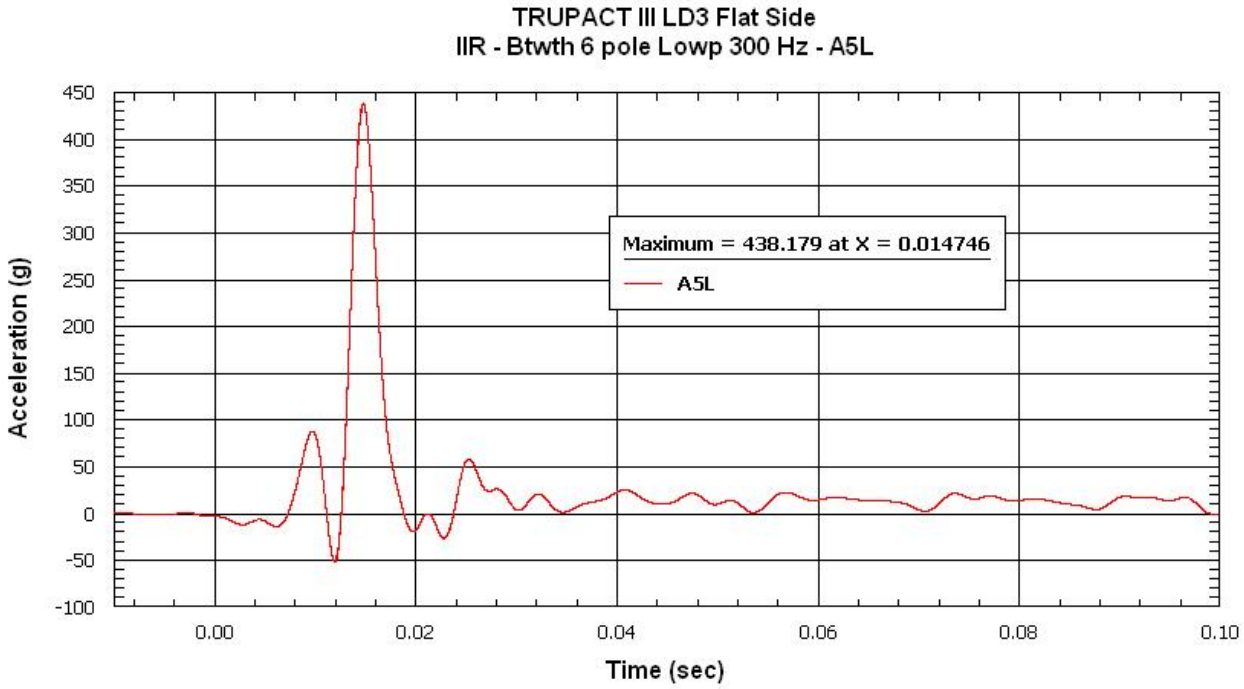
TRUPACT III LD3 Flat Side
IIR - Btwth 6 pole Lowp 300 Hz - A5L
Maximum = 438.179 at X = 0.014746
A5L
Acceleration (g)
Time (sec)
450
400
350
300
250
200
150
100
50
0
-50
-100
0.00
0.02
0.04
0.06
0.08
0.10

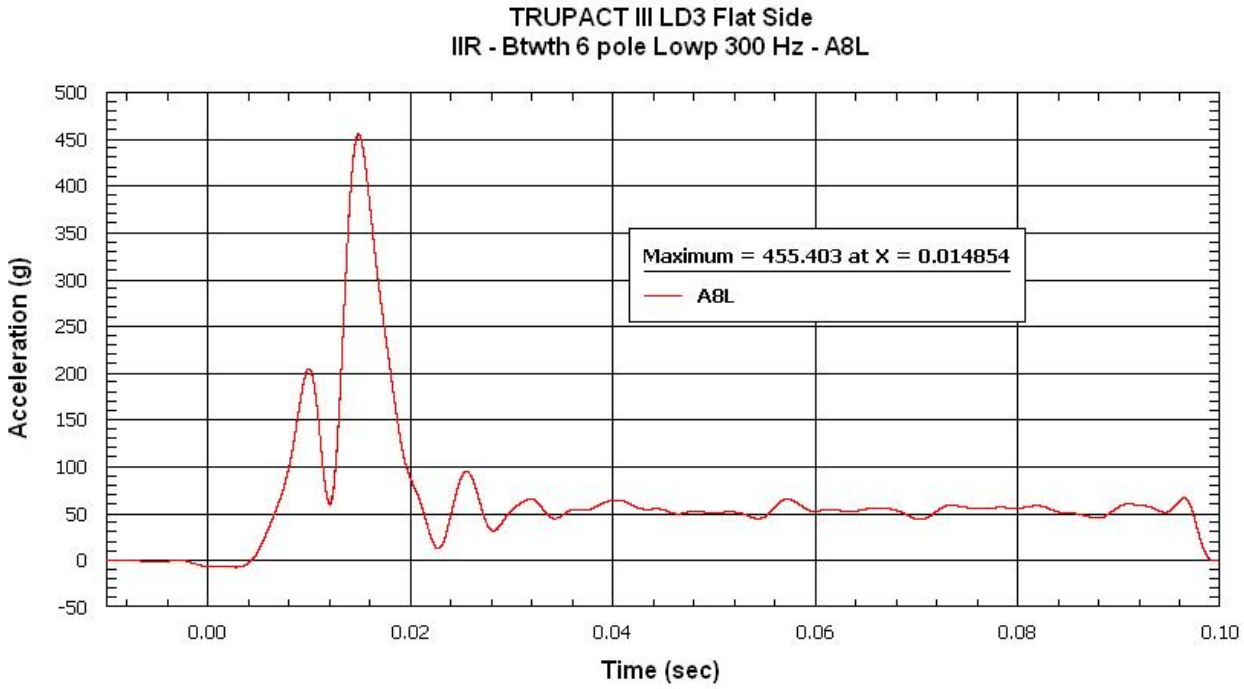
TRUPACT III LD3 Flat Side
IIR - Btwth 6 pole Lowp 300 Hz - A8L
Maximum = 455.403 at X = 0.014854
A8L
Acceleration (g)
Time (sec)
500
450
400
350
300
250
200
150
100
50
0
-50
0.00
0.02
0.04
0.06
0.08
0.10

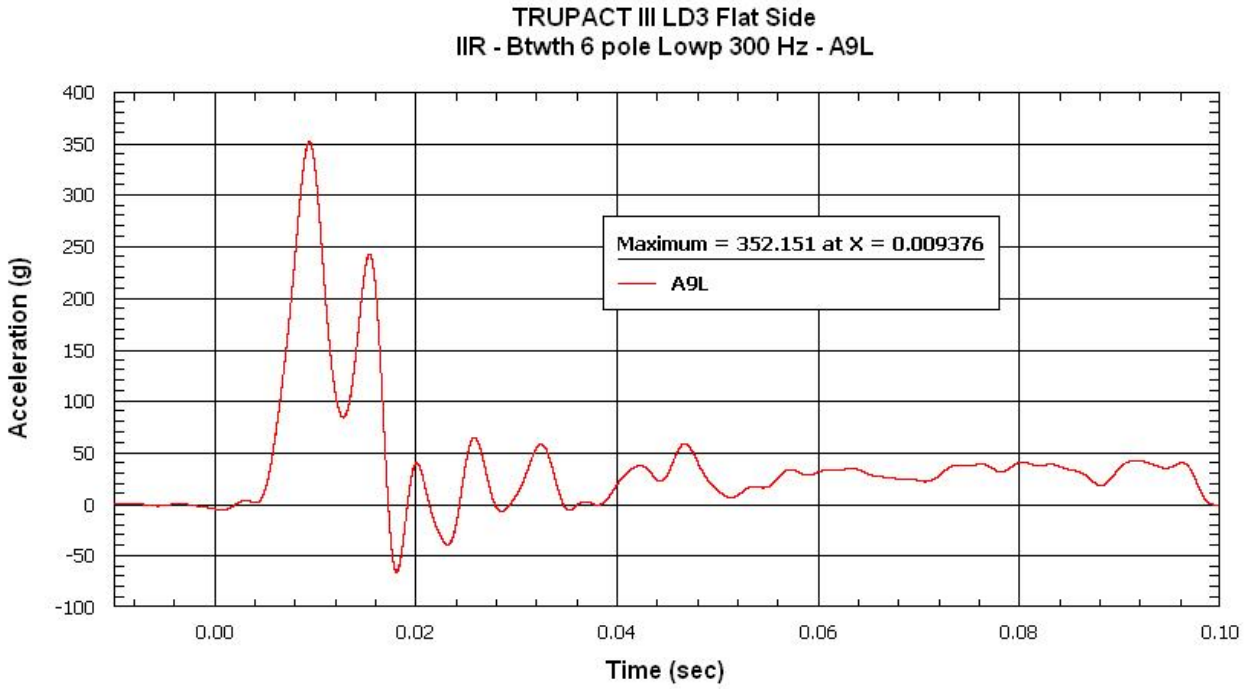
TRUPACT III LD3 Flat Side
IIR - Btwth 6 pole Lowp 300 Hz - A9L
Maximum = 352.151 at X = 0.009376
A9L
Acceleration (g)
Time (sec)
400
350
300
250
200
150
100
50
0
-50
-100
0.00
0.02
0.04
0.06
0.08
0.10

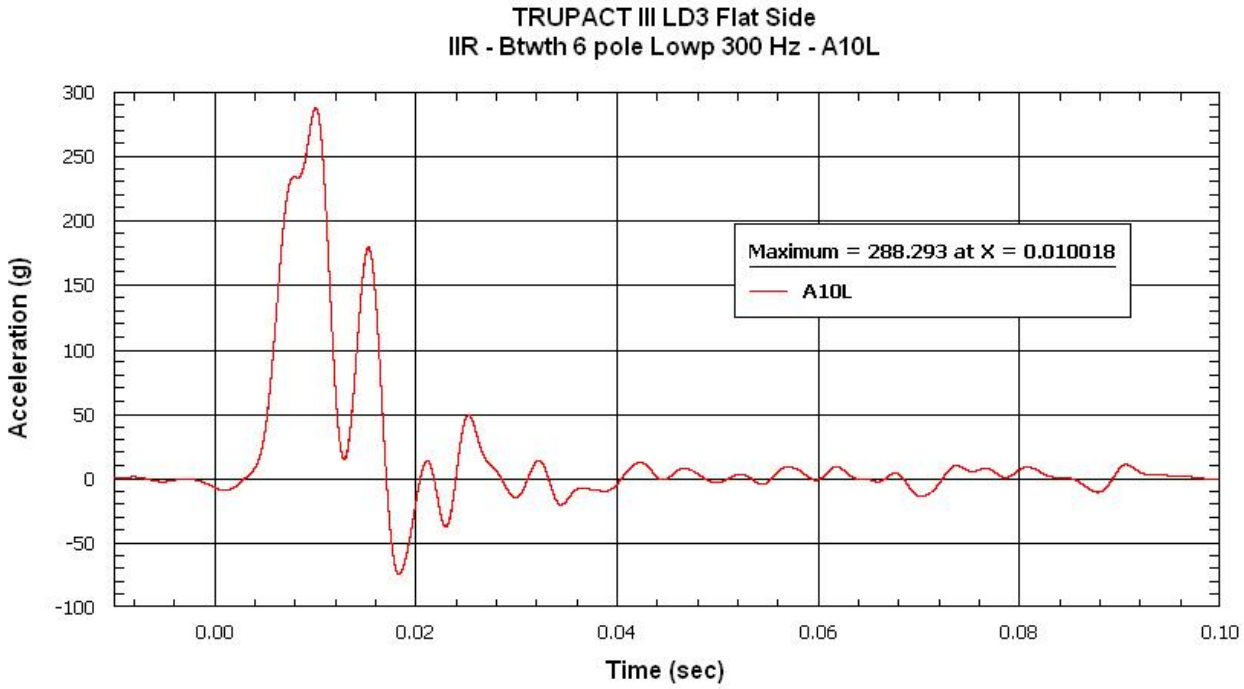
TRUPACT III LD3 Flat Side
IIR - Btwth 6 pole Lowp 300 Hz - A10L
Maximum = 288.293 at X = 0.010018
A10L
Acceleration (g)
Time (sec)
300
250
200
150
100
50
0
-50
-100
0.00
0.02
0.04
0.06
0.08
0.10

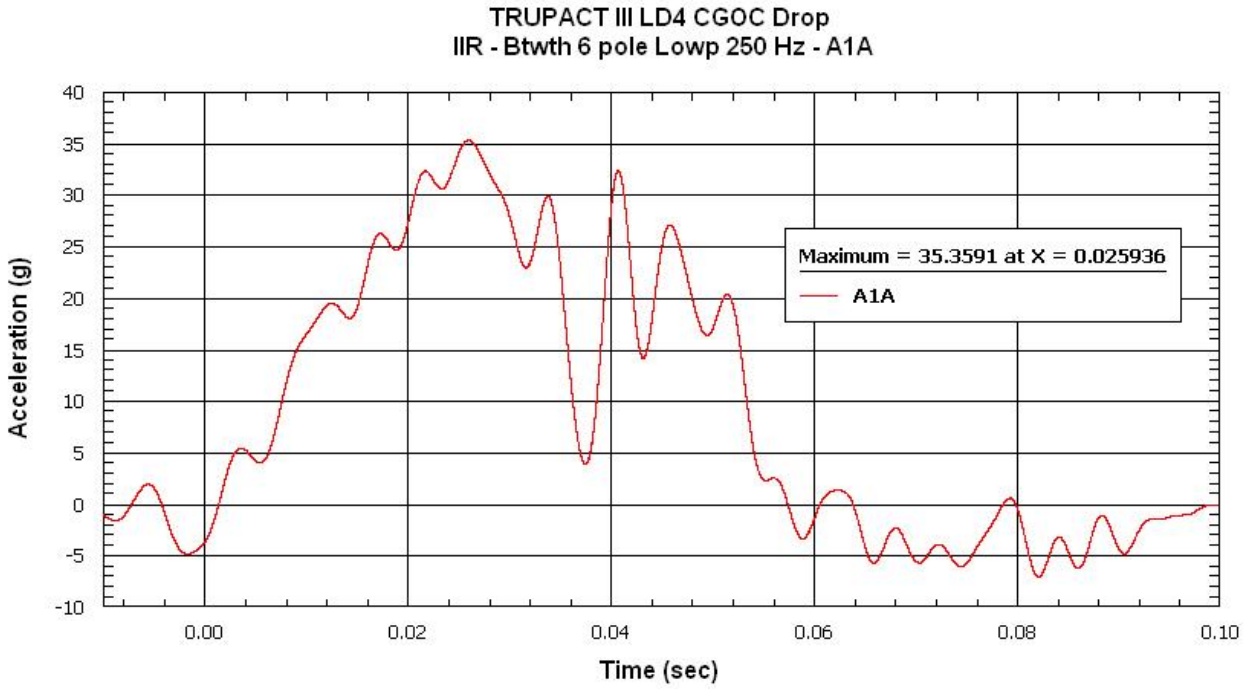
TRUPACT III LD4 CGOC Drop
IIR - Btwth 6 pole Lowp 250 Hz - A1A
Acceleration (g)
Time (sec)
Maximum = 35.3591 at X = 0.025936
A1A
40
35
30
25
20
15
10
5
0
-5
-10
0.00
0.02
0.04
0.06
0.08
0.10

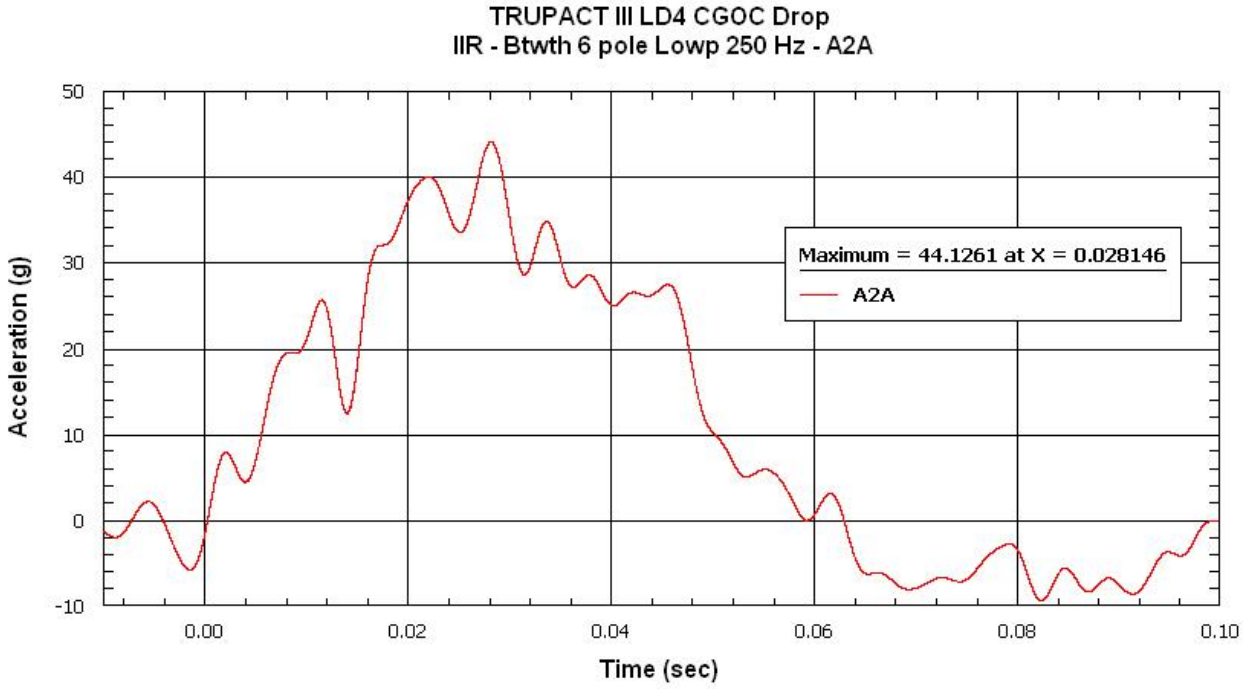
TRUPACT III LD4 CGOC Drop
IIR - Btwth 6 pole Lowp 250 Hz - A2A
Acceleration (g)
Time (sec)
Maximum = 44.1261 at X = 0.028146
A2A
50
40
30
20
10
0
-10
0.00
0.02
0.04
0.06
0.08
0.10

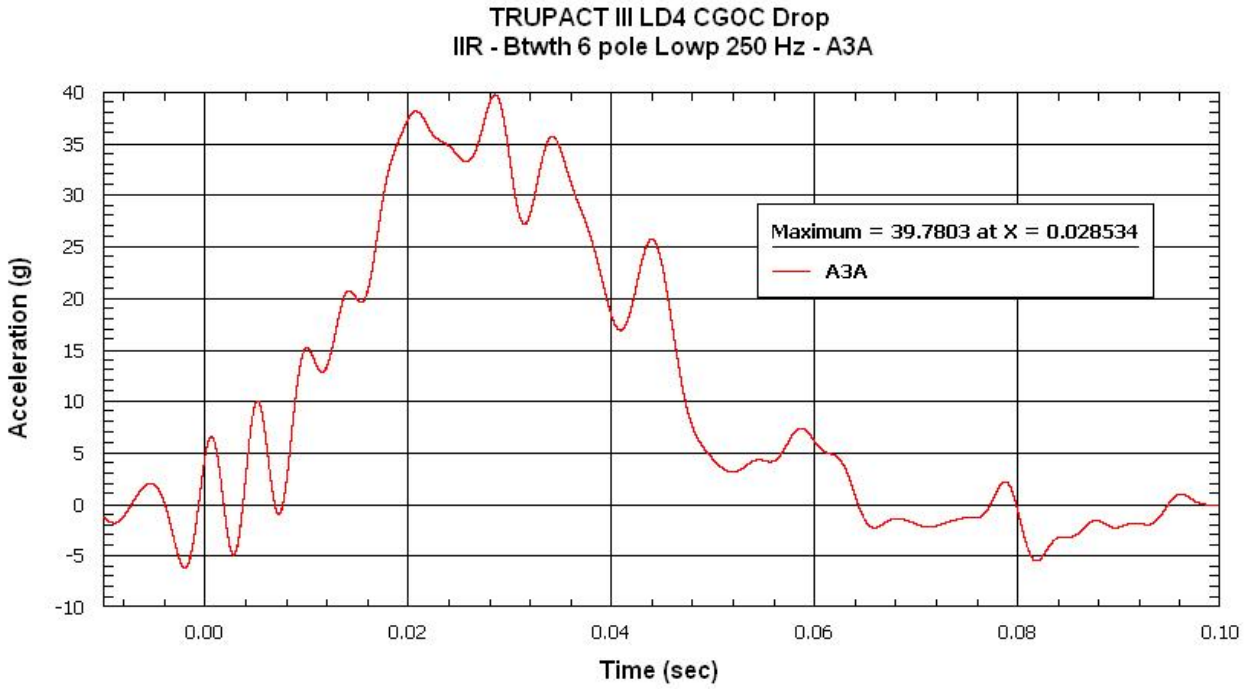
TRUPACT III LD4 CGOC Drop
IIR - Btwth 6 pole Lowp 250 Hz - A3A
Maximum = 39.7803 at X = 0.028534
A3A
Acceleration (g)
Time (sec)
40
35
30
25
20
15
10
5
0
-5
-10
0.00
0.02
0.04
0.06
0.08
0.10

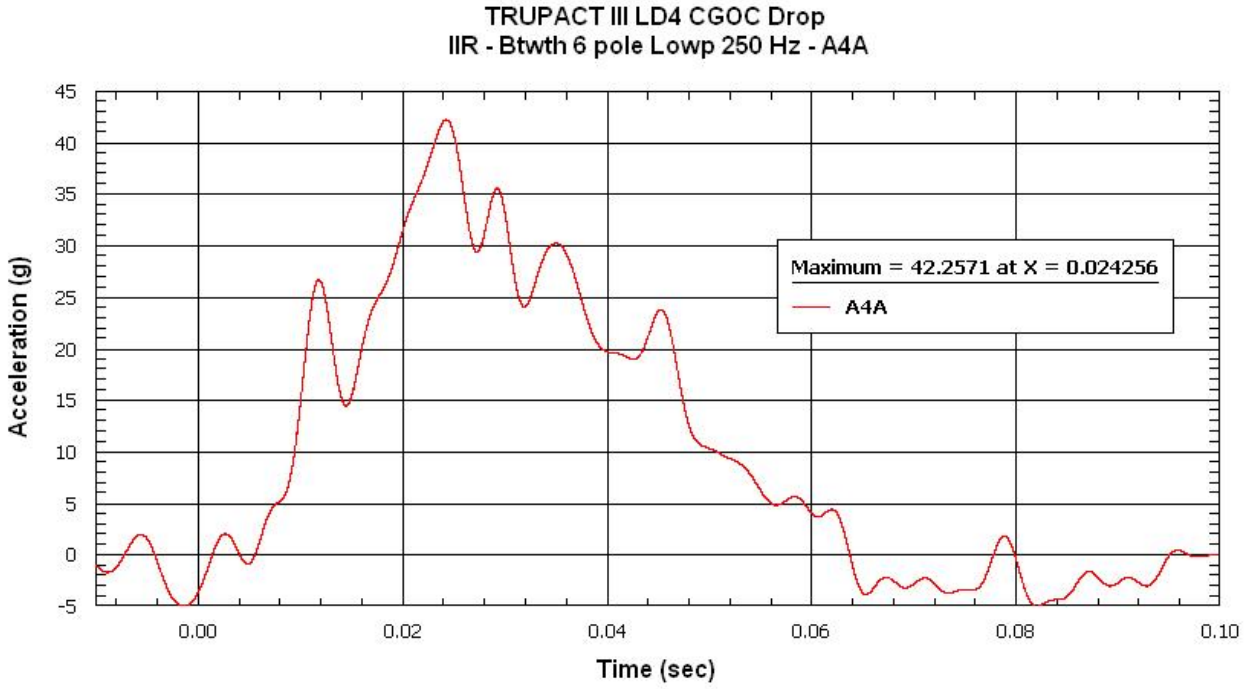
TRUPACT III LD4 CGOC Drop
IIR - Btwth 6 pole Lowp 250 Hz - A4A
Maximum = 42.2571 at X = 0.024256
A4A
Acceleration (g)
Time (sec)
45
40
35
30
25
20
15
10
5
0
-5
0.00
0.02
0.04
0.06
0.08
0.10

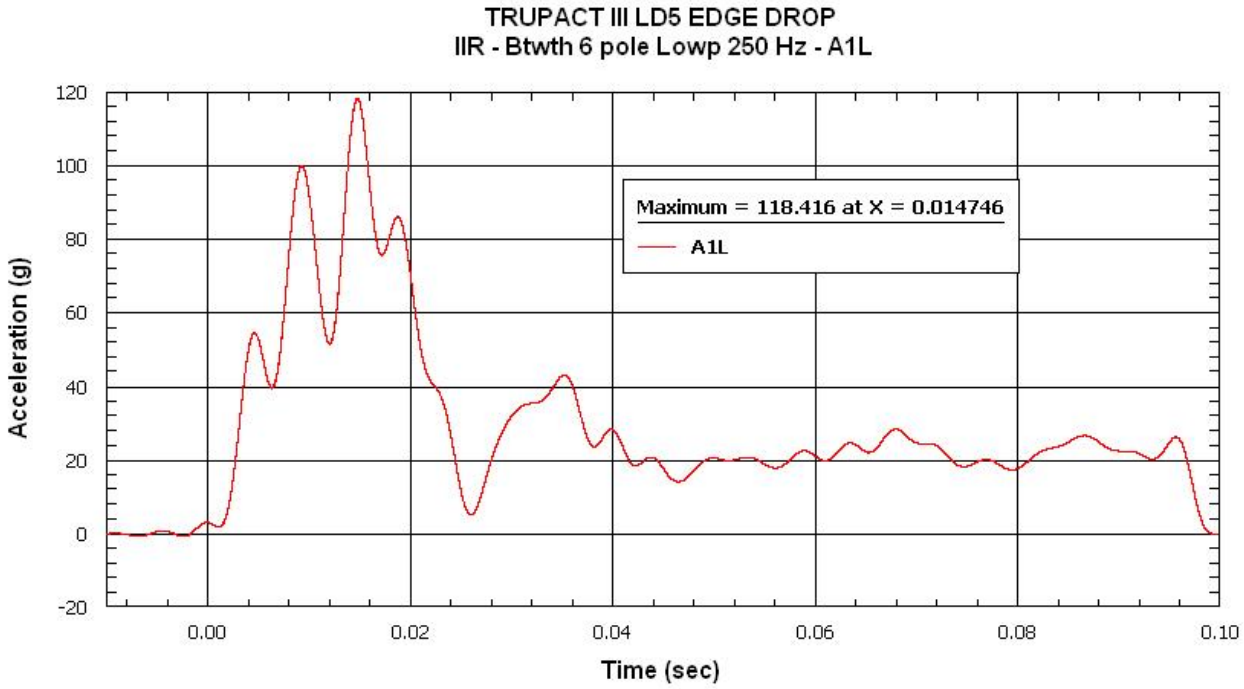
TRUPACT III LD5 EDGE DROP
IIR - Btwth 6 pole Lowp 250 Hz - A1L
Maximum = 118.416 at X = 0.014746
A1L
Acceleration (g)
Time (sec)
120
100
80
60
40
20
0
-20
0.00
0.02
0.04
0.06
0.08
0.10

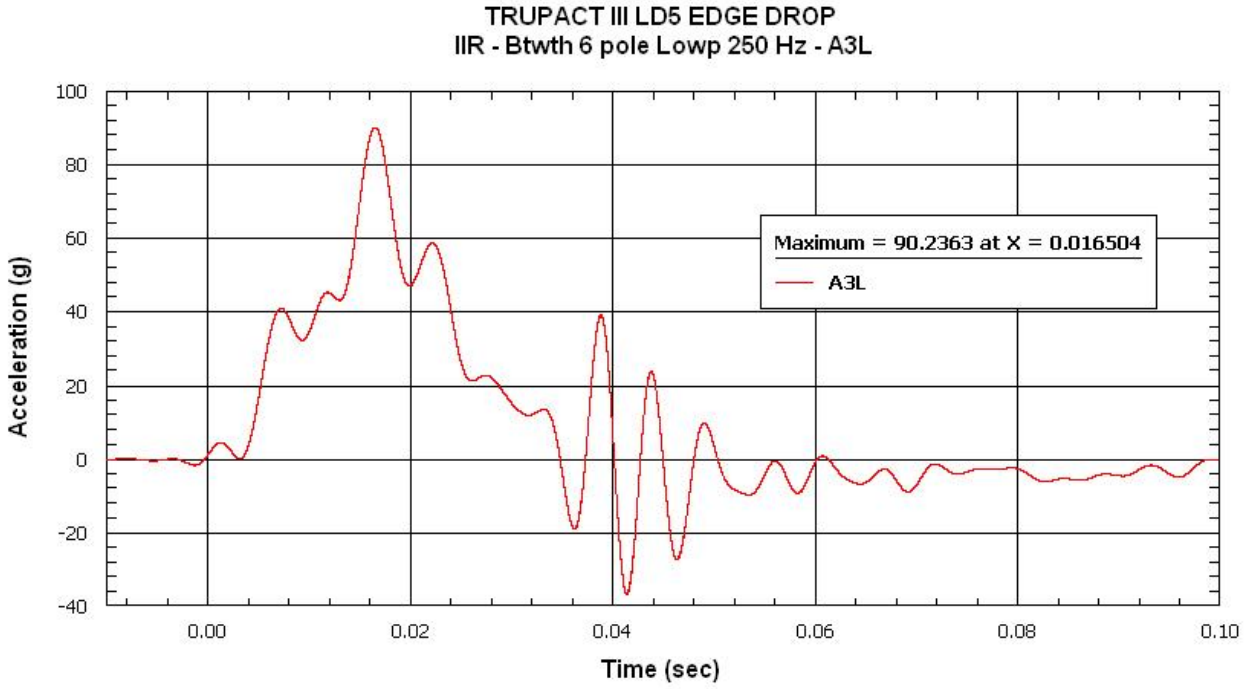
TRUPACT III LD5 EDGE DROP
IIR - Btwth 6 pole Lowp 250 Hz - A3L
Maximum = 90.2363 at X = 0.016504
A3L
Acceleration (g)
Time (sec)
100
80
60
40
20
0
-20
-40
0.00
0.02
0.04
0.06
0.08
0.10

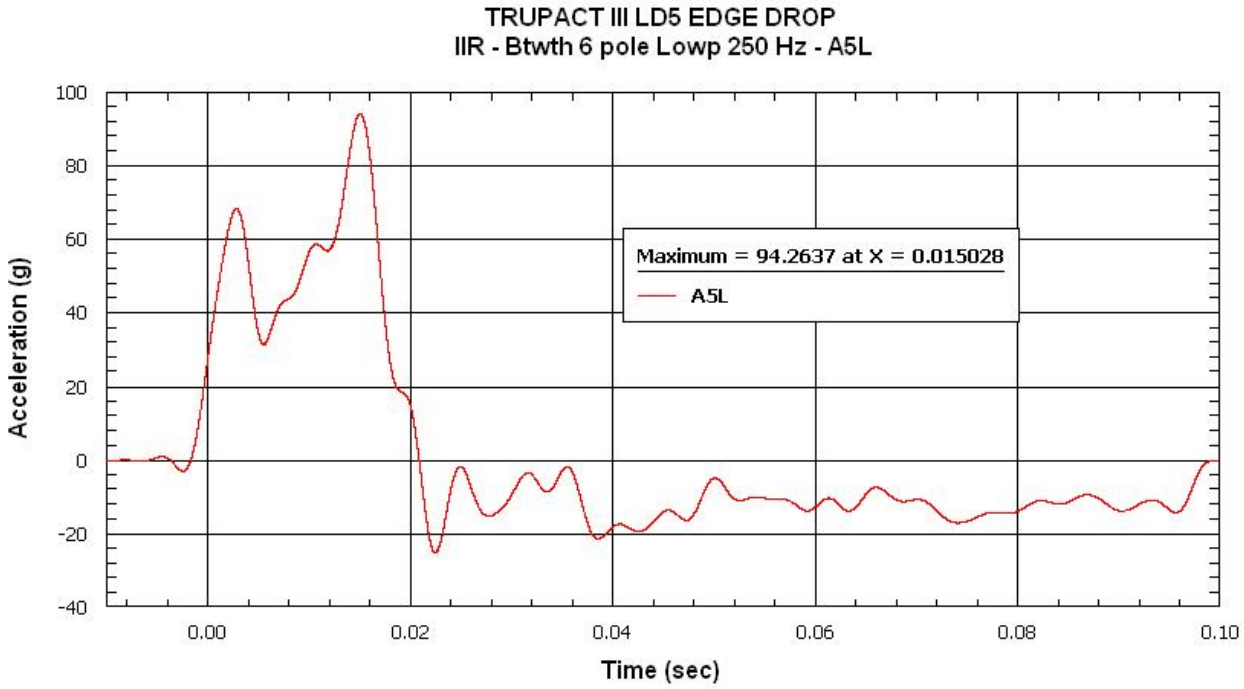
TRUPACT III LD5 EDGE DROP
IIR - Btwth 6 pole Lowp 250 Hz - A5L
Maximum = 94.2637 at X = 0.015028
A5L
Acceleration (g)
Time (sec)
100
80
60
40
20
0
-20
-40
0.00
0.02
0.04
0.06
0.08
0.10

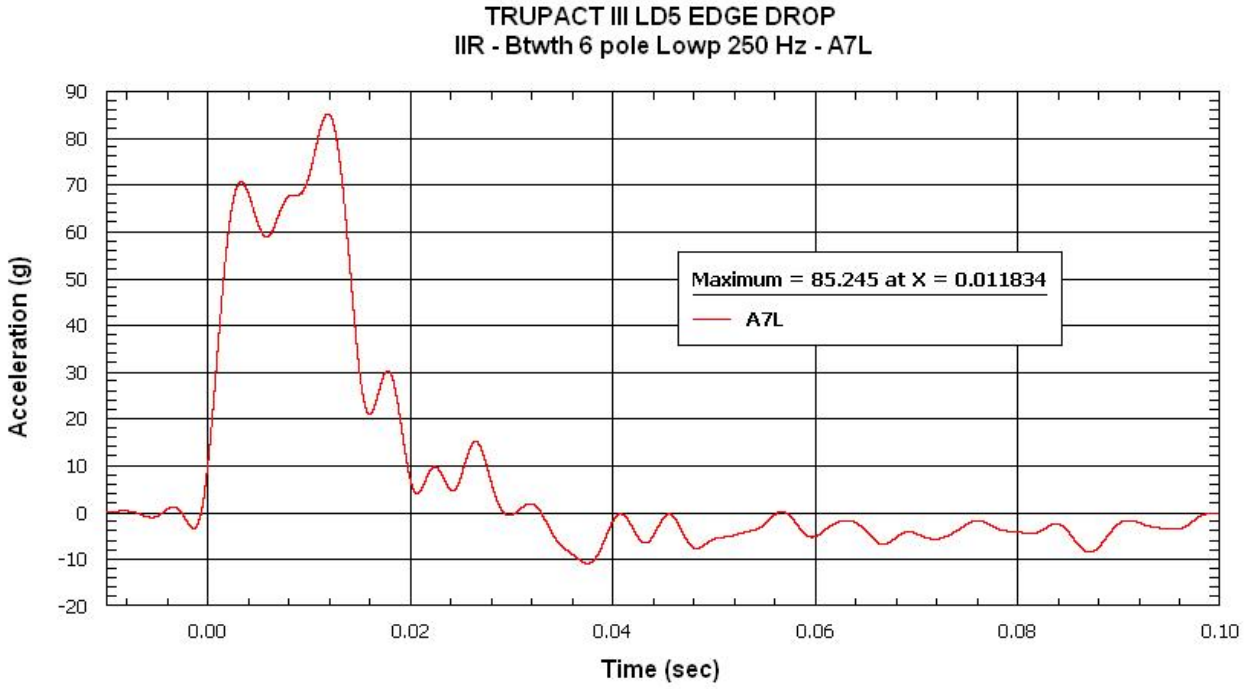
TRUPACT III LD5 EDGE DROP
IIR - Btwth 6 pole Lowp 250 Hz - A7L
Maximum = 85.245 at X = 0.011834
A7L
Acceleration (g)
Time (sec)
90
80
70
60
50
40
30
20
10
0
-10
-20
0.00
0.02
0.04
0.06
0.08
0.10

This page intentionally left blank.

2.12.4 HAC Immersion Buckling Evaluation

2.12.4.1 Introduction

The purpose of this evaluation is to determine the buckling characteristics of the containment structural assembly (CSA) walls due to the immersion requirement for hypothetical accident conditions (HAC) of 150 kPa, gauge, per 10 CFR §71.73(c)(6)[1]. This condition conservatively envelops the increased external pressure condition for normal conditions of transport (NCT) of 140 kPa, absolute, per 10 CFR §71.71(c)(4). The geometry design input is extracted from the general arrangement drawings in Appendix 1.3.1, *Packaging General Arrangement Drawings*. NOTE: All technical references are to be found in Section 2.12.4.5, *References*.

2.12.4.2 Mechanical Properties

The CSA walls are fabricated entirely from Alloy UNS S31803 stainless steel. Material properties utilized in this appendix are extracted from Table 2.2-1 and Table 2.2-2 of Section 2.2, *Mechanical Properties of Materials*.

2.12.4.3 Conditions Analyzed

The CSA structure will be evaluated in this calculation for the following conditions:

1. Buckling analysis of CSA containment sheets.
2. Buckling analysis of sidewall.
3. Stress due to pressure load.
4. Transverse shear stiffness of core.
5. Effect of initial deflections.

2.12.4.4 Calculations

2.12.4.4.1 Buckling Analysis of CSA Containment Sheets

The critical buckling condition is the hypothetical accident condition of immersion of at least 15 m head of water as defined in 10 CFR §71.73(c)(6). The equivalent external pressure and temperature is 150 kPa and 71 °C, respectively.

The sidewall is the largest sheet and as such, will be the bounding case for buckling under the action of edge loads and the design pressure load. The edge loads result from the pressure loads on the adjacent end, top, and bottom sheets.

For conservatism, assume that the height of the sidewall extends from the center of the bottom sheet to the center of the top sheet. Additionally, assume that the length extends from the center of the end sheet to the bolted O-ring seal flange. For purposes of calculating edge loads, the width of

[1] Title 10, Code of Federal Regulations, Part 71 (10 CFR 71), *Packaging and Transportation of Radioactive Material*, 01–01–09 Edition.

the top/bottom sheet is assumed to extend from the center of one sidewall to the center of the other sidewall. These dimensions are as follows:

H = height of sidewall = 2,140 mm

L = length of sidewall = 2,860 mm

W = width of top/bottom sheet = 1,980 mm

Referring to Figure 2.12.4-1, assume that the pressure load acting on Area 1 of the end sheet loads the end edges of the sidewall. Assume that the pressure load on Area 2 of the top sheet loads the top and bottom edges.

The areas, edge loads per unit length, and stresses acting on the end edges are calculated as follows:

A_1 = Area 1 (See Figure 2.12.4-2) = area of two triangles plus one rectangle
$= 2(1/2)(990)^2 + 160(990) = 1.139 \times 10^6$ mm^2

P = external pressure = 150 kPa = 0.150 MPa = 0.150 N/mm^2

N_y = edge load per unit length in y-direction (perpendicular to core longitudinal axis)

$$= \frac{PA_1}{H} = \frac{0.150\left(1.139\times10^6\right)}{2140} = 79.8 \text{ N/mm}$$

σ_y = edge stress in y-direction (perpendicular to core longitudinal axis)

$$= \frac{N_y}{2t_1} = \frac{79.8}{2(8)} = 5.0 \text{ MPa}$$

The areas, edge loads per unit length, and stresses acting on the top/bottom edges are calculated as follows:

A_2 = Area 2 (See Figure 2.12.4-3) = 2 $(1/2)(990)^2 + 880(990) = 1.851 \times 10^6$ mm^2

N_x = edge load per unit length in the x-direction (parallel to core longitudinal axis)

$$= \frac{PA_2}{L} = \frac{0.150\left(1.851\times10^6\right)}{2{,}860} = 97.1 \text{ N/mm}$$

σ_x = edge stress in x-direction (parallel to core longitudinal axis)

$$= \frac{N_x}{2t_1} = \frac{97.1}{2(8)} = 6.1 \text{ MPa}$$

2.12.4.4.2 Buckling Analysis of Sidewall

The buckling analysis of the sidewall will be performed as follows:

1) Calculate the buckling stress for biaxial compression using the method presented in Reference 2.
2) Calculate the face sheet stress due to the pressure load acting normal to the surface.
3) Calculate the amplification effect of edge loads upon the stress calculated in Step 2 using the combined load formula from Reference 3.
4) Add the amplified stress due to normal pressure to the stress due to edge loads.

5) Calculate a factor of safety using the applied stress from Step 4 and an allowable stress equal to the buckling stress from Step 1.

2.12.4.4.3 Buckling Stress for Biaxial Compression

The following quantities per the notation of Reference 2 will be needed:

a = sheet dimension in x-direction = 2,140 mm

b = sheet dimension in y-direction = 2,860 mm

a/b = 0.75

t = face sheet thickness = 8 mm

c = core height measured between face sheets (See Fig. 2.12.4-7) = 124 mm

E = modulus of elasticity of face sheet material = 19.2×10^4 MPa

μ = Poisson's ratio of face sheet material = 0.3 (Poisson's ratio was taken to be 0.3 since Figure 2.12.4-4 used later is based on this value. This value is slightly higher than the 0.29 value given in Table 1. Per Table 2 of Reference 2, the buckling coefficient decreases with increasing Poisson's ratio, so it is conservative to use the higher value.)

D = bending rigidity of facing sheets about sandwich centroidal axis

$$= \frac{E(t)(c+t)^2}{2(1-\mu^2)} = \frac{19.2\times10^4(8)(124+8)^2}{2(1-0.3^2)} = 1.471\times10^{10} \text{ N-mm}$$

U = transverse shear stiffness of core

= D_{Qy} = 2.050×10^4 N/mm (See Section 2.12.4.4.5, *Transverse Shear Stiffness of Core*)

J = sandwich stiffness parameter

$$= \frac{U(b)^2}{\pi^2(D)} = \frac{2.050\times10^4(2{,}860)^2}{\pi^2(1.471\times10^{10})} = 1.15$$

Buckling coefficients can be obtained from Figure 8(b) of Reference 2 (Figure 2.12.4-4 herein). This figure applies for a/b = 1.0 which is conservative for the aspect ratio of 0.75 for this analysis.[2] The equations for the buckling coefficients are:

$$K_x = \frac{N_x(b)^2}{\pi^2(D)} \qquad K_y = \frac{N_y(b)^2}{\pi^2(D)}$$

From the equations above, the ratio of the buckling coefficients is

$$\frac{K_y}{K_x} = \frac{N_y}{N_x} = \frac{79.8}{97.1} = 0.822$$

Construct a line with this slope on Figure 2.12.4-4 and read the values for K_x and K_y at the intersection of this line and the curve for J = 1.15, as illustrated in Figure 2.12.4-4. The buckling coefficients are:

[2] The conservatism is evident by comparison with Figure 8(a) of Reference 2, for which the aspect ratio is 0.5 and which yields larger critical buckling loads.

$$K_x = 1.35 \qquad K_y = 1.11$$

The critical buckling loads can be obtained from the equations above for K_x and K_y.

$$(N_x)_{cr} = \frac{\pi^2 (D)(K_x)}{(b)^2} = \frac{\pi^2 (1.471\times10^{10})(1.35)}{(2{,}860)^2} = 2.40\times10^4 \text{ N/mm}$$

$$(N_y)_{cr} = \frac{\pi^2 (D)(K_y)}{(b)^2} = \frac{\pi^2 (1.471\times10^{10})(1.11)}{(2{,}860)^2} = 1.97\times10^4 \text{ N/mm}$$

The critical buckling stress, $(\sigma_{cr})_x$, will be calculated based on the assumption that only the face sheets react the edge loads. This is conservative since the loads shared by the core are neglected.

$$(\sigma_{cr})_x = \frac{(N_x)_{cr}}{2(t)} = \frac{2.40\times10^4}{2(8)} = 1{,}500 \text{ MPa}$$

This stress exceeds the yield stress of 419 MPa at 71 °C indicating that the buckling is inelastic. The critical inelastic buckling stress can be calculated by using the tangent modulus instead of the elastic modulus. The tangent modulus is calculated by an iterative process from the true stress-strain curve for Alloy UNS S31803 material taken from Table 2.2-2 of Section 2.2, *Mechanical Properties of Materials*. True stress-strain and engineering stress-strain are essentially equivalent in the region of low strain under consideration. The data in the region of interest is:

True Strain	True Stress, MPa
0.0008	152
0.0016	276
0.0023	345
0.0042	421

These points are fit to the equation $\sigma = 164.02 ln(\varepsilon) + 1328.4$, with a correlation coefficient of 0.992. The derivative of this equation gives the tangent modulus for a given strain level. At a strain level of 0.00328, the stress is 390 MPa and the tangent modulus is $E_t = 5.0\times10^4$ MPa. Multiplying the elastically calculated buckling stress by the ratio of the tangent modulus to the elastic modulus gives the critical inelastic buckling stress, $(\sigma_{cri})_x$:

$$(\sigma_{cri})_x = (E_t/E)\,(\sigma_{cr})_x = (5.0\times10^4/19.2\times10^4)(1{,}500) = 391 \text{ MPa}$$

Note that the critical inelastic buckling stress value of 391 MPa is essentially equal to the stress value of 390 MPa from the stress-strain curve indicating that no further iterations are necessary.

The critical buckling load is:

$$(N_x)_{cr} = (\sigma_{cri})_x(2)(t) = 391(2)(8) = 6{,}256 \text{ N/mm}$$

2.12.4.4.4 Stress Due to Pressure Load

Consider a strip of unit width taken from the middle of the sidewall, as shown in Figure 2.12.4-5. The strip will be analyzed as a simply supported beam with uniform load, which is conservative since the end support of the sidewall is neglected. The uniform load is:

$$\omega = \text{P (unit width)} = 0.150\ (1) = 0.150\ \text{N/mm}$$

The maximum moment, which occurs at midspan, is:

$$M_{max} = \frac{\omega(H)^2}{8} = \frac{0.150(2{,}140)^2}{8} = 8.587 \times 10^4\ \text{N - mm}$$

The bending cross-section is shown in Figure 2.12.4-6. It is conservatively assumed that the face sheets resist all the bending. No structural credit is assumed for the core. Also, the moment of inertia of the face sheets about their individual centroidal axes is conservatively neglected.

The area of one face sheet per unit width is:

$$A = 1.0\ (8) = 8.0\ \text{mm}^2$$

The distance between the centroids of the face sheets is d = 132 mm. The moment of inertia of the cross-section is:

$$I = 2(A)\left(\frac{d}{2}\right)^2 = \frac{A(d)^2}{2} = \frac{8.0(132)^2}{2} = 69{,}700\ \text{mm}^4$$

The distance from the neutral axis to the centroid of a face sheet is:

$$c = \frac{d}{2} = \frac{132}{2} = 66\ \text{mm}$$

The stress in the face sheet is then:

$$\sigma_b = \frac{M(c)}{I} = \frac{8.587 \times 10^4 (66)}{69{,}700} = 81.3\ \text{MPa}$$

This stress is amplified by the presence of edge loads. Formula 8:5 from Reference 3 is used to calculate the amplified stress, σ_{ba}:

$$\sigma_{ba} = \frac{\sigma_b}{1 - \frac{N_x}{(N_x)_{cr}}} = \frac{81.3}{1 - \frac{97.1}{6{,}256}} = 82.6\ \text{MPa}$$

The combined stress resulting from normal plus edge loads is:

$$\sigma = \sigma_{ba} + \sigma_x = 82.6 + 6.1 = 88.7\ \text{MPa}$$

The factor of safety against buckling is

$$FS = \frac{(\sigma_{cr})_x}{\sigma} = \frac{391}{88.7} = 4.41$$

This is considerably in excess of the minimum factor of safety of 2.00 for NCT and 1.34 for HAC per Section -1400 of Reference 6. Note that the result for NCT is quite conservative, since it assumes an external pressure of 150 kPa gauge, whereas the required pressure per 10 CFR §71.71(c)(4) is only 140 kPa absolute.

2.12.4.4.5 Transverse Shear Stiffness of Core

The transverse shear stiffness will be calculated using the method presented in Reference 1. A symmetric core is assumed even though there is no crest flat in this case. This assumption is judged to be conservative for the following reasons:

1) Unequal crests and troughs have very little effect on the value of the transverse shear stiffness factor "S" for the geometry of this case (See Figure 4(c) of Reference 1).
2) The method of Reference 1 assumes that the core is attached to the face sheets at the mid-lengths of the trough and crest flats. This configuration is a more flexible geometry than the present case because the core length is longer and the face sheet span between attachment points is greater. The additional flexibility results in a lower value of transverse shear stiffness, which is conservative.
3) In the analysis that follows, a very conservative value of 20 was extracted from Figure 2.12.4-8 for the factor "S". If the curve is extrapolated, a value greater than 30 is obtained.

Dimensions

t_c = core thickness = 4 mm

h_c = vertical core height from crest centerline to centerline at trough (See Fig. 2.12.4-7) = 120 mm

h = distance between middle surfaces of face sheets = 132 mm

t_1 = thickness of face 1 = 8 mm

t_2 = thickness of face 2 = 8 mm

2p = corrugation pitch = 164 mm

p = 164/2 = 82 mm

R_{c1} = radius of corrugation at face 1 = 4 mm

R_{c2} = radius of corrugation at face 2 = 4 mm

θ = angle between corrugation side & face sheet = $\tan^{-1}$ (124/55) = 66.1° (See Figure 2.12.4-7)

f_1 = face width of corrugation at face 1

f_2 = face width of corrugation at face 2 (assume $f_1 = f_2$)

Dimensional Ratios

$h_c/t_c = 120/4 = 30$

$t_c/t_1 = 4/8 = 0.5$

$p/h_c = 82/120 = 0.683$

$R_{c1}/h_c = R_{c2}/h_c = 4/120 = 0.0333$

As previously noted, the modulus of elasticity for the core material (E_c) at 71 °C is 19.2×10^4 MPa.

The formula for transverse shear stiffness contains a factor "S" that can be obtained from charts in the reference above. The Figure 3 charts of Reference 1 are for $R_{c1} = R_{c2} = 0.18\ h_c$. For this analysis, $R_{c1} = R_{c2} = 0.0333\ h_c$. Results for $R_{c1} = R_{c2} \neq 0.18\ h_c$ are presented in the reference where the effect on "S" is seen to be small. Thus, it will be sufficiently accurate to use the Figure 3 charts.

Figure 3(c) of Reference 1 for $t_c/t_1 = 0.50$ and $h_c/t_c = 30$, included as Figure 2.12.4-8, applies for this case. For $p/h_c = 0.683$ and $\theta = 66.1°$, the value of "S" is off the upper end of the chart. The upper chart value of S = 20 will be conservatively used.

The transverse shear stiffness, D_{Qy}, is calculated from the following formula:

$$D_{Qy} = S(h)\frac{E_c}{\left(1-\mu_c^2\right)}\left(\frac{t_c}{h_c}\right)^3 = 20(132)\frac{19.2 \times 10^4}{\left(1 - 0.29^2\right)}\left(\frac{4}{120}\right)^3 = 2.050 \times 10^4 \text{ N/mm}$$

2.12.4.4.6 Effect of Initial Deflections

The effect of initial deflections of the sidewall on the critical buckling load will be evaluated. Initial deflections can occur during the manufacturing process and are controlled by flatness tolerances on the fabrication drawings. The total deflection of a sheet with an initial deflection under the action of edge loads can be calculated from Equation 6.3.7 of Reference 5. The equation is:

$$W + W_o = \frac{W_o}{1 - \frac{N_x}{(N_x)_{cr}}}$$

where: $W + W_o$ = total deflection

W_o = initial deflection

W = additional deflection due to edge loads acting on a sheet with initial deflection W_o

$\frac{N_x}{(N_x)_{cr}}$ = ratio of applied edge load to critical edge load

Note that this equation is similar to the one used in Section 2.12.4.4.4, *Stress Due to Pressure Load,* to calculate the effect of the pressure load acting on the surface of the sidewall.

The stress due to the combined effect of edge loads and initial deflection W_o results from the additional deflection W only. In order to calculate this stress, the equation above will be solved for W. The result is:

$$W = \left[\frac{\frac{N_x}{(N_x)_{cr}}}{1 - \frac{N_x}{(N_x)_{cr}}}\right] W_o$$

The edge load values are:

N_x = 97.1 N/mm (See Section 2.12.4.4.1, *Buckling Analysis of CSA Containment Sheets*)

$(N_x)_{cr}$ = 6,256 N/mm (See Section 2.12.4.4.3, *Buckling Stress for Biaxial Compression*)

The ratio of edge loads is:

$$\frac{N_x}{(N_x)_{cr}} = \frac{97.1}{6{,}256} = 0.0155$$

Substituting this value into the above equation yields:

$$W = \left[\frac{0.0155}{1 - 0.0155}\right] W_o = 0.0157\ W_o$$

The stress associated with the deflection W will be calculated by multiplying W by the ratio of stress to deflection for the uniformly loaded strip analyzed in Section 2.12.4.4.4, *Stress Due to Pressure Load*. The stress for the strip was determined to be:

$$\sigma_b = 81.3 \text{ MPa}$$

The deflection for a uniformly loaded strip is:

$$\delta = \frac{5(\omega)(H)^4}{384(E)(I)}$$

where: $\omega = 0.150$ N/mm

$H = 2{,}140$ mm

$E = 19.2 \times 10^4$ MPa

$I = 69{,}700$ mm^4

Substituting values into the above equation yields:

$$\delta = \frac{5(0.150)(2140)^4}{384(19.2\times10^4)(69{,}700)} = 3.06 \text{ mm}$$

The ratio of stress to deflection is:

$$\frac{\sigma_b}{\delta} = \frac{81.3}{3.06} = 26.6 \text{ MPa/mm}$$

The stress due to deflection W is:

$$\sigma_w = 26.6\ W = 26.6\ (0.0157)W_o = 0.418W_o$$

This stress will be added to the combined stress $\sigma = 88.7$ MPa from Section 2.12.4.4.4, *Stress Due to Pressure Load*, for a total stress of:

$$\sigma_{tot} = 88.7 + 0.418W_o$$

An allowable initial deflection can be calculated by equating the total stress above to the allowable stress. The allowable stress is 391 MPa from Section 2.12.4.4.3, *Buckling Stress for Biaxial Compression*.

$$\sigma_{tot} = \sigma_{all} \Rightarrow 88.7 + 0.418(W_o)_{all} = 391$$

Solving for $(W_o)_{all}$ yields the following:

$$(W_o)_{all} = \frac{391 - 88.7}{0.418} = 723 \text{ mm}$$

The allowable initial deflection is large because the applied edge loads are very small compared to the critical edge loads for buckling. For this case, the ratio $N_x/(N_x)_{cr}$ is 0.0155.

Since the manufacturing tolerance on sheet flatness is much smaller than the allowable initial deflection calculated above, it is concluded that initial deflections due to the manufacturing process will have an insignificant effect on the critical buckling load.

2.12.4.5 References

1. Libove, C. and Hubka, R.E., *Elastic Constants for Corrugated-Core Sandwich Plates*, NACA TN 2289, 1951.
2. Harris, L.A. and Auelmann, R.R., *Stability of Flat, Simply Supported Corrugated-Core Sandwich Plates Under Combined Loads*, Journal of the Aero/Space Sciences, Vol. 27, No. 7, pp. 525-534, July, 1960.
3. MIL-HDBK-23A, *Structural Sandwich Composites*, U.S. Dept. of Defense, 1968.
4. American Society of Mechanical Engineers (ASME) Boiler and Pressure Vessel Code, Section II, *Materials*, Part D, *Properties*, 2004 Edition, 2005 and 2006 Addenda.
5. Plantema, F. J., *Sandwich Construction*, John Wiley and Sons, Inc, New York, 1966.
6. Code Case N–284–1, Metal Containment Shell Buckling Design Methods, Class MC, Section III, Division 1, ASME Boiler & Pressure Vessel Code.

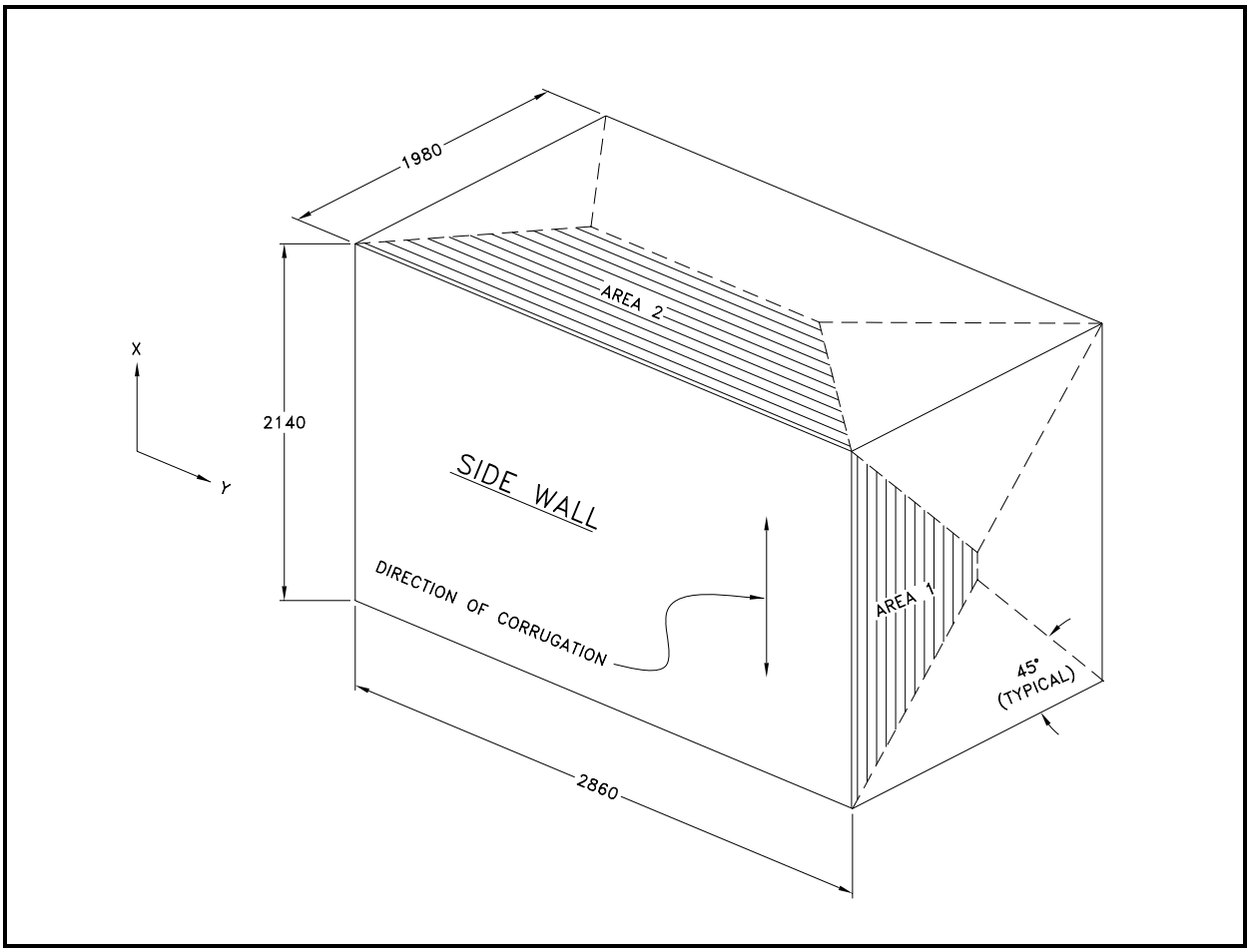

Figure 2.12.4-1 – View of Sidewalls and Adjacent Panels Showing Areas Used to Calculate Edge Loads

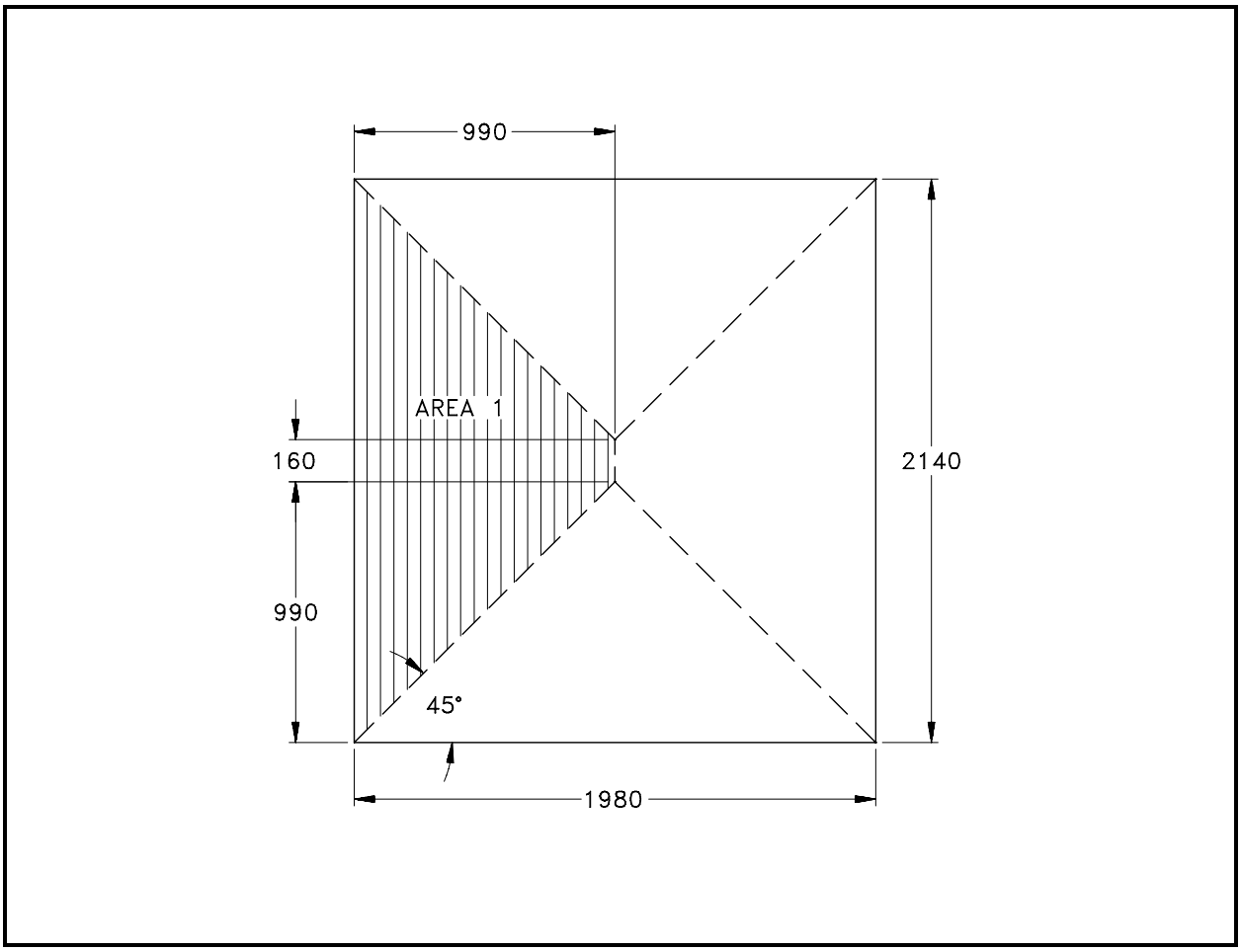

Figure 2.12.4-2 – View of Area 1 on End Sheet Used to Calculate End Edge Load on Sidewall

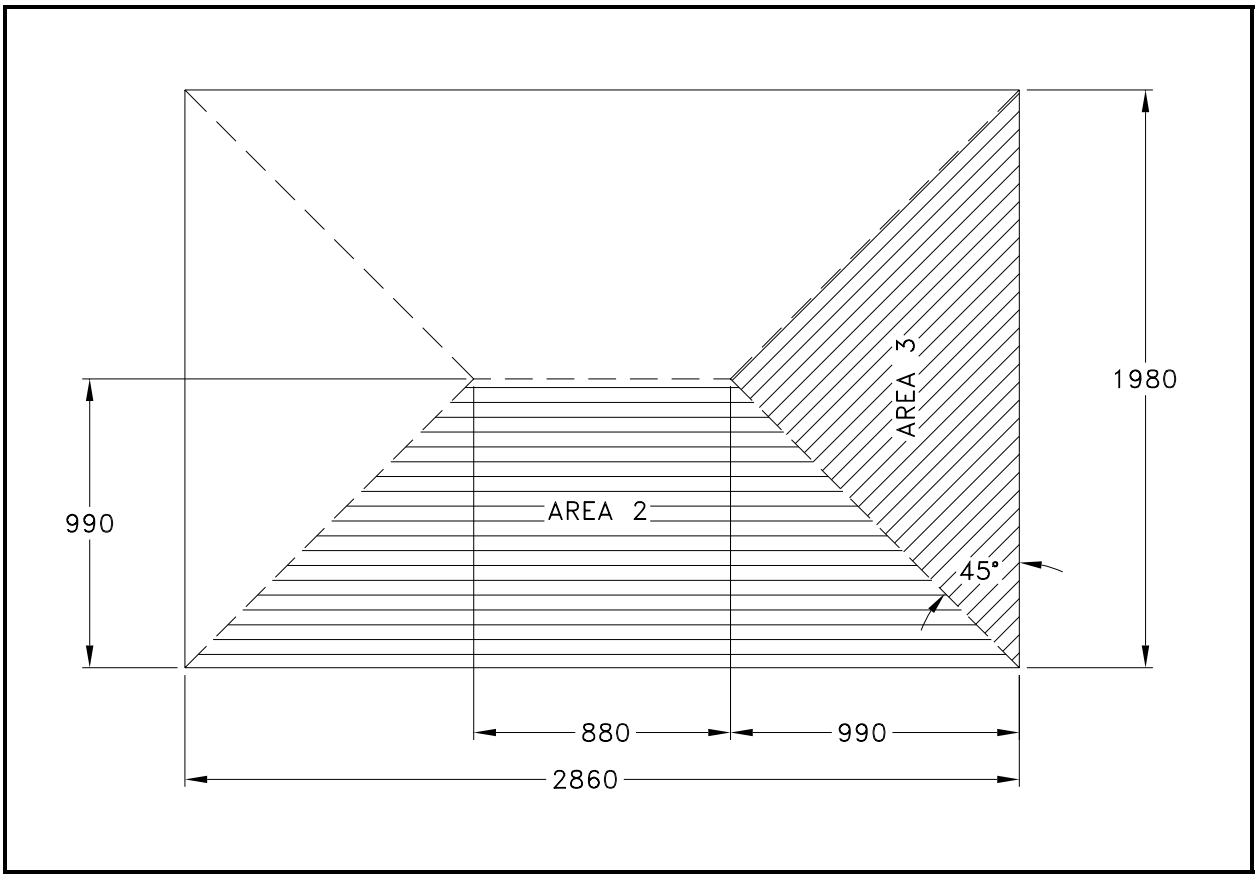

Figure 2.12.4-3 – View of Area 2 on Top Sheet Used to Calculate Top/Bottom Edge Loads on Sidewall

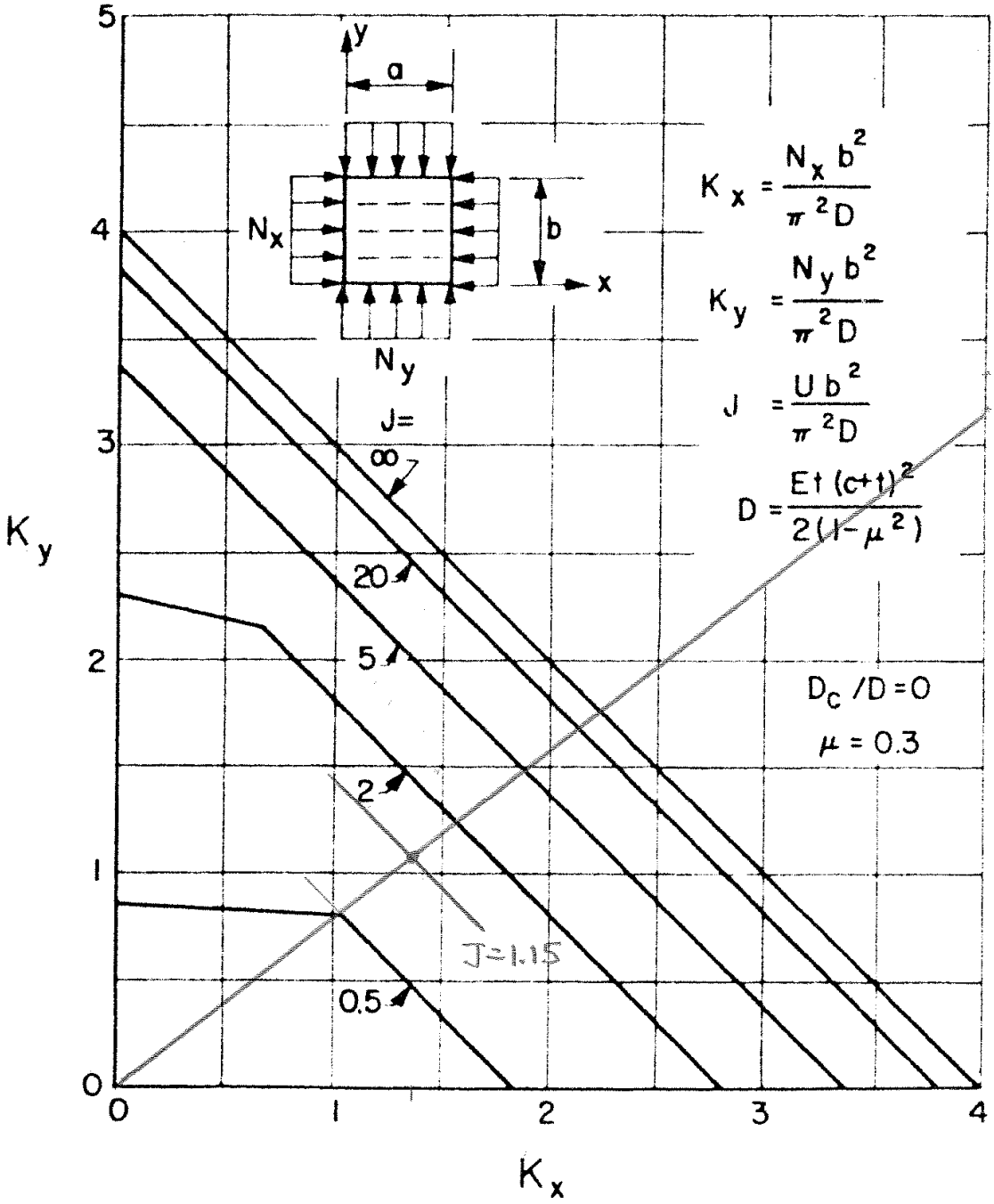

Figure 2.12.4-4 – Buckling Coefficients for Biaxial Compression (a/b = 1) [Figure 8(b) from Reference 2]

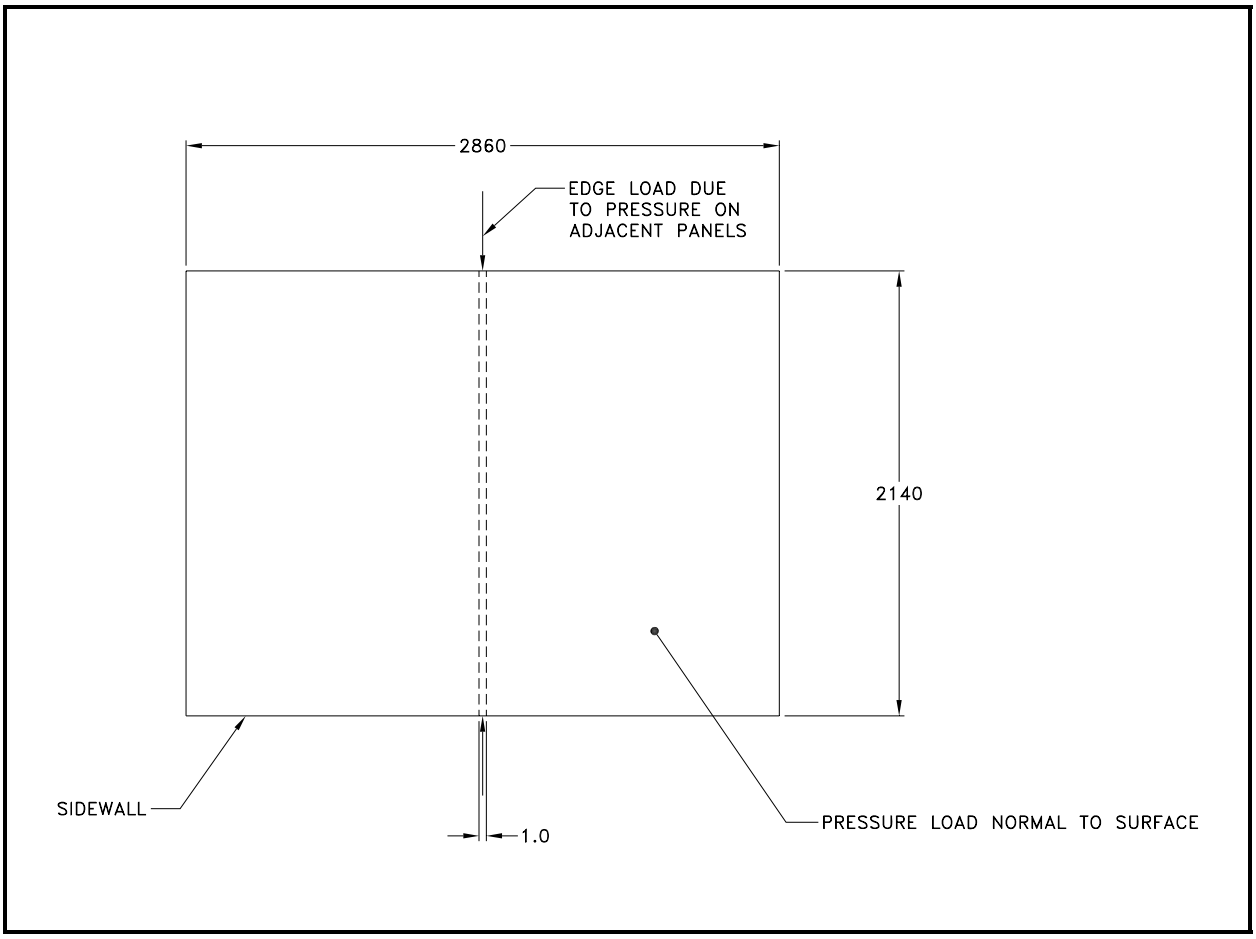

Figure 2.12.4-5 – View of Sidewall Showing Strip of Unit Width

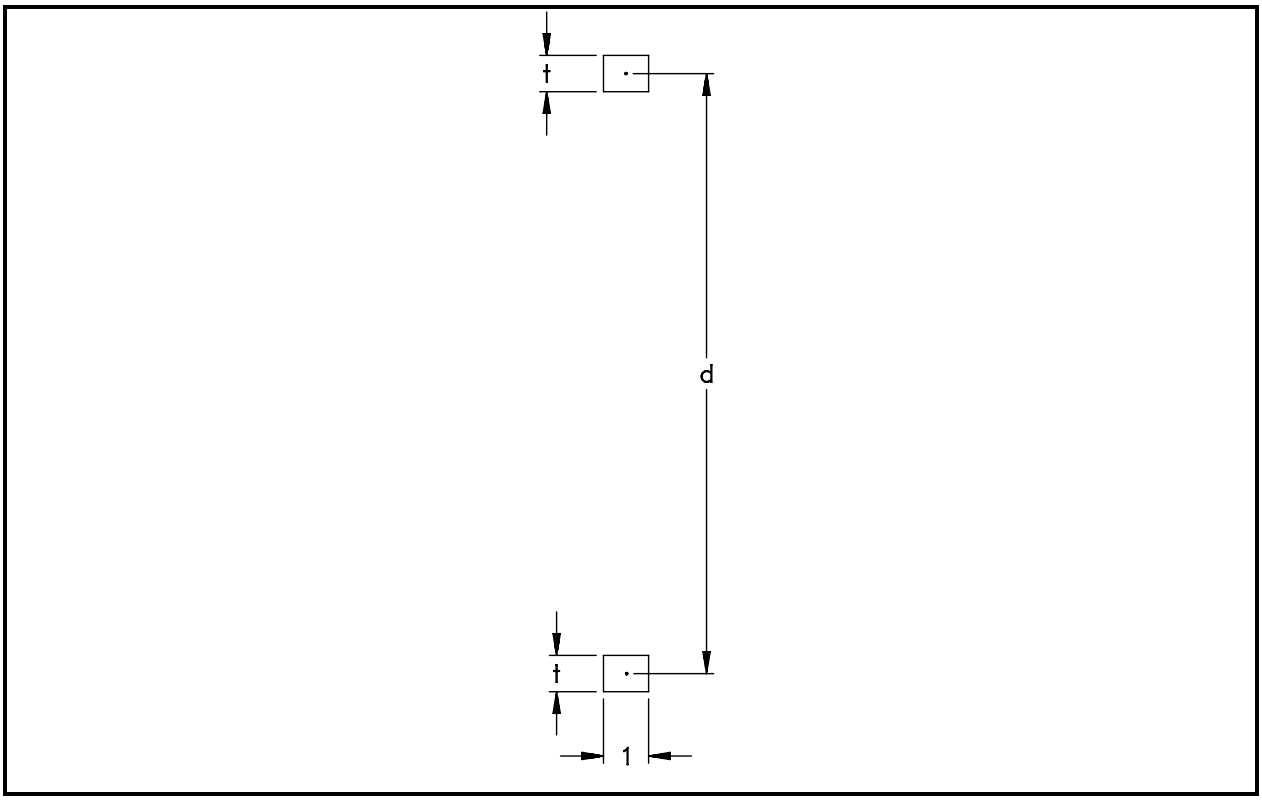

Figure 2.12.4-6 – Bending Cross-Section

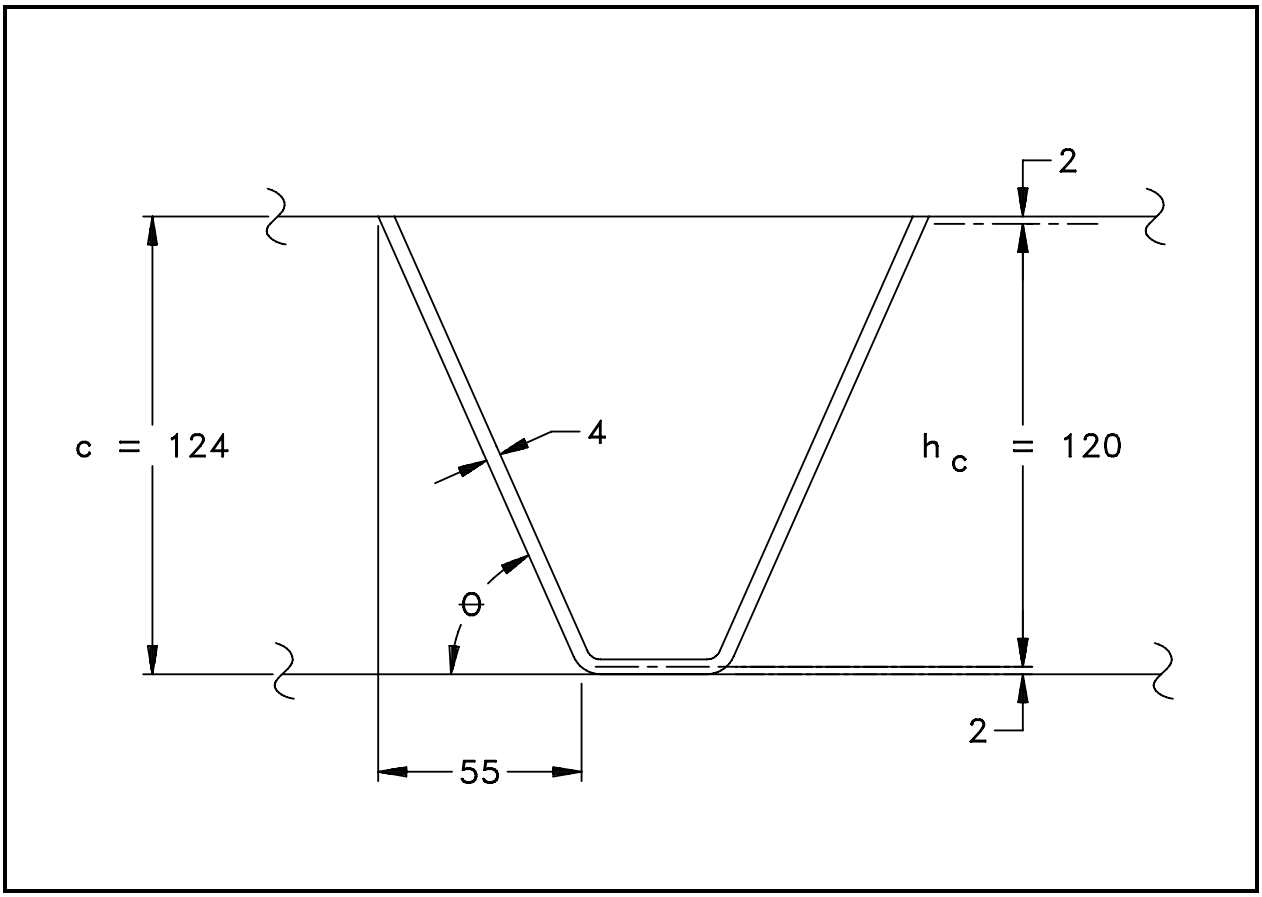

Figure 2.12.4-7 – V-Stiffener Core Geometry

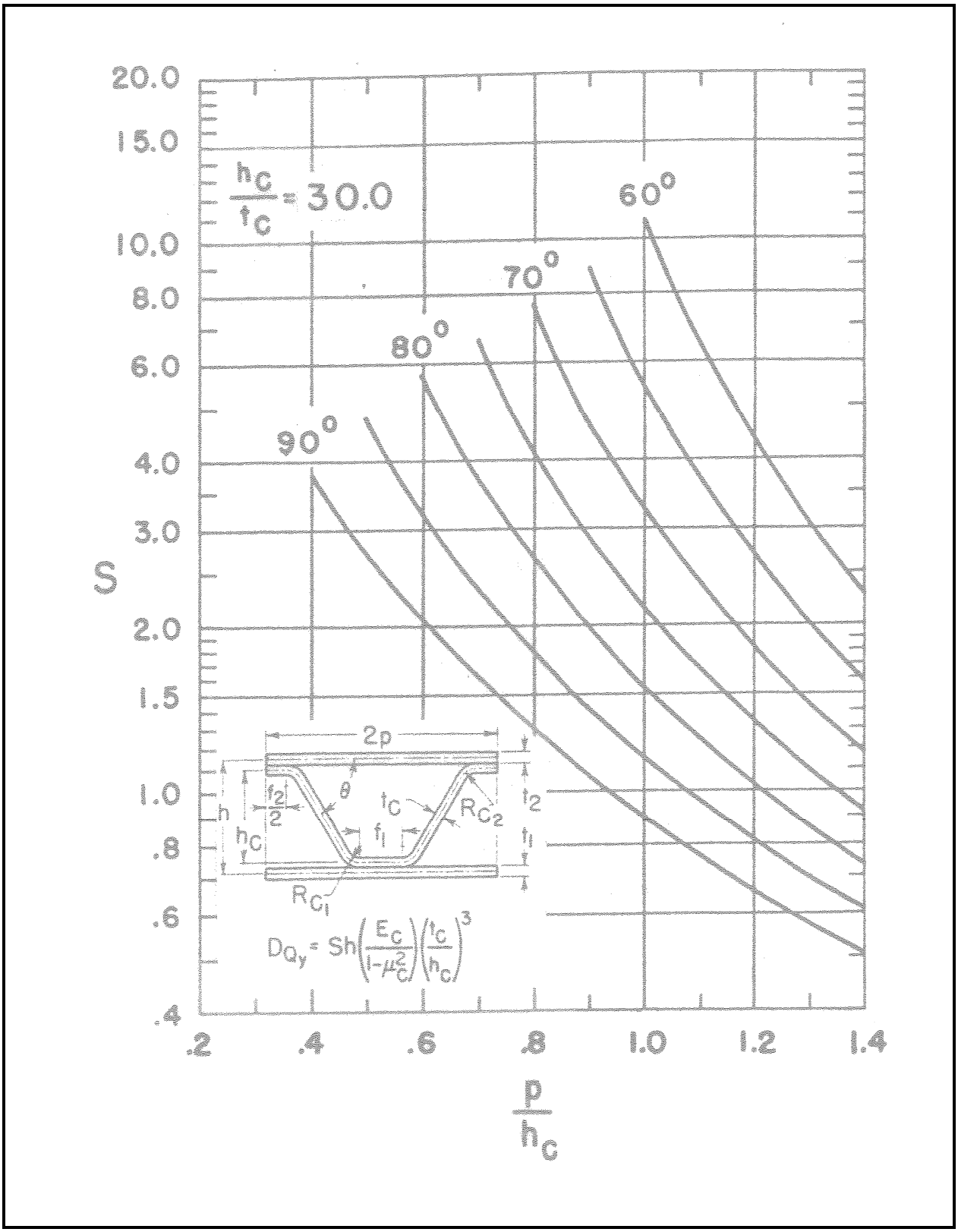

Figure 2.12.4-8 – Chart for Evaluation Coefficient S in Formula for D_{Qy} ($t_c/t_1 = 0.5$) [Figure 3(c) of Ref. 1]

This page intentionally left blank.

2.12.5 Closure Lid Debris Shield

2.12.5.1 Introduction

This section presents a demonstration of the effectiveness of the debris shield design by analysis. The debris shield performance was demonstrated by test using CTU-2 as discussed in Appendix 2.12.6, *Certification Tests on CTU-2*. Note, all references to certification testing in this appendix indicate the first certification test series using CTU-1.

The purpose of the debris shield is to prevent the contamination of the containment O-ring seal with any particulate matter (i.e., debris) which might be present within the payload cavity. As a result of certain HAC free drop impacts, a transient opening of the closure joint could occur, allowing the debris to be deposited on the containment O-ring seal, potentially preventing a leaktight condition. The debris shield utilized in the TRUPACT–III blocks the access of any debris to the vicinity of the closure joint, thus preventing contamination of the seal.

2.12.5.2 Contamination of the Containment O-ring Seal During Certification Testing

The tests performed on the first certification test unit (CTU-1) are fully discussed in Appendix 2.12.3, *Certification Tests on CTU-1*. As detailed therein, the post-test helium leakage rate testing of the closure lid containment O-ring seal was not successful due to the presence of small debris particles lodged between the elastomer seal surface and the mating body flange. The source of the particles was the aluminum bars which were used for the simulated payload. Upon inspection, the particles were found to be spread over the entire closure joint, including both the containment and test O-ring seals.

During disassembly of the closure lid, it was discovered that a number of the closure bolts, particularly on the right side, had become bent. However, the presence of the debris was the only reason for the inability of the CTU to pass the leakage rate test. After inspection of the closure joint was complete, the exposed sealing surfaces were wiped clean (O-rings were not removed for cleaning), and the lid re-attached with reduced bolt preload. Two reduced-preload tests were performed:

1. All 44 closure bolts were tightened to 149 N-m, or approximately one-sixth of the average measured residual torque of all 44 bolts of 898 N-m. This torque was chosen because it was equal to the lowest residual preload of any bolt. The helium leakage rate test was repeated, and the containment O-ring seal was found to be leaktight.
2. Only the bolts in the four corners of the lid were installed, again tightened to 149 N-m. In this case, the total closure force was only 1.5% of the force that would be applied by all 44 bolts tightened to the average measured residual torque of 898 N-m. The helium leakage rate test was repeated, and the containment O-ring seal was again found to be leaktight.

The helium leakage rate test results are presented in Section 2.12.3.8.1, *Leakage Rate Tests*. Note that, since the pressure within the payload cavity was atmospheric during these tests, there was no assistance from atmospheric pressure in obtaining a leaktight seal, nor was there any assistance from gravity, since the package was horizontal. Note further that the only leakage rate test failure occurred with debris on the seal; both tests performed after removal of the debris were successful. From these two supplemental leakage rate tests, it can be concluded that only a

very small clamping force is needed to ensure a leaktight closure joint, as long as the seals are free of contamination. Therefore, to ensure a leaktight condition of the TRUPACT–III, it will be sufficient to prevent debris contamination of the containment O-ring seal.

Before developing the design criteria for the debris seal, a thorough investigation of the debris phenomena was performed. The intrusion of debris into the closure joint was found to depend on several factors:

- *Generation of debris.* Because several free drops were performed, a large number of collisions among the simulated payload aluminum bars and between the bars and the payload cavity walls occurred, generating a quantity of small aluminum shards and flakes. Numerous re-orientations of the CTU allowed some debris to accumulate next to the closure joint, in the crevice between the closure lid shear lip and the body wall.
- *Transient separation of the closure joint.* In certain free drop impacts, a small transient opening of the closure joint can occur, large enough to allow the passage of debris particles, and lasting on the order of 10 – 15 milliseconds. See Section 2.12.5.5, *Finite Element End Drop Analysis*, and Section 2.12.5.6, *Finite Element Side Drop Analysis*, for an investigation of this phenomenon.
- *Elastomer non-response*. The elastomer material from which the O-ring seals are made cannot elastically respond in a 10 millisecond timeframe. The O-rings remained in a compressed configuration, thus briefly opening a gap across the seals. Because the opening was largest at the inside, the gap at the test seal was somewhat smaller than the gap at the containment seal.
- *Internal design pressure*. The internal design pressure, which was present in the CTU, is 172 kPa. Since the containment seal is a pressure boundary, the differential pressure across the containment seal would be equal to the design pressure. In the transient separation event, escaping air flushed the debris into the closure joint, and onto the O-ring seals.
- *Sliding motions*. Lateral motions of the lid in subsequent free drops or puncture drops could have transported more debris into the sealing nip.

Identification of a specific drop test as the primary driver for debris contamination cannot readily be made. Note is made of the fact that a hard vacuum (160 millitorr or less) was successfully applied to the annulus between the containment and test O-ring seals after the first two 9-m free drops (the lid-down and the side-down drops, LD2 and LD3), but the vacuum could not be achieved after completion of the remaining two 9-m free drops (the side-edge and CG-over-corner drops, LD5 and LD4). If the vacuum test can be taken as a surrogate for the complete helium leakage rate test (experience demonstrates that it can), then the loss of leaktight condition occurred sometime during the last two 9-m free drops.

The certification test program was somewhat unique in that several free drops were performed, allowing debris to be generated over time, and possibly intruding more than once. The packaging regulations require only a single free drop and a single puncture drop. However, the presence of some kind of debris in normal use cannot be ruled out, and if present in the right place and in the right quantity, a single free drop could allow debris contamination of the seals and a possible loss of the leaktight condition. Therefore a debris shield is needed.

2.12.5.3 Debris Shield Design Criteria

The purpose of the TRUPACT–III debris shield is to prevent any debris which may be present in the packaging from contaminating the containment seal in the event of a transient separation of the closure joint, such as could occur in the HAC free drop. To accomplish this task, the following safety-related design criteria have been identified (Table 2.12.5-1).

Table 2.12.5-1 – Debris Shield Design Criteria

Environment	*Temperature:* Per Regulatory Guide 7.8, the temperature range is between a minimum temperature of -29 ºC (-40 ºC for the normal cold condition) and a maximum ambient temperature of 38 ºC with full solar. According to Section 3.1.3, *Summary Tables of Temperatures*, the maximum NCT hot temperature of the containment seal, which may be assumed valid for the debris shield, is 52.6 ºC. *Pressure:* The design pressure of the TRUPACT–III is 172 kPa, gage. However, as discussed below, the debris shield should be designed to not retain this pressure.
Material	The material used must be capable of instantaneous response, or else not depend upon elastic response for its function. The material must be strong and durable.
Relative Position/Motion	The debris shield must accommodate the possible range of position of the closure lid relative to the body, and must also accommodate any relative motions arising from transient impact events which lead to closure joint separation. This requirement is discussed in more detail below.
Physical Constraints	The debris shield must not reduce the shear area or bearing area of the closure lid shear lip. It must be compatible with the size of the payload container and the installation of the lid. It must not prevent helium from approaching the containment O-ring seal during helium leakage rate testing. It should be vented so that pressure is nominally equal on both sides (to reduce the mechanical forces on the shield and to eliminate a significant driving force for debris to pass the shield).
Reliability	The debris shield must be reliable and easy to use. It must be protected from damage under normal use and under normal and accident conditions of transport. It must not be damaged by motions of the roller floor, pallet, or payload container during NCT and HAC events. Damage to the shield must be readily detectable and repairable.

As shown in Table 2.12.5-1, the debris shield must accommodate the relative motions which could occur between the closure lid and body. These include the lateral position of the lid within the limits established by the lid shear lip, as well as the axial motions resulting from the transient elastic motions of the lid during HAC free drop events.

As shown in the drawings in Section 1.3.1, *Packaging General Arrangement Drawings*, the clearance between the outer dimension of the lid shear lips and the body flange opening (equivalent to the total range of lateral motion of the lid) is 6 mm in both the side-to-side and up-and-down directions.

The bounding axial motions are defined by the two free drop orientations having the maximum cold impact: one, the lid end down, and two, the flat side down orientation. These orientations represent the largest possible deformations at the closure joint because they combine the largest free drop impacts with a direction of impact force oriented normal to the largest panels of the containment structural assembly (CSA).

The lid end down case is equivalent to CTU free drop orientation LD2. A dynamic finite element model of this case is described in Section 2.12.5.5, *Finite Element End Drop Analysis*. In this orientation, the lid deflects outward, resulting in a rotation of the lid flange away from the body flange. The maximum transient dynamic relative motion at the debris shield is calculated to be 0.78 mm.

The flat side down case is equivalent to CTU free drop orientation LD3. A quasi-dynamic finite element model of this case is described in Section 2.12.5.6, *Finite Element Side Drop Analysis*. In this orientation, the large flat side impacts the ground and deflects downward, resulting in a rotation of the body flange away from the lid flange. The maximum transient dynamic relative motion at the debris shield is calculated to be 3.0 mm. This value will therefore be used as a bounding design criterion for axial debris shield function.

2.12.5.4 Debris Shield Design

The debris shield is shown in a section view in Figure 2.12.5-1, and consists of a receptacle, a holder, and an insert. The receptacle is attached to each side of the body opening, and the holder is integral with the closure lid shear lip. The insert is made from silicone rubber foam having a U-shaped cross-section which is attached to the holder using adhesive double-sided tape on each leg. The insert is therefore carried with the lid. The insert interfaces with a 15-mm wide groove in the receptacle. When the lid is installed, the insert component is inserted into the receptacle. The debris shield incorporates two functional principles: a foam rubber-to-steel seal, and a labyrinth configuration.

The total free-state thickness of the foam insert plus the holder is equal to 18 mm (two 7-mm thicknesses of foam plus the 4 mm center holder). Since the receptacle opening width is 15 mm, the nominal compression of the foam when assembled is 1.5 mm per side, or 1.5/7 = 21%. Note that, since the debris shield has two equivalent sides, a seal is maintained regardless of the lateral location[1] of the holder: any compression lost on one side because of a lateral shift of the holder is gained on the opposite side of the holder. The maximum shift from nominal position is 3 mm, based on the total possible lateral clearance between the lid shear lips and the body opening, equal to 6 mm. If the lid shifted laterally by 3 mm in either direction, a 1.5 mm gap would open up on one side, but a compression of (1.5 + 3) = 4.5 mm (equivalent to 4.5/7 = 64%) would occur on the opposite side. See Figure 2.12.5-2. Of note, during normal operation, the lid lateral position is controlled to within ±1 mm by the two closure lid guide pins. Therefore, the maximum lateral lid displacement of ±3 mm is to be expected only in a HAC free drop event.

The receptacle has an approximately 11.5-mm long straight section, ensuring that the shielding function will occur even if the insert is withdrawn somewhat from the receptacle, also depicted

[1] As used here, 'lateral' means any direction which is parallel to the closure flange sealing surface.

in the figure. Note that the bounding axial movement of the holder relative to the receptacle under HAC free drop conditions of 3 mm is equal to only one-fourth of the straight section. A lead-in on the receptacle opening ensures that the insert will move smoothly into and out of the receptacle without binding or damage. Both the holder and the receptacle are made from the same material as the CSA, i.e., UNS S31803 duplex stainless steel (the receptacle may optionally be made from Type 304/304L material). The receptacle is connected to the body inner flange side using groove and fillet welds, and the holder is integral with the closure lid lip.

The labyrinth configuration alluded to above is achieved by requiring any debris to make at least four right angle turns in order to pass by the shield, as illustrated in Figure 2.12.5-3. This feature provides extra assurance that any debris cannot reach the containment O-ring seal.

Also shown in Figure 2.12.5-1 is a cross section of the lid shear lip. To accommodate the holder design, the tapered lead-in portion of the shear lip, which was present in the CTU, was removed. However, the width of the straight portion of the shear lip (10 mm), representing the bearing area between the lip and the mating body flange under lateral HAC loading, is unchanged. The same thing is true for the shear lip shear width (measured in the plane of the lid) of 20 mm. Therefore, the lid shear lip will have the same bearing area and shear strength as the CTU. Also note the presence of a filtered vent passage across the shear lip shown in Figure 2.12.5-1. There are two vent passages per side for a total of eight. Each hole is fitted with a 5/16-inch (7.94-mm) diameter porous polyethylene filter, and used to maintain equal pressure on both sides of the debris shield.

To protect the debris shield from damage from the payload in normal operation or in a hypothetical accident, nominally 1-inch by 3-inch wide (25.4 mm by 76.2 mm) ASTM Type 304L steel guide bars are welded longitudinally to the sides of the CSA containment sheets. There are three bars on each side, and two on the top. No bars are needed on the bottom, since the roller floor and pallet fully protect the debris shield components from contact with the payload. The bars run the full length of the payload cavity, and are located to align with the 1.5-inch (38.1-mm) wide, hollow tube bumpers which are integral parts of the SLB2 payload container. They are connected to the inner CSA wall using fillet welds. The function of the guide bars is to prevent excessive local loading of the debris shield in a HAC free drop which could affect the body flange/sealing surface geometry. They also keep the SLB2 from getting trapped behind the rear edge of the debris shield, which could lead to damage to the shield in a free drop having a vertical impact force component. Since this is the case, no evaluation of loading of the debris shield in a direction parallel to the package axis needs to be performed. However, the SLB2 can apply lateral impact loads to the debris shield and guide bars, and a finite element analysis of this loading condition is given in Section 2.12.5.7, *Finite Element Payload Interaction Analysis*. As shown in that section, under cold side impact loading, the flange remains elastic, and there is no permanent reduction in containment O-ring seal compression. Therefore, interaction between the payload and the CSA, the debris shield, and the guide bars is of no concern.

The design of the debris shield is evaluated in Table 2.12.5-2. As shown, the design meets all of the design requirements listed in Table 2.12.5-1.

Table 2.12.5-2 – Debris Shield Design Evaluation

Environment	*Temperature:* Silicone foam rubber can easily function at the environmental extremes of -40 ºC to 52.6 ºC. *Pressure:* The presence of the filtered passages in the shear lip prevents any differential pressure across the debris shield.
Material	Since any lateral movement of the closure lid will cause an increase in the debris shield compression on one side or the other, and since any axial movement of the lid can be accommodated without a change in compression due to the receptacle's straight sides, function of the seal does not depend on elastic unloading response of the insert foam material.
Relative Position/Motion	Since there is no differential pressure driving force across the debris shield, only a very small region of contact between the receptacle and the insert is needed to block transport of debris. The conservatively calculated maximum axial motion is 3 mm (see Section 2.12.5.3, *Debris Shield Design Criteria*), which is significantly smaller than the length of the straight sides of the receptacle of 11.5 mm. The full lateral motion of ±3 mm can be accommodated resulting in seal contact and compression on at least one side of the insert. Therefore, debris will be blocked assuming worst-case relative motion in any direction between the closure lid and the body.
Physical Constraints	The bearing area and shear area of the closure lid shear lip are unchanged from the CTU. The design allows access for the SLB2 payload container and easy installation of the closure lid. The vent passages in the shear lip prevent a differential pressure across the debris shield, and allow passage of helium tracer gas to the containment seal during leakage rate testing.
Reliability	The debris shield is protected from payload interactions by means of the guide bars attached to the walls of the payload cavity as described above and in Section 2.12.5.7, *Finite Element Payload Interaction Analysis*. In normal operation, the debris shield insert may be readily inspected for any damage prior to use and replaced if necessary.

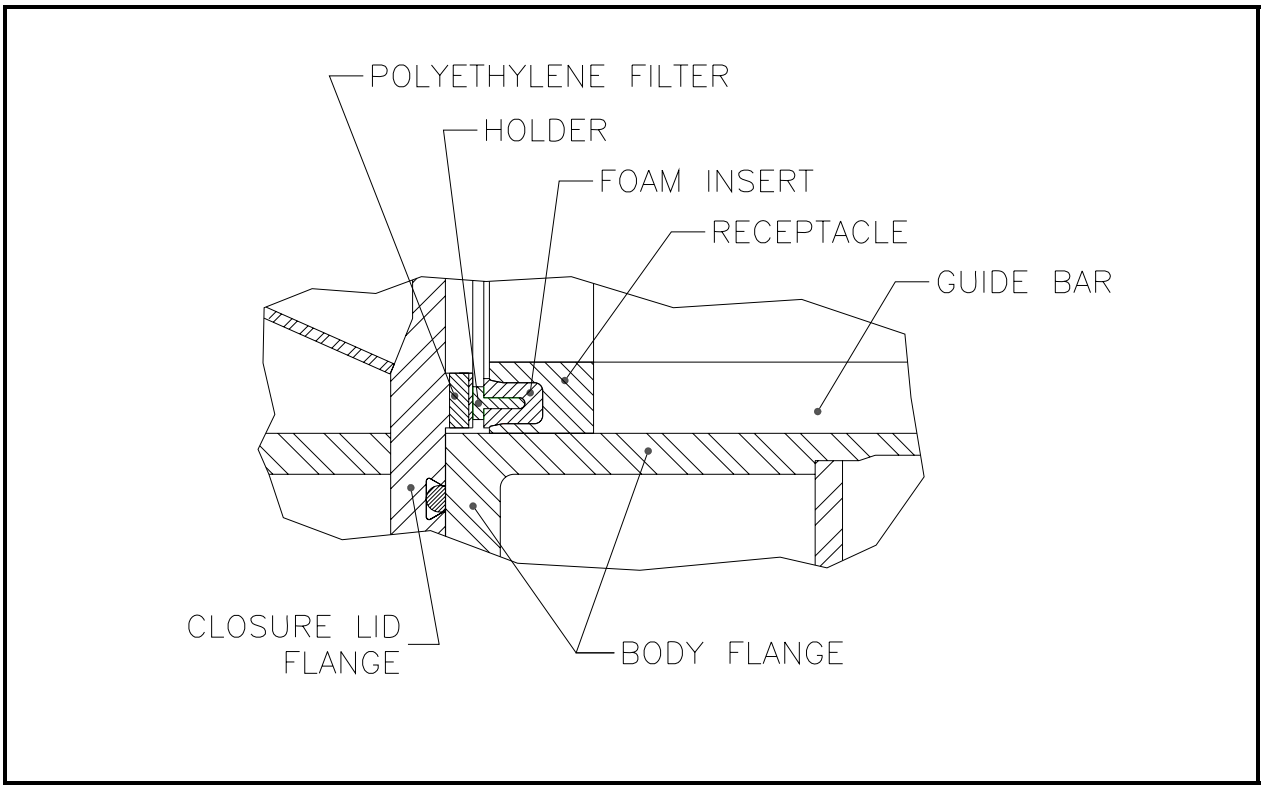

Figure 2.12.5-1 – Debris Shield Cross Sectional View

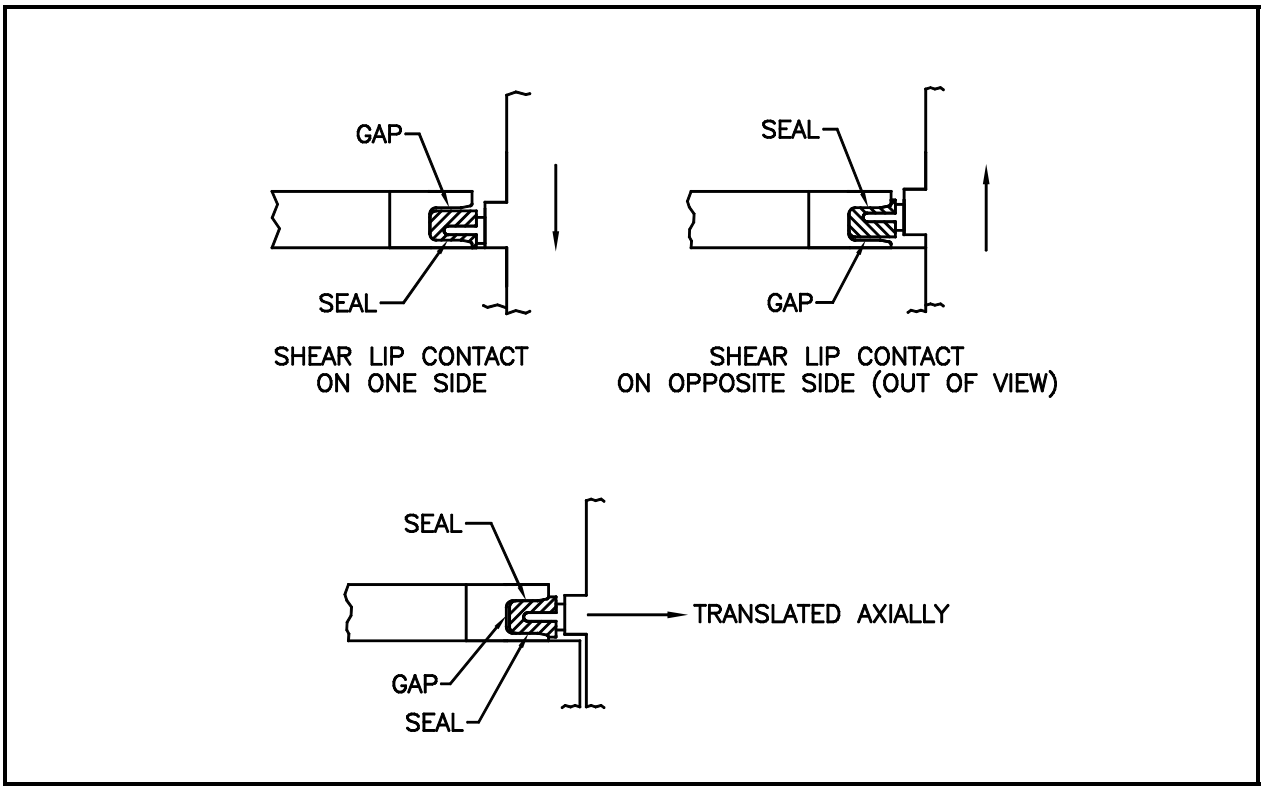

Figure 2.12.5-2 – Debris Shield with Bounding Displacements

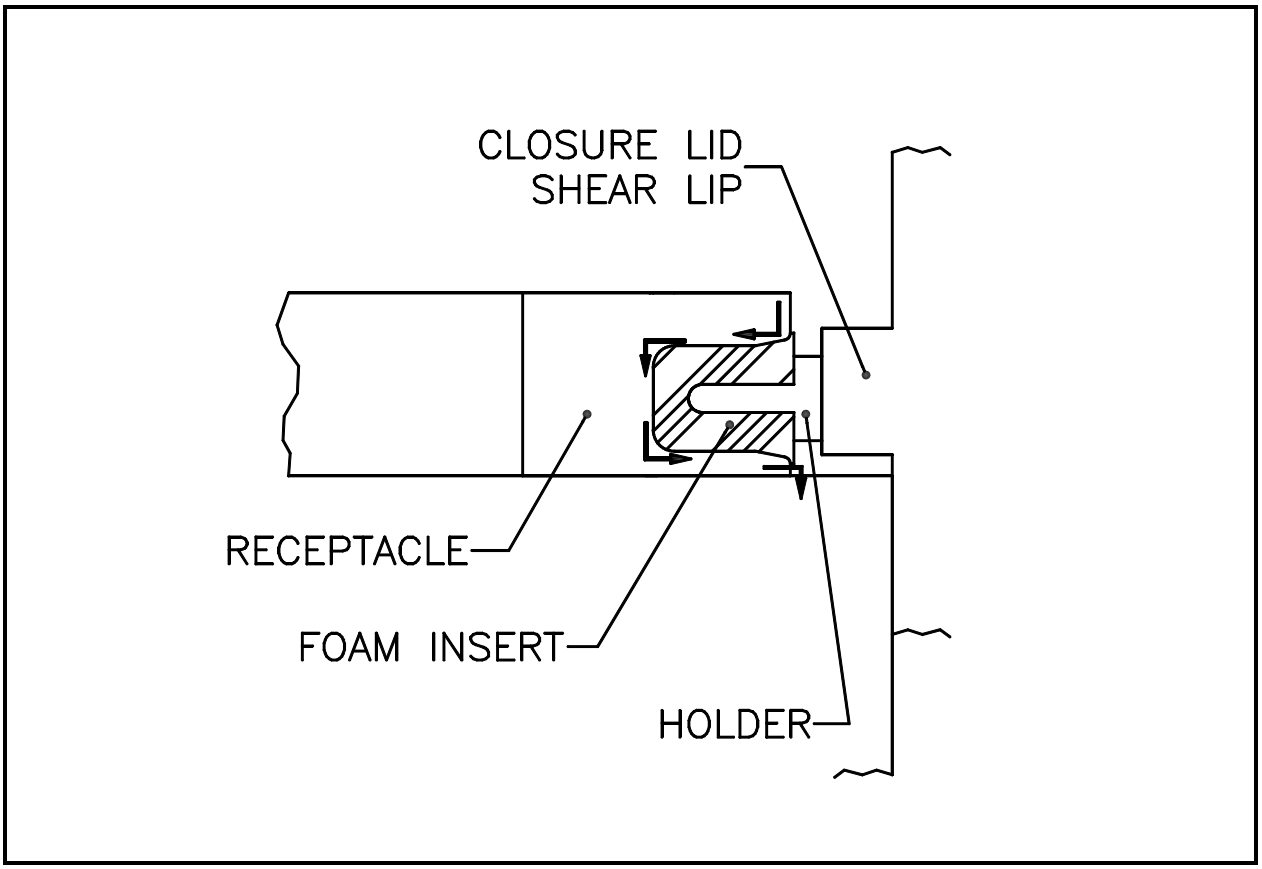

Figure 2.12.5-3 – Debris Shield Showing Labyrinth Configuration

2.12.5.5 Finite Element End Drop Analysis

In the vertical, lid-down HAC free drop orientation, the closure lid is loaded as a membrane by its own weight and the weight of the payload. As the lid deflects under load, a small rotation of the lid flange occurs, resisted by the closure bolts and pivoting about the outside edge of the flange. The containment O-ring seal, located near the inner edge of the flange, briefly separates from the body flange (which remains essentially undeformed). A finite element model using LS-DYNA version LS970s was used to investigate the behavior of the lid and associated parts. The purpose of the investigation was to establish the maximum relative motion which will occur at the debris shield under the cold end drop impact. This data point serves as input to the design of the debris shield. Note, however, that the relative motion calculated in this section is bounded by the larger value calculated in Section 2.12.5.6, *Finite Element Side Drop Analysis*.

The LS-DYNA model was a fully dynamic, explicit formulation of the package vertical, lid-down impact event. The model was constructed in quarter-symmetry. The two planes of symmetry were the longitudinal vertical and horizontal center planes of the package. To simplify modeling and analysis, the length was limited to a total of 614 mm measured from the flange joint. This length included three complete sidewall V-stiffeners. Neglecting the structure above this point (i.e., towards the closed end of the CSA) was not significant since the only result taken from the output is the behavior at the closure, including deformation of the lid flange which might lead to a gap at the containment O-ring and motion at the debris shield. All of the necessary weight was included or otherwise accounted for as described below. Geometry plots of the model are shown in Figure 2.12.5-4 and Figure 2.12.5-5. Model dimensions conform to the drawings given in Appendix 1.3.1, *Packaging General Arrangement Drawings*, and are shown on Figure 2.12.5-6 and Figure 2.12.5-7. Modeled part thicknesses are included in Table 2.12.5-3. The shell elements were defined at the mid-thickness of the structural elements. This may result in small differences between modeled dimensions and actual dimensions. However, such differences are negligible and will not affect results.

The inner and outer sheets, the flange plates, and the V-stiffeners were modeled using four-node Belytschko-Tsay shell elements, with five integration points through the thickness. The tube located in the lid bolting flange which carries the bolt load between the outer and inner surfaces of the lid flange was modeled using the same elements. The bolts were modeled using 8-noded constant stress solid elements with Flanagan-Belytschko hourglass control. The outer end of the bolt was joined to the outer surface of the closure lid flange (the bolt head) and the inner end joined to the body flange at the bolting boss. The 70-mm diameter bolting boss connected the front and rear faces of the body flange, and was constructed using the same solid elements as the bolts. The annular region between the bolt outer diameter and the bolt tube in the closure lid was modeled as rigid, to avoid the creation of a relatively weak diaphragm that does not exist in the prototype. The resulting FEA model correctly models the CSA stiffness and permits a determination of the deformation of the lid flange under the applied impact loading. Stresses are not evaluated since this orientation was physically tested in the certification test program as discussed in Section 2.12.3, *Certification Test Results*, and since only a design input value for the debris shield is required.

The standard nominal preload of 222,000 N was modeled with a target bolt prestress of 314 MPa, whereas 307 MPa (2.2% lower) was actually obtained in the analysis. For the desired output of maximum lid flange deflection, the slightly lower bolt preload is conservative. An internal pressure

of 172 kPa was applied to the lid and sides of the CSA. To balance the pressure on the lid, equivalent forces were applied to the top edge of the CSA inner sheet.

With the exception of the energy-absorbing triangular prism on the bottom of the model, the overpack structures were not explicitly modeled. The weight of the closed end overpack is, however, included in the model. The weight of the overpack sides, cheeks, and overpack cover weight are not included since these items will be self-supporting against the impact surface. The weight of the closed end overpack was 2,860 kg. The weight of the CSA structure (not including the lid) was bounded by 6,390 kg. The weight of the lid was 1,900 kg. Material densities were adjusted to match these weights, as shown in Table 2.12.5-3. The weight of the maximum payload was 5,175 kg. The payload was applied to the lid using discrete mass elements, uniformly distributed over the inside of the lid surface.

The material property of all components except the bolts and bolt sleeves was a bilinear kinematic stress-strain curve which utilizes a tangent modulus obtained from:

$$E_{TAN} = \frac{(S_u - S_y)}{\left(\varepsilon_u - \frac{S_y}{E}\right)}$$

where S_u is the ultimate true stress, S_y is the yield true stress (obtained at a true strain of 0.0047), and ε_u is the ultimate true strain, found for -29 ºC in Table 2.2-2 as 888.8 MPa, 528.8 MPa, and 0.2231, respectively. E is found from Table 2.2-1 as $19.8(10^4)$ MPa. Using this data, the tangent modulus E_{TAN} = 1,633 MPa. Bolts and bolt sleeves were assumed elastic, as confirmed by model output.

Vibration damping in the TRUPACT–III is significant, since a) the payload will typically consist of loose objects, b) the impact energy will be absorbed by the crush of polyurethane foam and the deformation of steel, and c) the closure lid is a bolted flange joint. In the model, an effective damping value of 9.3% was used, which is considered relatively low for conditions existing within the packaging.

The model was decelerated by the crush of material in the triangular prism shown in part (c) of Figure 2.12.5-5. The material was constructed of 8-noded solid *MAT_CRUSHABLE_FOAM elements that were undamped. This region simulated the triangular regions of 0.16 kg/dm^3 foam in the four corners of the overpack cover (adjacent to the octagonal recess). The foam material stress-strain curve consisted of a single plateau value which was adjusted until the target acceleration of 204g (equal to the impact measured in the identical full-scale free drop test LD2) was approximately achieved. The rigid body acceleration was measured using the body side walls (since they would have little vibrational response), and equaled 211.3g, thus slightly in excess of the target. The impact velocity was 13.29 m/s, consistent with a 9-m free drop.

The TRUPACT–III package is designed such that under end drop loading, the impact forces tend to support the closure lid, restricting its deformation. This is shown schematically in Figure 2.12.5-8(a), where contact would occur between (1) the impact limiter and the container lid, and (2) between the container lid and the container body. In this analysis, the impact absorbing triangular prism was connected directly to the CSA body flange, thus conservatively leaving the closure lid unsupported and maximizing lid deformation (and relative motion at the debris shield) under impact loads. This is shown schematically in Figure 2.12.5-8(b).

The transient maximum relative displacement at the containment O-ring was extracted in three locations: the center of the long side of the lid (maximum magnitude), the center of the short side, and at the corner. These and additional results are given in Table 2.12.5-4. A plot of the relative motion between the body flange and closure lid flange at the containment O-ring at the center of the long lid side is given in Figure 2.12.5-9.

As can be seen from the table, the transient dynamic motion at the containment O-ring was very small. Since the lid flange pivots about its outer edge, the motion at the debris shield is:

$$Z_{DS-End} = \frac{X_{P-DS}}{X_{P-CO}} Z_{CO} = 0.78 \text{ mm}$$

where the distance between the outer edge of the lid and the debris shield, $X_{P\text{-}DS}$ = 145 mm, the distance between the outer edge of the lid and the containment O-ring, $X_{P\text{-}CO}$ = 110 mm, and the maximum transient motion at the containment O-ring, Z_{CO} = 0.59 mm from Table 2.12.5-4. The value of 0.78 mm is the relative motion which must be accommodated by the debris shield during the vertical, lid-down, maximum-impact free drop. Note also that the maximum transient bolt stress, 465 MPa, is considerably less than the yield strength of ASTM A320, L43 bolting material from Table 2.2-4, justifying the elastic treatment of the bolts in the model.

Input and output files for all LS-DYNA analysis computer runs are included on a DVD attached to this appendix.

Table 2.12.5-3 – LS-DYNA Model Part Identification and Mass Listing

As Modeled Container Mass / Weight						[WI_Trupact3_Results-0.xls]Model_Mass		
Part ID	Description / Structural Component		Modeled Thickness	Wt. / Load (1/4 Sym.) Mass	Pounds	Model Color	(x4) Full Structure	Actual
1	Ribs (Lid)	Lid	4 mm	61.58 kg	135.8 lb	Red	--	--
2	Inner Plate	Lid	12 mm	92.47 kg	203.9 lb	Blue	--	--
3	Outer Plate	Lid	12 mm	108.32 kg	238.9 lb	Green	--	--
4	Flange	Lid Flange	16 mm	113.39 kg	250.1 lb	Yellow	--	--
5	Flange (Inner Plate)	Lid Flange	20 mm	46.75 kg	103.1 lb	Brown	--	--
6	Impact Limiter (Lower)	--	n/a (1)	9.95 kg	21.9 lb	Red	--	--
7	Impact Limiter (Upper)	--	n/a (1)	28.98 kg	63.9 lb	Blue	--	--
8	Pipe	Lid Flange	10 mm	19.39 kg	42.8 lb	Green	--	--
9	Bolts	--	n/a (1)	9.09 kg	20.0 lb	Yellow	--	--
10	Container Flange (Face)	Container Flange	20 mm	39.17 kg	86.4 lb	Lt. Brown	--	--
11	Container Flange (Backside)	Container Flange	10 mm	19.59 kg	43.2 lb	Red	--	--
12	Side Walls	Container	8 mm	2,071 kg	4,568.0 lb	Light Blue	--	--
13	Side Wall Ribs	Container	4 mm	66.23 kg	146.1 lb	Green	--	--
14	Rigid (Bolt Heads)	Lid Flange	n/a (2)	5.06 kg	11.2 lb	Yellow	--	--
15	Bar (Threaded Inserts)	--	n/a (1)	47.32 kg	104.4 lb	Tan	--	--
16	Container Flange (Sides)	Container Flange	15 mm	68.45 kg	151.0 lb	Purple	--	--
17	Ground	--	n/a	n/a	n/a	Orange	--	--
Subtotals								
A.	Lid (complete), Parts 1, 2, 3, 4, 5, 8, 9, & 14			456 kg	1,006 lb	--	1,824 kg	1,900 kg
B.	Container (w/o Lid), Parts 10, 11, 12, 13, 15, & 16			2,312 kg	5,099 lb	--	9,248 kg	9,250 kg
C.	Total Container (Parts 1 - 5 & 8 - 17)			2,768 kg	6,105 lb	--	11,072 kg	11,150 kg
Contents (Lumped/Discrete Masses)								
D.	SAR Payload			1293.9 kg	2,853 lb	--	5,176 kg	5,175 kg
E.	CTU Payload			1686.7 kg	3,720 lb	--	6,747 kg	6,745 kg
Package + Payload (1/4 Symmetry Model)								
F.	Standard (STD) Payload: (C + D)			4,062 kg	8,958 lb	--	16,248 kg	--
G.	CTU Payload (C + E)			4,455 kg	9,824 lb	--	17,819 kg	--
Notes:								
1.	Thickness not applicable, modeled with solid elements.							
2.	Modeled as rigid.							
3.	Masses in this table are from the summaries included in the LS-DYNA output files (NLS_CTU_314MPa_1.out)							

Table 2.12.5-4 – End Drop Transient Maximum Results

Location	Value
At containment O-ring:	
Center of long lid side[1]	0.59 mm
Center of short lid side[1]	0.35 mm
Corner of lid[1]	0.06 mm
Center of lid[2]	4.83 mm
Maximum closure bolt stress	465 MPa

Notes:

1. Relative displacement between CSA body flange and closure lid flange.
2. Relative displacement between CSA body flange and geometric center of lid.

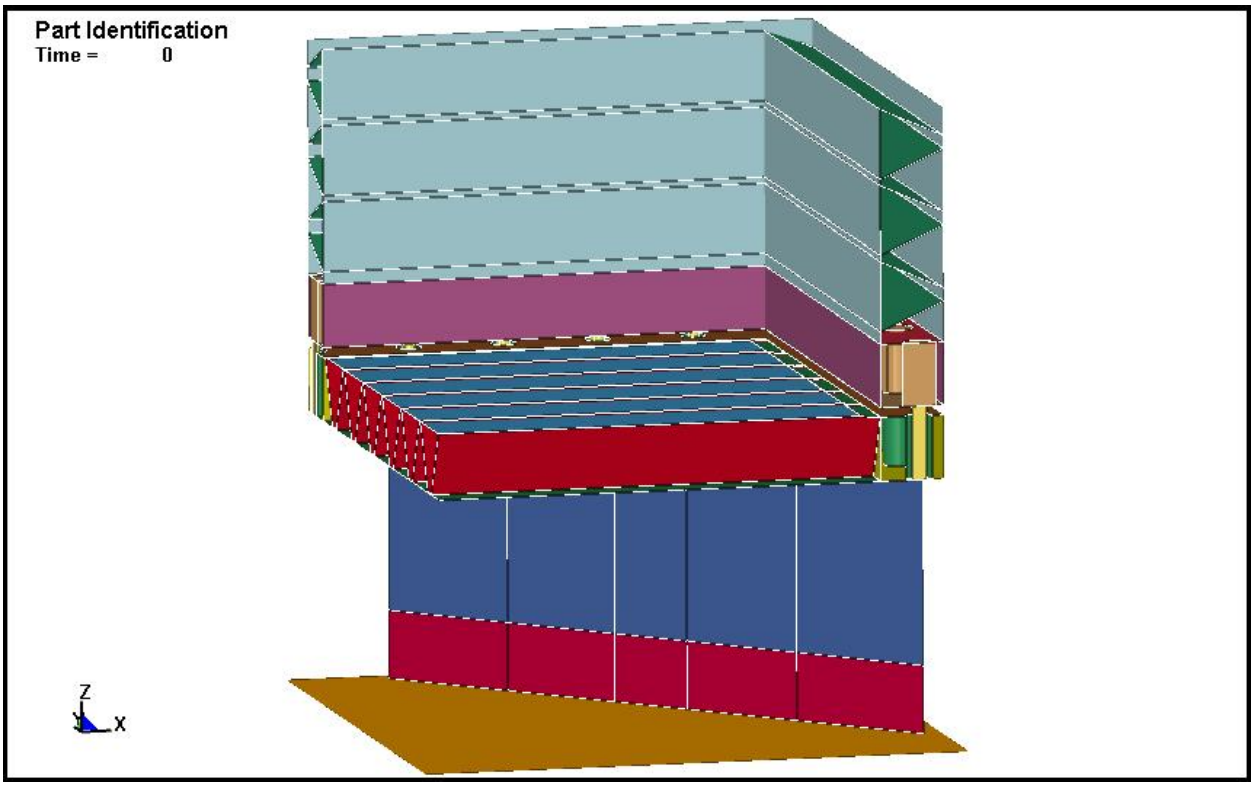

Figure 2.12.5-4 – LS-DYNA End Drop Model

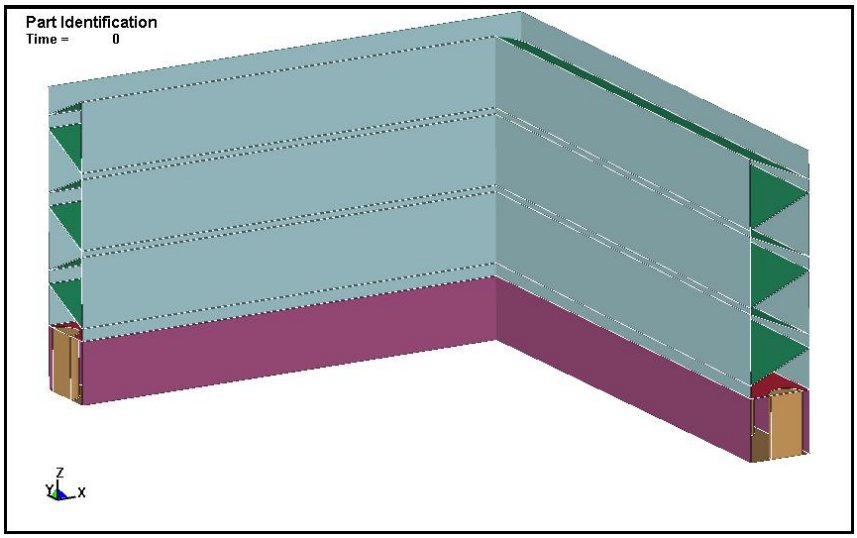

(A) Container Side Wall
(Parts 10, 11, 12, 13, 15, & 16)

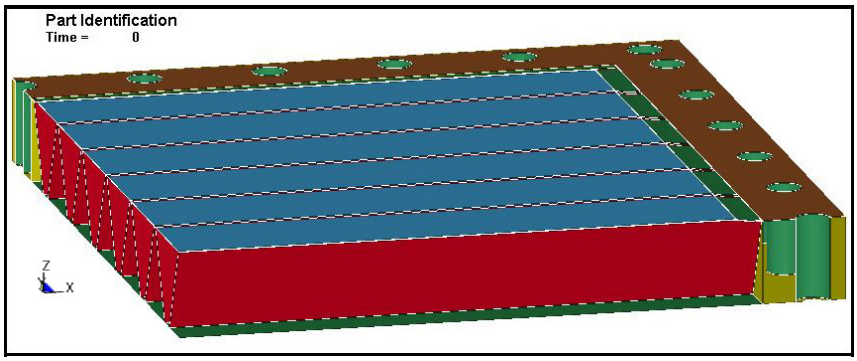

(B) Container Lid
(Parts 1,2,3,4,5,8, & 14)
(Bolts (part 9) not shown)

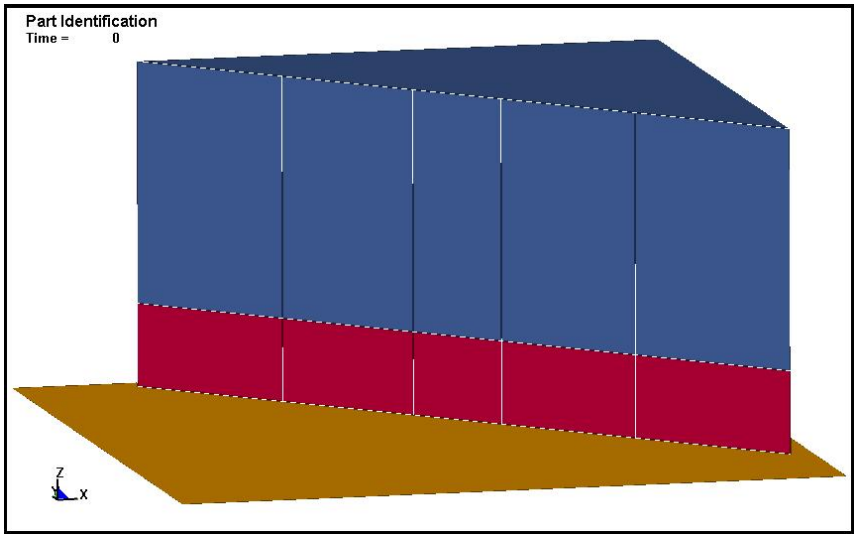

(C) Impact Limiters & Ground
(Parts 6, 7, & 17)

Figure 2.12.5-5 – LS-DYNA Model Components

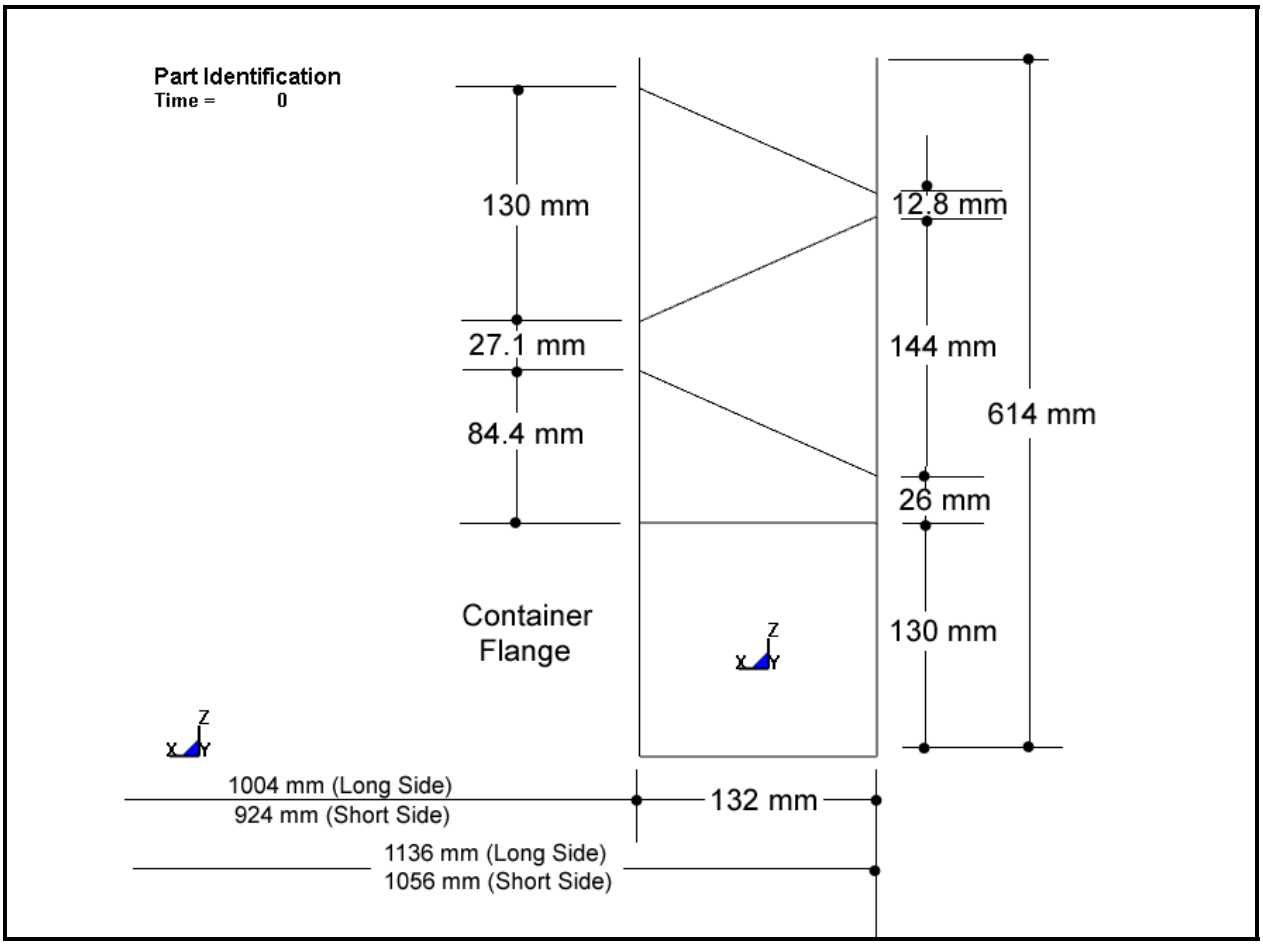

Figure 2.12.5-6 – LS-DYNA Model - Side View of Container with Modeled Dimensions

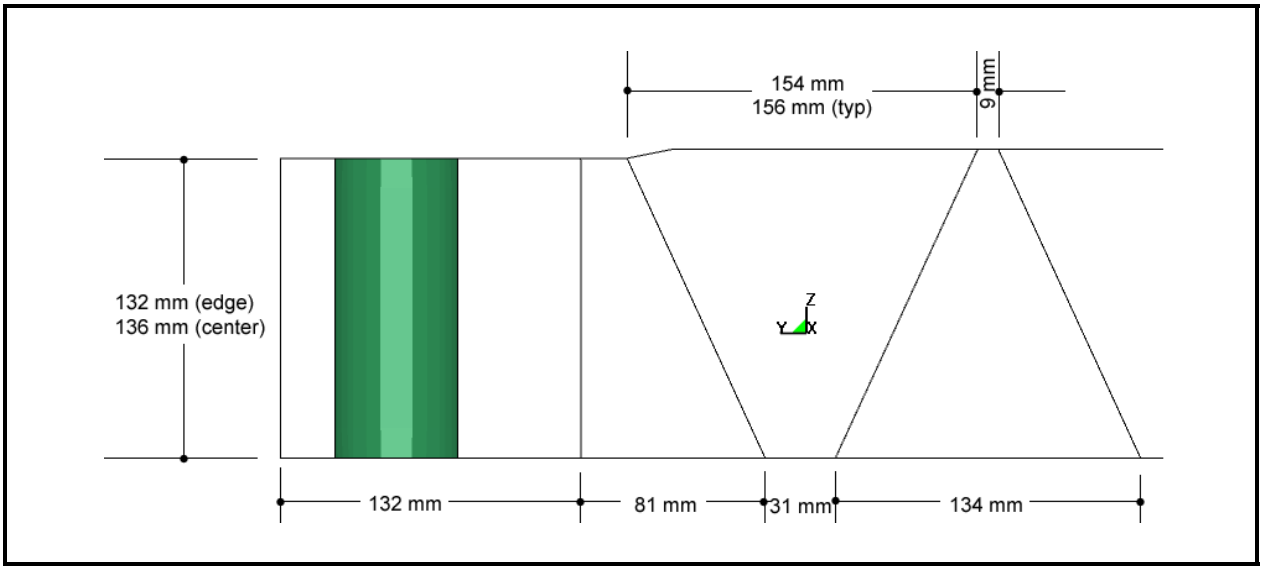

Figure 2.12.5-7 – LS-DYNA Model – Section Through Lid With Modeled Dimensions

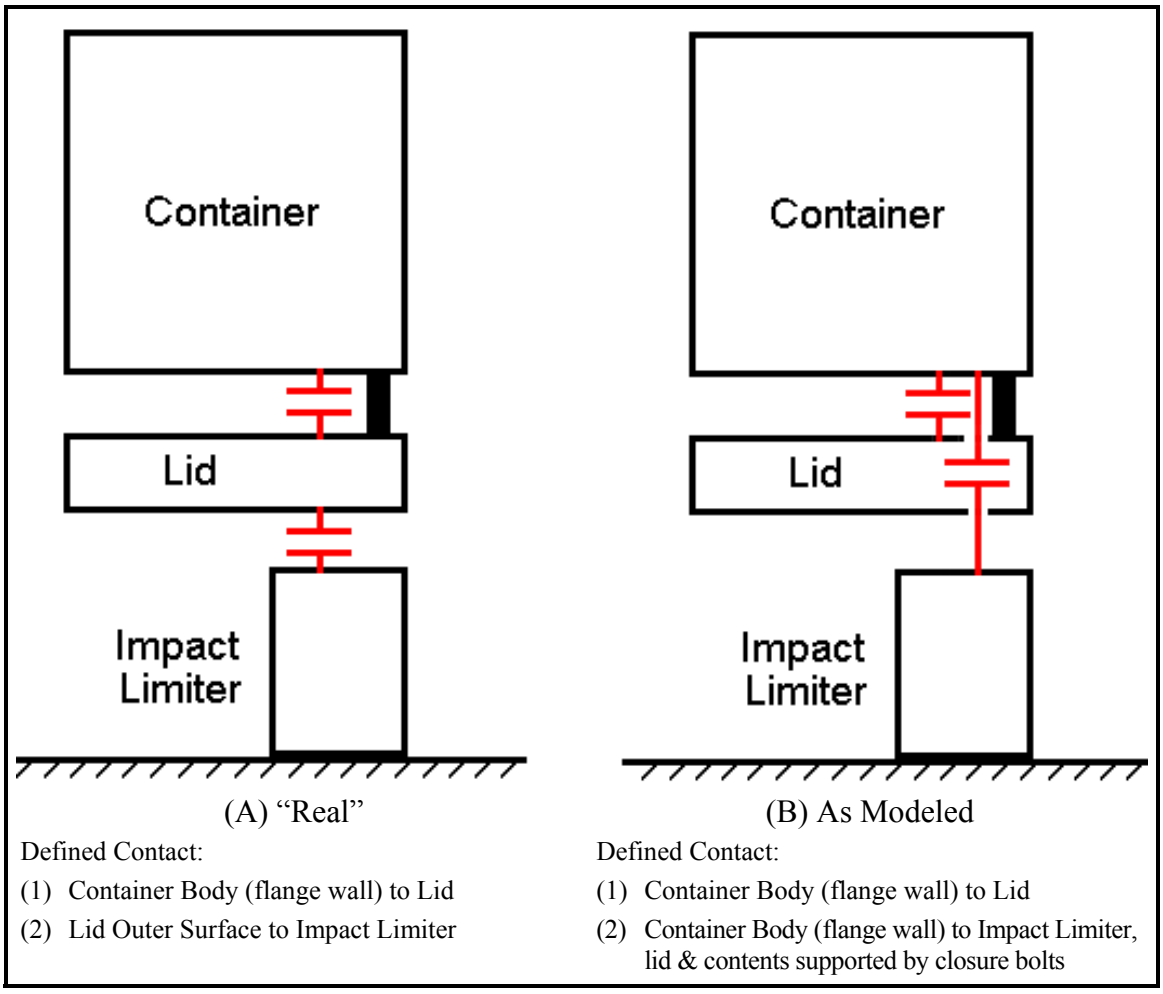

(A) "Real"

Defined Contact:

(1) Container Body (flange wall) to Lid

(2) Lid Outer Surface to Impact Limiter

(B) As Modeled

Defined Contact:

(1) Container Body (flange wall) to Lid

(2) Container Body (flange wall) to Impact Limiter, lid & contents supported by closure bolts

Figure 2.12.5-8 – Contact Definitions

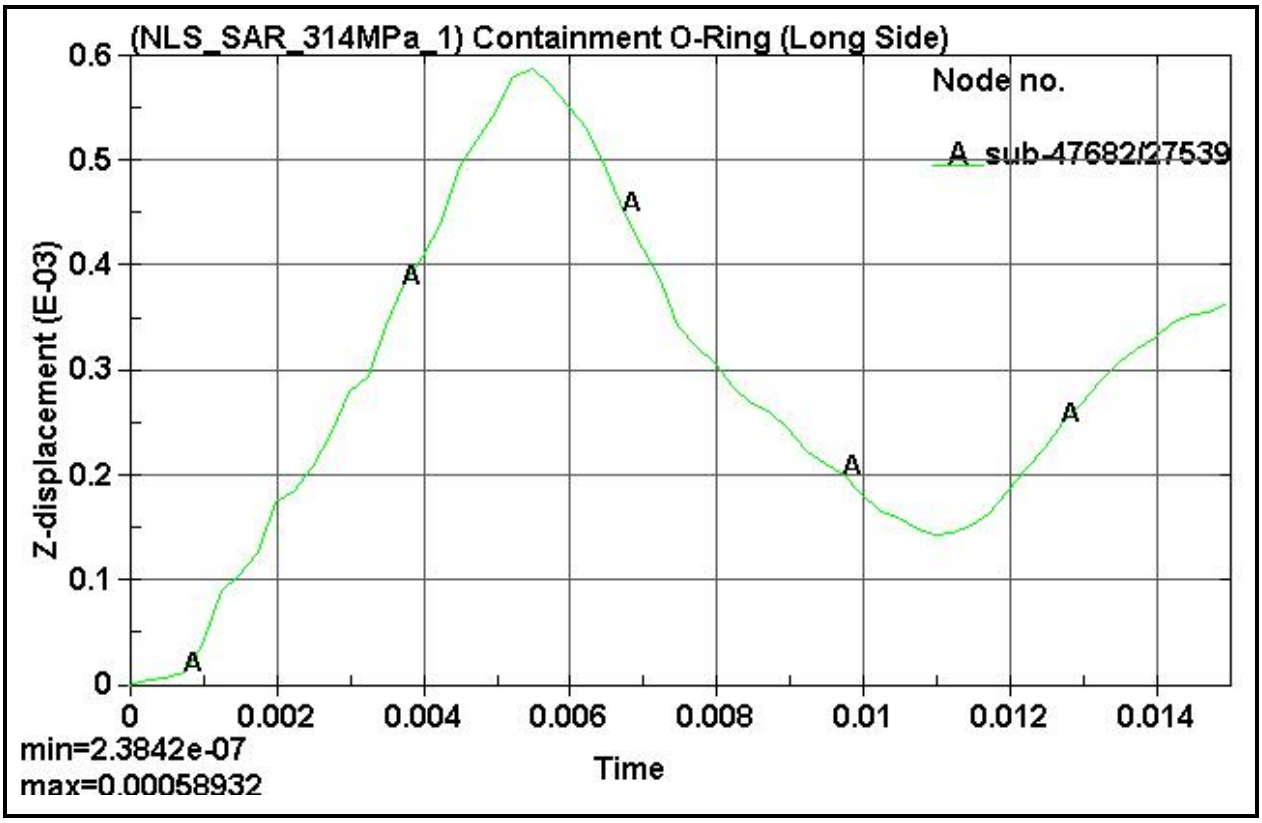

Figure 2.12.5-9 – Transient Maximum Relative Displacement at the Containment O-ring

2.12.5.6 Finite Element Side Drop Analysis

In the horizontal, side-down HAC free drop orientation, the CSA sidewall is loaded as a membrane by its own weight and the weight of the payload. As the sidewall deflects under load, a small rotation of the body flange occurs relative to the closure lid. Note that this side orientation is the inverse of the vertical, lid-down case, in which the closure lid flange rotated relative to an essentially undeformed body flange (see Section 2.12.5.5, *Finite Element End Drop Analysis*). Here, the body flange rotates relative to an essentially undeformed closure lid flange. In both cases, the pivot point of contact between the two flanges is at the outside edge of the flanges. Similar to the end drop case, the containment O-ring seal, located in the lid near the inner edge of the flange, briefly separates from the body flange. A fully elastic, quasi-static finite element model using ANSYS® Version 8.0 was used to evaluate the body flange rotation. The purpose of the analysis was to establish the maximum relative motion which will occur at the debris shield under the cold side drop impact. This data point serves as input to the design of the debris shield.

The body flange rotation was determined using a half symmetry model of the CSA as shown in Figure 2.12.5-9 and Figure 2.12.5-10. The closure lid was not modeled. Since the presence of the lid, attached by the closure bolts, would have the effect of reducing body flange rotation, its absence was conservative. The model used a combination of shell and beam elements to approximate the CSA wall stiffness. The walls of the model used shell elements having a thickness which gave the same bending stiffness as the CSA inner and outer sheets. The model walls were placed on the CSA wall centerplane locations. The stiffness of the V-stiffeners was added to the model by means of beam elements having the bending stiffness of a V-stiffener, placed at the stiffener locations in the walls. The body flange was also modeled as shell elements based on the calculated bending stiffness of the actual body flange. The resulting FEA model correctly models the CSA stiffness and permits a determination of the deformation of the body flange under the applied impact loading. Stresses are not evaluated since this orientation was physically tested in the certification test program as discussed in Section 2.12.3, *Certification Test Results*, and since only a design input value for the debris shield is required. The use of an elastic model is justified based on the results of the testing, which showed no inelastic behavior of the side wall (see Section 2.12.3.8.2, *CTU Measurements*.) The stiffness of the debris shield and guide bars was conservatively neglected in the model, but their weight was included.

The CSA wall, flange, and V-stiffener stiffness and equivalent element properties were calculated as follows. First, the wall bending moment of inertia was calculated for one V-stiffener span including the V-stiffener. A second calculation of the moment of inertia was made, excluding the V-stiffener. The difference between the two results was the moment of inertia of the V-stiffener itself. A set of calculations was performed for both the side and back walls, since the V-stiffener design and pitch of the stiffeners is slightly different. The equivalent thickness of the model wall shell elements is found by equating the moment of inertia of a solid plate over the V-stiffener pitch width to the moment of inertia of the wall excluding the V-stiffener, or:

$$\frac{b \times t_{eq}^3}{12} = I_{ev}$$

where b is the V-stiffener pitch, I_{ev} is the moment of inertia excluding the V-stiffener, and t_{eq} is the shell element thickness. Solving for t_{eq}:

$$t_{eq} = \sqrt[3]{\frac{I_{ev} \times 12}{b}}$$

The calculations for the side wall, back wall, and flange are summarized in Table 2.12.5-5, using information in Figure 2.12.5-11, Figure 2.12.5-12, and Figure 2.12.5-13.

The model has symmetry boundary conditions in the y-z plane. The three edges nearest the ground (back, side, and flange) are restrained in the vertical y-direction. Full support of the front flange at the open end is conservative for the purposes of determining flange rotation, since any motion of the flange perpendicular to the ground would reduce the amount of rotation. The back lower edge is also restrained in the axial z-direction for model stability. The model impact surface (CSA large external side) is supported by a 1.0 MPa pressure to simulate the partial support of the 0.10 kg/dm^3 polyurethane foam underneath. From Table 2.2-5, the 0.10 kg/dm^3 foam has an initial crush strength of approximately 1.0 MPa.

The weight of the CSA of 6,786 kg (3,393 kg in half symmetry) is evenly distributed over the model elements[2]. A pseudo-density is calculated based on the weight and the model volume, and which is then acted on by the impact acceleration. The weight of the payload of 5,175 kg (2,588 kg in half symmetry) is evenly distributed over the elements on the lower side wall, and is additive to the self-weight of the lower side wall. The weight of the overpack skin and puncture-resistant plate which are supported by the upper side wall is added to the model upper side wall elements. (The weight of the 0.10 kg/dm^3 polyurethane foam and of the balsa wood on the top wall is negligible.) The specific weight added to the elements (386 kg) is based on the model wall length and width dimensions, the steel plate thicknesses of 10mm and 6mm, and a density of 7.89 kg/dm^3.

The model is loaded with a 172 kPa internal pressure and an acceleration of 407g, as measured in the HAC cold flat side drop (LD3). The model is elastic, using a modulus of elasticity at -29 ºC of 19.8(10^4) MPa from Table 2.2-1 and a Poisson's ratio of 0.3.

The resulting maximum rotation of the body flange was equal to 0.02003 radians, located at the center of the lower body flange as shown in Figure 2.12.5-14. The maximum deflection of the side wall was 16.4 mm (shown in Figure 2.12.5-15 as 0.647 inches). Since the width of the body flange is 140 mm, and the distance from the inner surface of the CSA and the center of the debris shield is 13 mm, the transient motion which must be accommodated by the debris shield in a maximum-impact side drop is:

$$Z_{DS-Side} = 0.02003 \times (140 + 13) = 3 \text{ mm}$$

For establishment of the debris shield design criteria, $Z_{DS\text{-}Side}$ governs over the value $Z_{DS\text{-}End}$ = 0.78 mm calculated above in Section 2.12.5.5, *Finite Element End Drop Analysis*.

Input and output files for this computer run are included on a DVD attached to this appendix.

[2] The CSA weight used in this analysis is 396 kg greater than the weight of 6,390 kg used in the end drop analysis (see Section 2.12.5.5, *Finite Element End Drop Analysis*). This difference is equal to the weight of the debris shield and guide bars. That weight was not included in the end drop analysis because it would not affect the closure lid behavior, but was included here because it would affect side wall behavior.

Table 2.12.5-5 – Shell Element Calculation Results

	Side Wall	Back Wall	Body Flange
V- stiffener pitch or width, b, mm	164	165	145
I_{wv}, mm^4	$13.186(10^6)$	$13.290(10^6)$	
I_{ev}, mm^4	$11.451(10^6)$	$11.521(10^6)$	
I_{vr}, mm^4	$1.735(10^6)$	$1.769(10^6)$	
I_{Flange}, mm^4			$20.412(10^6)$
t_{eq}, mm	94.3	94.3	119.1

Note: The smaller side wall V- stiffener moment of inertia, $I_{vr} = 1.735(10^6)$ mm^4, is conservatively used for all V- stiffeners.

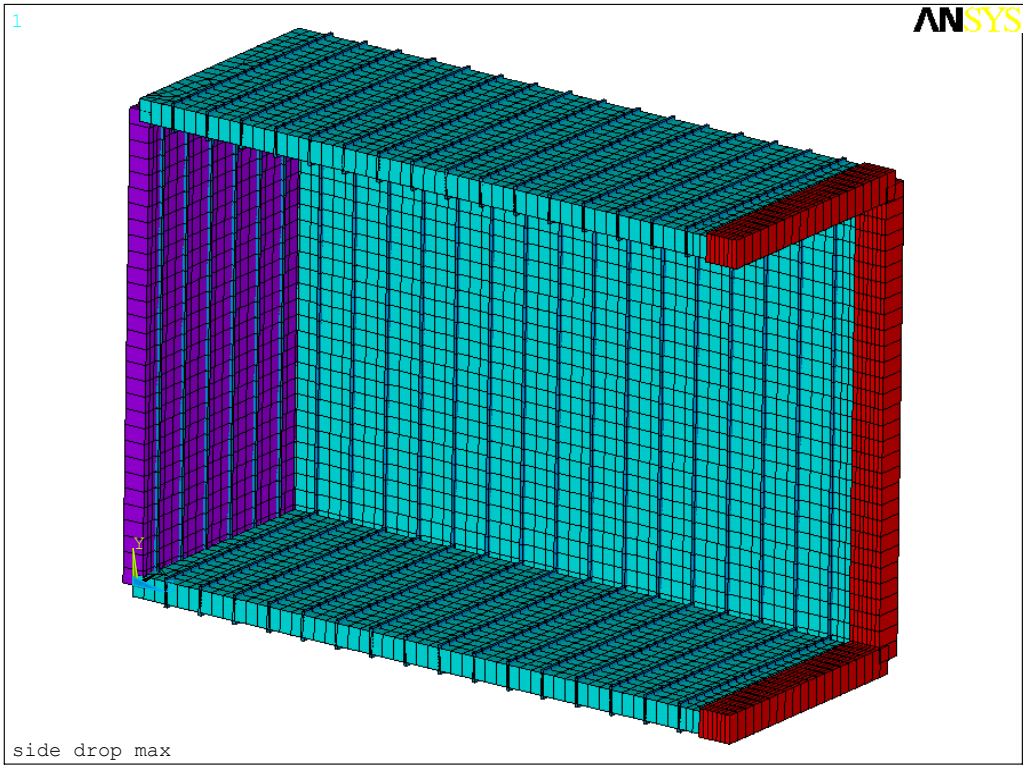

Figure 2.12.5-9 – Half Symmetry Model of the CSA Body Showing Thickness

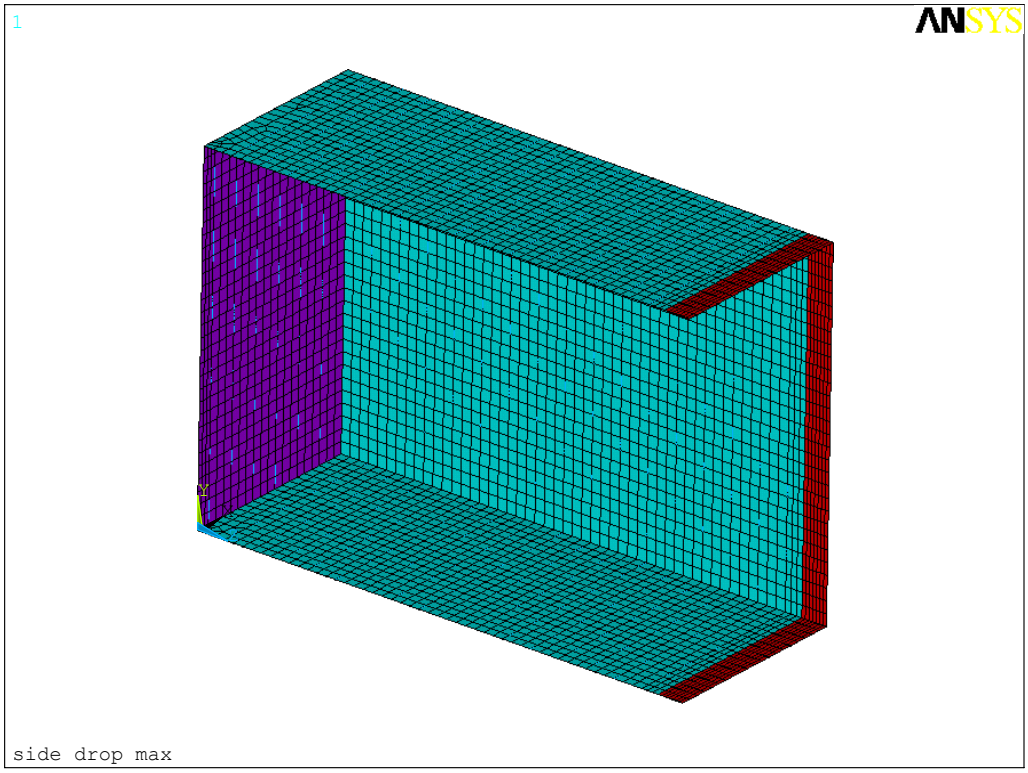

Figure 2.12.5-10 – Model of the CSA Body, Element Plot

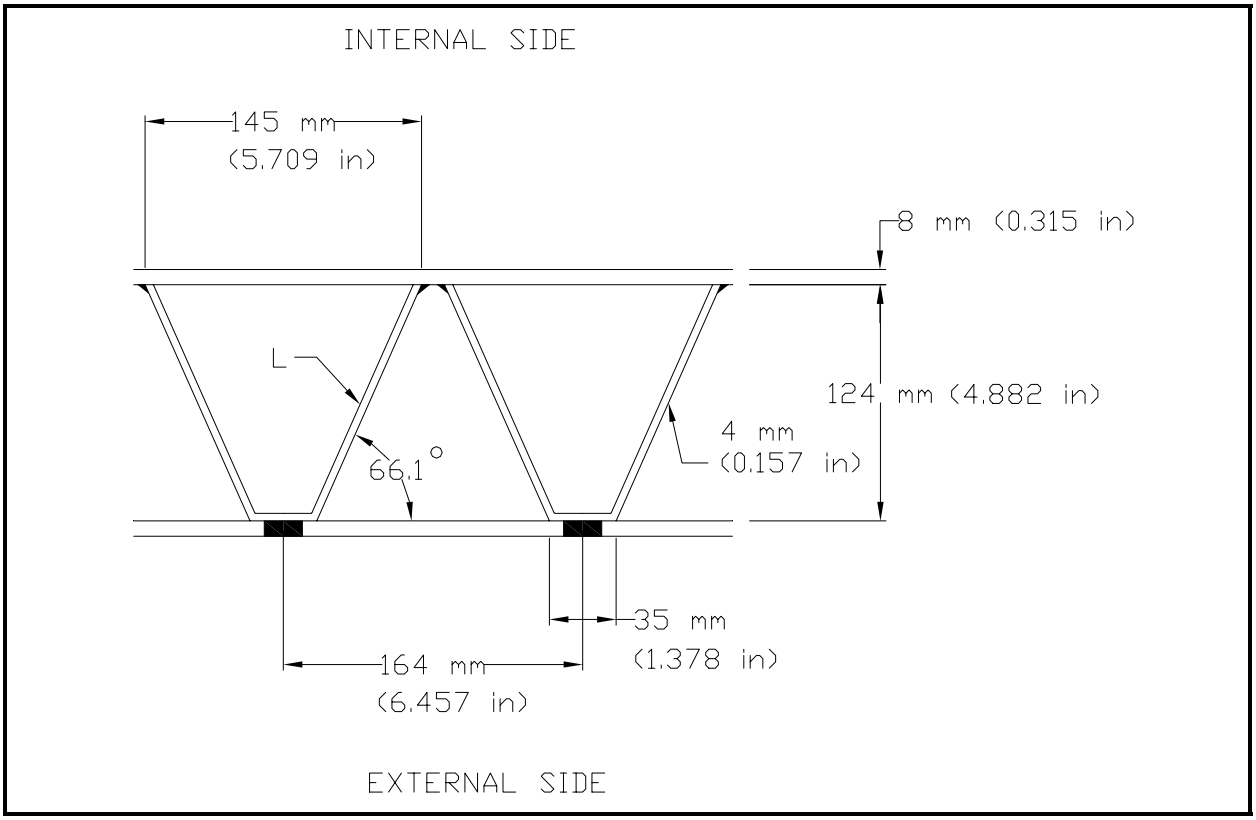

Figure 2.12.5-11 – Side Wall Cross-section Details

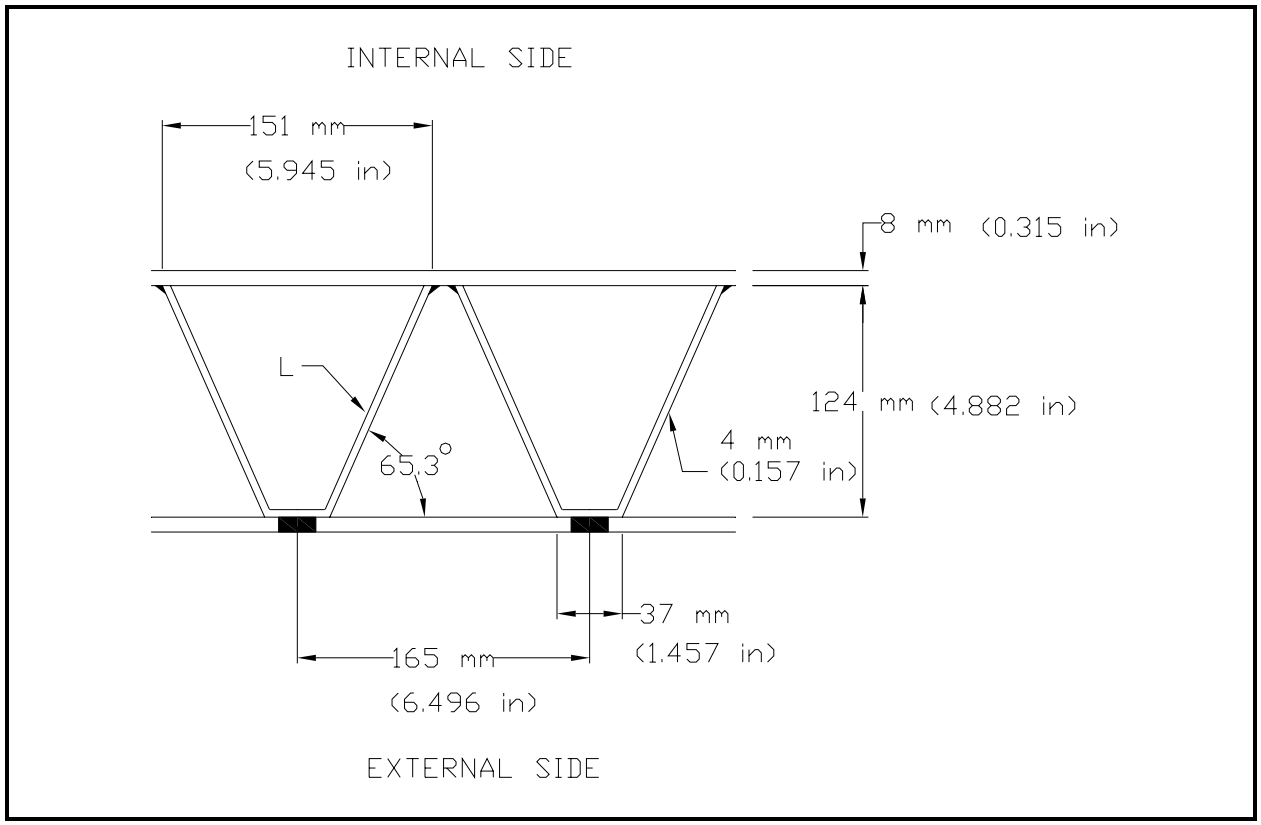

Figure 2.12.5-12 – Back Wall Cross-section Details

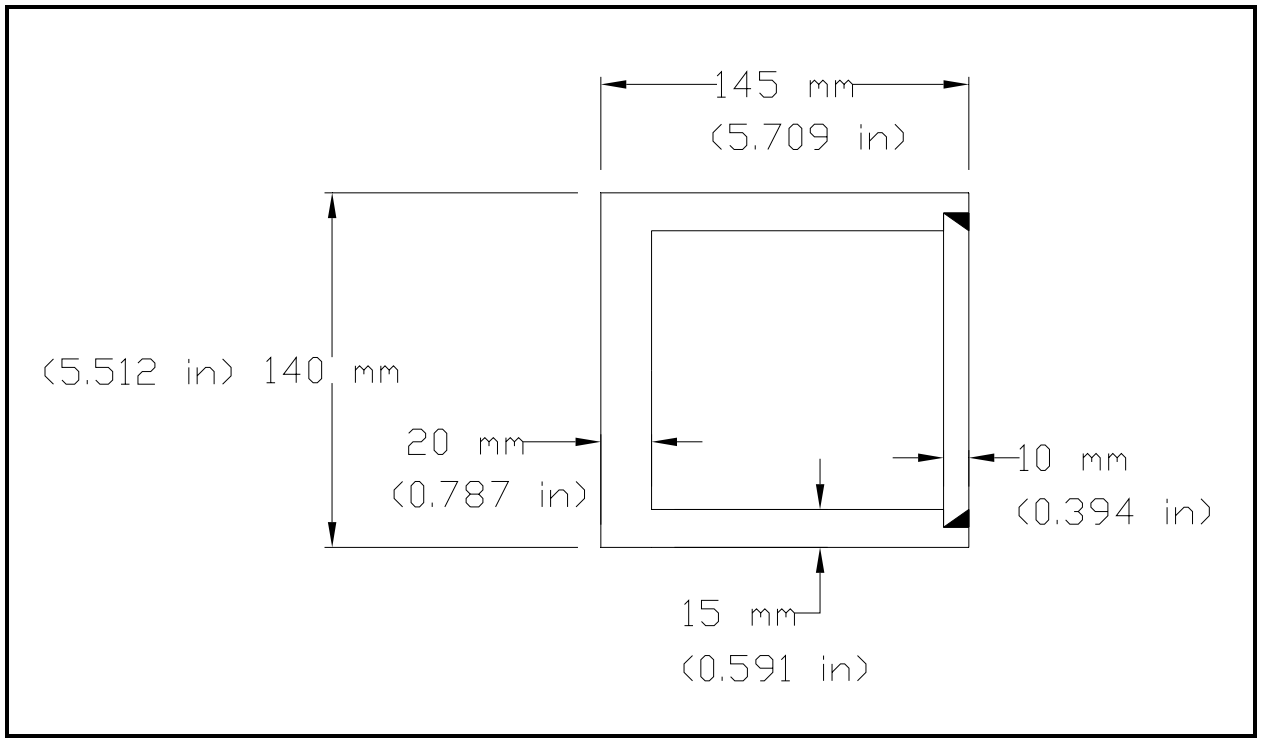

Figure 2.12.5-13 – Flange Cross-section Details

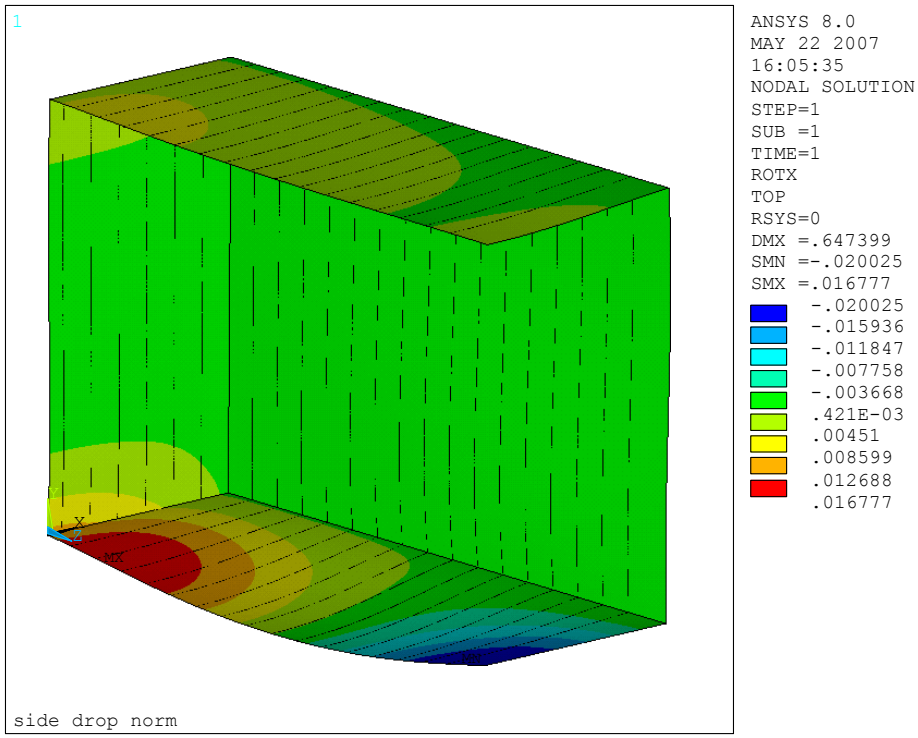

Figure 2.12.5-14 –Flange Rotation (ROTX, Radians)

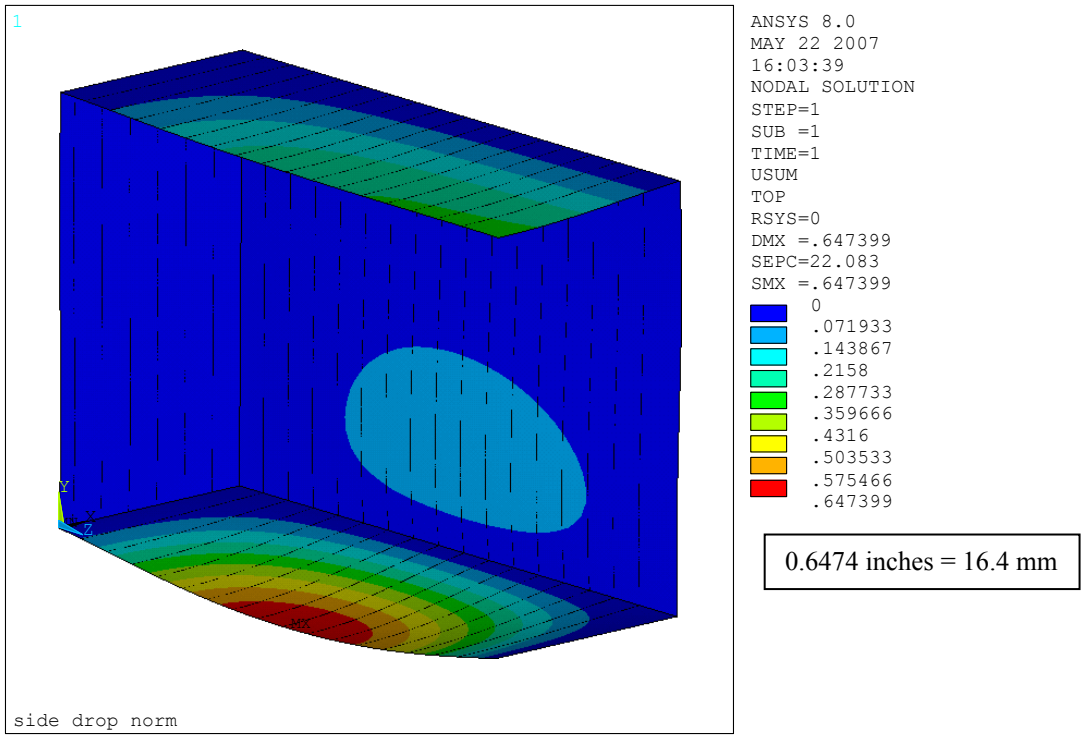

Figure 2.12.5-15 – Maximum Side Wall Displacement, Inches/mm

2.12.5.7 Finite Element Payload Interaction Analysis

The presence of the debris shield on the inside surface of the CSA body flange creates the potential for permanent deformation of the flange sealing surface due to locally high loads being applied by the payload in the HAC free drop. The analysis presented in this section demonstrates that any permanent deformations of the sealing surfaces are negligible in the worst-case interaction between the payload and the CSA.

Due to the design and placement of the guide bars, the SLB2 payload container cannot become trapped behind the debris shield, and consequently, cannot apply any axial impact loads to the debris shield. The only direction from which significant loads are applied to the debris shield and guide bars is from the side (i.e., perpendicular to the plane of the CSA wall). This analysis evaluates the response of the debris shield, guide bars, and body flange when impacted by a maximum-weight SLB2 in the cold side drop impact. Note that this analysis is focused on the potential for containment O-ring compression reduction as a result of the concentrated forces on the guide bars and debris shield. By inspection of Figure 2.12.5-1, a compressive load on the debris shield could, at most, deform the receptacle 'c-section' toward a closed position. This would tend to compress the debris shield foam rubber insert, which would not inhibit the function of the debris shield. Therefore, the function of the debris shield cannot be affected by payload interactions.

There are three guide bars on each TRUPACT–III side wall, located to coincide with the bumpers on the SLB2 container. In a side drop, the bumpers will contact the guide bars. Since the SLB2 wall section is relatively thin, it will deform under impact, and some load could be carried by the containment wall in between the guide bars. In this analysis, however, it is assumed that all of the SLB2 inertia load is carried only by the bars, thus conservatively concentrating the load. The maximum weight of a SLB2 is 4,763 kg. Since the measured impact in the cold, flat side impact in the certification test LD3 was 407g, the maximum impact load is:

$$F = 4{,}763 \times 407 \times 9.81 = 19.017\left(10^6\right) \text{N}$$

Since each bumper is 2,743.2 mm long and 38.1 mm wide (108 inches by 1.5 inches), the uniform pressure on the guide bars is:

$$P = \frac{F}{2{,}743.2 \times 38.1 \times 3} = 60.651 \text{ MPa}$$

Since the bumpers are tubes made of mild carbon steel having a wall thickness of only 1.5 mm (0.06 inches), they will deform under loading, and the uniform load distribution is justified. Conservatively, the analysis assumed a pressure loading of 68.95 MPa (10,000 psi).

The finite element model was built using ANSYS® Version 8.0 and is shown in Figure 2.12.5-16 and Figure 2.12.5-17. The model is built with symmetry: one longitudinal edge is at the center of a guide bar, and the opposite longitudinal edge coincides with the center of the span between two adjacent guide bars. Since the guide bars are separated by 17 inches, the model is 8.5 inches wide. The flange face is included at one end of the model, and the other end extends towards the rear of the package by the distance of one full V-stiffener beyond the rear edge of the flange. Note that the minimum flange face thickness of 20 mm was conservatively used (other dimensions are nominal). Conservatively, the stiff bolting boss located in the flange is omitted from the model. Since the closure lid does not affect the loading of the flange by the payload,

the closure lid is also omitted. However, a rigid lid closure flange is assumed in calculating the maximum reduction in containment O-ring compression as described below.

The model uses solid 3-D elements in conjunction with 3-D point to surface contact elements. The guide bar is fully separate from the flange, and conservatively not attached to the flange, inner sheet, or debris shield. It is held in place only by the symmetry constraints and the applied load. In practice, the guide bar is attached by fillet welds to the CSA side wall, but the successful omission of these welds in the model demonstrates that they are not structural in nature and do not need to be subject to stress limits. In a similar manner, the debris shield receptacle is not attached to the flange, except for two coupled nodes at the center span symmetry edge. These couples help the model solve while not interfering with the action of the debris shield at the loaded area of interest. Therefore, the debris shield welds are also non-structural. The V-stiffener is coupled to the inner sheet at both sides of the "v" to account for the fillet welds, while the base of the stiffener is coupled at the center of the flat to the outer sheet to account for the plug welds.

Both symmetry edges of the model have symmetry boundary conditions. The side of the model furthest from the flange face has constraints in the x-direction, which models the connection of the guide bar, inner, and outer sheets to the rest of the CSA walls. The flange face is free. The model is supported vertically in the y-direction. Two versions of support are used with different types of vertical support. Version A supports the model across the entire bottom surface including the flange and entire CSA outer sheet. Version B supports the model across the CSA outer sheet and flange back wall, but the bottom surface of the flange, including the bottom edge of the flange face, is free. The purpose of the two runs is to examine the difference between the two extreme cases of full flange support and no flange support. Free drop testing indicates that the flange is reasonably well supported in a side drop, but both extremes are conservatively investigated.

The 68.95 MPa pressure calculated above was applied to the top of the debris shield and guide bar. The pressure begins at the solid part of the debris shield and runs the entire length of the guide bar. Pressure is not applied above the open C-section of the debris shield since an insignificant load could be transferred down into the flange from this area due to plastic deformation of the C-section upper leg. (As discussed above, any such deformation would be in the direction to close the C-section, and would therefore not inhibit the function of the debris shield.) The width of the pressure application is 19 mm, which is equal to one half-symmetry width of the bumper of the SLB2. The loading is concentrated on the guide bars and on the debris shield in order to determine whether deleterious permanent plastic deformations of the CSA body flange could result.

Nonlinear true stress-strain properties for ASTM Type 304L (guide bars) and UNS S31803 stainless steel (debris shield and all other CSA components) is taken from Table 2.2-2 for a temperature of -29 ºC. The cold temperature corresponds to the maximum impact loading. That is the most critical condition, since with increasing temperature, the impact loading would fall faster than would the steel properties due to the stronger temperature dependence of polyurethane foam.

Allowable stress limits are developed using Table 2.1-1. Since the output stresses are in the form of true stress, the allowables must also have the same basis. For UNS S31803 steel, the last data point in Table 2.2-2 for -29 ºC corresponds to the minimum elongation (minimum ultimate strain) of 25%. Therefore, the true ultimate stress for UNS S31803 is 888.8 MPa. For ASTM Type 304L stainless steel, the linearly extrapolated engineering ultimate strength is 515.9 MPa, using values at 38 ºC and 93 ºC from Table 2.2-3. The minimum elongation (minimum ultimate strain) for Type 304L is 40%. The engineering ultimate strength was converted to true ultimate strength using:

$$S_{u-true} = S_{u-eng}\left(1 + e_{eng}\right) = 722.3 \text{ MPa}$$

where $S_{u\text{-}eng}$ = 515.9 MPa and e_{eng} = 0.40. From Table 2.1-1, the maximum primary stress intensity is limited to $0.9S_u$. (The membrane allowable stress is applicable primarily to pressure vessels and is not used here.) The allowable stresses therefore are:

	Stress Criteria	Allowable Stress
UNS S31803	0.9 × 888.8	799.9 MPa
ASTM Type 304L	0.9 × 722.3	650.1 MPa

The analysis was performed in two steps. First, the full quasi-static impact load was applied. From this run, maximum stresses and deflections were extracted, representing the transient maximum values during the impact event. A second load step was made with the load reduced to nearly zero (an approximately 1% load is required to maintain model stability since some parts are unconnected), representing the permanent deformation state of the components. These results were examined to find the maximum permanent variation in flatness of the body flange, measured between the most outwardly-deformed point anywhere on the flange (which serves to locate the flat closure lid flange surface) and the least outwardly-deformed point on a line which corresponds to the mating surface of the containment O-ring. This total difference is equal to the reduction in containment O-ring compression which would be expected to result from the worst-case interaction between the payload and the debris shield and guide bars. Note that this analysis does not purport to show the minimum state of O-ring compression under accident conditions. The leaktightness of the containment seal, in the absence of debris, was demonstrated by full-scale testing (see Section 2.12.3.8.1, *Leakage Rate Tests*). Instead, this analysis evaluates only the differential effect on O-ring compression of the interaction with the payload under HAC impact. It demonstrates that the presence of the debris shield and guide bars does not affect the leaktight capability of the TRUPACT–III.

Since the width across the lid from center-to-center of the containment O-ring groove is 1,888 mm, and the width of the CSA opening is 1,840 mm, the location of the containment O-ring mating line on the body flange, measured from the inner edge of the body flange, is:

$$(1{,}888 - 1{,}840)/2 = 24 \text{ mm}$$

Deformations perpendicular to the body flange face are in the model x-direction; outward-bulging deformations are negative. The maximum reduction in compression of the containment O-ring is therefore found using:

$$\left[\text{Greatest } (-x) \text{ deformation of the body flange surface}\right] \textit{ minus}$$

$$\left[\text{Least } (-x) \text{ deformation on a line 24 mm from flange top edge}\right]$$

Results are shown in Table 2.12.5-6 for Version A (fully supported flange) and in Table 2.12.5-7 for Version B (unsupported flange). Plots of stress intensity for each component for Version A are provided in Figure 2.12.5-18 to Figure 2.12.5-22, and for Version B in Figure 2.12.5-25 to Figure 2.12.5-29. Plots of the body flange face deformation for Version A are provided in Figure 2.12.5-23 (under full transient load) and Figure 2.12.5-24 (unloaded, post-impact), and for Version B in Figure 2.12.5-30 (under full transient load) and Figure 2.12.5-31 (unloaded, post-impact).

As shown in Table 2.12.5-6 and Table 2.12.5-7, a positive margin of safety on maximum stress exists in both cases, having a minimum value of +0.23. It is also noteworthy that the stresses in the debris shield and the body flange are elastic in nature, based on the engineering yield strength of UNS S31803 stainless steel, given in Table 2.2-1 as 448 MPa at a conservative temperature of 38 ºC. The flange components are here specified as the 20-mm thick flange front wall and the inner and outer, 15-mm thick flange plates. Only the guide bar and the inner CSA sheet behind the flange structure have stresses above the yield point (but below the nonlinear allowable stress), and the regions above yield are relatively small. This statement applies to both Version A and Version B.

Also shown in the tables is the maximum reduction of containment O-ring compression (column 4, lower half of table, labeled 'Net displacement, mm'). From Table 2.12.5-7 (Version B, unsupported flange), the reduction in the fully loaded transient condition was 0.07 mm, or only 0.58% in terms of the compression of the 12 mm diameter O-ring. In the unloaded, post-impact condition, the reduction was 0.0017 mm, which is equivalent to essentially no reduction in compression. These values are trivial with regard to the leaktight compression criteria determined in Section 2.12.2, *Elastomer O-ring Seal Performance Tests*.

Therefore, since the body flange stresses are elastic, and other nonlinear maximum stresses meet allowable stress criteria, and the maximum effect on O-ring compression is trivial, the interaction between the payload and the CSA is of no concern.

Input and output files for this computer run are included on a DVD attached to this appendix.

Table 2.12.5-6 – Version A (Fully Supported Flange)

Component	Maximum Stress Intensity, MPa	Allowable Stress, MPa	Margin of Safety
Debris Shield	311.2 *(elastic)*①	799.9	+1.57
Guide Bar	262.7	650.1	+1.47
Flange components	330.1 *(elastic)*①	799.9	+1.42
Inner and outer CSA sheets behind flange	471.2	799.9	+0.70
V-stiffener	650.2	799.9	+0.23
Loading Case	**Max overall displace-ment of flange face, mm**	**Min displacement of flange face at O-ring, mm**	**Net displace-ment, mm**
Full Transient Load	-0.06764	-0.00902	0.05862
Unloaded	-0.00115	-0.00061	0.00054

Notes:

1. Although the stress is elastic in this case, the inelastic stress criterion is applied for consistency with the rest of the model.

Table 2.12.5-7 – Version B (Unsupported Flange)

Component	Maximum Stress Intensity, MPa	Allowable Stress, MPa	Margin of Safety
Debris Shield	342.3① *(elastic)*②	799.9	+1.34
Guide Bar	261.2	650.1	+1.49
Flange components	381.3 *(elastic)*②	799.9	+1.10
Inner and outer CSA sheets behind flange	557.1	799.9	+0.44
V-stiffener	650.2	799.9	+0.23
Loading Case	**Max overall displacement of flange face, mm**	**Min displacement of flange face at O-ring, mm**	**Net displacement, mm**
Full Transient Load	-0.07206	-0.00153	0.07053
Unloaded	-0.00223	-0.00053	0.00170

Notes:

1. Coupled nodes for debris shield furthest from applied load are removed from the stress plot, since the local stresses at the coupled nodes are artificial.
2. Although the stress is elastic in this case, the inelastic stress criterion is applied for consistency with the rest of the model.

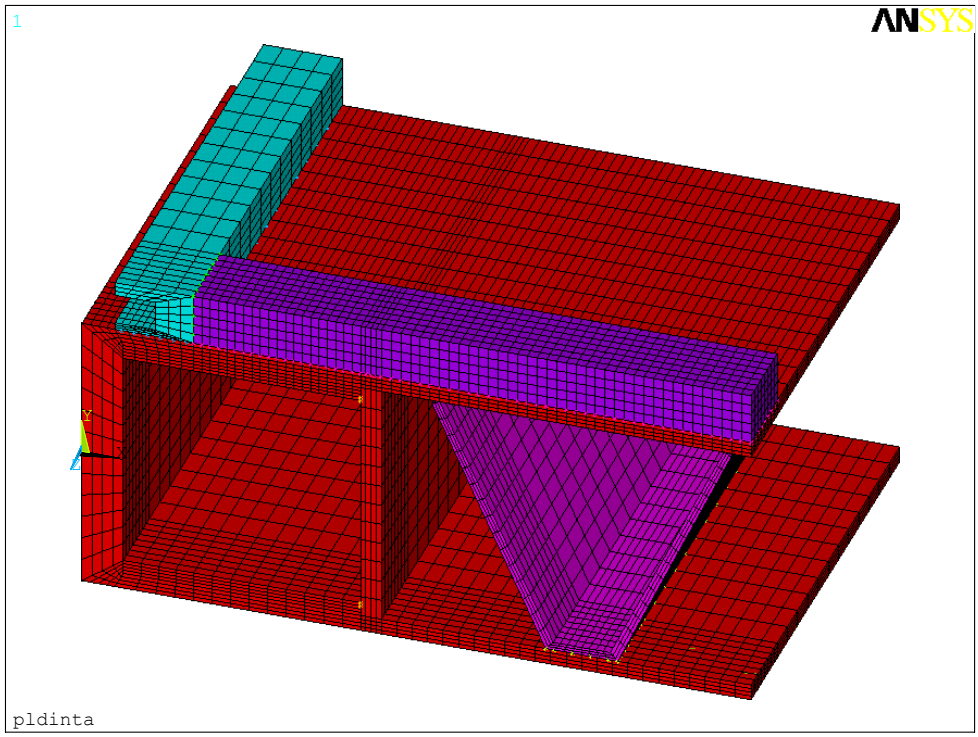

Figure 2.12.5-16 – Payload Interaction Model, Isometric Plot

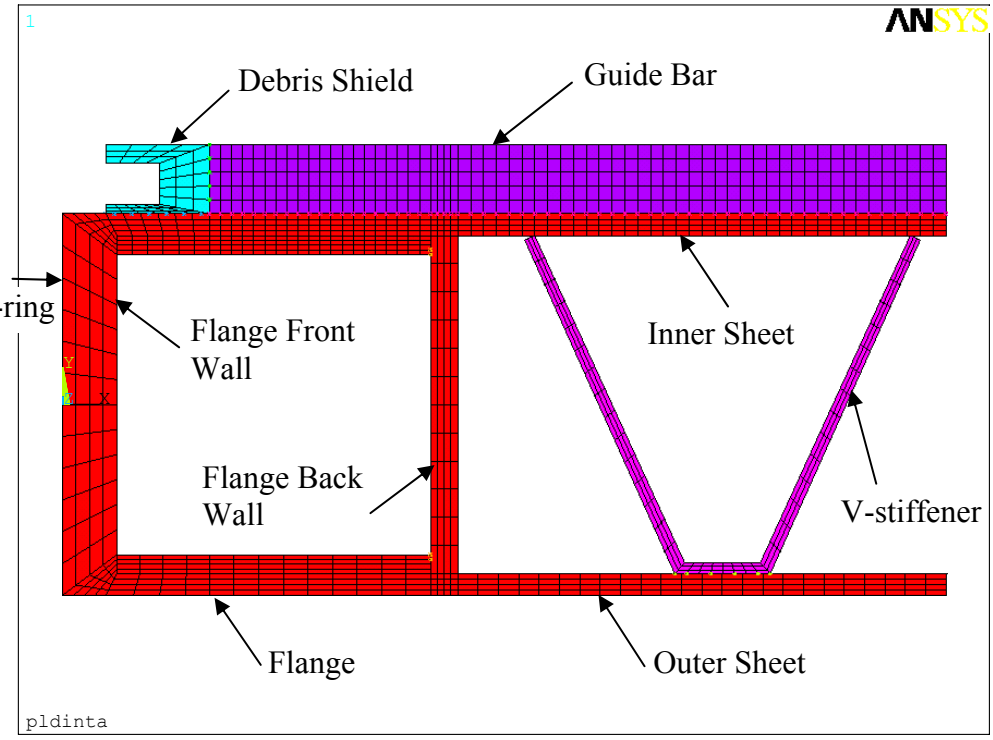

Figure 2.12.5-17 – Element Plot – Cross-section of Body Side Flange

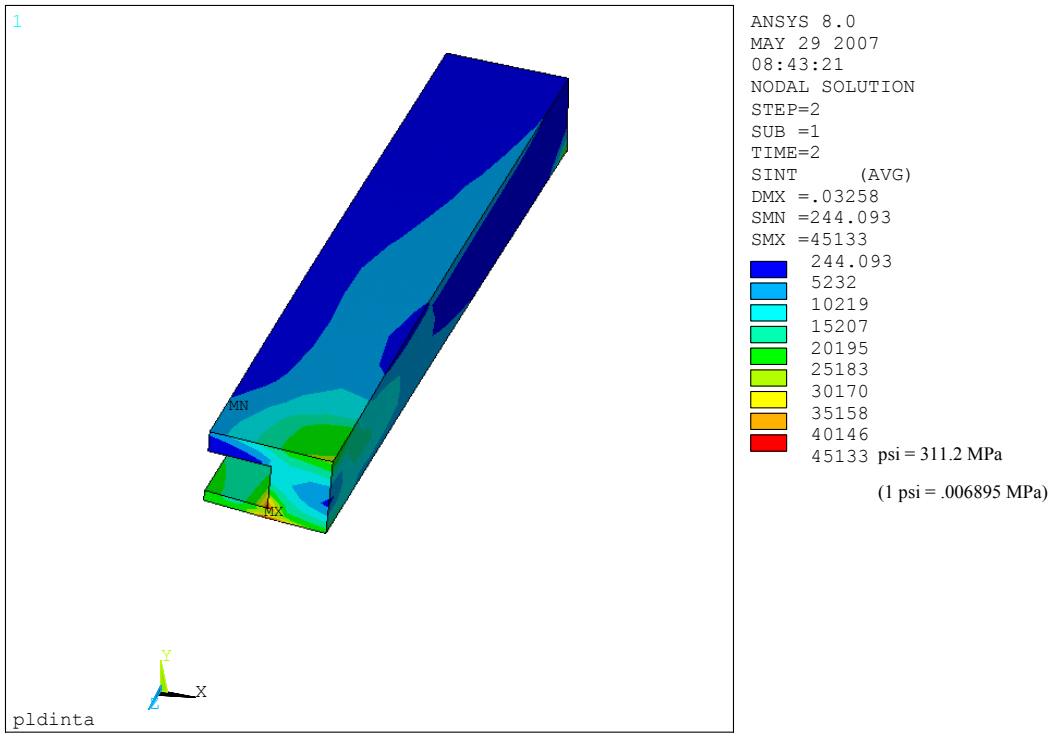

Figure 2.12.5-18 – Debris Shield Receptacle Stress Intensity, Version A

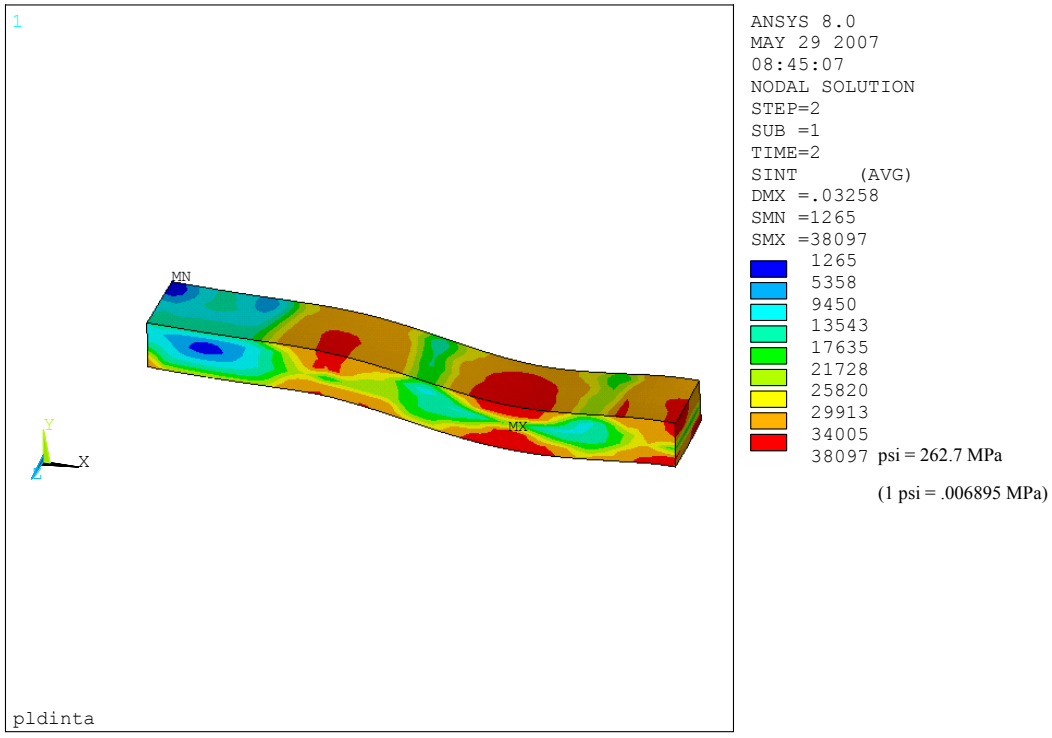

Figure 2.12.5-19 – Guide Bar Stress Intensity, Version A

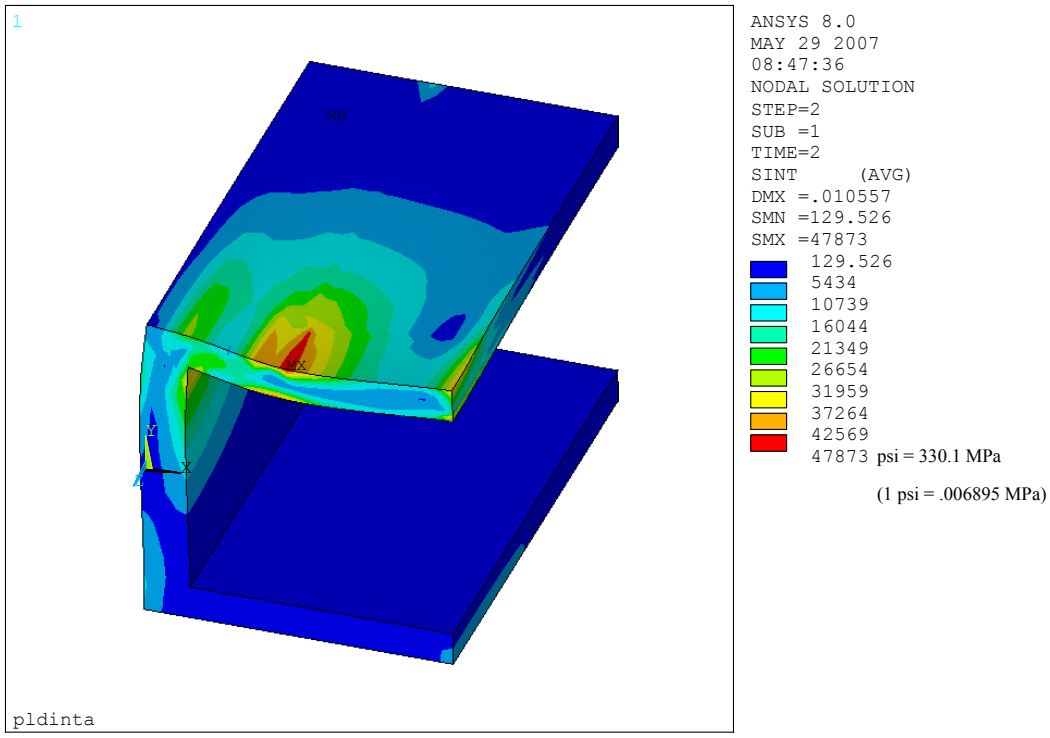

Figure 2.12.5-20 – Flange Component Stress Intensity, Version A

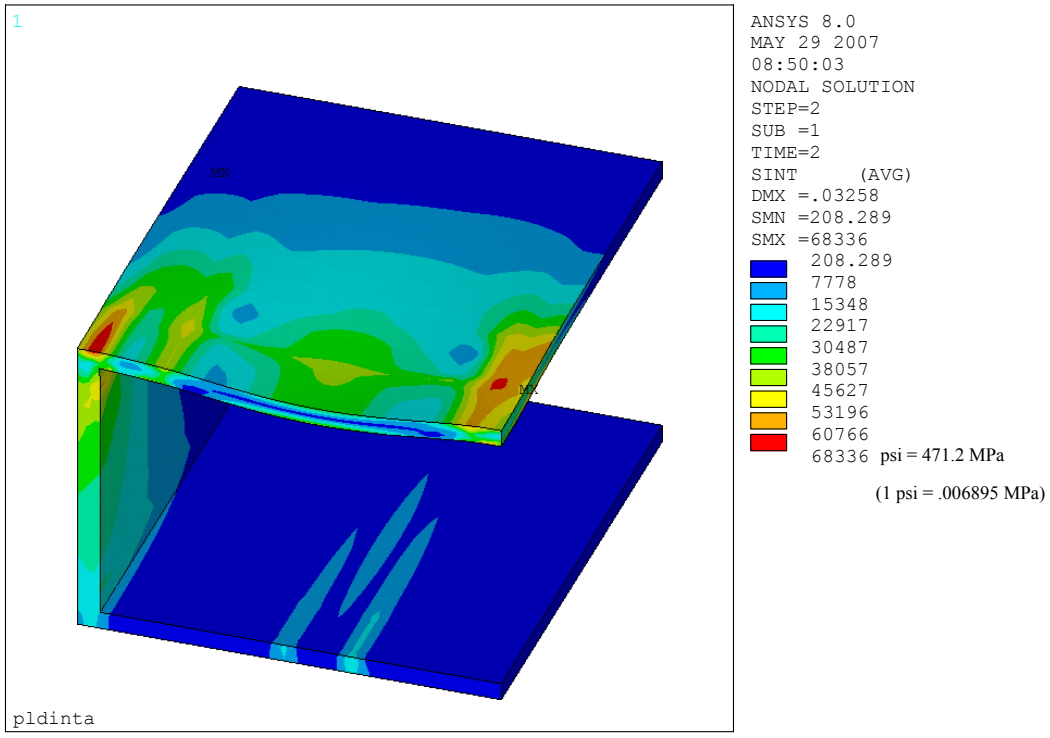

Figure 2.12.5-21 – Flange Rear Wall, Inner, and Outer Sheet Stress Intensity, Version A

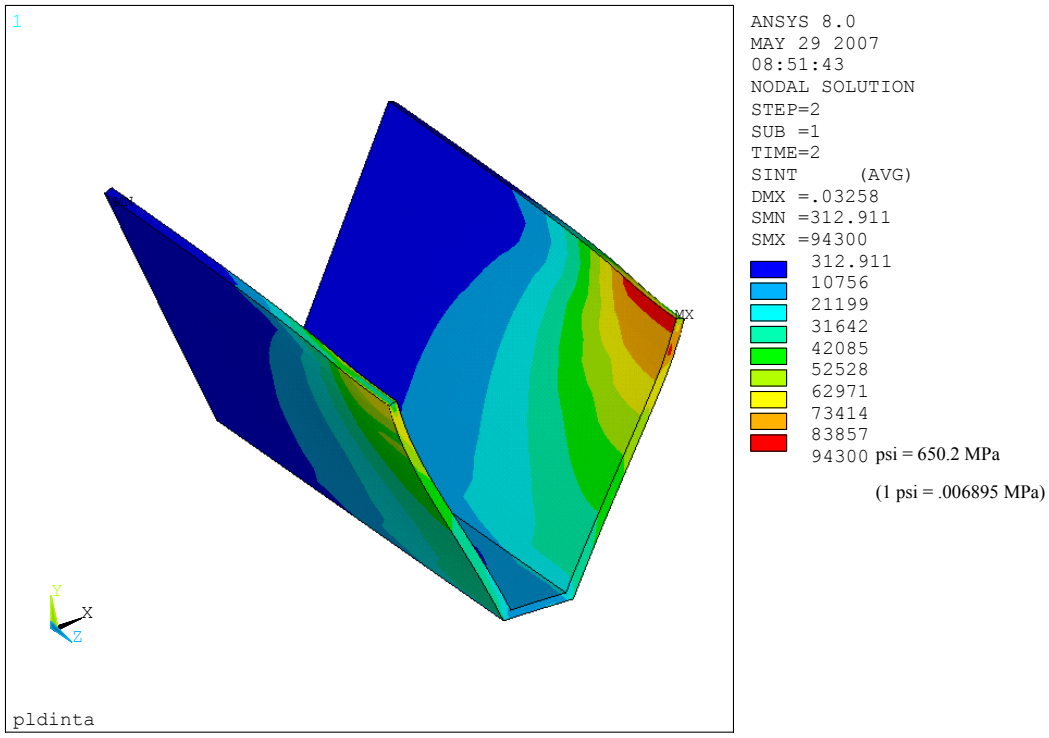

Figure 2.12.5-22 – V-stiffener Stress Intensity, Version A

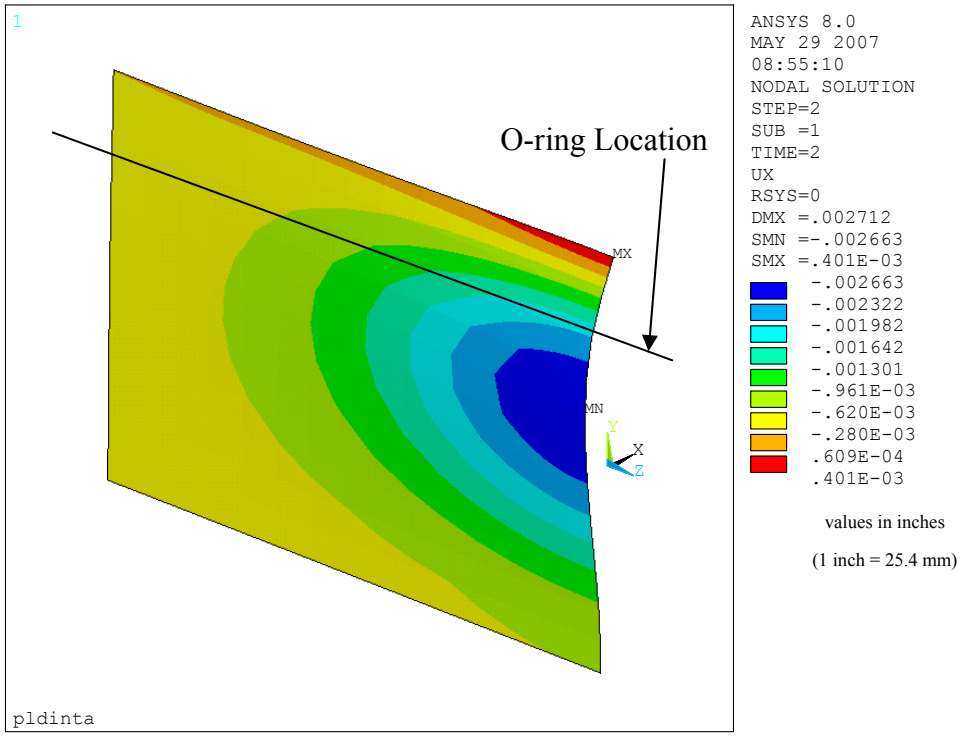

Figure 2.12.5-23 – Flange Face Deformation (Full Load), Version A

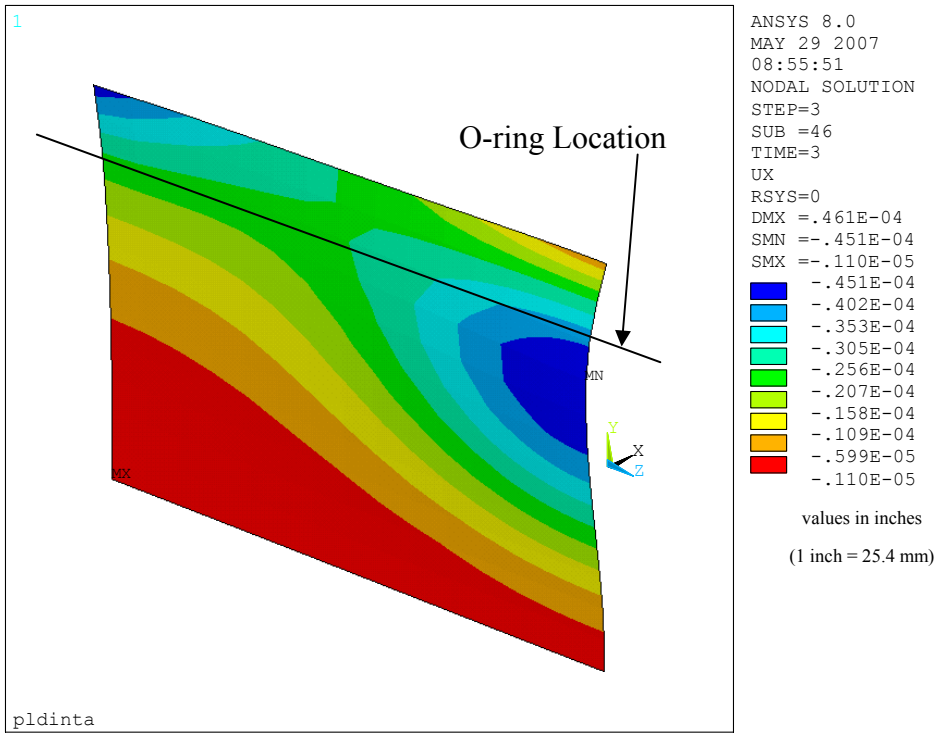

Figure 2.12.5-24 – Flange Face Deformation (Unloaded), Version A

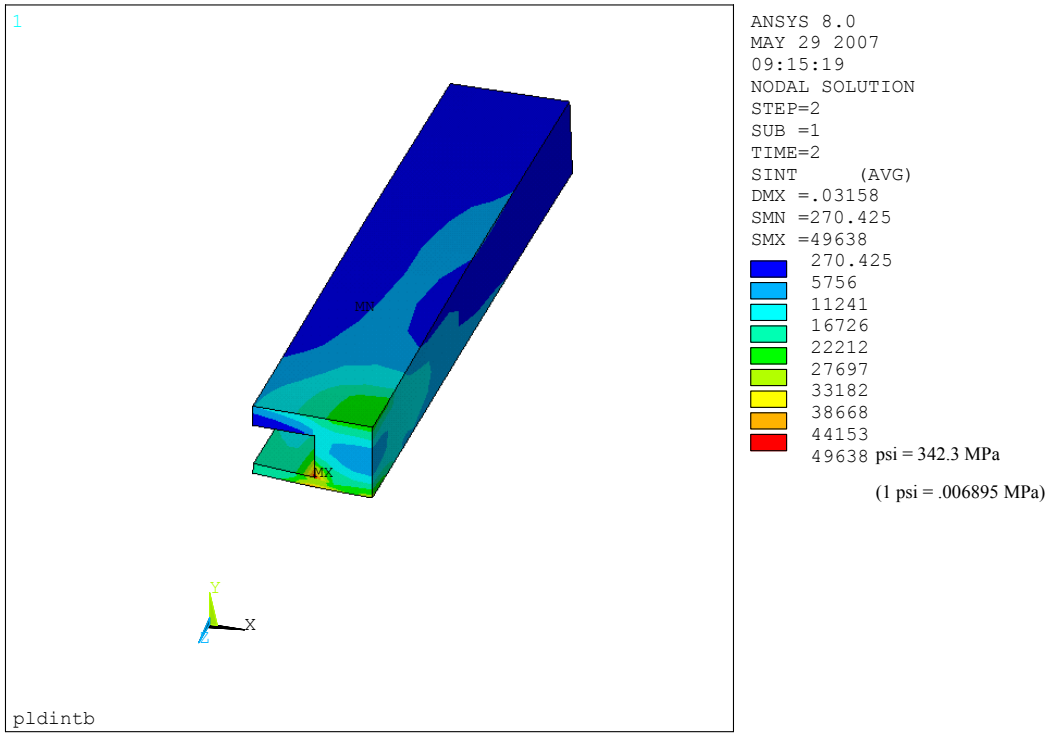

Figure 2.12.5-25 – Debris Shield Receptacle Stress Intensity, Version B

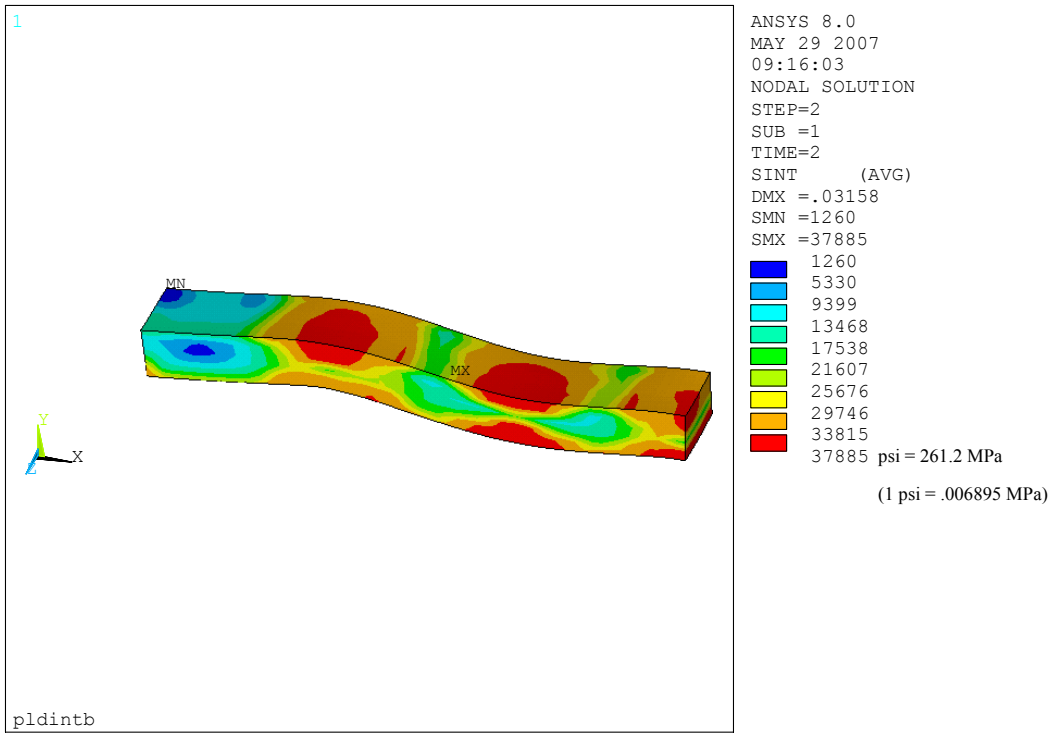

Figure 2.12.5-26 – Guide Bar Stress Intensity, Version B

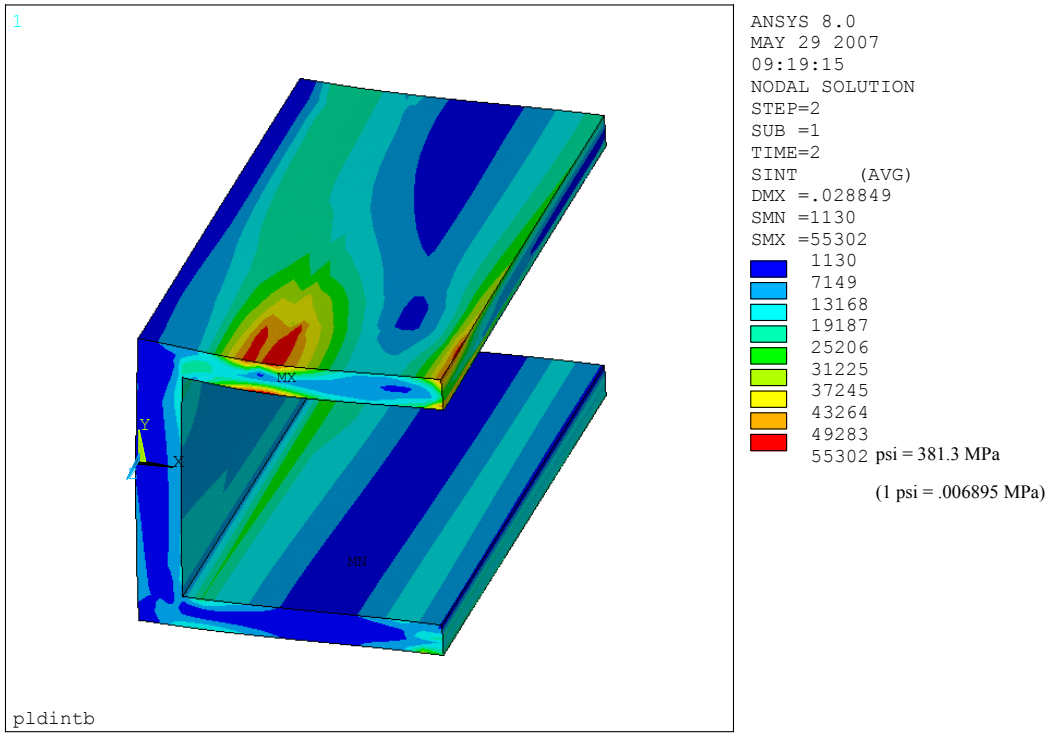

Figure 2.12.5-27 – Flange Component Stress Intensity, Version B

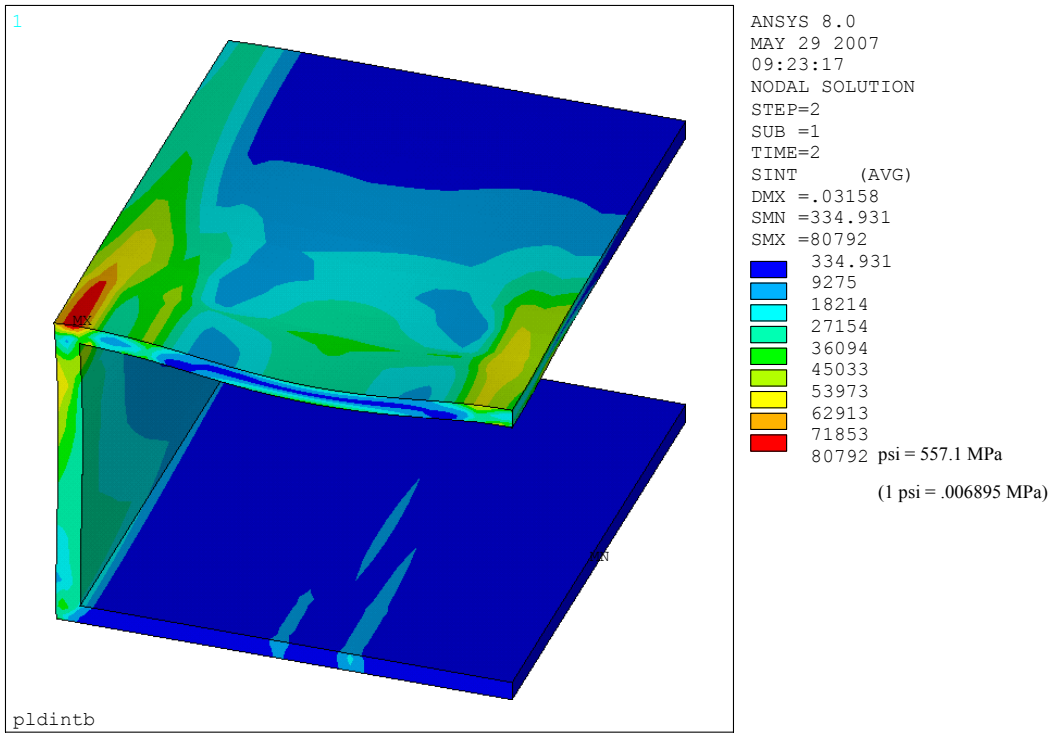

Figure 2.12.5-28 – Flange Rear Wall, Inner, and Outer Sheet Stress Intensity, Version B

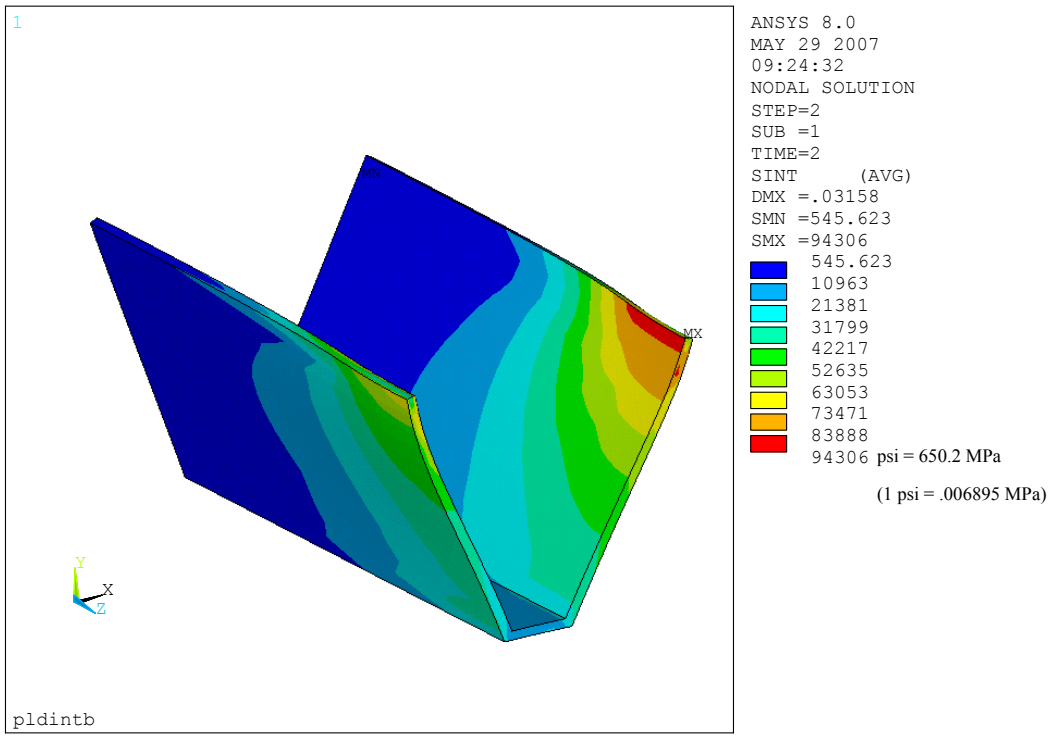

Figure 2.12.5-29 – V-stiffener Stress Intensity, Version B

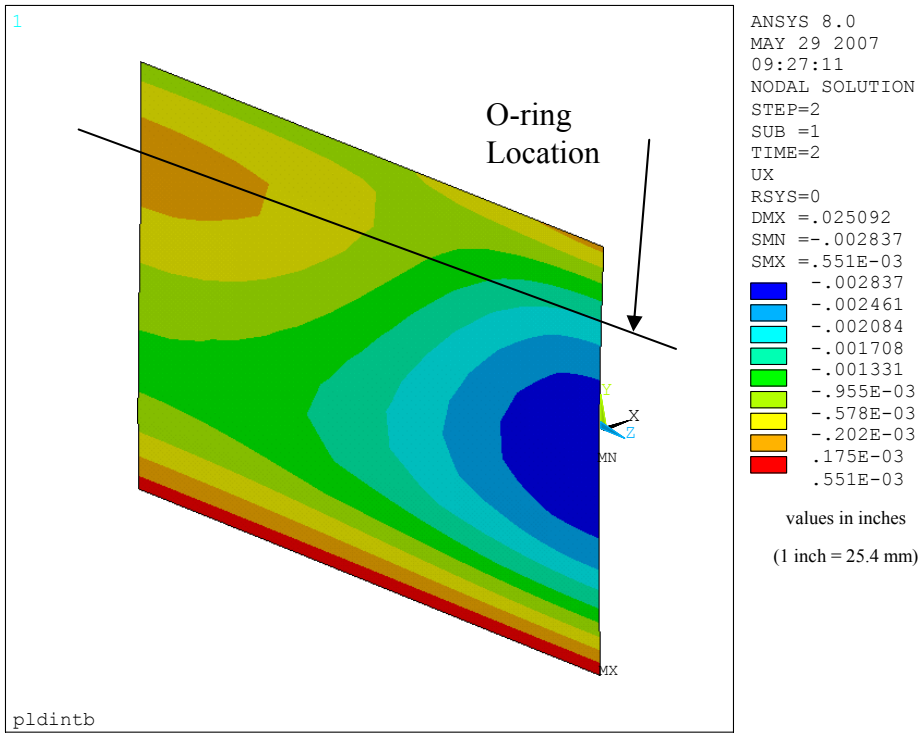

Figure 2.12.5-30 – Flange Face Deformation (Full Load), Version B

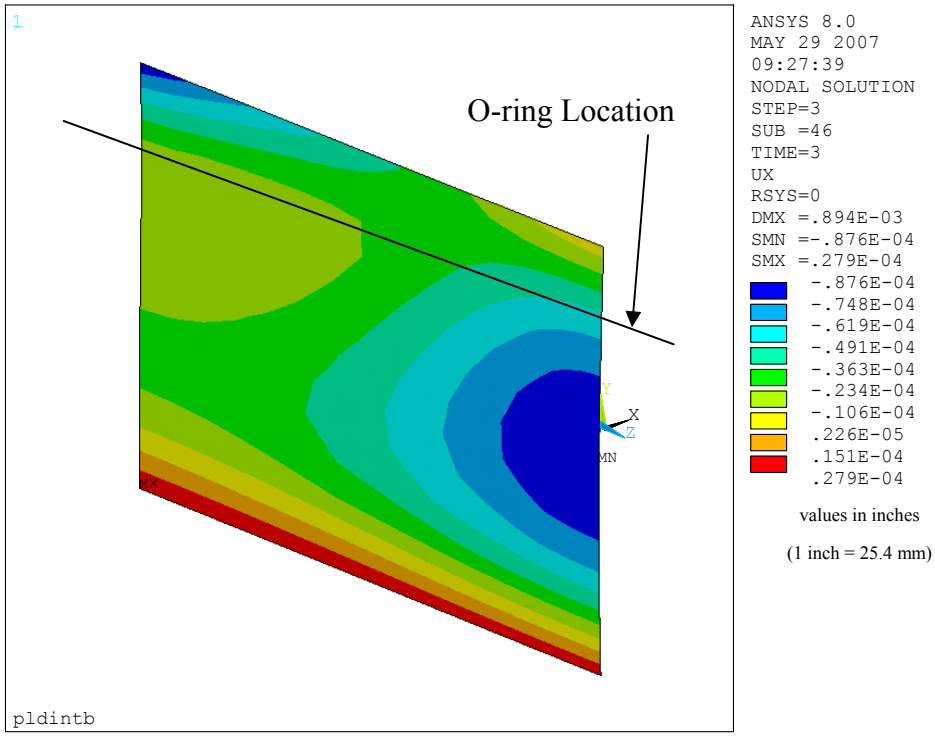

Figure 2.12.5-31 – Flange Face Deformation (Unloaded), Version B

2.12.6 Certification Tests on CTU-2

This appendix presents the results of supplementary tests that address the free drop and puncture test performance requirements of 10 CFR 71[1]. The test was performed using a written test plan[2] and procedure[3]. This appendix summarizes the information presented in the test report[4] for the second TRUPACT–III certification test unit (serial number CTU-2).

2.12.6.1 Introduction

Demonstration of the compliance of the design of the TRUPACT–III transportation package with the requirements of 10 CFR §71.73 was primarily achieved using formal certification testing on two test units, CTU-1 and CTU-2. Results of testing on CTU-1 are documented in Appendix 2.12.3, *Certification Tests on CTU-1*. The testing on CTU-2 consisted of one 9-m free drop and two 1-m puncture drops, in order to ensure a leaktight condition after the worst-case series of HAC events. CTU-2 differed from CTU-1 primarily by including the debris shield that was designed after CTU-1 was tested, and by using a roller floor, pallet, and loaded SLB2 container instead of loose metal bars as contents. This appendix describes the results of the testing, including post-test measurements and evaluations. The primary success criterion was that, subsequent to all free drop and puncture testing, the containment boundary, including the closure lid and vent port seals, be leaktight per ANSI N14.5[5]. Other supporting data, including accelerations and physical measurements, was collected as described herein.

CTU-2, like CTU-1, was fabricated in prototypic full-scale, which was in full compliance with the drawings given in Section 1.3.1, *Packaging General Arrangement Drawings,* except for differences noted and justified below.

2.12.6.2 Test Facilities

Test facilities used for the supplemental testing on CTU-2 are the same as described in Section 2.12.3.2, *Test Facilities*.

2.12.6.3 Test Unit Configuration

CTU-2 was an essentially prototypic, full-scale model of the TRUPACT–III package, fabricated according to the drawings given in Section 1.3.1, *Packaging General Arrangement Drawings*.

---

[1] Title 10, Code of Federal Regulations, Part 71 (10 CFR 71), *Packaging and Transportation of Radioactive Material*, 01–01–09 Edition.

[2] *TRUPACT–III Transportation Package Certification Test Plan for Supplementary Tests in 2009*, PKG–TP–SPC–005, Rev. 1, AREVA Federal Services LLC.

[3] *TRUPACT–III Transportation Package Certification Test Procedure for Supplementary Tests in 2009*, PKG–TP–SPC–006, Rev. 2, AREVA Federal Services LLC.

[4] *TRUPACT–III Transportation Package Certification Test Report for Supplementary Tests in 2009*, PKG–TR–SPC–004, AREVA Federal Services LLC.

[5] "Leaktight" is a leakage rate not exceeding 1×10^{-8} Pascals – cubic meters per second (Pa–m^3/s), air, as defined in ANSI N14.5–1997 (or later), *American National Standard for Radioactive Materials – Leakage Tests on Packages for Shipment,* American National Standards Institute, Inc. (ANSI).

Prior to testing, a certificate of conformance was issued. Any differences between CTU-2 and a regular production TRUPACT–III unit are discussed and justified below.

1. The CTU utilized no thread inserts. The production unit inserts are stronger than threads made directly in the parent material. However, the production unit thread inserts are optional, therefore the CTU conservatively represented the minimum pull-out strength possible in a production unit.
2. To ensure conservative leakage rate measurement of the CTU containment O-ring seal, care was taken to ensure that the compression of the seal was below the minimum compression of the production unit seal of 27.8%. Therefore, the containment O-ring groove in the closure lid was fabricated with a depth greater than shown on the production unit drawings. The as-built depth of the containment seal O-ring groove varied between 8.76 and 8.84 mm, for an average of 8.80 mm. The average cross-sectional diameter of the containment O-ring was 12.04 mm. The diameter reduction due to the circumferential stretch, as shown in Section 4.1.3.1, *Seals*, is 1.5%. Therefore the installed cross-sectional diameter of the O-ring was:

   $$D_R = (1 - 0.015)D = 11.86 \text{ mm}$$

   where D = 12.04 mm. The compression of the test O-ring was:

   $$C = \left[1 - \left(\frac{d}{D_R}\right)\right] \times 100 = 25.8\%$$

   where d = 8.80 mm. This is conservatively less than the minimum standard production unit containment seal compression of 27.8%, as shown in Section 4.1.3.1, *Seals*.
3. Special vent and test ports were added to the side of the CTU that do not occur on the production unit. These were provided to allow leakage rate testing of the CTU without the need to remove the overpack cover or disturb the prototypic vent and test ports. They were located away from structural damage areas, and did not affect the behavior of the CTU.
4. The CTU did not have guide bars or plastic plates across the rear wall of the payload cavity. The guide bars do not play a significant role in package resistance to damage, and their only purpose is to limit the axial free play of the payload container in the cavity. Based on the length of the payload cavity of the CTU and the length of the SLB2 test unit, the average axial space present was 57 mm. The maximum space allowed in a production unit is 28 mm, as discussed in Section 1.2.1.1, *Body*. Since the axial free play of the payload container was approximately twice the maximum amount allowed in a production model, this difference is conservative.
5. Several minor package features were omitted from the CTU: Package nameplate, tamper-indicating device, ISO corner drain holes, and paint. Lack of these items did not affect the outcome of the certification tests.
6. Small steel accelerometer mounting blocks and threaded steel lifting bosses were attached to the outside surface of the CTU. Also, six swivel hoist rings and mounting bases, weighing a total of 120 kg, were attached to the CTU. These items were not involved with any test damage, and their weight was insignificant, so they did not affect test results.

7. The debris shield seal holder located on the closure lid shear lip may be made utilizing three different configurations, as shown on Drawing 51199-SAR, Sheet 14, Zone A-1/5:
    - Optional Configuration 1 was utilized for CTU-2 in which the holder was made from A240/A479 Type 304/304L material in a welded configuration. The shear lip height was 10 mm. This configuration may be used for initial fabrication or repair. UNS S31803 material may also be used for configuration 1.
    - Optional Configuration 2 utilizes a non-welded configuration in which the holder is integral with the shear lip which is made from UNS S31803 material. The shear lip height is 14 mm. This is justified since the use of a stronger material in a non-welded configuration, with a taller shear lip (greater contact area) is conservative vis-à-vis the test.
    - Optional Configuration 3 utilizes a holder made from UNS S31803 material which is welded to the top of the shear lip. This is justified since the final configuration, which uses a full-thickness weld, is structurally the same as Configuration 2. This configuration may be used for initial fabrication or repair.
8. The guide bars which are located on the inside walls of the payload cavity were located approximately 13 mm below the location shown on the SAR drawings. In spite of this, the square tube bumpers on the SLB2 properly interfaced with the guide bars during the test.
9. The bolting bosses in the body flange included 35 mm diameter × 40 mm deep holes on the back side (towards the inside of the flange). These holes had no effect on test results.
10. Several nonconformances were encountered during fabrication of the CTU. All are recorded in the data package for the CTU, and were dispositioned according to the Quality Assurance program and approved by AFS. The nonconformances were very minor in nature and did not have a significant effect on the performance of the CTU during testing. The most significant nonconformances are noted in the following list.
    - The CSA body face flange thickness for the CTU ranged from 27 – 31 mm, compared to the specified thickness of 20 – 30 mm. This difference is negligible.
    - The 28.5 mm thick lifting plate on each ISO corner was to be welded to the 8 mm thick side plate using an 8 mm groove weld from the outside only. The actual components featured an additional 6 mm fillet backing weld on the inside of the ISO corner weldment. This had a negligible effect on the strength of the ISO corner component.
    - Due to welding-related distortion, the outside surface of the CSA top, bottom, and side surfaces were out–of–flat by 8 mm, which required the addition of small pieces of 8–mm plate to bridge the gap between the square frame containing the overpack cover bolt bosses on the front end to the CSA body.
    - The 3–piece polyurethane glued foam assembly in the right front cheek broke at the glue line, and was installed without repair of the joint. This had no effect on the test results, since the right cheek was not deformed by any of the tests.
    - To prevent out-gassing from behind the debris shield receptacle (which would lead to a high background reading in the payload cavity and interfere with the ability to perform the metallic containment boundary leakage rate testing), epoxy material was applied at various places to the receptacle attachment welds and inside the receptacle

opening where the receptacle component was thinned or locally penetrated during machining of the opening. This localized use of epoxy had no effect on debris shield performance or on any other test results.

- The bars from which the debris shield receptacle were machined did not match up properly at the four corners. The resulting gaps were filled using epoxy.
- Due to welding-related distortion, the width between the front cheeks on the CTU where they weld to the CSA measured 2105 mm on the top versus the specified width of 2120 ±10 mm (which applies at the attachment of the cheeks to the CSA). To permit assembly of the overpack cover between the cheeks, the width of the overpack cover was locally reduced by a total of approximately 10 mm. This change was made only to the lips of the overpack cover (a region 272 mm long, measured from the bolting flange). The resulting lateral fit up gaps between the overpack cover and the cheek inside dimension were measured and are recorded in Table 2.12.6-4.
- The CTU utilized 15 mm plate thickness for the puncture resistant plates in the rear octagon (item 19, see sheet 5, zone C-1 of drawing 51199-SAR in Section 1.3.1, *Packaging General Arrangement Drawings*) and in the overpack cover (item 19, see sheet 17, zone C-3). In addition, the CTU utilized 15 mm plate thickness for the inner and outer body flange plates (item 19, see sheet 21, zone C/D-5). The list of materials on sheet 1 of the drawing shows that 16 mm thickness material (item 23) may optionally be used in place of item 19. This potential increase in thickness (nominally only 6.7%) is structurally conservative and will have a negligible effect on the outcome of any test. In the body flange position, the resulting small increase in stiffness effectively reduces deformations that might occur during a HAC event. In the puncture-resistant plate positions, a slightly greater resistance to puncture will result. Thus, the potential substitution of a 16 mm thickness for 15 mm plates is acceptable.
- The CTU used a nominal 40 mm thick plate in the vent port region of the closure lid. The plate can vary from 37 to 52 mm in thickness. This variation in thickness, primarily to the plus-side, will not affect the leaktight performance of the closure lid or of the vent port.
- The CTU was fabricated using a drawing that limited the opening width of the closure lid main O-ring grooves (designated P1 and P2), at the narrow part of the dovetail shape, to a maximum of 11.30 mm. Drawing 51199-SAR, sheet 13, and associated flag note 52, identifies that the O-ring groove may be up to 11.35 mm wide. The difference in width, equal to 0.05 mm (0.002 inch), does not affect the depth of the O-ring groove or the location of the sides of the groove. The only effect is on the outer opening, which serves to retain the O-ring when the lid is removed. The small increase in width will not materially affect the ability of the dovetail shape to retain the O-ring, and has no effect on the performance of the O-ring in service.
- The CTU was fabricated using a drawing which specified the dimensions of the rectangular groove located between the main O-ring grooves on the closure lid of 1 ±0.2 mm × 4 ±0.2 mm (applying block tolerances). The only purpose of the groove is to allow for sensing helium during leakage rate testing of the main containment O-ring seal. For this function, such tight control of the tolerance is not necessary. Drawing 51199-SAR, sheet 13, zone

C-2/3, shows a dimension of 1 ±0.2 mm × 4 ±0.4 mm for this rectangular groove. This difference will have no effect on the stated function of the groove.

Prior to any certification testing, the CTU was subject to acceptance testing, including a lifting load test, an internal pressure (1.5 times MNOP) test, and leakage rate tests of the containment boundary.

The test payload included a prototypic roller floor, pallet, and SLB2, shown in Figure 2.12.6-3. The SLB2 was loaded with a quantity of square-ended, two-inch and four-inch diameter aluminum bars. Approximately one quart of debris was added to the payload cavity of the CTU (outside the SLB2). The debris was composed of crushed concrete and fine grinding grit found in the fabrication shop, and was poured into the cavity just before the final installation of the closure lid. It was placed primarily in the gap between the lower front debris shield receptacle bar and the roller floor, and between the two side walls and the roller floor nearest the opening. The debris is shown on white paper in Figure 2.12.6-9 and shown in the CTU cavity in Figure 2.12.6-10. Weights are detailed in Table 2.12.6-1. The gross weight of CTU-2 was 25,154 kg, slightly more than the maximum gross weight of the TRUPACT–III package of 25,000 kg.

2.12.6.4 Instrumentation

2.12.6.4.1 Accelerometers

Four single axis piezoresistive accelerometers were utilized to record the free drop impact. Accelerometers were not used for the puncture drop tests. The accelerometers were attached to solid stainless steel blocks that were attached by screws and epoxy to the outer sheet on the body at the locations shown in Figure 2.12.6-1. Data was recorded and conditioned by a calibrated stand-alone Spectral Dynamics data acquisition system. A Fast Fourier Transform (FFT) of the raw data was performed to determine the appropriate cutoff, or filtering frequency. The accelerometer data was filtered using a six-pole Butterworth filter with the cutoff set at 200 Hz.

2.12.6.4.2 Thermocouples

Type K thermocouples were installed as shown in Figure 2.12.6-2 to measure the temperature of the polyurethane foam in the critical region near the impact event on the lower left corner of the CTU. The data was monitored during the chilling period, and continued until impact.

2.12.6.5 Initial Test Conditions

2.12.6.5.1 Internal Pressure

Since internal pressure has the effect of increasing the stress on the containment boundary, the CTU was pressurized to an internal pressure of 170 kPa at a temperature of -4 ºC, which conservatively exceeded the design pressure of 172 kPa at 21 ºC. Since resistance to puncture is not significantly affected by internal pressure, the CTU was not pressurized for the puncture tests. Since the pressure is only an initial condition, monitoring the pressure was not performed.

2.12.6.5.2 Temperature

As discussed in Section 2.7.1.1.3, *Free Drop Test on CTU-2*, the maximum damage from the c.g.-over-corner free drop will occur at the minimum regulatory temperature condition of -29 ºC. The actual temperature of the energy-absorbing material in free drop test LD91 is recorded in Section 2.12.6.7.1, *Free Drop, CG-Over-Corner, Overpack Cover Down, HAC (LD91)*. Prevailing temperature was used for all puncture drop tests.

2.12.6.6 Certification Tests Performed

The evaluation and selection of tests to be performed for certification testing is discussed in Section 2.7.1, *Free Drop*, and Section 2.7.3, *Puncture*. One HAC free drop and two puncture drops were performed, as summarized in Table 2.12.6-2. The free drop is designated LD91 and is shown schematically in Figure 2.12.6-4. The punctures are designated LP91 and LP92, and shown schematically in Figure 2.12.6-5 and Figure 2.12.6-6, respectively.

2.12.6.7 Test Results

After each of the tests, a vacuum was placed between the closure lid seals as an approximate confirmation of the sealing integrity of the containment seal, using the special test port on the CTU side. The vacuum achieved in each case is recorded in the sections below. For the puncture tests, the internal pressure was bled off to a value nominally equal to atmospheric.

Prior to performing any tests, helium leakage rate tests were performed on the containment metallic boundary, the main O-ring seal, and the sampling/vent port plug O-ring seal according to an approved procedure. Photos of certification testing are provided in Figure 2.12.6-7 to Figure 2.12.6-20.

2.12.6.7.1 Free Drop, CG-Over-Corner, Overpack Cover Down, HAC (Test LD91)

Test LD91 was a free drop from a conservative height of 9.2 m, with the CTU axis oriented approximately 47º to the ground, striking the lower left corner of the package as shown in Figure 2.12.6-4. The center of gravity of the package was over the point of initial impact. The average temperature of thermocouples T1, T2, and T7 was -33.6 ºC. These temperatures represent both shallow and deep readings in the corner of the package. The ambient temperature was 5.6 ºC. Accelerations were obtained from gages A1 through A4. The raw signals were filtered at 200 Hz, and the resulting acceleration plots are shown in Section 2.12.6.9, *Acceleration Time History Plots*. The shapes of the accelerometer curves were not consistent with each other, nor (with one exception) were the recorded peaks as high as expected. The resulting curve which best fit the expectation based on the high speed video and on the results obtained from CTU-1 was accelerometer A1. This was also the highest acceleration. The impact was therefore considered to be best characterized by the A1 result, and the results of A2 – A4 were not used. The accelerometers were mounted with their measuring axis parallel to the package axis; the resulting acceleration perpendicular to the ground was found using:

$$A1_{\perp} = \frac{A1}{\cos(43)} = 80.8\text{g}$$

where A1 is the filtered accelerometer peak value from the table below, and the axial direction is oriented at an angle of 90º – 47º = 43º to the vertical as defined in Figure 2.12.6-4.

A1	A2	A3	A4	$A1_{\perp}$
59.1	(25.8)	(37.1)	(33.7)	**80.8**

The impact caused a triangular flat region having dimensions of 737 mm along the overpack cover, 864 mm along the bottom, and 787 mm along the left side of the CTU. The damage to the overpack cover included a gap of up to 70 mm at the center between the cheek and the overpack cover left edge, see Figure 2.12.6-12. The gap exposed some foam, but narrowed to nearly zero a short distance from the surface. No significant weld seam failures were noted from this test. A hard vacuum of below 200 millitorr was obtained between the closure lid seals as a preliminary confirmation of leak tightness. Photos of the damage are shown in Figure 2.12.6-11 and Figure 2.12.6-12.

2.12.6.7.2 Puncture Drop On CG-over-Corner Damage (Test LP91)

The drop height for this test was one meter. The ambient temperature for this test was 15 ºC and the package surface temperature was 19 ºC. The CTU was rigged as shown in Figure 2.12.6-5. The bar was 762 mm long (above the baseplate). The puncture bar struck on the overpack cover portion of the prior c.g.-over-corner free drop (LD91) damage. The depth of puncture, measured to the center of the damage hole in an axial direction from the undeformed surface of the overpack cover, was 146 mm. The damage loosened the entire lower quadrant of the overpack cover outer sheet and a significant portion of the low density (0.16 kg/dm^3) foam fell out. The bar corner partially sheared into the 6-mm thick puncture resistant plate located between the low density and high density (0.48 kg/dm^3) foam by an amount of 38 mm. However, little of the high density foam was exposed and essentially none was lost. A hard vacuum of 224 millitorr was obtained between the closure lid seals as a preliminary confirmation of leak tightness. The puncture bar remained intact after the impact. A photograph of the damage is shown in Figure 2.12.6-13.

2.12.6.7.3 Puncture Drop On CTU Bottom (Test LP92)

The drop height for this test was one meter. The ambient temperature for this test was 12 ºC, and the package surface temperature was 15 ºC. The bar was 965 mm long (above the baseplate). The puncture bar struck as shown in Figure 2.12.6-6, with the edge of the bar placed approximately 476 mm from the closed outer end of the package, with the package inclined 40º from the horizontal. The bar penetrated the outer skin and impacted the CSA outer structural sheet, creating a crack in the weld between the structural sheet and the rear diagonal corner stiffener of the CSA, and in some of the adjacent plug welds which connect the outer structural sheet to the V-stiffener nearest the impact. This condition required weld repairs in order to support helium leakage rate testing of the containment boundary structure. (The CSA outer wall structure must be capable of retaining the helium test gas for the containment boundary leakage rate test to be performed.) However, there was no evidence of any dent or bulge in the CSA inner (containment) sheet at the puncture site. In addition, the containment boundary was leaktight as discussed in Section 2.12.6.8.1, *Leakage Rate Tests*. A hard vacuum of below 250 millitorr was obtained between the closure lid seals as a preliminary confirmation of leak tightness. The puncture bar remained intact after the impact. The damage is shown in Figure 2.12.6-14 and Figure 2.12.6-15. Figure 2.12.6-15 shows the cracked outer structural sheet weld.

2.12.6.8 Leakage Rate Tests and Post-Test Measurements

2.12.6.8.1 Leakage Rate Tests

Post-test leakage rate testing of the containment boundary was performed using helium tracer gas and a mass spectrometer leak detector (MSLD). The leaktight criterion was 2.2×10^{-8} Pa-m^3/s, He. All tests were successful. Testing result details are provided in Table 2.12.6-3. The testing consisted of three elements:

- Closure lid containment O-ring seal
- Vent port containment O-ring seal
- Metallic portion of the containment boundary

2.12.6.8.1.1 Closure Lid and Vent Port Containment O-ring Seals

The closure lid and vent/test port containment seals were both tested by connecting a MSLD to the space between the containment seal and the test seal and then filling the payload cavity with helium. Testing was performed at the prevailing ambient temperature of the fabrication shop. This test was equivalent to a test at the minimum regulatory temperature of -20 ºF due to the intentionally low O-ring compression used in the CTU. As shown in Section 2.12.6.3, *Test Unit Configuration*, the room-temperature compression of the closure lid containment O-ring in the CTU was 25.8%, and the minimum room-temperature compression in a prototypic unit is 27.8%. The reduction in compression in the seal at a temperature of -29 ºC (caused by thermal contraction of the rubber) may be inferred to be approximately 1%, based on the calculation performed in Section 2.12.2.6, *Test Results*, for a temperature of -40 ºC. Therefore, a prototypic unit at a temperature of -29 ºC would have a minimum compression of 27.8 – 1 = 26.8%, which is 1% greater than the compression in the CTU at the test temperature. Therefore testing the CTU at room temperature was conservative. The leakage rate of both containment seals was acceptable as shown in Table 2.12.6-3.

2.12.6.8.1.2 Metallic Containment Boundary

The metallic portion of the containment boundary was tested by connecting a MSLD to the payload (interior) cavity and then replacing the air in the annulus between the containment and structural sheets of the CSA with helium. Helium could then pass through any openings in the containment boundary to the inside of the package, and register on the MSLD connected to the cavity. In order to achieve the required vacuum in the payload cavity to support the leakage rate test and to ensure there were no obstructions to any potential leak paths, the closure lid was removed, the contents were removed, and the payload cavity was thoroughly cleaned. The lid was then reinstalled and the bolts tightened to approximately 400 N-m, which was conservatively much less than the measured minimum residual torque for any bolt (see Section 2.12.6.8.2.1, *Overpack Cover and Closure Lid Observations*). Since the leakage rate tests of the closure lid O-ring and vent port seals had already been completed, removal of the closure lid had no effect on any test. Further, a leak in the metallic boundary, had one existed, would not be affected by the removal of the closure lid, of the contents, or by the cleaning. The leakage rate was acceptable as shown in Table 2.12.6-3.

2.12.6.8.2 CTU Measurements

Besides measurement of the damage reported above, various measurements were taken of the CTU during disassembly as discussed below.

2.12.6.8.2.1 Overpack Cover and Closure Lid Observations

The gaps between the overpack cover and the cheeks were measured in several locations before and after the test, and reported in Table 2.12.6-4. The results show that the cover moved away from the impact, and the total gap width decreased, as expected. It is concluded that the cover did not move very far as a result of the tests.

The lid moved slightly relative to the body as demonstrated by the scribe line offsets. On assembly, four scribe lines were made between the lid and body. After the test, the scribe lines were offset by 1.3 mm top left; 1.8 mm top right; 0.25 – 0.50 mm lower left; and 0 – 0.13 mm lower right. The lid appeared to have moved to the left, i.e, toward the c.g.-over-corner impact (test LD91).

It was noted that a 0.102 mm thick feeler gauge could not be inserted between the lid and body flanges (with one very limited exception) along the top and bottom flanges. The sides were not checked due to the presence of the cheeks. It is thus concluded that the closure lid flange was in clamped contact with the body flange. As noted in Section 2.12.6.8.2.2, *Observations with the Closure Lid Removed*, some galling of the flanges near the bolt holes testified to a high clamping force during the test.

None of the bolt heads had rotated, based on the location of the rotational index marks, and based on the residual torques. Residual torques were checked in the clockwise direction by applying a torque of 1,356 N-m to each bolt. No bolts rotated as a result of this torque application. Residual loosening torque was recorded as the largest counter-clockwise torque value obtained during removal of the bolts. Of note, all bolts were tested for loosening torque without significantly reducing the preload of any. Only after checking the residual loosening torque of all bolts were any bolts significantly loosened and removed. The residual loosening torques varied between a minimum of 1,112 N-m and a value greater than 1,356 N-m (which was the maximum capacity of the torque wrench used for this test). The average was 1,260 N-m, which is equal to 1,260/1,600×100 = 79% of the original tightening torque value of 1,600 N-m. Residual torques are given in Table 2.12.6-5.

There was some interference between the overpack cover cups and the closure bolt washers on about 61% of the bolts, from bolt no. 13 on the right side, down the right side, across the bottom, and up the left side as far as bolt no. 40[6]. Washer nos. 41 on the left side, up through no. 12 on the top, had no interference with the cups. The struck location was uniformly between 6:30 O'clock and 7:00 O'clock, which indicates that the overpack cover slid primarily upward and slightly to the right, away from the free drop impact. The washers showed no evidence of denting or imprinting from the bolt head or lid hole, and no out-of-flat deformation. Only a little scuffing/galling from use was evident. The greatest displacement of washers relative to the lid surface occurred centered on the lower left corner impact zone. For bolt no. 33 (lower left corner, adjacent to the impact), the washer displaced approximately 0.5 mm toward the upper right. However, none of the bolts were bent. Bolt nos. 31 through 35 showed no runout when checked using a V-block and dial indicator. None of the bolt heads were struck by the cups, only

[6] Bolt no. 1 is the leftmost bolt on the top side, and numbered clockwise.

some washers as stated. Typical evidence of interference between an overpack cover cup and a washer is shown in Figure 2.12.6-16.

2.12.6.8.2.2 Observations with the Closure Lid Removed

The debris shield was in good condition and protected the containment O-ring seal from contact with any of the debris which had been introduced into the payload cavity before testing. The only anomaly was that on the top side, the foam rubber component appeared to have caught an edge – apparently the edge of the receptacle – during lid assembly or removal and pulled away from the holder on the outside (nearest the flange). However, most of the silicone foam rubber in the affected sections was still compressed in the receptacle as designed, and the shield function was unaffected. There was a small pile of debris on the inside of the shield on the lid as shown in Figure 2.12.6-17, which functioned properly in preventing access of the debris to the containment seal.

The metallic portion of the containment boundary was in good condition. There was no evidence of any bulge in the inner containment wall at the site of puncture LP92. There was a little galling between the lid and body appearing next to some of the bolt holes, indicating good clamping force local to the bolts, as shown in Figure 2.12.6-18. There was also a narrow line of scuffing across the top flange. There were no deformations on the closure lid or in the body cavity due to contact with the SLB2 except for a dent in the debris shield receptacle on the left side at the elevation of the SLB2 lid as shown in Figure 2.12.6-19. This condition did not affect the function of the debris shield, since it locally increased the compression of the foam rubber shield.

Measurements of the payload cavity, shown in Table 2.12.6-6, demonstrate essentially no change to the cavity due to the test impacts. The small differences which were noted (up to two millimeters) are considered to be measurement anomalies, rather than evidence of permanent deformation. A view of the cavity with all of the contents removed is shown in Figure 2.12.6-20.

The SLB2, roller floor, and pallet were in very good condition after the test. The payload bars caused the panel walls of the SLB2 to bulge outward from the impact, and the lower of the three square tube bumpers were flattened on the front face and left side. (The level of the payload bars did not reach the middle or upper bumpers, and thus, they were not deformed.) One bar poked through the front panel of the SLB2 at the bottom. The roller floor and pallet were fully functional during removal of the SLB2 from the CTU.

Table 2.12.6-1 – CTU-2 Weight

Component	Weight, kg
Empty CTU, without closure lid or overpack cover	14,506
Closure lid and (44) closure bolts	1,796
Overpack cover and 10 attachment bolts	2,758
Empty Package Sum	19,060
Roller floor	235
Pallet	196
Loaded SLB2 (must weigh 4,763 kg minimum)	5,543
Contents Sum	5,974
Large swivel hoist rings (6)	120
Total CTU-2 Weight (must weigh 25,000 kg minimum)	25,154

Table 2.12.6-2 – CTU-2 Test Summary

Test	Description[1]	Orientation	Temperature[2]	Accelerometers & Direction	Temperature Monitors
LD91	CG-over-corner, overpack cover down, HAC	CTU axis inclined 47º from horizontal, impacting on lower left corner. See Figure 2.12.6-4.	Cold	A1 thru A4	T1, T2 & T7
LP91	On c.g.-over-corner damage	Impact on crushed corner at same orientation as test LD91, through CG. See Figure 2.12.6-5.	Prevailing	NA	NA
LP92	On bottom wall	Impact on bottom wall, aiming at puncture-resistant plate gap. CTU axis at 40º to horizontal. See Figure 2.12.6-6.	Prevailing	NA	NA

Notes:
1. HAC free drop height 9.2 m.
2. Recorded temperatures of the energy absorbing material are reported in Section 2.12.6.7.

Table 2.12.6-3 – Leakage Rate Test Results

Test Date	Test Performed	Adjusted Leak Rate (Pa-m^3/s, He)[1]	Pass/Fail
12/10/09	Metallic containment boundary	1.7×10^{-9}	Pass
12/2/09	Closure lid containment seal	Zero[2]	Pass
12/2/09	Vent port containment seal	Zero[2]	Pass

Notes:
1. Pass criterion equals 2.2×10^{-8} Pa-m^3/s, He.
2. Zero leakage rate means no detectable leakage on the range tested (10^{-9} Pa-m^3/s, He).

Table 2.12.6-4 – Overpack Cover Gap Measurements, mm

	Pre-test		Post-test	
	Left Cheek	Right Cheek	Left Cheek	Right Cheek
Top: rear	5	5	3	2
Top: front	20	20	14	18
Front: top	20	23	13	17
Front: bot	24	15	Not Accessible	13
Front: max	27	22	30	18
Front: min	13	13	13	13
Bot: rear	3	2	10[2]	0[2]
Bot: front	10[1]	9[1]	Not Accessible	Not Accessible
Cover surface to cheek surface (axial)	+8[3]	+15	+17	+12

Notes:
1. Measured approximately 305 mm from front face.
2. At back corner.
3. A positive sign indicates protrusion beyond the cheek ends.

Table 2.12.6-5 – Closure Lid Bolt Residual Torques (Loosening), N-m

Bolt No.	Residual Torque, Top Flange	Bolt No.	Residual Torque, Right Flange	Bolt No.	Residual Torque, Bot. Flange	Bolt No.	Residual Torque, Left Flange
1	1,248	12	1,187	23	1,268	34	1,248
2	1,288	13	1,227	24	1,295	35	1,112
3	1,281	14	>1,356	25	>1,356	36	1,193
4	>1,356	15	1,248	26	1,220	37	1,207
5	1,200	16	1,254	27	1,248	38	1,220
6	1,302	17	1,315	28	1,193	39	1,295
7	1,200	18	1,302	29	1,173	40	1,268
8	1,261	19	>1,356	30	1,295	41	>1,356
9	1,248	20	1,153	31	>1,356	42	1,302
10	1,220	21	1,302	32	1,153	43	1,288
11	>1,356	22	1,193	33	1,302	44	1,220

Note: Note: All closure bolts were tested for residual tightening (clockwise) torque up to a value of 1,356 N-m (1,000 ft-lb). When 1,356 N-m was applied to the bolts clockwise, none of the bolts rotated. The values in this table are the residual loosening (counter-clockwise) torque. See Section 2.12.6.8.2.1 for a definition of these quantities.

Table 2.12.6-6 – Payload Cavity Measurements, mm

Measurement	Pre-test	Post-test
Width, 100 mm from Top	1,840	1,840
Width, 100 mm from Bottom	1,840	1,840
Height, 100 mm from Left	2,000	2,001
Height, 100 mm from Right	2,000	2,002
Diagonal, LL to UR	2,701	2,701
Diagonal, UL to LR	2,703	2,703
Depth, center left wall, 100 mm from wall	2,791	2,791
Depth, center top wall, 100 mm from wall	2,794	2,794
Depth, center right wall, 100 mm from wall	2,793	2,791
Depth, center bottom wall, 100 mm from wall	2,789	2,790

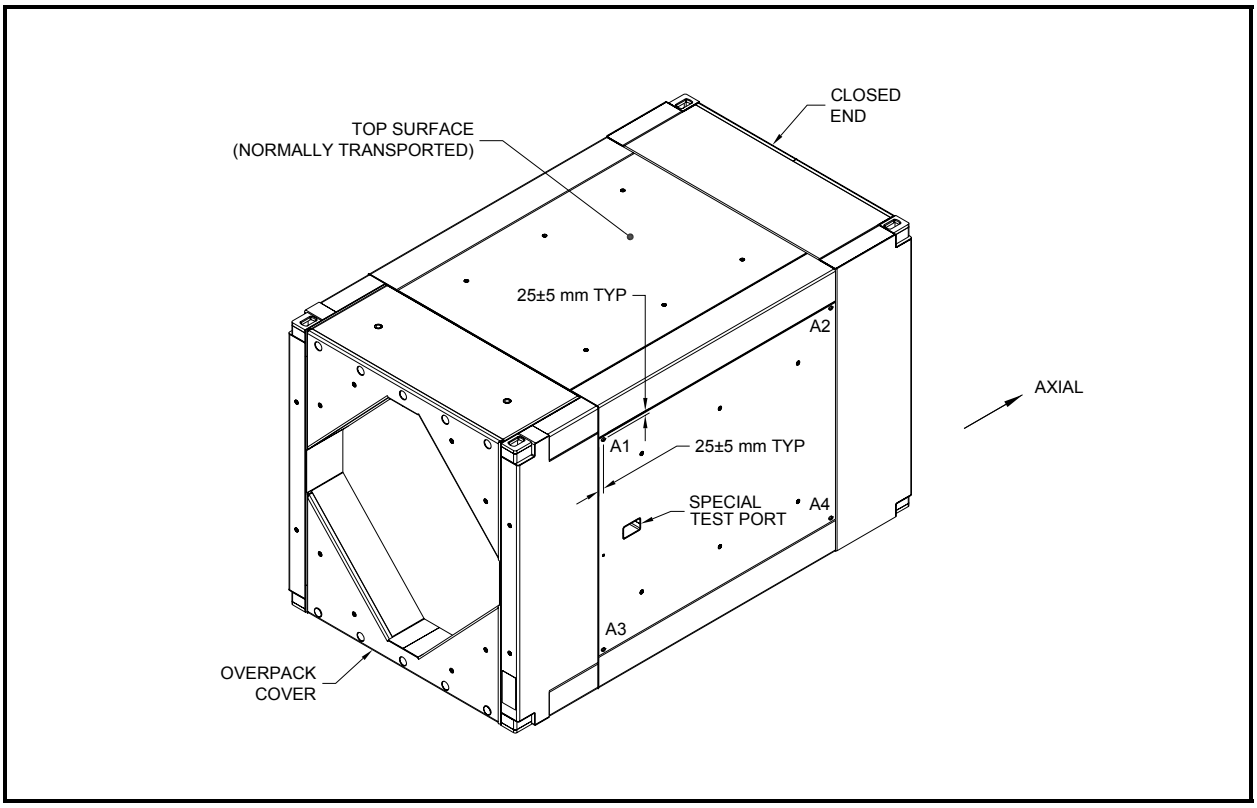

Figure 2.12.6-1 – Accelerometer Locations

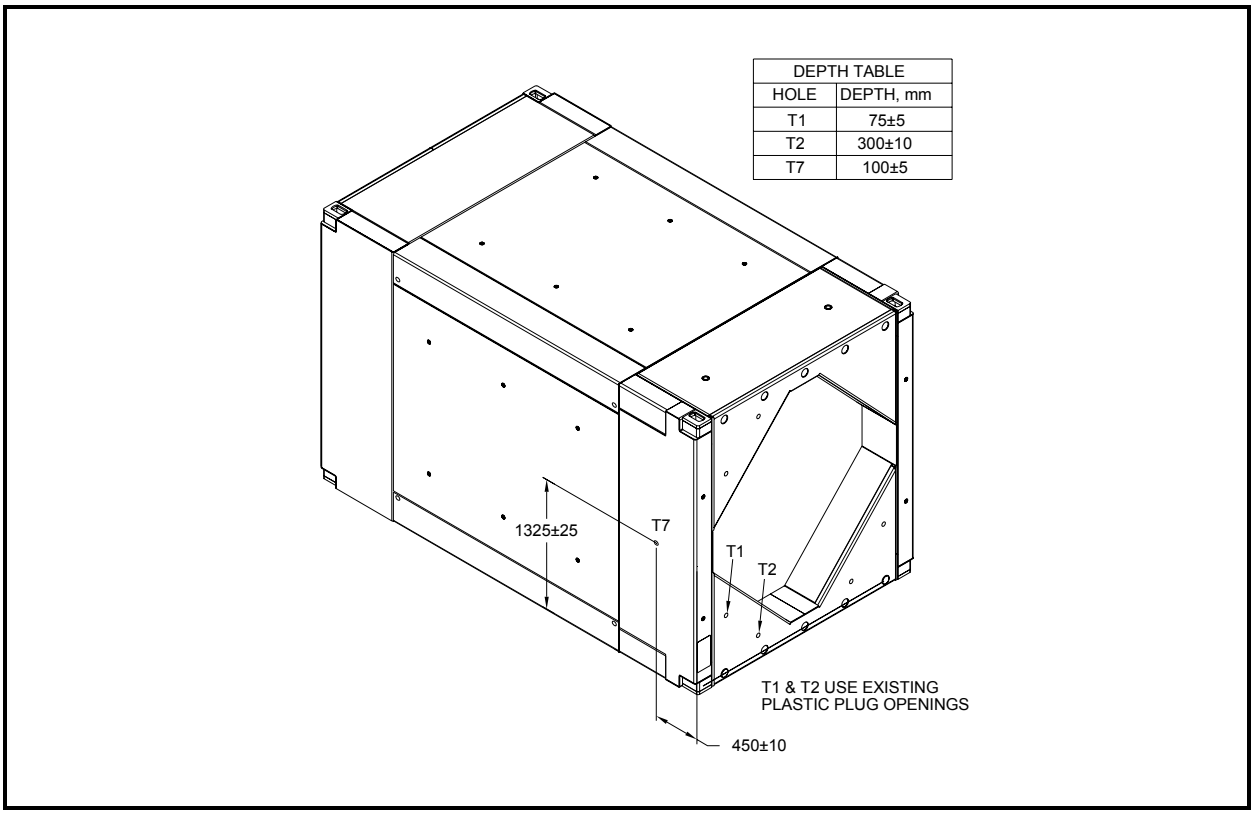

Figure 2.12.6-2 – Thermocouple Locations

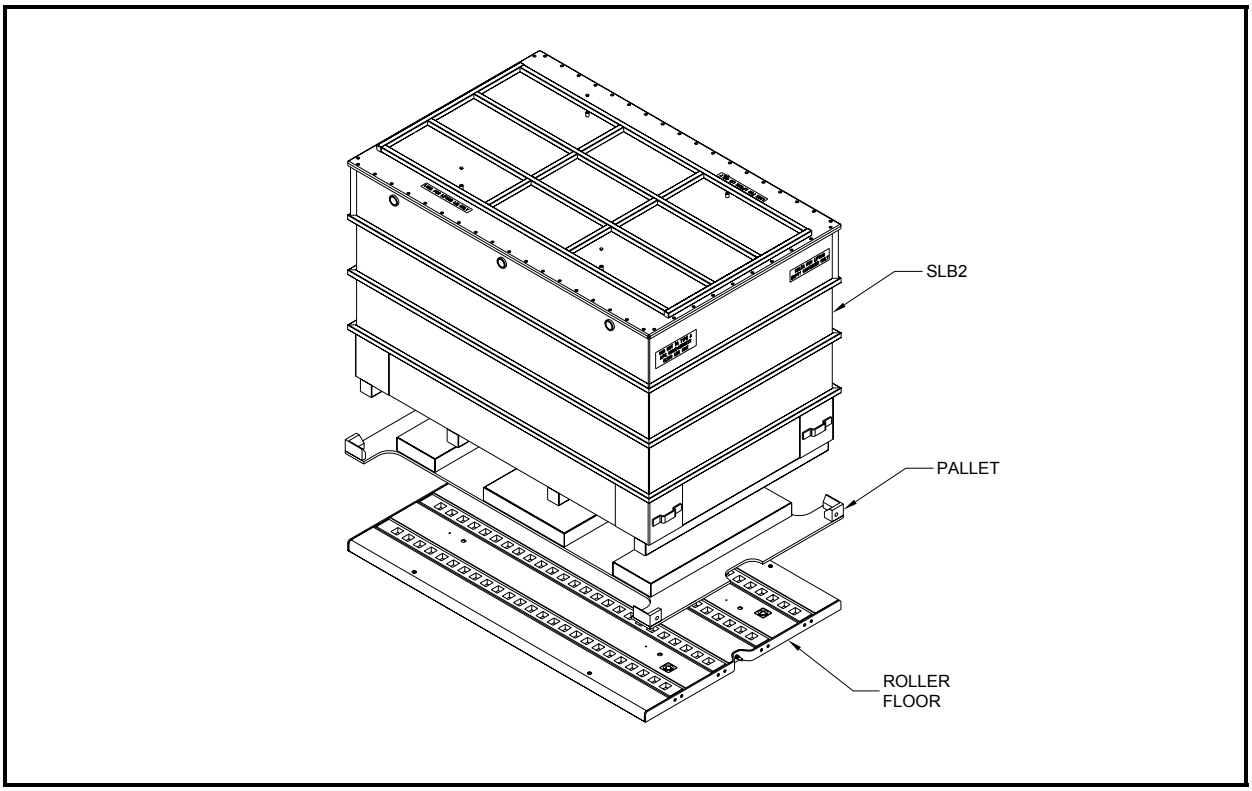

Figure 2.12.6-3 – CTU-2 Contents

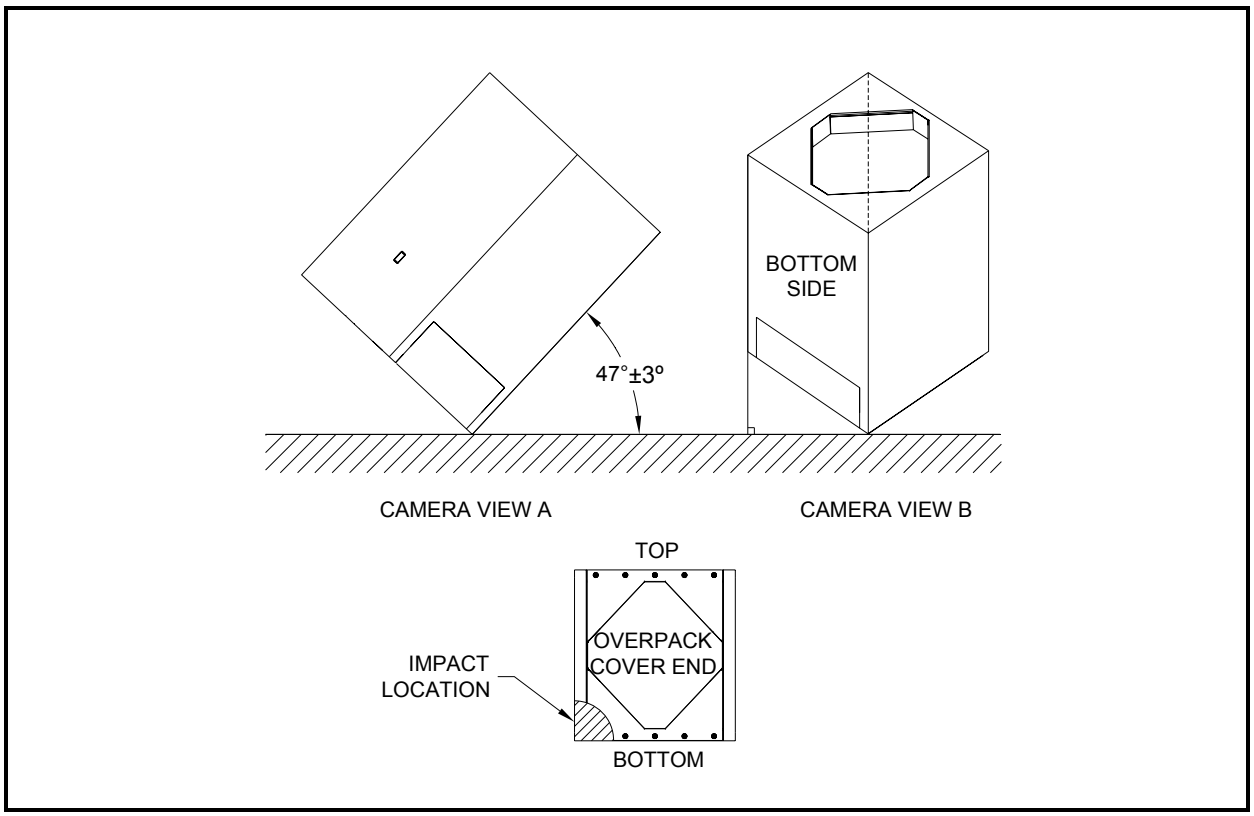

Figure 2.12.6-4 – CG-Over-Corner Free Drop Orientation, Test LD91

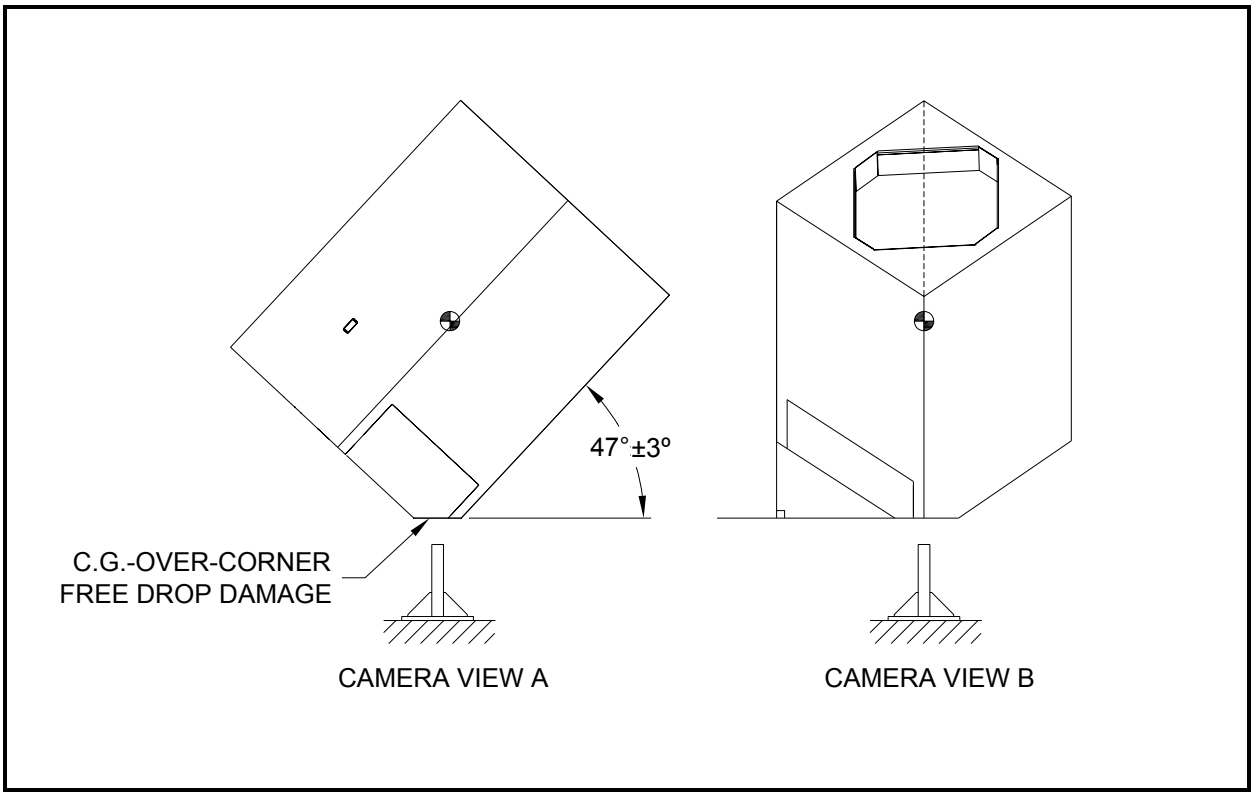

Figure 2.12.6-5 – Puncture on Prior CG-Over-Corner Damage, Test LP91

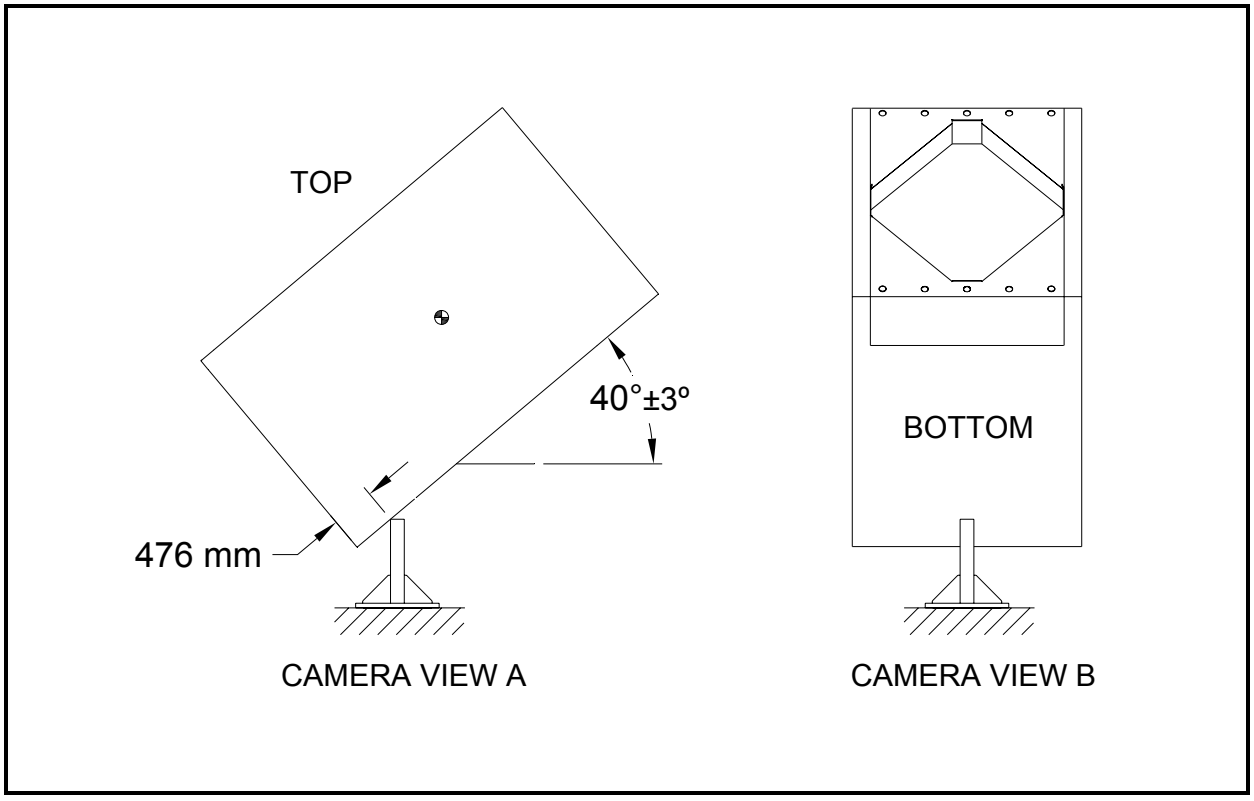

Figure 2.12.6-6 – Puncture on Bottom, Test LP92

Figure 2.12.6-7 – Aluminum Bars Inside the SLB2

Figure 2.12.6-8 – SLB2 and Pallet Installed in the Payload Cavity

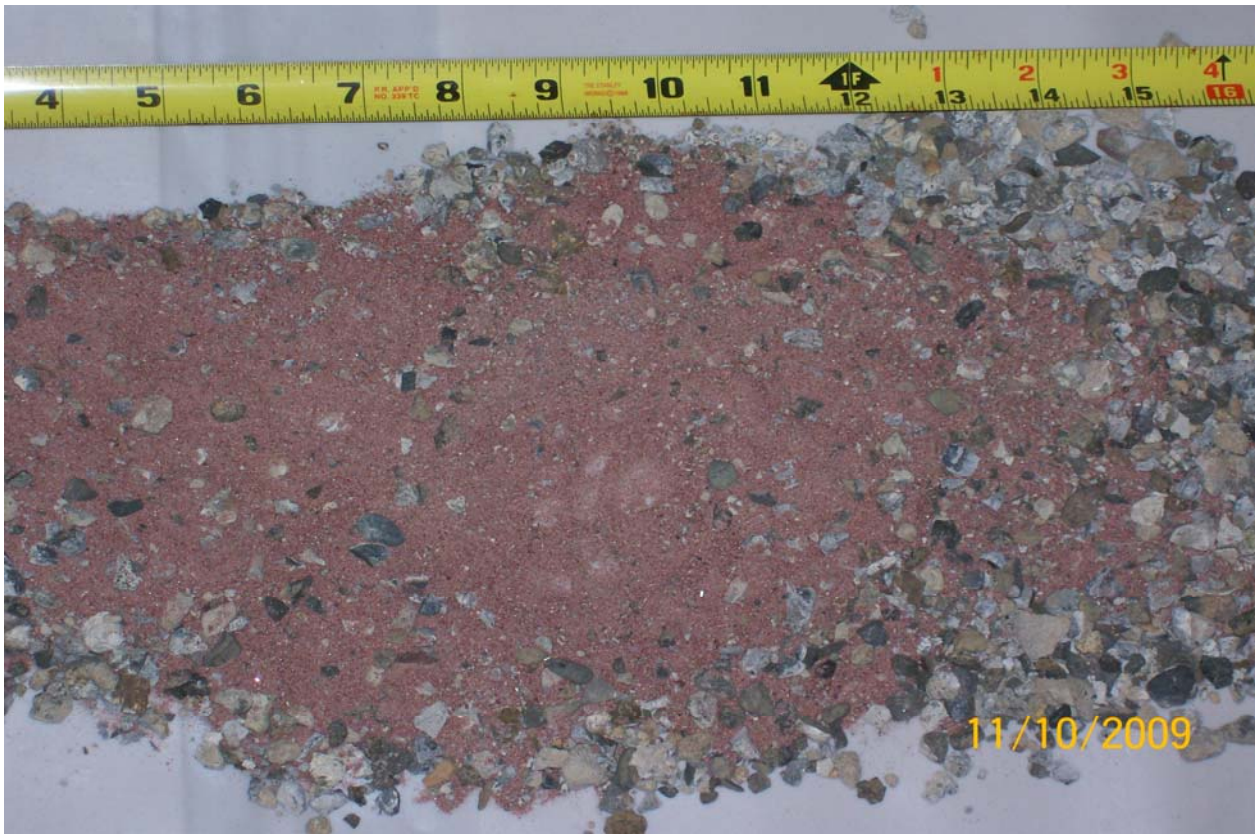

Figure 2.12.6-9 – Test Debris Used in CTU-2

Figure 2.12.6-10 – Part of the Debris Between Roller Floor and Sidewall

Figure 2.12.6-11 – Test LD91, CG-Over-Corner Free Drop Damage

Figure 2.12.6-12 – Test LD91, CG-Over-Corner Free Drop Damage, Detail

Figure 2.12.6-13 – Test LP91, CG-Over-Corner Puncture Damage

Figure 2.12.6-14 – Test LP92, Puncture on Bottom Wall Damage

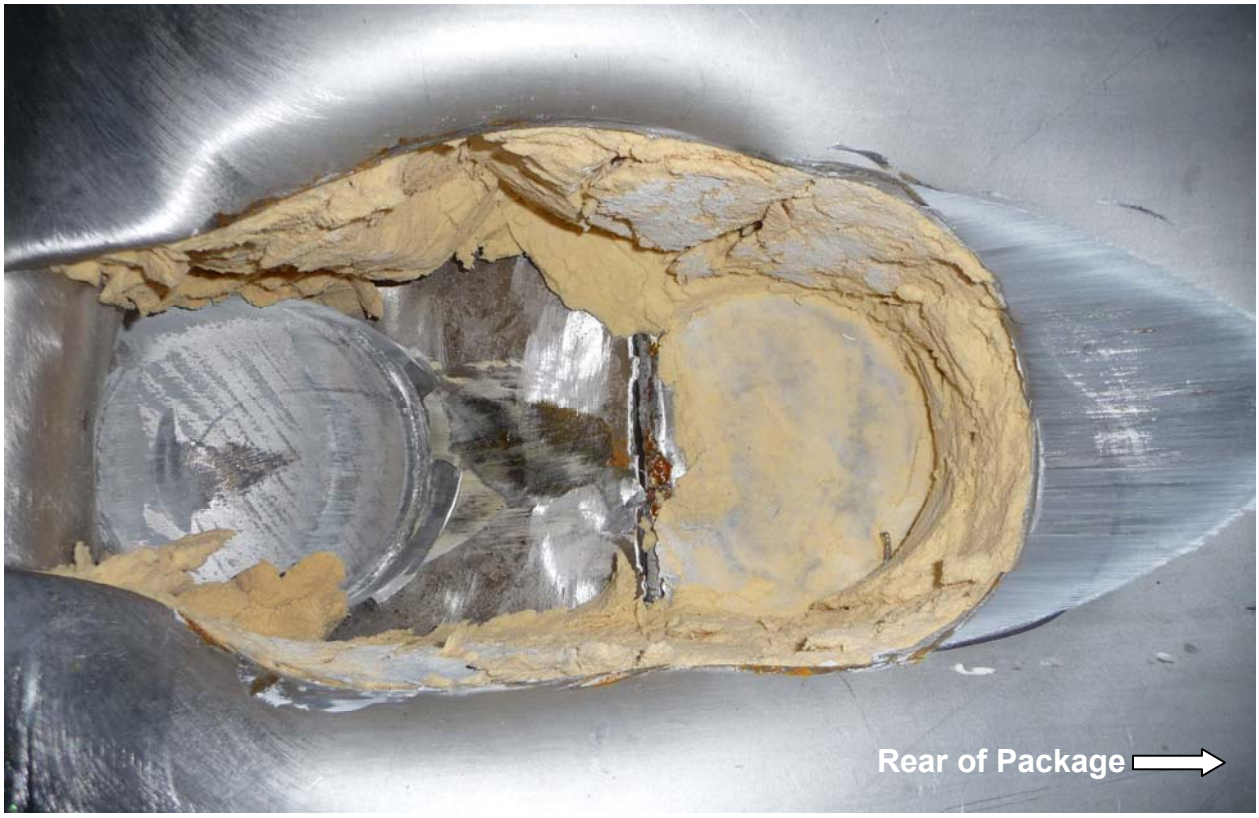

Figure 2.12.6-15 – Test LP92, Puncture on Bottom Wall Damage, Detail

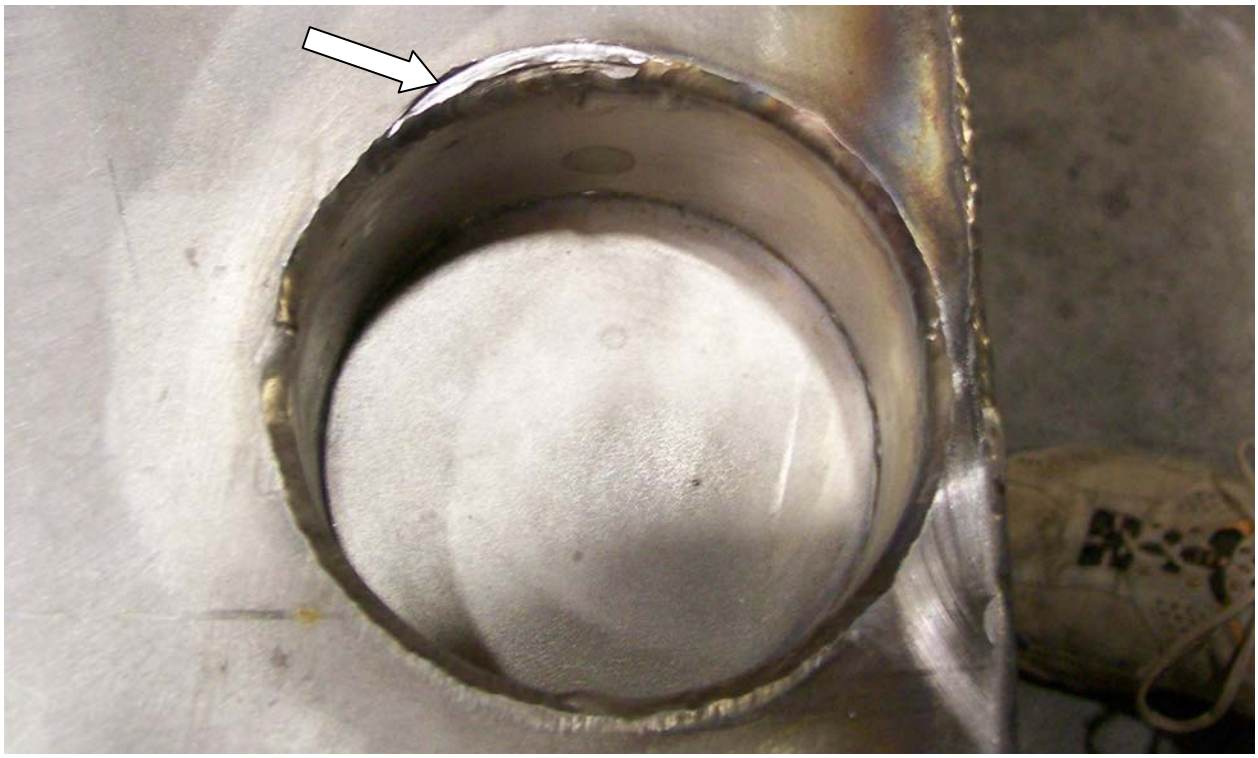

Figure 2.12.6-16 – Typical Damage to Overpack Cover due to Interference with Closure Bolt Washers

Figure 2.12.6-17 – Debris and Debris Shield (red) Upon Closure Lid Removal

Figure 2.12.6-18 – Galling on Flange Around Closure Bolt Holes

Figure 2.12.6-19 – Dent in Debris Shield Receptacle Caused by SLB2

Figure 2.12.6-20 – Payload Cavity with All Contents Removed

2.12.6.9 Acceleration Time History Plots (Free Drop Test LD91)

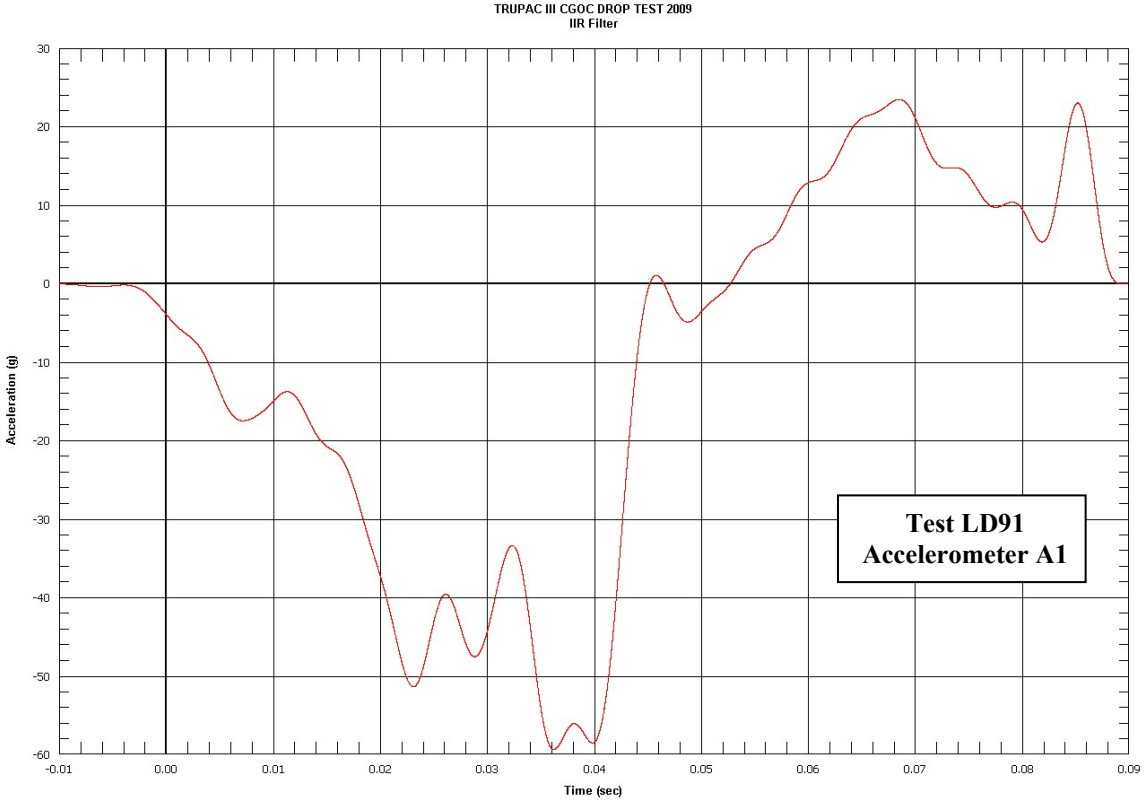

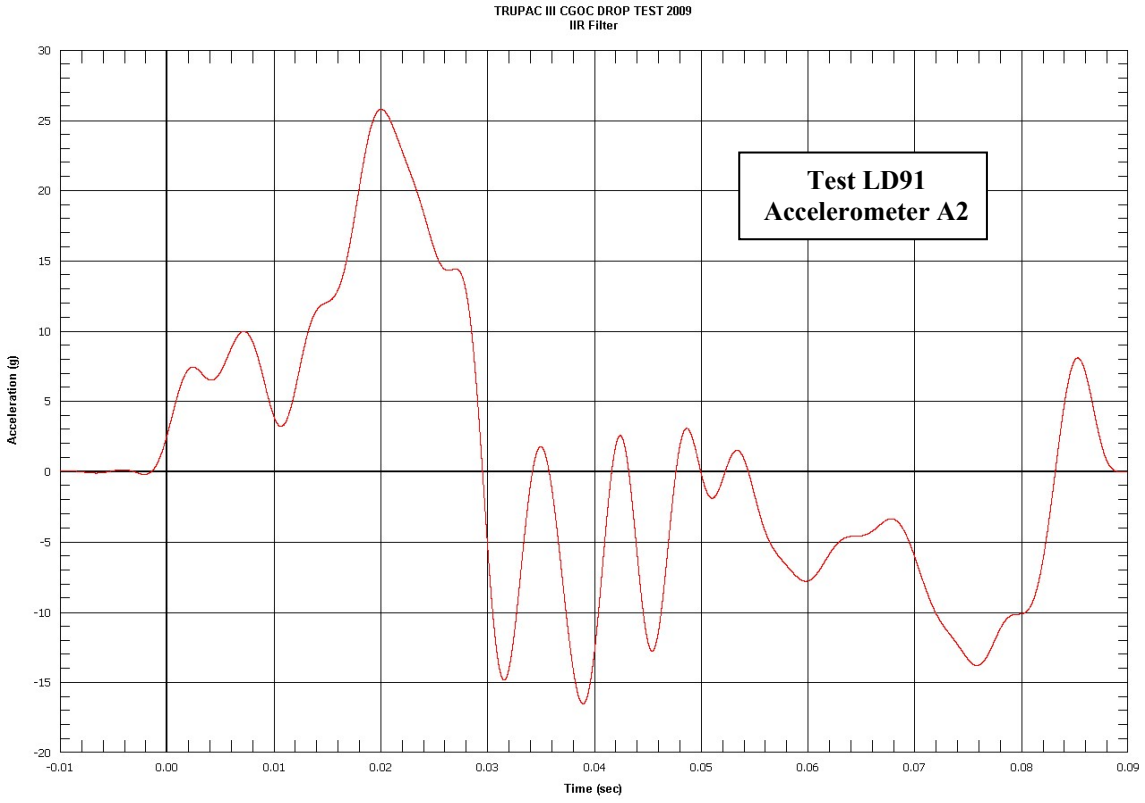

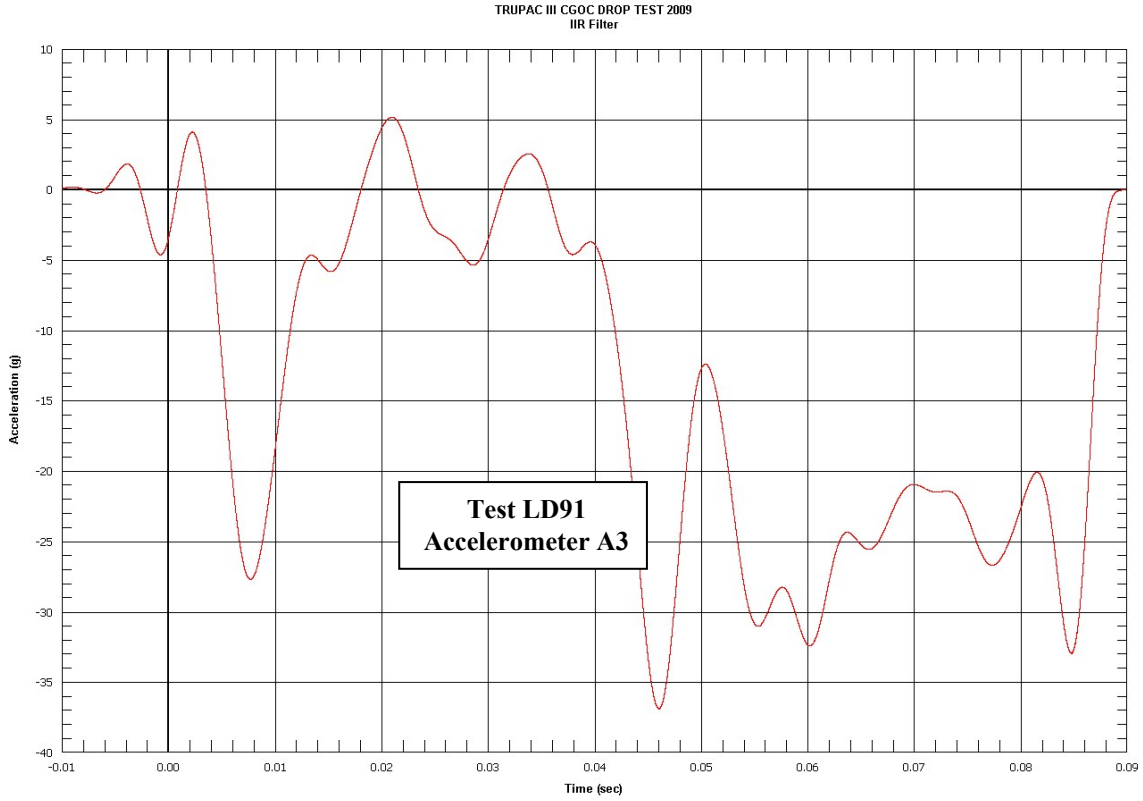
TRUPAC III CGOC DROP TEST 2009
IIR Filter
Acceleration (g)
Time (sec)
Test LD91
Accelerometer A3

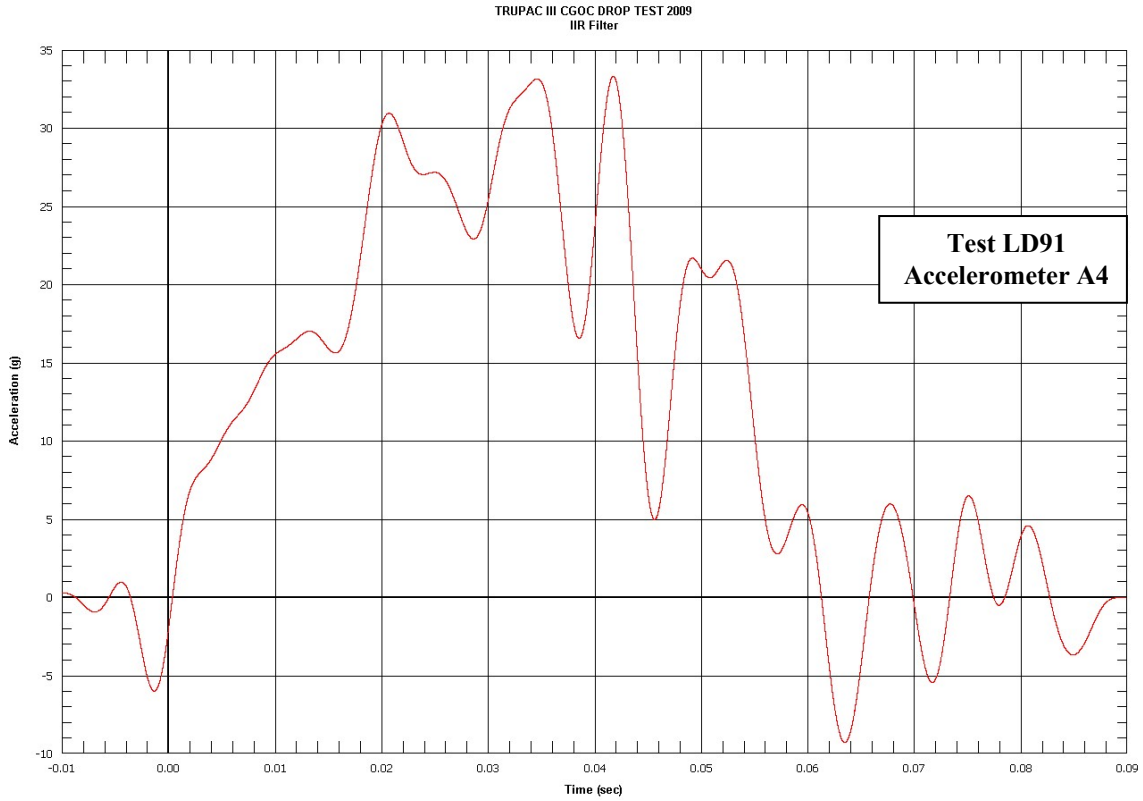
TRUPAC III CGOC DROP TEST 2009
IIR Filter
Acceleration (g)
Time (sec)
Test LD91
Accelerometer A4

This page intentionally left blank.

2.12.7 Closure Lid, Bolt, and Washer Interaction

2.12.7.1 Introduction

This appendix demonstrates that the TRUPACT–III lid closure bolt washer is not the weakest link in the closure joint, i.e., not the first component to yield under HAC loadings. The other components in the joint include the lid, bolt, and body flange. For the purposes of this analysis, the body flange is assumed to be rigid. The purpose of this analysis is to show that:

- With increasing load on the closure joint, the first component to incur permanent deformation is the bolt, not the washer.
- If an initially preloaded closure joint were to be loaded up to the yield load of the bolt, and then released, the residual preload on the joint is over 90% of the initial preload force.

The closure joint, including representations of the lid, bolt, and washer, is analyzed using a Finite Element Analysis (FEA) model. The model is evaluated using the FEA program ANSYS® Version 11.0. This analysis assumes the lid moves parallel to the bolt axis, without flange rotation. While some rotation will occur under circumstances of lid loading in an impact, this analysis is intended only to demonstrate the general robustness of the closure joint, and that the washer is not the weakest component in the joint. The actual performance of the closure under HAC free drop impacts is discussed in detail in Section 2.7.1, *Free Drop*.

Dimensions of the components are taken from Appendix 1.3.1, *Packaging General Arrangement Drawings*. The lid is a machined weldment comprised of duplex stainless steel Type UNS S31803. The portion of the lid represented in the FEA model is primarily the lid bolt tube, as discussed below. The closure lid bolts are socket head cap screws with M36 x 4 threads and a 30 mm shank diameter. The bolt material is ASTM A320 Grade L43. The washers are M36 x 6 mm thick with a 64 mm outer diameter. The washer material is age-hardened stainless steel, ASTM A564 Grade 630 Condition H1025. The bolt installation torque is 1,600 N-m. The bolt preload is calculated in Section 2.6.1.6, *Closure Bolts*, to be 222.2 kN.

Material properties are evaluated at the NCT hot condition of 71 °C. Material properties for the lid are taken from Table 2.2-1 and Table 2.2-2. The material properties for the bolt and washer are taken from Table 2.2-4 and Table 2.2-8, respectively. The temperature-interpolated values are shown Table 2.12.7-1.

2.12.7.2 Finite Element Analysis Methodology

The FEA model consists of a 2-D axisymmetric representation of the bolt, washer, and lid. The bolt and lid are only modeled in sufficient length such that stresses surrounding the washer contact region are not influenced by the model boundary constraints. Similarly, the lid bolt tube is modeled with a larger outer diameter. A value of 102 mm instead of 64 mm was used in order to include a reasonable representation of the 20 mm thick top plate of the lid that is adjacent to the washer bearing area. This prevents a discontinuity in the model at the outer edge of the washer bearing area with the lid. The increased stiffness of the lid bolt tube due to the larger outer diameter is reasonable with respect to the stiffness of the boxed outer section of the lid and conservative with respect to determining if the washer will yield.

Three parts are defined in the model as described in Table 2.12.7-2, and each part is meshed with PLANE82 2-D 8-Node structural solid elements. The interaction between the bolt and washer, and washer and lid, are modeled with contact elements. CONTA172 2D 3-Node surface-to-surface contact elements are used in conjunction with TARGE169 2-D target segments. Friction is conservatively neglected. The element mesh is sized such that the region of interest around the washer is very refined and slowly transitions to coarser density away from the washer. The 2-D axisymmetric model has 4,693 nodes, 1,444 structural elements and 100 contact elements. The bolt is constrained in the x-direction (radial) along its axis for the axisymmetric condition. The bolt and lid have y-direction (vertical) displacement constraints along their bottom nodes. The lid is also constrained in the x-direction along its bottom nodes. The washer is only restrained by the bolt and lid contact forces. The FEA model is shown Figure 2.12.7-1 and Figure 2.12.7-2.

To analyze the bolt joint and washer capability, the model is solved in a series of steps to represent a generic hypothetical drop condition. First, the bolt is preloaded such that the tensile force is approximately 222.2 kN, which corresponds to the nominal preload torque of 1,600 N-m. The lid is then displaced into the preloaded bolt such that the tensile force in the bolt is approximately 491.9 kN, which is the force necessary for the bolt shank to reach the material yield strength. The lid is then released to its original position and the bolt is left with residual preload. Finally, the bolt is released to its original position and only parts that exceeded their yield strength show residual stresses. The arbitrary displacements necessary to induce the preload and yield load in the bolt are determined iteratively until the model reaction forces match the desired values. To represent this series of conditions the model is solved in four sequential load steps:

1. Lid is constrained and the lower end of the bolt shank is displaced downward to apply the initial preload force.

2. The lid is displaced upward parallel to the bolt axis while the bolt is constrained in the initial preload location, to apply a tensile force in the bolt such that the shank approximately reaches the bolt material yield strength.

3. The lid is returned to its originally constrained preload location, which leaves the bolt with a residual preload.

4. The bolt is returned to its original location, thus releasing the residual preload.

Since the bolt shank is loaded up to the material yield strength, the model uses nonlinear material properties. For the lid, the UNS S31803 stress-strain data shown in Table 2.2-2 is in the form of true stress and strain. The multilinear kinematic hardening (KINH) material type is used. The bolt and washer material properties are defined using the bilinear kinematic hardening (BKIN) material type. The bolt and washer material properties in Table 2.12.7-1 are used to develop the true material yield strength and tangent modulus required for the BKIN material type.

Bolt Material A320 Gr. L43:

True Yield Strength: $S_{yt} = S_y\left(1+\left(\frac{S_y}{E}+0.002\right)\right) = 696\left(1+\left(\frac{696}{18.8\left(10^4\right)}+0.002\right)\right) = 700 \text{ MPa}$

True Ultimate Strength: $S_{ut} = S_u\left(1+e_u\right) = 862\left(1+0.16\right) = 999.9 \text{ MPa}$

True Yield Strain: $\varepsilon_{yt} = \ln(1+e_y) = \ln\left(1+\left(\frac{696}{18.8(10^4)}+0.002\right)\right) = 0.00569$

True Ultimate Strain: $\varepsilon_{ut} = \ln(1+e_u) = \ln(1+0.16) = 0.148$

Tangent Modulus: $E_{tan} = \frac{S_{ut}-S_{yt}}{\varepsilon_{ut}-\varepsilon_{yt}} = \frac{999.9-700}{0.148-0.00569} = 2{,}107.4 \text{ MPa}$

Washer Material A564 Gr. 630 Condition H1025:

True Yield Strength: $S_{yt} = S_y\left(1+\left(\frac{S_y}{E}+0.002\right)\right) = 948\left(1+\left(\frac{948}{19.3(10^4)}+0.002\right)\right) = 954.6 \text{ MPa}$

True Ultimate Strength: $S_{ut} = S_u(1+e_u) = 1{,}069(1+0.12) = 1{,}197.3 \text{ MPa}$

True Yield Strain: $\varepsilon_{yt} = \ln(1+e_y) = \ln\left(1+\left(\frac{948}{19.3(10^4)}+0.002\right)\right) = 0.00689$

True Ultimate Strain: $\varepsilon_{ut} = \ln(1+e_u) = \ln(1+0.12) = 0.113$

Tangent Modulus: $E_{tan} = \frac{S_{ut}-S_{yt}}{\varepsilon_{ut}-\varepsilon_{yt}} = \frac{1{,}197.3-954.6}{0.113-0.00689} = 2{,}287.2 \text{ MPa}$

2.12.7.3 Finite Element Analysis Results

The stress intensities for each part at each load step are listed in Table 2.12.7-3 and shown in Figure 2.12.7-3 through Figure 2.12.7-10. The stress intensities show the washer does not yield for a hypothetical condition where the bolt is loaded to its yield strength. The washer maximum stress is 758.9 MPa, which is less than the engineering yield strength of 948 MPa at 71 ºC. The bolt shank measured 691.6 MPa, which is approximately the bolt engineering yield stress of 696 MPa. The discontinuity between the bolt head and shank exceed the yield strength as expected. The lid tube also shows minor yielding with a residual stress of 100.9 MPa after the bolt is unloaded.

The bolt reaction loads are listed in Table 2.12.7-4. The reduction in bolt preload force is less than 10% of the initial preload force after being loaded up to its yield strength.

$$\text{Reduction of Preload} = \frac{222.6-201.4}{222.6} \times 100 = 9.5\,\%$$

2.12.7.4 Closure Lid, Bolt, and Washer Interaction Summary

The FEA results show that none of the TRUPACT–III closure lid components experiences significant permanent deformation when a load equal to the bolt shank yield load is applied to the joint. Local yielding in the sharp corner under the bolt head and at the outer sharp edge of the bolt head does occur, but yield of the washer does not occur. Very limited yielding in the lid surface

also occurs. The insignificance of these deformations is demonstrated by the fact that, after the full loading sequence has been applied, the initial preload force applied to the bolt has been reduced by only 9.5%. Therefore, the components of the lid closure joint are adequately designed. Adequacy of the joint to maintain closure in the worst-case HAC free drop is demonstrated by test.

Table 2.12.7-1 – Bolt and Washer Material Properties at 71 ºC

Bolt Material A320 Gr. L43[1]	
Yield Strength, MPa	696
Ultimate Strength, MPa	862
Elastic Modulus, MPa	18.8×10^4
Elongation[3] (%)	16
Washer Material A564 Gr. 630 H1025[2]	
Yield Strength, MPa	948
Ultimate Strength, MPa	1,069
Elastic Modulus, MPa	19.3×10^4
Elongation[3] (%)	12

Notes:

1. Material properties interpolated using data from Table 2.2-4.
2. Material properties interpolated using data from Table 2.2-8.
3. The total elongation is from ASME B&PV Code, Section II, Part A.

Table 2.12.7-2 – Model Parts

Part #	Description	Material Size (mm)	Material Type
1	Washer	M36 x 6 THK	ASTM A564 Gr. 630 H1025
2	Lid, Tube	44 ID	ASTM A240/A479 UNS S31803
3	Bolt, SHCS	M36 x 4, 30 OD Shank	ASTM A320 Gr. L43

Table 2.12.7-3 – Maximum Stress Intensity Results Summary, MPa

Load Step	Washer	Lid	Bolt Head	Bolt Shank
1, Bolt preload	389.3	393.2	709.6	314.4
2, Bolt yield load	758.9	540.3	835.1	691.6
3, Bolt residual preload	353.6	248.2	420.8	284.5
4, Bolt unloaded	0	100.9	599.9	0

Table 2.12.7-4 – Reaction Load Summary

Load Step	Bolt Force, kN
1, Bolt preload	222.6①
2, Bolt yield load	489.7②
3, Bolt residual preload	201.4
4, Bolt unloaded	0

Notes:

1. Adequately close to the target preload of 222.2 kN.
2. Adequately close to the target yield load of 491.9 kN.

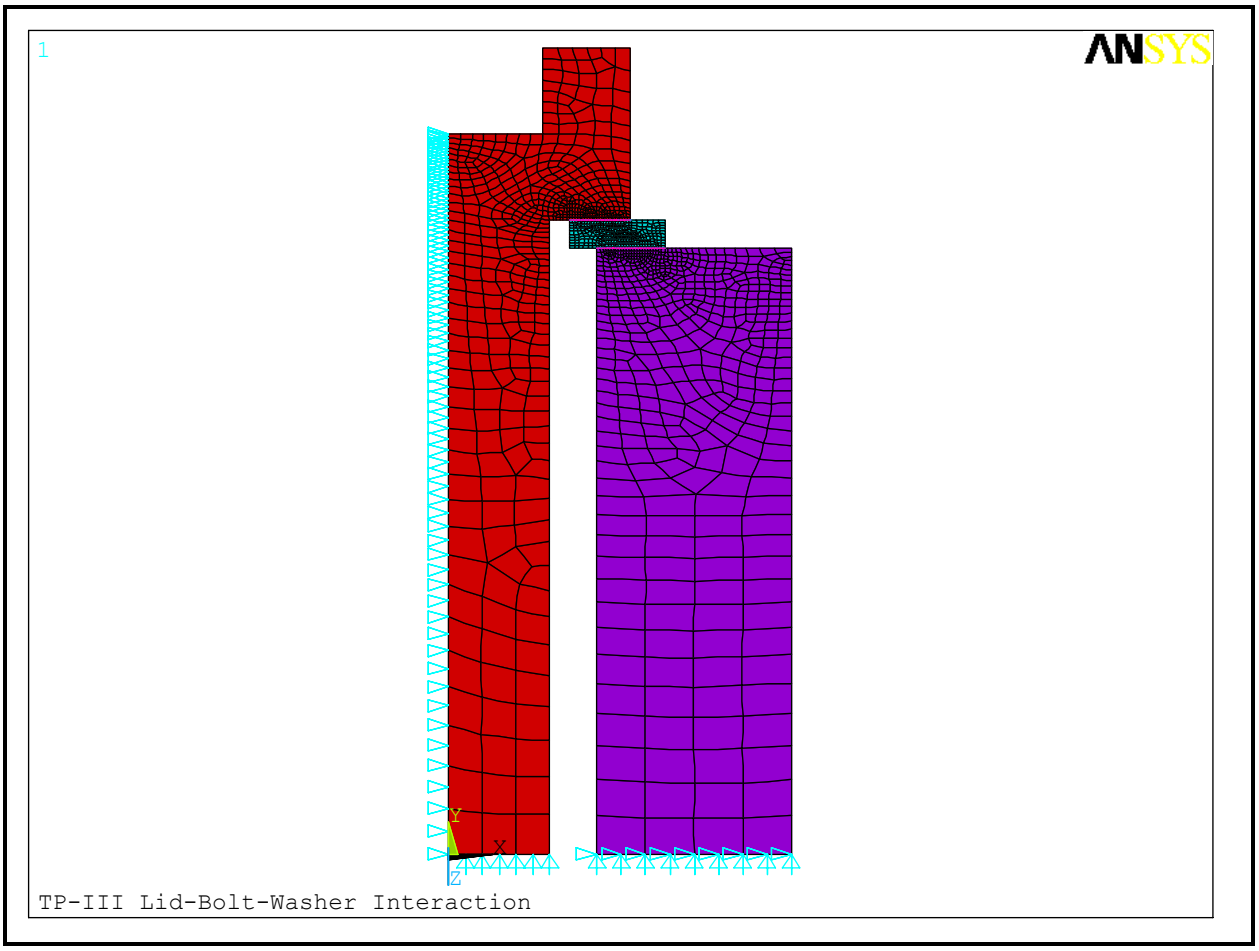

Figure 2.12.7-1 – ANSYS® Model Element Plot with Boundary Constraints

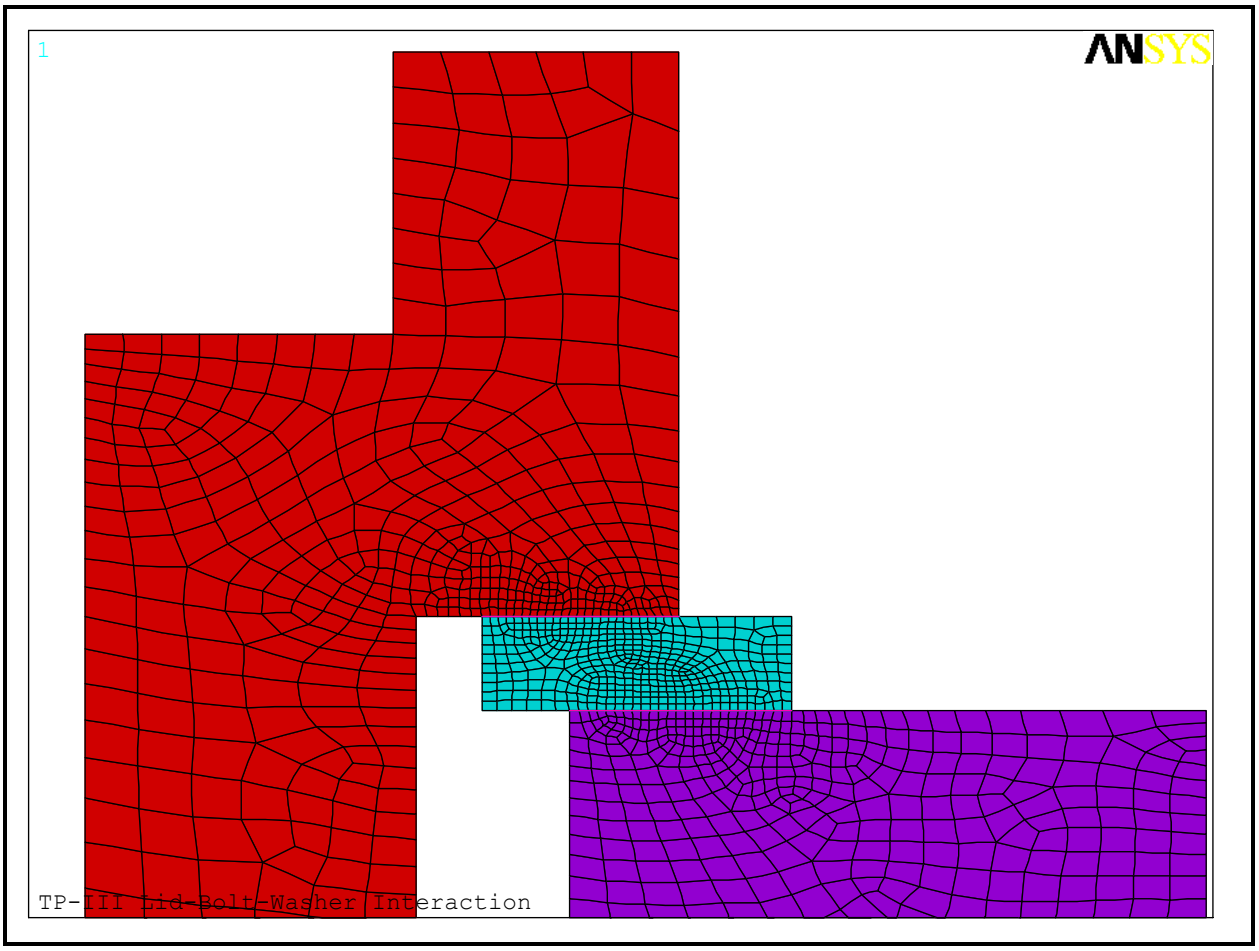

Figure 2.12.7-2 – ANSYS® Model with Washer Detail Element Plot

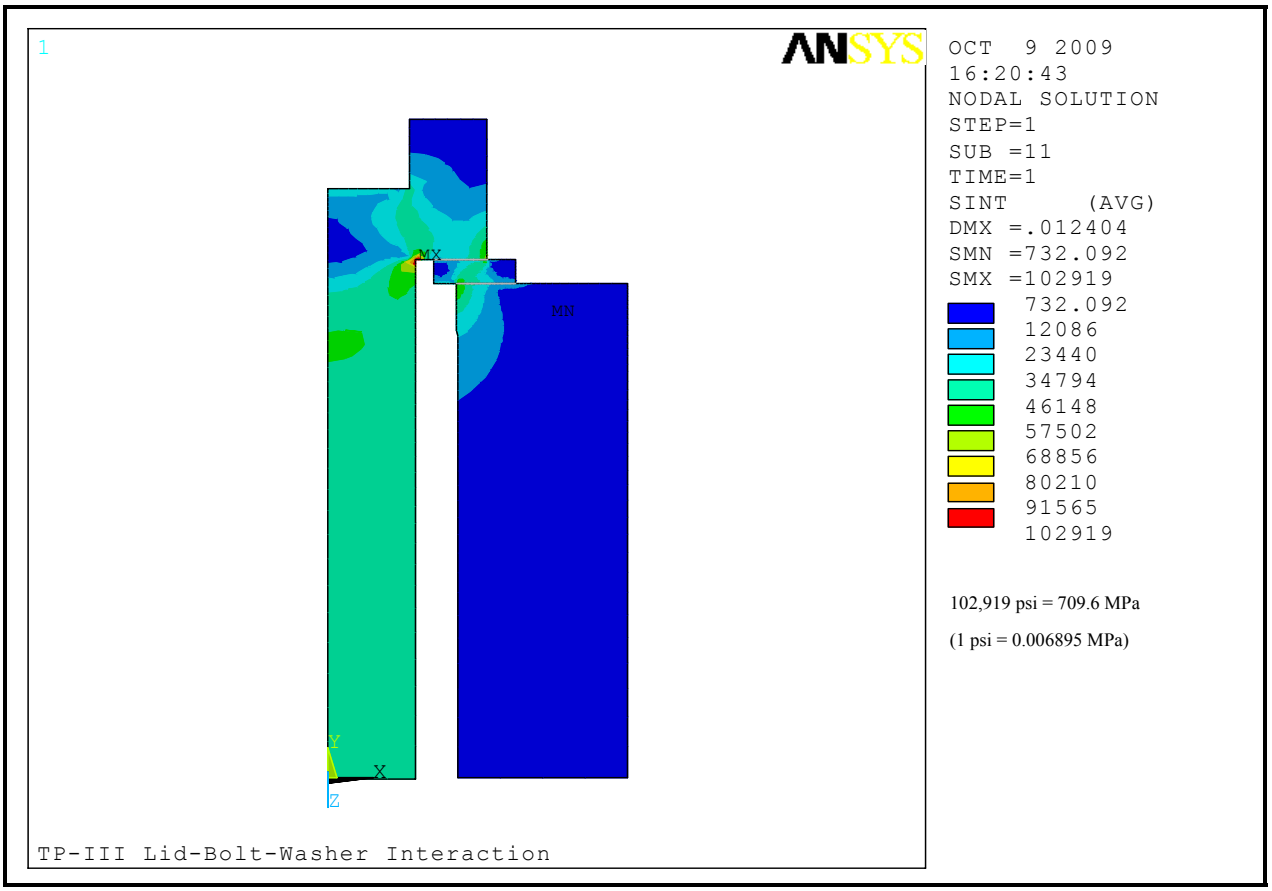

Figure 2.12.7-3 – Preload Stress Intensity Model View

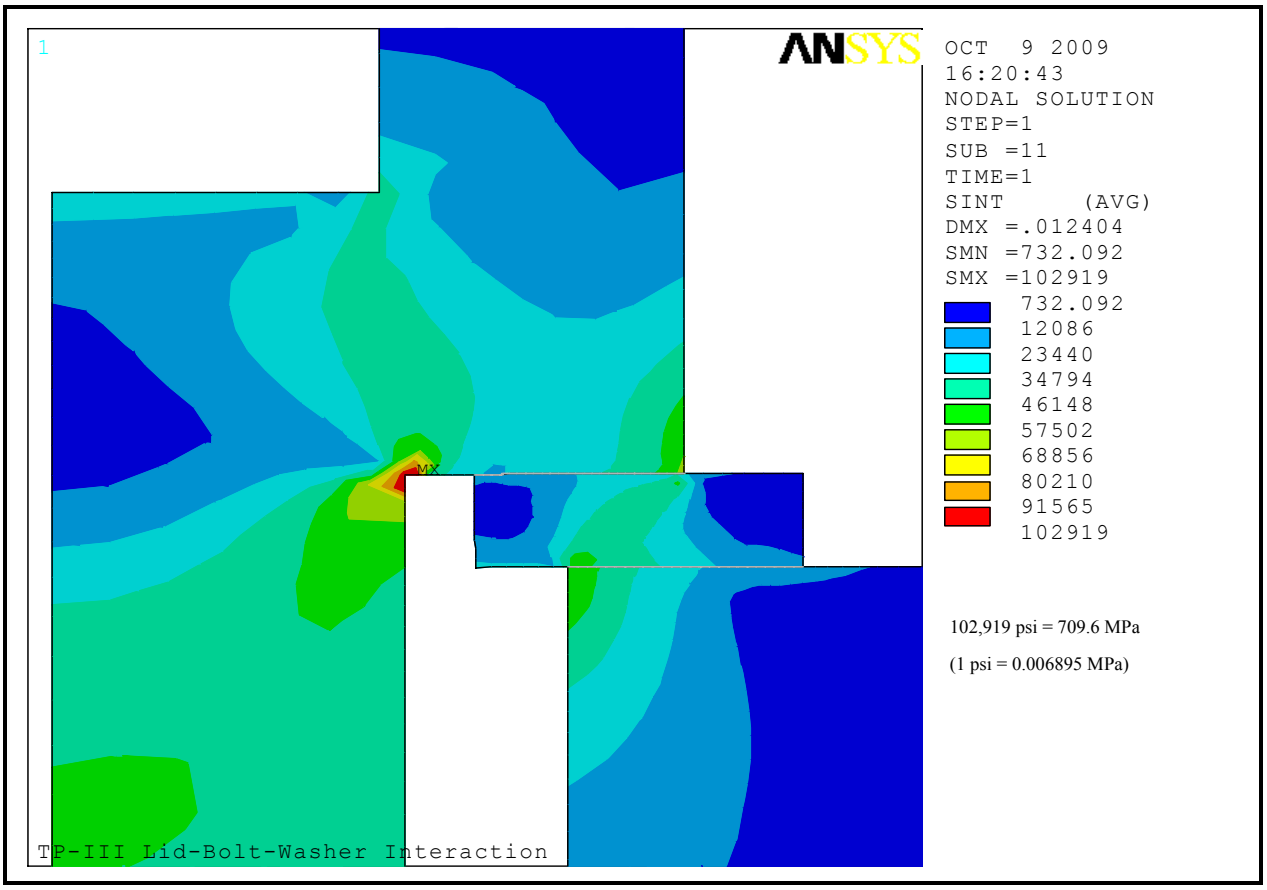

Figure 2.12.7-4 – Preload Stress Intensity Detail View

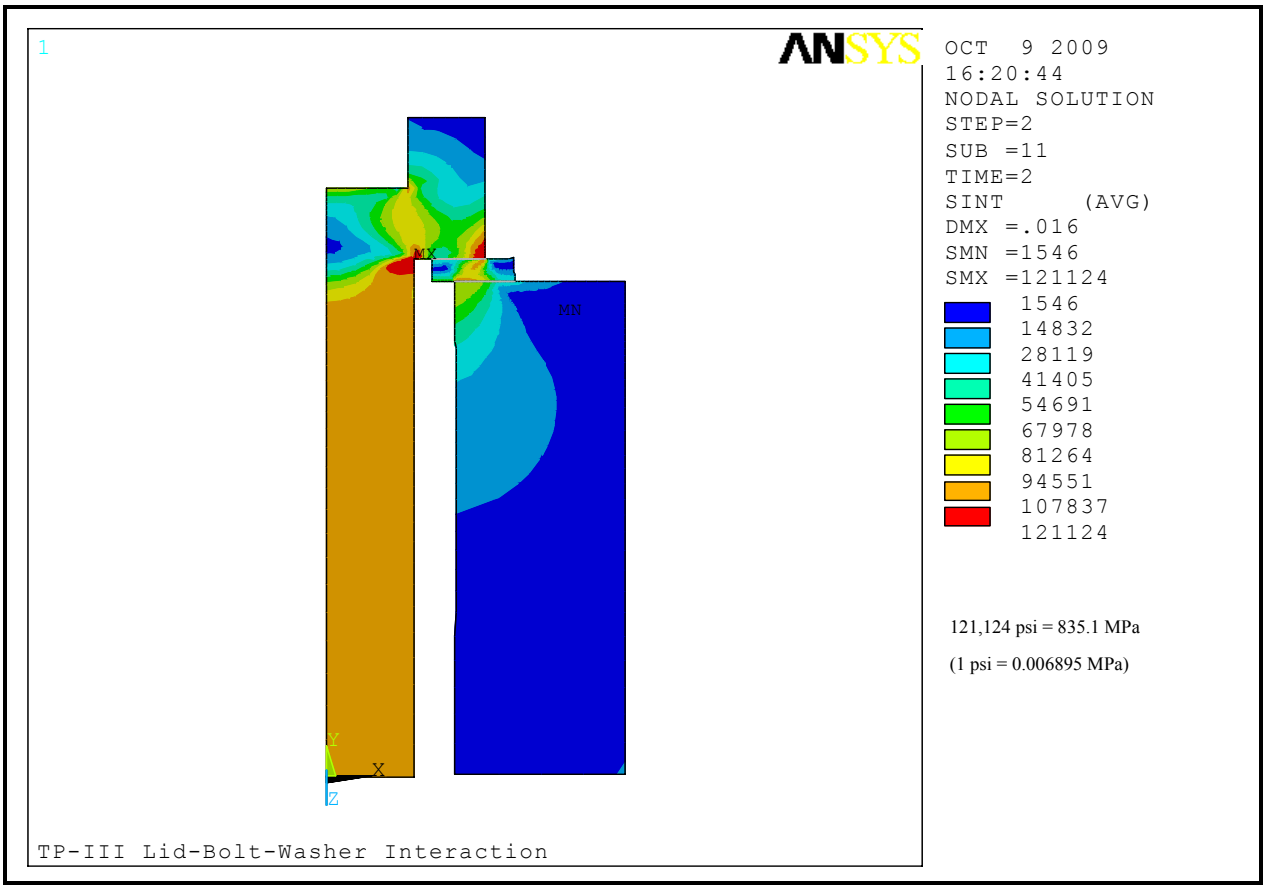

Figure 2.12.7-5 – Yield Load Stress Intensity Model View

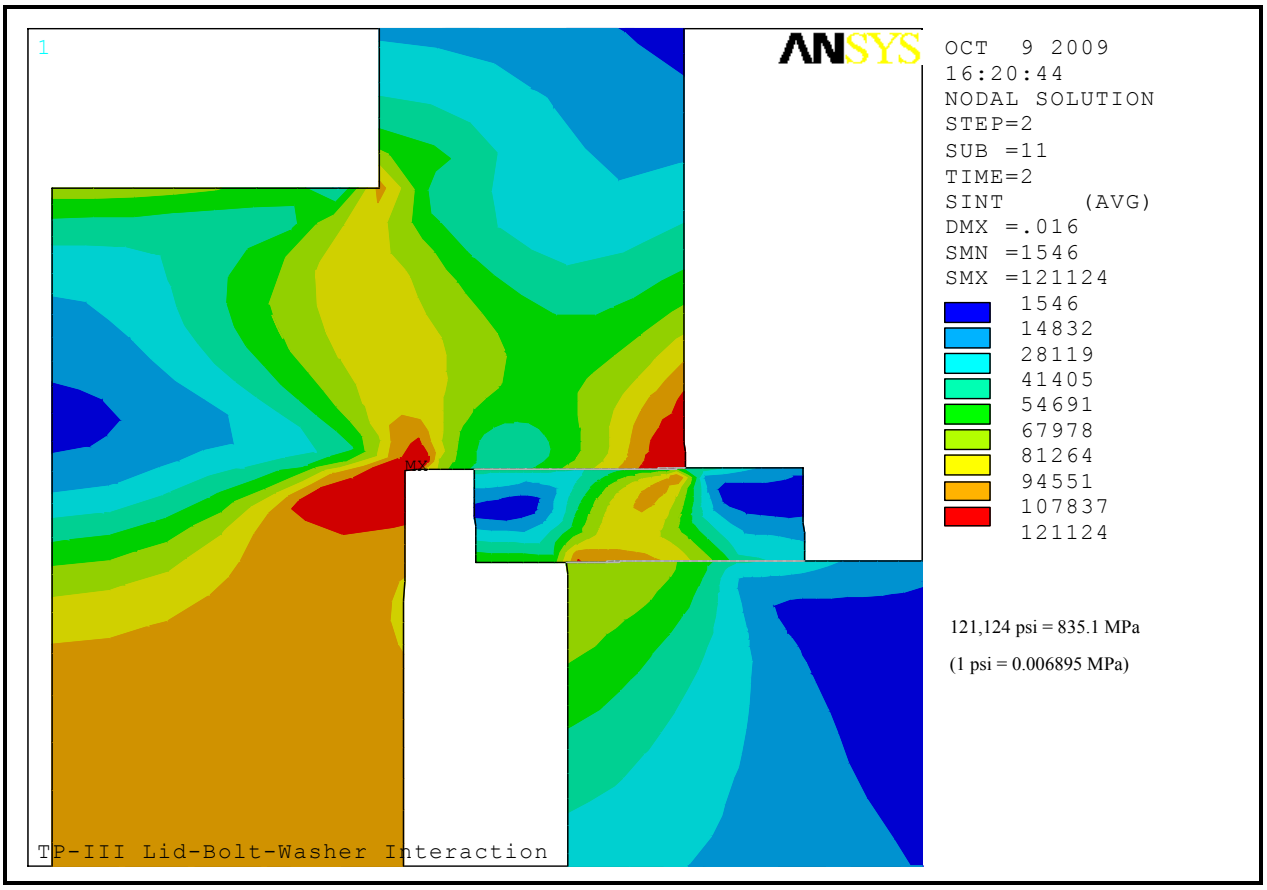

Figure 2.12.7-6 – Yield Load Stress Intensity Detail View

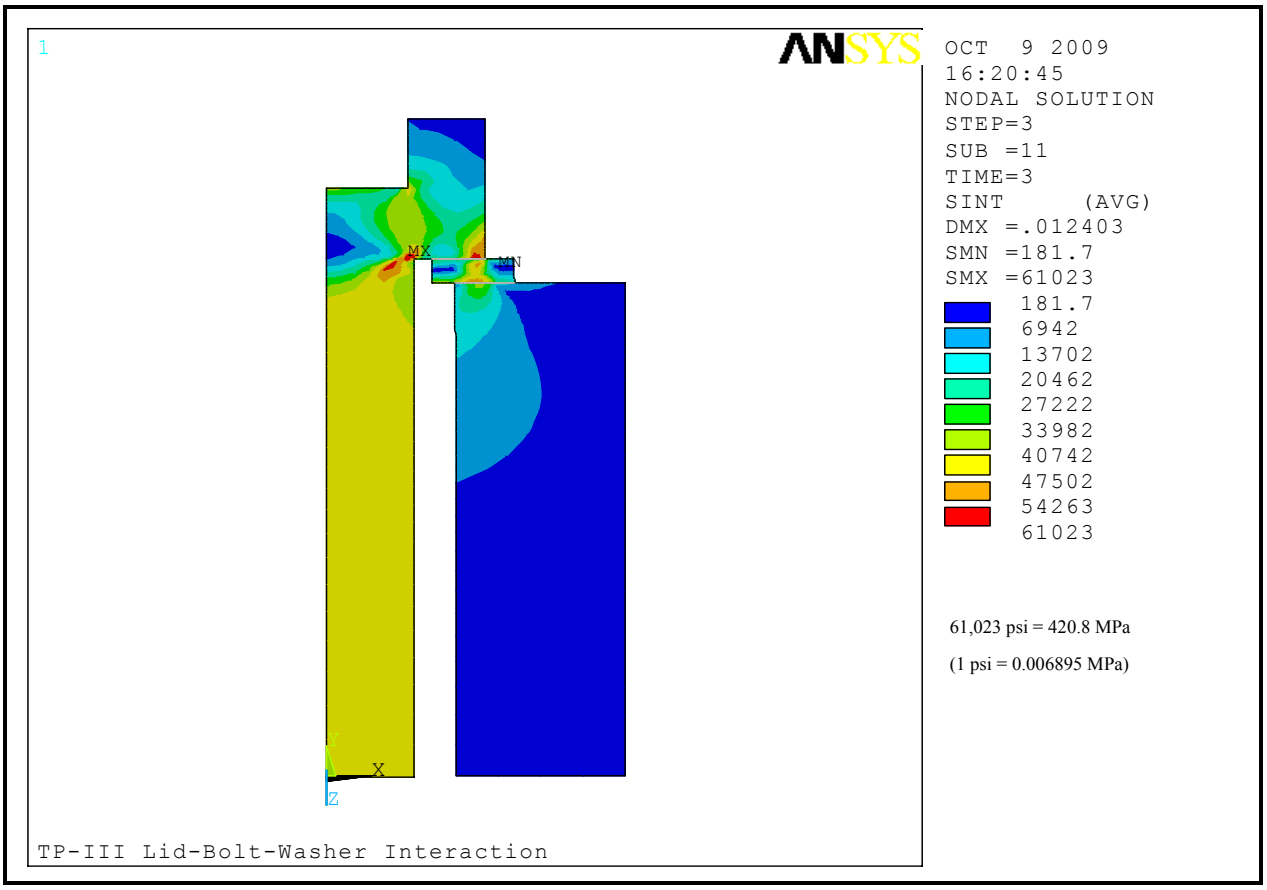

Figure 2.12.7-7 – Residual Preload Load Stress Intensity Model View

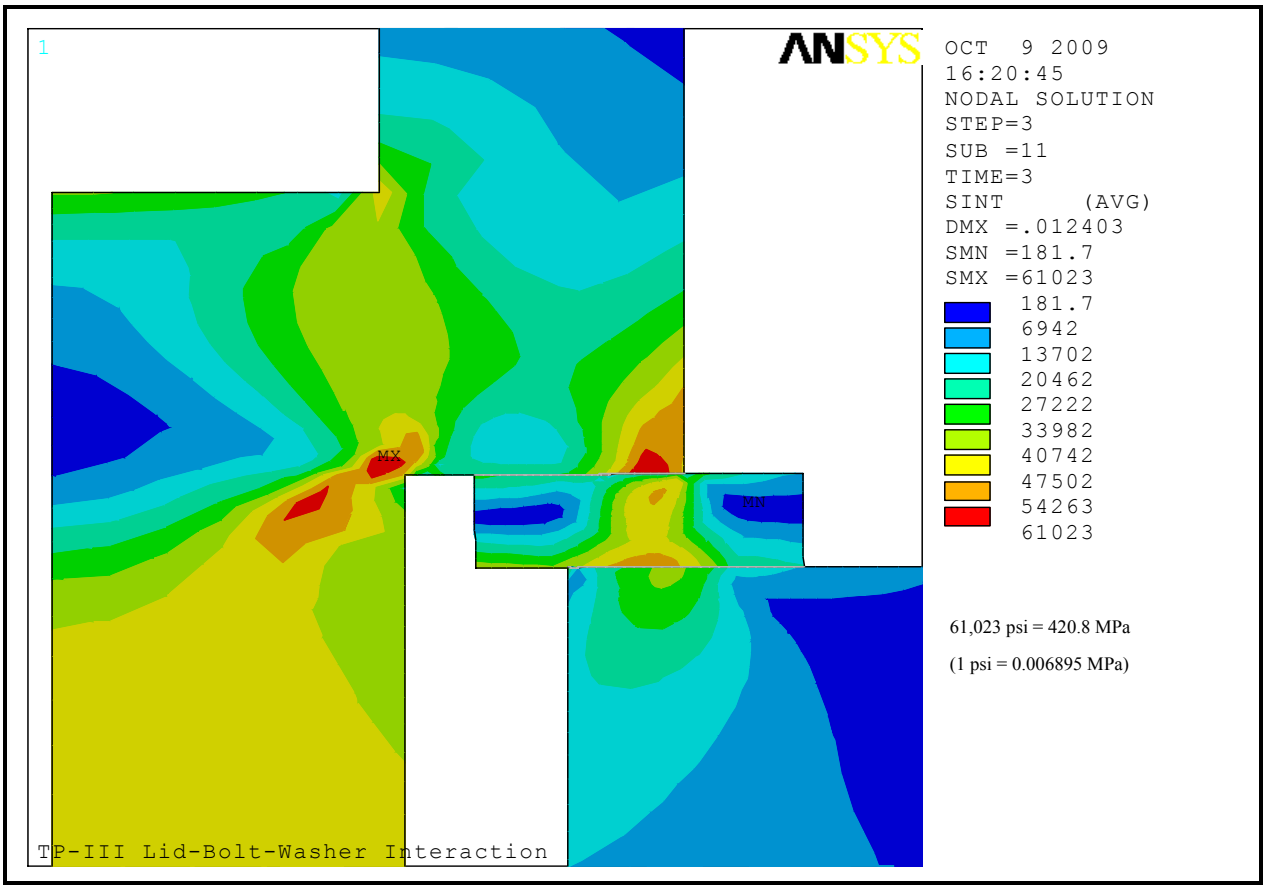

Figure 2.12.7-8 – Residual Preload Load Stress Intensity Detail View

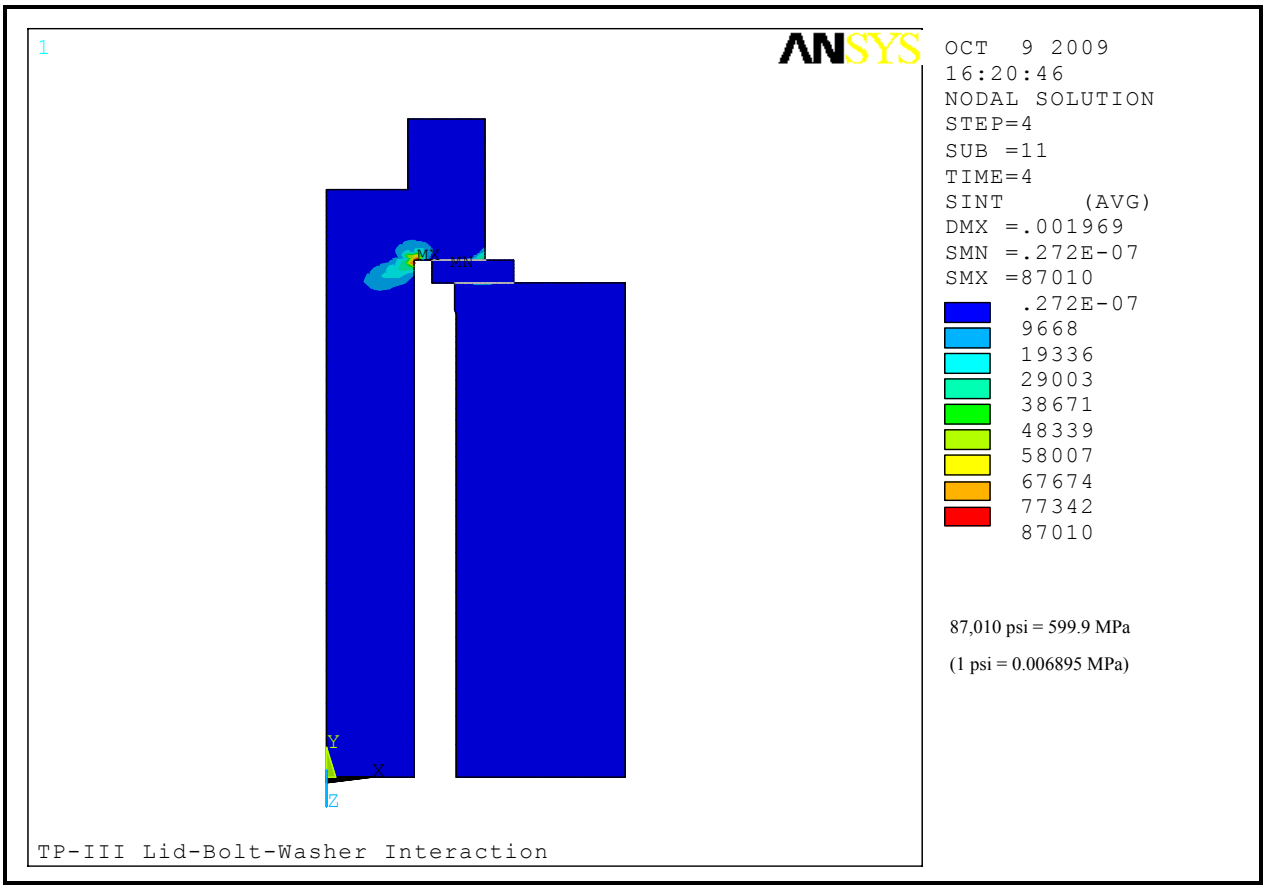

Figure 2.12.7-9 – Unloaded Residual Stress Intensity Model View

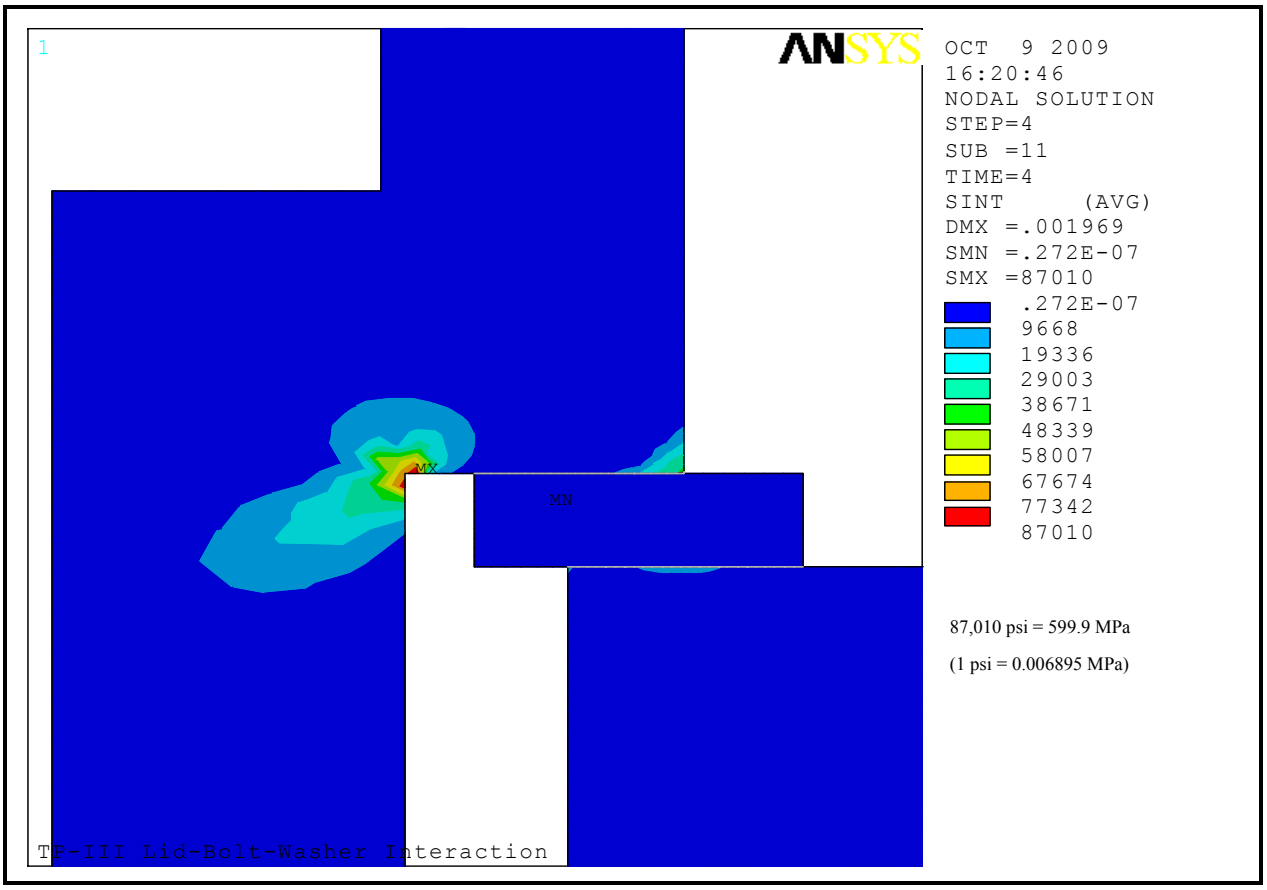

Figure 2.12.7-10 – Unloaded Residual Stress Intensity Detail View

This page intentionally left blank.

3.0 THERMAL EVALUATION

This chapter identifies and describes the principal thermal design aspects of the TRUPACT–III package. Further, this chapter presents the evaluations that demonstrate the thermal safety of the TRUPACT–III packaging and compliance with the thermal requirements of 10 CFR 71[1] when transporting a payload of contact-handled (CH) transuranic (TRU) waste generating a maximum of 80 watts of decay heat. Specifically, all package components are shown to remain within their respective temperature limits under the design basis normal conditions of transport (NCT). Further, per 10 CFR §71.43(g), the maximum accessible package surface temperature is demonstrated to be less than 50 °C for the maximum decay heat loading, an ambient temperature of 38 °C, and no insolation.

The bulk temperature of the impact absorbing foam is shown to be less than 65 °C, based on the NCT maximum temperature conditions. As such, the foam will retain sufficient structural integrity to protect the payload during the subsequent hypothetical accident condition (HAC) drop scenarios described in Chapter 2.0, *Structural Evaluation*. Finally, the package is shown to structurally withstand the damage arising from the HAC drop scenarios and retain sufficient thermal protection to maintain all package component temperatures within their respective short term limits during the regulatory fire event and the post-fire package cool-down period.

3.1 Description of Thermal Design

The TRUPACT–III packaging, as illustrated in Figure 1.1-1 through Figure 1.1-7 from Section 1.1, *Introduction*, is a rectangular body assembly with a bolted, flat closure lid and an energy absorbing overpack cover that protects the closure lid. The body assembly consists of an integral, energy-absorbing and thermally-protective overpack structure that surrounds and protects a rigid containment structural assembly (CSA) from the hypothetical accident conditions of transport (HAC). The external dimensions of the package are 4,288 mm long × 2,500 mm wide × 2,650 mm high, while the internal dimensions of the payload compartment are 2,790 mm long × 1,840 mm wide × 2,000 mm high. The maximum gross shipping weight of the package is 25,000 kg, with an empty weight of approximately 19,790 kg.

The primary heat transfer mechanisms within the TRUPACT–III packaging are conduction and radiation, while the principal heat transfer from the exterior of the packaging is via convection and radiation to the ambient environment. The potential for convective heat transfer within the payload cavity is conservatively neglected due to the relatively close coupling of the bodies within the package cavity.

3.1.1 Design Features

The TRUPACT–III package (see Figure 1.1-1 and Figure 1.1-2) is designed as a totally passive thermal system. The principal thermal characteristic of the TRUPACT–III package is that the structure of both the overpack and CSA are fabricated of relatively light weight sheetmetal. This design feature results in a package design that exhibits a rapid thermal response for the overpack sheetmetal under

[1] Title 10, Code of Federal Regulations, Part 71 (10 CFR 71), *Packaging and Transportation of Radioactive Material*, 01–01–09 Edition.

transient heat loads. The CSA is thermally protected from temperature swings on the package exterior through the balsa wood and polyurethane foam used to provide thermal and impact protection.

3.1.1.1 TRUPACT–III Packaging

CSA

The CSA (the body plus the bolted closure lid) is a rigid, lightweight, and high strength structure fabricated of Alloy UNS S31803 stainless steel. The inner wall of the CSA serves as the containment boundary for the package. Surrounding the 8-mm inner containment stainless steel sheets is an 8-mm stainless steel structural sheet that is attached to the containment sheets via V-shaped, 4-mm thick stainless steel stiffener ribs. Continuous seam welds attach the 4-mm thick ribs to the containment sheet, while 20-mm plug welds spaced approximately 55-mm apart are utilized to attach the ribs to the structural sheet. The overall cross-sectional thickness of the CSA body is 140-mm. Guide bars with a cross section of 25 mm × 76 mm are attached to the side, back, and roof of the CSA inner cavity. The guide bars are made of ASTM Type 304/304L stainless steel and are located to correspond to the bumpers on the SLB2 payload container.

The containment boundary of the CSA is formed by the following components:

- the inner stainless steel sheets of the CSA body (four sides plus the closed end),
- the closure lid inner sheet,
- the inner O-ring seal located in the outer flange of the closure lid,
- the vent port insert located in the closure lid,
- the vent port insert inner O-ring seal.

Packaging Overpack

The CSA is surrounded on the sides by an overpack of 109 to 114-mm thick polyurethane foam (nominal density of 0.10 kg/dm^3), followed by a 10-mm puncture resistant stainless steel sheet, then a 60-mm thick layer of low density balsa wood, and, finally, a 6-mm outer stainless steel sheet. The exterior surface of the outer sheet is painted white, with the coating being optional for the bottom surfaces. The steel sheets are fabricated of Alloy UNS S31803 stainless steel. The 109-mm foam thickness is used on the top and bottom of the package, while the sides of the package use a 114-mm thick foam layer. Figure 1.1-3 illustrates the typical buildup of components through a typical package section.

While the CSA is essentially surrounded by low thermal conductivity material (i.e., the polyurethane foam and balsa wood), the 6-mm support sheets connecting each edge of the CSA to the exterior of the package (see Figure 3.1-1) provide a direct heat transfer path between the CSA and the exterior surface of the package. As seen from the figure, the 6-mm support sheets are an integral part of the corner sheet metal component. This feature, plus the use of a continuous weld at the joint with the CSA structural sheet, provides a direct, metallic heat transfer path between the CSA and outer sheet. The impact protection at the corners is enhanced by the use of a higher density polyurethane foam (nominal density of 0.29 kg/dm^3) than that used along the sides of the package.

Packaging Closures

The ends of the package are similar to each other in construction and design layout. The principal differences are that the closure lid end contains the temperature sensitive O-ring seals and is more

complex in its design due to its ability to be removed. As such, while the following discussion is specific to the closure lid end, it is generally applicable to the design of the closed end as well.

The closure lid is fabricated in a similar manner as the sidewalls of the CSA body. However, for additional rigidity, the inner and outer sheets are 12-mm thick vs. the 8-mm thick sheets used for the CSA body sidewalls. In addition, the structural sheet of the closure lid is fabricated of multiple sheetmetal strips vs. a continuous sheet. The V-stiffeners are attached to the outside of the inner (containment) sheet using continuous fillet welds, while the outer structural sheets are connected to each other and the V-stiffeners using continuous slot welds (as opposed to the plug welds used for the CSA body). The total thickness of the lid is 148-mm, the width is 2,108 mm, and the height is 2,280 mm. The perimeter of the lid assembly is formed by a rigid box beam flange that incorporates two dovetail grooves to retain the containment and test O-rings and which mates with a similar box beam flange on the CSA body.

The closure lid incorporates a debris shield to protect the containment O-ring from debris originating from the payload. The debris shield assembly consists of a holder, a U-shaped foam insert, and the receptacle. The debris shield extends inward from the shear lip of the closure lid and mates with a receptacle mounted on the sides of the CSA inner cavity (see Figure 1.1-7). The holder is fabricated of UNS S31803 duplex stainless steel, the receptacle is UNS S31803 or Type 304L stainless steel, and the foam insert is made of silicone foam rubber. Double-sided tape is used to mount the foam insert to the holder. Each of the four shear lips features two, 5/16-inch (7.9 mm) diameter filters made from porous polyethylene. These filtered passages prevent a pressure differential across the debris shield and permit helium to reach the containment O-ring seal during leakage rate testing.

A 200-mm × 320-mm recess located in the lower right-hand corner of the lid contains the vent port and the seal test port. The vent port, which is a containment boundary penetration, is closed by an aluminum-bronze insert and sealed by a O-ring seal. The containment, test, and vent port O-ring seals are fabricated from butyl rubber. The closure lid is attached to the CSA body by forty-four (44) bolts fabricated from ASTM A320, L43 alloy steel. Figure 1.1-5 illustrates a cross-section through the closure lid and the interface between lid and the CSA structure.

Impact and thermal protection of the closure lid is provided by the overpack cover assembly. Figure 3.1-2 illustrates an elevation view, while a perspective view is provided in Figure 1.1-1. Because of the diamond shaped recessed region incorporated into the design, the cross-section through the assembly is not uniform. Figure 3.1-3 illustrates the cross-section through the assembly along a section cut line depicted in Figure 3.1-2.

The recessed region of the overpack cover assembly utilizes a 6-mm thick outer sheet backed by a 60-mm thick layer of low-density balsa wood which, in turn, is backed by a 120-mm thick layer of polyurethane foam. The balsa wood and polyurethane foam materials are separated by a 15-mm thick stainless steel sheet to provide resistance to the HAC puncture drop accidents. An additional 6-mm thick sheet is used at the backside of the overpack cover to enclose the polyurethane foam and form the surface which is secured against the outer surface of the closure lid.

The outer region of the overpack cover assembly utilizes an 8-mm thick outer sheet. The joints at the edges of the outer sheets used a rolled, overlapping joint to provide additional tear resistance when deformed under the HAC drop events. The outer sheet is backed by a 140-mm thick layer of medium density polyurethane foam (nominal density of 0.16 kg/dm^3) which, in turn, is backed by a 380-mm

thick layer of higher density polyurethane foam (nominal density of 0.48 kg/dm^3). The layers of polyurethane foam are separated by a 6-mm thick stainless steel sheet to provide resistance to the HAC puncture drop accidents. To provide additional thermal protection around the perimeter of the closure lid where the containment O-ring seals are used, a 42-mm layer of calcium silicate insulation is used. The calcium silicate insulation is covered by a 16-mm thick stainless steel protection plate to provide impact protection to the underlying insulation. Similarly, the upper and lower extensions on the overpack cover assembly incorporate a 30-mm layer of calcium silicate insulation backed by 16-mm thick protection plate to provide lateral protection to the overlapped edges of the closure lid.

Packaging Cheeks

The extensions or 'cheeks' at the end of the package (see Figure 1.1-1 and Figure 3.1-4) provide additional impact protection and serve as lifting points for the package. The outer plates of the cheeks vary in thickness from approximately 2 to 8-mm, but are typically 6-mm or 8-mm. A 140-mm thick layer of medium density polyurethane foam (nominal density of 0.16 kg/dm^3) is used at the ends of the extensions, while the remainder of the extension is filled with high density polyurethane foam (nominal density of 0.48 kg/dm^3). A 30-mm layer of calcium silicate insulation backed by 16-mm thick protection plate provides lateral thermal protection to the overlapped edges of the closure lid.

3.1.1.2 Payload Configuration

As described in Section 1.2.2, *Contents*, the users of the TRUPACT–III package must comply with the payload requirements outlined in the TRUPACT–III TRAMPAC document[2]. That document specifies the Standard Large Box 2 (SLB2) as the only permissible waste box payload container to be utilized with the TRUPACT–III package. The SLB2 containers are fabricated of painted carbon steel and have outside dimensions of 2,743-mm (108-in) long, 1,753-mm (69-in) wide and 1,854-mm (73-in) tall. The containers are designed to be either top or bottom loaded and to accommodate a variety of CH-TRU waste. Figure 3.1-5 illustrates a prototypic top-loading SLB2 container. The waste may either be placed directly into the SLB2 container, or be housed within other containers which, in turn, are placed into the SLB2 container.

Because of the potential variability in the configuration of the waste stream to be loaded in a SLB2 container, a hypothetical waste box which provides a conservative lower bound on the waste stream volume expected to be transported within a SLB2 container is assumed. The dimension of the hypothetical waste box is 965 mm × 965 mm × 1,727 mm (i.e., 3 ft, 2 inches × 3 ft, 2 inches × 5 ft, 8 inches). This hypothetical waste box payload geometry represents 23% of the total available waste volume within the SLB2 container and bounds both the credible volumetric heat loading and the credible non-uniform distribution of decay heat generating waste within the SLB2 container. The hypothetical waste box is assumed to be horizontally and axially centered within the SLB2 container and to be resting against the bottom of the SLB2 container. This placement yields the maximum expected separation distance between the payload and the interior of the TRUPACT–III cavity.

Section 3.5.2.1, *Description of Thermal Model for NCT Conditions*, provides additional details of the payload modeling.

[2] U.S. Department of Energy (DOE), *TRUPACT–III TRU Waste Authorized Methods for Payload Control (TRUPACT–III TRAMPAC)*, U.S. Department of Energy, Carlsbad Field Office, Carlsbad, New Mexico.

3.1.2 Content's Decay Heat

The maximum decay heat dissipated by the contents of the TRUPACT–III payload will be 80 watts or less. Further, the decay heat is assumed to be uniformly distributed within the reduced hypothetical payload volume discussed above. The use of a uniform volumetric heat generation is justified by the following considerations:

1) first, the region of uniform volumetric heat generation is confined to a reduced, hypothetical volume that represents only 23% of the actual payload volume within the SLB2 container (see discussion in Section 3.1.1.2, *Payload Configuration*),
2) the thermal conductivity of the entire volume within the SLB2 container is conservatively assumed to be equal to air. Since the actual payload will have an effective bulk thermal conductivity substantially higher than air due to the presence of metals and/or other materials, the peak temperature predicted using the SAR assumptions will bound the peak payload temperature for any credible decay heat distribution within the SLB2 container based on an even greater non-uniform decay heat distribution and the actual payload thermal conductivity.

3.1.3 Summary Tables of Temperatures

Table 3.1-1 presents a summary of the maximum temperatures determined for the major components of the TRUPACT–III packaging under NCT and HAC conditions with an internal decay heat load of 80 watts. As seen from the table, the peak temperature for all components remain within their respective limits for both NCT and HAC conditions. Therefore, the TRUPACT–III Package design complies with the thermal requirements of 10 CFR 71.

Further details of the NCT results, plus those for lower decay heat loads, are presented in Section 3.3, *Thermal Evaluation for Normal Conditions of Transport*. Similarly, further discussion of the HAC thermal analysis is provided in Section 3.4, *Thermal Evaluation for Hypothetical Accident Conditions*.

3.1.4 Summary Tables of Maximum Pressures

The maximum normal operation pressure (MNOP) developed during the maximum shipping period is limited by administrative controls to 172 kPa gauge. The maximum pressure developed under HAC conditions will be 249.3 kPa gauge, or a + 45% increase from its maximum pre-fire level. Table 3.1-2 presents a summary of the maximum package pressures.

The primary mechanism for potential flammable gas generation in TRU wastes is radiolysis[2], while gas generation via chemical, biological, and thermal mechanisms are insignificant. The methods of compliance and verification for gas generation issues are provided in the TRAMPAC document[2].

Table 3.1-1 – Summary of Maximum Package Temperatures

Location / Component	Temperatures (°C)			
			Maximum Allowable [3]	
	NCT Hot [1,2]	HAC [2]	NCT	HAC
Bounding Waste Box Payload				
- Maximum	162.2	177	230	230
- Bulk Avg.	90.4	107	230	230
Standard Large Box (SLB2) Payload				
- Maximum sidewall	62.3	89	230	230
- Minimum sidewall (coincident) [4]	52.9	54	230	230
- Avg. sidewall	54.9	60	230	230
- Bulk Avg. (of void only)	55.4	76	230	230
- Bulk Avg. (of total volume) [5]	63.0	83	230	230
Containment O-ring Seal	52.6	95	107	204
Sampling/Vent Port O-ring Seal	51.2	80	107	204
Debris Shield	52.6	95	120	-
CaSi (Seal Protection) Insulation	60.9	688	982	982
CSA Structural Sheet (includes Lid outer sheet),	57.6	689 (Max) [6] 75 (Avg)	316	725 for < 1 hour / 316
CSA Containment Sheet (includes Lid inner sheet)				
- Maximum	55.6	222	316	316
- Minimum (coincident) [4]	50.4	51	316	316
CSA Lid Bolts	53.4	187	427	316
Outer Skin				
- Package Body, Peak	86.6	800	121	1,370
- Package Cheek, Peak	77.8	800	121	1,370
- Package Cover, Peak	84.2	800	121	1,370
Last-a-Foam				
- Package Body, Peak/Avg.	67.3 / 51.9	684 / 96	260 / 65	-
- Package Corner, Peak/Avg.	82.4 / 52.3	797 / 189	260 / 65	-
- Package Cheek, Peak/Avg.	77.3 / 49.7	800 / 373	260 / 65	-
- Overpack Cover Outer Area, Peak/Avg.	83.6 / 52.4	792 / 169	260 / 65	-
- Overpack Cover Recess Area, Peak/Avg.	58.6 / 50.5	695 / 99	260 / 65	-
Balsa				
- Package Body, Peak/Avg.	86.2 / 55.3	793 / 455	100 / 65	-
- Overpack Cover, Peak/Avg.	66.9 / 51.3	784 / 449	100 / 65	-

Notes:

1) Peak temperatures determined assuming one SLB2, diurnal insolation cycle, and a constant ambient temperature of 38 ºC.
2) For conservatism, the decay heat is confined to a bounding minimum sub-volume within the SLB2. This sub-volume represents 23% of the total available volume. The remaining SLB2 volume is assumed to have zero decay heat and the thermal properties of air.
3) Maximum allowable temperatures are established in Section 3.2.2, *Technical Specifications of Components*.
4) The listed minimum temperature is taken at the same time point (i.e., 'coincident') as the listed maximum temperature as opposed to the actual minimum temperature occurring during the diurnal cycle.
5) Bulk average temperature computed assuming SLB2 internal volume of 7,394 liters and a bounding waste box volume of 1,609 liters.
6) The peak CSA structural sheet temperature occurs at the location of the puncture bar damage and lasts less than 1 hour. The temperature for the remaining portions of the structural sheet is substantially lower as demonstrated by the average temperature value.

Table 3.1-2 – Summary of Maximum Pressures

Condition	CSA Cavity Temperature	Pressure
NCT Hot	59 °C	172 kPa gauge
HAC Hot	153 °C	249.3 kPa gauge

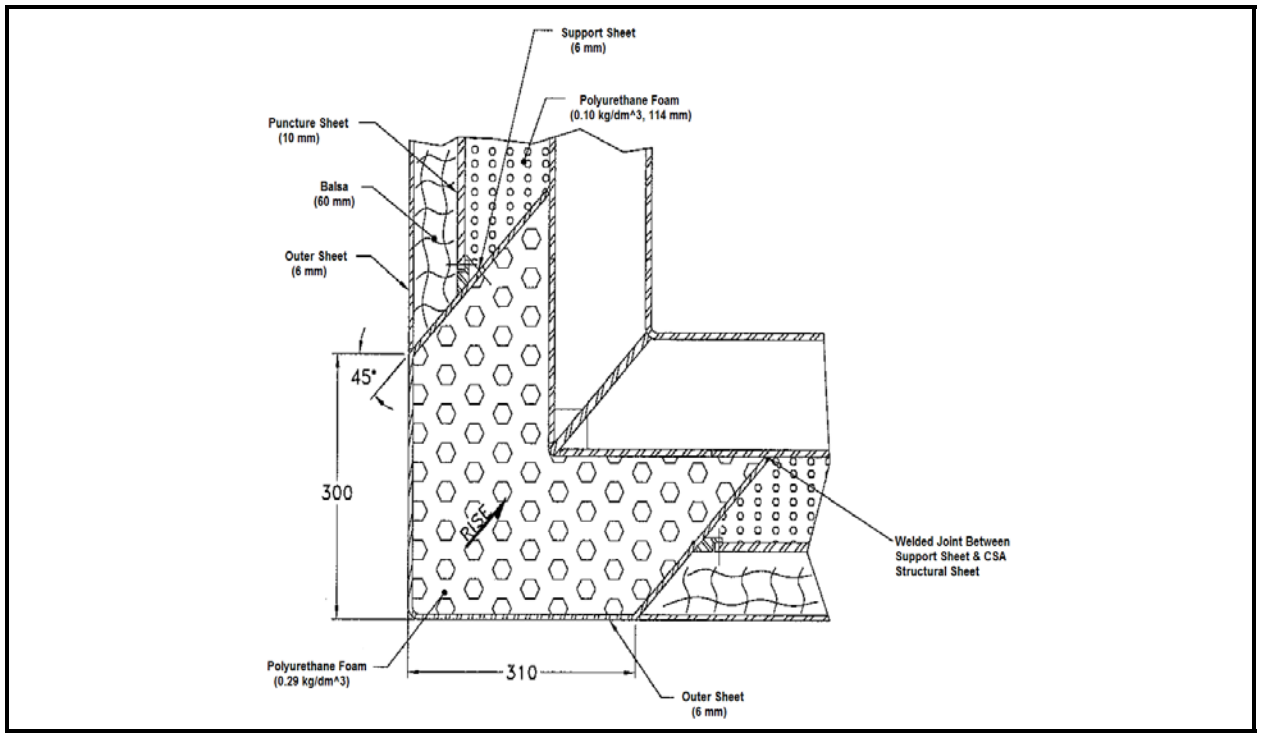

Figure 3.1-1 – Package Corner Detail

Security-Related Information
Figure Withheld Under 10 CFR 2.390

Figure 3.1-2 – Overpack Cover Elevation

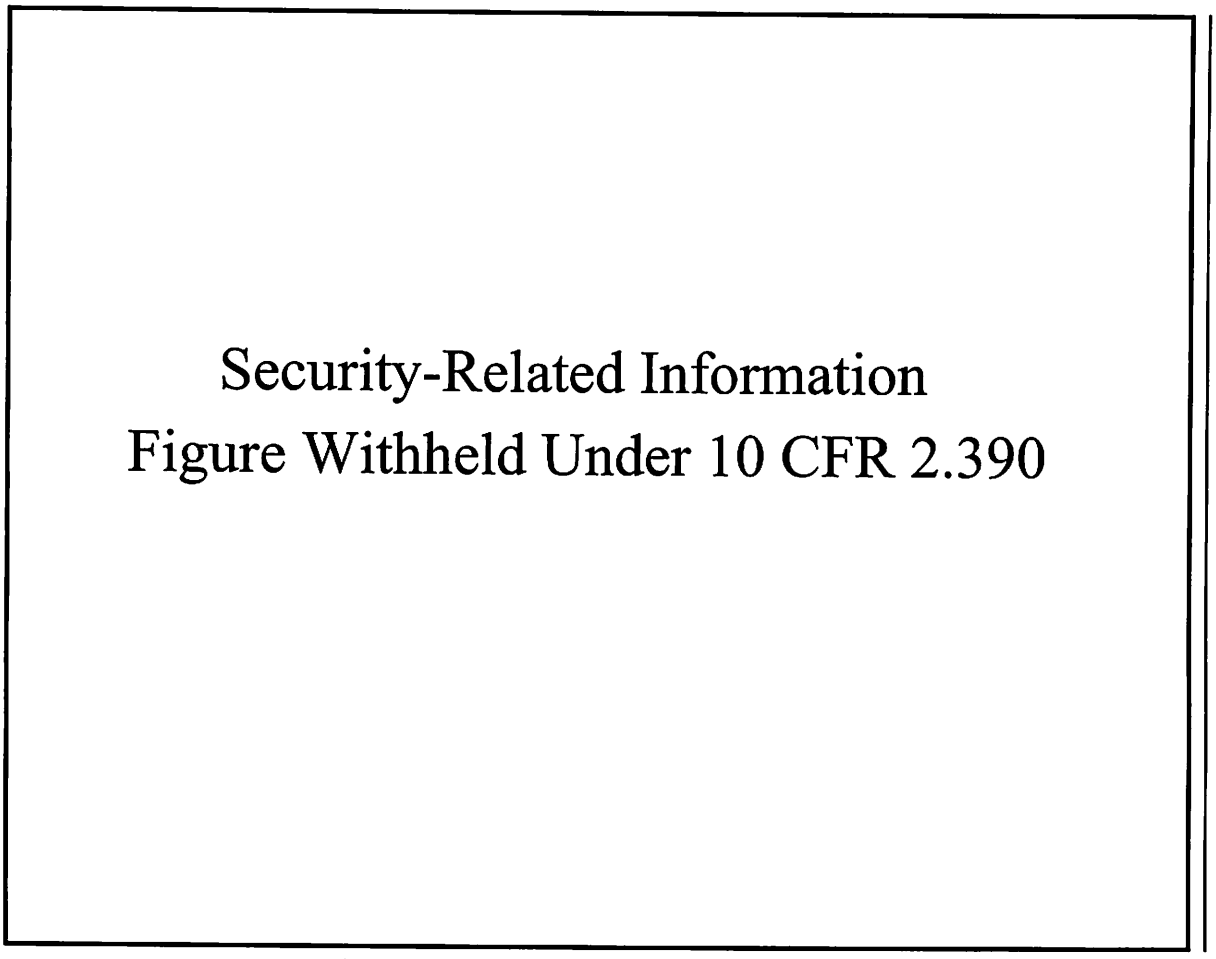

(See Figure 3.1-2 for depiction of section cut line.)

Figure 3.1-3 – Overpack Cover, Section Cut A-A

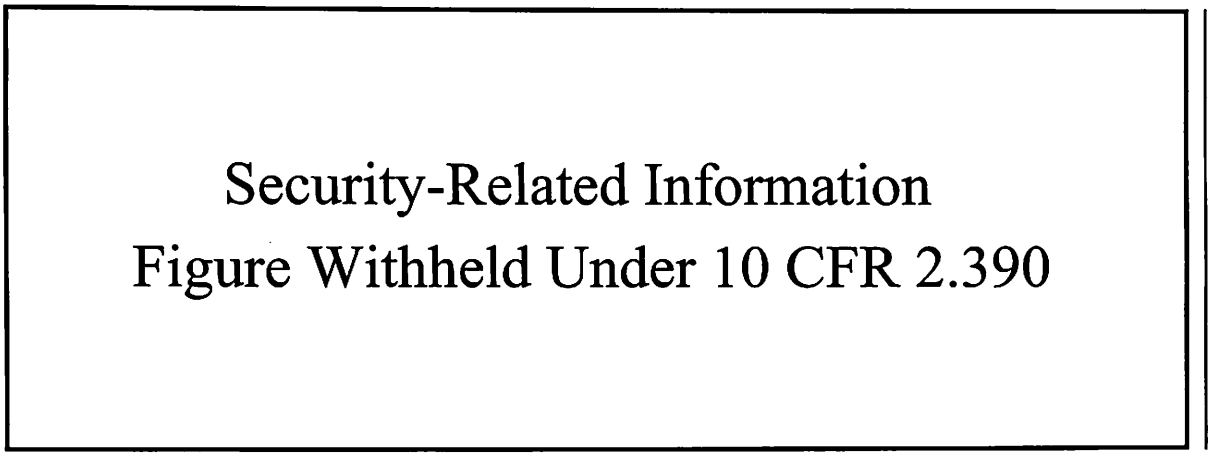

Figure 3.1-4 – Package Cheek Cross-Section

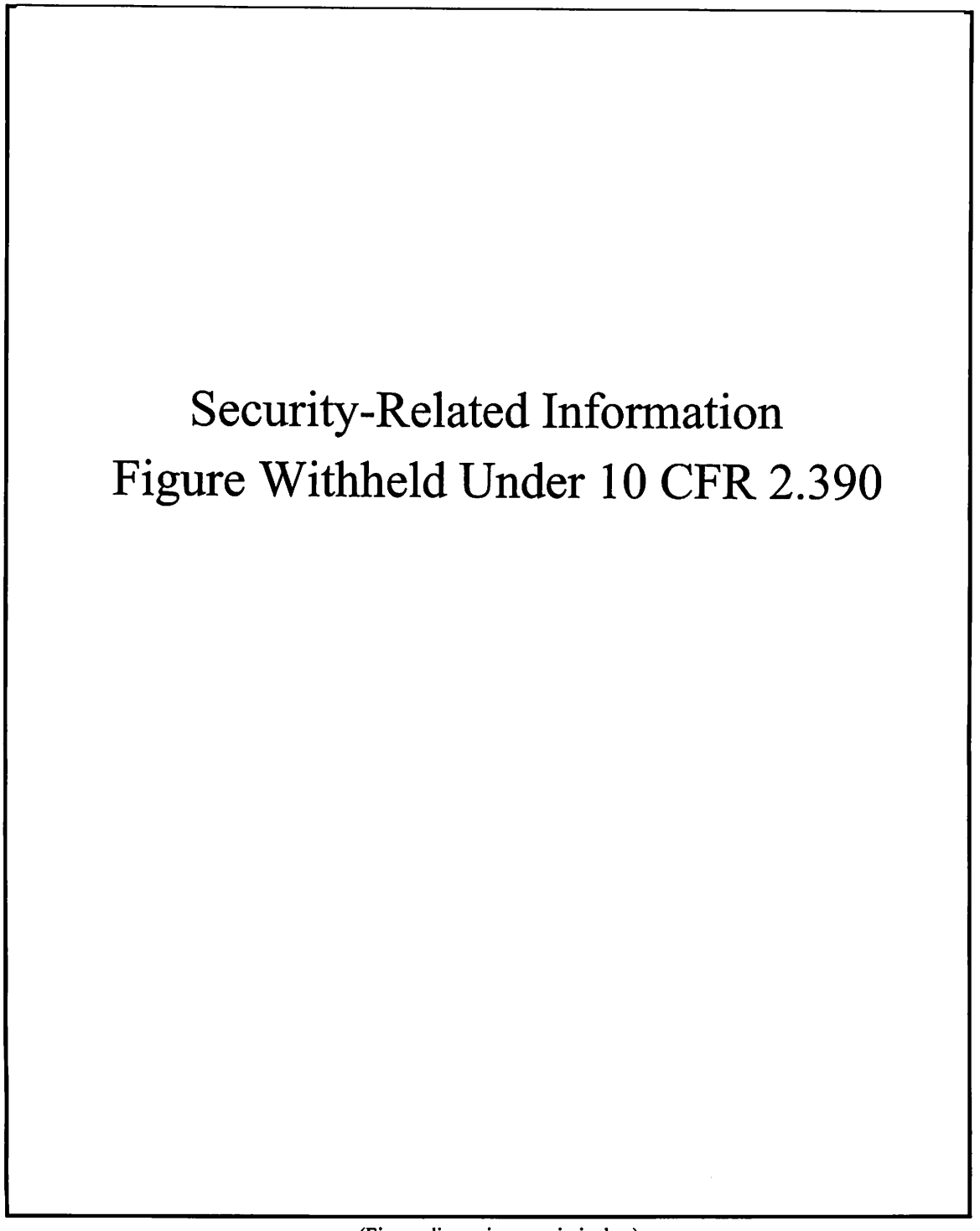

(Figure dimensions are in inches)

Figure 3.1-5 – Top-Loading SLB2 Waste Container

3.2 Material Properties and Component Specifications

The thermally significant materials used in the fabrication of the TRUPACT–III include the following:

- Alloy UNS S31803 used for all plate and sheet material
- ASTM Type 304/304L stainless steel used for parts made from round stock and any round tubes
- ASTM A320 L43 alloy steel, used for closure lid and overpack cover attachment bolts
- Balsa, used in the impact structure for the CSA body and the end overpacks
- Polyurethane foam, used in the body overpack and in the overpack cover
- Calcium silicate insulation, used for thermal protection around lid containment seal
- Air at atmospheric pressure, which fills all void volumes
- Closed-cell silicone foam and polyethylene used for the debris shield
- Plastic material (i.e., nylon, polyethylene, or polyurethane) attached to the guide bars

In addition to the above materials, the SLB2 waste boxes are assumed to be fabricated principally from ASTM A-36 carbon steel, while the roller floor is assumed to be fabricated of 6061 aluminum.

3.2.1 Material Properties

The thermal properties for the Alloy UNS S31803 and ASTM Type 304/304L stainless steels are provided in Table 3.2-1 as a function of temperature. The thermal properties, including thermal conductivity and specific heat, are taken from Table TCD of the ASME Boiler and Pressure Vessel Code[1] for material groups K and J, respectively. Since the NCT analysis requires evaluations for ambient temperatures down to -40 °C, the ASME table values are extrapolated to provide data for this temperature condition. The density of Alloy UNS S31803 stainless steel is 7.89 g/cm^3 and the density of the ASTM Type 304L stainless steel is 8.0 g/cm^3, as taken from an on-line database[2].

Instead of modeling the exact geometry of the structure for the CSA sidewall and lid, as illustrated in Figure 1.1-4, effective thermal properties were developed which permit the structures to be simulated as homogeneous solids. The effective thermal properties are based on the properties for Alloy UNS S31803 stainless steel and consist of a set of temperature dependant, anisotropic (i.e., directional dependant) thermal conductivities, a volume weighted density, and temperature dependant specific heat values. See Section 3.5.2.4, *Effective Thermal Properties for Corrugated Wall/Lid Structures*, for a discussion of the methodology used to develop these values. Table 3.2-2 and Table 3.2-3 present the computed effective thermal properties for the prototypic container wall and closure lid structures, respectively.

[1] American Society of Mechanical Engineers (ASME) Boiler and Pressure Vessel Code, Section II, *Materials*, *Part D – Properties*, Table TCD, 2004 Edition, 2005 and 2006 Addenda, New York, NY.

[2] Matweb, Online Material Data Sheets, www.matweb.com.

In a similar fashion, the box beam structures used at the end of the CSA body and around the perimeter of the closure lid are modeled using effective thermal properties. These effective properties are computed as a fraction of those for an equivalent volume of solid Alloy UNS S31803 stainless to account for the geometry of the structures. Section 3.5.2.5, *Effective Thermal Properties for CSA End Detail & Lid Perimeter*, presents the methodology used to develop these fractional multipliers with the computed values presented in Table 3.2-4.

The thermal properties for the ASTM A320 L43 (AISI 4340) alloy steel, as taken from Table TCD of the ASME Boiler and Pressure Vessel Code[1] for material group D, are presented in Table 3.2-5 as a function of temperature. The ASME table values are extrapolated to provide data for the -40°C temperature condition. A density of 7.86 g/cm^3 is used for the ASTM A320 Type L43 material, per an on-line database[2]. Similarly, the thermal properties for the carbon steel used for the SLB2 waste container and the aluminum used in the roller floor and the payload pallets are also taken from taken from the ASME Boiler and Pressure Vessel Code with their density based on an on-line database[2]. Table 3.2-6 and Table 3.2-7 present the thermal properties for 6061 aluminum and SA-36 carbon steel, respectively.

The thermal properties for the polyurethane foam, balsa, and calcium silicate insulation are assumed to be constant with temperature under NCT conditions. The values assumed for this analysis are presented in Table 3.2-8. Since the polyurethane foam used for the TRUPACT–III package is based on a proprietary formulation, the thermal properties for the four densities of polyurethane foam used are obtained from the manufacturer's on-line website[3]. These proprieties remain essentially constant over the range of temperatures encountered during NCT operations. The performance of the polyurethane foam under HAC conditions is addressed in Section 3.5.4, *'Last-A-Foam' Response under HAC Condition*.

The property values for balsa are based on information from the database for the SCALE computer code[4] which gives a thermal conductivity for balsa wood across its grain as approximately 0.05 W/m-K. Another database[5] gives a maximum ratio of 2.8 for the 'with-grain' versus the 'cross-grain' properties and indicates that the variation in property values may be of up to ±20%. Based on this guidance, the thermal conductivity for balsa obtained from the SCALE database is reduced to 0.0415 W/m-K to account for material variability. This value is conservatively used under NCT for both grain directions. For HAC conditions, where the concern is heat into the package, the SCALE database value of 0.05 W/m-K is multiply by 2.8 (for grain effects) and increased by 20% (for property variability effects), to yield a maximum expected thermal conductivity of 0.168 W/m-K. See Section 3.5.2.6, *Description of Thermal Model for HAC Conditions*, for a more detailed discussion of how the exposed and unexposed sections of balsa wood are modeled under HAC conditions.

[3] Last-A-Foam™ FR3700 On-line Data Sheet, www.generalplastics.com

[4] NuReg/CR-0200, Vol. 3, Rev. 6, SCALE, *A Modular Code System for Performing Standardized Computer Analyses for Licensing Evaluation*.

[5] *Wood Handbook--Wood As An Engineering Material*, General Technical Report #FPL-GTR-113. Madison, WI: U.S. Department of Agriculture, Forest Service, Forest Products Laboratory, 1999.

The calcium silicate insulation data presented in Table 3.2-8 is taken from a prototypic vendor's product sheet[6] for calcium silicate insulation with a nominal density of 0.45 kg/dm^3. The specific heat of the material is based on test data[7] obtained for generically similar materials.

The thermal properties of air are based on curve fits[8] and are presented in Table 3.2-9. Since the debris shield is not directly modeled, the thermal properties for closed-cell silicone foam and polyethylene are not needed. The same is true for the plastic material used on the surface of the guide bars at the closed end of the payload cavity. Instead, the temperatures for these components are assumed to be equal to the maximum of the surrounding structures.

The tested emissivity of as-received Type 304 stainless steel[9] varied from 0.25 to 0.28. Since Type 304 and Alloy UNS S31803 stainless steel are similar in chemical composition, they can be expected to exhibit similar emissivity properties. For the purpose of this evaluation, an emissivity of 0.25 is conservatively used for the emittance from all interior radiating stainless steel surfaces under NCT conditions.

The outer skin of the package will be coated with a white coating, with the coating being optional for the bottom surfaces. While the presence of a white coating[10] could increase the emittance of the outer skin to as high as 0.92 and reduce the solar absorptivity to as low as 0.20, conservative values of 0.8 and 0.52 (i.e., the same as uncoated stainless steel[11]), respectively, are used for these parameters. Besides allowing for flexibility in selecting a coating type, this assumption provides an allowance for degradation of the coating under ultraviolet exposure and for the accumulation of dirt and grime under transport conditions.

Exposure of the coating to the elevated temperatures experienced during the HAC event will blacken the coating and soot may accumulate on the surface. While it is possible that the coating could fail during the fire, thus exposing the underlying stainless steel surface with its associated lower emissivity, such a failure is not a certainty. Therefore, for the purpose of this analysis, an emissivity of 0.90 is used for all exterior surfaces during the regulatory transient fire condition. Further, as a result of oxidation under high temperatures, the inside surface of the outer skin will see an increase in its emittance from the 0.25 value assumed for NCT conditions to a conservatively high value of 0.60[12].

---

[6] Product sheet for Super Firetemp® M, Industrial Insulation Group, Fruita, CO, www.iig-llc.com.

[7] Ohmura, Tsuboi, Onondera, and Tomimura, *Specific Heat Measurements of High Temperature Thermal Insulations by Drop Calorimeter Method*, International Journal of Thermalphysics, Vol. 24, No. 2, March 2003.

[8] Rohsenow, Hartnett, and Choi, *Handbook of Heat Transfer*, 3rd edition, McGraw-Hill Publishers, 1998.

[9] Frank, R. C., and W. L. Plagemann, *Emissivity Testing of Metal Specimens*. Boeing Analytical Engineering coordination sheet No. 2-3623-2-RF-C86-349, August 21, 1986. Testing accomplished in support of the TRUPACT-II design program.

[10] Gilmore, D. G., Editor, Satellite Thermal Control Handbook, The Aerospace Corporation Press, El Segundo, CA, 1994.

[11] Tables 399 and 402, G. G. Gubareff, J. E. Janssen, and R. H. Torborg, *Thermal Radiation Properties Survey*, 2nd Edition, Honeywell Research Center, 1960.

[12] Tables 148 and 149, G. G. Gubareff, J. E. Janssen, and R. H. Torborg, *Thermal Radiation Properties Survey*, 2nd Edition, Honeywell Research Center, 1960.

For the purposes of this evaluation, an emissivity of 0.9[13] is assumed for the balsa surfaces at all temperatures. The same reference indicates that the other non-metallic solids used in the package, such as the polyurethane foam and the calcium silicate insulation, will exhibit a similar emissivity of 0.9 since these materials have a similar color and surface roughness.

The radiation properties of the SLB2 payload container is based on emissivity values of approximately 0.70 for "light-scale" or "rusted" surfaces[9] and values of approximately 0.82 or higher for various paints/coatings[10]. A value of 0.78 provides a conservative lower bound for the normally painted surface.

Table 3.2-10 presents a summary of the emittance and absorptivity data used for the NCT analysis. Specific changes to these values to account for the thermal conditions existing for the hypothetical fire are addressed in Section 3.4.2, *Fire Test Conditions* and Section 3.5.2.6, *Description of Thermal Model for HAC Conditions*.

3.2.2 Technical Specifications of Components

The materials used in the TRUPACT–III that are considered temperature sensitive are the Alloy UNS S31803 stainless steel, the butyl rubber seals, the silicone foam and porous polyethylene used in the debris shield for the CSA, the coating used on the outer skin, the balsa wood, and the rigid polyurethane foam components. The minimum allowable service temperature for all TRUPACT–III components is below the minimum -40°C thermal load condition.

Stainless steel exhibits material property variations within the operating temperature range of the transportation cask. In compliance with the ASME B&PV Code[14], an upper temperature limit of 316 °C (600 °F) has been placed on the use of the Alloy UNS S31803 stainless steel. This temperature point represents the maximum temperature listed for the material in the ASME Code Case N-635-1. Studies[15] have shown that duplex steels, such as Alloy UNS S31803, may experience a transition from ductile to brittle fracture if exposed to temperatures in excess of 300 °C (572 °F) for extended periods of time. The phenomenon consists of two hardening and embrittlement processes that may occur when the material is heated: (a) sigma phase (σ) precipitation in the range of 700 °C to 900 °C and (b) precipitation of a Cr-rich phase (α') in the range of 300 °C to 600 °C. The (α') precipitation leads to a progressive hardening and reduction of the material toughness. This precipitation occurs by spinodal decomposition, a mechanism by which the ferrite phase decomposes into a Cr-rich phase (α') and a Fe-rich phase. Because this reaction occurs more rapidly at 475 °C, this process is also known as "475 °C embrittlement". However this phase separation may also occur after thousands of hours at exposure temperatures as low as 300 °C, after about 11 hours at an exposure temperature of 650 °C, or after approximately 1 hour at an exposure temperature of 725 °C.

The maximum allowable temperature for the ASTM Type 304/304L stainless steel and the ASTM A320 L43 alloy steel used for structural purposes is 427 °C (800 °F)[16]. Both the Alloy

[13] Table 5-2, Kreith, Frank, *Principles of Heat Transfer*, 3rd edition, Harper & Row, 1973.

[14] American Society of Mechanical Engineers (ASME) Boiler & Pressure Vessel Code, Section III, *Code Case N-635-1*.

[15] Weng, K., Chen, T., and Yang, J, *The High-Temperature and Low-Temperature Aging Embrittlement in a 2205 Duplex Stainless Steel*, Bulletin of the College of Engineering, N.T.U., No. 89, October 2003, pp. 45–61.

[16] ASME Boiler & Pressure Vessel Code, Section II, Part D, 2004 Edition, with 2005 and 2006 Addendum.

UNS S31803 and ASTM Type 304/304L stainless steels have a melting point above 1,370 °C. The ASME limits on allowable temperature apply only to conditions where the component's structural properties are required to accommodate the structural loads arising from the respective operating mode or a load combination (such as NCT and HAC drop accidents).

Therefore, based on the above paragraphs, the temperature criteria applied to the various steel components of the package are as follows. A long-term temperature limit of 316 °C is used for the Alloy UNS S31803 stainless steel utilized for the CSA and the closure lid. While a 427 °C long-term temperature limit is applicable for the ASTM Type 304/304L and ASTM A320 L43 steels, a 316 °C long-term temperature limit is conservatively applied instead for consistency with the UNS S31803 limit. The 316 °C limit is also conservatively used for the short-term limit under HAC conditions for all UNS S31803, ASTM Type 304/304L, and A320 L43 steels with the exception of the small region of the CSA structural sheet affected by the puncture bar damage and the outer sheets of the package. For the portion of the CSA structural sheet affected by the puncture bar damage, the allowable short-term limit is based on the time-at-temperature exposure criterion summarized above. This variable temperature versus time criteria is used to assess the potential for incurring a ductile-to-brittle transition (i.e., embrittlement) when the CSA structural steel exceeds the long-term 316 °C temperature limit. A short-term limit of 1,370 °C is applied for the outer sheets of the package.

The outer surface coating has a continuous temperature range of -40 °C to 121 °C, with a maximum intermittent temperature rating of 135 °C[17]. Extended operations above 135 °C can be expected to result in the coating losing its surface adherence and flaking off. In compliance with 10 CFR §71.43(g), the maximum temperature of any accessible outer surface is further limited to 50 °C under NCT conditions when insolation is not present.

The butyl rubber O-rings used for the containment seals have a continuous service temperature range of approximately -54 ºC to +107 ºC[18]. The material is compatible with higher temperatures if the exposure period to the elevated temperatures is kept correspondingly shorter. Testing performed in support of the certification of the TRUPACT–II package and the Radioisotope Thermoelectric Generator (RTG) Transportation System Packaging[19] demonstrated the material's ability to maintain a leak tight containment boundary under a combination of elevated temperatures, time duration, and minimum seal compression. The testing demonstrated that the butyl rubber compound has a minimum temperature rating of 221 ºC for exposure durations of 1 hour or less and 204 °C for exposures of 8 hours or less. For the purposes of this evaluation, the Butyl rubber O-rings are assumed to have an upper temperature limit of 204 °C for exposures of 8 hours or less, a maximum continuous rating of 107 °C, and a lower temperature limit of -54 °C. See Section 2.12.2, *Elastomer O-ring Seal Performance Tests*, for a further discussion of the thermal performance of Butyl rubber O-ring seals.

[17] Based on typical epoxy based coating performance based on the Tnemec line of epoxy coatings, Tnemec Company Inc. Kansas City, MO 64120-1323, www.tnemec.com.

[18] Parker O-Ring Handbook, ORD 5700/USA, 2007, www.parker.com.

[19] DOE Docket No. 94-6-9904, *Radioisotope Thermoelectric Generator Transportation System Safety Analysis Report for Packaging*, WHC-SD-RTG-SARP-001, prepared for the U.S. Department of Energy Office of Nuclear Energy under Contract No. DE-AC06-87RL10930 by Westinghouse Hanford Company, Richland, WA.

The silicone foam used in the debris shield assembly for the CSA has a recommended service temperature range of -50 to 200°C[20]. Under intermittent use, the allowable temperature range increases to -75 to 260°C. The porous polyethylene used to prevent a pressure gradient and allow the flow of helium across the debris shield during leak testing has a recommended service temperature range similar to HDPE (high density polyethylene), or -60 to 120 °C[2]. The melting point for HDPE is 135 °C[2]. Since the function of the debris shield is required only for the NCT and pre-fire HAC conditions, the appropriate temperature limit for the debris shield is -60 to 120 °C to protect the porous polyethylene. The same temperature limit applies to the plastic material on the guide bars. No temperature limit exists for the HAC fire condition as the debris shield and the plastic material on the guide bars may fail under this condition with no consequence for the safety of the packaging.

The calcium silicate insulation has a recommended maximum service temperature of 982 °C[6]. There is no minimum recommended service temperature.

Wood will degrade under elevated temperature, with the severity of the degradation depending on the temperature level achieved, the length of exposure, and the availability of oxygen[5]. While permanent reduction in strength can occur for prolonged exposure to temperatures >65 °C, significant thermal degradation occurs at temperatures >100 °C when the chemical bonds begin to break. As the temperature increases, the level and rate of decomposition also increases until at a temperature of approximately 450 °C the decomposition process forms volatile and flammable gases which can ignite and begin a self-sustaining process if sufficient oxygen is present. For the purposes of this evaluation, the maximum allowable temperature for the balsa wood under NCT conditions is assumed to be 100 °C for peak temperatures based on the onset of chemical decomposition and 65 °C for average temperatures based upon loss of strength considerations. No short-term temperature limit is applied to the balsa wood since the material is not required to survive the HAC fire event.

Section 3.5.4, *'Last-A-Foam' Response under HAC Condition*, describes the behavior of the rigid polyurethane foam as a function of temperature. Based on this information, an NCT temperature limit of approximately 260 °C is used to avoid non-reversible changes in the thermal properties. No temperature limit exists under HAC conditions since the thermal decomposition of the foam material plays a significant role in the level of thermal protection the material provides to underlying foam material and components. A design limit of 65 °C for the bulk average foam temperature under NCT conditions is imposed for this evaluation to establish a lower bound on the foam's structural properties which decrease with increased temperature level.

The maximum payload temperature is assumed to be 230 °C based on the commonly accepted auto-ignition temperature for paper.

[20] Product Cut Sheet, SS30 Expanded, Closed-Cell Silicone Sponge / Foam, Innovation in Polymer Technology, 41 Industrial Drive, Exeter, NH, 03833, www.ipotec.com.

Table 3.2-1 – Thermal Properties of Stainless Steels

Material	Temperature (ºC)	Density (kg/dm^3)	Thermal Conductivity W/m-K	Specific Heat (J/g-K)
Alloy UNS S31803 Stainless Steel ①	-40	7.89	13.56	0.492
	21.1		14.19	0.502
	37.8		14.37	0.504
	93.3		15.23	0.516
	148.9		16.10	0.527
	204.4		16.96	0.538
	260.0		17.65	0.542
	315.6		18.52	0.551
	371.1		19.38	0.560
	426.7		20.08	0.564
	537.8		21.63	0.578
	648.9		23.19	0.587
	760.0		24.75	0.602
	815.6		25.44	0.604
ASTM Type 304/304L Stainless Steel ②	-40.0	8.00	14.25	0.469
	21.1		14.88	0.478
	37.8		15.06	0.480
	93.3		16.10	0.500
	148.9		16.96	0.514
	204.4		18.00	0.528
	260.0		18.87	0.538
	315.6		19.56	0.545
	371.1		20.42	0.553
	426.7		21.11	0.556
	537.8		22.85	0.570
	648.9		24.23	0.578
	760.0		25.79	0.589
	815.6		26.48	0.594

Notes:

① Data based on ASME Boiler and Pressure Vessel Code, Section II, *Materials*, *Part D – Properties*, Table TCD, Material Group K, 2004 Edition, 2005 and 2006 Addenda, New York.

② Data based on ASME Boiler and Pressure Vessel Code, Section II, *Materials*, *Part D – Properties*, Table TCD, Material Group J, 2004 Edition, 2005 and 2006 Addenda, New York.

Table 3.2-2 – Effective Thermal Properties for Corrugated Wall Structure

Temperature (ºC)	Density (kg/dm^3)	Thermal Conductivity, (W/m-K)			Specific Heat (J/g-K)
		'Thru Wall'①	'Along Wall'①	'Axial'①	
-40	1.33	0.62	2.28	1.55	0.492
21.1		0.70	2.41	1.62	0.502
93.3		0.84	2.56	1.74	0.516
204.4		1.16	2.85	1.94	0.538
315.6		1.60	3.11	2.12	0.551
426.7		2.20	3.37	2.29	0.564
537.8		2.97	3.63	2.47	0.578
648.9		3.92	3.90	2.65	0.587
760.0		5.08	4.16	2.83	0.602

Note: ① For horizontal walls of the CSA, the 'Thru Wall' conductivity is aligned with y-axis of model, 'Along Wall' is aligned with x-axis of the model, and 'Axial' is aligned with the z-axis of model. For vertical walls of the CSA, the 'Thru Wall' conductivity is aligned with x-axis of model, 'Along Wall' is aligned with y-axis of the model, and 'Axial' is aligned with the z-axis of model.
② See Appendix 3.5.2.4, *Effective Thermal Properties for Corrugated Wall/Lid Structures*, for the development of the effective thermal properties.

Table 3.2-3 – Effective Thermal Properties for Corrugated Lid Structure

Temperature (ºC)	Density (kg/dm^3)	Thermal Conductivity, (W/m-°K)			Specific Heat (J/g-K)
		'Thru Wall'①	'Along Wall'①	'Axial'①	
-40	1.69	0.65	2.91	2.20	0.492
21.1		0.74	3.04	2.30	0.502
93.3		0.89	3.26	2.47	0.516
204.4		1.23	3.64	2.75	0.538
315.6		1.71	3.97	3.00	0.551
426.7		2.35	4.30	3.26	0.564

Note: ① 'Thru Wall' is aligned with z–axis of model, 'Along Wall' is aligned with x–axis of the model, and 'Axial' is aligned with y–axis of model.
② See Appendix 3.5.2.4, *Effective Thermal Properties for Corrugated Wall/Lid Structures*, for the development of the effective thermal properties.

Table 3.2-4 – Effective Thermal Properties for CSA End & Lid Perimeter Structures

Structure	Density Multiplier ①	Thermal Conductivity Multiplier ①			Specific Heat Multiplier ①
		'Axial' ②	'Transverse' ②	'Along' ②	
CSA End	0.455	0.318	0.200	0.321	1.0
Lid Perimeter	0.495	0.308	0.270	0.368	1.0

Note: ① The table values represent multiplier factors to be applied against the thermal property values presented in Table 3.2-1 to yield the appropriate temperature dependant properties for the subject structure. See Section 3.5.2.5, *Effective Thermal Properties for CSA End Detail & Lid Perimeter*, for development of the table values.
② The 'Axial' value is for heat transfer aligned with the z-axis of the model. The 'Transverse' value is for heat transfer perpendicular to the face of the structures (i.e., from inside to outside). The 'Along' value is for heat transfer around the perimeters of the structures.

Table 3.2-5 – Properties of Type A320 L43 Bolt Material

Temperature (ºC)	Density (kg/dm^3)	Thermal Conductivity W/m-K	Specific Heat (J/g-K)
-40.0	7.86	35.54	0.401
21.1		36.17	0.437
37.8		36.35	0.447
93.3		36.86	0.473
148.9		37.21	0.494
204.4		37.21	0.514
260.0		37.04	0.534
315.6		36.52	0.556
371.1		35.83	0.581
426.7		34.96	0.607
537.8		33.06	0.673
648.9		31.15	0.800
760.0		27.00	1.823
815.6		26.48	0.663

Note: Data based on ASME Boiler and Pressure Vessel Code, Section II, *Materials*, *Part D – Properties*, Table TCD, Material Group D, 2004 Edition, 2005 and 2006 Addenda, New York

Table 3.2-6 – Properties of Type 6061 Aluminum

Temperature (ºC)	Density (kg/dm^3)	Thermal Conductivity (W/m-K)	Specific Heat (J/g-K)
-40	2.70	161.3	0.866
21.1		166.3	0.893
37.8		167.7	0.901
65.6		169.6	0.914
93.3		171.3	0.924
121.1		172.7	0.935
148.9		174.1	0.946
176.7		175.3	0.956
204.4		176.4	0.962

Note: Data based on ASME Boiler and Pressure Vessel Code, Section II, *Materials*, *Part D – Properties*, Table TCD, 2004 Edition, 2005 and 2006 Addenda, New York.

Table 3.2-7 – Properties of ASTM SA-36 Carbon Steel

Temperature (ºC)	Density (kg/dm^3)	Thermal Conductivity (W/m-K)	Specific Heat (J/g-K)
-40	7.86	45.35	0.390
21.1		47.25	0.439
37.8		47.77	0.453
93.3		48.11	0.487
148.9		47.25	0.512
204.4		45.86	0.531
260.0		44.48	0.550
315.6		43.10	0.570
371.1		41.71	0.594

Note: American Society of Mechanical Engineers (ASME) Boiler and Pressure Vessel Code, Section II, *Materials*, *Part D – Properties*, Table TCD, Material Group B, 2004 Edition, 2005 and 2006 Addenda, New York.

Table 3.2-8 – Thermal Properties of Non-Metallic Materials

Material	Temperature (ºC)	Density (kg/dm^3)	Thermal Conductivity W/m-K	Specific Heat (J/g-K)	Comments
Polyurethane Foam	-	0.48	0.068	1.477	NCT properties
	-	0.29	0.046	1.477	“
	-	0.16	0.031	1.477	“
	-	0.10	0.029	1.477	“
Balsa	-	0.12	0.0415	1.8	NCT properties
	-	0.12	0.168	1.8	HAC properties
Calcium Silicate Insulation	20	0.45	0.083	0.95	Values for 20 and 500°C extrapolated from the available data
	93		0.088		
	204		0.095		
	316		0.105		
	427		0.115		
	500		0.121		

Table 3.2-9 – Thermal Properties of Air

Temperature (ºC)	Thermal Conductivity[1] (W/m-°C)	Specific Heat[1] (J/g-K)	Dynamic Viscosity[1] (N-s/m^2 × 10^6)	Density (kg/dm^3)	Prandtl Number[3]	Coef. of Thermal Exp. (1/K)
-40	0.0209	1.0042	15.1836	Use Ideal Gas Law with Molecular wt = 28.966 g/mole	Compute as $Pr = c_p\mu/k$	Compute as β = 1/(°C+273.15)
-18	0.0227	1.0045	16.3407			
10	0.0248	1.0055	17.240			
38	0.0269	1.0071	19.0445			
93	0.0308	1.0121	21.5246			
149	0.0345	1.0191	23.8271			
204	0.0381	1.0278	25.9852			
260	0.0415	1.0378	28.0186			
316	0.0449	1.0488	29.9337			
371	0.0482	1.0606	31.7442			
427	0.0514	1.0730	33.4732			
482	0.0545	1.0857	35.1352			
538	0.0576	1.0986	36.7350			
649	0.0634	1.1242	39.7662			
760	0.0688	1.1487	42.6006			
816	0.0713	1.1603	43.9535			

Table 3.2-10 – Thermal Radiative Properties for NCT

Material	Assumed Conditions	Assumed Emissivity (ε)	Absorptivity (α)
Containment & Structural Sheets (UNS S31803 Stainless Steel) ①	Slightly oxidized, < 121 °C	0.25	---
Outer Sheet, Exterior Surface (Coated UNS S31803 Stainless Steel) ②	White coating	0.8	0.52
Outer Sheet, Interior Surface (UNS S31803 Stainless Steel) ①	Slightly oxidized, < 121 °C	0.25	---
Balsa Wood ③	Untreated	0.90	---
Polyurethane Foam & Calcium Silicate Insulation ③	---	0.90	---
SLB2 ④	Painted carbon steel	0.78	---
Bounding Waste Box ③	Wood or paper	0.90	---
Ambient Environment	---	1.00	N/A

Notes:

① Testing[9] indicates values of 0.25 to 0.28 for "as-received" stainless steel. An emissivity value of 0.25 represents a conservative lower-bound value for the unfinished stainless steel surfaces, leading to conservatively higher temperatures for NCT.

② Based on conservative estimate for emissivity and absorptivity. See Section 3.2.1, *Material Properties*, for more discussion.

③ The emissivity of 0.90 is a representative value for wood and most non-metallic solids (e.g., polyurethane foam & calcium silicate insulation)[13].

④ Emissivity values of approximately 0.70 for "light-scale" or "rusted" surfaces[9] and values of approximately 0.82 or higher for various paints/coatings[10]. A value of 0.78 provides a conservative lower bound for the normally painted surface.

3.3 Thermal Evaluation for Normal Conditions of Transport

This section presents the thermal analysis methodology and the evaluation results for the thermal performance of the TRUPACT–III package under NCT conditions to demonstrate compliance with the requirements of 10 CFR §71.43(g) and §71.71. The thermal evaluations are performed for the recommended design basis NCT cases[1] using conservative analytical techniques to assure that all materials are maintained within their applicable minimum and maximum allowable temperature during all modes of operation.

The analytical thermal model of the TRUPACT–III is developed for use with the Thermal Desktop® [2] and SINDA/FLUINT[3] computer programs. The SINDA/FLUINT and Thermal Desktop® computer programs have been validated for safety basis calculations for nuclear related projects[4,5]. Together, the Thermal Desktop® and SINDA/FLUINT codes provide the capability to simulate steady-state and transient temperatures using temperature dependent material properties and heat transfer via conduction, convection, and radiation. Complex algorithms may be programmed into the solution process for the purposes of computing heat transfer coefficients as a function of the local geometry, gas thermal properties as a function of temperature, and pressure.

The thermal model of the TRUPACT–III package defines a quarter symmetry model of the package's closure end (i.e., symmetrical about the package axial axis and 180° symmetry about the package vertical axis). This modeling choice captures the thermally sensitive seal region at the package closure lid and allows the incorporation of varying insolation loads that will occur at the top, sides, and ends of the package and the adiabatic conditions assumed to exist over the bottom surface of the package. The modeling assumes that the TRUPACT–III operations are conducted with the package in its normal, horizontal orientation. Appendix 3.5.2, *Thermal Model Details*, provides details of the thermal model used for the NCT evaluation.

3.3.1 Heat and Cold

3.3.1.1 Maximum NCT Temperatures

The thermal evaluation of the TRUPACT–III package with the SLB2 payload for the NCT Hot condition assumes a constant ambient air temperature of 38°C and regulatory insolation that follows a sine curve distribution. Given the relatively low thermal mass of the package exterior, the analysis is conducted as a transient simulation to properly account for the diurnal solar loading on the thermal response of the package. Figure 3.3-1 illustrates the expected warm up transient for

[1] Regulatory Guide 7.8, *Load Combinations for the Structural Analysis of Shipping Casks for Radioactive Material*, Revision 1, U. S. Nuclear Regulatory Commission, March 1989.

[2] Thermal Desktop®, Versions 4.8/5.1, Cullimore & Ring Technologies, Inc., Littleton, CO, 2005/2008.

[3] SINDA/FLUINT, Systems Improved Numerical Differencing Analyzer and Fluid Integrator, Versions 4.8/5.1, Cullimore & Ring Technologies, Inc., Littleton, CO, 2005/2008.

[4] Software Validation Test Report for Thermal Desktop® and SINDA/FLUINT, Version 4.8, Packaging Technology, Inc., File No. TR-VV-05-001, Rev. 1.

[5] AFS-TR-VV-006, Rev. 0, Thermal Desktop and SINDA/FLUINT Testing and Acceptance Report, V5.1, Windows XP, AREVA Federal Services LLC, September 2008.

the TRUPACT–III package loaded with a single SLB2 container dissipating 80 watts of decay heat. The package and payload are assumed to begin the transient at a uniform temperature of 20ºC at the time of loading. The transient is conducted for a period of 18 days with the resulting temperatures plotted for every 6 hours until the last 48 hours when the output interval is decreased to every 1/2-hour to more accurately define the diurnal temperature response.

As seen from the figure, the maximum container skin temperature reaches a repeatable cycle within the first 2 or 3 days of the transient, while the internal package components (see the curves for the CSA containment sheet and the SLB2 shell) require in excess of 10 days to achieve the majority of their temperature rise and over 15 days to attain their maximum temperatures. Further, while an approximate 35ºC swing in the exterior skin temperature will occur over each 24 hour period, the temperatures within the CSA will be essentially constant due to the insulating nature of the overpack. The relatively high temperature seen for the bounding waste box is due to the assumption that the thermal conductivity within the waste box and the SLB2 container is equal to that of air with no convection. As such, large thermal gradients are required to dissipate even low power levels.

Figure 3.3-2 illustrates the associated thermal response for the foam and balsa wood components of the package during the same time frame and for the closure and vent port/sampling seals. The temperature response is similar in that in excess of 10 days is required for the majority of the temperature increase to be attained and over 15 days are required to reach the maximum temperature levels.

A summary of the temperature results for this evaluation, plus those achieved for decay heat loads of 40 and 20 watts are presented in Table 3.3-1. As seen from the table, the level of payload decay heat loading has only a slight effect on the peak package temperatures. Instead, the package temperature levels achieved are driven primarily by the ambient conditions. The peak temperatures achieved for all of the components are significantly below the allowable temperature limits. The O-rings used on the containment boundaries remain well within the allowable temperature limits under NCT conditions. The same is true for the temperature sensitive components of the debris shield assembly. It should be noted that, since the debris shield assembly is not explicitly represented by the thermal model, its temperature is assumed to be the same as the containment O-ring due to their proximity.

The evaluation strategy of centering of the hypothetical waste box within the CSA was chosen to yield the maximum payload temperature and, thus, the highest level of CSA pressurization for a given decay heat loading. While positioning the hypothetical waste box against the forward wall of the SLB2 container could yield a higher containment seal temperature, the effect would be minor. First, even if the SLB2 container were slid against the CSA lid, direct contact between the SLB2 container (and the hypothetical waste box within it) and the lid would be highly limited by the 'bumpers' on the SLB2 container. These 38 mm square, thin walled, hollow tubes around the sides and ends of the SLB2 container (see Figure 3.1-5) will effectively maintain a 38 mm wide air gap between the SLB2 container and the lid. Second, the maximum SLB2 container sidewall temperature noted in Table 3.3-1 is 62.3 °C. This maximum temperature occurs where the hypothetical waste box is touching the SLB2 container wall and, as such, represents the maximum temperature the CSA lid could reach under the extreme scenario where the hypothetical waste box is located against the forward SLB2 container wall, the SLB2 container is slid against the CSA lid, and the thermal resistance of the thin walled, hollow tube bumpers is ignored. Further, contact with the CSA lid will act to lower the temperature level within both the SLB2 container and the

waste box such that the actual peak lid temperature would be between 62.3 °C and the 52.6 °C reported in Table 3.1-1 for the containment seal. In any case, the maximum seal temperature would still remain well below its established 107 °C temperature limit for NCT conditions.

To assess the effect of assuming no air gaps between the component interfaces, the various air gap conductors within the NCT thermal model were converted to direct contact conductors and the NCT evaluation for the 80 W decay heat payload repeated. As expected, the elimination of the thermal resistance associated with the air gaps resulted in the peak component temperatures decreasing. However, the level of decrease noted is less than 1 °C indicating that the size of the air gap is not thermally significant for this package due to a combination of its low decay heat loading, the surface area of the package for dissipating the heat through, and the metallic heat transfer path between the CSA and outer sheet provided by the corner ribs.

Figure 3.3-3 and Figure 3.3-4 present perspective views of the temperature distribution within the packaging and within the packaging and payload, respectively, for the 80 watt decay heat case at approximately mid-day during the diurnal cycle. The temperature distribution illustrates the heating due to a combination of decay heat and insolation on the external surfaces. As seen, the peak package temperature occurs at the outer skin due to the solar heating of the horizontal, flat surfaces. Those portions of the package that have a vertical orientation or are shaded exhibit temperatures that are 30 to 40ºC cooler. The temperature variation across the face of the closure end impact structure is due to the variation of solar loading on each of the surfaces because of the orientation and the self-shading by portions of the structure. The presence of the puncture resistant sheets and the joint between the overpack cover and the package overpack structure can be seen in the temperature distribution illustrated in Figure 3.3-3. The temperature distribution illustrated in Figure 3.3-4 demonstrates that the principal thermal gradient within the packaging occurs between the center of the payload and the CSA containment sheet. As stated before, this relatively large thermal gradient occurs because of the assumption that the thermal conductivity within the CSA cavity is equal to that of still air.

The evaluation of the package's thermal performance for the NCT Hot condition without insolation is conducted to confirm the package design complies with the requirements of 10 CFR §71.43(g)[6]. As seen from the summary of component temperatures presented in Table 3.3-2, the maximum temperature of all accessible surfaces are below the allowable limit of 50°C for non-exclusive packages.

3.3.1.2 Minimum NCT Temperatures

The minimum temperature distribution for the packaging occurs with a zero decay heat load and an ambient air temperature of -40 °C per 10 CFR §71.71(c)(2). The steady-state analysis of this condition requires no thermal calculations to be performed. Instead, it is assumed that all package components achieve the -40 °C temperature under steady-state conditions. As discussed in Section 3.2.2, *Technical Specifications of Components*, the -40 °C temperature is within the allowable range of all components.

As a potential initial condition for all normal or accident events, a minimum uniform temperature of -29 °C and no insolation must be considered per 10 CFR §71.71(b) and §71.73(b). Table 3.3-3

[6] Title 10, Code of Federal Regulations, Part 71 (10 CFR 71), *Packaging and Transportation of Radioactive Materials*, United States Nuclear Regulatory Commission (USNRC), 01–01–09 Edition.

presents a summary of the resulting temperatures with 80, 40, and 20 watt payload decay heat loads and the evaluated SLB2 payload configuration. All component temperatures are within the allowable temperature limits.

3.3.2 Maximum Normal Operating Pressure

The maximum normal operation pressure (MNOP) developed during the maximum shipping period is limited to 172 kPa gauge by design. The pressure developed will be a function of the initial quantity of air filling the TRUPACT–III cavity, the quantity of gas generated by the waste stream in the payload containers, the thermal expansion of the gases under operating conditions, and the amount of water vapor that may exist within the package. The chemical, biological, and thermal mechanisms of gas generation within the payload are insignificant with radiolysis being the primary mechanism for potential flammable gas generation in TRU wastes[7].

The TRUPACT–III TRAMPAC[7] describes the basis for computing the maximum amount of gas that can be generated from any source within the payload based on the contribution of each component contributing to the total pressure in the package. The relatively low temperature attained within the CSA indicates that outgassing will not occur from either the silicone foam or porous polyethylene used in the debris shield nor will it occur from the plastic material used on the CSA's guide bars

[7] U.S. Department of Energy (DOE), *TRUPACT–III TRU Waste Authorized Methods for Payload Control (TRUPACT–III TRAMPAC)*, U.S. Department of Energy, Carlsbad Field Office, Carlsbad, New Mexico.

Table 3.3-1 – NCT Hot Temperatures w/ SLB2 Payload

Location / Component	Temperatures (°C)[1]			
	80 Watts [2]	40 Watts [2]	20 Watts [2]	Maximum Allowable [3]
Bounding Waste Box Payload				
- Maximum	162.2	108.5	79.2	230
- Bulk Avg.	90.4	69.8	59.0	230
Standard Large Box (SLB2) Payload				
- Maximum sidewall	62.3	54.5	51.8	230
- Minimum sidewall (coincident) [4]	52.9	50.0	48.5	230
- Avg. sidewall	54.9	51.5	49.8	230
- Bulk Avg. (of void only)	55.4	51.9	50.1	230
- Bulk Avg. (of total volume) [5]	63.0	55.8	52.0	230
Containment O-ring Seal	52.6	51.4	50.9	107
Sampling/Vent Port O-ring Seal	51.2	49.1	48.0	107
Debris Shield	52.6	51.4	50.9	120
CaSi (Seal Protection) Insulation	60.9	60.3	59.9	982
CSA Structural Sheet [6]	57.6	56.5	55.9	316
CSA Containment Sheet				
- Maximum	55.6	53.3	52.6	316
- Minimum (coincident) [4]	50.4	48.5	47.3	316
CSA Lid				
- Maximum	56.1	54.8	54.1	316
- Lid Bolt Maximum	53.4	52.4	51.9	316
Outer Skin				
- Package Body, Peak	86.6	86.5	86.5	121
- Package Cheek, Peak	77.8	77.8	77.7	121
- Package Cover, Peak	84.2	84.2	84.2	121
Last-a-Foam				
- Package Body, Peak/Avg.	67.3 / 51.9	66.6 / 50.3	66.2 / 49.4	260 / 65
- Package Corner, Peak/Avg.	82.4 / 52.3	82.3 / 51.1	82.3 / 50.5	260 / 65
- Package Cheek, Peak/Avg.	77.3 / 49.7	77.2 / 49.4	77.2 / 49.3	260 / 65
- Overpack Cover Outer Area, Peak/Avg.	83.6 / 52.4	83.6 / 51.8	83.6 / 51.5	260 / 65
- Overpack Cover Recess Area, Peak/Avg.	58.6 / 50.5	58.0 / 49.4	57.7 / 48.8	260 / 65
Balsa				
- Package Body, Peak/Avg.	86.2 / 55.3	86.1 / 54.5	86.1 / 54.2	100 / 65
- Overpack Cover, Peak/Avg.	66.9 / 51.3	66.6 / 51.0	66.5 / 50.9	100 / 65

Notes:

1) Peak temperatures determined assuming one SLB2, diurnal cycle for insolation, and a constant ambient temperature of 38 ºC.
2) For conservatism, the decay heat is confined to a bounding minimum sub-volume within the SLB2. This sub-volume represents 23% of the total available volume. The remaining SLB2 volume is assumed to have zero decay heat and the thermal properties of air.
3) Maximum allowable temperatures are established in Section 3.2.2, *Technical Specifications of Components*.
4) The listed minimum temperature is taken at the same time point (i.e., 'coincident') as the listed maximum temperature as opposed to the actual minimum temperature occurring during the diurnal cycle.
5) Bulk average temperature computed assuming SLB2 internal volume of 7,394 liters and a bounding waste box volume of 1,609 liters.
6) The peak CSA structural sheet temperature occurs at joint with overpack cover where enclosing sheet metal and corner ribs form thermal bridges to outer skin. Generally, the CSA structural sheet temperature is within 1ºC of containment sheet temperature.

Table 3.3-2 – NCT Hot, No Solar Temperatures w/ SLB2 Payload

Location / Component	Temperatures (°C)[1]			
	80 Watts [2]	40 Watts [2]	20 Watts [2]	Maximum Allowable [3]
Bounding Waste Box Payload				
- Maximum	155.1	100.3	70.2	230
- Bulk Avg.	81.9	60.8	49.6	230
Standard Large Box (SLB2) Payload				
- Maximum sidewall	54.6	46.5	42.2	230
- Minimum sidewall	42.0	39.9	38.9	230
- Avg. sidewall	45.0	41.5	39.6	230
- Bulk Avg. (of void only)	45.3	41.6	39.7	230
- Bulk Avg. (of total volume) [4]	53.3	45.8	41.9	230
Containment O-ring Seal	42.6	40.2	39.0	107
Sampling/Vent Port O-ring Seal	42.2	40.0	38.9	107
Debris Shield	42.6	40.2	39.0	120
CaSi (Seal Protection) Insulation	42.0	39.9	38.8	982
CSA Structural Sheet [5]	44.2	41.0	39.4	316
CSA Containment Sheet				
- Maximum	44.7	41.3	39.5	316
- Minimum	40.3	39.1	38.4	316
CSA Lid				
- Maximum	43.6	40.7	39.2	316
- Lid Bolt Maximum	42.8	40.3	39.1	316
Outer Skin				
- Package Body, Peak	41.9	39.8	38.8	50
- Package Cheek, Peak	41.5	39.7	38.7	50
- Package Cover, Peak	42.2	40.0	38.9	50
Last-a-Foam				
- Package Body, Peak/Avg.	44.2 / 41.2	41.0 / 39.5	39.4 / 38.6	260 / 65
- Package Corner, Peak/Avg.	43.4 / 40.4	40.6 / 39.1	39.2 / 38.4	260 / 65
- Package Cheek, Peak/Avg.	40.6 / 38.4	39.2 / 38.1	38.5 / 37.9	260 / 65
- Overpack Cover Outer Area, Peak/Avg.	41.4 / 39.0	39.6 / 38.4	38.7 / 38.1	260 / 65
- Overpack Cover Recess Area, Peak/Avg.	42.2 / 40.1	40.0 / 39.0	38.9 / 38.4	260 / 65
Balsa				
- Package Body, Peak/Avg.	42.3 / 39.4	40.0 / 38.6	38.9 / 38.2	100 / 65
- Overpack Cover, Peak/Avg.	39.2 / 38.5	38.5 / 38.1	38.1 / 38.0	100 / 65

Notes:

1) Peak temperatures determined assuming one SLB2, diurnal cycle for insolation, and a constant ambient temperature of 38 ºC.
2) For conservatism, the decay heat is confined to a volume within the SLB2 defined by the bounding waste box form (i.e., 965mm × 965mm × 1,727mm). This bounding volume is assumed to be centered within the SLB2 in the lateral and axial directions and to be resting against the bottom of the SLB2. The remaining volume of the SLB2 is assumed to have zero watts of decay heat and the thermal properties of air.
3) Maximum allowable temperatures are established in Section 3.2.2, *Technical Specifications of Components*. Maximum outer skin temperature limited to 50 ºC in compliance with the requirements of §71.43(g).
4) Bulk average temperature computed assuming SLB2 internal volume of 7,394 liters and a bounding waste box volume of 1,609 liters.
5) The peak CSA structural sheet temperature occurs at joint with overpack cover where enclosing sheet metal and corner ribs form thermal bridges to outer skin. Generally, the CSA structural sheet temperature is within 1ºC of containment sheet temperature.

Table 3.3-3 – NCT Cold Temperatures w/ SLB2 Payload

Location / Component	Temperatures (°C)[1]			
	80 Watts [2]	40 Watts [2]	20 Watts [2]	Minimum Allowable [3]
Bounding Waste Box Payload				
- Maximum	108.7	46.4	10.9	<-40
- Bulk Avg.	25.7	0.2	-13.8	<-40
Standard Large Box (SLB2) Payload				
- Maximum sidewall	-3.9	-15.7	-22.2	<-40
- Minimum sidewall	-23.2	-26.0	-27.5	<-40
- Avg. sidewall	-19.3	-24.0	-26.5	<-40
- Bulk Avg. (of void only)	-18.7	-23.7	-26.3	<-40
- Bulk Avg. (of total volume) [4]	-9.0	-18.5	-23.6	<-40
Containment O-ring Seal	-23.5	-26.2	-27.6	<-40
Sampling/Vent Port O-ring Seal	-23.9	-26.4	-27.7	<-40
Debris Shield	-23.5	-26.2	-27.6	<-40
CaSi (Seal Protection) Insulation	-24.3	-26.6	-27.8	<-40
CSA Structural Sheet [5]	-21.8	-25.4	-27.2	<-40
CSA Containment Sheet				
- Maximum	-21.4	-25.2	-27.1	<-40
- Minimum	-26.1	-27.5	-28.2	<-40
CSA Lid				
- Maximum	-22.4	-25.7	-27.3	<-40
- Lid Bolt Maximum	-23.3	-26.1	-27.6	<-40
Outer Skin				
- Package Body, Peak	-24.1	-26.5	-27.7	<-40
- Package Cheek, Peak	-24.7	-26.8	-27.9	<-40
- Package Cover, Peak	-24.0	-26.5	-27.7	<-40
Last-a-Foam				
- Package Body, Peak/Avg.	-21.8 /-25.1	-25.4 /-27.0	-27.2 /-28.0	<-40
- Package Corner, Peak/Avg.	-22.7 /-26.0	-25.8 /-27.5	-27.4 /-28.2	<-40
- Package Cheek, Peak/Avg.	-25.8 /-28.2	-27.4 /-28.6	-28.2 /-28.8	<-40
- Overpack Cover Outer Area, Peak/Avg.	-24.9 /-27.5	-26.9 /-28.2	-28.0 /-28.6	<-40
- Overpack Cover Recess Area, Peak/Avg.	-24.0 /-26.3	-26.5 /-27.6	-27.7 /-28.3	<-40
Balsa				
- Package Body, Peak/Avg.	-23.7 /-27.0	-26.3 /-28.0	-27.7 /-28.5	<-40
- Overpack Cover, Peak/Avg.	-27.3 /-28.1	-28.1 /-28.5	-28.6 /-28.8	<-40

Notes:

1) Peak temperatures determined assuming one SLB2, no insolation, and a constant ambient temperature of -29 ºC. Minimum temperature of all components is ≥ -29 ºC.
2) For conservatism, the decay heat is confined to a volume within the SLB2 defined by the bounding waste box form (i.e., 965mm × 965mm × 1,727mm). This bounding volume is assumed to be centered within the SLB2 in the lateral and axial directions and to be resting against the bottom of the SLB2. The remaining volume of the SLB2 is assumed to have zero watts of decay heat and the thermal properties of air.
3) Minimum allowable temperatures are established in Section 3.2.2, *Technical Specifications of Components*.
4) Bulk average temperature computed assuming SLB2 internal volume of 7,394 liters and a bounding waste box volume of 1,609 liters.
5) The peak CSA structural sheet temperature occurs at joint with overpack cover where enclosing sheet metal and corner ribs form thermal bridges to outer skin. Generally, the CSA structural sheet temperature is within 1ºC of containment sheet temperature.

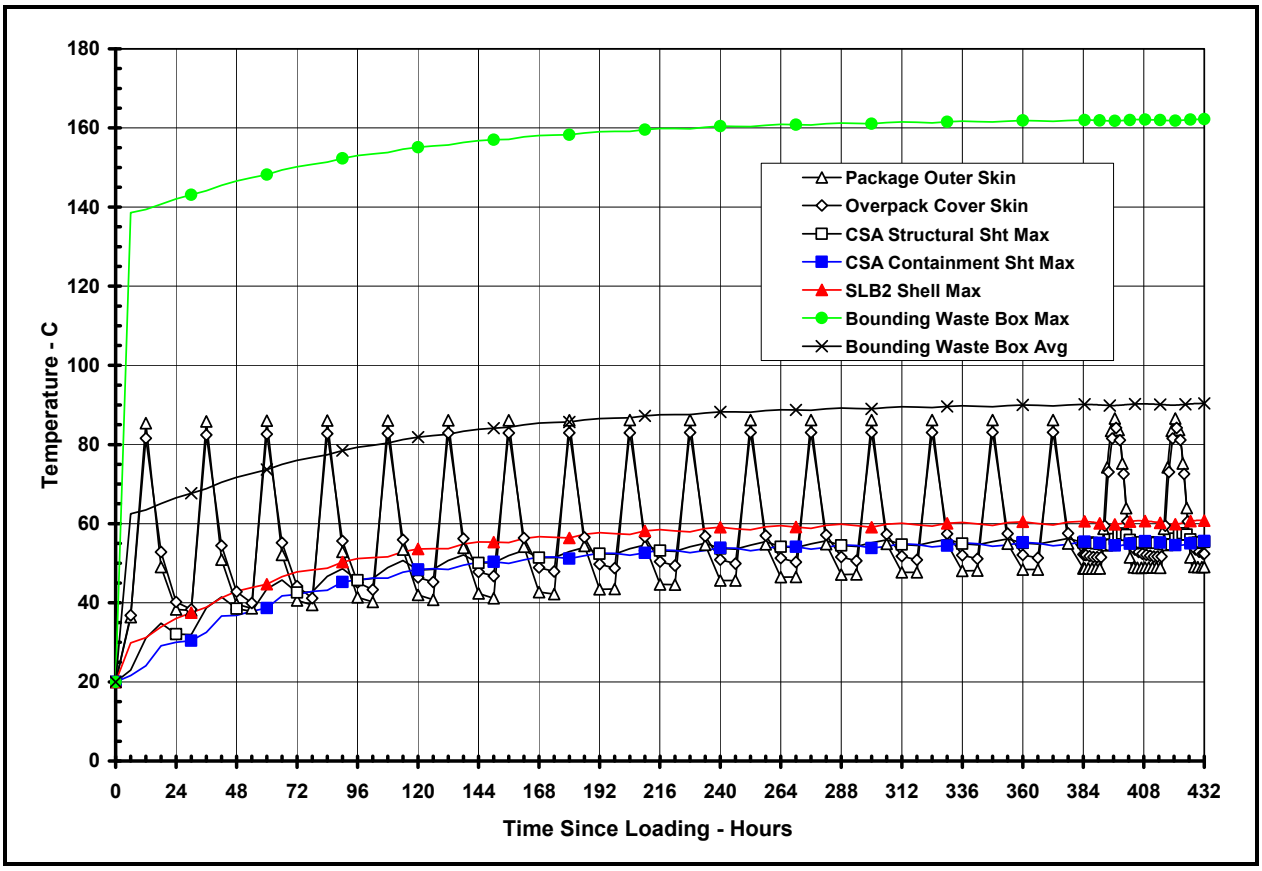

Figure 3.3-1 – Transient Package Thermal Response with 80 Watt SLB2 Payload

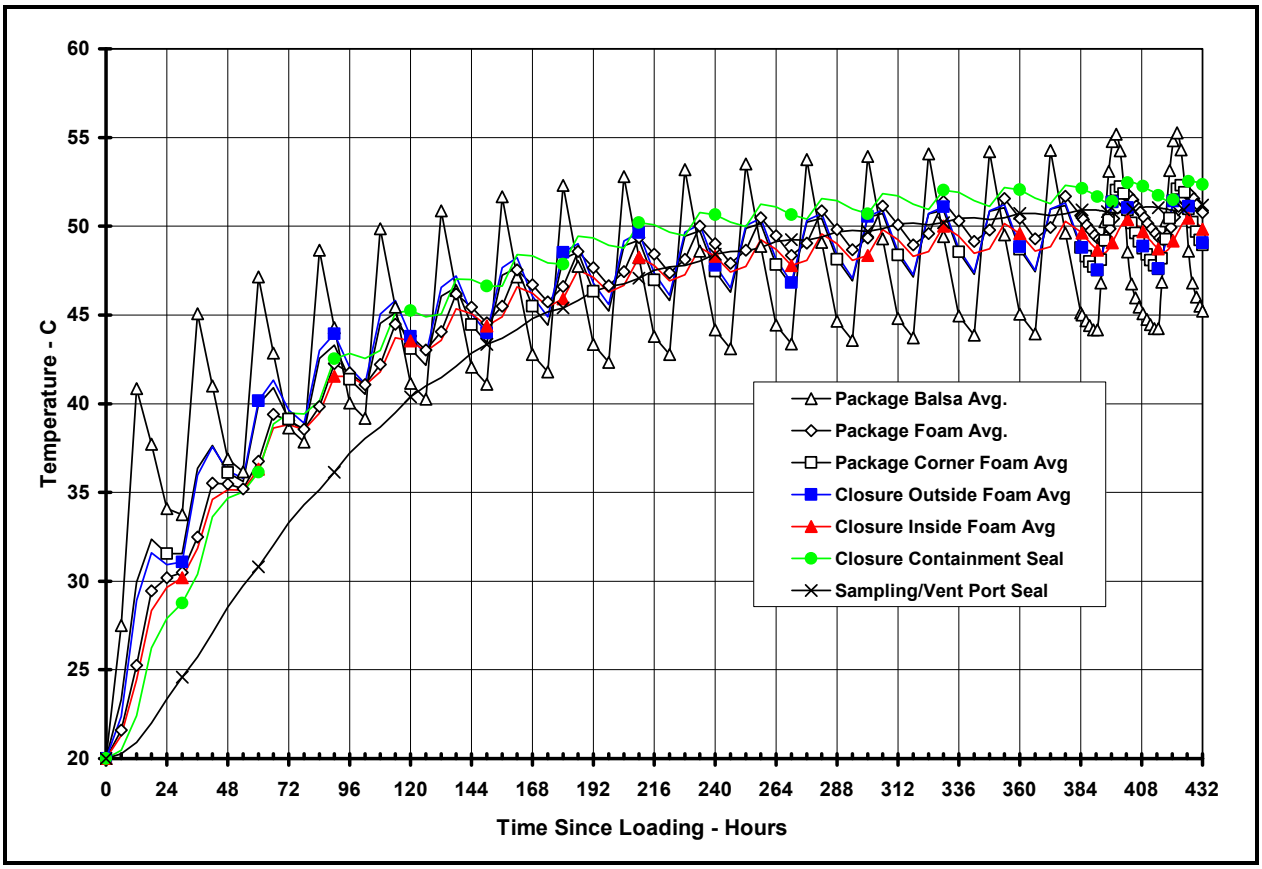

Figure 3.3-2 – Transient Foam, Balsa, and Seal Thermal Response with 80 Watt SLB2 Payload

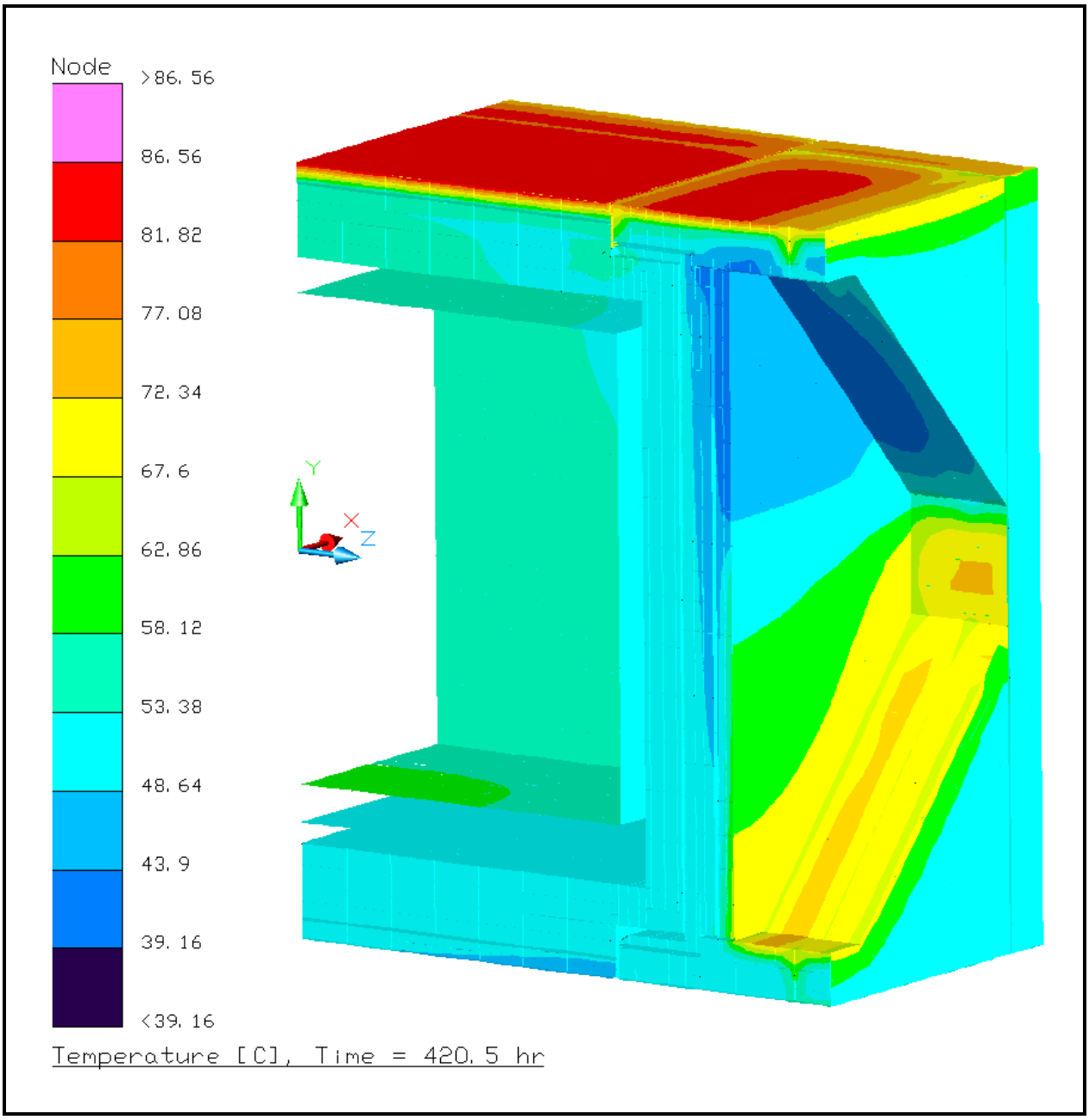

Figure 3.3-3 – Temperature Distribution within Packaging

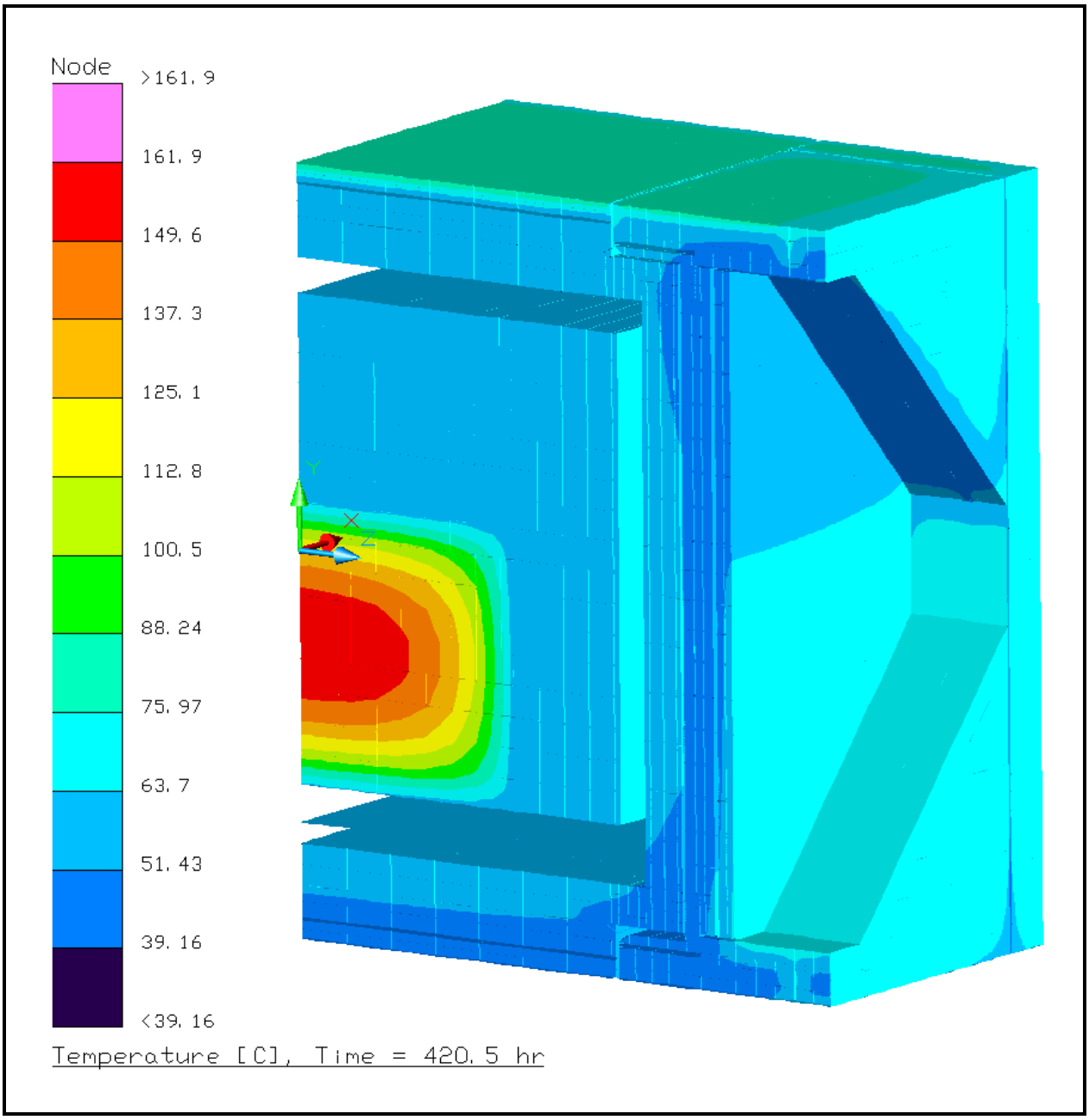

Figure 3.3-4 – Temperature Distribution within Packaging and Payload

This page intentionally left blank.

3.4 Thermal Evaluation for Hypothetical Accident Conditions

This section presents the evaluation methodology and results for the thermal analysis of the TRUPACT–III package under the hypothetical accident condition (HAC) specified in 10 CFR §71.73(c)(4) [1]. The evaluation is based on an analytical model of the TRUPACT–III package which takes into account the damage expected to the package as result of the HAC free and puncture bar drops that precede the fire event, as well as the changes expected to the thermal characteristics and survivability of the various package components.

3.4.1 Initial Conditions

The initial conditions of the TRUPACT–III package prior to the HAC fire event is based on drop testing of two full scale certification test units (i.e., CTU-1 and CTU-2) to establish the expected level of damage sustained by the package as a result of the NCT and HAC free and puncture drop tests. Section 2.7, *Hypothetical Accident Conditions*, documents the series of accident drops conducted on the test articles. Section 3.5.3, *Review of TRUPACT–III Package Full Scale Drop Test Results*, provides a further overview of the test results and the rationale for selecting the worst-case damage scenario based on the test results.

Based on the referenced evaluation of the potential package damage, it is concluded that the bounding damage scenario for the TRUPACT–III package will consist of an oblique free drop on the side-edge of the package (test LD5, see Section 2.7.1.1.2(B), *Drops on the Sides*), followed by a puncture bar impact just aft of the cheek to body joint. The oblique free drop on the side-edge of the package will impart the most significant damage over the greatest surface area compared to any of the other free drop scenarios, while the puncture bar impact location will generate the greatest level of damage in comparison with the other puncture bar impacts and places that damage as close to the thermally sensitive closure seals as feasible. It is further assumed that the TRUPACT–III package will come to rest in a horizontal position prior to the initiation of the fire. Since the package geometry is nearly symmetrical about its axis, there are no significant thermal differences whether the package is right-side up, up-side down, or even on its side. The potential for the SLB2 payload being re-positioned depending upon the package orientation is not significant to the peak temperatures developed under HAC conditions given the payload's relatively low shell temperatures noted for the NCT conditions.

The temperature of the package components prior to the start of the HAC fire event are based on those observed for the 424 hour point in the transient NCT Hot analysis presented in Section 3.3.1.1, *Maximum NCT Temperatures*, for a payload of one SLB2 with a maximum decay heat load of 80 watts. While the effects of solar radiation may be neglected before and during the thermal test [2], the initial package condition for the HAC thermal event for this evaluation are conservatively based the presence of insolation prior to the fire event. It should be noted that an exact temperature match between the maximum temperatures from the NCT results and the HAC pre-fire initial temperatures does not occur since, given the diurnal cycle used for the insolation

[1] Title 10, Code of Federal Regulations, Part 71 (10 CFR 71), *Packaging and Transportation of Radioactive Material*, United States Nuclear Regulatory Commission (USNRC), 01–01–09 Edition.

[2] NUREG-1609, *Standard Review Plan for Transportation Packages for Radioactive Material*, U.S. Regulatory Commission, Office of Nuclear Materials Safety and Standards, March 1999.

loading, each package component reaches its peak temperature at a different time point. As such, while the selected time point in the NCT transient used for the HAC pre-fire temperatures occurs when the CSA is reaching its maximum temperature, the outer shell temperatures of the package are slightly below their noted peak temperatures. This difference is not significant since the outer shell temperature quickly rises when exposed to the HAC fire event.

3.4.2 Fire Test Conditions

The thermal performance of the TRUPACT–III package under HAC conditions is evaluated using an analytical thermal model. The HAC model is a modified version of the quarter symmetry NCT model described in Appendix 3.5.2.1, *Description of Thermal Model for NCT Conditions*. This is appropriate since the use of a quarter symmetry model to simulate the non-symmetric damages arising from the HAC drop events is inherently conservative. The primary modifications made to the NCT model for the HAC modeling consist of the following:

- Simulated the worst-case HAC free and puncture drops consisting of an oblique side-edge drop and subsequent puncture bar damage adjacent to the side-edge damage and just aft of the cheek to body joint (see Figure 3.5-16). As described in Appendix 3.5.2.6, *Description of Thermal Model for HAC Conditions*, the oblique side-edge drop creates a flattened region approximately 305 mm (12 inches) wide along the package length, reducing to approximately 178 mm (7 inches) wide at the cheek areas due to the additional structure and the higher density polyurethane foam used in the cheeks. The puncture bar damage is assumed to have penetrated both the outer skin and the underlying 10 mm thick puncture-resistant plate and to have opened a hole in the outer skin that is approximately 254 mm (10 inches) long by 178 mm (7 inches) wide following the package rotation after impact. While the hole in the underlying 10 mm thick puncture-resistant plate and polyurethane foam was 178 mm (7 inches) in diameter, or 54% of the opening in the outer skin, the full 254 mm x 178 mm opening is assumed all the way to the surface of the CSA for conservatism. Further, all compacted material within the affected area is assumed to have fallen out prior to the HAC fire, thus exposing the underlying CSA surface to the HAC environment. These assumptions provide a significant level of conservatism.
- Changed the thermal conductivity of the balsa wood from the value consistent with the low end of the observed range to a value that represent the high end of the range,
- Increased the emissivity of the external surfaces from 0.8 to 0.9 to account for possible soot accumulation on the surfaces,
- The balsa wood surfaces adjacent to undamaged portions of the outer skin will be charred from the HAC fire, but not consumed due to the lack of air. However, since the thermal conductivity of solid wood is greater than that for charred wood, the thermal properties of undamaged wood are assumed for computing the heat flow into the package. Exposed sections of balsa wood are conservatively assumed to be fully consumed at the start of the fire,
- Replaced the assumed air gaps between the layered components of the package side wall with direct contact,

- Replaced the adiabatic boundary condition applied to the bottom of the package for NCT conditions with convective and radiation thermal conductors to the ambient,
- Apply convection heat transfer coefficients between the package and the ambient that are appropriate for gas velocities of 10 m/sec during the 30-minute fire event[3]. The elevated convection heat transfer rate is conservatively applied to the surfaces of the CSA exposed by the puncture bar attack, even though convection will be significantly reduced by the recessed cavity formed by the puncture bar damage. Convection coefficients based on still air are assumed following the 30-minute fire event,
- An 800 ºC ambient condition with an effective emissivity of 1.0 is used to simulate the elevated temperature of the fire for convective and radiation heat transfer during the 30-minute fire event. The ambient condition is re-set at the end of the 30-minute fire to the pre-fire ambient condition of 38 ºC with an effective emissivity of 1.0 and with the addition of insolation.

3.4.3 Maximum Temperatures and Pressure

3.4.3.1 Maximum HAC Temperatures

Figure 3.4-1 presents the thermal response curves for selected package components to the simulated HAC fire event. As illustrated in the figure, while the exterior of the package quickly rises to nearly the temperature of the fire, the CSA containment sheet and its enclosed SLB2 payload container and bounding waste box configuration show only moderate thermal response to the presence of the 30-minute fire event. The noted transient response reflects the significant thermal protection afforded to the CSA and its payload by the presence of the outer skin, the balsa wood, polyurethane foam, and the calcium silicate insulation.

This result is further illustrated by the perspective and reverse perspective views presented in Figure 3.4-2 of the temperature distribution in the TRUPACT–III Package after 30 minutes of exposure to the HAC fire. The figure clearly shows that the balsa wood and polyurethane foam limits the elevated temperatures resulting from the fire event to narrow regions adjacent to the outer shell. The presence of the 6-mm puncture resistant sheet in the overpack cover can be seen via the thermal path it provides between the layers of polyurethane foam. Similar thermal paths occur at the corner ribs and the end sheets separating the package body and the overpack cover.

This thermal protection of the CSA is further illustrated by the temperature response curves presented in Figure 3.4-3 and the temperature distribution illustrated in Figure 3.4-4. As seen from the figures, the maximum temperature noted on the CSA occurs only on the structural sheet and only for the relatively small portion of the CSA affected by the puncture bar damage. In addition to the region of elevated temperature caused by the puncture bar damage, Figure 3.4-4 also shows a smaller region of slightly elevated temperature approximately mid-height on the CSA. This region of slightly elevated temperature results from heat conducted axially into the package via the exposed sheet metal of the recessed area of the overpack cover (see Figure 3.5-2) and the opposing sheet metal in the package cheek area and not as the result of the HAC free or puncture bar damage.

[3] Schneider, M.E and Kent, L.A., *Measurements Of Gas Velocities And Temperatures In A Large Open Pool Fire, Heat and Mass Transfer in Fire* - HTD Vol. 73, 1987, ASME, New York, NY.

Figure 3.4-5 presents an enlarged view of the portion of the CSA affected by the puncture bar damage and which exceeds the NCT design limit of 316 °C. The region of elevated temperatures is predicted to extend only a short distance below the structural sheet and does not extend to the containment sheet. The large thermal gradient through the segment of the CSA wall affected by the puncture bar attack depicted in Figure 3.4-5 results from the 'corrugated' makeup of the 140 mm thick CSA wall (see Appendix 3.5.2.4, *Effective Thermal Properties for Corrugated Wall/Lid Structures*, for details). In this type of construction, the structural sheet of the CSA is separated from the containment sheet by a 124-mm airspace and 4-mm thick V-stiffeners inclined at an approximately 67 degree angle. The V-stiffeners act as a thermal shield by preventing direct radiation heat transfer between the structural and containment sheets, while their thinness, length, and stainless steel makeup greatly restrict heat conduction between the sheets.

As discussed in Section 3.2.2, *Technical Specifications of Components*, the NCT 316 ºC temperature limit for the CSA represents the maximum temperature for continuous use listed for the material in the ASME Code Case N-635-1 and not the limit under the transient HAC conditions. The temperature limit under HAC is established to avoid what is known as "475 ºC Embrittlement". Section 3.2.2 indicates that an aging time of 1 hour at 725 ºC (i.e., a temperature that bounds the peak predicted CSA temperature) or approximately 11 hours at 650 ºC is required to transition from ductile to brittle fracture. Per Figure 3.4-3, the entire time the peak CSA structural sheet temperature is above 650 ºC is only about 30 minutes, while the CSA containment sheet remains well below 316 ºC. As such, while a reduction in ductility may occur for the section of the CSA structural sheet affected by the elevated temperature, full embrittlement of the CSA steel is not expected due to insufficient aging time at temperature. No loss in ductility and no embrittlement of the CSA containment boundary will occur since its peak temperature remains well below the continuous use temperature of 316ºC for the Alloy UNS S31803 stainless steel.

The significance of possible CSA steel embrittlement is further reduced by the fact that the fire test is the last hypothetical accident condition which is applicable per 10 CFR 71 (i.e., no post-fire drop events are considered plausible). As such, the only subsequent structural loads occurring for the package will arise from 1 g recovery operations. Therefore, even if a reduction in ductility does occur over the small portion of the structural shell affected by the puncture bar damage, no safety impact will result since sufficient package ductility will remain to allow recovery operations.

As demonstrated by the temperature response curves presented in Figure 3.4-3, the containment and sampling/vent port seals show only a limited temperature affect from the HAC fire event. The maximum temperature of 95 ºC attained by the CSA debris shield is well below the intermittent use temperature for the silicone foam and porous polyethylene used in the debris shield. Therefore, while a potential failure of the debris shield poses no safety concern for the HAC fire event, the relatively low temperature attained also indicates that no out–gassing from this material which could lead to pressurization of the CSA cavity will occur.

The thermal protection afforded by the TRUPACT–III design is further illustrated by Figure 3.4-6 which illustrates the average temperature response within the balsa wood and polyurethane foam components. The fact that the average balsa wood temperature remains near or below 450 ºC is significant in that temperatures in excess of this are required to reduce the wood structure to char. As such, while the outer layer of the balsa may be charred, it is expected that un-damaged balsa will exist below that. Further, the fact that the average temperature of the polyurethane foam in the package body and corner segments is below 190 ºC indicates that the

bulk of the polyurethane foam will not experience any significant decomposition as the result of exposure to the HAC fire event since significant decomposition begins at approximately 354 °C (see Section 3.5.4, *'Last-A-Foam' Response under HAC Conditions*).

While the HAC evaluation assumes no air gaps between the balsa and polyurethane foam components and the metallic surfaces of the package, the peak predicted HAC temperatures are not seen as being affected by the presence or absence of air gaps between the modeled components. This conclusion is based on the fact that the peak CSA temperature occurs at the location of the puncture bar damage where the surface of the CSA is directly exposed to the HAC environment and not at locations that underlie the other model segments. Further, as demonstrated by the sensitivity analysis conducted under the NCT evaluations, the effect of the assumed air gaps for NCT had a thermally insignificant effect on the NCT results (i.e., less than 1 °C).

Table 3.4-1 summarizes the peak component temperatures expected during the HAC fire event. As seen from the table, with the exception of a limited surface area on the CSA structural sheet, all components exhibit large thermal margins between the noted peak temperatures and the associated maximum allowable temperatures for the component. As explained above, while a small region of the CSA structural sheet may experience a reduction in ductility due to being heated above 316 ºC, full embrittlement of the steel is not expected due to the limited time at temperature and no significant impact is expected on post-accident handling or the ability of the CSA to maintain containment of the payload. Therefore, the TRUPACT–III Package design is seen as complying with the thermal limits established for operation under the short-term conditions existing for the HAC fire event. Further, given the conservative method of analysis, the pedigree of the thermal properties assumed for the various components, and the level of the thermal margins (as presented in Table 3.4-1), this conclusion is seen as being unaffected by any potential uncertainties in the method or basis of analysis.

While the peak HAC temperature of 688 ºC predicted for the calcium silicate (CaSi) exceeds the range of the temperature dependant properties provided in Section 3.2.1, *Material Properties*, no significant impact on the thermal performance of the package results for several reasons. First, relative to the metallic components, the change in thermal conductivity of CaSi with temperature is small. Second, the elevated temperature occurs for only a limited time under the HAC temperature which, when combined with the low conductivity of the CaSi material, means that both the extent of the CaSi material affected by the peak temperature and the time duration of the elevated temperature are both limited. Finally, the location of the CaSi material is remote from the area on the package experiencing the maximum temperatures (see Figure 3.4-4).

Given the relative light weight structure of the TRUPACT–III package, the peak temperature results for the cold weather conditions will be similar to those seen for the HAC hot condition presented above. Further, since the thermal gradients that may exist within the package structure are very limited due to the thickness of the metal sheets used in its fabrication, no significant increase in thermal stresses will occur for the HAC cold condition from those observed under the evaluated HAC hot condition. As such, no specific analysis is presented for the HAC cold condition.

3.4.3.2 Maximum HAC Pressure

The maximum internal pressure within the CSA during the HAC event is determined in the same manner as for NCT (see Section 3.3.2, *Maximum Normal Operating Pressure*). Based on the

conservative assumption that the TRUPACT–III package has reached its MNOP pressure of 172 kPa gauge due to gas generation just prior to the initiation of the fire, the predicted pressure increase within the CSA due to heat up from its pre-fire, steady-state level is computed via the ideal gas law as follows:

$$\text{pressure increase during fire} = \frac{p_{\text{Pre-fire}}\left(T_{\text{Void Volume Fire}} + 273.15\,\text{K}\right)}{\left(T_{\text{Void Volume Pre-fire}} + 273.15\,\text{K}\right)} - p_{\text{Pre-fire}}$$

$$\text{where,}\quad T_{\text{Void Volume Fire}} = \frac{83 + 222}{2} = 153\ ^{\circ}\text{C}$$

$$T_{\text{Void Volume Pre-Fire}} = \frac{63 + 55}{2} = 59^{\circ}\text{C}$$

$$\text{and,}\quad p_{\text{Pre-fire}} = 101.3 + 172 = 273.3\,\text{kPa}$$

As such, the maximum pressure increase during the fire transient is 77.3 kPa, yielding a peak HAC pressure of 249.3 kPa gauge. This pressure increase value is conservative in that the analysis is based on maximum of non-coincidental peak temperatures and the fact that the peak temperature of the CSA containment sheet is used as opposed to an area weighted average temperature.

The relatively low temperature attained within the CSA indicates that no significant out–gassing will occur from the silicone foam and porous polyethylene used for the debris shield or the plastic material used on the CSA's guide bars which could lead to pressurization of the CSA cavity. As explained in Section 3.3.2, *Maximum Normal Operating Pressure*, compliance with the limitation on the buildup of flammable mixtures within the package is ensured by administrative controls on the payloads that are permitted to be loaded. See Section 3.3.2 for more discussion.

3.4.4 Maximum Thermal Stresses

As shown in Section 3.4.3.2, *Maximum HAC Pressure*, the internal pressure within the payload cavity will increase by a maximum of 77.3 kPa, or +45% from its maximum pre-fire level, due to the HAC thermal event. As such, pressure stresses due to the HAC thermal event increase a corresponding maximum of 45%. This level of pressurization is within the capability of the CSA as demonstrated in Section 2.7.4.3, *Stress Calculations*. Further, since the TRUPACT–III package is fabricated principally of sheet metal and relatively thin structural steel shapes, the thermal stresses developed within any component during the HAC fire event will be low and not significant to the safety of the package.

Table 3.4-1 – HAC Temperatures w/ SLB2 Payload

Location / Component	Temperatures (°C)			
	Pre-fire [1,2]	End of Fire [2]	Peak [2]	Maximum Allowable [3]
Bounding Waste Box Payload				
- Maximum	162	163	177	230
- Bulk Avg.	90	92	107	230
Standard Large Box (SLB2) Payload				
- Maximum sidewall	62	83	89	230
- Minimum sidewall (coincident)	53	54	54	230
- Avg. sidewall	55	59	60	230
- Bulk Avg. (of void only)	55	59	76	230
- Bulk Avg. (of total volume) [4]	63	66	83	230
Containment O-ring Seal	52	63	95	204
Sampling/Vent Port O-ring Seal	51	53	80	204
Debris Shield	52	63	95	-
CaSi (Seal Protection) Insulation	61	688	688	982
CSA Structural Sheet (includes Lid outer sheet), - Peak/Avg. [5]	58 / 52	689 / 73	689 / 75	725 for < 1 hour / 316
CSA Containment Sheet (includes Lid inner sheet)				
- Maximum	55	216	222	316
- Minimum (coincident)	50	51	51	316
CSA Lid Bolts	53	187	187	316
Outer Skin				
- Package Body, Peak	71	800	800	1,370
- Package Cheek, Peak	69	800	800	1,370
- Package Cover, Peak	73	800	800	1,370
Last-a-Foam				
- Package Body, Peak/Avg.	66 / 52	684 / 75	684 / 96	-
- Package Corner, Peak/Avg.	60 / 55	797 / 189	797 / 189	-
- Package Cheek, Peak/Avg.	69 / 52	800 / 373	800 / 373	-
- Overpack Cover Outer Area, Peak/Avg.	73 / 52	792 / 168	792 / 169	-
- Overpack Cover Recess Area, Peak/Avg.	58 / 50	695 / 70	695 / 99	-
Balsa				
- Package Body, Peak/Avg.	73 / 54	793 / 455	793 / 455	-
- Overpack Cover, Peak/Avg.	64 / 51	784 / 449	784 / 449	-

Notes:

1) Initial temperatures based on SLB2 with 80 watt decay heat load at the 424 hour point in the transient NCT Hot analysis.
2) For conservatism, the decay heat is confined to a bounding minimum sub-volume within the SLB2. This sub-volume represents 23% of the total available volume. The remaining SLB2 volume is assumed to have zero decay heat and the thermal properties of air.
3) Maximum allowable temperatures are established in Section 3.2.2, *Technical Specifications of Components*.
4) Bulk average temperature computed assuming SLB2 internal volume of 7,394 liters and a bounding waste box volume of 1,609 liters.
5) The peak CSA structural sheet temperature occurs at the location of the puncture bar damage and lasts less than 1 hour. The peak temperature for the remaining portion of the structural sheet is substantially lower as demonstrated by the average temperature value.

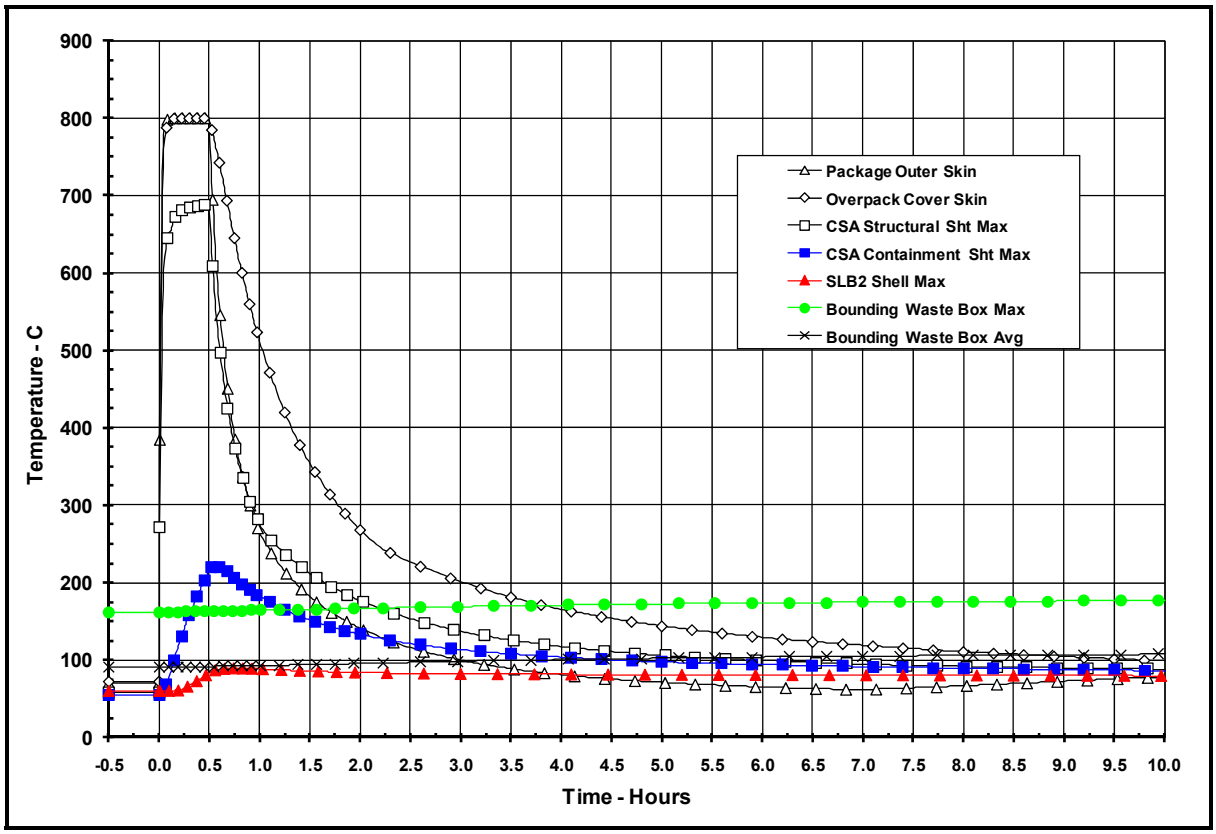

Figure 3.4-1 – TRUPACT–III Package HAC Temperature Response

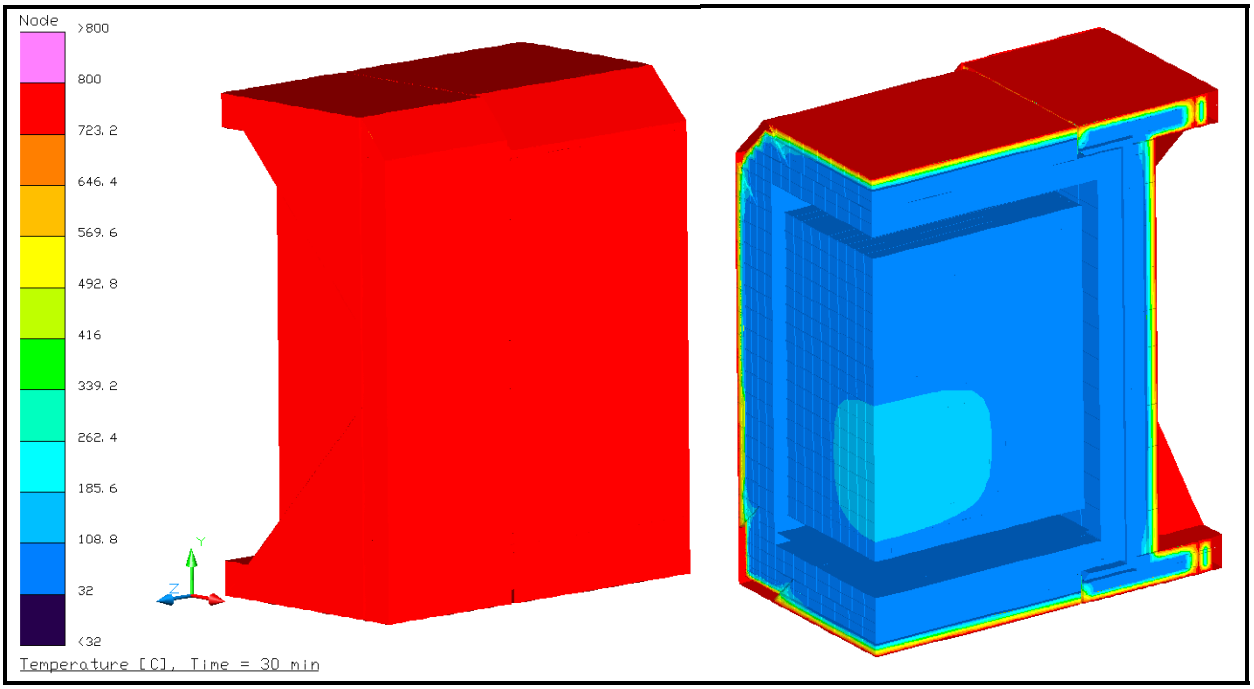

(Note: the positive y-axis is oriented towards the top of the package and the positive z-axis towards the package closure end)

Figure 3.4-2 – Temperature Distribution at End of 30 Minute Fire Event, Perspective and Reverse Perspective Views

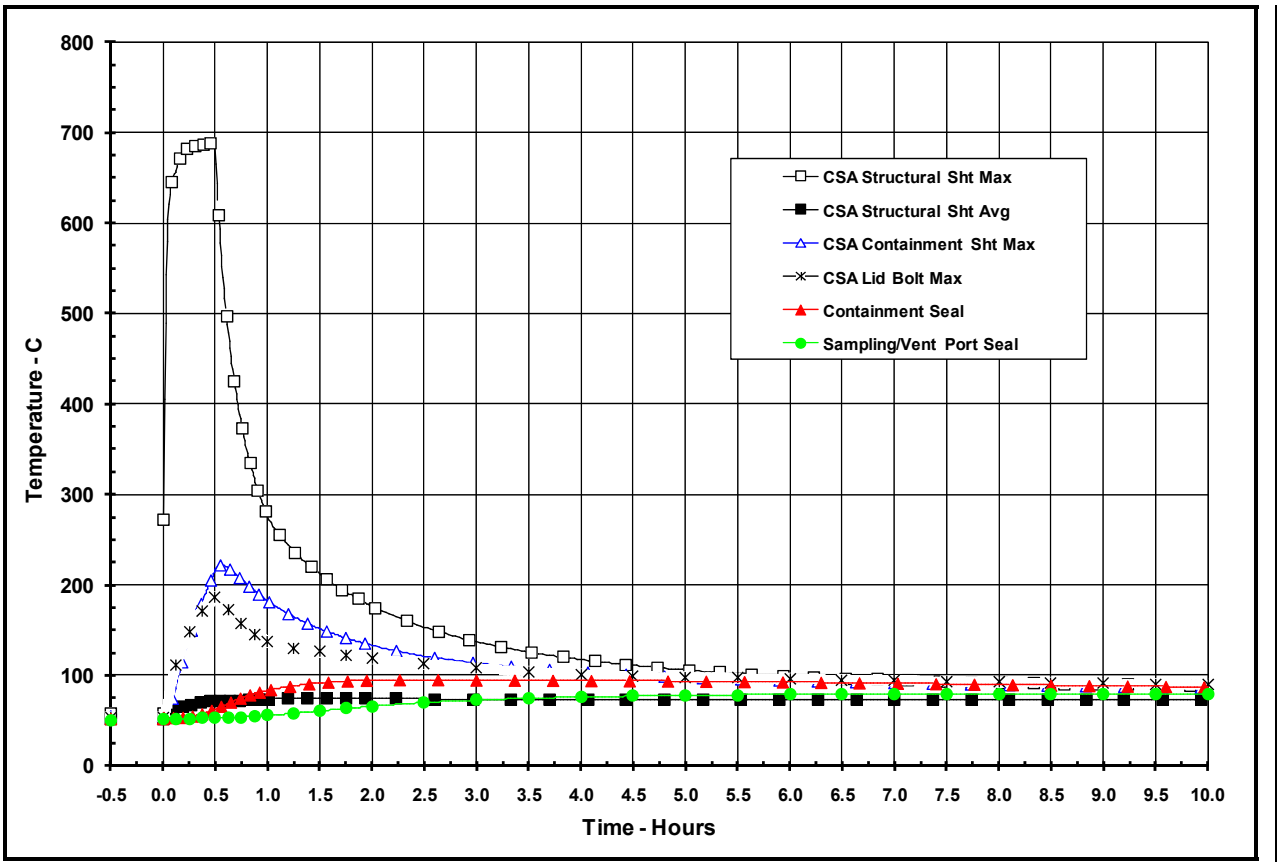

Figure 3.4-3 – Temperature Response of CSA to HAC Fire Event

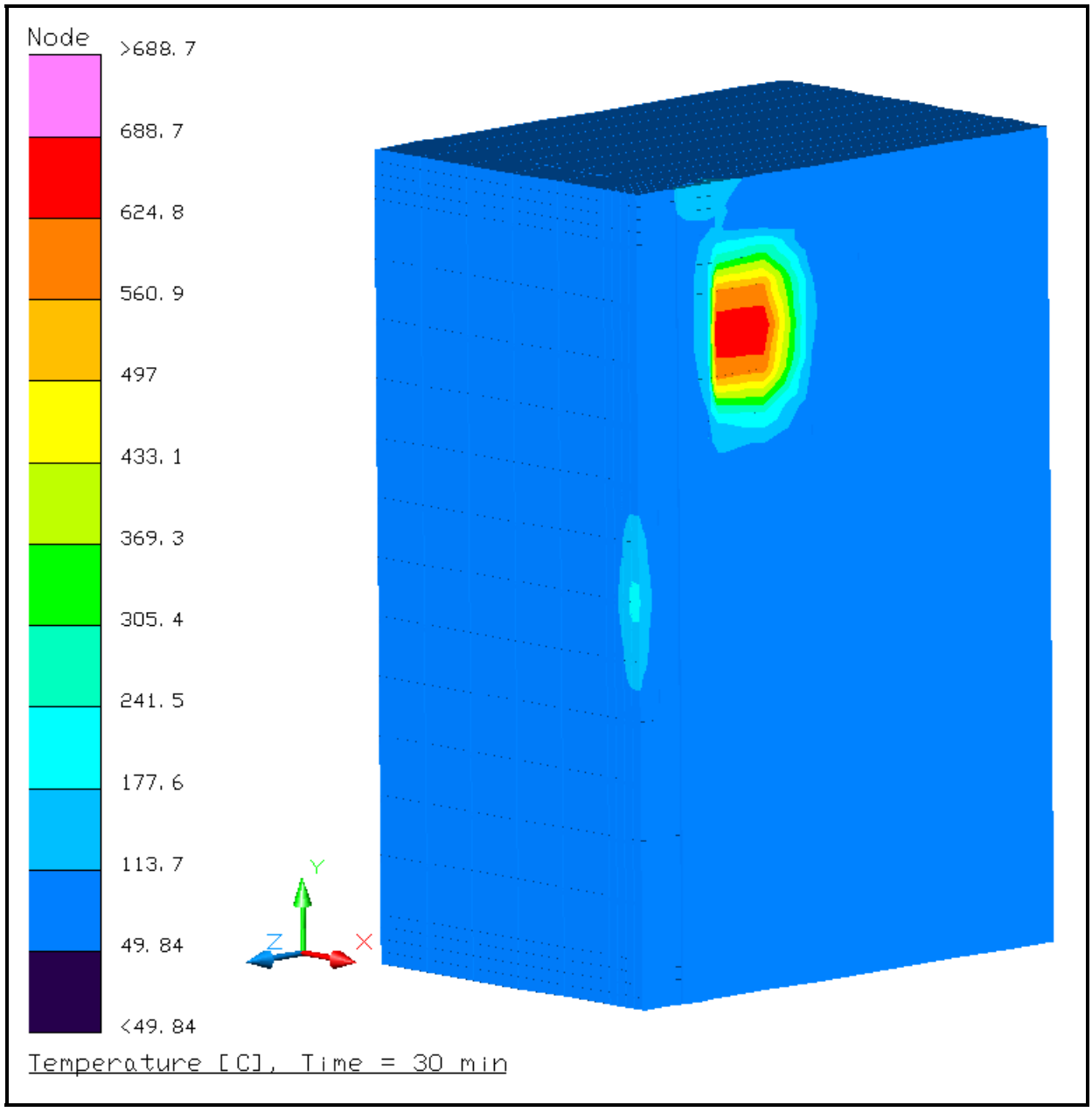

(Note: the positive y-axis is oriented towards the top of the package and the positive z-axis towards the package closure end)

Figure 3.4-4 – CSA Exterior Temperature Distribution at End of 30 Minute Fire Event

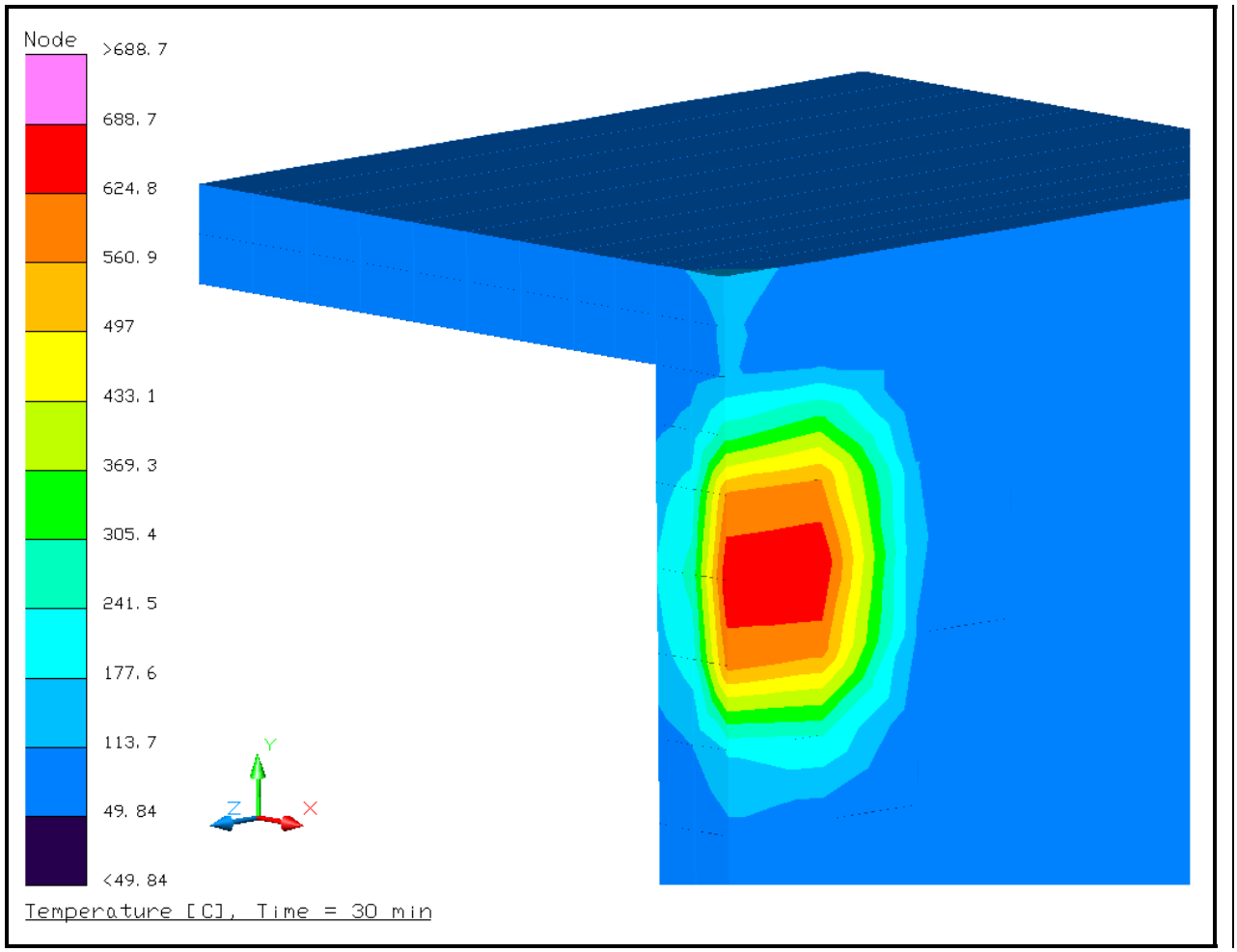

(Note: the positive y-axis is oriented towards the top of the package and the positive z-axis towards the package closure end)

Figure 3.4-5 – Temperature Distribution through CSA Wall at End of 30 Minute Fire Event

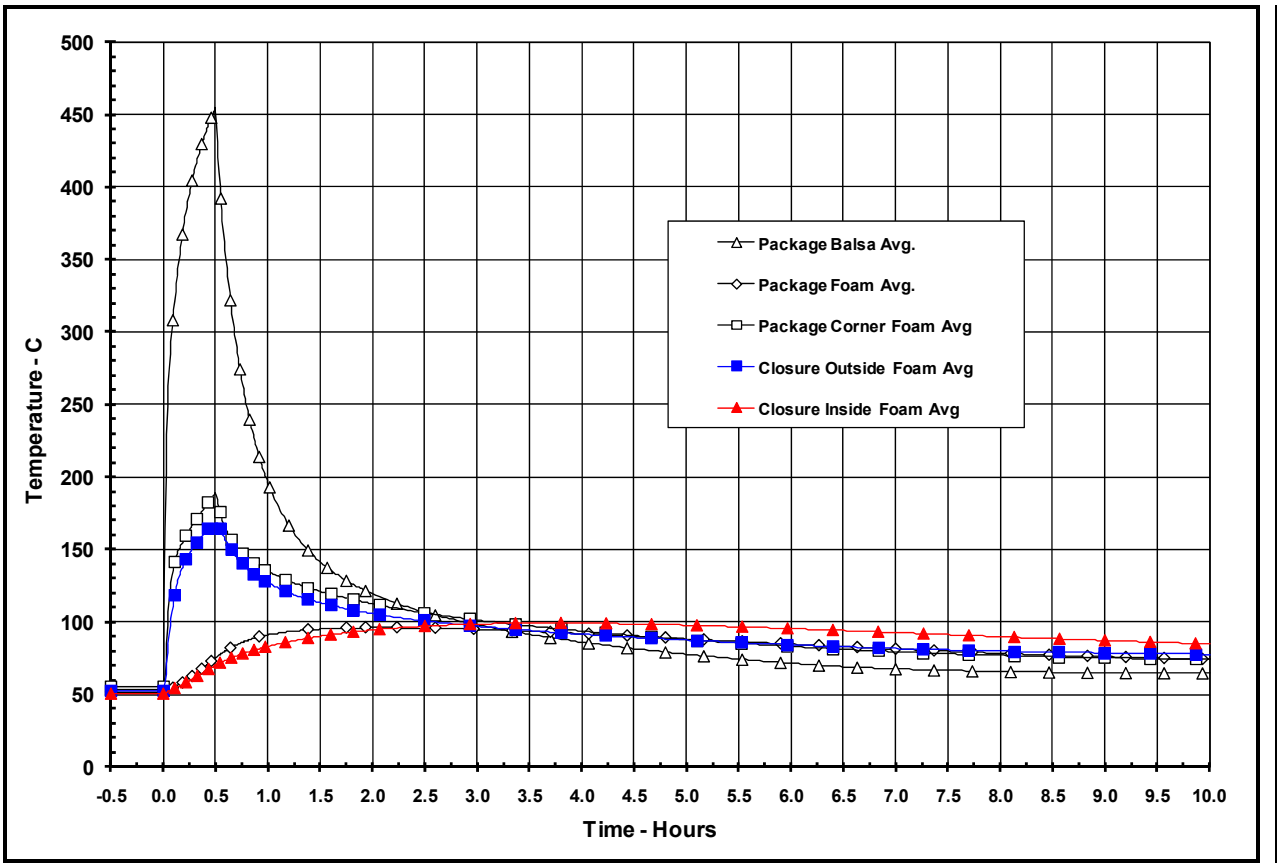

Figure 3.4-6 – Temperature Response of Package Polyurethane Foam and Balsa Wood Components to HAC Fire Event

3.5 Appendices

3.5.1 Computer Analysis Results

3.5.2 Thermal Model Details

3.5.3 Review of TRUPACT–III Package Full–Scale Drop Test Results

3.5.4 'Last-A-Foam' Response Under HAC Conditions

This page intentionally left blank.

3.5.1 Computer Analysis Results

Due to the size and number of the output files associated with each analyzed condition, results from the computer analysis are provided on a DVD–R.

This page left intentionally blank.

3.5.2 Thermal Model Details

The analytical thermal model of the TRUPACT–III package was developed for use with the Thermal Desktop®[1] and SINDA/FLUINT[2] computer programs. These programs are designed to function together to build, exercise, and post-process a thermal model. The Thermal Desktop® computer program is used to provide graphical input and output display function, as well as computing the radiation exchange conductors for the defined geometry and optical properties. Thermal Desktop® is designed to run as an AutoCAD® application. As such, all of the CAD tools available for generating geometry within AutoCAD® can be used for generating a thermal model. In addition, the use of the AutoCAD® layers tool presents a convenient means of segregating the thermal model into its various elements.

The SINDA/FLUINT computer program is a general purpose code that handles problems defined in finite difference (i.e., lumped parameter) and/or finite element terms and can be used to compute the steady-state and transient behavior of the modeled system. Although the code can be used to solve any physical problem governed by diffusion-type equations, specialized functions used to address the physics of heat transfer and fluid flow make the code primarily a thermal code.

The SINDA/FLUINT and Thermal Desktop® computer programs have been validated for safety basis calculations for nuclear related projects[3,4].

Together, the Thermal Desktop® and SINDA/FLUINT codes provide the capability to simulate steady-state and transient temperatures using temperature dependent material properties and heat transfer via conduction, convection, and radiation. Complex algorithms may be programmed into the solution process for the purposes of computing heat transfer coefficients as a function of the local geometry, gas thermal properties as a function of species content, temperature, and pressure, or, for example, to estimate the effects of buoyancy driven heat transfer as a function of density differences and flow geometry.

3.5.2.1 Description of Thermal Model for NCT Conditions

The thermal model of the TRUPACT–III package defines a quarter symmetry model of the package's closure end (i.e., symmetrical about the package axial axis and 180° symmetry about the package vertical axis). This modeling choice captures the thermally sensitive seal region at the package's closure lid and allows the incorporation of varying insolation loads that will occur at the top, sides, and ends of the package and the adiabatic conditions assumed to exist over the bottom surface of the package. Program features within the Thermal Desktop® computer program automatically compute the various areas, lengths, thermal conductors, and view factors involved in determining the individual elements that make up the thermal model of the complete

[1] Thermal Desktop®, Version 4.8/5.1, Cullimore & Ring Technologies, Inc., Littleton, CO, 2005/2008.

[2] SINDA/FLUINT, Systems Improved Numerical Differencing Analyzer and Fluid Integrator, Version 4.8/5.1, Cullimore & Ring Technologies, Inc., Littleton, CO, 2005/2008.

[3] Software Validation Test Report for Thermal Desktop® and SINDA/FLUINT, Version 4.8, Packaging Technology, Inc., File No. TR-VV-05-001, Rev. 1.

[4] AFS-TR-VV-006, Rev. 0, Thermal Desktop and SINDA/FLUINT Testing and Acceptance Report, V5.1, Windows XP, AREVA Federal Services LLC, September 2008.

assembly. The modeling assumes that the TRUPACT–III operations are conducted with the package in its normal, horizontal orientation.

Figure 3.5-1 illustrates a perspective view of the three dimensional thermal model developed for the purposes of this calculation. The origin of the thermal model axis is located at the center of the package, with the positive x-axis pointing towards the right side of the package (when facing the closure end), the positive y-axis pointing towards the top of the package and the positive z-axis pointing towards the closure end of the package. The model is composed of solid and plate type elements to represent the various package components. Thermal communication between the various components is via conduction, convection, radiation, and surface-to-surface contact. A total of approximately 14,700 thermal nodes, 9,300 planar elements, and 11,300 solids are used in the model to provide thermal resolution. One boundary node is used to represent the ambient environment for convection purposes and a second boundary node is used to represent the ambient temperature for the purpose of radiation heat transfer. An effective emissivity of 1.0 is assumed for the hypothetical fire.

The balsa wood, the polyurethane foam, and the calcium silicate insulation used in the packaging are installed as individual components. Therefore, direct contact between the various packaging layers may be relatively low, depending on the 'tightness' of the fit up. To reflect this situation, the interface with the components fabricated of these materials is treated as an air gap with conductance across the gap computed as a function of the thermal conductivity of air and an assumed gap thickness. Radiation heat transfer is ignored for conservatism. A nominal gap width of 0.5-mm is used between the layered components of the package side walls, with an assumed gap width of 0.5-mm to 1-mm used at the other various material interfaces.

A comparison of the thermal model configuration, illustrated by Figure 3.5-2 to Figure 3.5-9, with the TRUPACT–III package design, as defined by Figure 1.1-1 through Figure 1.1-6 from Section 1.1, *Introduction*, and Figure 3.1-1 to Figure 3.1-5, demonstrates that the placement and geometry of the major components of the package are individually captured in the thermal model. The design features captured include the recessed overpack cover, the puncture resistant sheets, and the calcium silicate insulation protection plates. In addition, the thermal connection between the structural shell of the CSA and the outer skin of the package via the 6-mm support ribs at the corners of the package is accurately represented in the model (see Figure 3.5-3). These support ribs provide a significant thermal bridge, in relation to the level of the payload decay heat load, between the CSA and the ambient.

Payload Container Thermal Model

As discussed in Section 3.1.1.2, *Payload Configuration*, the only payload form currently planned for the TRUPACT–III package is one (1) SLB2 container. Since the SLB2 containers may contain a variety of TRU waste and that waste may either be placed directly into the SLB2 container or be housed within other containers, the thermal model is set up to simulate either an SLB2 container completely filled with waste, or an SLB2 container containing waste that is confined within a small region of the SLB2 (i.e., 965-mm × 965-mm × 1,727-mm, or approximately 23% of the total SLB2 container volume) for the given decay heat loading. See Section 3.1.1.2, *Payload Configuration*, and Section 3.1.2, *Content's Decay Heat*, for a description and justification of this bounding waste form.

Figure 3.5-10 illustrates the 1/4-symmetry thermal modeling of the SLB2 container with its enclosed hypothetical bounding waste box form and the roller floor pallet system. The figure shows the external surface of the SLB2 container and the enclosed hypothetical bounding waste

box. While the decay heat is assumed to be evenly distributed over the volume of the bounding waste box form, it actually represents a non-uniform heat distribution within the SLB2 container since the bounding waste box form is only 23% of the available waste volume within the SLB2 container. Heat transfer within the bounding waste box volume is via conduction only, based on the thermal properties of air. Heat transfer between the surface of the bounding waste box form and the internal surfaces of the SLB2 container are assumed to be via conduction and radiation across the void air volume. The hypothetical waste box is assumed to be horizontally and axially centered within the SLB2 container and to be resting against the bottom of the SLB2 container. This placement yields the maximum expected separation distance between the payload and the interior of the TRUPACT–III.

The heat transfer between the exterior of the SLB2 container and the interior cavity of the TRUPACT–III is computed based on conduction and radiation across the void air volume. The SLB2 container may either be 'rolled' into the package via a roller floor pallet or slid into the package onto a floor pallet structure with similar dimensions and thermal resistance. The pallet structure is simulated as two 4.75-mm thick aluminum sheets separated by a 66.7-mm airspace. The thermal properties of Type 6061 aluminum are assumed. Conductance between the upper and lower sheets of the pallet structure is modeled via conductors which simulate the heat transfer through the air gap and the vertical metal 'legs' of the pallet structure. Credit is taken for direct contact heat transfer between the pallet structure and the bottom of the CSA interior, but only over that portion of the support rail surface area that actually makes contact with the CSA. No credit is taken for direct contact heat transfer between the SLB2 container and roller floor. Instead, the heat transfer is modeled as conduction and radiation across an approximately 130-mm airspace representing a conservative estimate of the standoff height of the SLB2 container above the roller floor, plus an allowance for the separation distance between the hypothetical waste box and the base of the SLB2 container.

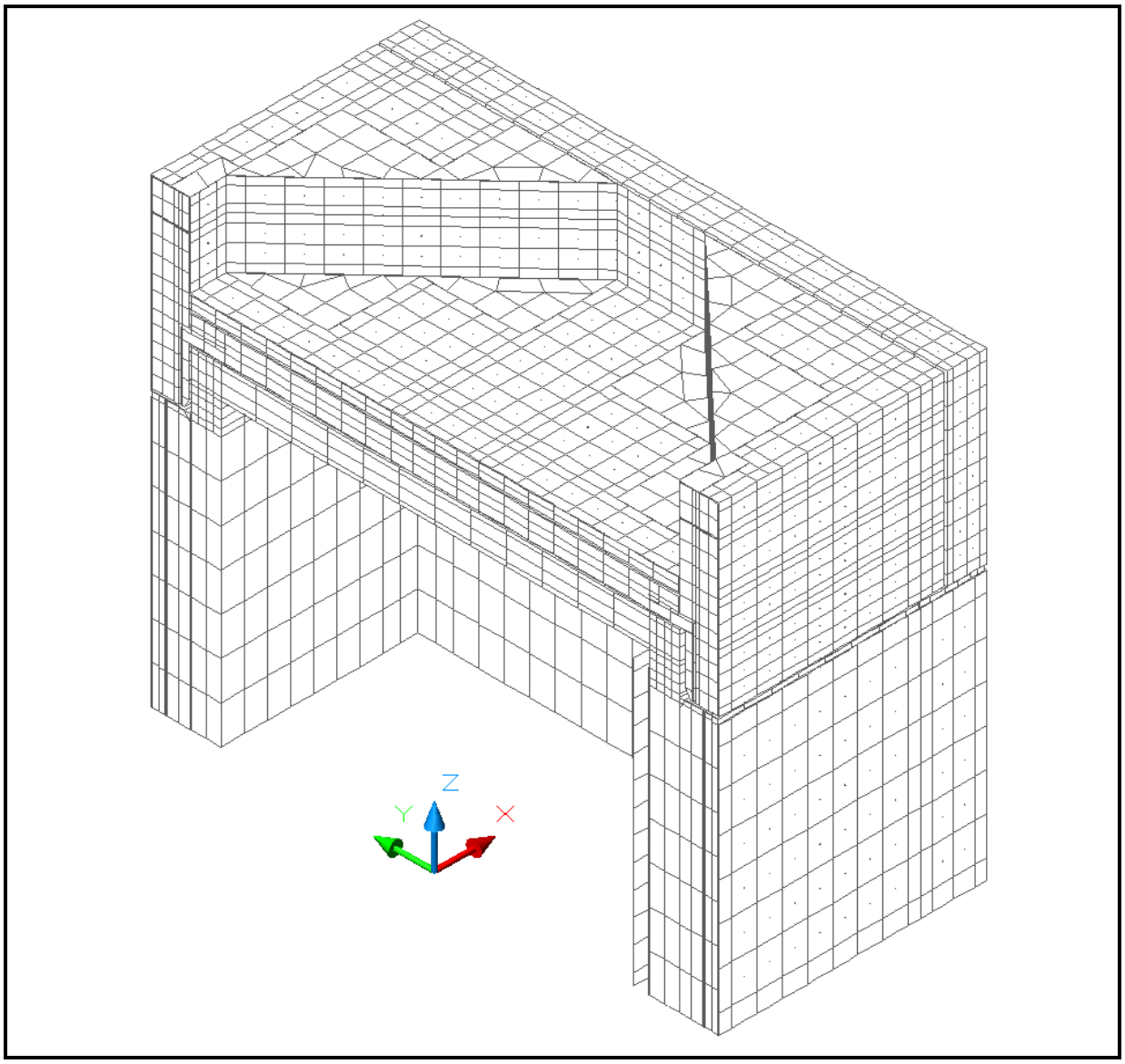

(Note: the positive y-axis is oriented towards the top of the package and the positive z-axis towards the package closure end)

Figure 3.5-1 – Perspective View of One-Quarter Symmetry TRUPACT–III Thermal Model

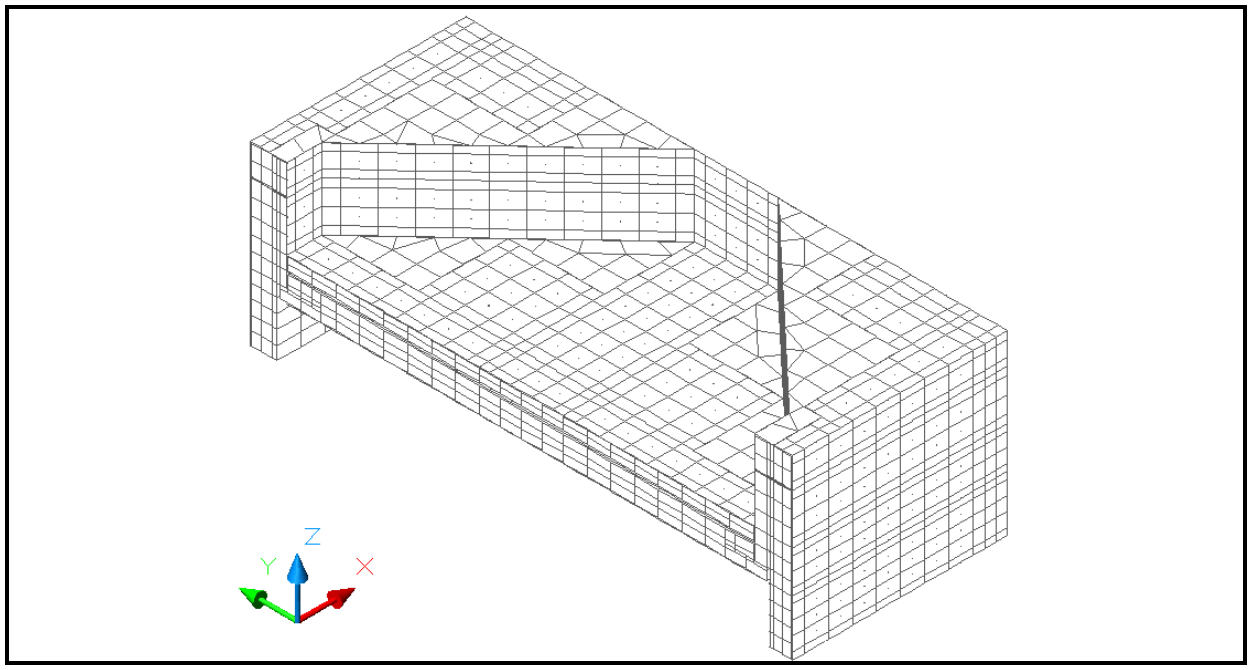

Figure 3.5-2 – Perspective View of Modeled Closure End

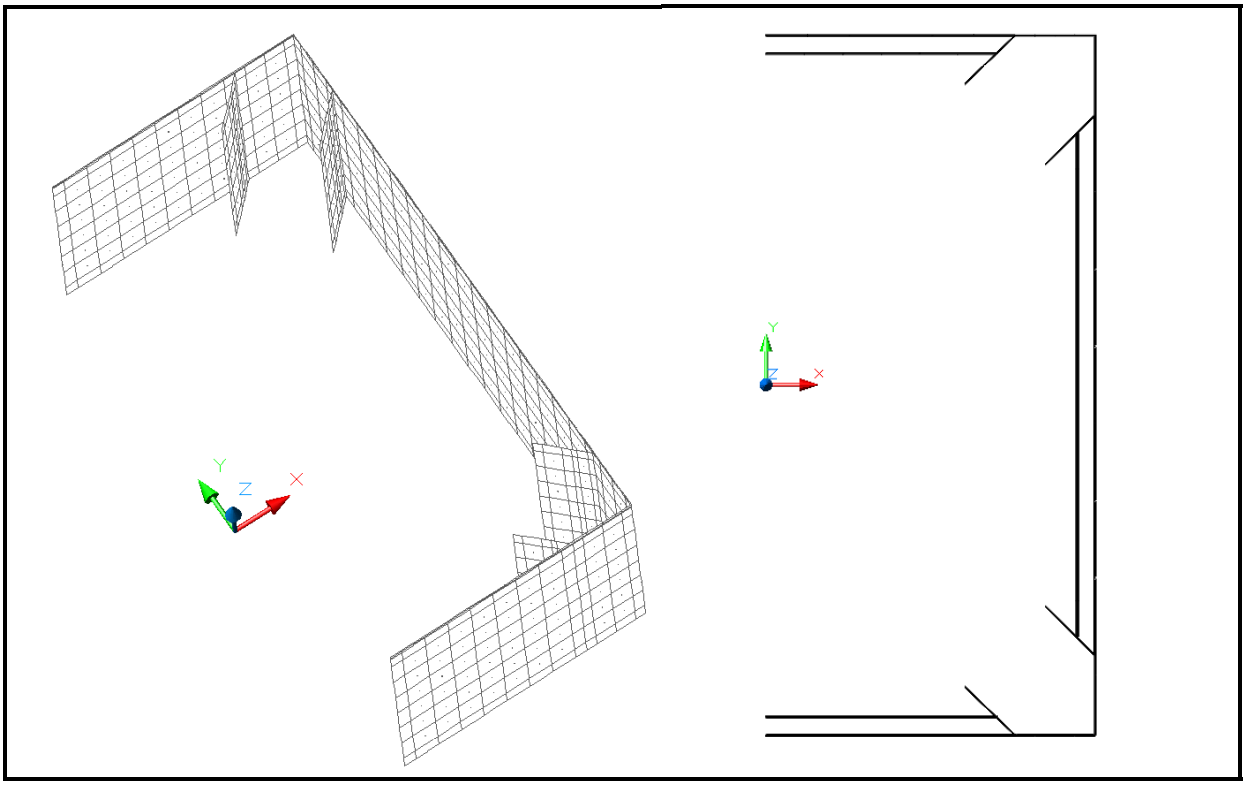

(Note: the positive y-axis is oriented towards the top of the package and the positive z-axis towards the package closure end)

Figure 3.5-3 – Perspective and Plan Views of Modeled Outer Skin, Puncture Protection Plate, and Corner Ribs

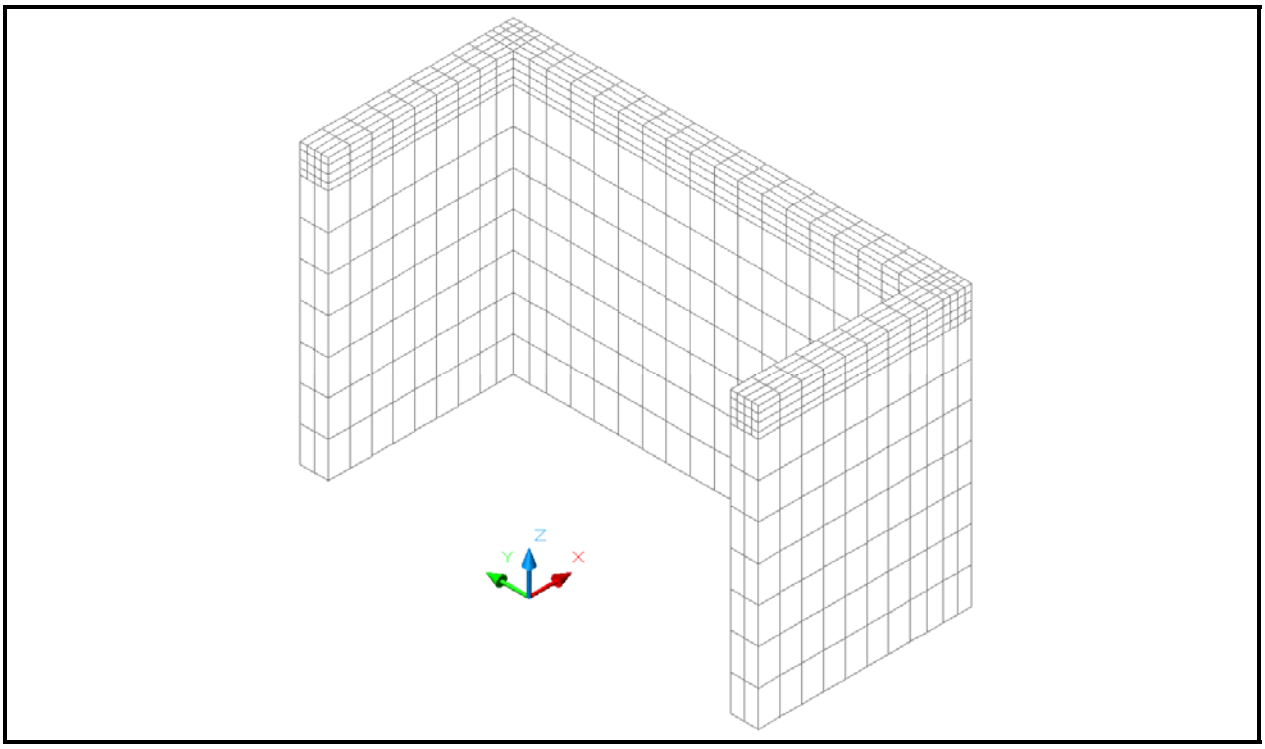

Note: the positive y-axis is oriented towards the top of the package and the positive z-axis towards the package closure end)

Figure 3.5-4 – Perspective View of CSA Thermal Model

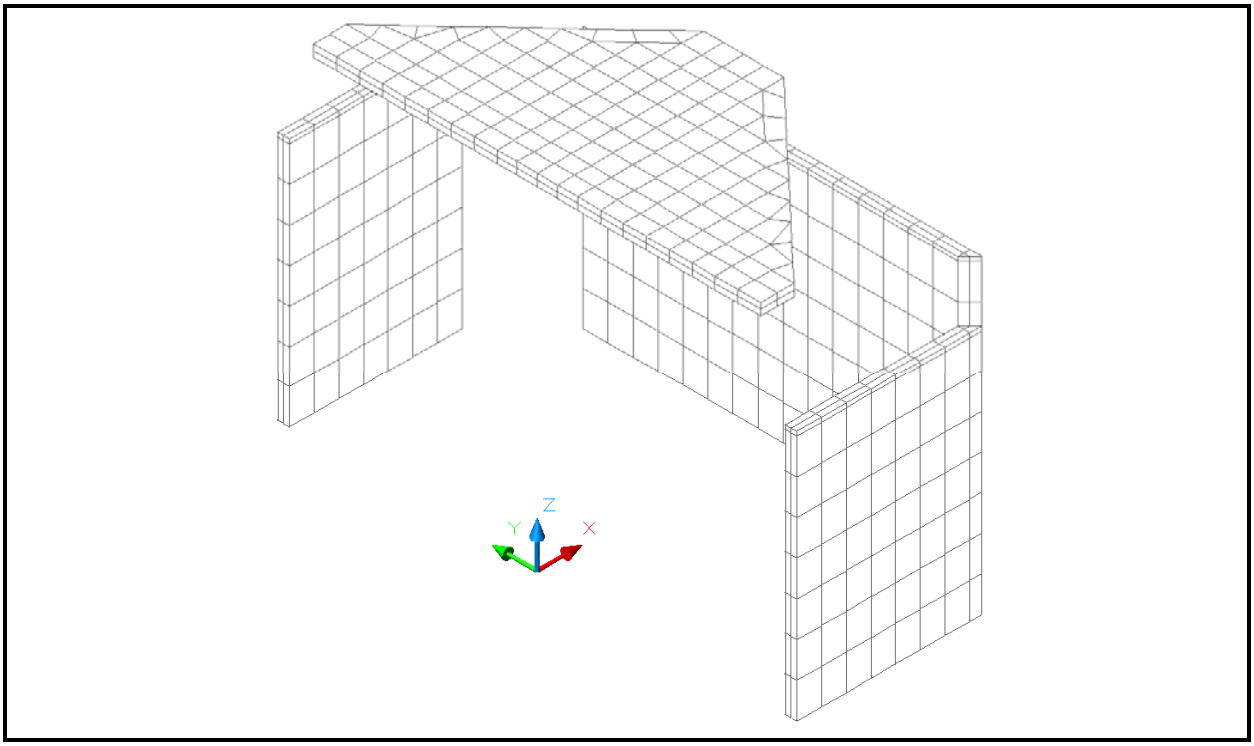

(Note: the positive y-axis is oriented towards the top of the package and the positive z-axis towards the package closure end)

Figure 3.5-5 – Perspective View of Modeled Balsa

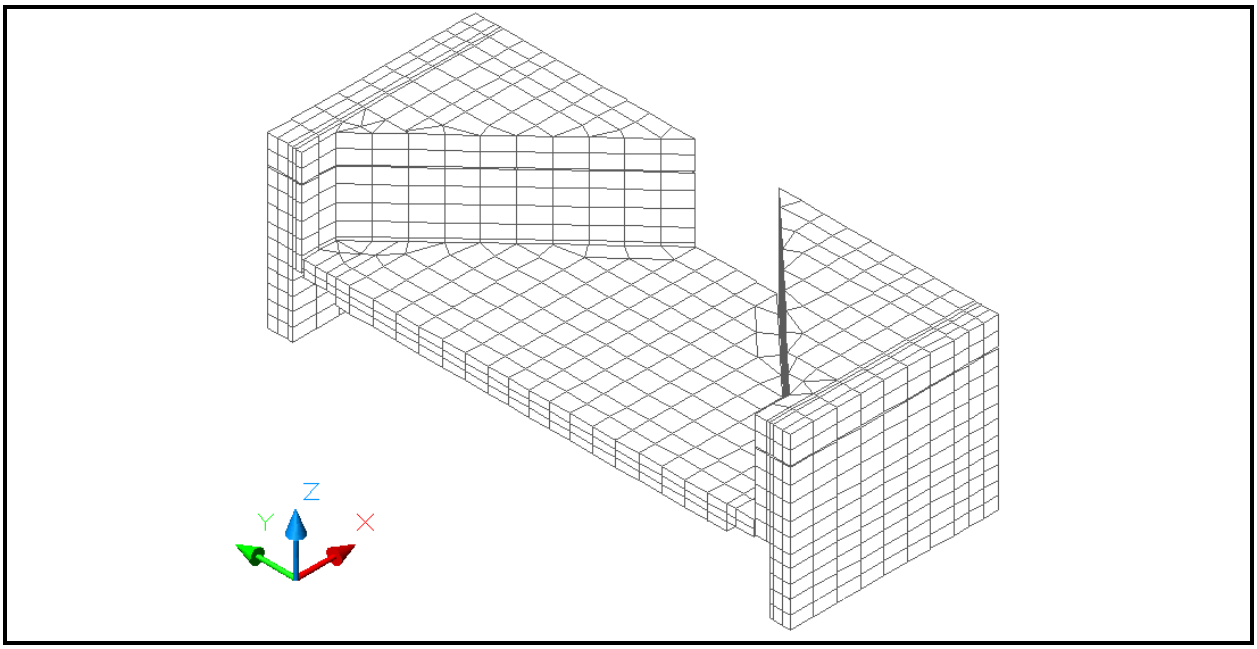

Note: the positive y-axis is oriented towards the top of the package and the positive z-axis towards the package closure end)

Figure 3.5-6 – Perspective View of Modeled Closure End Polyurethane Foam

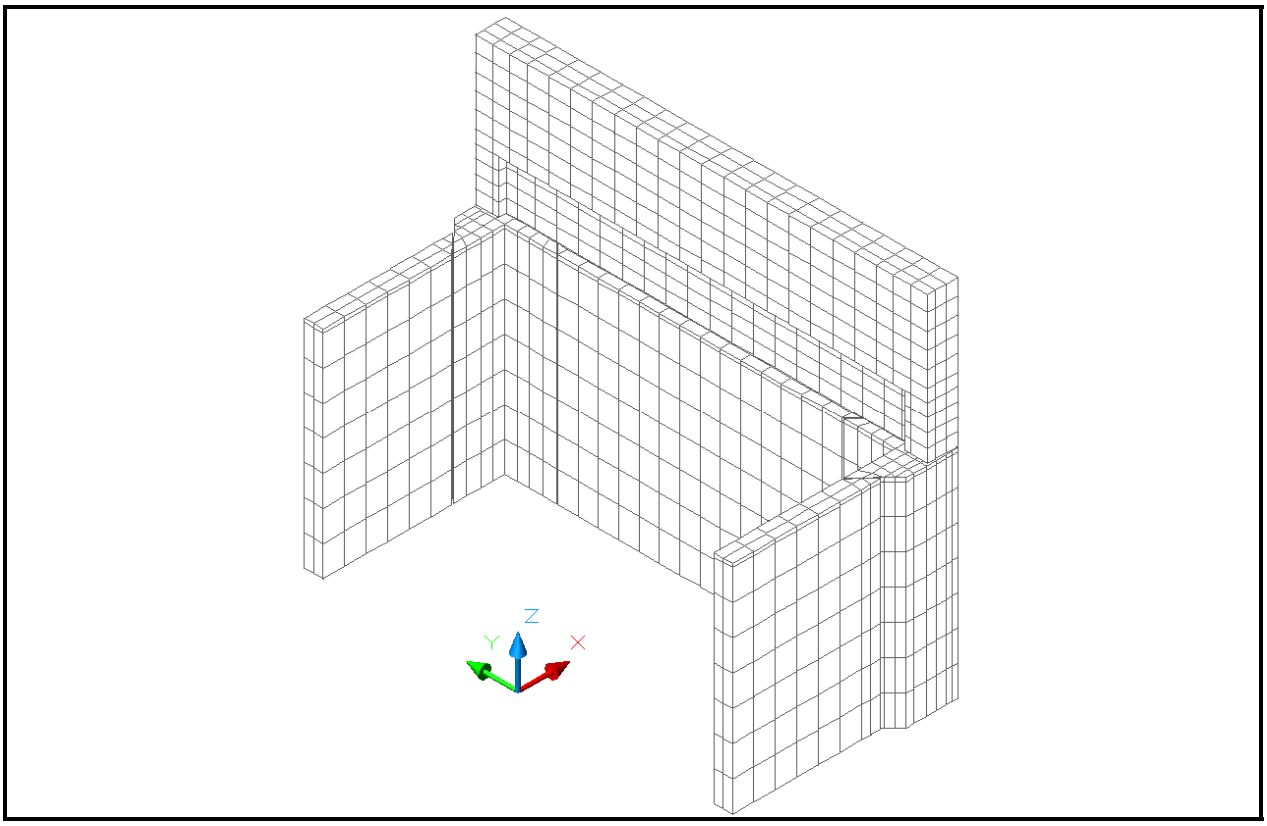

(Note: the positive y-axis is oriented towards the top of the package and the positive z-axis towards the package closure end)

Figure 3.5-7 – Perspective View of Modeled Package Polyurethane Foam

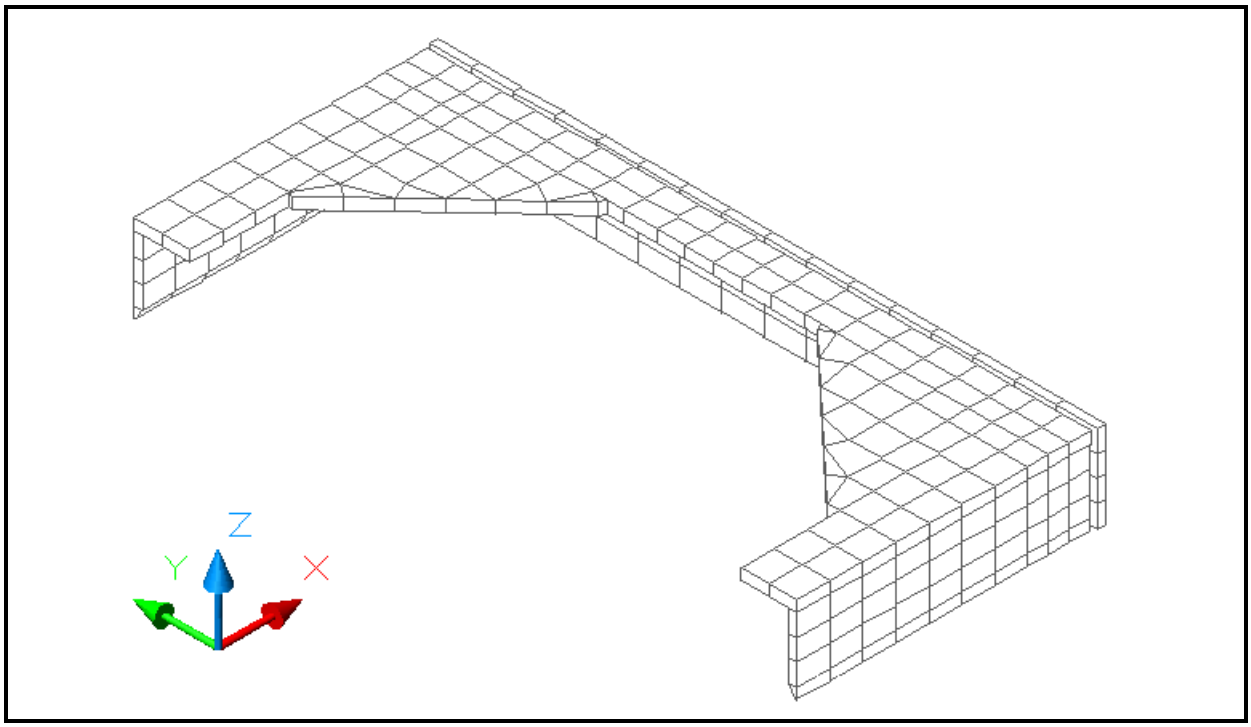

Note: the positive y-axis is oriented towards the top of the package and the positive z-axis towards the package closure end)

Figure 3.5-8 – Perspective View of Modeled Calcium Silicate Insulation

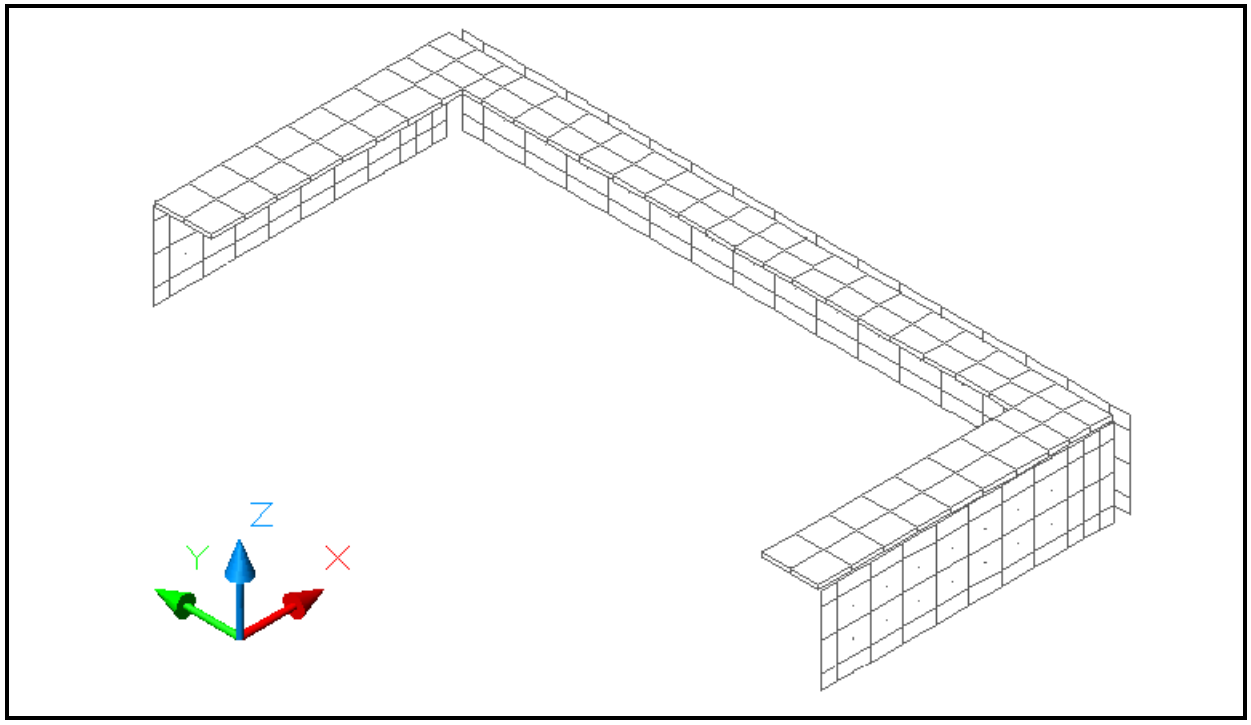

(Note: the positive y-axis is oriented towards the top of the package and the positive z-axis towards the package closure end.)

Figure 3.5-9 – Perspective View of Modeled 16-mm Protection Plates

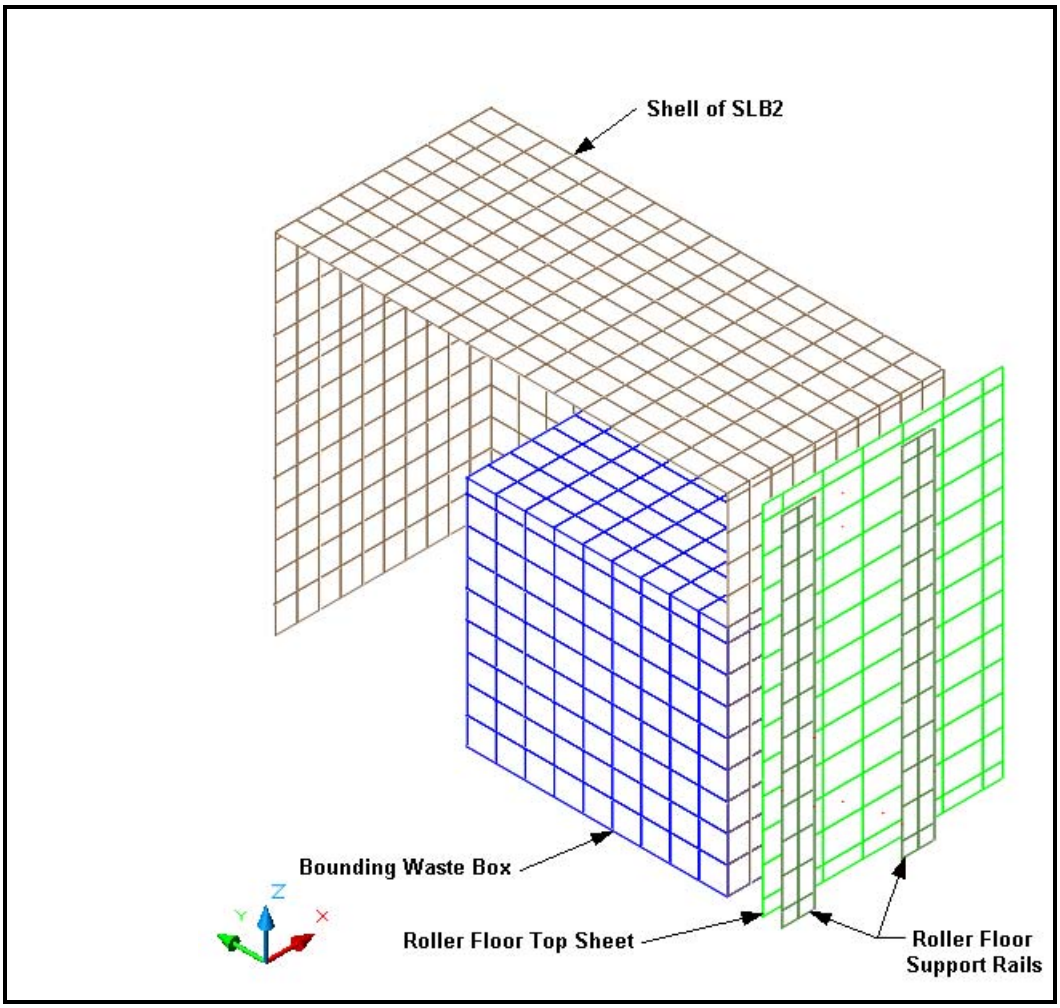

(Note: the positive y-axis is oriented towards the top of the package and the positive z-axis towards the package closure end)

Figure 3.5-10 – SLB2 Model (Shown with Hypothetical Bounding Waste Box Form and Roller Floor)

3.5.2.2 Convection Coefficient Calculation

The convective heat transfer coefficient, h_c, has a form of:

$$h_c = Nu \frac{k}{L}$$

where k is the thermal conductivity of the gas at the mean film temperature and L is the characteristic length of the vertical or horizontal surface.

Natural convection from each surface is computed based on semi-empirical relationships using the local Rayleigh number and the characteristic length for the surface. The Rayleigh number is defined as:

where $$Ra_L = \frac{\rho^2 g_c \beta L^3 \Delta T}{\mu^2} \times Pr$$

g_c = gravitational acceleration, 9.81 m/s^2

β = coefficient of thermal expansion, K^{-1}

ΔT = temperature difference, °C

ρ = density of air at the film temperature, g/m^3

μ = dynamic viscosity, N-s/m^2

Pr = Prandtl number = (c_p μ) / k

L = characteristic length, m

k = thermal conductivity of air film temperature, W/m-K

c_p = specific heat, J/g-°C

Ra_L = Rayleigh #, based on length 'L'

Note that k, c_p, and μ are each a function of air temperature as taken from Table 3.2-9. Values for ρ are computed using the ideal gas law, β for an ideal gas is simply the inverse of the absolute temperature of the gas, and Pr is computed using the values for k, c_p, and μ from Table 3.2-9. Unit conversion factors are used as required to reconcile the units for the various properties used.

The natural convection from a discrete vertical surface is computed using Equation 4-33 of Rohsenow, et. al. [5], which is applicable over the range 1 < Rayleigh number (Ra) < 10^{12}:

$$Nu^T = \overline{C}_L Ra^{1/4}$$

$$\overline{C}_L = \frac{0.671}{\left(1 + \left(0.492/Pr\right)^{9/16}\right)^{4/9}}$$

$$Nu_L = \frac{2.0}{\ln\left(1 + 2.0/Nu^T\right)}$$

$$Nu_t = \frac{C_t^V Ra^{1/3}}{\left(1 + 1.4x10^9\ Pr/\ Ra\right)}$$

[5] Rohsenow, Hartnett, and Choi, *Handbook of Heat Transfer*, 3rd edition, McGraw-Hill Publishers, 1998.

$$C_t^V = \frac{0.13\,Pr^{0.22}}{\left(1+0.61\,Pr^{0.81}\right)^{0.42}}\left[1+0.78\left(\frac{T_{wall}}{T_\infty}-1\right)\right]$$

where T_{wall} and T_∞ are in terms of absolute temperature.

$$Nu = \frac{h_c L}{k} = \left[(Nu_L)^6 + (Nu_t)^6\right]^{1/6}$$

Natural convection from horizontal surfaces is computed from Equations 4.39 and 4.40 of Rohsenow, et. al.[5], and Equations 3.34 to 3.36 of Guyer [6], where the characteristic dimension (L) is equal to the plate surface area divided by the plate perimeter. For a heated surface facing upwards or a cooled surface facing downwards and Ra > 1:

$$Nu = \frac{h_c L}{k} = \left[(Nu_L)^{10} + (Nu_t)^{10}\right]^{1/10}$$

$$Nu_L = \frac{1.4}{\ln\left(1+1.677/\left(\overline{C_L}Ra^{1/4}\right)\right)}$$

$$\overline{C_L} = \frac{0.671}{\left[1+(0.492/Pr)^{9/16}\right]^{4/9}}$$

$$Nu_t = 0.14Ra^{1/3}$$

For a heated surface facing downwards or a cooled surface facing upwards and $10^3 < Ra < 10^{10}$, the correlation is as follows:

$$Nu = Nu_L = \frac{2.5}{\ln\left(1+2.5/Nu^T\right)}$$

$$Nu^T = \frac{0.527}{\left(1+(1.9/Pr)^{9/10}\right)^{2/9}}Ra^{1/5}$$

The forced convection coefficients applied during the HAC fire event are computed using the relationships in Table 6-5 of *Principles of Heat Transfer*[7] for flat surfaces where the characteristic dimension (L) is equal to the length along the surface. For Reynolds number (Re) < 5×10^5 and Prandtl number (Pr) > 0.1:

$$Nu = 0.664\,Re_L^{0.5}\,Pr^{0.33}$$

For Reynolds number (Re) > 5×10^5 and Prandtl number (Pr) > 0.5:

$$Nu = 0.036\,Pr^{0.33}[Re_L^{0.8} - 23{,}200]$$

[6] Guyer, E.C., *Handbook of Applied Thermal Design*, McGraw-Hill, Inc., 1989.

[7] Kreith, Frank, *Principles of Heat Transfer*, 3rd edition, Harper & Row, 1973.

3.5.2.3 Insolation Loads

The thermal loading on the TRUPACT–III during NCT arises from insolation on the outer skin of the package and, to a much lesser degree, from the decay heat of the payload. The 10CFR71.71(c)(1) insolation values represent the total insolation over a 12-hour period. The presence of the balsa wood and polyurethane foam in the package wall and shock absorbing structures will thermally isolate the interior of the package from the external environment. The presence of these materials and the relatively thin exterior skin of the package will result in the peak surface temperatures of the package responding rapidly to changes in the external environment. As such, transient modeling of the insolation loading provides the best means of capturing both the peak temperatures near the exterior of the package while not underestimating the peak payload temperatures and vice-versa.

A sine wave model is used to simulate the variation in the applied insolation on the surfaces of the package over a 24-hour period, except that when the sine function is negative, the insolation level is set to zero. The timing of the sine wave is set to achieve its peak at 12 pm and peak value of the curve is adjusted to ensure that the total energy delivered matched the values in 10 CFR §71.71(c)(1). As such, the total energy delivered in one day by the sine wave solar model is given by:

$$\int_{6\cdot hr}^{18\cdot hr} Q_{peak}\cdot\sin\left(\frac{\pi\cdot t}{12\cdot hr}-\frac{\pi}{2}\right)dt=\left(\frac{24\cdot hr}{\pi}\right)\cdot Q_{peak}$$

Using the expression above for the peak rate of insolation, the peak rates for top and side insolation may be calculated as follows:

$$Q_{top}=\left(800\frac{cal}{cm^2}\right)\cdot\left(\frac{\pi}{24\,hr}\right) \qquad Q_{top}=1.218\times10^{-3}\frac{W}{mm^2}$$

$$Q_{side}=\left(200\frac{cal}{cm^2}\right)\cdot\left(\frac{\pi}{24\,hr}\right) \qquad Q_{side}=3.045\times10^{-4}\frac{W}{mm^2}$$

Conversion factors of 1 cal/sec. = 4.1868 W and 1 cal/cm^2-hr = 1.163 x 10^{-5} W/mm^2 are used in the above calculation. These peak rates are multiplied by the sine function to create the top and side insolation values as a function of time of day.

3.5.2.4 Effective Thermal Properties for Corrugated Wall/Lid Structures

The walls and lid of the TRUPACT–III container are corrugated structures comprised of inner and outer plates separated by V-stiffeners on approximately 164-mm centers. The enclosed void volumes are filled with air at atmospheric pressure. Figure 1.1-5 from Section 1.1, *Introduction*, illustrates a typical cross-section of the container wall and closure lid. The overall 140-mm wall thickness of the container wall is comprised of two 8-mm sheets and 4-mm thick V-stiffeners inclined at an approximately 67 degree angle. The closure lid has a similar cross-section, except that the inner and outer plates are 12-mm thick and the V-stiffeners are on 165-mm centers.

Modeling the exact geometry of the container's wall and lid structures would be node intensive and unnecessary, given the relatively low temperature gradients expected. Instead, a set of effective thermal properties are developed which permits the walls and lid to be simulated as

homogeneous solids. The effective thermal properties, based on the temperature dependant properties for Alloy UNS S31803 stainless steel, consists of a set of anisotropic (i.e., direction dependant) thermal conductivities, an effective density value, and specific heat values. Figure 3.5-11 illustrates the thermal model segment used to develop the effective thermal properties for the prototypic wall section. A similar thermal model, but with the appropriate dimensional changes, is used to compute the effective thermal properties for the lid section.

The Figure 3.5-11 model segment represents a symmetrical section of the container wall that is 164-mm long × 164-mm wide × 140-mm thick (132-mm between the centerlines of the inner and outer walls). A total of approximately 300 nodes are used to represent the temperature distribution across the wall/rib surfaces and the enclosed air volume. A constant heat flux condition is assumed on the inner wall of the model segment, while a constant temperature condition is assumed on the outer wall. Adiabatic boundary conditions are assumed at the remaining four edges of the modeled segment. Perfect connection between the ends of the V-stiffeners and the containment sheet is assumed to simulate the continuous seam welds, while the plug welded connection between the flat of the V-stiffeners and the structural sheet is modeled using contact elements.

Computation of the effective thermal properties in the 'along' direction (i.e., into the page for the Figure 3.5-11 plan view) is based on an area weighted average of the material cross-sections. For the wall segments with 8-mm thick inner and outer plates the effective thermal conductivity is computed as:

$$\text{Area}_{\text{cross-section}} \times k_{\text{along-wall}} = \text{Area}_{\text{inner/outer plates}} \times k_{\text{318 Stainless steel}} + \text{Area}_{\text{ribs}} \times k_{\text{318 Stainless steel}}$$

$$(164\,\text{mm} \times 140\,\text{mm}) \times k_{\text{along-wall}} = (2 \times 164\,\text{mm} \times 8\,\text{mm}) \times k_{\text{318 Stainless steel}} + (2 \times 136.694\,\text{mm} + 35\,\text{mm}) \times 4\,\text{mm} \times k_{\text{318 Stainless steel}}$$

$$k_{\text{along-wall}} = 0.16801 \times k_{\text{318 Stainless steel}}$$

It should be noted that the 136.694 mm dimension in the above equation is obtained from the modeled length of the 'v' in the thermal model.

The contributions of the air and radiation are conservatively ignored. The effective thermal conductivity for the lid structure is higher due to the 50% greater thickness in the inner and outer plates. The effective thermal conductivity for the 'along' direction of the lid is:

$$(165\,\text{mm} \times 148\,\text{mm}) \times k_{\text{along-lid}} = (2 \times 165\,\text{mm} \times 12\,\text{mm}) \times k_{\text{318 Stainless steel}} + (2 \times 139.715\,\text{mm} + 39\,\text{mm}) \times 4\,\text{mm} \times k_{\text{318 Stainless steel}}$$

$$k_{\text{along-lid}} = 0.21432 \times k_{\text{318 Stainless steel}}$$

The 139.715 mm dimension in the above equation is obtained from the modeled length of the 'v' in the thermal model.

The effective thermal properties in the 'axial' direction of the container wall (i.e., across the Figure 3.5-11 plan view) is computed in a similar fashion via the following equation:

$$\text{Area}_{\text{cross-section}} \times k_{\text{axial-wall}} = \text{Area}_{\text{inner/outer plates}} \times k_{\text{318 Stainless steel}}$$

$$(\text{unit length} \times 140\,\text{mm}) \times k_{\text{axial-wall}} = 2 \times (\text{unit length} \times 8\,\text{mm}) \times k_{\text{318 Stainless steel}}$$

$$k_{\text{axial-wall}} = 0.114286 \times k_{\text{318 Stainless steel}}$$

Again, the effective thermal conductivity for the lid structure is higher due to the thicker inner and outer plates. The effective thermal conductivity for the 'axial' direction of the lid is:

$$(\text{unit length} \times 148\,\text{mm}) \times k_{\text{axial-lid}} = 2 \times (\text{unit length} \times 12\,\text{mm}) \times k_{\text{318 Stainless steel}}$$

$$k_{\text{axial-lid}} = 0.162162 \times k_{\text{318 Stainless steel}}$$

As seen, these formulations for the 'axial' thermal conductivity conservatively ignore the contribution of ribs in addition to the contributions of the air and radiation.

In contrast to the 'along' and 'axial' thermal conductivity, the contributions of heat transfer through the enclosed air and radiation exchange is more significant for the computation of the effective thermal conductivity through the wall/lid structures (i.e., between the inner and outer plates). Further, the interaction between the ribs and the inner and outer plates is complex. As such, the 'thru' thermal conductivity was evaluated using the lumped model depicted in Figure 3.5-11 and the Thermal Desktop™ and SINDA/FLUINT™ programs. A constant heat flux condition is assumed on the inner wall, while a constant temperature condition is assumed on the outer wall. The constant heat flux condition was determined assuming the maximum payload heat load of 80 watts and an even distribution over the surface area of the container's sides, top, and ends (the floor is conservatively ignored given the presence of the roller floor and pallet). The resulting heat flux is equal to 80 watts/(2 × 2.790 m × 2.0 m + 2.790 m × 1.840 m + 2 × 2.0 m × 1.840 m), or 3.3821 watts/m^2. The thermal model was exercised for a range of boundary temperature conditions and the temperature results used to compute the effective 'thru' thermal conductivity for the CSA wall via the equation:

$$Q_{\text{thru-wall}} = \text{Section Area/Section Thickness} \times k_{\text{thru}} \times \Delta T$$

$$3.3821 \frac{\text{watts}}{\text{m}^2} \times (0.164\,\text{m})^2 = (164\,\text{mm} \times 164\,\text{mm})/140\,\text{mm} \times k_{\text{thru-wall}} \times (\text{Ave. Inner Wall Temp.} - \text{Ave. Outer Wall Temp.})$$

$$k_{\text{thru-wall}} = 0.090965\,\text{watts} \times 5.2052\,\text{m}^{-1}/(\text{Ave. Inner Wall Temp.} - \text{Ave. Outer Wall Temp.})$$

The 'thru' conductivity for the container lid is computed in a similar fashion, but with adjustment given its greater overall thickness, thicker inner and outer plates, and different rib geometry. The Figure 3.5-11 thermal model was modified for these geometry differences and the results of the Thermal Desktop™ and SINDA/FLUINT™ modeling used with the following equation:

$$k_{\text{thru-lid}} = 0.092078\,\text{watts} \times 5.4362\,\text{m}^{-1}/(\text{Ave. Inner Lid Temp.} - \text{Ave. Outer Lid Temp.})$$

Table 3.2-2 and Table 3.2-3 present the computed 'thru', 'along', and 'axial' thermal conductivity values for a range of temperatures based on the results of the Thermal Desktop® and SINDA/FLUINT modeling. The 'along' and 'axial' thermal conductivity values are computed using the thermal conductivity for Alloy UNS S31803 stainless steel (see Table 3.2-4) and the multiplication factors determined above. The effective densities of the container wall and lid sections are determined as volume weighted functions of the Alloy UNS S31803 stainless steel values where:

$$\text{Volume}_{\text{cross-section}} \times \rho_{\text{effective}} = \text{Volume}_{\text{inner/outer plates}} \times \rho_{\text{318 Stainless steel}} + \text{Volume}_{\text{ribs}} \times \rho_{\text{318 Stainless steel}}$$

Thus, $$\rho_{\text{wall-effective}} = 0.16801 \times \rho_{\text{318 Stainless steel}}$$

$$\rho_{\text{wall-effective}} = 1.33\ \text{kg/dm}^3$$

and $$\rho_{\text{lid-effective}} = 0.21432 \times \rho_{\text{318 Stainless steel}}$$

$$\rho_{\text{lid-effective}} = 1.69\ \text{kg/dm}^3$$

The specific heat of the container walls and lid are assumed to be the same as Alloy UNS S31803 stainless steel.

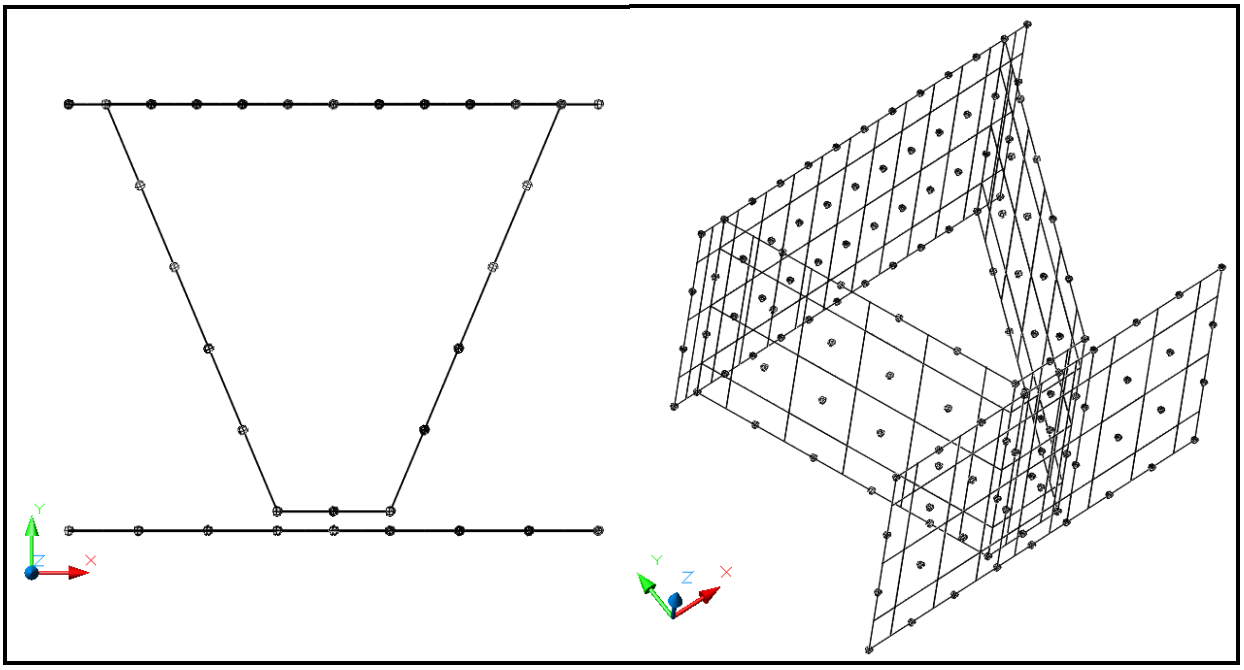

Figure 3.5-11 – Plan and Perspective Views of Container Wall Section Model for Effective Thermal Conductivity Calculation

3.5.2.5 Effective Thermal Properties for CSA End Detail & Lid Perimeter

CSA End Detail

The effective thermal properties for the walls of the CSA body developed in Section 3.5.2.4, *Effective Thermal Properties for Corrugated Wall/Lid structures*, are appropriate for defining the heat transfer through the CSA structure for all but the structural detail at the closure end. At this location, the structure is defined by a box beam structure as illustrated in Figure 3.5-12 and Figure 3.5-13. The design illustrated in these figures represents a slight modification from the preliminary design used to develop the thermal model (see Figure 3.5-14). The differences consist of a thickening of the front plate from 19 mm to 25 $\pm$ 5 mm and the elimination of the 35 mm lightening hole on the backside of the closure bolt bar stock. Since these design changes provide a greater thermal mass and a higher effective thermal conductance in the transverse direction, ignoring the design change is conservative for NCT conditions. The thermal gradients are low enough that a composite of the thermal properties for each location can be used to define the thermal performance of the structure around its entire circumference.

The effective thermal properties in the axial direction (i.e., along the z-axis of the package) in the segments not encompassing the closure bolt insertions can be defined on a per unit length as:

$$k_{axial} = \frac{\text{Actual Heat Transfer Area}}{\text{Full Area}} \times k_{318\,\text{Stainless steel}}$$

$$k_{axial} = \frac{(2 \times 15\,\text{mm}) \times 1\,\text{mm}}{140\,\text{mm} \times 1\,\text{mm}} \times k_{318\,\text{Stainless steel}}$$

$$k_{axial} = 0.2143 \times k_{318\,\text{Stainless steel}}$$

The bolt inserts are on 198 mm centers and are fabricated of 70 mm diameter bar stock with 35 mm diameter holes drilled from one direction. Therefore, the minimum axial heat transfer area of each bolt insert is:

$$\text{Area}_{insert} = \left[\left(\frac{70}{2}\right)^2 - \left(\frac{35}{2}\right)^2\right] \times \pi$$

$$\text{Area}_{insert} = 2{,}886.3\,\text{mm}^2$$

Therefore, the effective axial heat transfer, including the effect of the bolt inserts, is:

$$k_{axial} = \frac{(2 \times 15\,\text{mm} \times 198\,\text{mm} + 2{,}886.3\,\text{mm}^2)}{140\,\text{mm} \times 198\,\text{mm}} \times k_{318\,\text{Stainless steel}}$$

$$k_{axial} = 0.318 \times k_{318\,\text{Stainless steel}}$$

The effective thermal properties in the transverse direction (i.e., vertically, across the plane of Figure 3.5-12 or Figure 3.5-13) can be defined in a similar manner. Conservatively ignoring the thicker front plate provided by the latest design iteration and using the Figure 3.5-14 design layout, the transverse thermal conductivity is defined as:

$$k_{transverse} = \frac{\text{Actual Heat Transfer Area}}{\text{Full Area}} \times k_{318\ \text{Stainless steel}}$$

$$k_{transverse} = \frac{(19\ \text{mm} + 10\ \text{mm}) \times 198\ \text{mm}}{145\ \text{mm} \times 198\ \text{mm}} \times k_{318\ \text{Stainless steel}}$$

$$k_{transverse} = 0.20 \times k_{318\ \text{Stainless steel}}$$

Finally, the effective thermal properties along the CSA's structural end detail (i.e., into the plane of Figure 3.5-12 or Figure 3.5-13) can be defined in a similar manner. While the holes in the structure for the lid bolts will have only a local effect, it is simpler and conservative to reduce the heat transfer area by their diameter. Based on this approach, the effective thermal conductivity is computed as:

$$k_{along} = \frac{\text{Actual Heat Transfer Area}}{\text{Full Area}} \times k_{318\ \text{Stainless steel}}$$

$$k_{along} = \frac{(19\ \text{mm} + 10\ \text{mm}) \times (140\ \text{mm - 35 mm for bolt holes}) + (2 \times 15\ \text{mm}) \times (145\ \text{mm - 19 mm - 10 mm})}{140\ \text{mm} \times 145\ \text{mm}} \times k_{318\ \text{Stainless steel}}$$

$$k_{along} = 0.321 \times k_{318\ \text{Stainless steel}}$$

The effective density of the CSA end detail is determined as a volume weighted function of the Alloy UNS S31803 stainless steel values where:

$$\text{Volume}_{section} \times \rho_{\text{CSA-effective}} = \text{Volume}_{\text{inner/outer plates}} \times \rho_{318\ \text{Stainless steel}} + \text{Volume}_{\text{bolt insert}} \times \rho_{318\ \text{Stainless steel}}$$

$$\rho_{\text{CSA-effective}} = \left[(19\ \text{mm} + 10\ \text{mm}) \times 140\ \text{mm} \times 198\ \text{mm} + (2 \times 15\ \text{mm} \times 116\ \text{mm}) \times 198\ \text{mm} + 2{,}886.3\ \text{mm}^2 \times 116\ \text{mm}\right] / (145\ \text{mm} \times 140\ \text{mm} \times 198\ \text{mm}) \times \rho_{318\ \text{Stainless steel}}$$

$$\rho_{\text{CSA-effective}} = 0.455 \times \rho_{318\ \text{Stainless steel}}$$

The specific heat is the same as Alloy UNS S31803 stainless steel.

Since ignoring the thicker front plate thickness is non-conservative for HAC conditions, the effective thermal properties used in the HAC modeling are re-computed based on the maximum dimensions depicted in Figure 3.5-12 and Figure 3.5-13.

$$k_{transverse} = \frac{((25 + 5)\ \text{mm} + 10\ \text{mm}) \times 198\ \text{mm}}{145\ \text{mm} \times 198\ \text{mm}} \times k_{318\ \text{Stainless steel}}$$

$$k_{transverse} = 0.276 \times k_{318\ \text{Stainless steel}}$$

$$k_{along} = \frac{(30\ \text{mm} + 10\ \text{mm}) \times (140\ \text{mm - 35 mm for bolt hole}) + (2 \times 15\ \text{mm}) \times (145\ \text{mm - 30 mm - 10 mm})}{140\ \text{mm} \times 145\ \text{mm}} \times k_{318\ \text{Stainless steel}}$$

$$k_{along} = 0.362 \times k_{318\ \text{Stainless steel}}$$

The thermal conductivity in the axial direction is the same as used for NCT conditions. For conservatism, the effective density computed for NCT conditions is used.

Lid Perimeter

The perimeter of the CSA closure lid incorporates a box beam edge detail as depicted in Figure 3.5-15. The effective thermal properties for this portion of the lid are computed in the same manner as that presented above for the CSA end structure. The effective thermal properties in the axial direction (i.e., along the z-axis of the package) in the segments not encompassing the closure bolt insertions can be defined on a per unit length as:

$$k_{axial} = \frac{\text{Actual Heat Transfer Area}}{\text{Full Area}} \times k_{318\ \text{Stainless steel}}$$

$$k_{axial} = \frac{(2 \times 16\,\text{mm}) \times 1\,\text{mm}}{140\,\text{mm} \times 1\,\text{mm}} \times k_{318\ \text{Stainless steel}}$$

$$k_{axial} = 0.229 \times k_{318\ \text{Stainless steel}}$$

The bolt inserts are on 198 mm centers and are fabricated of 64 mm diameter bar stock with a 44 mm inner diameter. Therefore, the area of each bolt insert is:

$$\text{Area}_{insert} = \left[\left(\frac{64}{2}\right)^2 - \left(\frac{44}{2}\right)^2\right] \times \pi$$

$$\text{Area}_{insert} = 1{,}696.5\,\text{mm}^2$$

Therefore, the effective axial heat transfer, including the effect of the bolt inserts, is:

$$k_{axial} = \frac{(2 \times 16\,\text{mm} \times 198\,\text{mm} + 1{,}696.5\,\text{mm}^2)}{140\,\text{mm} \times 198\,\text{mm}} \times k_{318\ \text{Stainless steel}}$$

$$k_{axial} = 0.290 \times k_{318\ \text{Stainless steel}}$$

It should be noted that the thermal model assumes that $k_{axial} = 0.308 \times k_{318\ \text{Stainless steel}}$ based on earlier assumptions regarding the geometry of the bolt inserts. The 0.308 multiplier factor represents an approximately 6% higher value than the correct multiplier factor of 0.290. Since the principal heat transfer concern for this package arises during the HAC fire event when heat is moving into the package, the use of the higher multiplier factor will provide a conservative estimate of the peak temperature achieved in the package closure seal.

The effective thermal properties in the transverse direction (i.e., vertically, across the plane of Figure 3.5-15) can be defined in a similar manner as:

$$k_{transverse} = \frac{\text{Actual Heat Transfer Area}}{\text{Full Area}} \times k_{318\ \text{Stainless steel}}$$

$$k_{transverse} = \frac{(20\,\text{mm} + 20\,\text{mm}) \times 198\,\text{mm}}{148\,\text{mm} \times 198\,\text{mm}} \times k_{318\ \text{Stainless steel}}$$

$$k_{transverse} = 0.270 \times k_{318\ \text{Stainless steel}}$$

Finally, the effective thermal properties along the perimeter of the lid (i.e., into the plane of Figure 3.5-15) can be defined in a similar manner as:

$$k_{along} = \frac{\text{Actual Heat Transfer Area}}{\text{Full Area}} \times k_{318\,\text{Stainless steel}}$$

$$k_{along} = \frac{(20\,\text{mm} + 20\,\text{mm}) \times (140\,\text{mm} - 36\,\text{mm}) + (2 \times 16\,\text{mm}) \times (148\,\text{mm} - 2 \times 20\,\text{mm})}{140\,\text{mm} \times 148\,\text{mm}} \times k_{318\,\text{Stainless steel}}$$

$$k_{along} = 0.368 \times k_{318\,\text{Stainless steel}}$$

The effective density of the lid perimeter detail is determined as a volume weighted function of the Alloy UNS S31803 stainless steel values where:

$$\text{Volume}_{\text{section}} \times \rho_{\text{lid-effective}} = \text{Volume}_{\text{inner/outer plates}} \times \rho_{318\,\text{Stainless steel}} + \text{Volume}_{\text{bolt insert}} \times \rho_{318\,\text{Stainless steel}}$$

Thus,

$$\rho_{\text{lid-effective}} = \left[(2 \times 20\,\text{mm} \times 140\,\text{mm}) \times 198\,\text{mm} + (2 \times 16\,\text{mm} \times 108\,\text{mm}) \times 198\,\text{mm} + 2{,}199.1\,\text{mm}^2 \times 108\,\text{mm}\right] / (148\,\text{mm} \times 140\,\text{mm} \times 198\,\text{mm}) \times \rho_{318\,\text{Stainless steel}}$$

$$\rho_{\text{lid-effective}} = 0.495 \times \rho_{318\,\text{Stainless steel}}$$

The specific heat is the same as Alloy UNS S31803 stainless steel.

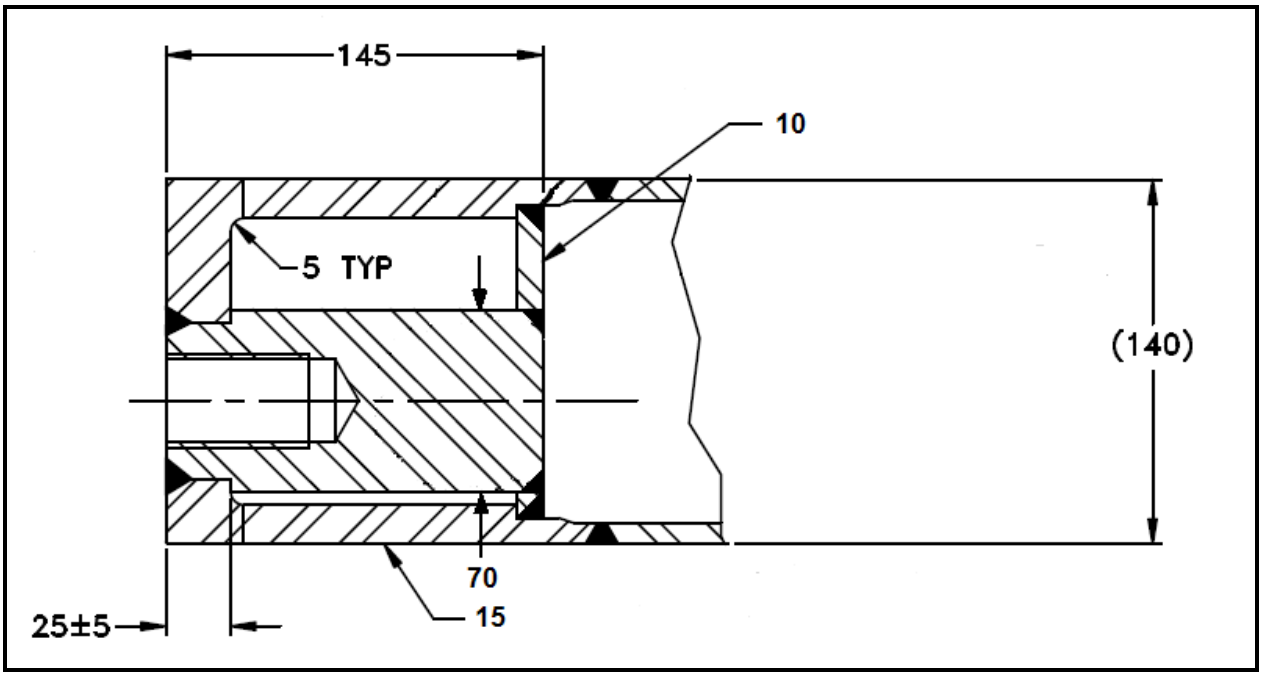

Figure 3.5-12 – CSA End Detail at Location of Closure Bolts

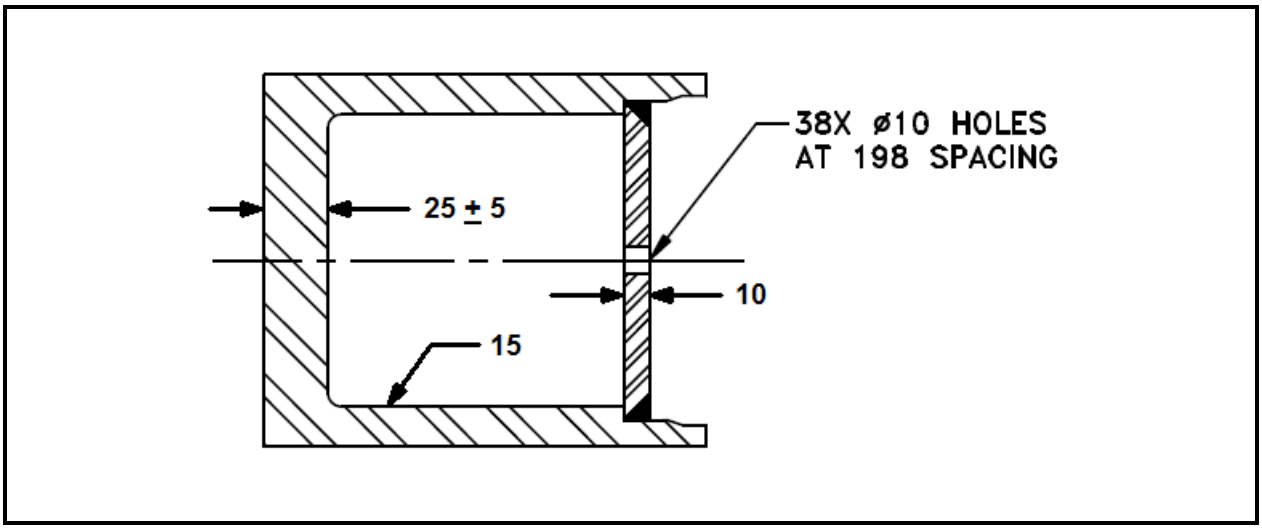

Figure 3.5-13 – CSA End Detail at Locations between Closure Bolts

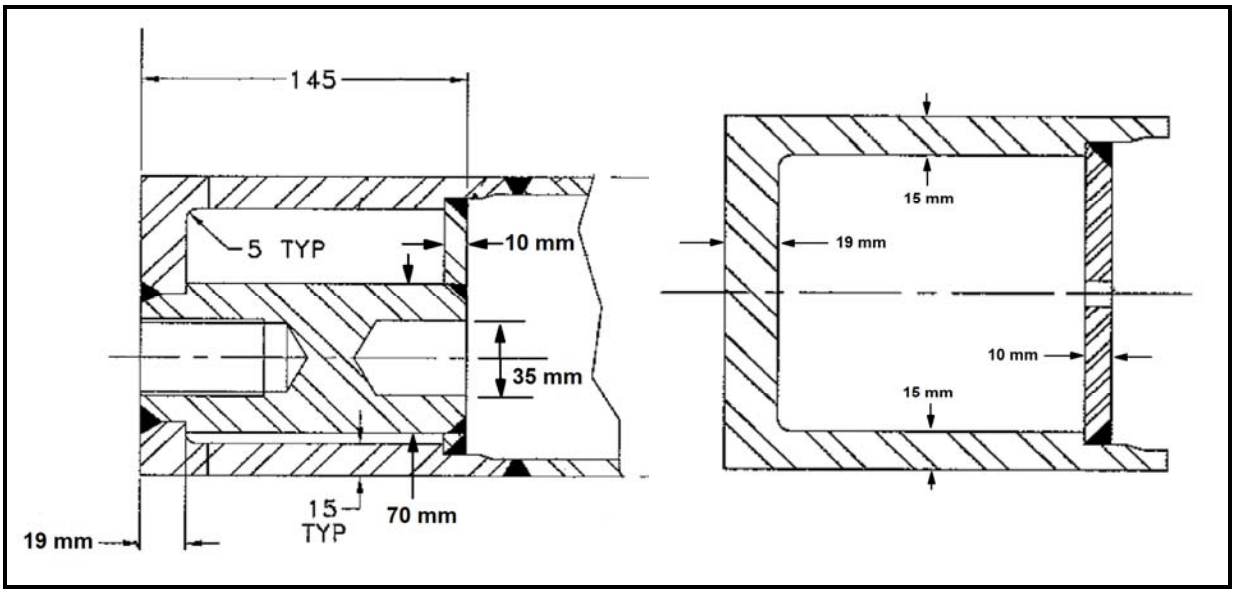

Figure 3.5-14 – Preliminary CSA End Detail as Modeled for NCT

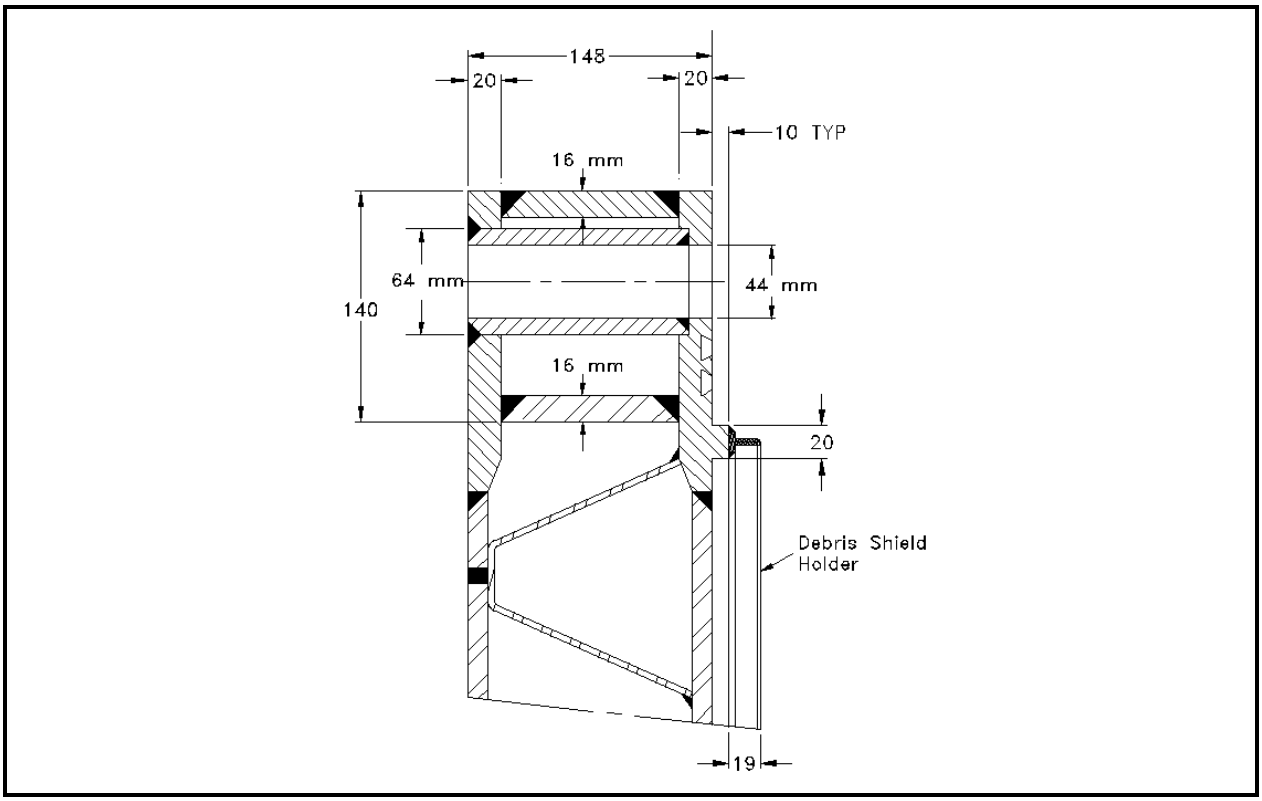

Figure 3.5-15 – Closure Lid Edge Detail

3.5.2.6 Description of Thermal Model for HAC Conditions

The analytical thermal model of the TRUPACT–III used for HAC conditions is a modified version of the quarter symmetry NCT model described in Section 3.5.2.1, *Description of Thermal Model for NCT Conditions*. This is appropriate since the use of a quarter symmetry model to simulate the non-symmetric damages arising from the HAC drop events is inherently conservative. The primary modifications made to the NCT model for the HAC modeling consist of the following:

- Simulated the worst-case HAC free and puncture drops consisting of an oblique side-edge drop and subsequent puncture bar damage adjacent to the side-edge damage and just aft of the cheek to body joint (see Figure 3.5-16 and the discussion below for details),
- Changed the thermal conductivity of the balsa wood from a value consistent with the low end of the observed range to a value that represents the high end of the range,
- Increased the emissivity of the external surfaces from 0.8 to 0.9 to account for possible soot accumulation on the surfaces,
- The balsa wood surfaces adjacent to undamaged portions of the outer skin will be charred from the HAC fire, but not consumed due to the lack of air. However, since the thermal conductivity of solid wood is greater than that for charred wood, the thermal properties of undamaged wood are assumed for computing the heat flow into the package,
- Replaced the assumed air gaps between the layered components of the package side wall with direct contact,
- Replaced the adiabatic boundary condition applied to the bottom of the package for NCT conditions with convective and radiation thermal conductors to the ambient,
- Apply convection heat transfer coefficients between the package and the ambient that are appropriate for gas velocities of 10 m/sec[8] during the 30-minute fire event. Convection coefficients based on still air are assumed following the 30-minute fire event,
- An 800 ºC ambient condition with an effective emissivity of 1.0 is used to simulate the elevated temperature of the fire for convective and radiation heat transfer during the 30-minute fire event. The ambient condition is re-set at the end of the 30-minute fire to the pre-fire ambient condition of 38 ºC with an effective emissivity of 1.0 and with the addition of insolation.

The presence of the outer skin, balsa, polyurethane foam, and calcium silicate insulation provides significant thermal protection to the TRUPACT–III package. The potential damage to these components arising from the hypothetical free drop and puncture bar accidents is established based on the results of a series of drop tests on a full-scale model of the TRUPACT–III package. A summary of the testing and the associated results is presented in Section 2.7, *Hypothetical Accident*

[8] Schneider, M.E and Kent, L.A., *Measurements Of Gas Velocities And Temperatures In A Large Open Pool Fire, Heat and Mass Transfer in Fire* - HTD Vol. 73, 1987, ASME, New York, NY.

Conditions. The drop tests covered a range of hypothetical free drop orientations and a series of puncture bar drops. Section 3.5.3, *Review of TRUPACT–III Package Full Scale Drop Test Results*, provides a further overview of the drop test results and justification for the selected bounding damage combination. Of the tested drop scenarios, the oblique drop on the side-edge of the package with a subsequent puncture bar attack just aft of the cheek to body joint (see Figure 3.5-24) is judged to be the most damaging to the thermally sensitive areas of the package. As discussed in Section 2.7.1.5.2, *Side-Edge Free Drop Extrapolation*, the oblique side-edge drop is expected to create a flattened region approximately 305 mm wide along the package length. The flattened region will be reduced to approximately 178 mm at the cheek areas due to the additional structure and the higher density polyurethane foam used in the cheeks. The minimum distance between the outer skin and the corner of the CSA is estimated to be 75 mm over the length of the package body and 65 mm between the outer skin and the corner of the protection plate enclosure (i.e., thermal shield) surrounding the calcium silicate insulation at the cheek areas. Additionally, the weld seam joining the outer skin of the front cheek with the outer skin of the package body is assumed to fail for a distance of approximately 914 mm creating an opening with a maximum width of 51 mm.

Consistent with the damage observed from the drop tests, the puncture bar is predicted to have penetrated both the outer skin and the underlying 10 mm thick puncture-resistant plate and to have opened a hole in the outer skin that is approximately 254 mm long by 178 mm wide. The hole in the underlying 10 mm thick puncture-resistant plate is approximately 178 mm in diameter. The puncture bar is conservatively assumed to have pulled out of the package prior to the start of the fire, thus fully exposing the damaged area to exposure to the fire environment. To maximize the potential effect on the package temperature, the simulated puncture drop damage is located directly below the chevron-shaped edge sheet and directly behind the cheek to package body junction. Locating the damage ahead of the joint would not be as thermally significant due to the presence of the 16-mm protection plate and the calcium silicate. Likewise, locating the puncture bar damage in the corner region would also not be as thermally significant since the higher foam density in this region would act to reduce penetration by the bar and the bar would contact the edge of the CSA obliquely and reduce the area of exposure.

Figure 3.5-16 presents an overview of the bounding damage inflicted on the package thermal model prior to the initiation of the HAC fire. To model the combined damage condition, the thermal model used for the NCT analysis was modified via the following steps:

a. the NCT thermal model was altered at one corner to reflect the flattening of the outer shell of the package expected to result from the 9 m free drop under NCT Hot conditions,
b. the underlying foam in the crushed corner regions is compressed by approximately 30% to yield an apparent density of 0.41 kg/dm^3. For conservatism, a lower bound density of 0.36 kg/dm^3 is used to estimate the recession depth of 42 mm within the foam under HAC conditions (see Section 3.5.4, *'Last-A-Foam' Response under HAC Condition*). Further, although the recession of the foam will occur over the 30 minute exposure to the HAC fire temperatures, for conservatism the full recession depth is assumed to occur at the start of the HAC fire event.
c. the foam at the undamaged corners of the package is likewise recessed at the start of the fire event to reflect the expected 60 mm of foam recession that is expected to occur over the entire HAC event for 0.25 kg/dm^3 density foam (representing the lower bound density for the corner region foam).

d. the foam in the cheek regions of the package is assumed to be crushed at the top and recessed at its exterior surfaces by 36 mm for the lower bound fabrication density of 0.41 kg/dm^3 for foam in this region. The remaining foam depth and recession depth are conservatively captured by the thermal model,

e. the 140 mm thick, 0.16 kg/dm^3 foam at the end of the closure overpack is assumed to have recessed by 60 mm,

f. the heat transfer between the ablated foam surfaces and the exterior skin of the package is modeled as a combination of radiation and conduction across an air filled gap

g. the puncture drop damage is simulated by fully exposing a surface area on the CSA measuring 179 mm wide by 239 mm directly to the HAC fire conditions. This surface area essentially matches the size of the damage noted to the outer skin from the puncture bar (i.e., 254 mm by 178 mm) and is nearly twice the size of the 178 mm diameter hole created in the 10 mm puncture-resistant sheet (see discussion of the puncture bar damage above). The 179 mm by 239 mm area was chosen for modeling since it matched the surface resolution available in the thermal model. No credit is taken for the potential shielding provided by the compacted foam, metal, etc. that may remain within the damaged area. This assumption, together with the larger hole assumed in the 10 mm puncture-resistant sheet, provides a significant level of conservatism on the effect of the HAC damage. Further, as discussed above, the surface area is located directly below the corner ribs and directly behind the cheek to package body junction. A view factor of 0.23 is assumed between the exposed CSA surface and the HAC fire based on a view factor calculation for parallel plates, the 179 mm by 239 mm dimensions of the hole, and the nominal 185 mm separation distance between the CSA surface and the outer sheet of the package skin,

h. the emissivity of the exterior surfaces of the package skin is increased to 0.90 (both sides),

i. the thermal conductivity of the balsa components is increased from the conservatively low value of 0.0415 W/m-K assumed for NCT conditions to a conservatively high value of 0.168 W/m-K,

j. given the package dimension, the package is assumed to be in its horizontal orientation during and the HAC event, and

k. the convection heat transfer coefficients are based on a gas velocity of 10 m/sec during the 30-minute fire event and still air afterwards. The elevated HAC convection heat transfer rate is conservatively applied to the surfaces of the CSA exposed by the puncture bar attack, even though convection will be significantly reduced within the recessed cavity created by the puncture bar attack.

l. the assumed air gaps between the layered balsa wood and polyurethane foam components and the metallic surfaces of the package side walls are replaced with direct contact.

Figure 3.5-17 presents an elevation view of the thermal model of the simulated damaged TRUPACT–III package along the package body. As seen from the figure, the model captures the flattened corner on the outer shell of the package that results from the oblique side-edge drop. In addition, the simulated ablation of the 0.29 kg/dm^3 polyurethane foam in the corners of the package is incorporated into the modeled geometry.

Figure 3.5-18 illustrates an elevation view through the HAC thermal model of the package cheek. The ablation of the 0.48 kg/dm^3 polyurethane foam used in the cheek is conservatively captured

using a lower bound foam density of 0.41 kg/dm^3 to yield a predicted 36 mm recession depth. The modeling also conservatively assumes that the 16-mm protection plate surrounding the calcium silicate insulation in the cheek has been uncovered by the foam ablation along its top surface. This assumption results in the top surface of the protection plate structure being exposed to conductive and radiation heat transfer with the outer skin of the cheek throughout the entire HAC fire event. In reality, this thermal exposure is not expected to occur or, if it did, only near the end of the 30-minute fire event.

Modeling of Balsa Wood Performance

Ignition of the balsa wood requires the wood to be subjected to sufficient heat and in an atmosphere with sufficient oxygen. The absence of either of these conditions will prevent the sustained combustion of the wood. Since the balsa wood components are encapsulated in metal, it will not ignite and it will not burn unless there is damage to the outer skin which allows the free passage of air. The openings created as the result of the melting of the plastic in the pressure relief fittings on the outer skin are not adequate to support active combustion of the wood. Likewise, with the exception of the failure of the weld seam joining the outer skin of the front cheek with the outer skin of the package body (see Figure 3.5-20), all other cracks or tears in the outer skin resulting from the HAC free drops are too small to support active combustion of the under lying wood.

The heat flux from the HAC fire through the outer skin will cause thermal decomposition of the exterior layers of the balsa wood components, resulting in the production of water vapor, carbon monoxide, and non-flammable and flammable volatiles. These gases will exit the package through the pressure relief fittings and may be ignited by the HAC fire. However, the absence of free air movement across the boundary formed by the outer skin will prevent combustion within the wood itself. As such, the pyrolysis process will remain endothermic, potentially resulting in a charred layer of wood, but no combustion. Further, since wood char has a lower thermal conductivity than virgin wood, the process will be self-limiting.

Therefore, the modeling approach used for the balsa wood contained within compartments whose boundaries have not been breached or where the level of breaching is considered insignificant is essentially the same as that used for NCT conditions. To bound the heat flux into the package, a thermal conductivity representing the high end of the observed range of values for balsa wood (see Table 3.2-8) is assumed. The density and specific heat values used for the NCT analyses are retained for the HAC analysis based on the assumptions that the wood will remain essentially intact and that any loss of wood density would also be accompanied by the endothermic process wherein the volatized material is expelled through the pressure relief ports in the outer skin, thus carrying with it a significant portion of the thermal energy passed into the wood. It is assumed for the purposes of this evaluation that this un-modeled mass transport of energy will offset the un-modeled reduction in density and change in specific heat values that would accompany the charring of the wood.

While the balsa wood contained within compartments whose boundaries have been breached could become involved in active combustion during the HAC fire event, the extent of the combustion will be severely restricted by the limited size of the openings. The largest breach noted from the drop tests was the failure of the weld seam joining the outer skin of the front cheek with the outer skin of the package body where the joint failed for a distance of approximately 914 mm creating an opening with a maximum width of 51 mm. The size of the

gap between the outer skin and the balsa wood reduced to zero approximately 150 to 175 mm from the edges of the tear. A revised weld joint design is expected to prevent this from occurring for the production units. However, for the purposes of the thermal modeling for the HAC evaluation this failure mode is conservatively assumed to exist and that the balsa wood contained in the affected compartment could ignite during the HAC fire.

However, given the limited free passage of air permitted by the size of the tear to the surface of the wood and the fact that the wood component exists as one, continuous block of balsa, it can be assumed that the balsa wood combustion in the vicinity of the weld failure would be limited to surface burning and that the extent of the balsa involved would extend no further than 250 mm from the edges of the tear. Any combustion and/or charring will be self-limiting since the developed char layer will insulate the underlying virgin wood and the presence of the sheetmetal encasement will protect the char layer. Further, even if active combustion were to occur, the thermally sensitive portion of the package (i.e., the CSA and the containment seals) are separated from the balsa wood in the package by a 10-mm thick puncture resistant sheet and a 109 to 114 mm thick layer of 0.10 kg/dm^3 polyurethane foam. As demonstrated by the discussion in Section 3.5.4, *'Last-A-Foam' Response under HAC Condition*, this combination of foam density and thickness is sufficient to protect the underlying CSA from excessive temperatures from a 30-minute fire event even if the balsa wood was not present and from any heat generated by the wood combustion. Therefore, when combined with the expected limited combustion of the balsa wood in the vicinity of the weld failure, the potential failure of the weld joint is not seen as having a significant impact on the peak temperatures within the thermally sensitive areas of the package. The same applies to the edges of the balsa wood exposed by the puncture bar attack.

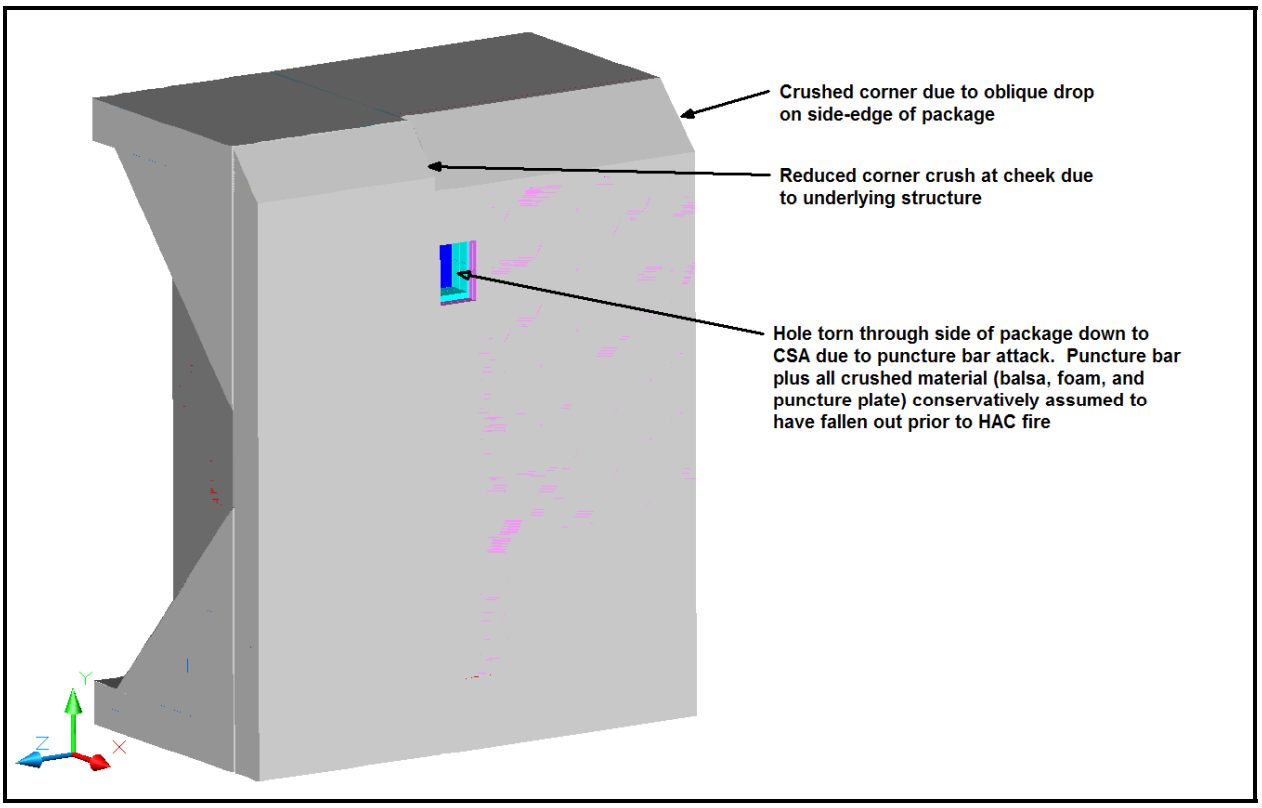

Figure 3.5-16 – Overview of Thermal Model of Damaged TRUPACT–III Package

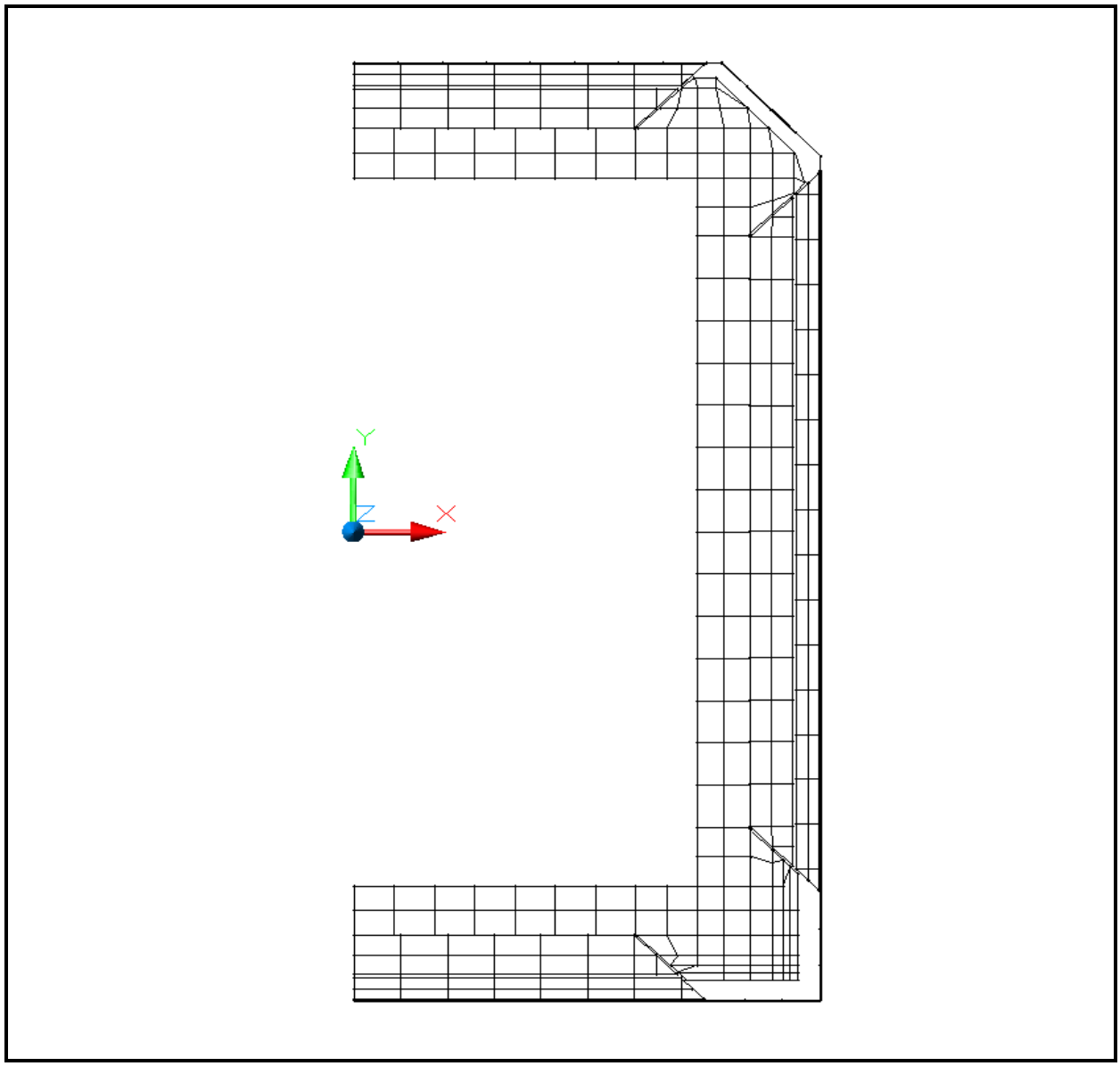

Figure 3.5-17 – Elevation View, Thermal Model of Damaged TRUPACT–III Package

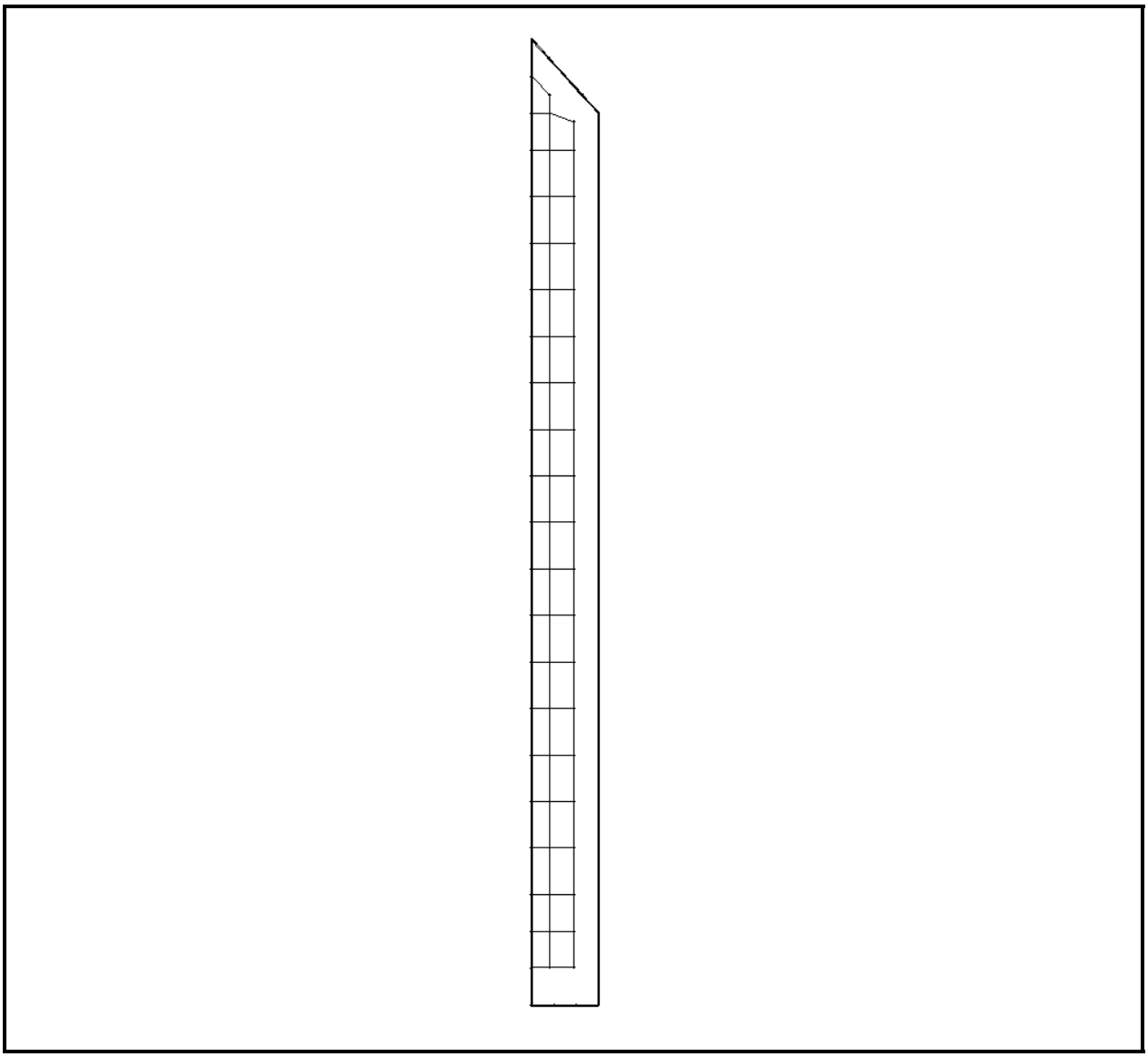

Figure 3.5-18 – Elevation View through Cheek of Damaged TRUPACT–III Thermal Model

This page intentionally left blank.

3.5.3 Review of TRUPACT–III Package Full–Scale Drop Test Results

The potential thermal damage to the TRUPACT–III package arising from the hypothetical free drop and puncture bar accidents is established based on the results of two series of drop tests on full-scale certification test units (i.e., CTU-1 and CTU-2) of the TRUPACT–III package, as described in Section 2.7, *Hypothetical Accident Conditions*. The following paragraphs examine the results of the tested drop scenarios from each test series and provide justification for the selected damage condition being bounding on the thermal performance of the package under HAC conditions.

NCT and HAC Free Drops

One (1) NCT and four (4) HAC free drops were carried out on the CTU-1 test unit. The NCT drop test was made from a height of 0.3 m (one foot) onto the overpack cover. Post-drop inspection indicated that the overpack cover, which had projected by approximately 22 mm beyond the end faces of the cheeks, had been crushed by approximately 7 mm. No other damage was noted. Based on exposed surface area, even less damage is expected for NCT free drops on the other faces of the package. As such, the NCT thermal model can conservatively assume un-damaged conditions as a basis of analysis.

The four (4) HAC free drop test scenarios consisted of: 1) vertical, overpack cover down (Ref. No. LD2), 2) horizontal, side of the package down (Ref. No. LD3), 3) CG-over-corner, overpack cover down (Ref. No. LD4), and 4) oblique side-edge of the package down (Ref. No. LD5). See the Section 2.7 for a full description of each drop orientation. Each free drop was from a height of 9 m (30 feet).

The LD2 test showed a total crush of 36 mm and cracks in the welds around the octagonal opening in the cover and at the ISO fittings of 51 mm to 152 mm long. In addition, the overpack body in the vicinity of the overpack bolts exhibited weld cracks of approximately 305 mm in length and a bulge in the outer skin of approximately 45 mm. This damage level is considered to be slight from a thermal point of view. The reduction in the depth of the foam insulation thickness is less than 7% (i.e., 36 mm vs. a total foam thickness of 140 + 380 = 520 mm, see Figure 3.1-3). Further, since the foam thickness is compacted and not physically lost, the principal thermal protection afforded by the foam under HAC conditions is essentially unaffected (see Section 3.5.4, *'Last-A-Foam' Response under HAC Condition*, for details). The noted cracks in the welds are too narrow to permit the hot gases from the fire event to penetrate the package boundary. As such, the package damage sustained under the vertical, overpack cover down (Ref. No. LD2) scenario is too limited to affect the HAC performance of the package.

The vertical, side of the package down (Ref. No. LD3) drop scenario resulted in the CSA moving towards the impact surface by approximately 7 mm. This movement is assumed to have occurred entirely via crushing of the polyurethane foam surrounding the package (see Figure 1.1-3 from Section 1.1, *Introduction*). In addition, the impact was noted as cracking the weld in the overpack outer skin at the joint between the cheek and the package body. The weld crack extended across the width of the chevron and had a maximum opening of approximately 25 mm. Both the reduction in the thickness of the polyurethane foam and the potential exposure of the polyurethane foam under the cracked weld are considered too minor to significantly affect the thermal performance of the package under HAC conditions.

The Ref. No. LD4 test scenario examined the potential damage arising from the CG-over-corner drop onto the overpack cover. While this drop scenario resulted in the greatest deflection from the original shell dimensions, the area of damage is limited and relatively remote from the thermally sensitive areas of the package. As documented in Section 2.7, *Hypothetical Accident Conditions*, the impact caused a triangular flattened region having a dimension of 1,054 mm diagonally across the overpack cover, 838 mm along the bottom, and 800 mm along the right side of the package. No significant weld seam failures were noted. Given this level of damage, no significant impact on the thermal performance of the package under HAC conditions is expected.

The final HAC free drop orientation examined using the CTU-1 test unit was the oblique side-edge of the package down (Ref. No. LD5). Except for the front and rear cheek areas, the impact caused a flattened region approximately 305 mm wide along the package length. The flattened region reduced to approximately 178 mm at the cheek areas. Figure 3.5-19 illustrates the damage caused by the Ref. No. LD5 free drop orientation. This degree of crush left a minimum distance of approximately 105 mm (as determined analytically, see Figure 3.5-21) between the outer skin and the corner of the CSA and approximately 95 mm (as measured during post-test disassembly, see Section 2.12.3.7.4, *Free Drop, Side-Edge HAC (Test LD5)*) between the outer skin and the corner of the protection plate enclosure surrounding the calcium silicate insulation. Additionally, as shown in Figure 3.5-20, the weld seam joining the outer skin of the front cheek with the outer skin of the package body failed for a distance of approximately 914 mm creating an opening with a maximum width of 51 mm. The gap developed between the outer skin and the balsa wood quickly decreased with distance from the tear until an essentially zero width gap was noted approximately 150 to 175 mm from the edges of the tear. Based on the level and extent of the damage and its proximity to the thermally sensitive areas of the package, the oblique side-edge of the package down drop scenario is seen as providing the bounding damage to the package resulting from the HAC free drop event.

The supplementary testing on CTU-2 repeated the LD4 CG-over-corner drop onto the overpack cover under the cold (i.e., -29 °C) foam temperature condition. The primary purpose of repeating this test scenario (test designation LD91) was to verify that the debris shield would exclude debris from entering the seal region during the package deflections occurring during the worst-case free drop event. The impact caused a triangular flat region having dimensions of 737 mm along the overpack cover, 864 mm along the bottom, and 787 mm along the left side of CTU-2. This level of damage is consistent with that seen from the LD4 test scenario for the testing on CTU-1 (see above). As with the original testing, no significant weld seam failures were noted from this supplementary testing and no significant impact on the thermal performance of the package under HAC conditions is expected.

HAC Puncture Drops

In addition to the free drops, the CTU-1 test article was subjected to four (4) puncture drop tests, all from a height of 1 meter. The drop orientations evaluated were 1) impact on the side damage, inclined at 20° from the horizontal (Ref. No. LP1), 2) impact on the recessed portion of the overpack cover, inclined at 25° from the vertical (Ref. No. LP2), 3) impact on the CG-over-corner damage (Ref. No. LP3), and 4) impact on the oblique side-edge damaged area, inclined at 30° from the horizontal (Ref. No. LP4).

The Ref. No. LP1 puncture drop resulted in penetration of both the outer skin and the underlying 10 mm thick puncture-resistant plate (see Figure 3.5-22 and Figure 3.5-23). The outer skin and balsa wood were 'cookie cut' and carried inward by the puncture bar. The cut section of balsa wood ended up as compressed disk, approximately 3 mm thick. The puncture-resistant plate was cut and then folded out of the way in a 'dog ear' fashion. The underlying foam was compressed and then shoved to the side as the package rotated after the puncture bar impacted with the CSA. While a dent approximately 51 mm deep was left in the CSA, there was no cutting or cracking of the CSA's outer skin. Post-impact rotation of the package resulted in enlarging the hole in the outer skin from approximately 178 mm in diameter to approximately 254 mm long by 178 mm wide. The hole in the 10 mm puncture-resistant plate was approximately 178 mm in diameter.

The Ref. No. LP2 puncture drop resulted in penetration of the outer skin and the balsa wood, but not the 15-mm puncture-resistant plate. A dent approximately 145 mm deep was left in the 15-mm puncture-resistant plate, with an associated dent of approximately 5 mm in the lid. Post-impact rotation of the package resulted in enlarging the original hole in the outer skin to approximately 360 mm long by 205 mm wide.

The third puncture bar drop scenario (Ref. No. LP3) attacked the CG-over-corner damage incurred from the LD4 free drop. The puncture bar struck near the center of the damage and created a further deformation over an area that is 178 mm in diameter and 102 mm deep. While the puncture bar locally compressed the material previously deformed by the LD4 free drop, it did not significantly increase the exposure of the underlying foam. As such, this puncture bar drop scenario was dropped from further consideration in determining the bounding damage scenario for the TRUPACT–III package.

The fourth puncture bar drop scenario (Ref. No. LP4) examined was the impact on the oblique side-edge damaged area. The bar penetrated the outer skin, creating a hole approximately 178 mm in diameter, and impacted the corner of the protection plate enclosure surrounding the calcium silicate insulation in the cheek. Post-impact inspection showed no damage to the calcium silicate insulation and only minor cracks in the protection plate welds.

The supplementary testing on CTU-2 repeated one puncture bar test from the test series on CTU-1 and addressed one additional scenario. The LP91 puncture test repeated the impact on the CG-over-corner damage addressed by the LP3 test in the CTU-1 test series. While the resultant damage loosened the lower quadrant of the overpack cover's outer sheet and a significant portion of the low density (0.16 kg/dm^3) foam fell out, little of the high density (0.48 kg/dm^3) foam was exposed and essentially none was lost. In addition, the corner of the puncture bar partially sheared into the 6-mm thick puncture resistant plate located between the low density and high density foam by 38 mm [1.5 inches]. Although the level of damage noted from the LP91 and LD91 drop combination is slightly worse than that seen for the original LP3 and LD4 drop combination on CTU-1, the level of remaining thermal protection is significant and no adverse affect on the TRUPACT–III seal region will occur.

The supplementary testing on CTU-2 added a puncture bar attack on the bottom side of the package that was not addressed by the original test series. Under the LP92 test, the puncture bar struck the package approximately 476 mm [18.7 inches] from the closed outer end of the package, with the package inclined 40º from the horizontal. The bar penetrated the outer skin and impacted the CSA outer structural sheet, creating a crack in the weld between the structural sheet and the rear diagonal corner stiffener of the CSA, and in some of the adjacent plug welds

which connect the outer structural sheet to the V-stiffener nearest the impact. However, there was no evidence of any dent or bulge in the CSA inner (containment) sheet at the puncture site and the containment boundary remained leak tight. Post-impact rotation of the package resulted in enlarging the hole in the outer skin from approximately 178 mm (7 inches) in diameter to approximately 318 mm (12.5 inches) long by 152 mm (6 inches) wide. The level of damage and the size of the CSA area exposed by the puncture bar is consistent with that seen for the LP1 test under the original testing on CTU-1. Given this and since the damage location is remote from the thermally sensitive area of the package (i.e., the containment seals), this puncture bar test was dropped from further consideration in determining the bounding damage scenario for the TRUPACT–III package.

Bounding Combined HAC Free and Puncture Drop Damage

Based on the above discussion, it is concluded that the bounding damage scenario for the TRUPACT–III package will consist of an oblique free drop on the side-edge of the package (Ref. No. LD5), followed by a puncture bar impact just aft of the cheek to body joint. The selected free drop and puncture drop damage scenarios will impart the most significant damage compared to the other free drop scenarios for the reasons described above.

Since the Ref. No. LD5 test was conducted at a corner foam temperature of approximately 7°C vs. the approximately 50°C average foam temperature expected under the NCT Hot condition of transportation and since the foam strength is a function of its temperature, post-test calculations (see Section 2.7.1.5.2, *Side-Edge Free Drop Extrapolation*) are used to extrapolate the package performance to the higher foam temperature. The maximum deformation at the NCT Hot condition is found by analysis to add an estimated 30 mm to the total crush depth. With this temperature correction, the minimum distance between the outer skin and the corner of the CSA is estimated to be 105 mm – 30 mm = 75 mm, while the distance between the outer skin and the corner of the protection plate enclosure surrounding the calcium silicate insulation will be 95 mm - 30 mm = 65 mm. The resulting level of crush in the underlying foam regions is estimated to be 30% along the CSA and 31.5% along the cheek. Figure 3.5-21 illustrates the crush lines as noted from the full-scale testing and as extrapolated for the foam temperatures predicted to occur at the NCT Hot conditions.

Of the puncture bar drop scenarios only two (Ref. No. LP1 and LP92) penetrated all the way through the package's thermal protection system. The others were stopped short by the puncture resistant plates and/or other package structures. However, it is noted that the location of both the Ref. No. LP1and LP92 impact damage are too far from the package closure seals to have any significant thermal effect beyond the localized heating of the CSA structural sheet. Instead, by hypothetically re-locating the impact location to just aft of the cheek to body joint on the package and just below the damage caused by the Ref. No. LD5 free drop damage scenario (see Figure 3.5-24), the combined damage would create the maximum thermal exposure of the package in the vicinity of the closure seals to the HAC fire environment that can be supported by observed results from the full-scale CTU drop tests. No temperature corrections are required for the puncture drop damage scenarios since the puncture resistance of the package is principally determined by the steel plates and not the polyurethane foam.

The bending of the puncture bar during the LP1 puncture attack (see Figure 3.5-22) did not lessen the damage to the package. The basis for this conclusion comes from the video record of the LP1

puncture event which shows that the package comes essentially to rest before beginning a relatively slow rotation off of the puncture bar. The video clearly shows that the package does not receive any support from the ground before the energy of the 1m free fall has been absorbed in the wall overpack/puncture-resistant structure. As the package rolled off of the bar, the package c.g. moved away from the bar axis, and the bar bent over. Once the bar begins to bend, the amount of damage to the package has reached its limit. This is also demonstrated in the video, where it is shown that no further damage is occurring to the package as the bar bends. Similarly, a longer bar would tend to bend sooner due to its longer moment arm and, as such, do less damage. For these reasons, a longer bar would have no effect on the puncture damage experienced in LP1. Review of the other punctures confirms that this conclusion is universally true of the puncture drop tests performed.

The observed damage resulting from the LP1 puncture bar attack is bounding for the damage that could be obtained by a similar puncture bar attack elsewhere on the side surface of the package and, as such, the simple transfer of the observed damage to the containment seal region provides a significant level of conservatism for the assumed HAC damage scenario for the containment seals. The basis for this conclusion is that the LP1 puncture bar attack was through the package's center of gravity to ensure that all of the energy from the 1m free fall was absorbed in the package structures and not partially dissipated via rotation of the package about the puncture bar impact point. Therefore, an actual puncture attack in the region of the containment seal would have exhibited less damage than seen for the LP1 puncture test, partly because the overpack wall structures are stiffer in the region of the containment seals, and partly because the axis of the puncture bar would not pass through the c.g. of the package since the package orientation would need to be on the order of 55º to the horizontal. An attack at such a steep angle would cause the puncture bar to either glance off of the surface, or simply bend out of the way and yield a significantly lower level of damage than observed for the LP1 puncture bar attack.

Figure 3.5-19 – Edge Deformation from LD-5 Free Drop Orientation

Figure 3.5-20 – Weld Tear from LD-5 Free Drop Orientation

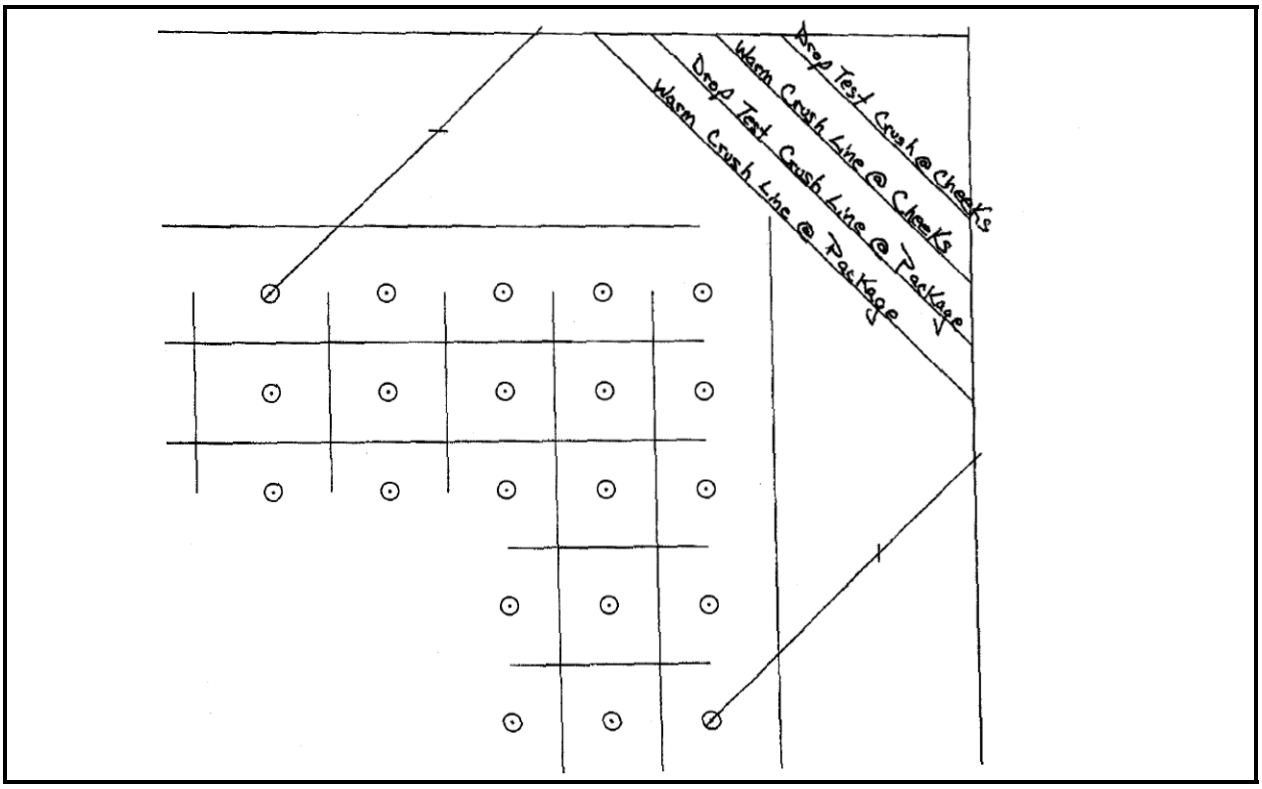

Figure 3.5-21 – Corner Crush Depths, Test and NCT Hot Conditions

Figure 3.5-22 – LP1 Puncture Bar Damage before Removal of Bar

Figure 3.5-23 – LP1 Puncture Bar Damage after Removal of Bar

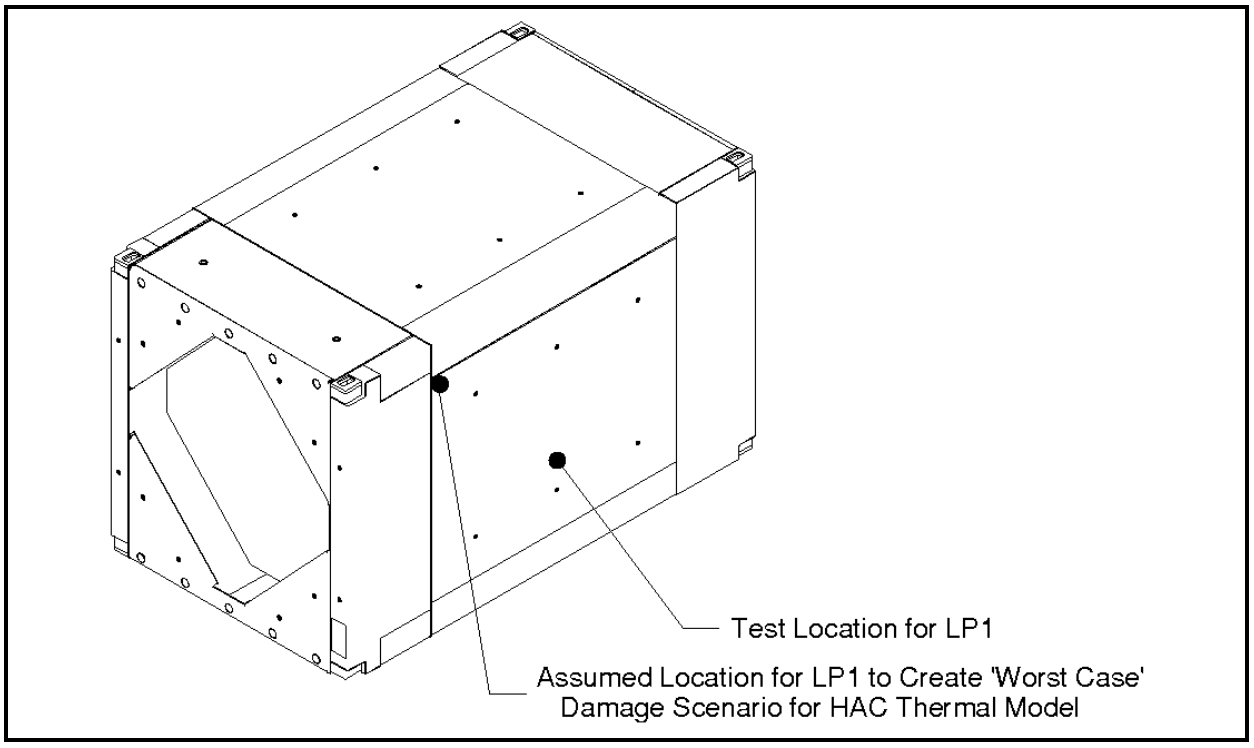

Figure 3.5-24 – Assumed Re-Location of LP1 Puncture Bar Damage

3.5.4 'Last-A-Foam' Response under HAC Conditions

The General Plastics LAST-A-FOAM® FR-3700 rigid polyurethane foam[1] has been used in numerous radioactive materials packages. The FR-3700 formulation is specially designed to allow predictable impact-absorption performance under dynamic loading, while also providing an intumescent char layer that insulates and protects the underlying materials, even when exposed to pool-fire conditions. Upon exposure to fire temperatures, this proprietary foam decomposes into an intumescent char that swells and tends to fill voids or gaps created by free drop or puncture bar damage. The thermal decomposition absorbs a significant amount of the heat transferred into the foam, which is then expelled from the package as a high temperature gas. At the same time, the resultant char layer shields the underlying undamaged foam from further direct exposure to the external high temperatures. This behavior has been observed in numerous fire tests of other packages.

Since the decomposition of the foam under elevated temperatures is an endothermic process, the foam is self-extinguishing and will not support a flame once the external fire is removed. However, the gases generated by the decomposition process are combustible and will burn under piloted conditions. Further, a portion of these generated gases could remain trapped within the charred layer of the foam for a period of time after the cessation of the HAC fire event and could support further combustion, although at a much reduced level, until a sufficient time has passed for their depletion from the cell structure.

The mechanisms behind the observed variations in the thermal properties and behavior of the FR-3700 foam at elevated temperatures are varied and complex and only limited research has been conducted in this area. As such, currently no definitive analytical model of the foam properties under HAC conditions exists. Instead, a combination of empirical data and modeling conservatism is used to simulate the thermal performance of the LAST-A-FOAM® FR-3700 polyurethane foam for this application.

A series of fire tests[2,3] conducted on 5-gallon cans filled with FR-3700 foam at densities from 0.107 to 0.412 kg/dm^3 helped define the expected performance of the foam under fire accident conditions. Under the fire tests, one end of the test articles (i.e., the "hot face" surface) was subjected to an open diesel fueled burner flame at temperatures of 980 to 1,200 ºC for 30+ minutes. A thermal shield prevented direct exposure to the burner flame on any surface of the test article other than the hot face. Each test article was instrumented with thermocouples located at various depths in the foam. In addition, samples of the foam were subjected to thermogravimetric analysis (TGA) to determine the thermal decomposition vs. temperature. The exposure temperatures for the TGA tests varied from 21 to 816 ºC and were conducted in both air and nitrogen atmospheres. The result for the nitrogen environment (see Figure 3.5-25) is more representative of the low oxygen environment existing within the enclosures encasing the foam components of the TRUPACT–III

[1] Last-A-Foam™ FR3700 On-line Data Sheet, www.generalplastics.com.

[2] "*Thermal Assault And Polyurethane Foam Evaluating Protective Mechanisms For Transport Containers*", C.L. Williamson, Z.L. Iams, General Plastics Manufacturing Company, Tacoma, WA, presented at Waste Management '05 Symposium, Tucson, AZ, 2005.

[3] "*Thermal Assault And Polyurethane Foam - Evaluating Protective Mechanisms*", C.L. Williamson, Z.L. Iams, General Plastics Manufacturing Company, Tacoma, WA, presented at PATRAM International Symposium, Berlin, Germany, 2004.

package. These test results indicate that the following steps occur in the thermal breakdown of the foam under the level of elevated temperatures reached during the HAC fire event:

- Below 120 °C, the variation in foam thermal properties with temperature are slight and reversible. As such, fixed values for specific heat and thermal conductivity are appropriate.
- Between 120 °C and 260 °C, small variations in foam thermal properties occur as water vapor and non-condensable gases are driven out of the foam. As such, fixed values for specific heat and thermal conductivity are also appropriate for this temperature range. Further, the observed changes are so slight that the same thermal properties used for temperatures below 120 °C may also be used to characterize the thermal performance of the foam between 120 °C and 260 °C.
- Irreversible thermal decomposition of the foam begins as the temperature rises above 260 °C and increases non-linearly with temperature. Based on the TGA testing (see Figure 3.5-25), approximately 2/3's of this decomposition occurs over a narrow temperature range centered about 354 °C.
- The decomposition is accompanied by vigorous out–gassing from the foam and an indeterminate amount of internal heat generation. The internal heat generation arises from the gases generated by the decomposition process that are combustible under piloted conditions. However, since the decomposition process is endothermic, the foam will not support combustion indefinitely. Further, the out gassing process removes a significant amount of heat from the package via mass transport.
- The weight loss due to out–gassing not only has direct affect on the heat flux into the remaining virgin foam, but changes the composition of the resulting foam char since the foam constituents are lost at different rates. This change in composition affects both the specific heat and the thermal conductivity of the foam char layer.
- As temperature continues to rise, the developing char layer begins to take on the characteristics of a gas-filled cellular structure where radiative interchange from one cell surface to another becomes the dominant portion of the overall heat transfer mechanism. This change in heat transfer mechanisms causes the apparent heat conductivity to take on a highly non-linear relationship with temperature.
- Finally, at temperatures above 675°C, the thermal breakdown of the foam is essentially completed and only about 5 to 10% of the original mass is left. In the absence of direct exposure to a flame or erosion by the channeling of the outgas products through the foam, the char layer will be the same or slightly thicker than the original foam depth. This char layer will continue to provide radiative shielding to the underlying foam material.

The sharp transition in the state of the foam noted in Figure 3.5-25 at or about 354 °C can be used to correlate the depth of the foam char and the occurrence of this temperature level within the foam. Figure 3.5-26 illustrates the relationship between foam recession (i.e., char depth) and foam density following exposure to a 30-minute fire as complied from a series of tests. The correlation between the foam recession depth and the foam density is expressed by the relation:

$$y = -0.94681 - 11.64 \times \log_{10}(x)$$

where, y = the recession depth, cm

x = foam density (g/cm^3)

Based on this correlation, the recession depth expected for the nominal 0.29 kg/dm^3 density foam used in the corner regions of the package is estimated to be 53 mm. Given that the fabrication tolerance for the foam density is $\pm$15%, the actual foam density may range from 0.25 to 0.33 kg/dm^3. The recession depth associated with the lower bound foam density of 0.25 kg/dm^3 is estimated to be 60 mm.

The expected worst case crush of the corner region foam is estimated to be approximately 30% (see Section 3.5.3, *Review of TRUPACT–III Package Full Scale Drop Test Results*). Since the package deflection would be accommodated by the compression of the corner foam, the density of the foam would increase from a lower bound density of 0.25 kg/dm^3 to an apparent density of 0.36 kg/dm^3. Since the recession depth for the foam is a function of its density, the recession depth for the 'crushed' foam will be approximately 42 mm.

The foam in the cheek region of the package has a nominal density of 0.48 kg/dm^3, except for a region 140 mm thick at the end of the cheek which has a nominal density of 0.16 kg/dm^3. The higher foam density in the cheek will yield a much smaller expected recession depth during the fire event than that expected for the corner region foam. At the nominal density of 0.48 kg/dm^3 the estimated recession depth will be 28 mm. The recession depth will increase to 36 mm at the lower bound fabrication density (-15%) of 0.41 kg/dm^3. The regions of the cheek crushed by the side-edge down drop will see a 31.5% increase in the nominal foam density of 48 kg/dm^3, or increase in the apparent density to approximately 0.70 kg/dm^3. Extrapolation of the recession depth relationship in Figure 3.5-26 to this density would yield an expected foam recession depth of only 8.6 mm. Even after accounting for the lower bound fabrication density, the increase in the apparent density would go from 0.41 kg/dm^3 to approximately 0.60 kg/dm^3 with an associated recession depth of 16 mm.

The 0.10 kg/dm^3 foam surrounding the CSA is 109 to 114 mm thick. Based on the recession depth correlation presented in Figure 3.5-26, a thickness of 107 mm is sufficient for the 0.10 kg/dm^3 foam to withstand a 30-minute regulatory fire event, even without the benefit of the 10 mm puncture-resistant sheet and the 60 mm thick balsa wood that lie between it and the outer skin. As such, local combustion within the balsa wood due to openings in the outer shell created by the drop damage will not create a thermal issue for the CSA.

An additional correction to the expected recession is required to account for the fact that the thermal testing upon which the recession depth correlation is based used a flame temperature 980 to 1,200 ºC, whereas the regulatory fire flame temperature is specified as 800 ºC[4]. The lower flame temperature will have a significant effect on the recession depth noted in the various foam components since the rate of heat transfer is directly related to the temperature of the flame. For example, the recession depth estimated for the nominal 0.29 kg/dm^3 density foam would be reduced from the 53 mm estimated by the correlation to less than 38 mm. For conservatism, a correction for the regulatory flame temperature is not applied for the purposes of this application.

[4] Title 10, Code of Federal Regulations, Part 71 (10 CFR 71), *Packaging and Transportation of Radioactive Material*, 01–01–09 Edition.

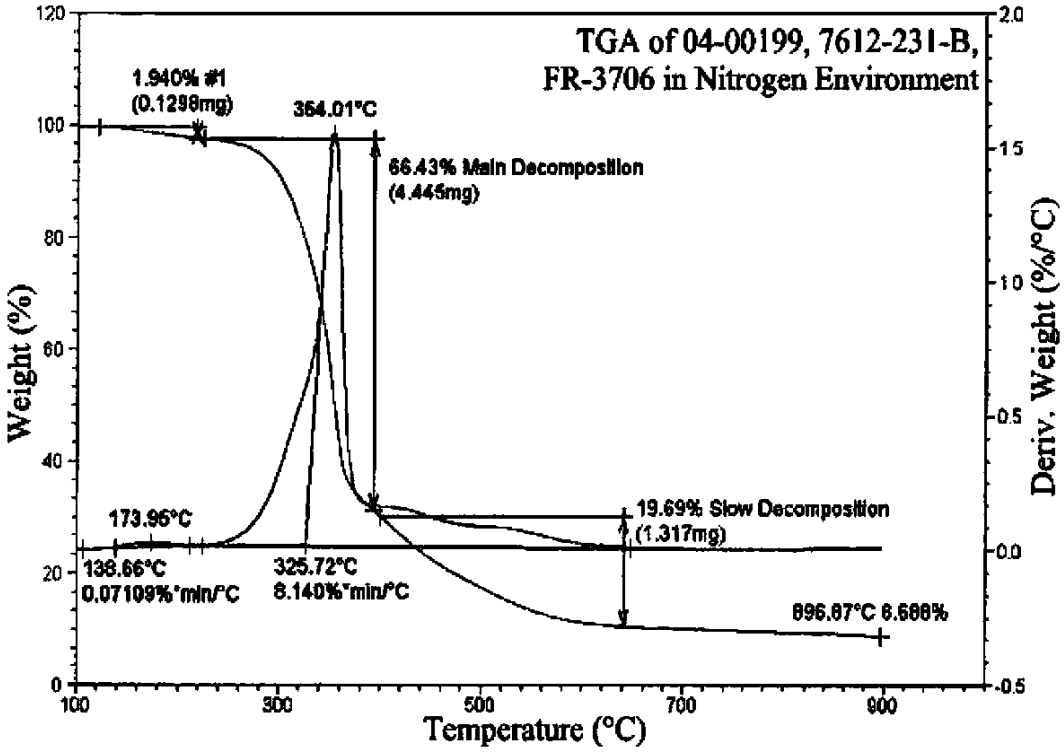

Figure 3.5-25 – TGA Analysis of Foam Decomposition in Nitrogen

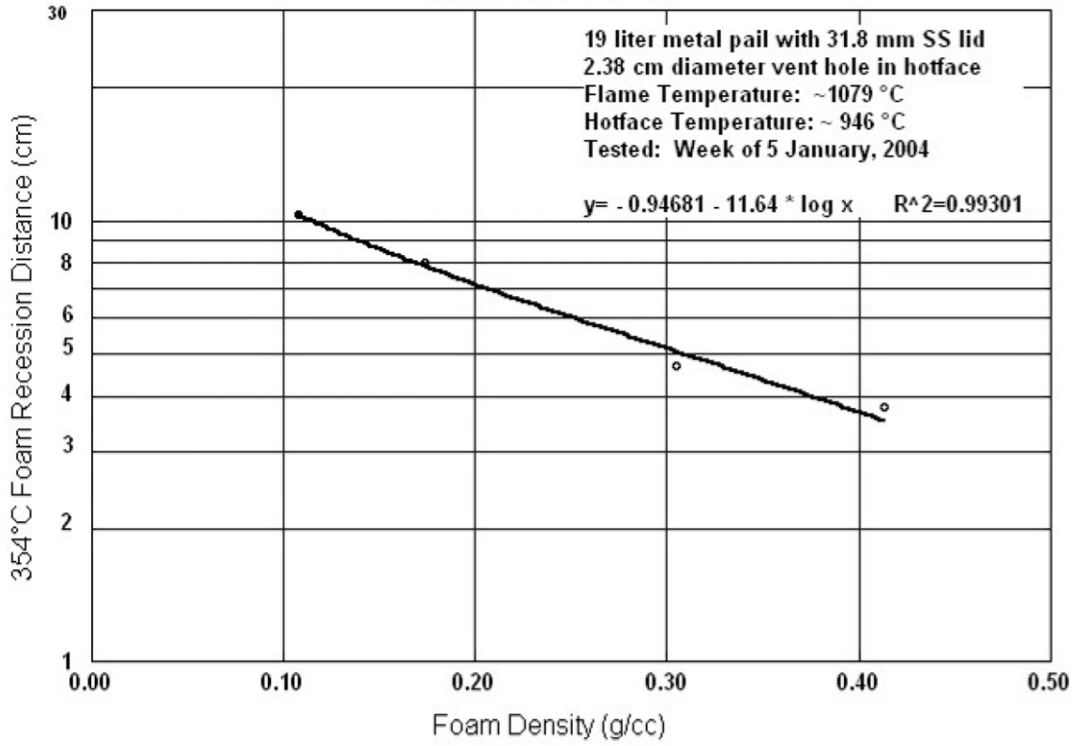

Figure 3.5-26 – Foam Recession vs. Density for 30-minute Fire

4.0 CONTAINMENT

4.1 Description of the Containment System

4.1.1 Containment Vessel

A single level of containment is established within the TRUPACT–III packaging. In general, the containment vessel is constructed primarily of Alloy UNS S31803 duplex stainless steel. The exceptions to the use of Alloy UNS S31803 stainless steel are so noted in the following detailed description.

The containment boundary of the TRUPACT–III packaging consists of the inner surfaces of the containment structural assembly (CSA). Specifically, the containment boundary is comprised of the inner rear wall, the inner side walls, the inner top and bottom walls, and the inner sheet of the closure lid. The containment boundary also includes those parts of the CSA body and closure lid flanges which are inboard of the containment (innermost) butyl O-ring seal. In addition, the containment boundary includes an aluminum bronze vent port insert with a mating inner butyl O-ring seal. A more detailed description of the containment boundary is provided in Section 1.2.1.1, *Body*, Section 1.2.1.2, *Closure Lid*, and in Appendix 1.3.1, *Packaging General Arrangement Drawings*.

4.1.2 Containment Penetrations

The only containment boundary penetrations into the containment vessel are the closure lid itself and the vent port. Each penetration is designed to demonstrate "leaktight" sealing integrity, i.e., a leakage rate not to exceed 1×10^{-8} Pa-m^3/s, air, as defined in ANSI N14.5[1].

4.1.3 Seals and Welds

4.1.3.1 Seals

The minimum and maximum compression for the TRUPACT–III containment O-ring seal are calculated based on the worst-case dimensions for the O-ring seal and groove as shown in Appendix 1.3.1, *Packaging General Arrangement Drawings*. The main closure lid containment O-ring seal has a diameter of 12 ± 0.15 mm. The groove into which the seal is placed has a depth of 8.27 ± 0.15 mm. The groove length, based on centerline dimensions of 1,888 × 2,048, with 50-mm corner radii, is:

$$L_G = 2(1{,}888 \text{ mm} + 2{,}048 \text{ mm}) - 8(50) + 2\pi\,(50 \text{ mm}) = 7{,}786 \text{ mm}$$

The inner diameter of the containment O-ring is 2,394 mm, or 2,394 + 12 = 2,406 mm on its centerline. The centerline length is therefore 2,406 × π = 7,559 mm, for a stretch of:

[1] ANSI N14.5–1997 (or later), *American National Standard for Radioactive Materials – Leakage Tests on Packages for Shipment,* American National Standards Institute, Inc. (ANSI).

$$S = \frac{(\text{Groove Length}) - (\text{O-ring Length})}{(\text{O-ring Length})} \times 100 = \frac{(7{,}786) - (7{,}559)}{(7{,}559)} \times 100 = 3.0\ \%$$

From Figure 3-3 for the calculated curve of the Parker O-ring Handbook[2], the resulting reduction in O-ring seal cross-sectional diameter is 1.5%. The reduced cross-sectional diameters, D_{Rmin} and D_{Rmax}, are therefore 1.5% less than the non-stretched diameters, ($D_{min} = 12 - 0.15 = 11.85$ mm) and ($D_{max} = 12 + 0.15 = 12.15$ mm), or:

$$D_{Rmin} = (1 - 0.015)D_{min} = 11.67 \text{ mm}$$

$$D_{Rmax} = (1 - 0.015)D_{max} = 11.97 \text{ mm}$$

The range of groove depths in the closure lid is:

minimum groove depth, $d_{min} = 8.27 - 0.15 = 8.12$ mm

maximum groove depth, $d_{max} = 8.27 + 0.15 = 8.42$ mm

Using these quantities, the maximum and minimum seal compression at ambient temperature, C_{seal}, is calculated as follows:

$$C_{seal} = \left[1 - \left(\frac{d}{D_R}\right)\right] \times 100$$

$$C_{seal\text{-}min} = \left[1 - \left(\frac{d_{max}}{D_{Rmin}}\right)\right] \times 100 = 27.8\%$$

$$C_{seal\text{-}max} = \left[1 - \left(\frac{d_{min}}{D_{Rmax}}\right)\right] \times 100 = 32.2\%$$

As shown in Section 2.12.2.6, *Test Results*, a room temperature compression of at least 19.8% is required to ensure that the minimum allowable compression of 18.5% exists at the minimum NCT temperature of -40 ºC. The minimum room temperature compression of 27.8% is well in excess of this value.

A summary of seal testing prior to first use, during routine maintenance, and upon assembly for transportation is as follows.

4.1.3.1.1 Fabrication Leakage Rate Tests

During fabrication and following the pressure testing per Section 8.1.3.2, *Containment Vessel Pressure Testing*, the CSA shall be leakage rate tested as delineated in Section 8.1.4, *Fabrication Leakage Rate Tests*. The fabrication leakage rate tests are consistent with the guidelines of Section 7.3 of ANSI N14.5. This leakage rate test verifies the containment integrity of the TRUPACT–III packaging to a leakage rate not to exceed 1×10^{-8} Pa–m^3/s, air.

[2] ORD 5700, *Parker O-ring Handbook*, 2007, Parker Hannifin Corporation, Cleveland, OH.

4.1.3.1.2 Maintenance/Periodic Leakage Rate Tests

Annually, or at the time of damaged containment seal replacement or sealing surface repair, the O-ring seals shall be leakage rate tested as delineated in Section 8.2.2, *Maintenance/Periodic Leakage Rate Tests*. The maintenance/periodic leakage rate tests are consistent with the guidelines of Section 7.4 of ANSI N14.5. This test verifies the sealing integrity of the closure lid and vent port containment seals to a leakage rate not to exceed 1×10^{-8} Pa–m^3/s, air.

4.1.3.1.3 Preshipment Leakage Rate Tests

Prior to shipment of the loaded TRUPACT–III package, the main inner O-ring seal and vent port insert O-ring seal shall be leakage rate tested per Section 7.4, *Preshipment Leakage Rate Test*. The preshipment leakage rate tests are consistent with the guidelines of Section 7.6 of ANSI N14.5. This test verifies the sealing integrity of the closure lid and vent port insert containment seals to a leakage rate sensitivity of 1×10^{-4} Pa–m^3/s, air.

The maintenance/periodic leakage rate tests, delineated in Section 8.2.2, *Maintenance/Periodic Leakage Rate Tests*, may be performed as an option, in lieu of the preshipment leakage rate tests.

4.1.3.2 Welds

All containment vessel body welds are full penetration welds that have been radiographed to ensure structural and containment integrity. Non-radiographed, safety related welds such as those that attach the V-stiffeners to their respective containment plates are examined using liquid penetrant testing on the final pass. All containment boundary welds are confirmed to be leaktight as delineated in Section 8.1.4, *Fabrication Leakage Rate Tests*.

4.1.4 Closure

With reference to Figures 1.1-1 and 1.1-2 in Chapter 1.0, *General Information*, the closure lid is secured to the body via forty-four (44) M36 × 4 socket head cap screws tightened to a torque of 1,600 ±120 N-m. Thus, the closure lid is securely attached. After completing the installation of the closure lid, the overpack cover is installed over the closure lid, which completely covers the lid and the vent port. The overpack cover is secured with ten (10), M36 × 4 socket head cap screws tightened to a torque of 1,600 ±120 N-m. Thus, the closure lid and the vent port cannot be inadvertently opened.

This page intentionally left blank.

4.2 Containment Under Normal Conditions of Transport

4.2.1 Containment of Radioactive Material

The results of the normal conditions of transport (NCT) structural and thermal evaluations performed in Section 2.6, *Normal Conditions of Transport*, and Section 3.3, *Thermal Evaluation for Normal Conditions of Transport*, respectively, and the results of full-scale structural testing presented in Appendix 2.12.3, *Certification Tests on CTU-1* and Appendix 2.12.6, *Certification Tests on CTU-2*, verify that there will be no release of radioactive materials per the "leaktight" definition of ANSI N14.5[1] under any of the NCT tests described in 10 CFR §71.71[2].

4.2.2 Pressurization of Containment Vessel

The maximum normal operating pressure (MNOP) of the CSA is 172 kPa per Section 3.3.2, *Maximum Normal Operating Pressure*. The design pressure of the CSA is 172 kPa. Based on the structural evaluations performed in Chapter 2.0, *Structural Evaluation*, pressure increases to 172 kPa will not reduce the effectiveness of the TRUPACT–III package to maintain containment integrity per Section 4.2.1, *Containment of Radioactive Material*.

4.2.3 Containment Criterion

At the completion of fabrication, the CSA shall be leakage rate tested as described in Section 4.1.3.1.1, *Fabrication Leakage Rate Tests*. For annual maintenance, the CSA shall be leakage rate tested as described in Section 4.1.3.1.2, *Maintenance/Periodic Leakage Rate Tests*. In addition, at the time of a seal replacement if other than during routine maintenance (e.g., if damage during assembly necessitates seal replacement), maintenance/periodic leakage rate testing shall be performed for the seal that is replaced. For verification of proper assembly prior to shipment, the CSA shall be leakage rate tested as described in Section 4.1.3.1.3, *Preshipment Leakage Rate Tests*.

[1] ANSI N14.5–1997 (or later), *American National Standard for Radioactive Materials – Leakage Tests on Packages for Shipment,* American National Standards Institute, Inc. (ANSI).

[2] Title 10, Code of Federal Regulations, Part 71 (10 CFR 71), *Packaging and Transportation of Radioactive Material*, 01–01–09 Edition.

This page intentionally left blank.

4.3 Containment Under Hypothetical Accident Conditions

4.3.1 Fission Gas Products

There are no fission gas products in the TRUPACT–III package payload.

4.3.2 Containment of Radioactive Material

The results of the hypothetical accident condition (HAC) structural and thermal evaluations performed in Section 2.7, *Structural Evaluation for Hypothetical Accident Conditions*, and Section 3.4, *Thermal Evaluation for Hypothetical Accident Conditions*, respectively, and the results of full-scale structural testing presented in Appendix 2.12.3, *Certification Tests on CTU-1* and Appendix 2.12.6, *Certification Tests on CTU-2*, verify that there will be no release of radioactive materials per the "leaktight" definition of ANSI N14.5[1] under any of the HAC tests described in 10 CFR §71.73[2].

[1] ANSI N14.5–1997 (or later), *American National Standard for Radioactive Materials – Leakage Tests on Packages for Shipment,* American National Standards Institute, Inc. (ANSI).

[2] Title 10, Code of Federal Regulations, Part 71 (10 CFR 71), *Packaging and Transportation of Radioactive Material*, 01–01–09 Edition.

This page intentionally left blank.

4.4 Leakage Rate Tests for Type B Packages

The TRUPACT–III package is leakage rate tested as described in Section 4.1.3.1, *Seals*, to meet the "leaktight" definition of ANSI N14.5[1].

[1] ANSI N14.5–1997 (or later), *American National Standard for Radioactive Materials – Leakage Tests on Packages for Shipment,* American National Standards Institute, Inc. (ANSI).

This page intentionally left blank.

5.0 SHIELDING EVALUATION

The compliance evaluation of the TRUPACT–III packaging with respect to the dose rate limits established by 10 CFR §71.47(a)[1] for normal conditions of transport (NCT) or 10 CFR §71.51(a)(2) for hypothetical accident conditions (HAC) is based on limiting the dose rate of the payload container, not crediting the use of supplemental shielding within the payload container, and relying on the additional dose rate attenuation inherit in the structural design of the packaging to ensure that the package dose rate requirements are satisfied.

Each contact-handled transuranic (CH-TRU) waste payload container, i.e., SLB2, as prepared for transport in a TRUPACT–III package, is limited such that the external radiation field, both gamma and neutron, shall be less than or equal to 2 milliSieverts per hour (mSv/hr) at the surface of the payload container. This dose rate limit is for the payload container prior to addition of any lead, steel or other shielding material to the payload container for *as-low-as-reasonably-achievable* (ALARA) dose reduction purposes during non-transport handling operations.

The TRUPACT–III packaging is not designed to provide any significant gamma or neutron shielding. Five essentially concentric stainless steel sheets comprise the TRUPACT–III structure, providing an overall composite thickness of 36 mm. A minimum of 109 mm of polyurethane foam and 60 mm of balsa wood occupies the remaining spaces between the containment structural assembly and outer sheet.

Prior to transport, the TRUPACT–III package shall be monitored on the semi-trailer or railcar for both gamma and neutron radiation to demonstrate compliance with 10 CFR §71.47. Since the TRUPACT–III package is not significantly deformed under NCT, the package will meet the dose rate limits for NCT if the measurements demonstrate compliance with the allowable dose rate levels in 10 CFR §71.47. The shielding Transport Index (TI), as defined in 10 CFR §71.4, will be determined by measuring the dose rate at a distance of one meter from the package surface per the requirements of 49 CFR §173.403[2].

Shielding materials are not specifically provided by the TRUPACT–III packaging, and none are permitted in the payload containers to meet the dose rate limits of 10 CFR §71.47 for NCT. Therefore, shielding provided by the stainless steel shells and polyurethane foam of the packaging is not needed to meet the higher dose rate limits after the HAC tests delineated in 10 CFR §71.73. This ensures that the post-HAC, allowable dose rate of 10 mSv/hr a distance of one meter from the package surface per 10 CFR §71.51(a)(2) will be met.

Even if payload material is released from a payload container during a HAC event, the post-HAC dose rate limit of 10 mSv/hr at one meter from the package surface will always be met. This is because each CH-TRU waste payload container must have a dose rate less than or equal to 2 mSv/hr on contact prior to the addition of any ALARA dose reduction shielding for non-transport handling operations prior to being loaded into the TRUPACT–III packaging. Since shielding within the payload container is not permitted to meet the transportation dose rate limits

[1] Title 10, Code of Federal Regulations, Part 71 (10 CFR 71), *Packaging and Transportation of Radioactive Material*, 01-01-09 Edition.

[2] Title 49, Code of Federal Regulations, Part 173 (49 CFR 173), *Shippers – General Requirements for Shipments and Packagings*, 10-01-09 Edition.

for NCT, release of the materials from the payload container during a HAC event will not increase the dose rate significantly or cause it to exceed the dose rate limit for HAC.

6.0 CRITICALITY EVALUATION

The following analyses demonstrate that the TRUPACT–III package complies with the requirements of 10 CFR §71.55 and §71.59[1]. The analyses presented herein demonstrate that the criticality requirements are satisfied when limiting the TRUPACT–III package to the fissile gram equivalent (FGE) limits provided in Table 6.1-1 for the payloads described in the *TRUPACT–III TRU Waste Authorized Methods for Payload Control (TRUPACT–III TRAMPAC)*[2]. The contents are manually compacted (i.e., not machine compacted) waste contaminated with fissile materials containing less than or equal to 1% by weight quantities of special reflector materials

6.1 Description of Criticality Design

6.1.1 Design Features

No special features are required to maintain criticality safety for any number of TRUPACT–III packages for both normal conditions of transport (NCT) and hypothetical accident conditions (HAC). The presence and location of the stainless steel containment vessel sheets and adjoining concentric sheet and plate structures are all that are required to maintain criticality safety.

6.1.2 Summary Table of Criticality Evaluation

The maximum results of the TRUPACT–III criticality calculations are summarized in Table 6.1-1 for four assumed Pu-240 loadings (0, 5, 15, and 25 g). As Pu-240 behaves neutronically as a poison, the FGE limit increases with increasing Pu-240 mass.

For a single TRUPACT–III package under NCT or HAC conditions, the maximum calculated k_s ($k+2\sigma$) value is 0.9335 when optimally moderated and reflected with a mixture of 25% polyethylene, 74% water, and 1% beryllium (by volume). This value is below the USL of 0.9392. Therefore, the requirements of 10 CFR §71.55 are met when the contents of a single TRUPACT–III package are limited to the values provided in Table 6.1-1.

For an infinite array of TRUPACT–III packages under NCT or HAC conditions, the maximum calculated k_s value is 0.9335 for optimal internal moderation and reflection with a mixture of 25% polyethylene, 74% water, and 1% beryllium (by volume) and optimal external interspersed moderation by water. As with the single package case, the k_s is below the USL of 0.9392. This maximum value occurs when each of the packages in the array is fully reflected (internally) and therefore isolated from each other.

Results indicate that the maximum reactivity of the package arrays is identical to that of the single-unit. This occurs because:

[1] Title 10, Code of Federal Regulations, Part 71 (10 CFR 71), *Packaging and Transportation of Radioactive Material*, 01–01–09 Edition.

[2] *TRUPACT–III TRU Waste Authorized Methods for Payload Control (TRUPACT–III TRAMPAC)*, U.S. Department of Energy, Carlsbad Field Office, Carlsbad, New Mexico.

- When internally reflected to the maximum extent, the fissile material regions of the array of TRUPACT–III packages are essentially isolated from each other, and
- When the fissile material region of each damaged or undamaged TRUPACT–III package is internally unreflected, interaction between TRUPACT–III packages is maximized. However, for the array of TRUPACT–III packages, interactive effects are not as great as the effect of full internal reflection.

Therefore, the requirements of 10 CFR §71.59 are met for arrays of TRUPACT–III packages when the contents of a single TRUPACT–III package is limited to the values provided in Table 6.1-1. Furthermore, a Criticality Safety Index (CSI) of zero (0.0) is justified because an infinite array of packages is utilized.

6.1.3 Criticality Safety Index

As noted in Section 6.1.2, an infinite array of packages is modeled for both NCT and HAC conditions. Therefore, the CSI = $50/\infty = 0.0$.

Table 6.1-1 – Summary of Criticality Evaluation

FGE Limit	**325**	**340**	**360**	**380**
Pu-240 Content (g)	**0**	**5**	**15**	**25**
Normal Conditions of Transport (NCT)				
Number of undamaged packages calculated to be subcritical	∞	∞	∞	∞
Single Unit Maximum k_s	0.9333	0.9335	0.9317	0.9319
Infinite Array Maximum k_s	0.9333	0.9335	0.9317	0.9319
Hypothetical Accident Conditions (HAC)				
Number of damaged packages calculated to be subcritical	∞	∞	∞	∞
Single Unit Maximum k_s	0.9333	0.9335	0.9317	0.9319
Infinite Array Maximum k_s	0.9333	0.9335	0.9317	0.9319
Upper Subcritical Limit (USL)	0.9392			

6.2 Fissile Material Contents

6.2.1 General

The contents are manually compacted (i.e., not machine compacted) waste contaminated with fissile materials containing less than or equal to 1% by weight quantities of special reflector materials. The payload within each TRUPACT–III package is held within a Standard Large Box 2 (SLB2). The SLB2 overall size envelope consists of a 108" length, 69" width, and 73" height. A single TRUPACT–III can transport one SLB2. The SLB2 is not modeled in the criticality evaluation.

The typical isotopic distribution of the waste is provided in Table 6.2-1. In accordance with ANSI/ANS-8.1[1], the quantities of all fissile isotopes other than Pu-239 present in the CH-TRU waste material and other authorized payloads may be converted to a fissile gram equivalent (FGE) of the most restrictive isotope for criticality evaluations. As noted in Table 6.1-1, the mass of the fissile contents ranges from 325 FGE Pu-239 with no Pu-240 up to 380 FGE Pu-239 with 25 g Pu-240.

If no credit is taken for the poisoning effects of Pu-240, all fissile material present in the package is modeled as Pu-239. If credit is taken for the poisoning effects of Pu-240, the fissile material is modeled as a mixture of Pu-239 and Pu-240. When developing the total FGE for an actual package, Pu-240 should be conservatively included in the total FGE even if credit is taken for its poisoning effects. In addition, in accordance with ANSI/ANS-8.1, Pu-241 is considered to be Pu-239 when computing plutonium mass values provided the Pu-240 concentration exceeds the Pu-241 concentration.

No credit is taken for parasitic neutron absorption in contact-handled transuranic (CH-TRU) waste materials and other authorized payloads, dunnage, or package contents for the base case with no Pu-240, except to the extent that the elements present in the moderator absorb neutrons. For cases with variable amounts of Pu-240, credit is taken for parasitic neutron absorption in this material.

The CH-TRU waste material and other authorized payloads may contain plastic materials such as anti-contamination clothing, plastic bags, and other plastic refuse. Plastic items present in the payload will be present with a low packing density. Because polyethylene is a superior moderator to water and leads to higher reactivities, the volume fraction of polyethylene used in TRUPACT–III criticality analysis must bound the polyethylene volume fraction expected in the waste stream. The volume fraction of polyethylene was experimentally determined, using hand-packing of surrogate waste forms, to be 13.36%[2]. Therefore, in all TRUPACT–III criticality models, a bounding value of 25% polyethylene (by volume) is utilized.

A small amount of special reflecting materials may be present in the waste stream as a result of cross-contamination. To bound the presence of small (< 1% of the waste mass) amounts of special reflectors, models are developed with 1% by volume beryllium in the fissile and reflector regions. ("Reflector" in this context is the region outside the fissile mass but within the inner cavity of the package.) Due to the

[1] ANSI/ANS-8.1-1998, *Nuclear Criticality Safety in Operations with Fissionable Materials Outside Reactors*, American Nuclear Society, September 1998.

[2] WP 08-PT.09, *Test Plan to Determine the TRU Waste Polyethylene Packing Fraction,* Washington TRU Solutions, LLC., Revision 0, June 2003.

large volume of the package, 1% by volume bounds 1% by weight. Special reflectors are discussed further in Section 6.2.2, *Special Reflectors*.

Therefore, to bound the presence of both plastics and special reflectors in the waste stream, the fissile material is both moderated and reflected with a mixture of 25% polyethylene, 74% water, and 1% beryllium (by volume) for both NCT and HAC conditions.

6.2.2 Special Reflectors

As noted above, this analysis considers the potential presence of a limited quantity of "special reflectors," which are materials that can credibly provide better than 25% polyethylene/75% water equivalent reflection and are not authorized for shipment in quantities that exceed 1% by mass except in specific configurations discussed below. An extensive study of special reflectors has been documented in report SAIC-1322-001[3], which was developed for a reflected sphere of 325 g Pu-239 for the TRUPACT–II package. As the TRUPACT–II and TRUPACT–III are both large cavity packages with similar payloads for the general case, the conclusions from SAIC-1322-001 are also applicable to the TRUPACT–III. Based on the results from SAIC-1322-001, Be, BeO, C, D_2O, MgO, and depleted U (less than 0.72 wt.% and greater than or equal to 0.3 wt.% U-235) are the only materials that can provide reflection equivalent to a 2 ft thickness of 25% polyethylene and 75% water mixture under any of the following conditions:

- Less than 15.9-mm thick at 100% of theoretical density[4] in the form of large solids
- Less than 17.5-mm thick at 70% of theoretical density in the form of tightly-packed particulate solids
- Less than 20% packing fraction at 609.6-mm thick in the form of randomly dispersed particulate solids

SAIC-1322-001 found that beryllium is the bounding special reflector as it provides the best reflection of the system resulting in the highest reactivity. In the current analysis, the utilization of 1% by volume beryllium in the models bounds the presence of up to 1% by mass quantities of special reflectors that are dispersed in the waste matrix.

The reference study, SAIC-1322-001, found that, with the exception of Be, adding special reflector materials to the fissile region reduced the reactivity of a single 325 FGE, 25% polyethylene/75% water reflected sphere. Thus, if it can be shown that a candidate special reflector other than Be is chemically or mechanically bound to the fissile material, or otherwise in a form which would not provide better than a 25% polyethylene/75% water equivalent reflection, the FGE limits developed using an assumption of 1% Be by mass will apply even in the presence of greater than 1% by mass quantities of the special reflector.

[3] Neeley, G. W., D. L. Newell, S. L. Larson and R. J. Green, *Reactivity Effects of Moderator and Reflector Materials on a Finite Plutonium System*, SAIC-1322-001 Revision 1, Science Applications International Corporation, Oak Ridge, Tennessee, May 2004.

[4] Theoretical densities used in the study are 1.85 g/cm^3 for Be, 2.69 g/cm^3 for BeO, 2.1 g/cm^3 for C, 1.1054 g/cm^3 for D_2O, 3.22 g/cm^3 for MgO, and 19.05 g/cm^3 for U.

As further discussed below, a consideration of each candidate special reflector in CH-TRU waste has been made, leading to the conclusion that, with the exception of Be and BeO, none will provide better than a 25% polyethylene/75% water equivalent reflection. Therefore, the current analysis utilizes a mixture of 25% polyethylene, 74% water, and 1% beryllium (by volume) for both the moderator and reflector, which bounds a 25% polyethylene/75% water mix. In summary, except for limiting TRUPACT–III shipments to 1% by weight quantities of Be and BeO, no specific controls on candidate special reflectors are needed.

The only "special reflectors" applicable to CH-TRU waste criticality analysis are Be, BeO, C, D_2O, MgO, and depleted U, when present in quantities greater than 1% by weight. Each special reflector with regard to its possible presence in CH-TRU waste is discussed below.

Beryllium and Beryllium Oxide – Be and BeO may be present in CH-TRU waste in quantities which exceed 1% by weight. However, for transport in the TRUPACT–III, Be and BeO are specifically limited to quantities not exceeding 1% by weight.

Carbon – Carbon is present as a constituent in CH-TRU waste but not in forms that can reconfigure as a reflector. For example: (1) Carbon may be present as graphite molds or crucibles. In these forms the carbon will be chemically and irreversibly bound to the plutonium or other fissile material and cannot be separated. (2) Carbon may be present in filter media as spent or activated carbon. The plutonium or other fissile material would then be attached to the carbon filter media and would not be easily separated. (3) Granular activated carbon (GAC) pads may also be present in an enclosed bag for the purpose of absorbing volatile organic compounds. Once the GAC pad is placed inside the payload container, there is no method for the carbon to fully surround the fissile material and reconfigure as a reflector. (4) Carbon may also be present in alloys, which are by definition chemically and/or mechanically bound. In summary, there is no identified mechanism that could cause the carbon in CH-TRU waste to be separated from the fissile material and to be reconfigured as a reflector.

Deuterium – The presence of liquid waste in the payload containers, except for residual amounts, is prohibited. As specified by the TRUPACT–III TRAMPAC, the total volume of residual liquid in a payload container shall be less than 1 percent (volume) of the payload container. This limitation on the authorized contents is such that deuterium will not be present in concentrations of greater than 1% by weight.

Magnesium Oxide – Magnesium oxides used in temperature control applications may be present in solid inorganic waste forms such as glass, metal, and pyrochemical salts. If present, magnesium oxide will be bound to the fissile material and would not be easily separated. Magnesium oxide used for neutralization in solidified material cannot be separated out as it is chemically reacted in the waste generation process. There is no identified mechanism that could cause the magnesium oxide in CH-TRU waste to be reconfigured as a reflector.

Depleted Uranium – Depleted uranium may be present in CH-TRU waste, but it will be chemically and/or mechanically bound to the plutonium or physically inseparable because the densities of uranium and plutonium are similar. Separation by mechanical means or by leaching is extremely difficult and is considered highly unlikely in CH-TRU waste. Depleted uranium in CH-TRU waste will, therefore, not be separated from the fissile material and reconfigured as a reflector.

6.2.3 Fissile Material Modeling

It is assumed that when packaged, the fissile material is distributed throughout the waste volume. Under accident conditions, water in-leakage may cause some fissile material to migrate within the package interior. It is unlikely that a distributed volume of fissile material could coalesce into a single fuel lump, but such a scenario is conservatively assumed. Because the most conservative fissile geometry is a sphere, a spherical fissile geometry is utilized. Therefore, this geometry bounds the true NCT and HAC geometry of the fissile material, which would likely be highly distributed.

It is desired to compute the Pu number densities as a function of H/X, where X is the Pu-239 number density. To compute the number densities, the following gram densities are utilized: 1.0 g/cm^3 for water, 0.92 g/cm^3 for polyethylene, and 1.848 g/cm^3 for beryllium. As the H/X ratio becomes larger, the size of the fissile volume also becomes larger. The fissile material number densities are provided in Table 6.2-2 through Table 6.2-5 for a Pu-239 FGE limit of 325 g, 340 g, 360 g, and 380 g, respectively. Note that the number densities of the moderating elements (H, C, O, and Be) are not constant between the various cases. The reason for the slight variability in these number densities is that the volume displaced by the Pu (solid metal, density = 19.84 g/cm^3) is explicitly factored into the computations (e.g., the volume of Pu is subtracted from the total fissile volume, and the remaining volume is divided on a volume percentage between water, polyethylene, and beryllium.) However, because the Pu mass is relatively small, the moderator number densities are nearly constant.

Table 6.2-1 – Fissile Payload Composition (typical)

Nuclide	Weight-Percent
Pu-238	Trace
Pu-239	93.0
Pu-240	5.8
Pu-241	0.4
Pu-242	Trace
Am-241	Trace
All other fissile isotopes	0.7

Table 6.2-2 – Number Densities, 325 g Pu-239, 0 g Pu-240

H/X	Radius (cm)	Pu-239 (at/b-cm)	Pu-240 (at/b-cm)	H (at/b-cm)	Be (at/b-cm)	C (at/b-cm)	O (at/b-cm)
500	11.2286	1.3806E-04	0.0000E+00	6.9030E-02	1.2314E-03	9.8473E-03	2.4668E-02
600	11.9303	1.1510E-04	0.0000E+00	6.9062E-02	1.2320E-03	9.8518E-03	2.4679E-02
700	12.5580	9.8692E-05	0.0000E+00	6.9085E-02	1.2324E-03	9.8550E-03	2.4687E-02
800	13.1285	8.6377E-05	0.0000E+00	6.9102E-02	1.2327E-03	9.8575E-03	2.4693E-02
900	13.6533	7.6794E-05	0.0000E+00	6.9115E-02	1.2329E-03	9.8594E-03	2.4698E-02
1000	14.1406	6.9126E-05	0.0000E+00	6.9126E-02	1.2331E-03	9.8609E-03	2.4702E-02
1100	14.5965	6.2849E-05	0.0000E+00	6.9134E-02	1.2333E-03	9.8621E-03	2.4705E-02
1200	15.0255	5.7618E-05	0.0000E+00	6.9142E-02	1.2334E-03	9.8632E-03	2.4708E-02
1300	15.4313	5.3190E-05	0.0000E+00	6.9148E-02	1.2335E-03	9.8640E-03	2.4710E-02
1400	15.8169	4.9395E-05	0.0000E+00	6.9153E-02	1.2336E-03	9.8648E-03	2.4712E-02
1500	16.1845	4.6105E-05	0.0000E+00	6.9157E-02	1.2337E-03	9.8654E-03	2.4713E-02
1600	16.5361	4.3226E-05	0.0000E+00	6.9161E-02	1.2338E-03	9.8660E-03	2.4715E-02
1700	16.8734	4.0685E-05	0.0000E+00	6.9165E-02	1.2338E-03	9.8665E-03	2.4716E-02
1800	17.1977	3.8427E-05	0.0000E+00	6.9168E-02	1.2339E-03	9.8669E-03	2.4717E-02

Table 6.2-3 – Number Densities, 340 g Pu-239, 5 g Pu-240

H/X	Radius (cm)	Pu-239 (at/b-cm)	Pu-240 (at/b-cm)	H (at/b-cm)	Be (at/b-cm)	C (at/b-cm)	O (at/b-cm)
500	11.3989	1.3805E-04	2.0217E-06	6.9027E-02	1.2314E-03	9.8469E-03	2.4667E-02
600	12.1112	1.1510E-04	1.6856E-06	6.9060E-02	1.2320E-03	9.8515E-03	2.4678E-02
700	12.7484	9.8689E-05	1.4453E-06	6.9083E-02	1.2324E-03	9.8548E-03	2.4687E-02
800	13.3275	8.6375E-05	1.2649E-06	6.9100E-02	1.2327E-03	9.8572E-03	2.4693E-02
900	13.8603	7.6793E-05	1.1246E-06	6.9113E-02	1.2329E-03	9.8591E-03	2.4698E-02
1000	14.3550	6.9124E-05	1.0123E-06	6.9124E-02	1.2331E-03	9.8607E-03	2.4701E-02
1100	14.8177	6.2848E-05	9.2038E-07	6.9133E-02	1.2333E-03	9.8619E-03	2.4705E-02
1200	15.2533	5.7617E-05	8.4377E-07	6.9140E-02	1.2334E-03	9.8630E-03	2.4707E-02
1300	15.6652	5.3190E-05	7.7894E-07	6.9147E-02	1.2335E-03	9.8639E-03	2.4709E-02
1400	16.0566	4.9394E-05	7.2335E-07	6.9152E-02	1.2336E-03	9.8646E-03	2.4711E-02

Table 6.2-4 – Number Densities, 360 g Pu-239, 15 g Pu-240

H/X	Radius (cm)	Pu-239 (at/b-cm)	Pu-240 (at/b-cm)	H (at/b-cm)	Be (at/b-cm)	C (at/b-cm)	O (at/b-cm)
500	11.6184	1.3804E-04	5.7278E-06	6.9022E-02	1.2313E-03	9.8461E-03	2.4665E-02
600	12.3445	1.1509E-04	4.7755E-06	6.9055E-02	1.2319E-03	9.8509E-03	2.4677E-02
700	12.9939	9.8684E-05	4.0947E-06	6.9079E-02	1.2323E-03	9.8542E-03	2.4685E-02
800	13.5841	8.6371E-05	3.5838E-06	6.9097E-02	1.2326E-03	9.8568E-03	2.4692E-02
900	14.1271	7.6789E-05	3.1862E-06	6.9111E-02	1.2329E-03	9.8587E-03	2.4697E-02
1000	14.6313	6.9122E-05	2.8680E-06	6.9122E-02	1.2331E-03	9.8603E-03	2.4700E-02
1100	15.1029	6.2846E-05	2.6077E-06	6.9131E-02	1.2332E-03	9.8616E-03	2.4704E-02
1200	15.5468	5.7615E-05	2.3906E-06	6.9138E-02	1.2334E-03	9.8627E-03	2.4706E-02
1300	15.9667	5.3188E-05	2.2069E-06	6.9145E-02	1.2335E-03	9.8636E-03	2.4709E-02
1400	16.3656	4.9393E-05	2.0494E-06	6.9150E-02	1.2336E-03	9.8644E-03	2.4711E-02

Table 6.2-5 – Number Densities, 380 g Pu-239, 25 g Pu-240

H/X	Radius (cm)	Pu-239 (at/b-cm)	Pu-240 (at/b-cm)	H (at/b-cm)	Be (at/b-cm)	C (at/b-cm)	O (at/b-cm)
500	11.8300	1.3804E-04	9.0434E-06	6.9018E-02	1.2312E-03	9.8455E-03	2.4663E-02
600	12.5692	1.1509E-04	7.5398E-06	6.9051E-02	1.2318E-03	9.8503E-03	2.4675E-02
700	13.2304	9.8679E-05	6.4650E-06	6.9076E-02	1.2322E-03	9.8538E-03	2.4684E-02
800	13.8314	8.6367E-05	5.6583E-06	6.9094E-02	1.2326E-03	9.8564E-03	2.4691E-02
900	14.3842	7.6787E-05	5.0307E-06	6.9108E-02	1.2328E-03	9.8584E-03	2.4696E-02
1000	14.8975	6.9119E-05	4.5283E-06	6.9119E-02	1.2330E-03	9.8600E-03	2.4700E-02
1100	15.3778	6.2844E-05	4.1172E-06	6.9129E-02	1.2332E-03	9.8613E-03	2.4703E-02
1200	15.8297	5.7614E-05	3.7745E-06	6.9136E-02	1.2333E-03	9.8624E-03	2.4706E-02
1300	16.2572	5.3187E-05	3.4845E-06	6.9143E-02	1.2334E-03	9.8633E-03	2.4708E-02
1400	16.6634	4.9392E-05	3.2359E-06	6.9148E-02	1.2335E-03	9.8641E-03	2.4710E-02

6.3 General Considerations

Criticality calculations for the TRUPACT–III package are performed using the three-dimensional MCNP5 Monte Carlo program[1]. Descriptions of the packaging geometric models are given in Section 6.3.1, *Model Configuration*. The material properties for all non-fissile materials used in the models are provided in Section 6.3.2, *Material Properties*. The computer code and cross section libraries used are provided in Section 6.3.3, *Computer Codes and Cross-Section Libraries*. Finally, the most reactive configuration is discussed in Section 6.3.4, *Demonstration of Maximum Reactivity*.

6.3.1 Model Configuration

All relevant features of the TRUPACT–III package are modeled in MCNP. The key dimensions used in the MCNP models are summarized in Table 6.3-1 and discussed in the following paragraphs. The NCT single package model geometry is illustrated in Figure 6.3-1 and Figure 6.3-2.

The inner dimensions of the containment structural assembly (CSA) are 184 cm x 200 cm x 279 cm. The outer dimensions (width and height) of the CSA are 212 cm x 228 cm, with a modeled length of 308.6 cm. The CSA is comprised of two layers of 0.8 cm thick steel plate separated by corrugated steel. For the closure lid, the plates are 1.2 cm thick, with an overall lid thickness of 14.8 cm. The corrugated steel has a negligible impact on reactivity and is omitted from the MCNP models.

The CSA is protected by layers of foam and balsa on the top, bottom, and sides of the package. The foam is 10.9 cm thick on the top and bottom, and 11.4 cm thick on the sides. The foam and balsa are separated by a layer of steel 1.0 cm thick. The balsa is 6 cm thick on each of the four sides. The outer skin of the package is 0.6 cm thick steel. The overall width (x) and height (y) of the package are 250 cm and 265 cm.

On each end of the package is an overpack cover. The inner boundary of each overpack cover is hexagonal in shape, while the outer boundary is approximately square in shape. Through the centerline of the closure lid end overpack cover are layers of steel (0.6 cm), foam (12.0 cm), steel (1.5 cm), balsa (6.0 cm), and steel (0.6 cm). Through the edge of the closure lid end overpack cover are layers of steel (0.6 cm), calcium silicate (4.2 cm), steel (1.6 cm), foam (38.4 cm), steel (0.6 cm), foam (14.0 cm), and steel (0.8 cm). For simplicity, the "cheeks" of the front end are not modeled explicitly. Rather, the x and y dimensions of the main portion of the overpack cover are extended to fill this region. This simplification has a negligible impact on the results.

The rear end is similar to the closure lid end overpack cover, although it is integral to the package. Through the centerline of the rear end, the material thicknesses are the same, although the innermost layer of steel is absent. Through the edge of the rear end impact limiter are layers of foam (44.8 cm), steel (0.6 cm), foam (14.0 cm), and steel (0.8 cm). The 44.8 cm thickness for the foam is approximate and selected to give the correct overall package length (z) of 428.8 cm. Also, the cheeks are modeled in the same manner as the closure lid end overpack cover.

The dimensions listed in the preceding paragraph are consistent with the NCT models, for which crush damage is assumed to be negligible. For the HAC models, all foam and balsa are conservatively

[1] MCNP5, *MCNP – A General Monte Carlo N-Particle Transport Code, Version 5; Volume II: User's Guide*, LA-CP-03-0245, Los Alamos National Laboratory, April 2003.

replaced with water of variable density, see Figure 6.3-3. Also, although at most only one side of the package would exhibit crush, 2.54 cm of crush is applied to the top, bottom, and sides of the package, and 7.62 cm of crush is applied to the ends of the package. This crush is applied to the thickness of the balsa region in the HAC models. Note that the modeled crush depth bounds the results of the actual drop tests, which demonstrated little deflection. Refer to Section 2.7.1, *Free Drop*.

Note that foam of several different densities is utilized in the package design, ranging from a low density of 0.096 g/cm^3 (6 pcf) to a high density of 0.480 g/cm^3 (30 pcf). To be conservative and to maximize reflection in the single package cases, all foam is modeled with a density of 0.480 g/cm^3, which maximizes the hydrogen density in the foam. In addition, for simplicity the calcium silicate is simply modeled as foam in the NCT cases (variable density water in the HAC cases).

All single package models are reflected with 30.48 cm (12 inches) of water.

6.3.2 Material Properties

The TRUPACT–III is constructed primarily from UNS S31803 stainless steel plate, balsa wood, and polyurethane foam of several different densities.

MCNP accepts material input in a variety of formats. The method of input for each material has been selected both to be consistent with the source of the data and for computational convenience. For foam and stainless steel, elemental compositions are input as weight percents and the gram density is input on the MCNP cell cards. For water and balsa wood, elemental compositions are input as atoms per molecule and the gram density is input on the MCNP cell cards. For the source and internal reflector, number densities are explicitly computed and the total atom density is input on the MCNP cell cards. (The number densities for the source are provided in Section 6.2.3.)

Most of the steel plate used in the package is UNS S31803. The composition and density of S31803 are provided in Table 6.3-2 and is obtained from the Allegheny Ludlum Corporation[3].

Balsa wood is modeled with a density of 0.125 g/cm^3 and the chemical formula $C_6H_{10}O_5$. The S(α,β) card POLY.60T is used to simulate hydrogen bound to carbon. The standard composition for balsa is obtained from the SCALE material library[4].

Water is modeled with a density ranging up to 1.0 g/cm^3 and the chemical formula H_2O. The S(α,β) card LWTR.60T is used to simulate hydrogen bound to oxygen in water.

Polyurethane foam of several different densities is present in the package. The density ranges from a low density of 0.096 g/cm^3 (6 pcf) to a high density of 0.480 g/cm^3 (30 pcf). To be conservative, the NCT models utilize a density of 0.480 g/cm^3 for all foam. A high density bounds a low density because increasing the hydrogen concentration increases neutron reflection and hence reactivity, as demonstrated in Section 6.6. The foam composition is provided in Table 6.3-3. Because the composition is provided as ranges, the composition used in the analysis is

[3] Technical Data Blue Sheet for Stainless Steel AL 2205™ Alloy (UNS Designation S31803), Allegheny Ludlum Corporation, Pittsburgh, PA.

[4] *Standard Composition Library*, NUREG/CR-0200, Rev. 6, Volume 3, Section M8, ORNL/NUREG/CSD-2/V3/R6, September 1998.

selected to maximize the weight percent of hydrogen. The S(α,β) card POLY.60T is used to simulate hydrogen bound to carbon.

The internal reflector is a mixture of 25% polyethylene, 74% water, and 1% beryllium by volume. Because MCNP does not have a convenient method to input volume fractions, number densities are computed explicitly and are provided in Table 6.3-4. To compute the number densities, the following densities are utilized: 1.0 g/cm^3 for water, 0.92 g/cm^3 for polyethylene, and 1.848 g/cm^3 for beryllium. The S(α,β) card BE.60T is used to simulate metallic beryllium. Note that the hydrogen in the internal reflector may be bound to either carbon or oxygen. However, MCNP does not have the capability to utilize the two different S(α,β) cards for hydrogen bound to water and hydrogen bound to polyethylene in the same material. It is demonstrated in Section 6.4.1.1 that using either the card LWTR.60T or POLY.60T yields essentially identical results. LWTR.60T is used with the internal reflector (and source) for the models.

6.3.3 Computer Codes and Cross-Section Libraries

MCNP5 v1.30 is used for the criticality analysis. All cross sections utilized are at room temperature (293.6 K). The most recent cross sections available are used for each isotope. Most isotopes utilize ENDF/B-VI cross sections. ENDF/B-V elemental cross sections are utilized only when ENDF/B-VI elemental cross sections are not available. The Pu-239 cross sections are a preliminary version of ENDF/B-VII cross section set. Although the ENDF/B-VII cross section set had not been formally released with MCNP5 v1.30, LANL included this Pu-239 cross section because it showed significant improvements compared to the latest ENDF/B-VI Pu-239 cross section for certain LANL benchmark models. Titles of the cross sections utilized in the models have been extracted from the MCNP output and provided in Table 6.3-5. As discussed in Section 6.3.2, the S(α,β) cards LWTR.60T, POLY.60T, and BE.60T are utilized, as appropriate.

All cases are run with 1000 neutrons per generation for 510 generations, skipping the first 10, except as otherwise noted. The 1-sigma uncertainty is approximately 0.001 for all cases.

6.3.4 Demonstration of Maximum Reactivity

The fissile material in the limiting cases is both moderated and internally reflected with a mixture of 25% polyethylene, 74% water, and 1% beryllium (by volume). This composition is more reactive than simply moderating and internally reflecting with water.

The HAC array analysis demonstrates that reducing internal reflection reduces the reactivity, although neutronic interaction between packages may increase. Therefore, the most reactive condition is achieved by simply infinitely reflecting the most reactive single package geometry.

Although the package is leaktight, full inleakage of water is modeled in both the NCT and HAC cases. In the NCT cases, the foam and balsa are modeled explicitly, while in the HAC cases, foam and balsa are replaced with variable density water, and crush is modeled on all six sides to reduce the distance between fissile spheres in adjacent packages. Because the package is large and the NCT and HAC models are quite similar, there is no difference in reactivity between the NCT and HAC cases.

In the HAC array cases, various combinations of fissile sphere location and reflector density are used to maximize the reactivity, although the most reactive case is simply with a fully-reflected

fissile sphere at the center of the cavity. Because the cavity is large, the fissile material in each package is completely isolated from adjacent packages, and there is no difference in reactivity between the most reactive single package and array cases. The maximum reactivities of the four combinations of Pu-239/Pu-240 mass are also similar.

Table 6.3-1 – Key NCT As-Modeled Dimensions

Parameter	Value (cm)
Overall package width (x)	250.0
Overall package height (y)	265.0
Overall package length (z)	428.8
CSA cavity inner width (x)	184.0
CSA cavity inner height (y)	200.0
CSA cavity inner length (z)	279.0
CSA outer width (x)	212.0
CSA outer height (y)	228.0
CSA inner plate thickness	0.8
CSA outer plate thickness	0.8
Closure lid thickness	14.8
Closure lid plate thickness	1.2
Top/Bottom foam thickness	10.9
Side foam thickness	11.4
Steel thickness between foam and balsa	1.0
Top/Bottom/Side balsa thickness	6.0
Top/bottom/side outer steel thickness	0.6

(continued)

Table 6.3-1 – Key NCT As-Modeled Dimensions (concluded)

Parameter	Value (cm)
Closure Lid End Overpack Cover (centerline)	
Steel thickness	0.6
Foam thickness	12.0
Steel thickness	1.5
Balsa thickness	6.0
Steel thickness	0.6
Rear End Overpack Cover (centerline)	
Foam thickness	12.0
Steel thickness	1.5
Balsa thickness	6.0
Steel thickness	0.6
Closure Lid End Overpack Cover (outer edge)	
Steel thickness	0.6
Calcium silicate thickness	4.2
Steel thickness	1.6
Foam thickness	38.2
Steel thickness	0.6
Foam thickness	14.0
Steel thickness	0.8
Rear End Overpack Cover (outer edge)	
Foam thickness (from end of CSA) (Selected to give package length of 428.8 cm)	44.8
Steel thickness	0.6
Foam thickness	14.0
Steel thickness	0.8

Table 6.3-2 – UNS S31803 Composition

Component	UNS S31803 (Wt.%, Typical)
C	0.02
Si	0.4
P	0.025
Cr	22.4
Mn	0.70
Fe	67.194
Ni	5.8
N	0.16
S	0.001
Mo	3.3
Density (g/cm^3)	7.89

Table 6.3-3 – Polyurethane Foam Composition

Component	Wt.% Range	Modeled Wt.%
C	50 – 70	70
O	14 – 34	14
N	4 – 12	6
H	4 – 10	10
P	0 – 2	0
Si	< 1	0
Cl	< 0.18	0
Other	< 1	0
Maximum Density = 0.480 g/cm^3		

Table 6.3-4 – Internal Reflector Composition

Component	Number Density (atoms/b-cm)
H	6.9221E-02
Be	1.2348E-03
C	9.8745E-03
O	2.4736E-02
Total	1.0507E-01

Table 6.3-5 – Cross Section Libraries Utilized

Isotope/Element	Cross Section Label (from MCNP output)
1001.62c	1-h-1 at 293.6K from endf-vi.8 njoy99.50
4009.62c	4-be-9 at 293.6K from endf/b-vi.8 njoy99.50
6000.66c	6-c-0 at 293.6K from endf-vi.6 njoy99.50
7014.62c	7-n-14 at 293.6K from endf-vi.8 njoy99.50
8016.62c	8-o-16 at 293.6K from endf-vi.8 njoy99.50
14000.60c	14-si-nat from endf/b-vi
15031.66c	15-p-31 at 293.6K from endf-vi.6 njoy99.50
16000.62c	16-s-0 at 293.6K from endf/b-vi.8 njoy99.50
25055.62c	25-mn-55 at 293.6K from endf/b-vi.8 njoy99.50
24000.50c	njoy
26000.55c	njoy
28000.50c	njoy
42000.66c	42-mo-0 at 293.6K from endf-vi.0 njoy99.50
94239.69c	94-pu-239 at 293.6K from t16 pu239la7d njoy99.50
94240.66c	94-pu-240 at 293.6K from endf-vi.2 njoy99.50

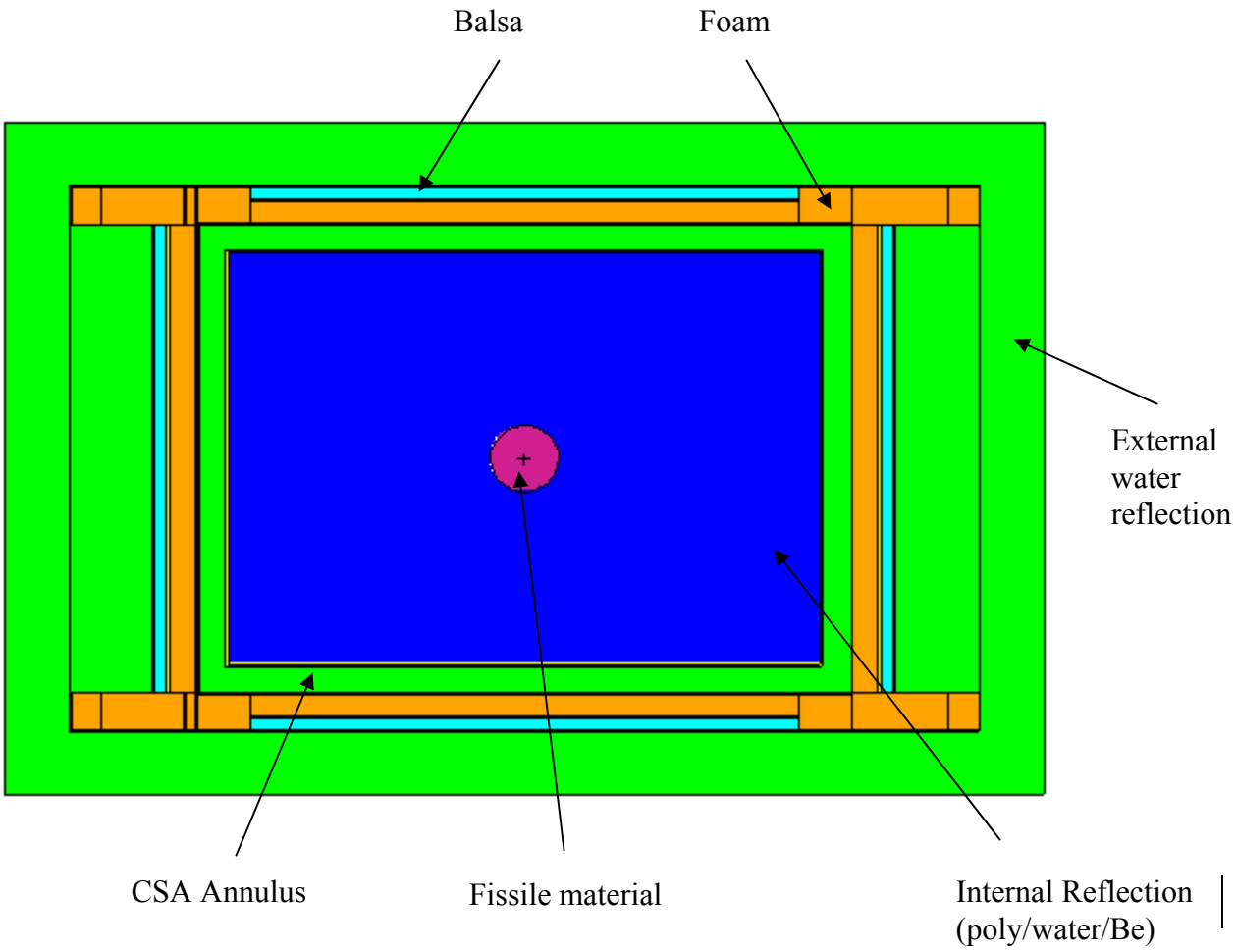

Figure 6.3-1 – NCT Single Package Model (z-y view)

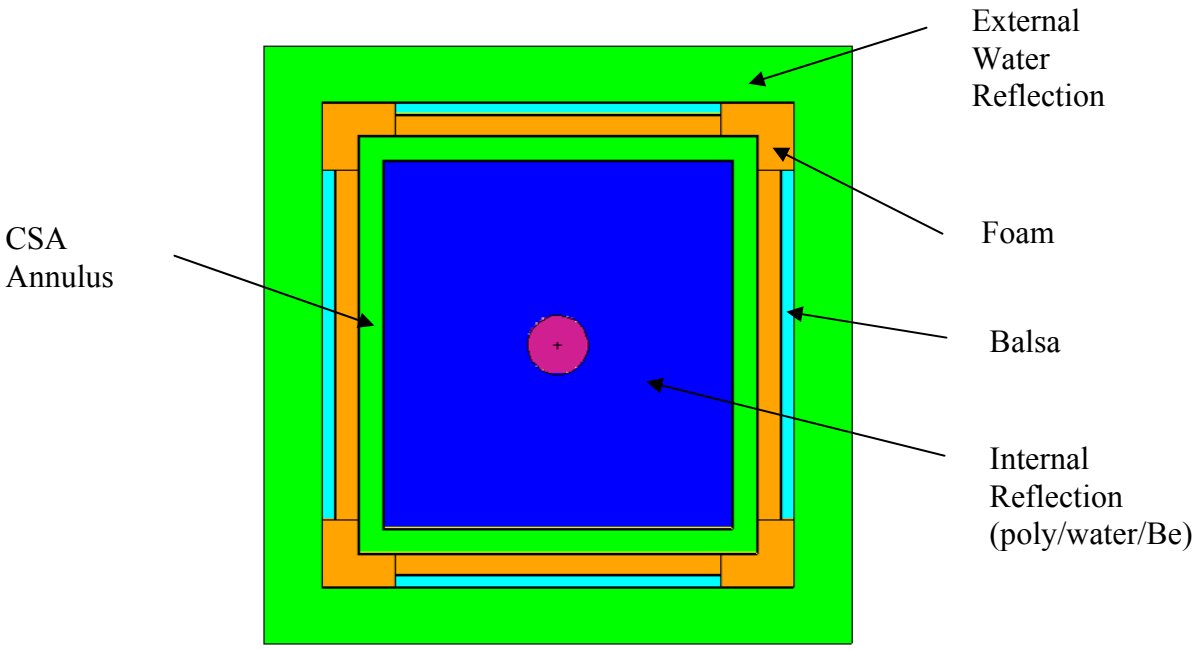

x-y view through center of package

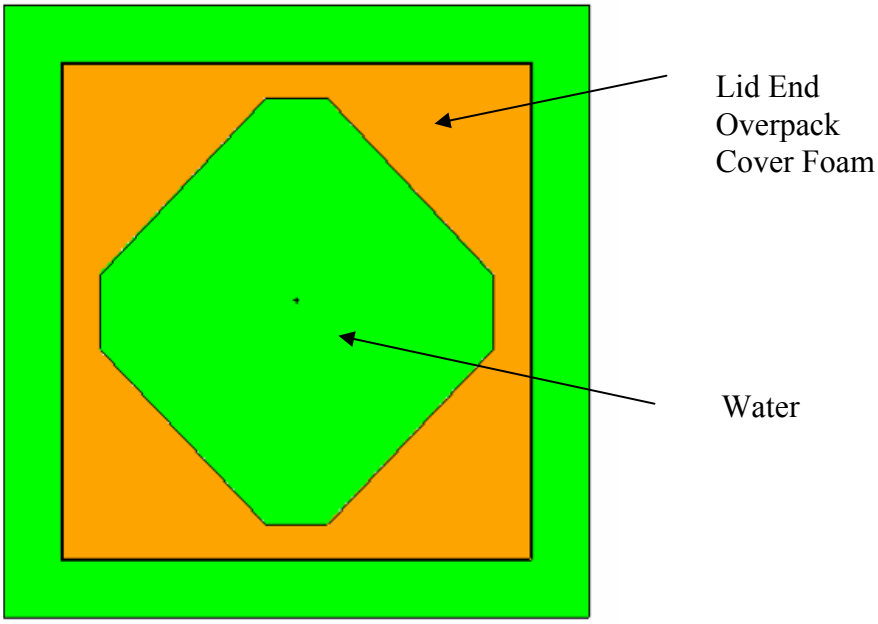

x-y view through lid end overpack cover

Figure 6.3-2 – NCT Single Package Model (x-y views)

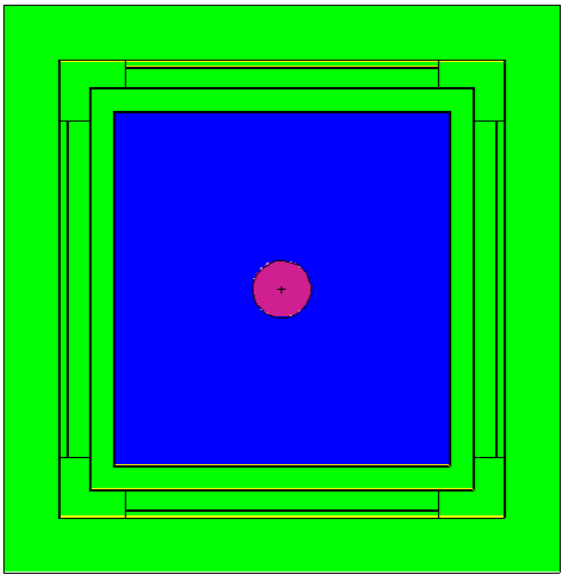

x-y view

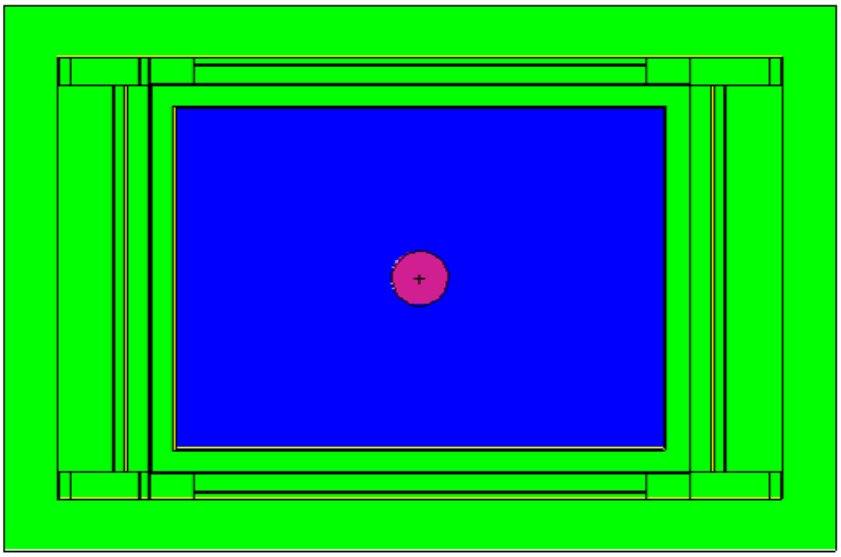

z-y view

Note: Foam and balsa have been replaced with water when compared to the NCT models. The package has also been crushed 2.54 cm on the top, bottom, and sides, and 7.62 cm on each end.

Figure 6.3-3 – HAC Single Package Model

6.4 Single Package Evaluation

Compliance with the requirements of 10 CFR 71 is demonstrated by analyzing optimally moderated damaged and undamaged, single-unit TRUPACT–III packages. The figures and descriptions provided in Section 6.3.1, *Model Configuration*, describe the basic geometry of the single-unit models.

6.4.1 Configuration

6.4.1.1 NCT Single Package Configuration

The geometry of the NCT single package configuration is discussed in Section 6.3.1. All relevant design features of the TRUPACT–III are modeled. The package is externally reflected with 30.48 cm of water. Although the package is leaktight, it is conservatively assumed that the package is also internally flooded with water, which is assumed to fill the CSA annulus as well as the cavity. Within the cavity itself, the internal reflector is modeled as a mixture of 25% polyethylene, 74% water, and 1% beryllium (by volume). This composition is also used to moderate the fissile material.

The fissile material is modeled as a sphere, which is the most reactive geometry possible. To maximize reflection, the sphere is modeled at the center of the cavity. The H/X ratio is varied between 500 and 1400 by adjusting the radius of the fissile sphere. Calculations are performed for four different FGE loadings and Pu-240 content: (1) 325 g Pu-239/0 g Pu-240, (2) 340 g Pu-239/5 g Pu-240, (3) 360 g Pu-239/15 g Pu-240, and (4) 380 g Pu-239/25 g Pu-240. The results are summarized in Table 6.4-1.

The proper use of S(α,β) cards is investigated for the 325 FGE series. By default, MCNP uses free gas treatment cross sections for all nuclides unless an S(α,β) card is specified to correct for the effects of binding the target atom to a specific molecule. For instance, BE.60T is used in the models to simulate metallic beryllium, and LWTR.60T is used in the pure water regions of the models. However, because the moderator and internal reflector are a mixture of both water and polyethylene, ~75% of the hydrogen atoms are bound to oxygen and ~25% of the hydrogen atoms are bound to carbon. For this reason, cases are run using the S(α,β) treatment for either water or polyethylene for the moderator/internal reflector, and the most reactive S(α,β) treatment is selected, as discussed in the following paragraph.

In Cases A1 through A10, the S(α,β) card LWTR.60T is used for both the fissile material and internal reflector. It is not possible to specify the S(α,β) cards LWTR.60T and POLY.60T in the same material. Therefore, additional cases are developed to investigate the impact on the reactivity of using these two S(α,β) cards individually. In Case A11, Case A5 is rerun with the POLY.60T card for the fissile material and internal reflector. K_s is lower (0.92900 vs. 0.93329), although the difference may be simply statistical fluctuation. To reduce the statistical uncertainty, Cases A11 and A5 are rerun as Cases A12 and A13, respectively, although the number of neutrons per cycle is increased by a factor of five. K_s values between Cases A12 and A13 are almost identical when the statistical uncertainty is reduced (0.92892 vs. 0.92901), and it is concluded that either LWTR.60T or POLY.60T may be used in the material cards for the fissile sphere and reflector. In the remaining cases (both HAC and NCT), LWTR.60T is used for fissile sphere and reflector materials.

Case A25 is the most reactive, with H/X=900 and k_s = 0.93354. This case has 340 g Pu-239 and 5 g Pu-240, although the maximum reactivities of the other FGE limits are similar. This result is below the USL of 0.9392.

6.4.1.2 HAC Single Package Configuration

The geometry of the HAC single package configuration is discussed in Section 6.3.1. It is essentially the same as the NCT configuration except that all foam and balsa components have been replaced with water, and the overall package dimensions have been crushed 2.54 cm on the top, bottom, and sides, and 7.62 cm on each end.

The single package HAC analysis is performed for 325, 340, 360, and 380 FGE. Results are provided in Table 6.4-2. The results are identical to the NCT single package results in all cases, indicating that the fissile sphere is so well reflected that essentially no neutrons are interacting with the package boundary. Case B15 is the most reactive, with H/X = 900 and k_s = 0.93354. This result is below the USL of 0.9392.

6.4.2 Results

Following are the tabulated results for the single package cases. The most reactive configuration in each table is listed in boldface.

Table 6.4-1 – NCT Single Package Results

Case ID	Filename	H/X	k	σ	k_s (k+2σ)
325 g Pu-239, 0 g Pu-240					
A1	ns_0g240_x0500	500	0.89611	0.00125	0.89861
A2	ns_0g240_x0600	600	0.91240	0.00126	0.91492
A3	ns_0g240_x0700	700	0.92548	0.00111	0.92770
A4	ns_0g240_x0800	800	0.93000	0.00124	0.93248
A5	**ns_0g240_x0900**	**900**	**0.93101**	**0.00114**	**0.93329**
A6	ns_0g240_x1000	1000	0.92669	0.00112	0.92893
A7	ns_0g240_x1100	1100	0.92192	0.00110	0.92412
A8	ns_0g240_x1200	1200	0.91987	0.00103	0.92193
A9	ns_0g240_x1300	1300	0.91286	0.00105	0.91496
A10	ns_0g240_x1400	1400	0.90661	0.00098	0.90857
A11	ns_0g240_x0900p	900	0.92674	0.00113	0.92900
A12	ns_0g240_x0900p_long	900	0.92786	0.00053	0.92892
A13	ns_0g240_x0900_long	900	0.92801	0.00050	0.92901
340 g Pu-239, 5 g Pu-240					
A21	ns_5g240_x0500	500	0.89458	0.00124	0.89706
A22	ns_5g240_x0600	600	0.91409	0.00122	0.91653
A23	ns_5g240_x0700	700	0.92270	0.00124	0.92518
A24	ns_5g240_x0800	800	0.92997	0.00116	0.93229
A25	**ns_5g240_x0900**	**900**	**0.93136**	**0.00109**	**0.93354**
A26	ns_5g240_x1000	1000	0.92922	0.00111	0.93144
A27	ns_5g240_x1100	1100	0.92648	0.00114	0.92876
A28	ns_5g240_x1200	1200	0.92055	0.00107	0.92269
A29	ns_5g240_x1300	1300	0.91337	0.00111	0.91559
A30	ns_5g240_x1400	1400	0.90735	0.00104	0.90943
360 g Pu-239, 15 g Pu-240					
A31	ns_15g240_x0500	500	0.89349	0.00126	0.89601
A32	ns_15g240_x0600	600	0.91135	0.00117	0.91369
A33	ns_15g240_x0700	700	0.92150	0.00123	0.92396
A34	ns_15g240_x0800	800	0.92647	0.00118	0.92883
A35	**ns_15g240_x0900**	**900**	**0.92943**	**0.00111**	**0.93165**
A36	ns_15g240_x1000	1000	0.92865	0.00113	0.93091
A37	ns_15g240_x1100	1100	0.92556	0.00111	0.92778
A38	ns_15g240_x1200	1200	0.92121	0.00109	0.92339
A39	ns_15g240_x1300	1300	0.91752	0.00099	0.91950
A40	ns_15g240_x1400	1400	0.91014	0.00100	0.91214

(continued)

Table 6.4-1 – NCT Single Package Results (concluded)

Case ID	Filename	H/X	k	σ	k_s (k+2σ)
380 g Pu-239, 25 g Pu-240					
A41	ns_25g240_x0500	500	0.89015	0.00128	0.89271
A42	ns_25g240_x0600	600	0.90726	0.00123	0.90972
A43	ns_25g240_x0700	700	0.92172	0.00116	0.92404
A44	ns_25g240_x0800	800	0.92644	0.00117	0.92878
A45	**ns_25g240_x0900**	**900**	**0.92966**	**0.00112**	**0.93190**
A46	ns_25g240_x1000	1000	0.92686	0.00118	0.92922
A47	ns_25g240_x1100	1100	0.92833	0.00110	0.93053
A48	ns_25g240_x1200	1200	0.92250	0.00105	0.92460
A49	ns_25g240_x1300	1300	0.91759	0.00104	0.91967
A50	ns_25g240_x1400	1400	0.91194	0.00106	0.91406

Table 6.4-2 – HAC Single Package Results

Case ID	Filename	H/X	k	σ	k_s (k+2σ)
325 g Pu-239, 0 g Pu-240					
B1	hs_0g240_x0500	500	0.89611	0.00125	0.89861
B2	hs_0g240_x0600	600	0.91240	0.00126	0.91492
B3	hs_0g240_x0700	700	0.92548	0.00111	0.92770
B4	hs_0g240_x0800	800	0.93000	0.00124	0.93248
B5	**hs_0g240_x0900**	**900**	**0.93101**	**0.00114**	**0.93329**
B6	hs_0g240_x1000	1000	0.92669	0.00112	0.92893
B7	hs_0g240_x1100	1100	0.92192	0.00110	0.92412
B8	hs_0g240_x1200	1200	0.91987	0.00103	0.92193
B9	hs_0g240_x1300	1300	0.91286	0.00105	0.91496
B10	hs_0g240_x1400	1400	0.90661	0.00098	0.90857
340 g Pu-239, 5 g Pu-240					
B11	hs_5g240_x0500	500	0.89458	0.00124	0.89706
B12	hs_5g240_x0600	600	0.91409	0.00122	0.91653
B13	hs_5g240_x0700	700	0.92270	0.00124	0.92518
B14	hs_5g240_x0800	800	0.92997	0.00116	0.93229
B15	**hs_5g240_x0900**	**900**	**0.93136**	**0.00109**	**0.93354**
B16	hs_5g240_x1000	1000	0.92922	0.00111	0.93144
B17	hs_5g240_x1100	1100	0.92648	0.00114	0.92876
B18	hs_5g240_x1200	1200	0.92055	0.00107	0.92269
B19	hs_5g240_x1300	1300	0.91337	0.00111	0.91559
B20	hs_5g240_x1400	1400	0.90735	0.00104	0.90943
360 g Pu-239, 15 g Pu-240					
B21	hs_15g240_x0500	500	0.89349	0.00126	0.89601
B22	hs_15g240_x0600	600	0.91135	0.00117	0.91369
B23	hs_15g240_x0700	700	0.92150	0.00123	0.92396
B24	hs_15g240_x0800	800	0.92647	0.00118	0.92883
B25	**hs_15g240_x0900**	**900**	**0.92943**	**0.00111**	**0.93165**
B26	hs_15g240_x1000	1000	0.92865	0.00113	0.93091
B27	hs_15g240_x1100	1100	0.92556	0.00111	0.92778
B28	hs_15g240_x1200	1200	0.92121	0.00109	0.92339
B29	hs_15g240_x1300	1300	0.91752	0.00099	0.91950
B30	hs_15g240_x1400	1400	0.91014	0.00100	0.91214
380 g Pu-239, 25 g Pu-240					
B31	hs_25g240_x0500	500	0.89015	0.00128	0.89271
B32	hs_25g240_x0600	600	0.90726	0.00123	0.90972
B33	hs_25g240_x0700	700	0.92172	0.00116	0.92404
B34	hs_25g240_x0800	800	0.92644	0.00117	0.92878
B35	**hs_25g240_x0900**	**900**	**0.92966**	**0.00112**	**0.93190**
B36	hs_25g240_x1000	1000	0.92686	0.00118	0.92922
B37	hs_25g240_x1100	1100	0.92833	0.00110	0.93053
B38	hs_25g240_x1200	1200	0.92250	0.00105	0.92460
B39	hs_25g240_x1300	1300	0.91759	0.00104	0.91967
B40	hs_25g240_x1400	1400	0.91194	0.00106	0.91406

This page intentionally left blank.

6.5 Evaluation of Package Arrays under Normal Conditions of Transport

6.5.1 Configuration

It is established in the HAC array analysis (Section 6.6) that the most reactive array configuration is with full density internal reflector and the fissile sphere in the center of the cavity. This configuration minimizes neutronic communication between packages. Because the NCT and HAC package geometry is very similar, this conclusion is also valid for the NCT array configuration. Therefore, it is sufficient to simply infinitely reflect the NCT single package models by removing the external water reflection and changing the six outer package surfaces to be reflective (i.e., mirror boundary condition). A series of cases is executed for each of the four FGE limits of interest over a range of H/X from 500 through 1400.

The results are provided in Table 6.5-1. The results are identical to the single package results, indicating that each package is essentially isolated from adjacent packages. Case C15 is the most reactive case, with $k_s = 0.93354$. This result is below the USL of 0.9392.

6.5.2 Results

The results for the NCT array cases are provided in the following table. The most reactive configurations are listed in boldface.

Table 6.5-1 – NCT Array Results

Case ID	Filename	H/X	k	σ	k_s (k+2σ)
325 g Pu-239, 0 g Pu-240					
C1	na_0g240_x0500	500	0.89611	0.00125	0.89861
C2	na_0g240_x0600	600	0.91240	0.00126	0.91492
C3	na_0g240_x0700	700	0.92548	0.00111	0.92770
C4	na_0g240_x0800	800	0.93000	0.00124	0.93248
C5	**na_0g240_x0900**	**900**	**0.93101**	**0.00114**	**0.93329**
C6	na_0g240_x1000	1000	0.92669	0.00112	0.92893
C7	na_0g240_x1100	1100	0.92192	0.00110	0.92412
C8	na_0g240_x1200	1200	0.91987	0.00103	0.92193
C9	na_0g240_x1300	1300	0.91286	0.00105	0.91496
C10	na_0g240_x1400	1400	0.90661	0.00098	0.90857
340 g Pu-239, 5 g Pu-240					
C11	na_5g240_x0500	500	0.89458	0.00124	0.89706
C12	na_5g240_x0600	600	0.91409	0.00122	0.91653
C13	na_5g240_x0700	700	0.92270	0.00124	0.92518
C14	na_5g240_x0800	800	0.92997	0.00116	0.93229
C15	**na_5g240_x0900**	**900**	**0.93136**	**0.00109**	**0.93354**
C16	na_5g240_x1000	1000	0.92922	0.00111	0.93144
C17	na_5g240_x1100	1100	0.92648	0.00114	0.92876
C18	na_5g240_x1200	1200	0.92055	0.00107	0.92269
C19	na_5g240_x1300	1300	0.91337	0.00111	0.91559
C20	na_5g240_x1400	1400	0.90735	0.00104	0.90943
360 g Pu-239, 15 g Pu-240					
C21	na_15g240_x0500	500	0.89349	0.00126	0.89601
C22	na_15g240_x0600	600	0.91135	0.00117	0.91369
C23	na_15g240_x0700	700	0.92150	0.00123	0.92396
C24	na_15g240_x0800	800	0.92647	0.00118	0.92883
C25	**na_15g240_x0900**	**900**	**0.92943**	**0.00111**	**0.93165**
C26	na_15g240_x1000	1000	0.92865	0.00113	0.93091
C27	na_15g240_x1100	1100	0.92556	0.00111	0.92778
C28	na_15g240_x1200	1200	0.92121	0.00109	0.92339
C29	na_15g240_x1300	1300	0.91752	0.00099	0.91950
C30	na_15g240_x1400	1400	0.91014	0.00100	0.91214
380 g Pu-239, 25 g Pu-240					
C31	na_25g240_x0500	500	0.89015	0.00128	0.89271
C32	na_25g240_x0600	600	0.90726	0.00123	0.90972
C33	na_25g240_x0700	700	0.92172	0.00116	0.92404
C34	na_25g240_x0800	800	0.92644	0.00117	0.92878
C35	**na_25g240_x0900**	**900**	**0.92966**	**0.00112**	**0.93190**
C36	na_25g240_x1000	1000	0.92686	0.00118	0.92922
C37	na_25g240_x1100	1100	0.92833	0.00110	0.93053
C38	na_25g240_x1200	1200	0.92250	0.00105	0.92460
C39	na_25g240_x1300	1300	0.91759	0.00104	0.91967
C40	na_25g240_x1400	1400	0.91194	0.00106	0.91406

6.6 Package Arrays under Hypothetical Accident Conditions

6.6.1 Configuration

The basic HAC infinite array model is developed by removing the external water reflector from the HAC single package model and changing the six outer package surfaces to be reflective. For the HAC configuration, all of the foam and balsa is replaced with variable density water.

When the package internal reflector is at maximum density, neutronic communication between packages is minimized. If the density of the internal reflector is reduced, more neutrons may escape to interact with fissile material in adjacent packages, although this condition may or may not be more reactive. Reactivity is also influenced by the location of the fissile sphere. If the fissile sphere is in the center of the package, it is unlikely the fissile sphere will interact with the fissile spheres in adjacent packages. Likewise, package to package interactions should be maximized if the fissile sphere is placed in the corner of the cavity, as this configuration effectively models eight fissile spheres in the closest possible proximity. However, placing the fissile sphere closer to the package walls increases parasitic absorption in the steel walls of the package, which tends to reduce the reactivity.

To investigate the effects of reduced internal reflector density and fissile sphere location, nine computational series are performed for the 325 FGE case. The results of the nine computational series are provided in Table 6.6-1 and are summarized below. The most reactive configuration is then utilized for the 340, 360, and 380 FGE analyses.

Series 1 (Cases D1 through D10): Series 1 is simply the infinitely reflected HAC single package case. The fissile sphere is in the center of the package, and all reflecting materials are at full density, including the internal reflector, all water within the package between the steel plates, and the water at the ends of the overpack covers (inside the octagonal regions).

Series 2 (Cases D11 through D20): Series 2 is the same as Series 1, except the water between the steel plates (including the CSA annulus) and water at the ends of the overpack covers are replaced with void. The internal reflector remains at full density. The purpose of this series is to investigate if reducing the hydrogenated material between the packages will increase reactivity by increasing interactions between packages.

Series 3 (Cases D21 through D30): Series 3 is the same as Series 1, except all hydrogenous reflector materials are voided, including the internal reflector. Therefore, the only hydrogenous materials are in the fissile sphere itself. This configuration would maximize package to package interactions.

Comparing Series 1, 2, and 3, the reactivites of Series 1 and 2 are identical. This indicates that the fissile sphere is fully reflected within the CSA cavity, and no neutrons at the package boundary are reflecting back into the fissile sphere. Series 3 is significantly less reactive than Series 1 or 2, although all hydrogenous materials are absent and neutrons are able to interact between adjacent packages.

Series 4 (Cases D31 through D40): Series 4 is the same as Series 1, except the fissile sphere is placed in the corner of the package, near the lid.

Series 5 (Cases D41 through D50): Series 5 is the same as Series 2, except the fissile sphere is placed in the corner of the package, near the lid.

Series 6 (Cases D51 through D60): Series 6 is the same as Series 3, except the fissile sphere is placed in the corner of the package, near the lid.

Comparing Series 4, 5, and 6, Series 4 and 5 are much more reactive than Series 6. Series 4 is slightly more reactive than Series 5, indicating that reflection outweighs package to package interactions when maximizing the reactivity. Series 4 is less reactive than Series 1, indicating that the center of the package is a more reactive location for the fissile sphere than the corner. It is expected that placing the fissile sphere in the corner may increase package to package interactions, but parasitic absorption in the steel components reduces the reactivity.

In Series 7, 8, and 9, a variety of hydrogenous material densities are examined with the fissile sphere in the center of the cavity.

Series 7 (Cases D61 through D70): Series 7 is the same as Series 1, but the densities of all cells containing hydrogenous reflector material are multiplied by 0.1.

Series 8 (Cases D71 through D80): Series 8 is the same as Series 1, but the densities of all cells containing hydrogenous reflector material are multiplied by 0.5.

Series 9 (Cases D81 through D90): Series 9 is the same as Series 1, but the densities of all cells containing hydrogenous reflector material are multiplied by 0.9.

The reactivities of Series 7, 8, and 9 are less than Series 1, although the reduced densities would presumably lead to greater package to package interactions. The reactivity becomes smaller as the density of hydrogenous materials decreases. This result again demonstrates that full-reflection rather than increased package to package interactions maximizes the reactivity.

An additional three miscellaneous cases (Cases D91, D92, and D93) are developed to examine scenarios in which the fissile sphere is in other locations. Full-reflection and H/X = 900 are utilized in these cases. In Case D91, the fissile sphere is placed midway between the corner and the center. K_s is identical between Cases D91 and D5, indicating that the fissile sphere does not need to be in the center of the cavity to be isolated from adjacent packages. In Case D92, the fissile sphere is located in a bottom end corner rather than a lid end corner, although the results are essentially identical (compare with Case D35). In Case D93, the fissile sphere is placed along an edge at the midplane of the package (z = 0), which effectively places four fissile spheres in close proximity. The results are essentially identical to cases with the fissile sphere in a corner.

The most reactive 325 FGE case is Series 1, Case D5, with $k_s = 0.93329$. This result is identical to the single package NCT result (Case A5), single package HAC result (Case B5), and NCT array result (Case C5) for 325 FGE. Although these cases all have slightly different package geometries and boundary conditions, neutronically the cases behave simply as a fissile sphere surrounded by a large reflector.

The Series 1 configuration is repeated for 340, 360, and 380 FGE, and the results are provided in Table 6.6-2. As with the 325 FGE cases, the results are identical to those obtained for the single package and NCT array cases.

Case E5 is the most reactive of all the HAC array cases, with $k_s = 0.93354$. This value is below the USL of 0.9392.

6.6.2 Results

Following are the tabulated results for the HAC array cases. The most reactive configurations in each table are listed in boldface.

Table 6.6-1 – HAC Array Results, 325 FGE

Case ID	Filename	H/X	k	σ	k_s (k+2σ)
Series 1: All hydrogenous materials are at full density, fissile sphere in center.					
D1	ha1_0g240_x0500	500	0.89611	0.00125	0.89861
D2	ha1_0g240_x0600	600	0.91240	0.00126	0.91492
D3	ha1_0g240_x0700	700	0.92548	0.00111	0.92770
D4	ha1_0g240_x0800	800	0.93000	0.00124	0.93248
D5	**ha1_0g240_x0900**	**900**	**0.93101**	**0.00114**	**0.93329**
D6	ha1_0g240_x1000	1000	0.92669	0.00112	0.92893
D7	ha1_0g240_x1100	1100	0.92192	0.00110	0.92412
D8	ha1_0g240_x1200	1200	0.91987	0.00103	0.92193
D9	ha1_0g240_x1300	1300	0.91286	0.00105	0.91496
D10	ha1_0g240_x1400	1400	0.90661	0.00098	0.90857
Series 2: The internal reflector is at full density, but the water between the steel plates (including the CSA annulus) and water at the ends of the overpack covers are replaced with void, fissile sphere in center.					
D11	ha2_0g240_x0500	500	0.89611	0.00125	0.89861
D12	ha2_0g240_x0600	600	0.91240	0.00126	0.91492
D13	ha2_0g240_x0700	700	0.92548	0.00111	0.92770
D14	ha2_0g240_x0800	800	0.93000	0.00124	0.93248
D15	**ha2_0g240_x0900**	**900**	**0.93101**	**0.00114**	**0.93329**
D16	ha2_0g240_x1000	1000	0.92669	0.00112	0.92893
D17	ha2_0g240_x1100	1100	0.92192	0.00110	0.92412
D18	ha2_0g240_x1200	1200	0.91987	0.00103	0.92193
D19	ha2_0g240_x1300	1300	0.91286	0.00105	0.91496
D20	ha2_0g240_x1400	1400	0.90661	0.00098	0.90857
Series 3: All hydrogenous reflector materials are voided, including the internal reflector, fissile sphere in center.					
D21	ha3_0g240_x0900	900	0.78658	0.00125	0.78908
D22	ha3_0g240_x1000	1000	0.79330	0.00115	0.79560
D23	ha3_0g240_x1100	1100	0.79903	0.00115	0.80133
D24	ha3_0g240_x1200	1200	0.80269	0.00114	0.80497
D25	**ha3_0g240_x1300**	**1300**	**0.80333**	**0.00111**	**0.80555**
D26	ha3_0g240_x1400	1400	0.80259	0.00107	0.80473
D27	ha3_0g240_x1500	1500	0.80154	0.00110	0.80374
D28	ha3_0g240_x1600	1600	0.79811	0.00101	0.80013
D29	ha3_0g240_x1700	1700	0.79598	0.00102	0.79802
D30	ha3_0g240_x1800	1800	0.79243	0.00097	0.79437

(continued)

Table 6.6-1 – HAC Array Results, 325 FGE

Case ID	Filename	H/X	k	σ	k_s (k+2σ)
Series 4: Same as Series 1, but with the fissile sphere in the corner.					
D31	ha4_0g240_x0500	500	0.88528	0.00124	0.88776
D32	ha4_0g240_x0600	600	0.90186	0.00120	0.90426
D33	ha4_0g240_x0700	700	0.91165	0.00118	0.91401
D34	ha4_0g240_x0800	800	0.91947	0.00118	0.92183
D35	**ha4_0g240_x0900**	**900**	**0.92013**	**0.00122**	**0.92257**
D36	ha4_0g240_x1000	1000	0.91989	0.00107	0.92203
D37	ha4_0g240_x1100	1100	0.91593	0.00106	0.91805
D38	ha4_0g240_x1200	1200	0.91322	0.00106	0.91534
D39	ha4_0g240_x1300	1300	0.90792	0.00111	0.91014
D40	ha4_0g240_x1400	1400	0.90049	0.00103	0.90255
Series 5: Same as Series 2, but with the fissile sphere in the corner.					
D41	ha5_0g240_x0500	500	0.86906	0.00124	0.87154
D42	ha5_0g240_x0600	600	0.89055	0.00126	0.89307
D43	ha5_0g240_x0700	700	0.90030	0.00118	0.90266
D44	ha5_0g240_x0800	800	0.90891	0.00122	0.91135
D45	ha5_0g240_x0900	900	0.91227	0.00115	0.91457
D46	**ha5_0g240_x1000**	**1000**	**0.91320**	**0.00116**	**0.91552**
D47	ha5_0g240_x1100	1100	0.91099	0.00109	0.91317
D48	ha5_0g240_x1200	1200	0.90539	0.00115	0.90769
D49	ha5_0g240_x1300	1300	0.90191	0.00108	0.90407
D50	ha5_0g240_x1400	1400	0.89597	0.00095	0.89787
Series 6: Same as Series 3, but with the fissile sphere in the corner.					
D51	ha6_0g240_x0900	900	0.81255	0.00121	0.81497
D52	ha6_0g240_x1000	1000	0.81993	0.00114	0.82221
D53	ha6_0g240_x1100	1100	0.82386	0.00120	0.82626
D54	ha6_0g240_x1200	1200	0.82417	0.00109	0.82635
D55	**ha6_0g240_x1300**	**1300**	**0.82757**	**0.00107**	**0.82971**
D56	ha6_0g240_x1400	1400	0.82444	0.00107	0.82658
D57	ha6_0g240_x1500	1500	0.82249	0.00110	0.82469
D58	ha6_0g240_x1600	1600	0.81590	0.00101	0.81792
D59	ha6_0g240_x1700	1700	0.81477	0.00097	0.81671
D60	ha6_0g240_x1800	1800	0.80818	0.00097	0.81012

(continued)

Table 6.6-1 – HAC Array Results, 325 FGE (concluded)

Case ID	Filename	H/X	k	σ	k_s (k+2σ)
Series 7: Same as Series 1, but the densities of all cells containing hydrogenous reflector material are multiplied by 0.1.					
D61	ha7_0g240_x0900	900	0.79687	0.00117	0.79921
D62	ha7_0g240_x1000	1000	0.80488	0.00125	0.80738
D63	ha7_0g240_x1100	1100	0.80883	0.00118	0.81119
D64	**ha7_0g240_x1200**	**1200**	**0.81085**	**0.00121**	**0.81327**
D65	ha7_0g240_x1300	1300	0.81091	0.00110	0.81311
D66	ha7_0g240_x1400	1400	0.80962	0.00113	0.81188
D67	ha7_0g240_x1500	1500	0.80756	0.00107	0.80970
D68	ha7_0g240_x1600	1600	0.80840	0.00103	0.81046
D69	ha7_0g240_x1700	1700	0.80257	0.00104	0.80465
D70	ha7_0g240_x1800	1800	0.79840	0.00100	0.80040
Series 8: Same as Series 1, but the densities of all cells containing hydrogenous reflector material are multiplied by 0.5.					
D71	ha8_0g240_x0500	500	0.83681	0.00135	0.83951
D72	ha8_0g240_x0600	600	0.85899	0.00120	0.86139
D73	ha8_0g240_x0700	700	0.87490	0.00123	0.87736
D74	ha8_0g240_x0800	800	0.88071	0.00120	0.88311
D75	ha8_0g240_x0900	900	0.88630	0.00124	0.88878
D76	ha8_0g240_x1000	1000	0.89035	0.00117	0.89269
D77	**ha8_0g240_x1100**	**1100**	**0.89127**	**0.00109**	**0.89345**
D78	ha8_0g240_x1200	1200	0.88734	0.00106	0.88946
D79	ha8_0g240_x1300	1300	0.88319	0.00107	0.88533
D80	ha8_0g240_x1400	1400	0.88007	0.00108	0.88223
Series 9: Same as Series 1, but the densities of all cells containing hydrogenous reflector material are multiplied by 0.9.					
D81	ha9_0g240_x0500	500	0.88810	0.00120	0.89050
D82	ha9_0g240_x0600	600	0.90529	0.00122	0.90773
D83	ha9_0g240_x0700	700	0.91734	0.00118	0.91970
D84	ha9_0g240_x0800	800	0.92253	0.00116	0.92485
D85	**ha9_0g240_x0900**	**900**	**0.92303**	**0.00117**	**0.92537**
D86	ha9_0g240_x1000	1000	0.92118	0.00109	0.92336
D87	ha9_0g240_x1100	1100	0.91848	0.00108	0.92064
D88	ha9_0g240_x1200	1200	0.91604	0.00109	0.91822
D89	ha9_0g240_x1300	1300	0.90980	0.00104	0.91188
D90	ha9_0g240_x1400	1400	0.90314	0.00103	0.90520
Miscellaneous					
D91	ha10_0g240_x0900_p1	900	0.93101	0.00114	0.93329
D92	ha10_0g240_x0900_p2	900	0.92125	0.00118	0.92361
D93	ha10_0g240_x0900_p3	900	0.92221	0.00109	0.92439

Table 6.6-2 – HAC Array Results (340, 360, 380 FGE)

Case ID	Filename	H/X	k	σ	k_s (k+2σ)
340 g Pu-239, 5 g Pu-240					
E1	ha_5g240_x0500	500	0.89458	0.00124	0.89706
E2	ha_5g240_x0600	600	0.91409	0.00122	0.91653
E3	ha_5g240_x0700	700	0.92270	0.00124	0.92518
E4	ha_5g240_x0800	800	0.92997	0.00116	0.93229
E5	**ha_5g240_x0900**	**900**	**0.93136**	**0.00109**	**0.93354**
E6	ha_5g240_x1000	1000	0.92922	0.00111	0.93144
E7	ha_5g240_x1100	1100	0.92648	0.00114	0.92876
E8	ha_5g240_x1200	1200	0.92055	0.00107	0.92269
E9	ha_5g240_x1300	1300	0.91337	0.00111	0.91559
E10	ha_5g240_x1400	1400	0.90735	0.00104	0.90943
360 g Pu-239, 15 g Pu-240					
E11	ha_15g240_x0500	500	0.89349	0.00126	0.89601
E12	ha_15g240_x0600	600	0.91135	0.00117	0.91369
E13	ha_15g240_x0700	700	0.92150	0.00123	0.92396
E14	ha_15g240_x0800	800	0.92647	0.00118	0.92883
E15	**ha_15g240_x0900**	**900**	**0.92943**	**0.00111**	**0.93165**
E16	ha_15g240_x1000	1000	0.92865	0.00113	0.93091
E17	ha_15g240_x1100	1100	0.92556	0.00111	0.92778
E18	ha_15g240_x1200	1200	0.92121	0.00109	0.92339
E19	ha_15g240_x1300	1300	0.91752	0.00099	0.91950
E20	ha_15g240_x1400	1400	0.91014	0.00100	0.91214
380 g Pu-239, 25 g Pu-240					
E21	ha_25g240_x0500	500	0.89015	0.00128	0.89271
E22	ha_25g240_x0600	600	0.90726	0.00123	0.90972
E23	ha_25g240_x0700	700	0.92172	0.00116	0.92404
E24	ha_25g240_x0800	800	0.92644	0.00117	0.92878
E25	**ha_25g240_x0900**	**900**	**0.92966**	**0.00112**	**0.93190**
E26	ha_25g240_x1000	1000	0.92686	0.00118	0.92922
E27	ha_25g240_x1100	1100	0.92833	0.00110	0.93053
E28	ha_25g240_x1200	1200	0.92250	0.00105	0.92460
E29	ha_25g240_x1300	1300	0.91759	0.00104	0.91967
E30	ha_25g240_x1400	1400	0.91194	0.00106	0.91406

6.7 Fissile Material Packages for Air Transport

This section does not apply for the TRUPACT–III package, because air transport is not claimed.

This page intentionally left blank.

6.8 Benchmark Evaluations

The Monte Carlo computer program MCNP5 v1.30 is utilized for this benchmark analysis. MCNP has been used extensively in criticality evaluations for several decades and is considered a standard in the industry.

ENDF/B-VI cross sections are used for most isotopes, although ENDF/B-V elemental cross sections are utilized when ENDF/B-VI elemental cross sections are not available. Also, the Pu-239 cross sections represent a preliminary version of the ENDF/B-VII cross section set. Although the ENDF/B-VII cross section set had not been formally released with MCNP5 v1.30, LANL included this Pu-239 cross section because it showed significant improvements compared to the latest ENDF/B-VI Pu-239 cross section for certain LANL benchmark models. All cross sections utilized are at room temperature. A listing of the cross section libraries used in the TRUPACT–III analysis is provided in Table 6.3-5. These cross sections are consistent with the cross sections utilized in the benchmarks.

The ORNL USLSTATS code[1] is used to establish a USL for the analysis. USLSTATS provides a simple means of evaluating and combining the statistical error of the calculation, code biases and benchmark uncertainties. The USLSTATS calculation uses the combined uncertainties and data to provide a linear trend and an overall uncertainty. Computed multiplication factors, k_{eff}, for the package are deemed to be adequately subcritical if the computed value of k_s is less than or equal to the USL as follows:

$$k_s = k_{eff} + 2\sigma \leq USL$$

The USL includes the combined effects of code bias, uncertainty in the benchmark experiments, uncertainty in the computational evaluation of the benchmark experiments, and an administrative margin. This methodology has accepted precedence in establishing criticality safety limits for transportation packages complying with 10 CFR 71.

6.8.1 Applicability of Benchmark Experiments

The critical experiment benchmarks are selected from the International Handbook of Evaluated Criticality Safety Benchmark Experiments[2] based upon their similarity to the TRUPACT–III package and contents. The important parameters of the package configuration are homogeneous mixtures of plutonium, water and/or polyethylene. Benchmark experiments that utilize plutonium solutions with beryllium reflectors are also desired because the TRUPACT–III may contain up to 1% beryllium by weight.

Two-hundred (200) plutonium solution benchmarks are selected from the Handbook[3]. No thermal benchmarks that utilize plutonium with beryllium reflectors are available, although U-233/beryllium benchmarks are described in U233-SOL-THERM-015. Note that four of the 31

[1] USLSTATS, *USLSTATS: A Utility To Calculate Upper Subcritical Limits For Criticality Safety Applications,* Version 1.4.2, Oak Ridge National Laboratory, April 23, 2003.

[2] *International Handbook of Evaluated Criticality Safety Benchmark Experiments*, Nuclear Energy Agency, NEA/NSC/DOC(95)03, September 2004.

[3] Note that PU–SOL–THERM–024, Case 6, is not included in the benchmark evaluation because the EALF for this case is an order of magnitude higher than the other plutonium cases.

U-233 benchmarks from U233-SOL-THERM-015 are rejected because there is no beryllium present in these cases. Therefore, twenty-seven (27) U-233 benchmarks are selected that utilize beryllium reflectors, for a total of 227 benchmark experiments. The titles for all utilized experiments are listed in Table 6.8-1.

Care must be exercised in the application of the U-233/beryllium benchmarks because the introduction of U-233 cross sections introduces a new source of uncertainty. The uncertainties added by including the U-233 benchmarks are evaluated by examining 70 U-233 benchmarks that do not use beryllium reflectors. These additional benchmarks, however, are not considered part of the TRUPACT–III benchmark set. Note that the four benchmarks rejected from U233-SOL-THERM-015 because they did not contain beryllium are included in this set. The titles for all U-233 experiments that do not utilize beryllium are also included in Table 6.8-1.

6.8.2 Bias Determination

The USL is calculated by application of the USLSTATS computer program. USLSTATS receives as input the k_{eff} as calculated by MCNP, the total 1-σ uncertainty (combined benchmark and MCNP uncertainties), and a trending parameter. Three trending parameters have been selected: (1) H/fissile atom ratio (abbreviated as H/X), (2) Pu240/Pu ratio, and (3) Energy of the Average neutron Lethargy causing Fission (EALF).

The only trending parameter used for both the plutonium and U-233 benchmarks is EALF. The U-233 benchmarks are not considered when trending with respect to H/X as the optimum H/X range will be significantly different for a U-233 system vs. a plutonium system. Also, the U-233 benchmarks are not considered when trending with the Pu240/Pu parameter, as this parameter has no meaning for the U-233 benchmarks.

The uncertainty value, σ_{total}, assigned to each case is a combination of the benchmark uncertainty for each experiment, σ_{bench}, and the Monte Carlo uncertainty associated with the particular computational evaluation of the case, σ_{MCNP}, or:

$$\sigma_{total} = (\sigma_{bench}^2 + \sigma_{MCNP}^2)^{½}$$

These values are input into the USLSTATS program in addition to the following parameters, which are the values recommended by the USLSTATS user's manual[4]:

- P, proportion of population falling above lower tolerance level = 0.995 (note that this parameter is required input but is not utilized in the calculation of USL Method 1)
- α, confidence on proportion P = 0.95 (note that this parameter is required input but is not utilized in the calculation of USL Method 1)
- 1-γ, confidence on fit = 0.95
- Δk_m, administrative margin used to ensure subcriticality = 0.05.

These data are followed by triplets of trending parameter value, computed k_{eff}, and uncertainty for each case. The USL Method 1 performs a confidence band analysis on the data for the

[4] USLSTATS is described in Appendix C, *User's Manual for USLSTATS V1.0*, in NUREG/CR-6361 *Criticality Benchmark Guide for Light-Water-Reactor Fuel in Transportation and Storage Packages*, March 1997.

trending parameter. The USL generated for each of the three trending parameters utilized is provided in Table 6.8-2. Note that several different trending analyses are performed for the EALF parameter in order to determine which benchmarks are dominating the USL computation for this parameter. The application of these equations in the determination of the USL is discussed in the following section. All benchmark data used as input to USLSTATS are reported in Table 6.8-3 for the plutonium benchmarks, Table 6.8-4 for the U-233/Be benchmarks, and Table 6.8-5 for the U-233/no Be benchmarks.

H/X

The ratio of the hydrogen number density (H) to the fissile number density (X) is used as the first trending parameter. Only the 200 plutonium benchmarks are utilized for this parameter. Both Pu-239 and Pu-241 are summed to determine the value of X for each experiment, although the Pu-241 number densities in the experiments are negligible. The USL1 value is a constant value of 0.9392 over the entire range. When the data is plotted, as shown in Figure 6.8-1, $R^2 = 0.0368$, indicating essentially no correlation between this variable and the calculated benchmark results.

The TRUPACT–III cases have an H/X range from 500 to 1800, which is within the range of the benchmark experiments.

Pu-240/Pu

Pu-240 weight fraction within the Pu is used as the second trending parameter. Only the 200 plutonium benchmarks are utilized for this parameter. The USL1 value is a constant value of 0.9396 over the entire range. When the data is plotted, as shown in Figure 6.8-2, $R^2 = 0.0038$, indicating essentially no correlation between this variable and the calculated benchmark results.

The TRUPACT–III cases utilize three discreet Pu-240/Pu ratios, 5/345 = 0.014, 15/375 = 0.04, and 25/405 = 0.062. These three ratios fall within the range of the benchmark experiments.

Energy of Average Lethargy of Fission (EALF)

The EALF is used as the third trending parameter for the benchmark cases. The EALF comparison provides a means to observe neutron spectral dependencies or trends. This parameter is examined for several different combinations of benchmark experiments to determine which benchmarks are dominating the USL computation for this parameter.

All 227 benchmark experiments are utilized in the first study (EALF1). When the data is plotted, as shown in Figure 6.8-3, $R^2 = 0.5319$, indicating high correlation between this variable and the calculated benchmark results. However, this correlation exists only for EALF values above 3.5×10^{-7} MeV. At the high end of the energy range, the USL = 0.9171, which is a low result. However, for EALF values below 3.5×10^{-7} MeV, the USL is a constant value of 0.9385. Examining the EALF data shown in Table 6.8-3 and Table 6.8-4, it is apparent that many of the U-233 benchmarks have a higher EALF than the plutonium benchmarks. Also, as several of the U-233 benchmarks have k_{eff} as low as ~0.97, the U-233 benchmarks depress the USL at the higher energy range.

When the EALF trending is performed for only the 200 plutonium benchmarks (EALF2), the USL over the entire energy range is a constant 0.9396. Conversely, when the EALF trending is performed for only the 27 U-233 benchmarks (EALF3), the trending is again poor, with a minimum USL of 0.9136.

Clearly, the U-233/Be benchmarks are distorting the EALF results. There may be a number of reasons for the poor U-233/Be benchmark results, including: (1) uncertainties in the U-233 cross sections, (2) uncertainties in the beryllium cross sections, or (3) experimental errors. To examine the bias in the U-233 cross sections, an additional 70 U-233 benchmark experiments are developed that do not use beryllium. These cases are summarized in Table 6.8-5. Note that six of these benchmarks are intermediate spectrum benchmarks rather than thermal benchmarks, which is desirable because the experiments with harder spectra tend to have more inaccurate results. The percentages of fissions caused by thermal, intermediate, and fast neutrons are also included in the tables to further demonstrate the different spectrum of the U-233 cases.

When the EALF trending is performed for the 70 U-233 benchmarks without beryllium (EALF4), the trending is worse than case EALF1, with a minimum USL of 0.9028. Based on these results, it may be concluded that the U-233 cross sections have large uncertainties in the intermediate energy range that result in low values of k_{eff} for many of these benchmarks. In the thermal energy range, the U-233 cross sections appear to be acceptable.

Because the EALF1 result is biased by poor U-233 cross sections unrelated to the TRUPACT–III analysis, the U-233/Be benchmarks are screened to exclude any benchmark experiment with an EALF > 5×10^{-7} MeV, which excludes 15 of the U-233/Be cases with a harder spectra. When the EALF trending is performed for this reduced set of 212 "highly thermalized" benchmarks (EALF5), the USL is a constant value of 0.9393 over the entire energy range. When the data is plotted, as shown in Figure 6.8-4, $R^2 = 0.0096$, indicating essentially no correlation between EALF and the calculated benchmark results for the "highly thermalized" data set.

The TRUPACT–III models have EALF values of approximately 5×10^{-8} MeV, which is within the range of the benchmark experiments.

Recommended USL

The USL for H/X is a constant value of 0.9392, and the USL for Pu240/Pu is a constant value of 0.9396. For the EALF parameter, only the EALF2 (0.9396) and EALF5 (0.9393) results are applicable because the EALF1 and EALF3 results are biased by poor U-233 cross sections. Comparing these USL values, the minimum USL of 0.9392 is selected for the analysis. The selected USL is applicable over the parameter ranges of 4.1×10^{-8} MeV $\leq$ EALF $\leq 4.7 \times 10^{-7}$ MeV, $91 \leq H/X \leq 2800$, and $0.005 \leq Pu240/Pu \leq 0.23$.

Table 6.8-1 – Benchmark Experiments Utilized

Series	Title
Pu Benchmarks (including U-233 Benchmarks with Beryllium)	
PU-SOL-THERM-001	Water-Reflected 11.5-Inch Diameter Spheres Of Plutonium Nitrate Solutions
PU-SOL-THERM-002	Water-Reflected 12-Inch Diameter Spheres Of Plutonium Nitrate Solutions
PU-SOL-THERM-003	Water-Reflected 13-Inch Diameter Spheres Of Plutonium Nitrate Solutions
PU-SOL-THERM-004	Water-Reflected 14-Inch Diameter Spheres Of Plutonium Nitrate Solutions 0.54% To 3.43% Pu240
PU-SOL-THERM-005	Water-Reflected 14-Inch Diameter Spheres Of Plutonium Nitrate Solutions 4.05% And 4.40% Pu240
PU-SOL-THERM-006	Water-Reflected 15-Inch Diameter Spheres Of Plutonium Nitrate Solutions
PU-SOL-THERM-007	Water-Reflected 11.5-Inch Diameter Spheres Partly Filled with Plutonium Nitrate Solutions
PU-SOL-THERM-009	Unreflected 48-Inch-Diameter Sphere Of Plutonium Nitrate Solution
PU-SOL-THERM-010	Water-Reflected 9-, 10-, 11-, And 12-Inch-Diameter Cylinders Of Plutonium Nitrate Solutions
PU-SOL-THERM-011	Bare 16- And 18-Inch-Diameter Spheres Of Plutonium Nitrate Solutions
PU-SOL-THERM-014	Interacting Cylinders of 300-mm Diameter Spheres of Plutonium Nitrate Solution (115.1gPu/L) in Air
PU-SOL-THERM-015	Interacting Cylinders of 300-mm Diameter with Plutonium Nitrate Solution (152.5gPu/L) in Air
PU-SOL-THERM-016	Interacting Cylinders of 300-mm and 256-mm Diameters with Plutonium Nitrate Solution (152.5 and 115.1 gPu/L) and Nitric Acid (2n) in Air
PU-SOL-THERM-017	Interacting Cylinders of 256-mm and 300-mm Diameters with Plutonium Nitrate Solution (115.1 gPu/L) in Air
PU-SOL-THERM-020	Water-Reflected and Water-Cadmium Reflected 14-inch Diameter Spheres of Plutonium Nitrate Solutions
PU-SOL-THERM-021	Water-Reflected and Bare 15.2-inch Diameter Spheres of Plutonium Nitrate Solutions
PU-SOL-THERM-024	Slabs of Plutonium Nitrate Solutions Reflected by 1-inch Thick Plexiglas
U233-SOL-THERM-015	Uranyl-Fluoride (^{233}U) Solutions in Spherical Stainless Steel Vessels with Reflectors of Be, CH_2, and Be-CH_2 Composites – Part II (Excluding Cases 7, 10, 17, and 25)
U-233 Benchmarks Without Beryllium	
U233-SOL-THERM-001	Unreflected Spheres of ^{233}U Nitrate Solutions
U233-SOL-THERM-003	Paraffin-Reflected 5-, 5.4-, 6-, 6.6-, 7.5-, 8-, 8.5-, 9-, and 12-inch Diameter Cylinders of ^{233}U Uranyl Fluoride Solutions
U233-SOL-THERM-012	Water-Reflected Spherical Vessels Partially Filled or Filled with $^{233}UO_2(NO_3)_2$ Solution
U233-SOL-THERM-013	Unreflected Spherical Vessels Partially Filled or Filled with $^{233}UO_2(NO_3)_2$ Solution
U233-SOL-THERM-014	Lucite-Moderated and Unmoderated, Reflected and Non-Reflected Arrays of Bottles Containing Uranyl Nitrate (98.2 wt.% ^{233}U) solution.
U233-SOL-THERM-015	Uranyl-Fluoride (^{233}U) Solutions in Spherical Stainless Steel Vessels with Reflectors of Be, CH_2, and Be-CH_2 Composites – Part II (Cases 7, 10, 17, and 25)
U233-SOL-INTER-001	Uranyl-Fluoride (^{233}U) Solutions in Spherical Stainless Steel Vessels with Reflectors of Be, CH_2, and Be-CH_2 Composites – Part I

Table 6.8-2 – USL Trending Equations

Trending Parameter (P)	USL equation	Minimum USL Over Range of Applicability	Range of Applicability
H/X (200 Pu benchmarks)	0.9392	0.9392	90.899 ≤ P ≤ 2800.6
Pu240/Pu (200 Pu benchmarks)	0.9396	0.9396	4.95000E-3 ≤ P ≤ 0.23200
EALF1 (200 Pu and 27 U-233/Be benchmarks)	0.9385 0.9449 - 1.8443E+4*P	0.9385 0.9171	4.07630E-8 ≤ P ≤ 3.49827E-7 3.49827E-7 < P ≤ 1.51290E-6
EALF2 (200 Pu benchmarks)	0.9396	0.9396	4.07630E-8 ≤ P ≤ 4.65100E-7
EALF3 (27 U-233/Be benchmarks)	0.9355 - 1.4523E+4*P	0.9136	1.27400E-7 ≤ P ≤ 1.51290E-6
EALF4 (70 U-233/no Be benchmarks)	0.9273 0.9330 - 6.3995E+3*P	0.9273 0.9028	3.94770E-8 ≤ P ≤ 8.83898E-7 8.83898E-7< P ≤ 4.70670E-6
EALF5 (212 highly thermal Pu and U-233/Be benchmarks)	0.9393	0.9393	4.07630E-8 ≤ P ≤ 4.69400E-7

Table 6.8-3 – Plutonium Benchmark Experiment Data

No.	Filename	Thermal (<0.635 eV)	Inter (>0.635 eV, <100 KeV)	Fast (>100 KeV)	EALF (MeV)	H/X	Pu240/Pu	k_{eff}	σ MCNP	σ bench	σ total
1	pust001_c01	94.32%	5.02%	0.66%	8.736E-08	370.2	0.0465	1.00368	0.00103	0.0050	0.0051
2	pust001_c02	92.56%	6.53%	0.91%	1.107E-07	270.7	0.0465	1.00549	0.00103	0.0050	0.0051
3	pust001_c03	91.08%	7.81%	1.12%	1.335E-07	215.2	0.0465	1.00707	0.00102	0.0050	0.0051
4	pust001_c04	89.99%	8.77%	1.24%	1.503E-07	189.8	0.0465	0.99970	0.00098	0.0050	0.0051
5	pust001_c05	89.56%	9.13%	1.32%	1.582E-07	179.6	0.0465	1.00317	0.00103	0.0050	0.0051
6	pust001_c06	81.77%	15.69%	2.54%	3.464E-07	90.9	0.0465	1.00610	0.00099	0.0050	0.0051
7	pust002_c01	95.71%	3.81%	0.48%	7.080E-08	524.3	0.0311	1.00302	0.00098	0.0047	0.0048
8	pust002_c02	95.55%	3.96%	0.49%	7.236E-08	504.9	0.0311	1.00363	0.00096	0.0047	0.0048
9	pust002_c03	95.15%	4.30%	0.55%	7.730E-08	451.3	0.0311	1.00146	0.00099	0.0047	0.0048
10	pust002_c04	94.90%	4.51%	0.59%	8.064E-08	420.5	0.0311	1.00434	0.00097	0.0047	0.0048
11	pust002_c05	94.59%	4.78%	0.62%	8.432E-08	392.8	0.0311	1.00539	0.00103	0.0047	0.0048
12	pust002_c06	93.95%	5.35%	0.71%	9.228E-08	344.2	0.0311	1.00264	0.00097	0.0047	0.0048
13	pust002_c07	93.38%	5.84%	0.78%	9.965E-08	308.9	0.0311	1.00594	0.00098	0.0047	0.0048
14	pust003_c01	96.92%	2.75%	0.32%	5.778E-08	788.0	0.0175	1.00219	0.00091	0.0047	0.0048
15	pust003_c02	96.80%	2.85%	0.35%	5.905E-08	756.0	0.0175	1.00360	0.00090	0.0047	0.0048
16	pust003_c03	96.57%	3.05%	0.38%	6.149E-08	698.9	0.0311	1.00496	0.00088	0.0047	0.0048
17	pust003_c04	96.53%	3.09%	0.38%	6.226E-08	681.7	0.0311	1.00090	0.00094	0.0047	0.0048
18	pust003_c05	96.26%	3.33%	0.41%	6.484E-08	626.6	0.0311	1.00589	0.00094	0.0047	0.0048
19	pust003_c06	95.99%	3.57%	0.45%	6.861E-08	562.8	0.0311	1.00609	0.00095	0.0047	0.0048
20	pust003_c07	96.81%	2.83%	0.35%	5.877E-08	737.8	0.0311	1.00456	0.00094	0.0047	0.0048
21	pust003_c08	96.73%	2.91%	0.36%	5.950E-08	714.3	0.0311	1.00608	0.00095	0.0047	0.0048
22	pust004_c01	97.37%	2.36%	0.27%	5.309E-08	987.0	0.0054	1.00304	0.00087	0.0047	0.0048
23	pust004_c02	97.36%	2.36%	0.28%	5.329E-08	976.9	0.0418	0.99783	0.00084	0.0047	0.0048
24	pust004_c03	97.31%	2.41%	0.28%	5.415E-08	934.6	0.0450	0.99976	0.00091	0.0047	0.0048
25	pust004_c04	97.19%	2.52%	0.29%	5.528E-08	888.9	0.0326	0.99814	0.00090	0.0047	0.0048
26	pust004_c05	97.28%	2.44%	0.29%	5.408E-08	942.0	0.0363	0.99932	0.00089	0.0047	0.0048
27	pust004_c06	97.23%	2.48%	0.29%	5.436E-08	927.4	0.0050	1.00092	0.00084	0.0047	0.0048
28	pust004_c07	97.18%	2.52%	0.30%	5.530E-08	891.7	0.0050	1.00542	0.00085	0.0047	0.0048

No.	Filename	Thermal (<0.635 eV)	Inter (>0.635 eV, <100 KeV)	Fast (>100 KeV)	EALF (MeV)	H/X	Pu240/Pu	k_{eff}	σ MCNP	σ bench	σ total
29	pust004_c08	97.12%	2.57%	0.31%	5.596E-08	869.0	0.0050	1.00027	0.00091	0.0047	0.0048
30	pust004_c09	96.87%	2.80%	0.33%	5.822E-08	805.2	0.0153	1.00040	0.00091	0.0047	0.0048
31	pust004_c10	96.49%	3.14%	0.37%	6.260E-08	689.4	0.0251	0.99994	0.00091	0.0047	0.0048
32	pust004_c11	96.00%	3.57%	0.43%	6.794E-08	591.7	0.0233	0.99886	0.00090	0.0047	0.0048
33	pust004_c12	97.13%	2.56%	0.31%	5.550E-08	892.7	0.0316	1.00298	0.00089	0.0047	0.0048
34	pust004_c13	97.20%	2.49%	0.31%	5.502E-08	903.1	0.0335	0.99956	0.00089	0.0047	0.0048
35	pust005_c01	97.17%	2.53%	0.30%	5.501E-08	902.8	0.0403	1.00299	0.00088	0.0047	0.0048
36	pust005_c02	97.06%	2.62%	0.32%	5.635E-08	867.7	0.0403	1.00224	0.00091	0.0047	0.0048
37	pust005_c03	96.98%	2.69%	0.33%	5.714E-08	834.4	0.0403	1.00371	0.00085	0.0047	0.0048
38	pust005_c04	96.76%	2.89%	0.35%	5.937E-08	765.2	0.0403	1.00515	0.00086	0.0047	0.0048
39	pust005_c05	96.49%	3.13%	0.38%	6.242E-08	694.1	0.0403	1.00753	0.00090	0.0047	0.0048
40	pust005_c06	96.22%	3.37%	0.41%	6.536E-08	633.4	0.0403	1.00320	0.00090	0.0047	0.0048
41	pust005_c07	95.93%	3.62%	0.45%	6.871E-08	580.6	0.0403	1.00422	0.00092	0.0047	0.0048
42	pust005_c08	97.04%	2.65%	0.32%	5.620E-08	868.7	0.0403	0.99760	0.00089	0.0047	0.0048
43	pust005_c09	96.96%	2.71%	0.33%	5.743E-08	825.1	0.0403	1.00355	0.00087	0.0047	0.0048
44	pust006_c01	97.46%	2.28%	0.26%	5.194E-08	1061.1	0.0311	1.00032	0.00081	0.0035	0.0036
45	pust006_c02	97.42%	2.32%	0.27%	5.272E-08	1017.8	0.0311	1.00193	0.00085	0.0035	0.0036
46	pust006_c03	97.21%	2.49%	0.30%	5.489E-08	940.1	0.0311	1.00163	0.00086	0.0035	0.0036
47	pust007_c02	84.19%	13.67%	2.14%	2.753E-07	109.2	0.0457	1.00653	0.00108	0.0047	0.0048
48	pust007_c03	84.77%	13.16%	2.06%	2.617E-07	113.6	0.0457	1.00156	0.00101	0.0047	0.0048
49	pust007_c05	92.46%	6.62%	0.91%	1.120E-07	266.7	0.0457	1.00731	0.00105	0.0047	0.0048
50	pust007_c06	92.35%	6.71%	0.94%	1.135E-07	261.2	0.0457	1.00177	0.00105	0.0047	0.0048
51	pust007_c07	92.47%	6.61%	0.92%	1.121E-07	264.9	0.0457	1.00239	0.00101	0.0047	0.0048
52	pust007_c08	92.26%	6.79%	0.94%	1.147E-07	257.6	0.0457	0.99838	0.00103	0.0047	0.0048
53	pust007_c09	92.27%	6.78%	0.95%	1.142E-07	258.9	0.0457	0.99579	0.00103	0.0047	0.0048
54	pust007_c10	92.93%	6.21%	0.86%	1.055E-07	284.1	0.0457	0.99814	0.00102	0.0047	0.0048
55	pust009_c01	98.61%	1.25%	0.14%	4.129E-08	2646.2	0.0251	1.01561	0.00046	0.0033	0.0033
56	pust009_c02	98.67%	1.21%	0.13%	4.076E-08	2776.7	0.0251	1.01905	0.00044	0.0033	0.0033
57	pust009_c03	98.66%	1.21%	0.13%	4.091E-08	2800.6	0.0251	1.01843	0.00043	0.0033	0.0033
58	pust010_c1.09	92.62%	6.49%	0.89%	1.102E-07	266.9	0.0284	1.01699	0.00104	0.0048	0.0049

No.	Filename	Thermal (<0.635 eV)	Inter (>0.635 eV, <100 KeV)	Fast (>100 KeV)	EALF (MeV)	H/X	Pu240/Pu	k_{eff}	σ MCNP	σ bench	σ total
59	pust010_c1.11	95.43%	4.06%	0.51%	7.478E-08	485.0	0.0284	1.01117	0.00103	0.0048	0.0049
60	pust010_c1.12	95.90%	3.63%	0.46%	6.913E-08	543.4	0.0289	1.00888	0.00094	0.0048	0.0049
61	pust010_c2.09	94.21%	5.11%	0.68%	8.887E-08	356.9	0.0284	1.01255	0.00104	0.0048	0.0049
62	pust010_c2.11	95.88%	3.66%	0.46%	6.925E-08	558.1	0.0284	1.00903	0.00093	0.0048	0.0049
63	pust010_c2.12	96.28%	3.31%	0.42%	6.485E-08	618.3	0.0289	1.00885	0.00097	0.0048	0.0049
64	pust010_c3.09	95.47%	4.03%	0.50%	7.349E-08	484.2	0.0284	1.00708	0.00095	0.0048	0.0049
65	pust010_c3.11	95.94%	3.60%	0.46%	6.866E-08	558.1	0.0284	1.00814	0.00098	0.0048	0.0049
66	pust010_c3.12	96.71%	2.93%	0.36%	6.013E-08	728.1	0.0289	1.01223	0.00092	0.0048	0.0049
67	pust010_c4.11	96.16%	3.42%	0.42%	6.607E-08	605.9	0.0284	1.00125	0.00095	0.0048	0.0049
68	pust010_c4.12	97.08%	2.61%	0.31%	5.633E-08	849.7	0.0289	1.01133	0.00090	0.0048	0.0049
69	pust010_c5.11	96.42%	3.19%	0.39%	6.370E-08	665.4	0.0284	1.00383	0.00095	0.0048	0.0049
70	pust010_c6.11	94.88%	4.53%	0.59%	8.074E-08	414.3	0.0289	1.01311	0.00102	0.0048	0.0049
71	pust010_c7.11	95.80%	3.73%	0.47%	6.991E-08	535.2	0.0289	1.00202	0.00095	0.0048	0.0049
72	pust011_c1.16	96.47%	3.14%	0.39%	6.287E-08	764.8	0.0415	1.01190	0.00104	0.0052	0.0053
73	pust011_c1.18	97.55%	2.19%	0.26%	5.143E-08	1207.8	0.0418	0.99465	0.00089	0.0052	0.0053
74	pust011_c2.16	96.37%	3.23%	0.40%	6.398E-08	736.0	0.0415	1.01659	0.00105	0.0052	0.0053
75	pust011_c2.18	97.45%	2.28%	0.27%	5.232E-08	1151.4	0.0418	1.00113	0.00090	0.0052	0.0053
76	pust011_c3.16	96.20%	3.38%	0.42%	6.611E-08	691.5	0.0415	1.01758	0.00101	0.0052	0.0053
77	pust011_c3.18	97.46%	2.27%	0.27%	5.245E-08	1158.2	0.0418	0.99814	0.00089	0.0052	0.0053
78	pust011_c4.16	96.08%	3.48%	0.44%	6.716E-08	681.7	0.0415	1.01174	0.00102	0.0052	0.0053
79	pust011_c4.18	97.30%	2.41%	0.29%	5.385E-08	1099.7	0.0418	0.99478	0.00090	0.0052	0.0053
80	pust011_c5.16	95.47%	4.02%	0.51%	7.446E-08	574.5	0.0415	1.01009	0.00102	0.0052	0.0053
81	pust011_c5.18	97.20%	2.50%	0.30%	5.498E-08	1038.9	0.0418	1.00372	0.00089	0.0052	0.0053
82	pust011_c6.18	96.88%	2.79%	0.33%	5.857E-08	908.4	0.0418	1.00169	0.00095	0.0052	0.0053
83	pust011_c7.18	97.34%	2.38%	0.28%	5.345E-08	1102.6	0.0418	1.00119	0.00089	0.0052	0.0053
84	pust014_c01	89.53%	9.18%	1.29%	1.650E-07	219.5	0.0423	1.00488	0.00097	0.0032	0.0033
85	pust014_c02	89.57%	9.15%	1.28%	1.657E-07	219.5	0.0423	1.00463	0.00103	0.0032	0.0034
86	pust014_c03	89.61%	9.10%	1.29%	1.647E-07	219.5	0.0423	1.00539	0.00102	0.0032	0.0034
87	pust014_c04	89.63%	9.09%	1.28%	1.644E-07	219.5	0.0423	1.00613	0.00100	0.0032	0.0034
88	pust014_c05	89.54%	9.16%	1.30%	1.655E-07	219.5	0.0423	1.00581	0.00097	0.0032	0.0033

No.	Filename	Thermal (<0.635 eV)	Inter (>0.635 eV, <100 KeV)	Fast (>100 KeV)	EALF (MeV)	H/X	Pu240/Pu	k_{eff}	σ MCNP	σ bench	σ total
89	pust014_c06	89.51%	9.21%	1.29%	1.654E-07	219.5	0.0423	1.00398	0.00105	0.0032	0.0034
90	pust014_c07	89.49%	9.21%	1.30%	1.660E-07	219.5	0.0423	1.00741	0.00103	0.0043	0.0044
91	pust014_c08	89.48%	9.22%	1.30%	1.666E-07	219.5	0.0423	1.00259	0.00103	0.0032	0.0034
92	pust014_c09	89.51%	9.19%	1.30%	1.661E-07	219.5	0.0423	1.00220	0.00101	0.0032	0.0034
93	pust014_c10	89.56%	9.15%	1.29%	1.649E-07	219.5	0.0423	1.00385	0.00100	0.0032	0.0034
94	pust014_c11	89.55%	9.16%	1.28%	1.656E-07	219.5	0.0423	1.00190	0.00099	0.0032	0.0033
95	pust014_c12	89.63%	9.08%	1.29%	1.646E-07	219.5	0.0423	1.00429	0.00103	0.0032	0.0034
96	pust014_c13	89.51%	9.20%	1.29%	1.666E-07	219.5	0.0423	1.00489	0.00101	0.0043	0.0044
97	pust014_c14	89.49%	9.21%	1.30%	1.663E-07	219.5	0.0423	1.00222	0.00097	0.0043	0.0044
98	pust014_c15	89.55%	9.16%	1.29%	1.650E-07	219.5	0.0423	1.00438	0.00102	0.0043	0.0044
99	pust014_c16	89.53%	9.18%	1.28%	1.651E-07	219.5	0.0423	1.00480	0.00099	0.0043	0.0044
100	pust014_c17	89.62%	9.09%	1.29%	1.650E-07	219.5	0.0423	1.00566	0.00100	0.0043	0.0044
101	pust014_c18	89.52%	9.18%	1.31%	1.670E-07	219.5	0.0423	1.00697	0.00099	0.0043	0.0044
102	pust014_c19	89.49%	9.22%	1.29%	1.663E-07	219.5	0.0423	1.00308	0.00101	0.0043	0.0044
103	pust014_c20	89.61%	9.11%	1.29%	1.647E-07	219.5	0.0423	1.00522	0.00102	0.0043	0.0044
104	pust014_c21	89.51%	9.20%	1.29%	1.659E-07	219.5	0.0423	1.00065	0.00102	0.0043	0.0044
105	pust014_c22	89.58%	9.12%	1.29%	1.651E-07	219.5	0.0423	1.00489	0.00105	0.0043	0.0044
106	pust014_c23	89.57%	9.13%	1.30%	1.648E-07	219.5	0.0423	1.00311	0.00095	0.0043	0.0044
107	pust014_c24	89.48%	9.24%	1.28%	1.667E-07	219.5	0.0423	1.00655	0.00100	0.0043	0.0044
108	pust014_c25	89.55%	9.16%	1.29%	1.659E-07	219.5	0.0423	1.00300	0.00099	0.0043	0.0044
109	pust014_c26	89.55%	9.19%	1.27%	1.652E-07	219.5	0.0423	1.00375	0.00100	0.0043	0.0044
110	pust014_c27	89.57%	9.14%	1.29%	1.653E-07	219.5	0.0423	1.00333	0.00103	0.0043	0.0044
111	pust014_c28	89.54%	9.16%	1.30%	1.654E-07	219.5	0.0423	1.00272	0.00103	0.0043	0.0044
112	pust014_c29	89.57%	9.15%	1.29%	1.650E-07	219.5	0.0423	1.00411	0.00096	0.0043	0.0044
113	pust014_c30	89.47%	9.22%	1.31%	1.677E-07	219.5	0.0423	1.00449	0.00092	0.0043	0.0044
114	pust014_c31	89.49%	9.21%	1.29%	1.667E-07	219.5	0.0423	1.00232	0.00098	0.0043	0.0044
115	pust014_c32	89.45%	9.25%	1.29%	1.662E-07	219.5	0.0423	1.00402	0.00103	0.0043	0.0044
116	pust014_c33	89.49%	9.20%	1.31%	1.664E-07	219.5	0.0423	1.00139	0.00102	0.0043	0.0044
117	pust014_c34	89.54%	9.16%	1.30%	1.660E-07	219.5	0.0423	1.00232	0.00101	0.0043	0.0044
118	pust014_c35	89.53%	9.19%	1.29%	1.652E-07	219.5	0.0423	1.00100	0.00103	0.0043	0.0044

No.	Filename	Thermal (<0.635 eV)	Inter (>0.635 eV, <100 KeV)	Fast (>100 KeV)	EALF (MeV)	H/X	Pu240/Pu	k_{eff}	σ MCNP	σ bench	σ total
119	pust015_c01	86.45%	11.82%	1.73%	2.345E-07	162.1	0.0423	1.00710	0.00100	0.0038	0.0039
120	pust015_c02	86.45%	11.82%	1.73%	2.344E-07	162.1	0.0423	1.00682	0.00107	0.0038	0.0039
121	pust015_c03	86.42%	11.85%	1.73%	2.344E-07	162.1	0.0423	1.00433	0.00102	0.0038	0.0039
122	pust015_c04	86.44%	11.82%	1.74%	2.348E-07	162.1	0.0423	1.00335	0.00101	0.0038	0.0039
123	pust015_c05	86.45%	11.82%	1.73%	2.342E-07	162.1	0.0423	1.00464	0.00102	0.0038	0.0039
124	pust015_c06	86.57%	11.71%	1.72%	2.324E-07	162.1	0.0423	1.00569	0.00104	0.0038	0.0039
125	pust015_c07	86.39%	11.88%	1.74%	2.360E-07	162.1	0.0423	1.00606	0.00102	0.0047	0.0048
126	pust015_c08	86.36%	11.90%	1.74%	2.361E-07	162.1	0.0423	1.00472	0.00100	0.0047	0.0048
127	pust015_c09	86.40%	11.87%	1.74%	2.351E-07	162.1	0.0423	1.00390	0.00100	0.0047	0.0048
128	pust015_c10	86.44%	11.85%	1.71%	2.342E-07	162.1	0.0423	1.00324	0.00096	0.0047	0.0048
129	pust015_c11	86.35%	11.92%	1.73%	2.366E-07	162.1	0.0423	1.00305	0.00098	0.0047	0.0048
130	pust015_c12	86.41%	11.85%	1.74%	2.350E-07	162.1	0.0423	1.00363	0.00101	0.0047	0.0048
131	pust015_c13	86.41%	11.85%	1.74%	2.341E-07	162.1	0.0423	1.00516	0.00102	0.0047	0.0048
132	pust015_c14	86.46%	11.81%	1.73%	2.331E-07	162.1	0.0423	1.00479	0.00103	0.0047	0.0048
133	pust015_c15	86.44%	11.82%	1.74%	2.350E-07	162.1	0.0423	1.00633	0.00100	0.0047	0.0048
134	pust015_c16	86.33%	11.91%	1.76%	2.359E-07	162.1	0.0423	1.00369	0.00095	0.0047	0.0048
135	pust015_c17	86.45%	11.82%	1.73%	2.336E-07	162.1	0.0423	1.00491	0.00101	0.0047	0.0048
136	pust016_c01	86.45%	11.81%	1.74%	2.350E-07	162.1	0.0423	1.00255	0.00100	0.0043	0.0044
137	pust016_c02	86.46%	11.81%	1.73%	2.345E-07	162.1	0.0423	1.00330	0.00100	0.0043	0.0044
138	pust016_c03	86.50%	11.77%	1.73%	2.331E-07	162.1	0.0423	1.00691	0.00102	0.0043	0.0044
139	pust016_c04	86.41%	11.86%	1.74%	2.349E-07	162.1	0.0423	1.00516	0.00099	0.0043	0.0044
140	pust016_c05	89.48%	9.22%	1.30%	1.669E-07	219.5	0.0423	1.00269	0.00102	0.0038	0.0039
141	pust016_c06	89.53%	9.18%	1.30%	1.658E-07	219.5	0.0423	1.00380	0.00098	0.0038	0.0039
142	pust016_c07	89.57%	9.15%	1.28%	1.646E-07	219.5	0.0423	1.00446	0.00097	0.0038	0.0039
143	pust016_c08	89.59%	9.12%	1.30%	1.648E-07	219.5	0.0423	1.00486	0.00098	0.0038	0.0039
144	pust016_c09	89.54%	9.17%	1.29%	1.657E-07	219.5	0.0423	0.99743	0.00097	0.0033	0.0034
145	pust016_c10	89.56%	9.15%	1.29%	1.648E-07	219.5	0.0423	1.00293	0.00108	0.0033	0.0035
146	pust016_c11	89.54%	9.17%	1.30%	1.658E-07	219.5	0.0423	1.00495	0.00101	0.0033	0.0035
147	pust017_c01	89.56%	9.14%	1.30%	1.652E-07	219.5	0.0423	1.00226	0.00099	0.0038	0.0039
148	pust017_c02	89.55%	9.17%	1.28%	1.647E-07	219.5	0.0423	1.00284	0.00102	0.0038	0.0039

No.	Filename	Thermal (<0.635 eV)	Inter (>0.635 eV, <100 KeV)	Fast (>100 KeV)	EALF (MeV)	H/X	Pu240/Pu	k_{eff}	σ MCNP	σ bench	σ total
149	pust017_c03	89.60%	9.11%	1.29%	1.648E-07	219.5	0.0423	1.00406	0.00103	0.0038	0.0039
150	pust017_c04	89.64%	9.07%	1.29%	1.644E-07	219.5	0.0423	1.00493	0.00103	0.0038	0.0039
151	pust017_c05	89.55%	9.14%	1.31%	1.659E-07	219.5	0.0423	1.00075	0.00102	0.0038	0.0039
152	pust017_c06	89.49%	9.22%	1.30%	1.664E-07	219.5	0.0423	1.00415	0.00105	0.0038	0.0039
153	pust017_c07	89.58%	9.13%	1.29%	1.648E-07	219.5	0.0423	1.00166	0.00099	0.0038	0.0039
154	pust017_c08	89.49%	9.22%	1.29%	1.659E-07	219.5	0.0423	1.00606	0.00099	0.0038	0.0039
155	pust017_c09	89.61%	9.11%	1.28%	1.650E-07	219.5	0.0423	1.00394	0.00102	0.0038	0.0039
156	pust017_c10	89.55%	9.15%	1.30%	1.657E-07	219.5	0.0423	1.00505	0.00103	0.0038	0.0039
157	pust017_c11	89.58%	9.14%	1.28%	1.647E-07	219.5	0.0423	1.00530	0.00105	0.0038	0.0039
158	pust017_c12	89.62%	9.09%	1.28%	1.644E-07	219.5	0.0423	1.00372	0.00100	0.0038	0.0039
159	pust017_c13	89.51%	9.20%	1.29%	1.659E-07	219.5	0.0423	1.00392	0.00107	0.0038	0.0039
160	pust017_c14	89.47%	9.22%	1.30%	1.660E-07	219.5	0.0423	1.00446	0.00105	0.0038	0.0039
161	pust017_c15	89.54%	9.17%	1.29%	1.654E-07	219.5	0.0423	1.00542	0.00098	0.0038	0.0039
162	pust017_c16	89.54%	9.17%	1.29%	1.649E-07	219.5	0.0423	1.00437	0.00103	0.0038	0.0039
163	pust017_c17	89.58%	9.12%	1.29%	1.652E-07	219.5	0.0423	1.00435	0.00104	0.0038	0.0039
164	pust017_c18	89.58%	9.13%	1.30%	1.653E-07	219.5	0.0423	1.00637	0.00099	0.0038	0.0039
165	pust020_c01	96.20%	3.39%	0.41%	6.535E-08	633.1	0.0457	1.00313	0.00092	0.0059	0.0060
166	pust020_c02	96.35%	3.25%	0.40%	6.407E-08	651.5	0.0457	1.00550	0.00090	0.0059	0.0060
167	pust020_c03	96.82%	2.85%	0.34%	5.876E-08	783.7	0.0457	1.00118	0.00092	0.0059	0.0060
168	pust020_c05	95.32%	4.15%	0.53%	7.572E-08	485.1	0.0457	1.00201	0.00096	0.0059	0.0060
169	pust020_c06	95.10%	4.36%	0.54%	7.870E-08	474.0	0.0457	1.00549	0.00096	0.0059	0.0060
170	pust020_c07	96.68%	2.96%	0.36%	6.028E-08	759.3	0.0457	0.99646	0.00095	0.0059	0.0060
171	pust020_c08	93.12%	6.10%	0.77%	1.052E-07	359.7	0.0457	1.00363	0.00102	0.0059	0.0060
172	pust020_c09	95.33%	4.17%	0.51%	7.554E-08	566.5	0.0457	0.99706	0.00104	0.0059	0.0060
173	pust021_c01	96.18%	3.40%	0.43%	6.578E-08	699.6	0.0457	1.00682	0.00105	0.0032	0.0034
174	pust021_c02	96.51%	3.12%	0.37%	6.181E-08	795.3	0.0457	1.00906	0.00102	0.0032	0.0034
175	pust021_c03	83.73%	14.16%	2.11%	3.081E-07	131.4	0.0457	1.00651	0.00114	0.0065	0.0066
176	pust021_c04	97.44%	2.30%	0.26%	5.229E-08	1082.3	0.0457	1.00045	0.00084	0.0025	0.0026
177	pust021_c05	97.57%	2.18%	0.25%	5.094E-08	1120.9	0.0457	1.00528	0.00080	0.0025	0.0026
178	pust021_c06	95.86%	3.69%	0.45%	6.992E-08	579.4	0.0457	1.00634	0.00098	0.0044	0.0045

No.	Filename	Thermal (<0.635 eV)	Inter (>0.635 eV, <100 KeV)	Fast (>100 KeV)	EALF (MeV)	H/X	Pu240/Pu	k_{eff}	σ MCNP	σ bench	σ total
179	pust024_c01	78.85%	18.26%	2.89%	4.651E-07	108.9	0.1840	1.00026	0.00105	0.0062	0.0063
180	pust024_c02	78.95%	18.16%	2.89%	4.600E-07	108.9	0.1840	1.00056	0.00106	0.0062	0.0063
181	pust024_c03	78.99%	18.15%	2.86%	4.561E-07	108.9	0.1840	0.99979	0.00103	0.0062	0.0063
182	pust024_c04	79.09%	18.04%	2.87%	4.546E-07	108.9	0.1840	1.00131	0.00104	0.0062	0.0063
183	pust024_c05	79.16%	17.97%	2.87%	4.507E-07	108.9	0.1840	1.00011	0.00106	0.0062	0.0063
184	pust024_c07	86.15%	12.05%	1.80%	2.276E-07	179.2	0.1840	1.00906	0.0011	0.0053	0.0054
185	pust024_c08	86.18%	12.02%	1.79%	2.275E-07	179.2	0.1840	1.00681	0.00102	0.0053	0.0054
186	pust024_c09	86.20%	12.03%	1.76%	2.247E-07	179.2	0.1840	1.00898	0.00107	0.0053	0.0054
187	pust024_c10	86.33%	11.91%	1.76%	2.235E-07	179.2	0.1840	1.00715	0.00103	0.0053	0.0054
188	pust024_c11	86.34%	11.91%	1.75%	2.219E-07	179.2	0.1840	1.00898	0.00104	0.0053	0.0054
189	pust024_c12	86.45%	11.80%	1.75%	2.202E-07	179.2	0.1840	1.00713	0.00101	0.0053	0.0054
190	pust024_c13	86.37%	11.89%	1.74%	2.214E-07	179.2	0.1840	1.00657	0.00104	0.0053	0.0054
191	pust024_c14	83.56%	14.18%	2.27%	2.980E-07	152.9	0.2320	0.99988	0.00107	0.0053	0.0054
192	pust024_c15	83.60%	14.17%	2.23%	2.962E-07	152.9	0.2320	0.99923	0.00108	0.0053	0.0054
193	pust024_c16	83.68%	14.09%	2.23%	2.934E-07	152.9	0.2320	0.99979	0.0011	0.0053	0.0054
194	pust024_c17	83.84%	13.93%	2.22%	2.905E-07	152.9	0.2320	1.00347	0.00111	0.0053	0.0054
195	pust024_c18	93.94%	5.33%	0.73%	8.982E-08	457.4	0.1840	1.00364	0.00107	0.0051	0.0052
196	pust024_c19	93.95%	5.32%	0.72%	8.957E-08	457.4	0.1840	1.00523	0.00105	0.0051	0.0052
197	pust024_c20	93.97%	5.30%	0.73%	8.921E-08	457.4	0.1840	1.00623	0.00101	0.0051	0.0052
198	pust024_c21	93.98%	5.30%	0.72%	8.910E-08	457.4	0.1840	1.00463	0.00102	0.0051	0.0052
199	pust024_c22	94.03%	5.26%	0.71%	8.875E-08	457.4	0.1840	1.00530	0.00098	0.0051	0.0052
200	pust024_c23	94.00%	5.28%	0.72%	8.869E-08	457.4	0.1840	1.00358	0.00099	0.0051	0.0052

Table 6.8-4 – U-233 Benchmark Experiment Data (with Beryllium)

No.	Filename	Thermal (<0.635 eV)	Inter (>0.635 eV, <100 KeV)	Fast (>100 KeV)	EALF (MeV)	k_{eff}	σ MCNP	σ bench	σ total
201	ust015_c01	51.61%	45.08%	3.31%	1.114E-06	0.99327	0.00101	0.0075	0.0076
202	ust015_c02	50.16%	46.32%	3.51%	1.247E-06	0.98695	0.00102	0.0069	0.0070
203	ust015_c03	49.68%	46.68%	3.64%	1.314E-06	0.98732	0.00105	0.0055	0.0056
204	ust015_c04	58.25%	38.43%	3.32%	7.298E-07	0.98992	0.00095	0.0066	0.0067
205	ust015_c05	49.10%	47.11%	3.79%	1.385E-06	0.98658	0.00104	0.0063	0.0064
206	ust015_c06	48.70%	47.40%	3.90%	1.435E-06	0.97847	0.00103	0.0058	0.0059
207	ust015_c08	48.53%	47.41%	4.06%	1.488E-06	0.97451	0.00102	0.0048	0.0049
208	ust015_c09	48.38%	47.48%	4.15%	1.513E-06	0.96798	0.00102	0.0055	0.0056
209	ust015_c11	57.24%	40.07%	2.69%	7.003E-07	0.99395	0.00100	0.0068	0.0069
210	ust015_c12	56.02%	41.15%	2.83%	7.747E-07	0.99488	0.00102	0.0041	0.0042
211	ust015_c13	55.49%	41.57%	2.94%	8.148E-07	0.99382	0.00099	0.0055	0.0056
212	ust015_c14	63.58%	33.74%	2.68%	4.694E-07	0.99780	0.00095	0.0099	0.0099
213	ust015_c15	54.97%	41.97%	3.06%	8.520E-07	0.99208	0.00104	0.0070	0.0071
214	ust015_c16	54.76%	42.05%	3.19%	8.768E-07	0.99101	0.00102	0.0067	0.0068
215	ust015_c18	54.47%	42.23%	3.30%	9.073E-07	0.97410	0.00102	0.0051	0.0052
216	ust015_c19	54.43%	42.22%	3.36%	9.141E-07	0.97675	0.00106	0.0075	0.0076
217	ust015_c20	68.57%	29.72%	1.71%	2.920E-07	0.99786	0.00093	0.0069	0.0070
218	ust015_c21	67.50%	30.70%	1.81%	3.167E-07	1.00066	0.00102	0.0036	0.0037
219	ust015_c22	66.72%	31.40%	1.88%	3.340E-07	0.99732	0.00101	0.0060	0.0061
220	ust015_c23	66.32%	31.71%	1.97%	3.478E-07	0.99508	0.00100	0.0043	0.0044
221	ust015_c24	66.02%	31.96%	2.02%	3.566E-07	0.99074	0.00102	0.0029	0.0031
222	ust015_c26	79.37%	19.65%	0.98%	1.274E-07	0.99630	0.00092	0.0052	0.0053
223	ust015_c27	78.94%	20.04%	1.02%	1.314E-07	0.99994	0.00094	0.0079	0.0080
224	ust015_c28	78.68%	20.28%	1.05%	1.343E-07	0.99846	0.00089	0.0070	0.0071
225	ust015_c29	78.53%	20.39%	1.08%	1.361E-07	0.99818	0.00096	0.0062	0.0063
226	ust015_c30	78.41%	20.48%	1.11%	1.377E-07	0.99753	0.00097	0.0051	0.0052
227	ust015_c31	78.41%	20.43%	1.16%	1.379E-07	0.99385	0.00105	0.0023	0.0025

Table 6.8-5 – U-233 Benchmark Experiment Data (without Beryllium)

No.	Filename	Thermal (<0.635 eV)	Inter (>0.635 eV, <100 KeV)	Fast (>100 KeV)	EALF (MeV)	k_{eff}	σ MCNP	σ bench	σ total
228	ust015_c07	57.08%	39.48%	3.44%	8.016E-07	0.98486	0.00098	0.0051	0.0052
229	ust015_c10	52.16%	44.00%	3.84%	1.149E-06	0.98968	0.00110	0.0070	0.0071
230	ust015_c17	62.55%	34.65%	2.80%	5.116E-07	0.99702	0.00099	0.0050	0.0051
231	ust015_c25	72.66%	25.57%	1.78%	2.263E-07	0.99647	0.00096	0.0056	0.0057
232	ust001_c01	94.71%	5.08%	0.21%	3.948E-08	1.00136	0.00060	0.0031	0.0032
233	ust001_c02	94.53%	5.25%	0.22%	4.000E-08	1.00045	0.00060	0.0033	0.0034
234	ust001_c03	94.36%	5.41%	0.23%	4.060E-08	1.00082	0.00061	0.0033	0.0034
235	ust001_c04	94.16%	5.61%	0.23%	4.116E-08	1.00026	0.00062	0.0033	0.0034
236	ust001_c05	93.98%	5.78%	0.24%	4.172E-08	1.00013	0.00065	0.0033	0.0034
237	ust003_c40	69.08%	28.67%	2.25%	3.101E-07	1.00873	0.00112	0.0087	0.0088
238	ust003_c41	67.65%	30.05%	2.30%	3.427E-07	1.02347	0.00112	0.0151	0.0152
239	ust003_c42	68.08%	29.61%	2.31%	3.341E-07	1.00305	0.00118	0.0087	0.0088
240	ust003_c45	58.35%	38.09%	3.56%	7.600E-07	1.01077	0.00115	0.0126	0.0126
241	ust003_c55	55.20%	40.75%	4.05%	1.008E-06	1.01743	0.00111	0.0122	0.0123
242	ust003_c57	79.78%	19.01%	1.21%	1.294E-07	1.02347	0.00114	0.0087	0.0088
243	ust003_c58	85.19%	14.01%	0.81%	8.460E-08	1.01795	0.00107	0.0087	0.0088
244	ust003_c61	87.62%	11.74%	0.64%	6.949E-08	1.01112	0.00104	0.0087	0.0088
245	ust003_c62	89.03%	10.42%	0.56%	6.202E-08	1.01319	0.00098	0.0087	0.0088
246	ust003_c65	92.74%	6.92%	0.34%	4.633E-08	1.00900	0.00086	0.0087	0.0088
247	ust012_c01	75.96%	22.52%	1.52%	1.743E-07	0.99683	0.00117	0.0028	0.0030
248	ust012_c02	76.79%	21.74%	1.47%	1.643E-07	0.99704	0.00118	0.0025	0.0028
249	ust012_c03	78.26%	20.42%	1.32%	1.460E-07	1.00807	0.00114	0.0023	0.0026
250	ust012_c04	82.01%	16.96%	1.02%	1.078E-07	1.00021	0.00114	0.0015	0.0019
251	ust012_c05	84.03%	15.10%	0.87%	9.191E-08	1.00309	0.00112	0.0071	0.0072
252	ust012_c06	85.66%	13.58%	0.75%	8.082E-08	1.00495	0.00113	0.0010	0.0015
253	ust012_c07	90.87%	8.70%	0.43%	5.350E-08	1.00366	0.00101	0.0038	0.0039
254	ust012_c08	90.89%	8.67%	0.43%	5.351E-08	0.99846	0.00100	0.0048	0.0049
255	ust013_c01	76.82%	21.84%	1.34%	1.576E-07	1.00497	0.00106	0.0073	0.0074

No.	Filename	Thermal (<0.635 eV)	Inter (>0.635 eV, <100 KeV)	Fast (>100 KeV)	EALF (MeV)	k_{eff}	σ MCNP	σ bench	σ total
256	ust013_c02	76.77%	21.89%	1.34%	1.584E-07	1.00562	0.00103	0.0070	0.0071
257	ust013_c03	76.68%	21.99%	1.33%	1.585E-07	1.00512	0.00107	0.0069	0.0070
258	ust013_c04	76.86%	21.80%	1.34%	1.579E-07	1.00454	0.00107	0.0073	0.0074
259	ust013_c05	76.80%	21.86%	1.35%	1.578E-07	1.00773	0.00105	0.0067	0.0068
260	ust013_c06	77.32%	21.38%	1.31%	1.519E-07	1.00653	0.00099	0.0050	0.0051
261	ust013_c07	77.37%	21.33%	1.30%	1.512E-07	1.00837	0.00103	0.0054	0.0055
262	ust013_c08	77.43%	21.28%	1.29%	1.507E-07	1.00761	0.00101	0.0050	0.0051
263	ust013_c09	77.29%	21.40%	1.30%	1.519E-07	1.00543	0.00108	0.0045	0.0046
264	ust013_c10	77.38%	21.33%	1.29%	1.508E-07	1.00653	0.00106	0.0046	0.0047
265	ust013_c11	77.41%	21.29%	1.30%	1.513E-07	1.00482	0.00107	0.0054	0.0055
266	ust013_c12	77.40%	21.31%	1.30%	1.511E-07	1.00530	0.00101	0.0050	0.0051
267	ust013_c13	77.38%	21.32%	1.30%	1.519E-07	1.00384	0.00105	0.0062	0.0063
268	ust013_c14	77.28%	21.42%	1.30%	1.522E-07	1.00613	0.00101	0.0051	0.0052
269	ust013_c15	81.99%	17.04%	0.96%	1.056E-07	1.01973	0.00102	0.0077	0.0078
270	ust013_c16	84.13%	15.04%	0.82%	8.930E-08	0.99337	0.00102	0.0069	0.0070
271	ust013_c17	84.74%	14.47%	0.79%	8.566E-08	0.99574	0.00096	0.0052	0.0053
272	ust013_c18	85.50%	13.75%	0.76%	8.073E-08	0.99987	0.00097	0.0020	0.0022
273	ust013_c19	85.42%	13.83%	0.75%	8.095E-08	0.99661	0.00099	0.0089	0.0090
274	ust013_c20	88.95%	10.52%	0.53%	6.188E-08	0.99872	0.00092	0.0056	0.0057
275	ust013_c21	90.00%	9.53%	0.47%	5.686E-08	1.00412	0.00088	0.0034	0.0035
276	ust014_c01	59.84%	37.21%	2.95%	6.126E-07	0.97859	0.00104	0.0112	0.0112
277	ust014_c02	59.02%	37.94%	3.03%	6.516E-07	0.99304	0.00102	0.0112	0.0112
278	ust014_c03	69.43%	28.29%	2.27%	3.060E-07	1.01601	0.00092	0.0074	0.0075
279	ust014_c04	69.67%	28.08%	2.25%	3.002E-07	1.01238	0.00094	0.0089	0.0089
280	ust014_c05	71.04%	26.80%	2.16%	2.721E-07	1.01603	0.00091	0.0089	0.0089
281	ust014_c06	71.62%	26.25%	2.13%	2.618E-07	1.01415	0.00093	0.0089	0.0089
282	ust014_c07	72.11%	25.77%	2.12%	2.534E-07	1.00820	0.00089	0.0088	0.0088
283	ust014_c08	72.63%	25.30%	2.08%	2.437E-07	1.01384	0.00087	0.0091	0.0091
284	ust014_c09	69.60%	28.09%	2.31%	3.043E-07	1.01718	0.00093	0.0054	0.0055
285	ust014_c10	67.23%	30.34%	2.43%	3.602E-07	0.99953	0.00102	0.0108	0.0108

No.	Filename	Thermal (<0.635 eV)	Inter (>0.635 eV, <100 KeV)	Fast (>100 KeV)	EALF (MeV)	k_{eff}	σ MCNP	σ bench	σ total
286	ust014_c11	64.17%	33.24%	2.59%	4.441E-07	1.00298	0.00106	0.0126	0.0126
287	ust014_c12	69.34%	28.35%	2.30%	3.095E-07	1.01041	0.00099	0.0097	0.0098
288	ust014_c13	69.91%	27.80%	2.29%	2.981E-07	1.00589	0.00101	0.0104	0.0104
289	ust014_c14	70.28%	27.42%	2.31%	2.939E-07	1.00416	0.00098	0.0095	0.0096
290	ust014_c15	69.00%	28.62%	2.38%	3.217E-07	1.00117	0.00100	0.0098	0.0099
291	ust014_c16	61.16%	36.01%	2.83%	5.528E-07	0.98220	0.00106	0.0109	0.0110
292	usi001_c08	38.39%	54.72%	6.89%	4.520E-06	0.98014	0.00099	0.0056	0.0057
293	usi001_c16	49.52%	45.17%	5.31%	1.768E-06	0.97951	0.00099	0.0028	0.0030
294	usi001_c20	42.28%	51.78%	5.94%	3.021E-06	0.97843	0.00104	0.0056	0.0057
295	usi001_c23	36.51%	56.96%	6.54%	4.707E-06	0.98906	0.00103	0.0047	0.0048
296	usi001_c30	49.99%	45.54%	4.47%	1.471E-06	0.97677	0.00104	0.0053	0.0054
297	usi001_c33	45.08%	50.04%	4.88%	2.104E-06	0.99285	0.00105	0.0046	0.0047

This page intentionally left blank.

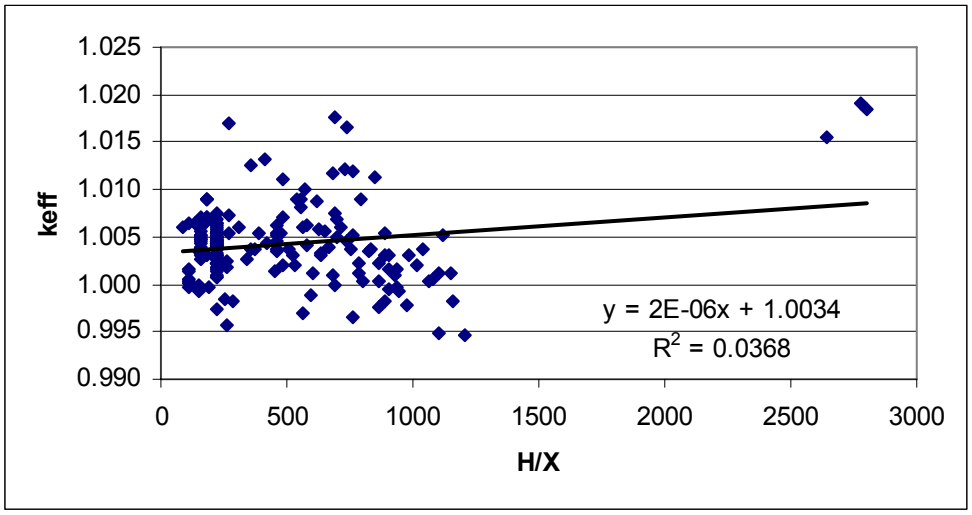

Figure 6.8-1 – Benchmark Data Trend for H/X

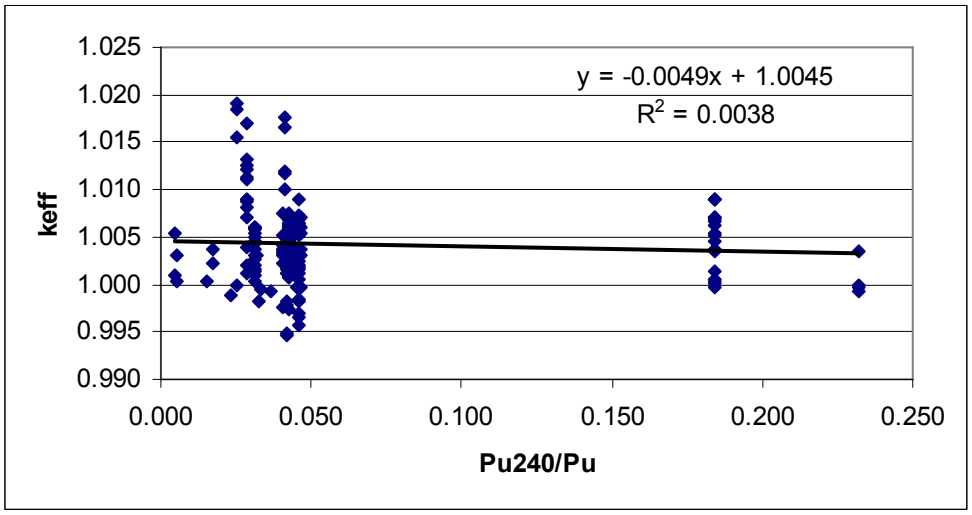

Figure 6.8-2 – Benchmark Data Trend for Pu240/Pu

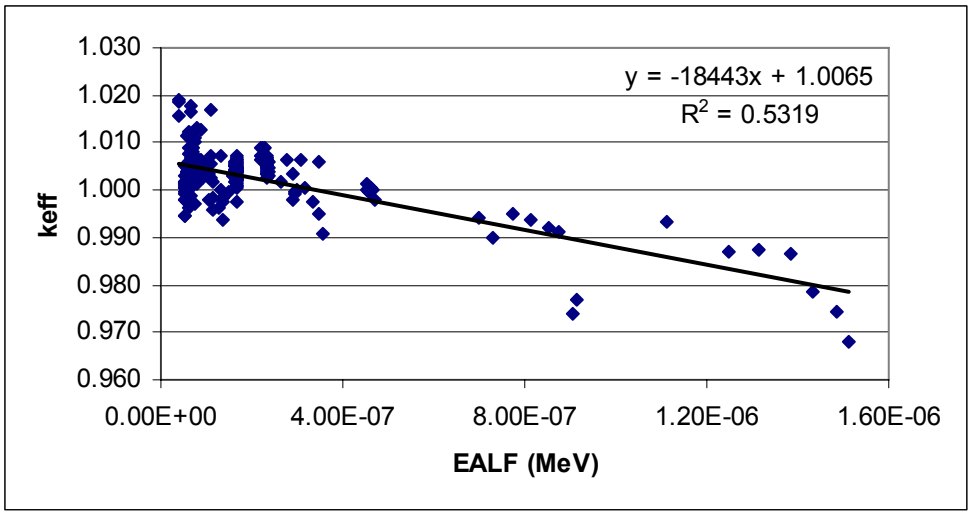

Figure 6.8-3 – Benchmark Data Trend for EALF1

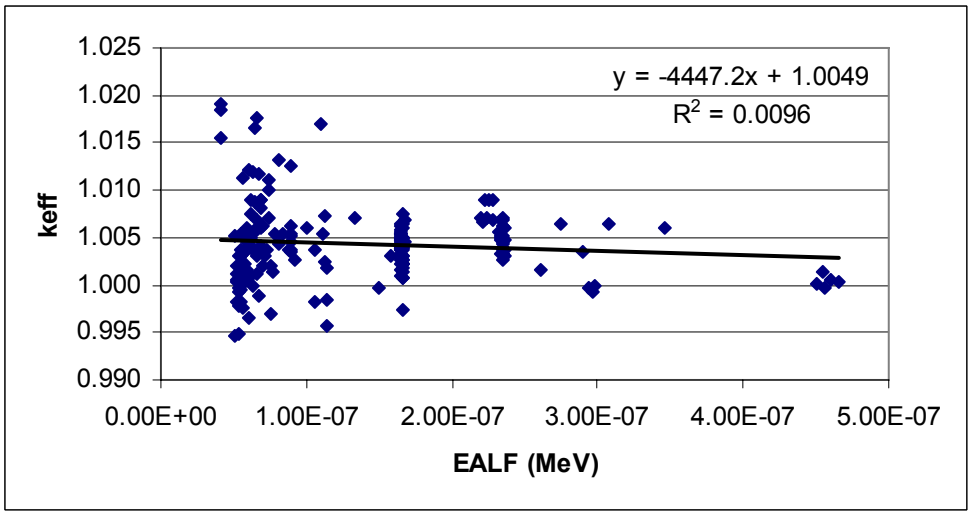

Figure 6.8-4 – Benchmark Data Trend for EALF5

6.9 Appendix

6.9.1 Sample Input File

A sample input file (filename ha_5g240_x0900) is provided for the most reactive HAC array case (Case E5 in Table 6.6-2).

ha_5g240_x0900

```
TRUPACT-III HA, H/X =  900 Pu239(g)= 340 Pu240(g)= 5
10      1 1.0498E-01 -5                              imp:n=1 $ source
11      2 1.0507E-01   10 -11 12 -13 14 -15 5              imp:n=1 $ CSA cavity
12      3 -7.89  (-10:11:-12:13:-14:15) 20 -21 22 -23 24 -25 imp:n=1 $ inner CSA steel
13      4 -1.0   (-20:21:-22:23:-24:25) 30 -31 32 -33 34 -35 imp:n=1 $ CSA annulus
14      3 -7.89  (-30:31:-32:33:-34:35) 40 -41 42 -43 44 -45 imp:n=1 $ outer CSA steel
20      4 -1.0   90 -91 43 -53 46 -47                       imp:n=1 $ side foam
21      4 -1.0   90 -91 52 -42 46 -47                       imp:n=1 $ side foam
22      4 -1.0   92 -93 50 -40 46 -47                       imp:n=1 $ side foam
23      4 -1.0   92 -93 41 -51 46 -47                       imp:n=1 $ side foam
30      3 -7.89  90 -91 53 -63 46 -47                       imp:n=1 $ foam/balsa steel
31      3 -7.89  90 -91 62 -52 46 -47                       imp:n=1 $ foam/balsa steel
32      3 -7.89  92 -93 60 -50 46 -47                       imp:n=1 $ foam/balsa steel
33      3 -7.89  92 -93 51 -61 46 -47                       imp:n=1 $ foam/balsa steel
40      4 -1.0   90 -91 63 -73 46 -47                       imp:n=1 $ balsa
41      4 -1.0   90 -91 72 -62 46 -47                       imp:n=1 $ balsa
42      4 -1.0   92 -93 70 -60 46 -47                       imp:n=1 $ balsa
43      4 -1.0   92 -93 61 -71 46 -47                       imp:n=1 $ balsa
50      4 -1.0   (91 -41 43 -73 46 -47):(41 -71 93 -73 46 -47) imp:n=1 $ corner foam
51      4 -1.0   (40 -90 43 -73 46 -47):(70 -40 93 -73 46 -47) imp:n=1 $ corner foam
52      4 -1.0   (91 -41 72 -42 46 -47):(41 -71 72 -92 46 -47) imp:n=1 $ corner foam
53      4 -1.0   (40 -90 72 -42 46 -47):(70 -40 72 -92 46 -47) imp:n=1 $ corner foam
54      4 -1.0   (-40:41:-42:43) 70 -71 72 -73 44 -46        imp:n=1 $ corner foam
55      4 -1.0   (-40:41:-42:43) 70 -71 72 -73 47 -45        imp:n=1 $ corner foam
56      3 -7.89  (-70:71:-72:73) 80 -81 82 -83 135 -213      imp:n=1 $ outer steel
c
c       Front Impact Limiter
c
100     3 -7.89  70 -71 72 -73 120 -44                          imp:n=1 $ 6 mm steel
101     4 -1.0   116 -112 114 -110 -111 -113 -115 -117 121 -120  imp:n=1 $ 120 mm foam
102     3 -7.89  116 -112 114 -110 -111 -113 -115 -117 122 -121  imp:n=1 $ 15 mm steel
103     4 -1.0   116 -112 114 -110 -111 -113 -115 -117 123 -122  imp:n=1 $ 60 mm balsa
104     3 -7.89  116 -112 114 -110 -111 -113 -115 -117 124 -123  imp:n=1 $ 6 mm steel
105     4 -1.0   116 -112 114 -110 -111 -113 -115 -117 135 -124  imp:n=1 $ water
106     4 -1.0   (-116:112:-114:110:111:113:115:117)
                  70 -71 72 -73 130 -120 imp:n=1 $ calcium silicate outer
107     3 -7.89  (-116:112:-114:110:111:113:115:117)
                  70 -71 72 -73 131 -130 imp:n=1 $ steel outer
108     4 -1.0   (-116:112:-114:110:111:113:115:117)
                  70 -71 72 -73 132 -131 imp:n=1 $ foam outer
109     3 -7.89  (-116:112:-114:110:111:113:115:117)
                  70 -71 72 -73 133 -132 imp:n=1 $ steel outer
110     4 -1.0   (-116:112:-114:110:111:113:115:117)
                  70 -71 72 -73 134 -133 imp:n=1 $ foam outer
111     3 -7.89  (-116:112:-114:110:111:113:115:117)
                  70 -71 72 -73 135 -134 imp:n=1 $ steel outer
c
c       Rear Impact Limiter
c
200     4 -1.0   116 -112 114 -110 -111 -113 -115 -117 45  -200  imp:n=1 $ 120 mm foam
201     3 -7.89  116 -112 114 -110 -111 -113 -115 -117 200 -201  imp:n=1 $ 15 mm steel
202     4 -1.0   116 -112 114 -110 -111 -113 -115 -117 201 -202  imp:n=1 $ 60 mm balsa
203     3 -7.89  116 -112 114 -110 -111 -113 -115 -117 202 -203  imp:n=1 $ 6 mm steel
204     4 -1.0   116 -112 114 -110 -111 -113 -115 -117 203 -213  imp:n=1 $ water
205     4 -1.0   (-116:112:-114:110:111:113:115:117)
```

```
                  70 -71 72 -73 45  -210 imp:n=1 $ foam outer
206     3 -7.89  (-116:112:-114:110:111:113:115:117)
                  70 -71 72 -73 210 -211 imp:n=1 $ steel outer
207     4 -1.0   (-116:112:-114:110:111:113:115:117)
                  70 -71 72 -73 211 -212 imp:n=1 $ foam outer
208     3 -7.89  (-116:112:-114:110:111:113:115:117)
                  70 -71 72 -73 212 -213 imp:n=1 $ steel outer
c
c       Reflection
c
999     0   -80:81:-82:83:-135:213 imp:n=0

5     so 13.8603     $ source
c
10    px -92 $ CSA inner cavity
11    px  92
12    py -100
13    py  100
14    pz -139.5
15    pz  139.5
c
20    px -92.8  $ CSA inner wall (8 mm)
21    px  92.8  $ 8 mm
22    py -100.8 $ 8 mm
23    py  100.8 $ 8 mm
24    pz -140.7 $ 12 mm
25    pz  140.3 $ 8 mm
c
30    px -105.2 $ CSA annulus
31    px  105.2
32    py -113.2
33    py  113.2
34    pz -153.1 $ CSA lid annulus
35    pz  153.5
c
40    px -106   $ CSA outer
41    px  106
42    py -114
43    py  114
44    pz -154.3 $ CSA lid
45    pz  154.3
46    pz -128.7 $ side balsa/foam extent
47    pz  128.7
c
50    px -117.4 $ 114 mm foam
51    px  117.4 $ 114 mm foam
52    py -124.9 $ 109 mm foam
53    py  124.9 $ 109 mm foam
c
60    px -118.4 $ 10 mm steel
61    px  118.4
62    py -125.9
63    py  125.9
c
70    px -121.86 $ 60 mm balsa with 1" crush
71    px  121.86 $ 1" crush
72    py -129.36 $ 1" crush
73    py  129.36 $ 1" crush
c
*80    px -122.46 $ 6 mm steel (outer)
*81    px  122.46
*82    py -129.96
*83    py  129.96
c
90    px -86.35  $ picked to match steel width
91    px  86.35
92    py -94.9
```

```
93    py  94.9
c
c      Front Impact Limiter Surfaces
c
110    px  104.8
111    p   104.8  19.95 0  16.2  113.7 0  16.2  113.7 1
112    py  113.7
113    p  -104.8  19.95 0 -16.2  113.7 0 -16.2  113.7 1
114    px -104.8
115    p  -104.8 -19.95 0 -16.2 -113.7 0 -16.2 -113.7 1
116    py -113.7
117    p   104.8 -19.95 0  16.2 -113.7 0  16.2 -113.7 1
c
120    pz  -154.9 $ 6 mm steel
121    pz  -166.9 $ 120 mm foam
122    pz  -168.4 $ 15 mm steel
123    pz  -174.4 $ 60 mm balsa
124    pz  -175.0 $ 6 mm plate
130    pz  -159.1 $ 42 mm calcium silicate outer
131    pz  -160.7 $ 16 mm steel outer
132    pz  -198.9 $ 382 mm foam outer
133    pz  -199.5 $ 6 mm steel
134    pz  -205.88 $ 140 mm foam (crushed 3")
*135    pz  -206.68 $ 8 mm steel
c
c      Rear Impact Limiter Surfaces
c
200    pz  166.3 $ 120 mm foam
201    pz  167.8 $ 15 mm steel
202    pz  173.8 $ 60 mm balsa
203    pz  174.4 $ 6 mm steel
210    pz  199.1 $ 448 mm foam outer (gives overall length of 4288 mm)
211    pz  199.7 $ 6 mm steel outer
212    pz  206.08 $ 140 mm foam (crushed 3")
*213    pz  206.88 $ 8 mm steel outer

mode  n
sdef pos=0 0 0 rad=d1
si1 13.8603
kcode 1000 1.0 10 510
m1      94239.69c 7.6793E-05 $ fuel
        94240.66c 1.1246E-06
        1001.62c 6.9113E-02
        4009.62c 1.2329E-03
        6000.66c 9.8591E-03
        8016.62c 2.4698E-02
c        total 1.0498E-01
mt1   lwtr.60t be.60t
m2    1001.62c  6.9221E-02 $ reflector
      4009.62c  1.2348E-03
      6000.66c  9.8745E-03
      8016.62c  2.4736E-02
c     total     1.0507E-01
mt2   lwtr.60t be.60t
m3    6000.66c  -0.02      $ S31803 steel
      14000.60c -0.4
      15031.66c -0.025
      24000.50c -22.4
      25055.62c -0.7
      26000.55c -67.194
      28000.50c -5.8
      16000.62c -0.001
      42000.66c -3.3
      7014.62c  -0.16
m4    1001.62c   2         $ water
      8016.62c   1
mt4   lwtr.60t
```

```
m5     6000.66c   6          $ balsa
       1001.62c   10
       8016.62c   5
mt5    poly.60t
m6     6000.66c   -70        $ foam
       8016.62c   -14
       7014.62c   -6
       1001.62c   -10
mt6    poly.60t
```

7.0 OPERATING PROCEDURES

7.1 Procedures for Loading the Package

This section delineates the procedures for loading a payload into the TRUPACT–III packaging, and leakage rate testing of the containment boundary O–ring seals. Hereafter, reference to specific TRUPACT–III packaging components may be found in Appendix 1.3.1, *Packaging General Arrangement Drawings*.

The loading operation shall be performed in a dry environment. In the event of precipitation during outdoor loading operations, precautions, such as covering the payload cavity opening shall be implemented to prevent water or precipitation from entering. If precipitation enters the cavity, the free–standing water shall be removed prior to loading the payload.

7.1.1 Removal of the TRUPACT–III Package from the Transport Trailer/Railcar

1. Remove any devices covering the four (4) ISO fittings located at the upper corners of the body as necessary to allow engagement of a lifting device with the ISO fittings.
2. Disengage the straps, tie–rods, or equivalent on the transport trailer or railcar, and if necessary or desired, remove the tie–down assembly from the package.

   CAUTION: Failure to disengage the straps or tie–rods may cause damage to the packaging and/or transport trailer/railcar.
3. Rig an overhead crane, or equivalent, with an appropriate lift fixture capable of handling the TRUPACT–III package.
4. Lower the lift fixture onto the package and engage each ISO corner fitting.
5. Lift the package from the transport trailer or railcar and move the package to the loading station.
6. Place the package in the loading station, disengage from the four (4) ISO corner fittings, and remove the lift fixture.

7.1.2 Overpack Cover Removal

1. Open the two (2) M36 threaded holes in the top of the overpack cover.
2. Install lifting hardware into the two (2) M36 threaded holes.
3. Rig an overhead crane, or equivalent, to the lifting hardware.
4. Remove the two (2) tamper–indicating seals (if installed), any optional plugs that are installed in the attachment bolt access tubes, and the ten (10) M36 attachment bolts (socket head cap screws) from the overpack cover.
5. Remove the overpack cover from the body. Store the overpack cover in a manner to minimize potential damage.

7.1.3 Closure Lid Removal

1. Remove the vent port locking ring and vent port dust plug. Open the vent port to allow the payload cavity to vent to atmosphere.
2. Install lifting hardware into the two (2) M36 threaded holes in the top of the closure lid. Rig an overhead crane, or equivalent, to the lifting hardware.
3. Remove the forty–four (44) M36 closure bolts (socket head cap screws) from the closure lid.
4. Remove the closure lid from the body. If necessary, separate the closure lid from the body using the four special M36 jacking threaded holes. Store the closure lid in a manner such that potential damage to the closure lid's sealing surface is minimized.

7.1.4 Loading the Payload into the TRUPACT–III Package

The following loading sequence requires that the payload has been properly prepared per the requirements of the *TRUPACT–III TRU Waste Authorized Methods for Payload Control (TRUPACT–III TRAMPAC)*[1].

1. Install sealing surface protectors onto the sealing flange of the body.
2. If not previously installed, install the roller floor (or equivalent payload loading system) in the payload cavity.
3. Connect an appropriate moving device to the loaded payload pallet.
4. Move the loaded payload pallet into the cavity until the payload is fully inserted into the payload cavity.
5. Ensure that a minimum of 2 mm axial clearance is present between any part of the SLB2 end face and the plane of the TRUPACT–III closure lid inner surface.

7.1.5 Closure Lid Installation

1. Visually inspect the closure bolts for wear or damage that could impair their function and, if necessary, replace or repair per the requirements of the drawings in Appendix 1.3.1, *Packaging General Arrangement Drawings*.
2. Visually inspect both closure lid main O–ring seals. If necessary, remove the O–ring seal(s) and clean the seal(s) and the sealing surface(s) on the closure lid and body to remove contamination. If, during the visual examination, it is determined that damage to the O–ring seal(s) and/or sealing surface(s) is sufficient to impair containment integrity, replace the damaged seal(s) and/or repair the damaged sealing surface(s) per Section 8.2.3.2.1, *Seal Area Routine Inspection and Repair*.
3. Visually inspect the O–ring seals on the vent port insert. If necessary, remove the O–ring seals, and clean the seals and sealing surfaces on the vent port insert and in the vent port to remove contamination. If, during the visual examination, it is determined that damage to the

[1] U.S. Department of Energy (DOE), *TRUPACT–III TRU Waste Authorized Methods for Payload Control (TRUPACT–III TRAMPAC)*, U.S. Department of Energy, Carlsbad Field Office, Carlsbad, New Mexico.

O–ring seal(s) and/or sealing surface is sufficient to impair containment integrity, replace the damaged seal(s) and/or repair the damaged sealing surface per Section 8.2.3.2.1, *Seal Area Routine Inspection and Repair*.

4. Visually inspect the debris shield foam insert and the eight (8) polyethylene filters for wear or damage that could impair their function and, if necessary, replace or repair per the requirements of the drawings in Appendix 1.3.1, *Packaging General Arrangement Drawings*.
5. As an option, remove and sparingly apply vacuum grease to the O–ring seals and/or sealing surfaces. Reinstall O–ring seals into the appropriate seal grooves in the closure lid and the vent port insert.
6. As an option, apply a silicone lubricant to the debris shield silicone foam insert.
7. If not previously installed, install lifting hardware into the two (2) M36 threaded holes in the top of the closure lid.
8. Remove the sealing surface protectors from the sealing flange of the body.
9. Visually inspect the guide pins and the threaded holes for the closure bolts on the body sealing flange for wear or damage that could impair their function and, if necessary, replace or repair per the requirements of the drawings in Appendix 1.3.1, *Packaging General Arrangement Drawings*.
10. Rig an overhead crane, or equivalent, to the lifting hardware. Install the closure lid onto the body.
11. Install the forty–four (44) M36 × 205 mm closure bolts (socket head cap screws) through the access tubes in the closure lid to secure the lid to the body. Tighten the closure bolts to 1,480 – 1,720 N–m (1,092 – 1,269 lb_f–ft) torque (lubricated).
12. Remove the lifting hardware.
13. If not previously installed, install the vent port retaining ring/insert assembly; tighten to 370 – 430 N–m (273 – 317 lb_f–ft) torque.
14. Leakage rate testing of the main containment O–ring seal and the vent port insert O–ring seal shall be performed based on the following criteria:
    a. If the inner main O–ring seal (containment) and/or vent port insert inner O–ring is replaced, or the corresponding sealing surface(s) were repaired, then perform the maintenance/periodic leakage rate test per Section 8.2.2.2, *Helium Leakage Rate Testing the Main Containment O–ring Seal*, or Section 8.2.2.3, *Helium Leakage Rate Testing the Vent Port Insert O–ring Seal* as appropriate.
    b. If there are no changes to the inner main O–ring seal (containment) or the vent port insert inner O–ring, and no repairs made to the corresponding sealing surfaces, then perform preshipment leakage rate testing per Section 7.4, *Preshipment Leakage Rate Test*, or per Section 8.2.2.2, *Helium Leakage Rate Testing the Main Containment O–ring Seal*, or Section 8.2.2.3, *Helium Leakage Rate Testing the Vent Port Insert O–ring Seal* as appropriate.

15. If not previously installed, install the seal test port plug; tighten to 8 – 12 N–m (5 – 9 lb_f–ft) torque.
16. Install the vent port locking ring; tighten to 370 – 430 N–m (273 – 317 lb_f–ft) torque.
17. Install the vent port dust plug; tighten to 90 – 110 N–m (66 – 81 lb_f–ft) torque.

7.1.6 Overpack Cover Installation

1. Visually inspect the M36 attachment bolts (socket head cap screws) for wear or damage that could impair their function and, if necessary, replace or repair per the requirements of the drawings in Appendix 1.3.1, *Packaging General Arrangement Drawings*.
2. If not previously installed, install lifting hardware into the two (2) M36 threaded holes in the top of the overpack cover.
3. Rig an overhead crane, or equivalent, to the lifting hardware. Install the overpack cover onto the body.
4. Install ten, M36 × 60 mm attachment bolts (socket head cap screws) in the overpack cover; tighten to 1,480 – 1,720 N–m (1,092 – 1,269 lb_f–ft) torque (lubricated).
5. Remove the lifting hardware, and install plastic plugs in the threaded holes.
6. If desired, install optional plugs into the overpack cover bolt access tubes.

7.1.7 Final Package Preparations for Transport (Loaded)

1. Install the two tamper–indicating devices (security seals) in the two overpack cover attachment bolt access tubes.
2. If the TRUPACT–III package is not already loaded onto and secured to the transport trailer or railcar, perform the following steps, as appropriate:
   a. Using an overhead crane, or equivalent, with a lift fixture of appropriate size, position the lift fixture on the top of the TRUPACT–III package and engage the ISO corner fittings. If the design of the tie–down frame allows, it may be pre–positioned on top of the TRUPACT–III package prior to positioning the lift fixture.
   b. Lift the loaded TRUPACT–III package, aligning the packaging over the tie–down points on the transport trailer or railcar.
   c. Disengage and remove the lift fixture from the top of the TRUPACT–III package.
   d. If not previously pre–positioned, install the tie–down assembly on top of the TRUPACT–III package. Install covers as/if necessary to disable the ISO fittings for use as a tie–down point.
   e. Secure the loaded TRUPACT–III package to the transport trailer or railcar using straps, tie–rods, or equivalent.
3. Monitor external radiation for each loaded TRUPACT–III package per the guidelines of 49 CFR §173.441[2].

[2] Title 49, Code of Federal Regulations, Part 173 (49 CFR 173), *Shippers–General Requirements for Shipments and Packagings*, 10–01–09 Edition.

4. Determine that surface contamination levels for each loaded TRUPACT–III package is per the guidelines of 49 CFR §173.443.
5. Determine the transport index for each loaded TRUPACT–III package per the guidelines of 49 CFR §173.403.
6. Complete all necessary shipping papers in accordance with Subpart C of 49 CFR 172[3].
7. TRUPACT–III package marking shall be in accordance with 10 CFR §71.85(c)[4] and Subpart D of 49 CFR 172. Package labeling shall be in accordance with Subpart E of 49 CFR 172. Package placarding shall be in accordance with Subpart F of 49 CFR 172.

[3] Title 49, Code of Federal Regulations, Part 172 (49 CFR 172), *Hazardous Materials Tables and Hazardous Communications Regulations*, 10–01–09 Edition.

[4] Title 10, Code of Federal Regulations, Part 71 (10 CFR 71), *Packaging and Transportation of Radioactive Material*, 01–01–09 Edition.

This page intentionally left blank.

7.2 Procedures for Unloading the Package

This section delineates the procedures for unloading a payload from the TRUPACT–III packaging. Hereafter, reference to specific TRUPACT–III packaging components may be found in Appendix 1.3.1, *Packaging General Arrangement Drawings*.

The unloading operation shall be performed in a dry environment. In the event of precipitation during outdoor unloading operations, precautions, such as covering the payload cavity shall be implemented to prevent water or precipitation from entering the cavity. If precipitation enters the cavity, the free–standing water shall be removed prior to installing the closure lid.

If the TRUPACT–III package will be unloaded while on the transport trailer or railcar, proceed directly to Section 7.2.2, *Overpack Cover Removal*.

7.2.1 Removal of the TRUPACT–III Package from the Transport Trailer/Railcar

1. Remove any devices covering the four (4) ISO fittings located at the upper corners of the body as necessary to allow engagement of a lifting device with the ISO fittings.
2. Disengage the straps, tie–rods, or equivalent on the transport trailer or railcar, and if necessary or desired, remove the tie–down assembly from the package.

   CAUTION: Failure to disengage the straps or tie–rods may cause damage to the packaging and/or transport trailer/railcar.
3. Rig an overhead crane, or equivalent, with an appropriate lift fixture capable of handling the TRUPACT–III package.
4. Lower the lift fixture onto the package and engage each ISO corner fitting.
5. Lift the package from the transport trailer or railcar and move the package to the unloading station.
6. Place the package in the unloading station, disengage from the four (4) ISO corner fittings, and remove the lift fixture.

7.2.2 Overpack Cover Removal

1. Open the two (2) M36 threaded holes in the top of the overpack cover.
2. Install lifting hardware into the two (2) M36 threaded holes in the top of the overpack cover.
3. Rig an overhead crane, or equivalent, to the lifting hardware.
4. Remove the two (2) tamper indicating seals, any optional plugs that are installed in the attachment bolt access tubes, and the ten (10) M36 attachment bolts (socket head cap screws) from the overpack cover.
5. Remove the overpack cover from the body. Store the overpack cover in a manner to minimize potential damage.

7.2.3 Closure Lid Removal

1. Remove the vent port locking ring and vent port dust plug. Open the vent port to allow the payload cavity to vent to atmosphere.
2. Install lifting hardware into the two (2) M36 threaded holes in the top of the closure lid. Rig an overhead crane, or equivalent, to the lifting hardware.
3. Remove the forty–four (44) M36 closure bolts (socket head cap screws) from the closure lid.
4. Remove the closure lid from the body. If necessary, separate the closure lid from the body using the four special M36 jacking threaded holes. Store the closure lid in a manner such that potential damage to the closure lid's sealing surface is minimized.

7.2.4 Unloading the Payload from the TRUPACT–III Package

1. Install sealing surface protectors to the sealing flange of the body.
2. Connect an appropriate moving device to the payload pallet.
3. Remove the loaded payload pallet from the payload cavity.

7.2.5 Closure Lid Installation

1. Visually inspect the closure bolts for wear or damage that could impair their function and, if necessary, replace or repair per the requirements of the drawings in Appendix 1.3.1, *Packaging General Arrangement Drawings*.
2. Visually inspect both closure lid main O–ring seals. If necessary, remove the O–ring seal(s) and clean the seal(s) and the sealing surface(s) on the closure lid and body to remove contamination. If, during the visual examination, it is determined that damage to the O–ring seal(s) and/or sealing surface(s) is sufficient to impair containment integrity, replace the damaged seal(s) and/or repair the damaged sealing surface(s) per Section 8.2.3.2.1, *Seal Area Routine Inspection and Repair*.
3. Visually inspect the O–ring seals on the vent port insert. If necessary, remove the O–ring seals, and clean the seals and sealing surfaces on the vent port insert and in the vent port to remove contamination. If, during the visual examination, it is determined that damage to the O–ring seal(s) and/or sealing surface is sufficient to impair containment integrity, replace the damaged seal(s) and/or repair the damaged sealing surface per Section 8.2.3.2.1, *Seal Area Routine Inspection and Repair*.
4. Visually inspect the debris shield foam insert and the eight polyethylene filters for wear or damage that could impair their function and, if necessary, replace or repair per the requirements of the drawings in Appendix 1.3.1, *Packaging General Arrangement Drawings*.
5. As an option, remove and sparingly apply vacuum grease to the O–ring seals and/or sealing surfaces. Reinstall O–ring seals into the appropriate seal grooves in the closure lid and the vent port insert.
6. As an option, apply a silicone lubricant to the debris shield silicone foam insert.

7. If not previously installed, install lifting hardware into the two (2) M36 threaded holes in the top of the closure lid.
8. Remove the sealing surface protectors from the sealing flange of the body.
9. Visually inspect the guide pins and the threaded holes for the closure bolts on the body sealing flange for wear or damage that could impair their function and, if necessary, replace or repair per the requirements of the drawings in Appendix 1.3.1, *Packaging General Arrangement Drawings*.
10. Rig an overhead crane, or equivalent, to the lifting hardware. Install the closure lid onto the body.
11. Install the forty–four (44) M36 × 205 mm closure bolts (socket head cap screws) through the access tubes in the closure lid to secure the lid to the body. Tighten the closure bolts to at least 800 N–m [590 lb_f–ft], but no more than 1,480 – 1,720 N–m [1,092 – 1,269 lb_f–ft] torque (lubricated).
12. If not previously installed, install the vent port retaining ring/insert assembly; tighten to 370 – 430 N–m (273 – 317 lb_f–ft) torque.
13. Install the vent port locking ring; tighten to 370 – 430 N–m (273 – 317 lb_f–ft) torque.
14. Install the vent port dust plug; tighten to 90 – 110 N–m (66 – 81 lb_f–ft) torque.
15. Remove the lifting hardware from the two (2) M36 threaded holes in the top of the closure lid.

7.2.6 Overpack Cover Installation

1. Visually inspect the M36 attachment bolts (socket head cap screws) for wear or damage that could impair their function and, if necessary, replace or repair per the requirements of the drawings in Appendix 1.3.1, *Packaging General Arrangement Drawings*.
2. If not previously installed, install the lifting hardware into the two (2) M36 threaded holes in the top of the overpack cover.
3. Rig an overhead crane, or equivalent, to the lifting hardware. Install the overpack cover onto the body.
4. Install ten, M36 × 60 mm attachment bolts (socket head cap screws) in the overpack cover; tighten to at least 800 N–m [590 lb_f–ft], but no more than 1,480 – 1,720 N–m [1,092 – 1,269 lb_f–ft] torque (lubricated).
5. Remove the lifting hardware, and install plastic plugs in the threaded holes.
6. If desired, install optional plugs into the overpack cover bolt access tubes.

7.2.7 Final Package Preparations for Transport (Unloaded)

1. If the TRUPACT–III packaging is not already loaded onto and secured to the transport trailer or railcar, perform the following steps, as appropriate:
   a. Using an overhead crane, or equivalent, with a lift fixture of appropriate size, position the lift fixture on the top of the TRUPACT–III packaging and engage the ISO corner fittings. If the design of the tie–down frame allows, it may be pre–positioned on top of the TRUPACT–III packaging prior to positioning the lift fixture.

b. Lift the TRUPACT–III packaging, aligning the packaging over the tie–down points on the transport trailer or railcar.

c. Disengage and remove the lift fixture from the top of the TRUPACT–III packaging.

d. If not previously pre–positioned, install the tie–down assembly on top of the TRUPACT–III packaging. Install covers as/if necessary to disable the ISO fittings for use as a tie–down point.

e. Secure the TRUPACT–III packaging to the transport trailer or railcar using straps, tie–rods, or equivalent.

2. Transport the TRUPACT–III packaging in accordance with Section 7.3, *Preparation of an Empty Package for Transport*.

7.3 Preparation of an Empty Package for Transport

Previously used and empty TRUPACT–III packagings shall be prepared and transported per the requirements of 49 CFR §173.428[1].

[1] Title 49, Code of Federal Regulations, Part 173 (49 CFR 173), *Shippers–General Requirements for Shipments and Packagings*, 10–01–09 Edition.

This page intentionally left blank.

7.4 Preshipment Leakage Rate Test

After the TRUPACT–III package is assembled and prior to shipment, leakage rate testing shall be performed to confirm proper assembly of the package following the guidelines of Section 7.6, *Preshipment Leakage Rate Test*, and Appendix A.5.2, *Gas Pressure Rise*, of ANSI N14.5[1].

7.4.1 Gas Pressure Rise Leakage Rate Test Acceptance Criteria

In order to demonstrate containment integrity in preparation for shipment, no leakage shall be detected when tested to a sensitivity of 1×10^{-4} reference Pascals – cubic meters per second (ref–Pa–m^3/s) [1×10^{-3} reference cubic centimeters per second (ref–cm^3/s)] air, or less, per Section 7.6, *Preshipment Leakage Rate Test*, of ANSI N14.5.

7.4.2 Determining the Test Volume and Test Time

1. Assemble a leakage rate test apparatus that consists of, at a minimum, the components illustrated in Figure 7.4–1, using a calibrated volume with a range of 100 – 500 cubic centimeters (6 – 31 cubic inches), and a calibrated pressure transducer with a minimum sensitivity of 0.013 kPa (100 millitorr). Connect the test apparatus to the test volume (i.e., the seal test port, or vent port insert, as appropriate).
2. Set the indicated sensitivity on the digital readout of the calibrated pressure transducer, ΔP, to, at a minimum, the resolution (i.e., sensitivity) of the calibrated pressure transducer (e.g., ΔP = 0.00013, 0.0013, or 0.013 kPa [1, 10, or 100 millitorr] sensitivity).
3. Open all valves (i.e., the vent valve, calibration valve, and vacuum pump isolation valve), and record ambient atmospheric pressure, P_{atm}.
4. Isolate the calibrated volume by closing the vent and calibration valves.
5. Evacuate the test volume to a pressure less than the indicated sensitivity on the digital readout of the calibrated pressure transducer or 0.10 kPa [0.76 torr], whichever is less.
6. Isolate the vacuum pump from the test volume by closing the vacuum pump isolation valve. Allow the test volume pressure to stabilize and record the test volume pressure, P_{test} (e.g., $P_{test} < 0.00013$ kPa [1 millitorr] for an indicated sensitivity of 0.00013 kPa [1 millitorr]).
7. Open the calibration valve and, after allowing the system to stabilize, record the total volume pressure, P_{total}.
8. Knowing the calibrated volume, V_c, calculate and record the test volume, V_t, using the following equation:

$$V_t = V_c\left(\frac{P_{atm} - P_{total}}{P_{total} - P_{test}}\right)$$

[1] ANSI N14.5–1997 (or later), *American National Standard for Radioactive Materials – Leakage Tests on Packages for Shipment,* American National Standards Institute, Inc. (ANSI).

9. Knowing the indicated sensitivity on the digital readout of the calibrated pressure transducer, ΔP, calculate and record the test time, t, using the following equation:

$$t = \Delta P(1.32)V_t$$

7.4.3 Performing the Gas Pressure Rise Leakage Rate Test

1. Isolate the calibrated volume by closing the calibration valve.
2. Open the vacuum pump isolation valve and evacuate the test volume to a pressure less than the test volume pressure, P_{test}, determined in Step 6 of Section 7.4.2, *Determining the Test Volume and Test Time*.
3. Isolate the vacuum pump from the test volume by closing the vacuum pump isolation valve. Allow the test volume pressure to stabilize and record the beginning test pressure, P_1. After a period of time equal to "t" seconds, determined in Step 9 of Section 7.4.2, *Determining the Test Volume and Test Time*, record the ending test pressure, P_2. To be acceptable, there shall be no difference between the final and initial pressures such that the requirements of Section 7.4.1, *Gas Pressure Rise Leakage Rate Test Acceptance Criteria*, are met.
4. If, after repeated attempts, the O–ring seal fails to pass the leakage rate test, replace the damaged seal and/or repair the damaged sealing surfaces per Section 8.2.3.2.1, *Seal Area Routine Inspection and Repair*. Perform verification leakage rate test per the applicable procedure delineated in Section 8.2.2, *Maintenance/Periodic Leakage Rate Tests*.

7.4.4 Optional Preshipment Leakage Rate Test

As an option to Section 7.4.3, *Performing the Gas Pressure Rise Leakage Rate Test*, Section 8.2.2, *Maintenance/Periodic Leakage Rate Tests*, may be performed.

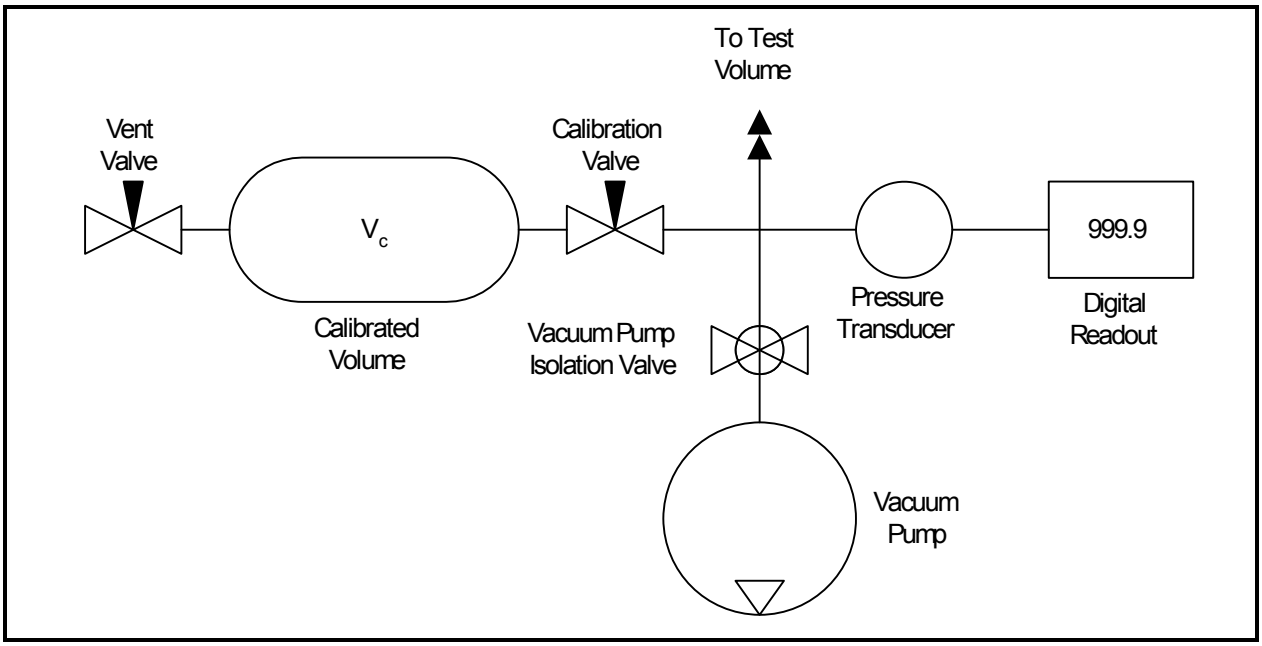

Figure 7.4-1 – Pressure Rise Leakage Rate Test Schematic

8.0 ACCEPTANCE TESTS AND MAINTENANCE PROGRAM

8.1 Acceptance Tests

Per the requirements of 10 CFR §71.85[1], this section discusses the inspections and tests to be performed prior to first use of the TRUPACT–III packaging. Acceptance criteria for all inspections and tests are found either on the drawings in Appendix 1.3.1, *Packaging General Arrangement Drawings,* or in the sections that follow. Deviations from requirements will be recorded and dispositioned in accordance with the cognizant quality assurance program.

8.1.1 Visual Inspections and Measurements

Each TRUPACT–III will be visually inspected and measured to ensure that all of the requirements delineated on the drawings in Appendix 1.3.1, *Packaging General Arrangement Drawings*, including but not limited to such items as materials, physical arrangement of components, quantities, dimensions, welds, and measurements, are satisfied.

8.1.2 Weld Examinations

The locations, types, and sizes of all welds will be identified and recorded to ensure compliance with the drawings in Appendix 1.3.1, *Packaging General Arrangement Drawings*. All welds in each TRUPACT–III packaging will be visually examined. With the exception of seal and specific non–structural welds, all welds will be liquid penetrant examined. In addition, all welds in the containment boundary will be examined by radiography. Alternatives to radiographic examination of containment boundary welds are delineated in General Note 48 on the drawings provided in Appendix 1.3.1, *Packaging General Arrangement Drawings*. Visual examination is performed according to AWS Specification D1.6[2]. Liquid penetrant, ultrasonic, and radiograph examinations are performed according to the relevant sections of the ASME code, as specified for each weld on the drawings.

8.1.3 Structural and Pressure Tests

8.1.3.1 Lifting Device Load Testing

From Section 2.1.3, *Weights and Center of Gravity*, the maximum weight of the TRUPACT–III is 25,000 kilograms (55,116 pounds). Each upper ISO corner fitting is designed to carry approximately 59% of the maximum lifted load, or 14,650 kg (32,298 lb). Each ISO corner fitting shall be load tested to 150% of the maximum working load, or at least 21,975 kg (48,447 lb), per ANSI N14.6[3].

---

[1] Title 10, Code of Federal Regulations, Part 71 (10 CFR 71), *Packaging and Transportation of Radioactive Material*, 01–01–09 Edition.

[2] ANSI/AWS D1.6:1999, *Structural Welding Code – Stainless Steel*, American Welding Society (AWS).

[3] ANSI N14.6–1993, *American National Standard for Radioactive Materials – Special Lifting Devices for Shipping Containers Weighing 10,000 Pounds (4,500 kg) or More*, American National Standard Institute, Inc. (ANSI).

Following load testing of the ISO corner fittings, all welds and adjacent base metal (minimum 13 mm [0.5 in.] on each side of the weld) directly related to the load testing of the fitting shall be visually inspected for plastic deformation or cracking in accordance with AWS D1.6, and liquid penetrant inspected per ASME B & PV Code, Section III[4], Division 1, Subsection NF, Article NF–5000, and Section V[5], Article 6, as delineated on the drawings in Appendix 1.3.1, *Packaging General Arrangement Drawings*. Indications of cracking or distortion shall be recorded and evaluated in accordance with the cognizant quality assurance program.

8.1.3.2 Containment Vessel Pressure Testing

Per the requirements of 10 CFR §71.85(b), the containment structural assembly (CSA) shall be pressure tested to 150% of the maximum normal operating pressure (MNOP) to verify structural integrity. The MNOP of the TRUPACT–III package is equal to 172 kPa (25 psig). Thus, the CSA shall be pressure tested to at least $172 \times 1.5 = 258$ kPa (37.5 psig).

Following pressure testing of the CSA, accessible base material and welds directly related to the pressure testing of the containment boundary sheets of the CSA shall be visually inspected for plastic deformation or cracking in accordance with AWS D.1.6, and liquid penetrant inspected per ASME B & PV Code, Section III, Division 1, Subsection NB, Article NB–5000, and Section V, Article 6, as delineated on the drawings in Appendix 1.3.1, *Packaging General Arrangement Drawings*. Indications of cracking or distortion shall be recorded and evaluated in accordance with the cognizant quality assurance program.

Leakage rate testing per Section 8.1.4, *Fabrication Leakage Rate Tests*, shall be performed after completion of pressure testing to verify package configuration and performance to design criteria.

8.1.4 Fabrication Leakage Rate Tests

This section provides the generalized procedure for fabrication leakage rate testing of the containment vessel boundaries and penetrations following the completion of fabrication. Fabrication leakage rate testing shall follow the guidelines of Section 7.3, *Fabrication Leakage Rate Test*, of ANSI N14.5[6].

Prior to leakage rate testing, internal components that are not permanently affixed to the containment plate, such as the payload, roller floor, and payload pallet, shall be removed. For ease of leakage rate testing, the interior surfaces of the CSA should be thoroughly cleaned. As an option, the debris shield insert may be omitted from the assembly for fabrication leakage rate tests.

Fabrication leakage rate testing shall be performed on the CSA. Three separate tests comprise the series. Each test shall meet the acceptance criteria delineated in Section 8.1.4.1, *Fabrication Leakage Rate Test Acceptance Criteria*.

---

[4] American Society of Mechanical Engineers (ASME) Boiler and Pressure Vessel Code, Section III, *Rules for Construction of Nuclear Power Plant Components*, 2004 Edition, 2005 and 2006 Addenda.

[5] American Society of Mechanical Engineers (ASME) Boiler and Pressure Vessel Code, Section V, *Nondestructive Examination*, 2004 Edition, 2005 and 2006 Addenda.

[6] ANSI N14.5–1997 (or later), *American National Standard for Radioactive Materials – Leakage Tests on Packages for Shipment,* American National Standards Institute, Inc. (ANSI).

8.1.4.1 Fabrication Leakage Rate Test Acceptance Criteria

1. To be acceptable, each leakage rate test shall demonstrate a leakage rate of 1×10^{-8} reference Pascals – cubic meter per second (Pa–m^3/s) [1×10^{-7} ref cm^3/s], air, or less, per Section 6.3, *Application of Referenced Air Leakage Rate (L_R)*, of ANSI N14.5.
2. In order to adequately demonstrate this leakage rate, the sensitivity of the leakage rate test procedure shall be 5×10^{-9} Pa–m^3/s (5×10^{-8} cm^3/s), air, or less, per Section 8.4, *Sensitivity*, of ANSI N14.5.
3. Failure to meet the stated leakage rate shall be recorded and evaluated in accordance with the cognizant quality assurance program.

8.1.4.2 Helium Leakage Rate Testing the Containment Structure Integrity

1. The fabrication leakage rate test of the containment structure shall be performed following the guidelines of Section A.5.3, *Gas Filled Envelope – Gas Detector*, of ANSI N14.5.
2. Remove the body helium fill access plugs (inner and outer) in the closure lid and the body helium fill port plug in the body.
3. The CSA shall be assembled with both main O–ring seals installed into the closure lid, and the O–ring identified for the B1 groove installed in the closure lid. Tighten the closure bolts to 1,480 – 1,720 N–m (1,092 – 1,269 lb_f–ft) torque as shown in Appendix 1.3.1, *Packaging General Arrangement Drawings*.
4. Remove the vent port locking ring, and back–off or remove the vent port retaining ring and vent port insert. Install an adapter to the vent port to allow gas flow to and from the cavity.
5. Install a helium mass spectrometer leak detector to the adapter on the vent port. Evacuate the payload cavity through the vent port until the vacuum is sufficient to operate the helium mass spectrometer leak detector.
6. Connect a vacuum pump to the outer body helium fill access port in the closure lid and evacuate the annulus (defined as the space within the sandwich construction of the CSA body and lid walls) to 90% vacuum or better (i.e., ≤10% ambient atmospheric pressure).
7. Provide a helium atmosphere inside the annulus by backfilling with helium gas to a pressure slightly greater than atmospheric pressure, i.e., +7, -0 kPa (+1, -0 psig).
8. Perform the helium leakage rate test to the requirements of Section 8.1.4.1, *Fabrication Leakage Rate Test Acceptance Criteria*. If, after repeated attempts, the CSA structure fails to pass the leakage rate test, isolate the leak path and, prior to repairing the leak path and repeating the leakage rate test, record on a nonconformance report and disposition prior to final acceptance in accordance with the governing quality assurance program.

8.1.4.3 Helium Leakage Rate Testing the Main Containment O–ring Seal

1. The fabrication leakage rate test of the main containment O–ring seal (inner) shall be performed following the guidelines of Section A.5.4, *Evacuated Envelope – Gas Detector*, of ANSI N14.5.
2. The CSA shall be assembled with both main O–ring seals installed into the closure lid. If not previously tightened, tighten the closure bolts to 1,480 – 1,720 N–m (1,092 – 1,269 lb_f–ft) torque as shown in Appendix 1.3.1, *Packaging General Arrangement Drawings*.
3. Remove the vent port locking ring, and back–off or remove the vent port retaining ring and vent port insert. Install an adapter to the vent port to allow gas flow to and from the cavity.
4. Connect a vacuum pump to the adapter on the vent port, and evacuate the payload cavity to 90% vacuum or better (i.e., ≤10% ambient atmospheric pressure).
5. Remove the seal test port plug in the closure lid. Install an adapter to the seal test port.
6. Install a helium mass spectrometer leak detector to the adapter on the seal test port. Evacuate through the seal test port until the vacuum is sufficient to operate the helium mass spectrometer leak detector.
7. Provide a helium atmosphere inside the payload cavity by backfilling with helium gas to a pressure slightly greater than atmospheric pressure, i.e., +7, -0 kPa (+1, -0 psig).
8. Perform the helium leakage rate test to the requirements of Section 8.1.4.1, *Fabrication Leakage Rate Test Acceptance Criteria*. If, after repeated attempts, the main containment O–ring seal fails to pass the leakage rate test, isolate the leak path and, prior to repairing the leak path and repeating the leakage rate test, record on a nonconformance report and disposition prior to final acceptance in accordance with the governing quality assurance program.

8.1.4.4 Helium Leakage Rate Testing the Vent Port Insert O–ring Seal

1. The fabrication leakage rate test of the vent port insert O–ring seal shall be performed following the guidelines of Section A.5.4, *Evacuated Envelope – Gas Detector*, of ANSI N14.5.
2. The closure lid shall be assembled with both main O–ring seals installed into the vent port insert. Assembly is as shown in Appendix 1.3.1, *Packaging General Arrangement Drawings*.
3. Remove the vent port locking ring and vent port dust plug. Ensure that the vent port retaining ring is tightened to 370 – 430 N–m (273 – 317 lb_f–ft) torque.
4. Install an adapter to the internal threads of the vent port insert.
5. Install a helium mass spectrometer leak detector to the adapter on the vent port. Evacuate through the vent port until the vacuum is sufficient to operate the helium mass spectrometer leak detector.
6. Install an evacuation envelope over the ∅50–mm vent port on the inside surface of the closure lid. If desired, the TRUPACT–III body may be utilized as the envelope.
7. Connect a vacuum pump to the evacuation envelope and evacuate the envelope to 90% vacuum or better (i.e., ≤10% ambient atmospheric pressure).
8. Provide a helium atmosphere inside the evacuation envelope by backfilling with helium gas to a pressure slightly greater than atmospheric pressure, i.e., +7, -0 kPa (+1, -0 psig).

9. Perform the helium leakage rate test to the requirements of Section 8.1.4.1, *Fabrication Leakage Rate Test Acceptance Criteria*. If, after repeated attempts, the vent port insert O–ring seal fails to pass the leakage rate test, isolate the leak path and, prior to repairing the leak path and repeating the leakage rate test, record on a nonconformance report and disposition prior to final acceptance in accordance with the governing quality assurance program.

8.1.5 Component Tests

8.1.5.1 Polyurethane Foam

This section establishes the requirements and acceptance criteria for installation, inspection, and testing of the rigid, closed–cell, polyurethane foam utilized within the TRUPACT–III packaging.

8.1.5.1.1 Introduction and General Requirements

The polyurethane foam used within the TRUPACT–III packaging is comprised of a specific "formulation" of foam constituents that, when properly apportioned, mixed, and reacted, produce a polyurethane foam material with physical characteristics consistent with the requirements given in this section. In practice, the chemical constituents are batched into multiple parts (e.g., parts A and B) for later mixing in accordance with a formulation. Therefore, a foam "batch" is considered to be a specific grouping and apportionment of chemical constituents into separate and controlled vats or bins for each foam formulation part. Portions from each batch part are combined in accordance with the foam formulation requirements to produce the liquid foam material for pouring into a component or box. Thus, a foam "pour" is defined as apportioning and mixing the batch parts into a desired quantity for subsequent installation (pouring). Finally, all contiguous pours into a single mold are termed a "bun".

The following sections describe the general requirements for constituent storage, and foam pour and test data records.

8.1.5.1.1.1 Polyurethane Foam Constituent Storage

The foam supplier shall certify that the polyurethane foam constituents have been properly stored prior to use, and that the polyurethane foam constituents have been used within their shelf life.

8.1.5.1.1.2 Polyurethane Foam Pour and Test Data Records

A production pour and testing record shall be compiled by the foam supplier during the foam pouring operation and subsequent physical testing. Upon completion of production and testing, the foam supplier shall issue a certification referencing the production record data and test data pertaining to each foamed component. At a minimum, relevant pour and test data shall include:

- formulation, batch, and pour numbers, with foam material traceability, and pour date,
- instrumentation description, serial number, and calibration due date,
- pour and test data (e.g., date, temperature, dimensional, and/or weight measurements, compressive stress, etc., as applicable), and
- technician and Quality Assurance/Quality Control (QA/QC) sign–off.

8.1.5.1.2 Physical Characteristics

The following subsections define the required physical characteristics of the polyurethane foam material used for the TRUPACT–III packaging design.

Testing for the various polyurethane foam physical characteristics is based on a "formulation", "batch", or "pour", as appropriate, as defined in Section 8.1.5.1.1, *Introduction and General Requirements*. The physical characteristics determined for a specific foam formulation are relatively insensitive to small variations in chemical constituents and/or environmental conditions, and therefore include physical testing only for leachable chlorides, thermal conductivity, and specific heat. Similarly, the physical characteristics determined for a batch are only slightly sensitive to small changes in formulation and/or environmental conditions during batch mixing, and therefore include physical testing only for flame retardancy. Finally, the physical characteristics determined for a pour are also only slightly sensitive to small changes in formulation and slightly more sensitive to variations in environmental conditions during pour mixing, and therefore include physical testing for density and compressive stress.

8.1.5.1.2.1 Physical Characteristics Determined for a Foam Formulation

8.1.5.1.2.1.1 Leachable Chlorides

Polyurethane foam material physical characteristic for leachable chlorides shall be determined once for a particular foam formulation. If multiple components are to utilize a specific foam formulation, then additional physical testing, as defined below, need not be performed.

1. The leachable chlorides test shall be performed using an ion chromatograph (IC) apparatus. The IC measures inorganic anions of interest (i.e., chlorides) in water. Description of a typical IC is provided in EPA Method 300.0[1]. The IC shall be calibrated against a traceable reference specimen per the IC manufacturer's operating instructions.
2. One test sample shall be taken from a pour for each foam formulation. The test sample shall be a cube with dimensions of 50 ±1 mm (2.00 ±0.03 in).
3. Place the test sample in a room (ambient) temperature environment (i.e., 20 ºC to 30 ºC [68 ºF to 86 ºF]) for sufficient time to thermally stabilize the test sample. Measure and record the room temperature to an accuracy of ±1 ºC (±2 ºF).
4. Obtain a minimum of 550 ml of distilled or de–ionized water for testing. The test water shall be from a single source to ensure consistent anionic properties for testing control.
5. Obtain a 400 ml, or larger, contaminant free container that is capable of being sealed. Fill the container with 250 ±3 ml of test water. Fully immerse the test sample inside the container for a duration of 72 ±3 hours. If necessary, use an inert standoff to ensure the test sample is completely immersed for the full test duration. Seal the container prior to the 72–hour duration.
6. Obtain a second, identical container to use as a "control". Fill the control container with 250 ±3 ml of the same test water. Seal the control container prior to the 72–hour duration.

[1] EPA Method 300.0, Revision 2.2 (October 1999), *Determination of Inorganic Anions by Ion Chromatography*, U.S. Environmental Protection Agency.

7. At the end of the test period, measure and record the leachable chlorides in the test water per the IC manufacturer's operating instructions. The leachable chlorides in the test water shall not exceed one part per million (1 ppm).
8. Should leachable chlorides in the test water exceed 1 ppm, measure and record the leachable chlorides in the test water from the "control" container. The difference in leachable chlorides from the test water and "control" water sample shall not exceed 1 ppm.

8.1.5.1.2.1.2 Thermal Conductivity

1. The thermal conductivity test shall be performed using a heat flow meter (HFM) apparatus. The HFM establishes steady state unidirectional heat flux through a test specimen between two parallel plates at constant but different temperatures. By measurement of the plate temperatures and plate separation, Fourier's law of heat conduction is used by the HFM to automatically calculate thermal conductivity. Description of a typical HFM test method is provided in ASTM C518[2]. The HFM shall be calibrated against a traceable reference specimen per the HFM manufacturer's operating instructions.
2. Three test samples shall be taken from the sample pour. Each test sample shall be of sufficient size to enable testing per the HFM manufacturer's operating instructions.
3. Place the test samples in a room (ambient) temperature environment (i.e., 20 ºC to 30 ºC [68 ºF to 86 ºF]) for sufficient time to thermally stabilize the test samples.
4. Measure and record the necessary test sample parameters as input data to the HFM apparatus per the HFM manufacturer's operating instructions.
5. Perform thermal conductivity testing and record the measured thermal conductivity for each test sample following the HFM manufacturer's operating instructions.
6. Determine and record the average thermal conductivity of the three test samples. The numerically averaged thermal conductivity of the three test samples shall lie within the ranges shown by Table 8.1–1.

8.1.5.1.2.1.3 Specific Heat

1. The specific heat test shall be performed using a differential scanning calorimeter (DSC) apparatus. The DSC establishes a constant heating rate and measures the differential heat flow into both a test specimen and a reference specimen. The DSC shall be calibrated against a traceable reference specimen per the DSC manufacturer's operating instructions.
2. Three test samples shall be taken from the sample pour. Each test sample shall be of sufficient size to enable testing per the DSC manufacturer's operating instructions.
3. Place the test samples in a room (ambient) temperature environment (i.e., 20 ºC to 30 ºC [68 ºF to 86 ºF]) for sufficient time to thermally stabilize the test samples.

[2] ASTM C518–04, *Standard Test Method for Steady–State Thermal Transmission Properties by Means of the Heat Flow Meter Apparatus*, American Society for Testing and Materials (ASTM).

4. Measure and record the necessary test sample parameters as input data to the DSC per the DSC manufacturer's operating instructions.
5. Perform specific heat testing and record the measured specific heat for each test sample following the DSC manufacturer's operating instructions.
6. Determine and record the average specific heat of the three test specimens. The numerically averaged specific heat of the three test samples shall be within the range between 1.12 and 1.86 J/g–ºC (0.27 and 0.44 Btu/lb–ºF).

8.1.5.1.2.2 Physical Characteristics Determined for a Foam Batch

Polyurethane foam material physical characteristics for flame retardancy shall be determined once for a particular foam batch based on the batch definition in Section 8.1.5.1.1, *Introduction and General Requirements*. If single or multiple components are to utilize a single foam batch, then additional flame retardancy testing, as defined below, need not be performed for each foam pour.

Polyurethane foam shall be tested for flame retardancy as follows:

1. Three test samples shall be taken from a pour from each foam batch. Each test sample shall be a rectangular prism with nominal dimensions of 13 mm (0.5 in) thick, 75 mm (3.0 in) wide, and a minimum length of 178 mm (7.0 in). In addition, individual sample lengths must not be less than the total burn length observed for the sample when tested.
2. Place the test samples in a room (ambient) temperature environment (i.e., 20 ºC to 30 ºC [68 ºF to 86 ºF]) for sufficient time to thermally stabilize the test samples. Measure and record the room temperature to an accuracy of ±1 ºC (±2 ºF).
3. Measure and record the length of each test sample to an accuracy of ±3 mm (±0.1 in).
4. Install an approximately 10–mm [3/8 in], or larger, Bunsen or Tirrill burner inside an enclosure of sufficient size to perform flame retardancy testing. Adjust the burner flame height to 38 ±5 mm (1½ ±1/8 in). Verify that the burner flame temperature is 850 ºC (1,562 ºF), minimum.
5. Support the test sample with the long axis oriented vertically within the enclosure such that the test sample's bottom edge will be 19 ±2 mm (3/4 ±1/16 in, see adjacent figure) above the top edge of the burner.

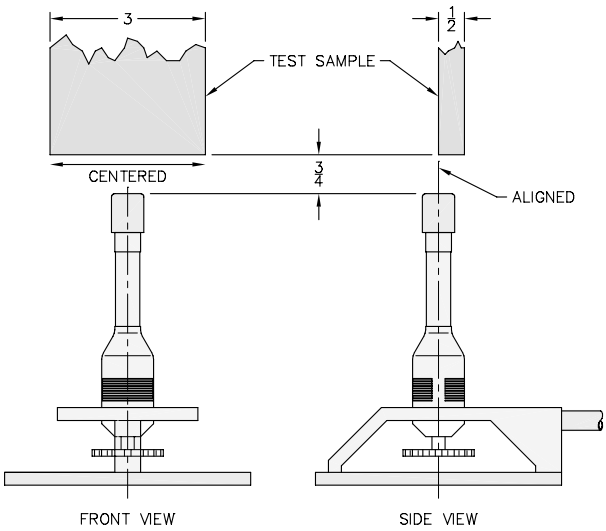

6. Move the burner flame under the test sample for an elapsed time of 60 ±3 seconds. As illustrated, align the burner flame with the front edge of the test sample thickness and the center of the test sample width.
7. Immediately after removal of the test sample from the burner flame, measure and record the following data:

a. Measure and record, to the nearest second, the elapsed time until flames from the test sample extinguish.

b. Measure and record, to the nearest second, the elapsed time from the occurrence of drips, if any, until drips from the test sample extinguish.

c. Measure and record, to the nearest 3 mm, the burn length following cessation of all visible burning and smoking.

8. Flame retardancy testing acceptance is based on the following criteria:

a. The numerically averaged flame extinguishment time of the three test samples shall not exceed fifteen seconds.

b. The numerically averaged flame extinguishment time of drips from the three test samples shall not exceed three seconds.

c. The numerically averaged burn length of the three test samples shall not exceed 150 mm (6.0 in).

8.1.5.1.2.3 Physical Characteristics Determined for a Foam Pour

8.1.5.1.2.3.1 Density

Polyurethane foam material physical characteristic for density shall be determined for each foam pour based on the pour definition in Section 8.1.5.1.1, *Introduction and General Requirements*.

1. Three test samples shall be taken from the foam pour. Each test sample shall be a rectangular prism with minimum nominal dimensions of 25 mm (1.0 in) thick (T) × 25 mm (1.0 in) wide (W) × 25 mm (1.0 in) long (L).
2. Place the test samples in a room (ambient) temperature environment (i.e., 20 ºC to 30 ºC [68 ºF to 86 ºF]) for sufficient time to thermally stabilize the test samples. Measure and record the room temperature to an accuracy of ±1 ºC (±2 ºF).
3. Measure and record the weight of each test sample to an accuracy of ±1 gram (±0.03 oz).
4. Measure and record the thickness, width, and length of each test sample to an accuracy of ±0.04 mm (±0.002 in).
5. Determine and record the room temperature density of each test sample utilizing the following formula:

$$\rho_{foam} = \frac{\text{Weight, g}}{\text{T} \times \text{W} \times \text{L, mm}^3} \times \frac{10^6 \text{ mm}^3/\text{dm}^3}{10^3 \text{ g/kg}}, \text{ kg/dm}^3$$

6. Determine and record the average density of the three test samples. The numerically averaged density of the three test samples shall be within ±15% of the specified nominal foam density.

8.1.5.1.2.3.2 Compressive Stress

1. Three test samples shall be taken from each foam pour. Each test sample shall be a rectangular prism with minimum nominal dimensions of 25 mm (1.0 in) thick (T) × 25 mm (1.0 in) wide (W) × 25 mm (1.0 in) long (L). The thickness dimension shall be the parallel–to–rise direction (for the perpendicular–to–rise direction, see below).
2. Place the test samples in a room (ambient) temperature environment (i.e., 20 ºC to 30 ºC [68 ºF to 86 ºF]) for sufficient time to thermally stabilize the test samples. Measure and record the room temperature to an accuracy of ±1 ºC (±2 ºF).
3. Measure and record the thickness, width, and length of each test sample to an accuracy of ±0.04 mm (±0.002 in).
4. Compute and record the surface area of each test sample by multiplying the width by the length (i.e., W × L).
5. Place a test sample in a Universal Testing Machine. Lower the machine's crosshead until it touches the test sample. Set the machine's parameters for the thickness of the test sample.
6. Determine and record the average parallel–to–rise compressive stress of the three test samples from each batch pour for each foam density. As shown in Table 8.1-2, the average parallel–to–rise compressive stress for each foam pour shall be the nominal compressive stress ±15% at strains of 10%, 40%, and 70% (60% for 0.48 kg/dm^3 [30 lb/ft^3] foam).
7. Determine and record the average parallel–to–rise compressive stress of all test samples from each foamed component. As shown in Table 8.1-2, the average parallel–to–rise compressive stress for all foam pours used in a single bun shall be the nominal compressive stress ±10% at strains of 10%, 40%, and 70% (60% for 0.48 kg/dm^3 [30 lb/ft^3] foam).
8. Data for compressive stress in the perpendicular–to–rise direction shall be obtained in an identical manner, using three additional test samples, except that the thickness dimension of the test samples shall be perpendicular to the foam rise direction. As shown in Table 8.1-3, the average perpendicular–to–rise compressive stress for each foam pour shall be the nominal compressive stress ±15% at strains of 10%, 40%, and 70% (60% for 0.48 kg/dm^3 [30 lb/ft^3] foam). As further shown in Table 8.1-3, the average perpendicular–to–rise compressive stress for all foam pours used in a single bun shall be the nominal compressive stress ±10% at strains of 10%, 40%, and 70% (60% for 0.48 kg/dm^3 [30 lb/ft^3] foam).

8.1.5.2 Balsa Wood

Balsa wood material physical characteristics for the following parameters shall be determined for each lot based on the following acceptance tests. All wood shall be free of gross defects and knots. Acceptable panel defects are as follows:

1. Cracks less than 1.5 mm (0.06 in) wide and less than 120 mm (4.72 in) long
2. A maximum of 4 cracks from 1.5 mm to 8 mm (0.06 in to 0.32 in) wide and less than 150 mm (6 in) long per panel.

8.1.5.2.1 Density

The density of each wood lot shall be determined in accordance with ASTM D2395[3], Method A. At least three test samples shall be taken from each lot of wood. The numerically averaged density of the test samples shall be within the range 0.11 ± 0.03 kg/dm³ (6.9 ±1.9 lb_m/ft^3).

8.1.5.2.2 Moisture Content

The moisture content of each wood lot shall be determined in accordance with ASTM D4442[4] or ASTM D4444[5]. At least three test samples shall be taken from each lot of wood. The moisture content shall be determined within 12 hours prior to being installed into the packaging. The moisture content for all wood samples shall not exceed 12%.

8.1.5.3 Butyl Rubber O–rings

Physical characteristics of butyl rubber containment O–ring seals for the following parameters shall be determined for each lot based on the following acceptance tests.

8.1.5.3.1 Durometer

The durometer of each lot of the butyl rubber material shall be determined in accordance with ASTM D2240[6]. Each lot of butyl rubber material shall have a hardness of 70 ±5 Shore A durometer (i.e., within the range of 65 to 75 Shore A durometer).

8.1.5.3.2 Tensile Strength and Elongation

The tensile strength of each lot of the butyl rubber material shall be determined in accordance with ASTM D412[7]. Each lot of butyl rubber material shall have a minimum tensile strength of 10 MPa (1,450 psi) and a minimum elongation of 250%.

8.1.5.3.3 Heat Resistance

The heat resistance of each lot of the butyl rubber material shall be determined in accordance with ASTM D573[8]. Each lot of butyl rubber material shall experience a maximum 10 Shore A durometer hardness increase, a maximum reduction in tensile strength of 25%, and a maximum reduction in ultimate elongation of 25%, when tested at 70 ºC (158 ºF).

---

[3] ASTM D2395–02, *Standard Test Methods for Specific Gravity of Wood and Wood–Based Materials*, American Society for Testing and Materials (ASTM).

[4] ASTM D4442–92(2003), *Standard Tests Methods for Direct Moisture Content Measurement of Wood and Wood–Based Materials*, American Society for Testing and Materials (ASTM).

[5] ASTM D4444–92(1998)e1, *Standard Tests Methods for Use and Calibration of Hand–Held Moisture Meters*, American Society for Testing and Materials (ASTM).

[6] ASTM D2240–05, *Standard Test Method for Rubber Property – Durometer Hardness,* American Society for Testing and Materials (ASTM).

[7] ASTM D412–98a(2002)e1, *Standard Test Methods for Vulcanized Rubber and Thermoplastic Rubbers and Thermoplastic Elastomers – Tension,* American Society for Testing and Materials (ASTM).

[8] ASTM D573–04, *Standard Test Method for Rubber – Deterioration in an Air Oven,* American Society for Testing and Materials (ASTM).

8.1.5.3.4 Compression Set

The compression set of each lot of the butyl rubber material shall be determined in accordance with Method B of ASTM D395[9]. After 22 hours at 70 ºC (158 ºF), each lot of butyl rubber material shall have a maximum compression set of 25%.

8.1.5.3.5 Cold Temperature Resistance

The cold temperature resistance of each lot of the butyl rubber material shall be determined in accordance with Method A, 9.3.2 of ASTM D2137[10]. After 3 minutes at -40 ºC (-40 ºF), each lot of butyl rubber material shall be non–brittle.

8.1.5.3.6 Cold Temperature Resiliency

The cold temperature resiliency of each lot of the butyl rubber material shall be determined in accordance with the TR–10 test of ASTM D1329[11]. Each lot of butyl rubber material shall be resilient at a test temperature of -50 ºC (-58 ºF) or less.

8.1.5.4 Calcium Silicate Insulation Board

This section establishes the requirements and acceptance criteria for inspection and testing of calcium silicate insulation board utilized within the TRUPACT–III packaging.

8.1.5.4.1 Composition

The insulation board supplier shall certify that the composition of the calcium silicate insulation board has a minimum fiber content of 95% mineral fibers.

8.1.5.4.2 Density

1. Three test samples shall be taken from each lot of calcium silicate insulation board. Each test sample shall be a rectangular prism with nominal dimensions of the sheet thickness (T) × 50 mm (2.0 in) wide (W) × 50 mm (2.0 in) long (L).
2. Place the test samples in a room (ambient) temperature environment (i.e., 20 ºC to 30 ºC [68 ºF to 86 ºF]) for sufficient time to thermally stabilize the test samples. Measure and record the room temperature to an accuracy of ±1 ºC (±2 ºF).
3. Measure and record the weight of each test sample to an accuracy of ±1 gram (±0.03 oz).
4. Measure and record the thickness, width, and length of each test sample to an accuracy of ±1 mm (0.04 in).

---

[9] ASTM D395–03, *Standard Test Methods for Rubber Property – Compression Set,* American Society for Testing and Materials (ASTM).

[10] ASTM D2137–94(2000), *Standard Test Methods for Rubber Property – Brittleness Point of Flexible Polymers and Coated Fabrics,* American Society for Testing and Materials (ASTM).

[11] ASTM D1329–02, *Standard Test Method for Evaluating Rubber Property – Retraction at Lower Temperatures (TR Test),* American Society for Testing and Materials (ASTM).

5. Determine and record the room temperature density of each test sample utilizing the following formula:

$$\rho_{cal\ sil} = \frac{\text{Weight, g}}{T \times W \times L,\ mm^3} \times \frac{10^6\ mm^3/dm^3}{10^3\ g/kg},\ kg/dm^3$$

6. Determine and record the average density of the three test samples. The numerically averaged density of the three test samples shall be 0.45 ±0.10 kg/dm^3 (28 ±6 lb$_m$/ft^3) (i.e., within the range of 0.35 to 0.55 kg/dm^3 [22 to 34 lb$_m$/ft^3]).

8.1.5.4.3 Thermal Conductivity

1. The thermal conductivity test shall be performed using a heat flow meter (HFM) apparatus. The HFM establishes steady state unidirectional heat flux through a test specimen between two parallel plates at constant but different temperatures. By measurement of the plate temperatures and plate separation, Fourier's law of heat conduction is used by the HFM to automatically calculate thermal conductivity. Description of a typical HFM test method is provided in ASTM C518. The HFM shall be calibrated against a traceable reference specimen per the HFM manufacturer's operating instructions.
2. Three test samples shall be taken from each lot of calcium silicate insulation board. Each test sample shall be of sufficient size to enable testing per the HFM manufacturer's operating instructions.
3. Place the test samples in a room (ambient) temperature environment (i.e., 20 ºC to 30 ºC [68 ºF to 86 ºF]) for sufficient time to thermally stabilize the test samples.
4. Measure and record the necessary test sample parameters as input data to the HFM apparatus per the HFM manufacturer's operating instructions.
5. Perform thermal conductivity testing and record the measured thermal conductivity for each test sample following the HFM manufacturer's operating instructions.
6. Determine and record the average thermal conductivity of the three test samples. The numerically averaged thermal conductivity of the three test samples shall be 0.085 ±0.017 W/m–K (0.59 ±0.12 Btu–in/hr–ft^2–ºF) (i.e., within the range of 0.068 to 0.102 W/m–K [0.47 to 0.71 Btu–in/(hr–ft^2–ºF)]).

8.1.6 Tests for Shielding Integrity

The TRUPACT–III packaging does not contain any biological shielding.

8.1.7 Thermal Acceptance Test

Material properties utilized in Chapter 3.0, *Thermal Evaluation*, are consistently conservative for the normal conditions of transport (NCT) and hypothetical accident condition (HAC) thermal analyses performed. With the exception of the tests required for polyurethane foam, wood, and calcium silicate insulation board, as shown in Section 8.1.5, *Component Tests*, specific acceptance tests for material thermal properties are not performed.

Table 8.1-1 – Foam Thermal Conductivity at 20 ºC to 30 ºC [68 ºF to 86 ºF]

Thermal Conductivity			
Density	**Nominal –20%**	**Nominal**	**Nominal +20%**
Kg/dm^3	**W/(m–K)**	**W/(m–K)**	**W/(m–K)**
0.10	0.024	0.030	0.036
0.16	0.025	0.031	0.037
0.29	0.038	0.047	0.056
0.48	0.055	0.069	0.083

Table 8.1-2 – Foam Compressive Strength, Parallel–to–Rise, at 20 ºC to 30 ºC [68 ºF to 86 ºF]

	Minimum		**Nominal**	**Maximum**	
	Nom. -15%	**Nom. -10%**		**Nom. +10%**	**Nom. +15%**
Strain	**Crush Strength, MPa (psi) (Note: Metric units govern)**				
Density 0.10 kg/dm^3 (6 lb/ft^3)					
10%	0.83 (120)	0.88 (128)	0.98 (142)	1.08 (157)	1.13 (164)
40%	0.89 (129)	0.95 (138)	1.05 (152)	1.16 (168)	1.21 (175)
70%	1.83 (265)	1.94 (281)	2.15 (312)	2.37 (344)	2.47 (358)
Density 0.16 kg/dm^3 (10 lb/ft^3)					
10%	1.96 (284)	2.07 (300)	2.30 (334)	2.53 (367)	2.65 (384)
40%	2.15 (312)	2.28 (331)	2.53 (367)	2.78 (403)	2.91 (422)
70%	5.59 (811)	5.92 (858)	6.58 (954)	7.24 (1,050)	7.57 (1,098)
Density 0.29 kg/dm^3 (18 lb/ft^3)					
10%	5.85 (848)	6.19 (898)	6.88 (998)	7.57 (1,098)	7.91 (1,147)
40%	7.16 (1,038)	7.58 (1,099)	8.42 (1,221)	9.26 (1,343)	9.68 (1,404)
70%	21.11 (3,061)	22.35 (3,241)	24.83 (3,600)	27.31 (3,560)	28.55 (4,140)
Density 0.48 kg/dm^3 (30 lb/ft^3)					
10%	15.27 (2,214)	16.17 (2,345)	17.97 (2,606)	19.77 (2,867)	20.67 (2,997)
40%	20.67 (2,997)	21.89 (3,174)	24.32 (3,526)	26.75 (3,879)	27.97 (4,056)
60%	38.16 (5,533)	40.40 (5,858)	44.89 (6,509)	49.38 (7,160)	51.62 (7,485)

Table 8.1-3 – Foam Compressive Strength, Perpendicular–to–Rise, at 20 ºC to 30 ºC [68 ºF to 86 ºF]

Strain	Minimum		Nominal	Maximum	
	Nom. -15%	Nom. -10%		Nom. +10%	Nom. +15%
	Crush Strength, MPa (psi) (Note: Metric units govern)				
Density 0.10 kg/dm^3 (6 lb/ft^3)					
10%	0.82 (119)	0.86 (125)	0.96 (139)	1.06 (154)	1.10 (160)
40%	0.86 (125)	0.91 (132)	1.01 (146)	1.11 (161)	1.16 (168)
70%	1.83 (265)	1.94 (281)	2.15 (312)	2.37 (344)	2.47 (358)
Density 0.16 kg/dm^3 (10 lb/ft^3)					
10%	1.96 (284)	2.07 (300)	2.30 (334)	2.53 (367)	2.65 (384)
40%	2.15 (312)	2.28 (331)	2.53 (367)	2.78 (403)	2.91 (422)
70%	5.69 (825)	6.02 (873)	6.69 (970)	7.36 (1,067)	7.69 (1,115)
Density 0.29 kg/dm^3 (18 lb/ft^3)					
10%	5.81 (842)	6.15 (892)	6.83 (990)	7.51 (1,089)	7.85 (1,138)
40%	7.10 (1,030)	7.52 (1,090)	8.35 (1,211)	9.19 (1,333)	9.60 (1,392)
70%	20.98 (3,042)	22.21 (3,220)	24.68 (3,579)	27.15 (3,937)	28.38 (4,115)
Density 0.48 kg/dm^3 (30 lb/ft^3)					
10%	15.30 (2,219)	16.20 (2,349)	18.00 (2,610)	19.80 (2,871)	20.70 (3,002)
40%	20.70 (3,002)	21.92 (3,178)	24.35 (3,531)	26.79 (3,885)	28.00 (4,060)
60%	38.42 (5,571)	40.68 (5,899)	45.20 (6,554)	49.72 (7,209)	51.98 (7,537)

This page intentionally left blank.

8.2 Maintenance Program

This section describes the maintenance program used to ensure continued performance of the TRUPACT–III package.

8.2.1 Structural and Pressure Tests

8.2.1.1 Containment Vessel Pressure Testing

Perform structural pressure testing on the containment vessel (i.e., the CSA) per the requirements of Section 8.1.3.2, *Containment Vessel Pressure Testing*, once every five years. Upon completing the structural pressure test, perform leakage rate testing per the requirements of Section 8.1.4, *Fabrication Leakage Rate Tests*.

8.2.1.2 Interior Cavity Surfaces Inspection

Annual inspection shall be performed of the accessible interior surfaces of the payload cavity for chemically induced corrosion. After removal of the payload loading system, perform a visual inspection for indications of interior surface corrosion. Should evidence of corrosion exist, a liquid penetrant inspection of the interior surfaces shall be performed per ASME Boiler and Pressure Vessel Code, Section V[1], Article 6, and ASME Boiler and Pressure Vessel Code, Section III[2], Division 1, Subsection NB, Article NB–5000. Indications of cracking or distortion shall be evaluated in accordance with the cognizant quality assurance program.

Once the packaging is placed into service, at a maximum interval of five (5) years, an examination shall be performed on the accessible interior surfaces for evidence of chemically induced stress corrosion. This examination shall consist of a liquid penetrant inspection of all accessible welds and adjacent base metal (minimum 13 mm [0.5 in.] on each side of the weld), and shall be performed per ASME Boiler and Pressure Vessel Code, Section V, Article 6, and ASME Boiler and Pressure Vessel Code, Section III, Division 1, Subsection NB, Article NB–5000, as delineated on the drawings in Appendix 1.3.1, *Packaging General Arrangement Drawings*. Indications of cracking or distortion shall be evaluated in accordance with the cognizant quality assurance program prior to implementing corrective actions.

8.2.2 Maintenance/Periodic Leakage Rate Tests

This section provides the generalized procedure for maintenance/periodic leakage rate testing of the containment vessel penetrations during routine maintenance, or at the time of seal replacement or

[1] American Society of Mechanical Engineers (ASME) Boiler and Pressure Vessel Code, Section V, *Nondestructive Examination*, 2004 Edition, 2005 and 2006 Addenda.

[2] American Society of Mechanical Engineers (ASME) Boiler and Pressure Vessel Code, Section III, *Rules for Construction of Nuclear Power Plant Components*, 2004 Edition, 2005 and 2006 Addenda.

seal area repair. Maintenance leakage rate testing shall follow the guidelines of Section 7.4, *Maintenance Leakage Rate Test*, and Section 7.5, *Periodic Leakage Rate Test*, of ANSI N14.5[3].

Maintenance/periodic leakage rate testing shall be performed on the main O–ring seal and vent port insert O–ring seal for the containment structural assembly (CSA) in accordance with Section 8.2.2.2, *Helium Leakage Rate Testing the Main Containment O–ring Seal*, and 8.2.2.3, *Helium Leakage Rate Testing the Vent Port Insert O–ring Seal*. Each leakage rate test shall meet the acceptance criteria delineated in Section 8.2.2.1, *Maintenance/Periodic Leakage Rate Test Acceptance Criteria*.

8.2.2.1 Maintenance/Periodic Leakage Rate Test Acceptance Criteria

Maintenance/periodic leakage rate test acceptance criteria are identical to the criteria delineated in Section 8.1.4.1, *Fabrication Leakage Rate Test Acceptance Criteria*.

8.2.2.2 Helium Leakage Rate Testing the Main Containment O–ring Seal

1. The maintenance/periodic leakage rate test of the main containment O–ring seal (inner) shall be performed following the guidelines of Section A.5.4, *Evacuated Envelope – Gas Detector*, of ANSI N14.5.
2. The CSA shall be assembled with both main O–ring seals installed into the closure lid. If not previously tightened, tighten the closure bolts to 1,480 – 1,720 N–m (1,092 – 1,269 lb_f–ft) torque as shown in Appendix 1.3.1, *Packaging General Arrangement Drawings*.
3. Remove the vent port locking ring and the vent port dust plug, and back–off or remove the vent port retaining ring and vent port insert. Install an adapter to the vent port to allow gas flow to and from the cavity.
4. Connect a vacuum pump to the adapter on the vent port, and evacuate the payload cavity to 90% vacuum or better (i.e., ≤10% ambient atmospheric pressure).
5. Remove the seal test port plug in the closure lid. Install an adapter to the seal test port.
6. Install a helium mass spectrometer leak detector to the adapter on the seal test port. Evacuate through the seal test port until the vacuum is sufficient to operate the helium mass spectrometer leak detector.
7. Provide a helium atmosphere inside the payload cavity by backfilling with helium gas to a pressure slightly greater than atmospheric pressure, i.e., +7, -0 kPa (+1, -0 psig).
8. Perform the helium leakage rate test to the requirements of Section 8.1.4.1, *Fabrication Leakage Rate Test Acceptance Criteria*. If, after repeated attempts, the main containment O–ring seal fails to pass the leakage rate test, isolate the leak path and, prior to repairing the leak path and repeating the leakage rate test, record on a nonconformance report and disposition prior to final acceptance in accordance with the cognizant quality assurance program.
9. If the vent port retaining ring/vent port insert was removed, remove the vent port adapter and re–install the vent port retaining ring/vent port insert; tighten to 370 – 430 N–m (273 – 317 lb_f–ft) torque.

[3] ANSI N14.5–1997 (or later), *American National Standard for Radioactive Materials – Leakage Tests on Packages for Shipment,* American National Standards Institute, Inc. (ANSI).

10. If the vent port retaining ring/vent port insert was not removed, tighten the vent port retaining ring/vent port insert to 370 – 430 N–m (273 – 317 lb_f–ft) torque using the vent port adapter.
11. Install the seal test port plug; tighten to 8 – 12 N–m (5 – 9 lb_f–ft) torque.
12. If the helium leakage rate testing of the vent port insert O–ring seal is to be performed immediately following this test, Steps 13 through 15 may be omitted.
13. If not previously removed, remove the vent port adapter.
14. Install the vent port locking ring; tighten to 370 – 430 N–m (273 – 317 lb_f–ft) torque.
15. Install the vent port dust plug; tighten to 90 – 110 N–m (66 – 81 lb_f–ft) torque.

8.2.2.3 Helium Leakage Rate Testing the Vent Port Insert O–ring Seal

The vent port insert O–ring seal test may be performed either with the closure lid assembled to or with the closure lid removed from the body of the TRUPACT–III packaging, as described in the following sections.

8.2.2.3.1 Testing with the Closure Lid Assembled to the Body

1. The maintenance/periodic leakage rate test of the vent port insert O–ring seal shall be performed following the guidelines of Section A.5.4, *Evacuated Envelope – Gas Detector*, of ANSI N14.5.
2. If this test immediately follows the testing from Section 8.2.2, *Helium Leakage Rate Testing the Main Containment O–ring Seal* (i.e., helium atmosphere already exists in the payload cavity, and the vent port retaining ring/vent port insert is closed and properly tightened), proceed to Step 9**.**
3. The CSA shall be assembled as shown in Appendix 1.3.1, *Packaging General Arrangement Drawings*.
4. Remove the vent port locking ring and vent port dust plug.
5. Install an adapter to the internal threads of the vent port and retract the vent port retaining ring/vent port insert to allow gas to flow to and from the payload cavity.
6. Connect a vacuum pump to the evacuation envelope and evacuate the envelope to 90% vacuum or better (i.e., ≤10% ambient atmospheric pressure).
7. Provide a helium atmosphere inside the payload cavity by backfilling with helium gas to a pressure slightly greater than atmospheric pressure, i.e., +7, -0 kPa (+1, -0 psig).
8. Utilizing an adaptor, tighten the vent port retaining ring to 370 – 430 N–m (273 – 317 lb_f–ft) torque.
9. If previously removed, install the vent port adapter to the vent port.
10. Install a helium mass spectrometer leak detector to the adapter on the vent port. Evacuate through the vent port until the vacuum is sufficient to operate the helium mass spectrometer leak detector.
11. Perform the helium leakage rate test to the requirements of Section 8.1.4.1, *Fabrication Leakage Rate Test Acceptance Criteria*. If, after repeated attempts, the vent port insert O–ring seal fails to pass the leakage rate test, isolate the leak path and, prior to repairing the leak path and repeating the leakage rate test, record on a nonconformance report and disposition prior to final acceptance in accordance with the cognizant quality assurance program.

12. Remove the vent port adapter.
13. Install the vent port locking ring; tighten to 370 – 430 N–m (273 – 317 lb_f–ft) torque.
14. Install the vent port dust plug; tighten to 90 – 110 N–m (66– 81 lb_f–ft) torque.

8.2.2.3.2 Testing with the Closure Lid Removed from the Body

As an alternative to Section 8.2.2.3.1, *Testing with the Closure Lid Assembled to the Body*, the vent port insert O–ring seal test may be performed with the assembled closure lid separate from the body. Operational steps are the same as established in Section 8.2.2.3.1, except that instead of utilizing the TRUPACT–III payload cavity to establish the required helium atmosphere, a localized envelope is established over the ∅50–mm vent port on the inside surface of the closure lid.

8.2.3 Component and Material Tests

8.2.3.1 Fasteners

All threaded components shall be inspected annually for deformed or stripped threads. Damaged components shall be repaired or replaced prior to further use. The threaded components to be visually inspected include the closure lid bolts, the overpack cover attachment bolts, the vent port insert, retaining ring, and locking ring, the vent port dust plug, the seal test port plug, the body helium fill access plugs, the body helium fill port plug, and all internal threads (i.e., holes and the optional threaded inserts, if applicable).

Regardless of condition, closure lid bolts and overpack cover attachment bolts shall be replaced after no more than 250 service cycles. A service cycle is defined as two tightening operations.

8.2.3.2 Seal Areas and Grooves

8.2.3.2.1 Seal Area Routine Inspection and Repair

Before each use and at the time of seal replacement, the sealing surfaces on the closure lid and body shall be visually inspected for damage that could impair the sealing capabilities of the TRUPACT–III packaging. Perform surface finish inspections for the body flange, and the O–ring grooves and mating sealing surfaces on the closure lid. Damage shall be corrected prior to further use (e.g., using emery cloth restore sealing surfaces) to the surface finish specified in Section 8.2.3.2.2, *Surface Finish of Sealing Areas*.

Upon completion of containment seal area repairs, perform a leakage rate test per the applicable section of Section 8.2.2, *Maintenance/Periodic Leakage Rate Tests*.

8.2.3.2.2 Surface Finish of Sealing Areas

The surface finish for the main O–ring sealing regions shall be a 0.8 micro–mm (32 micro–inches) finish, or better, to maintain package configuration and performance to design criteria. If the surface condition is determined to exceed 0.8 micro–mm (32 micro–inches), repair the surface per the requirements of Section 8.2.3.2.1, *Seal Area Routine Inspection and Repair*.

8.2.4 Thermal Tests

No thermal tests are necessary to ensure continued performance of the TRUPACT–III packaging.

8.2.5 Miscellaneous Tests

8.2.5.1 Valves and Rupture Discs

The TRUPACT–III packaging does not contain any valves or rupture discs on the containment vessel.

8.2.5.2 Gaskets

Containment boundary O–ring seals and the debris shield silicone foam insert shall be replaced within the 12–month period prior to shipment or when damaged (whichever is sooner), per the size and material requirements delineated on the drawings in Appendix 1.3.1, *Packaging General Arrangement Drawings*. Following containment O–ring seal replacement and prior to a loaded shipment, the new O–ring seals shall be leakage rate tested to the requirements of Section 8.2.2, *Maintenance/Periodic Leakage Rate Tests*.

8.2.5.3 Shielding

The TRUPACT–III packaging does not contain any biological shielding.

8.2.5.4 Passive Filters

The function of the passive polyethylene filters that are installed on the closure lid shall be verified within the 12–month period prior to shipment or when damaged (whichever is sooner). Verification of the passive filter function is determined by applying an air supply to one side of the filter to ensure air passes through the filter. Should a passive filter be determined to fail the function test or is damaged, the filter shall be replaced per the size and material requirements delineated on the drawings in Appendix 1.3.1, *Packaging General Arrangement Drawings*.

This page intentionally left blank.